ABSTRACT

Title of Dissertation:	SYNTHESIS AND MOLECULAR RECOGNITION PROPERTIES OF ACYCLIC CUCURBIT[N]URIL AND ITS DERIVATIVES
	Sandra A. Zebaze Ndendjio, Doctor of Philosophy, 2020
Dissertation directed by:	Professor Lyle Isaacs, Department of Chemistry & Biochemistry

The study of molecular containers has accelerated dramatically since the 1960's. The introduction of cucurbit[n]urils has contributed tremendously and continues to contribute to the expansion of the field. Chapter 1 introduces cucurbit[n]urils and their molecular recognition properties toward amino acids, peptides, and Insulin. Followed by an overview of the history of CB[n] and their analogs made with modified glycoluril backbone, solubilizing groups, alkyl arm linker, and type of aromatic arms.

Chapter 2 describes the application of the acyclic CB[n], Calabadion **1** and **2** for the molecular recognition of amino acids, peptides, and Insulin. The results show that **1** and **2** have preferential binding affinity toward aromatic (e.g. H-Phe-NH_2) and di-cationic (e.g. H-Lys-NH_2) amino acid amides. Electrostatic interactions between the tetraanionic **1** and **2** with the amino acid guests (in their N-acetylated,

zwitterionic, or CO-NH_2 forms) was demonstrated to dramatically influence the strength of the recognition process. The binding affinity of **1** and **2** toward insulin was compared to that of CB[7], respectively (K_a= 1.32 × 10^5 M^{-1} for **1**, 3.47 × 10^5 M^{-1} for **2**, and 5.59 × 10^5 M^{-1} for CB[7]) which showed comparable levels of affinity between these three hosts.

Chapter 3 introduces a new acyclic CB[n] featuring a central glycoluril trimer with sulfonated triptycene aromatic sidewalls. It was observed that the binding affinity increases as the alkyl chain length of the guest increases. An x-ray crystal structure reveals an overall out-of-plane distortion of the aromatic sidewalls and intermolecular packing driven by interactions between the external faces of the triptycene sidewalls. Finally, the trimer host was shown to bind strongly to fentanyl which suggests potential usage as in vivo reversal agent.

In chapter 4, an analog of **1** was synthesized in which the $(CH_2)_3$ linking group was removed. This structural change brings the anionic sulfate substituents closer to the electrostatically negative ureidyl C=O portals. We find that this new host displays preferential binding affinity toward quaternary ammonium ioins and a higher binding affinity toward dications compared to **1**. Most impressive are the nanomolar binding affinities toward rocuronium and vecuronium which suggests potential application for in vivo reversal agent.

SYNTHESIS AND MOLECULAR RECOGNITION PROPERTIES OF ACYCLIC CUCURBIT[N]URIL AND ITS DERIVATIVES

by

Sandra A. Zebaze Ndendjio

Dissertation submitted to the Faculty of the Graduate School of the
University of Maryland, College Park, in partial fulfillment
of the requirements for the degree of
Doctor of Philosophy
2020

Advisory Committee:
Professor Lyle Isaacs, Chair
Professor Jeffrey Davis
Professor Philip DeShong
Professor Myles Poulin
Professor Akua Asa-Awuku, Dean's representative

Dedication

To my parents, particularly, my mother Marie T. Lekane, but also my three siblings, Sonia Ndeloa, Wilfried Zebaze, and Rolling Zebaze, and my aunt Madeleine Dongmo.

Acknowledgements

I would like to thank my Ph.D. advisor Dr. Lyle Isaacs for his support, guidance and mentoring in the past five years. I'm forever thankful for the amazing opportunity that was offered to me by Dr. Isaacs, the chance to work in the forefront of scientific research. I experience many challenges, setbacks, and mental fatigues, but throughout it all Dr. Isaacs never gave up on me even when I was ready to abandon the project. Thanks to him, I learned to be resilient and rigorous. His strong work ethics became an example for me, as I learned to raise my own standard and develop a higher self-confidence. These priceless skills have made me into a better chemist.

I would like to acknowledge Dr. Philip DeShong who not only encouraged me during my undergraduate studies but continued to inspire and push me to reach my best during my graduate studies. Additionally, Dr. Herman Sintim who first introduced me to the world of research as an undergraduate student at the University of Maryland in College Park. My successful journey to my Ph.D. was made possible because of the financial support from the Ronald E. McNair program and the Louis-Stokes Alliance for Minority program (LSAMP), the National Science Foundation (CHE-1404911, CHE-1807486), the National Institutes of Health (GM132345, GM124270).

I would also like to thank former and current Isaacs group members, namely, Brittany Vinciguerra, Shweta Ganapati, David Sigwalt, Soumen Samanta, Xiaoyong Lu, Wenjin Liu, Weijian Xue, Nicholas Yvanez, Steven Murkli, Kimberly Brady, David King, Delaney Patterson, Ming Cheng, and Chunlin Deng. My labmates have

helped me tremendously when dealing with technical difficulties particularly with instrumentations and literature reviews for my research project. A special thank you to my undergraduate student Rohan Shah who has assisted me in setting up multiple experiments and running Isothermal Titration Calorimetric studies.

I would like to extend my sincere gratitude to Dr. Peter Zavalij and Dr. Fu Chen for assistance with X-ray crystallography and Nuclear Magnetic Resonance (NMR). I would also like to thank Dolores Jackson for emotional support and tips on time management, Dr. Theodore Kwaku-Dayie and all the members of the National Organization of Black Chemists and Chemical Engineers (NOBCChE) organization at the University of Maryland.

Finally, I would like to thank my family members in the United States, Cameroon, and Gabon. My mother and my aunt who have supported me from the beginning and brought me food when I was overwhelmed with work. My siblings for providing me with entertainment when I was stressing out with my research project. Jude Ndeloa who fixed my computer and my two nephews Ethan and Liam Ndeloa.

Table of Contents

List of Tables

Chapter 1

Chapter 2

Chapter 3

Chapter 4

List of Figures

Chapter 1

Chapter 2

Chapter 3

List of Schemes

Chapter 1

Chapter 3

Chapter 4

Chapter 5

List of Abbreviations

^{1}H NMR	proton nuclear magnetic resonance
^{13}C NMR	carbon-13 nuclear magnetic resonance
Å	angstrom
Ach	acetylcholine
br	broad
BSA	bovine serum albumin
CB[n]	cucurbit[n]uril
CD	cyclodextrin
d	doublet
DPT	2,7-dimethyldiazaphenanthrenium
D_2O	deuterium oxide
DMSO	dimethyl sulfoxide
DOSY	diffusion-ordered spectroscopy
ESI-MS	electrospray ionization-mass spectrometry
EtOH	ethanol
g	gram
H	hydrogen
h	hour
HCl	hydrochloric acid
H_2SO_4	sulfuric acid
HP-β-CD	hydroxypropyl-β-cyclodextrin

Hz	hertz
IR	infrared
ITC	isothermal titration calorimetry
J	coupling constant
K	kelvin
K_a	Binding affinity
kg	kilogram
M	molar
m	multiplet
M.p.	melting point
m/z	mass to charge ratio
M^+	molecular ion
Me	methyl
MeOH	methanol
MHz	megahertz
mg	milligram
min	minute
mL	milliliter
mM	millimolar
MW	molecular weight
M1	Motor 1
M2	Motor 2

M2C2	Motor 2 with a two-carbon long alkyl chain linker
M2C4	Motor 2 with a four-carbon long alkyl chain linker
MBBI	tetramethylbenzobis(imidazolium
MV	Methyl viologen
N	binding stoichiometry
NaOH	sodium hydroxide
NaH_2PO_4	sodium monophosphate
NMR	nuclear magnetic resonance
o	ortho
OH	Hydroxyl group
p	para
Ph	phenyl
ppm	parts per million
PXDA	para-xylylene diammonium ion
RT	room temperature
s	singlet
t	triplet
TFA	trifluoroacetic acid
USFDA	Food and Drug Administration
UV/Vis	Ultraviolet/ visible
$\Delta\delta$	change in chemical shift
ΔH	change in enthalpy

ΔG	Change in free energy
ΔS	change in entropy
μM	micromolar
π	pi

Chapter 1: Introduction to Molecular Containers

1.1 Introduction to Molecular Recognition

Supramolecular chemistry also known as "Chemistry beyond molecule" was first conceptualized by Prof. Dr. Jean-Marie Lehn. Prof. Lehn describes supramolecular chemistry as the study of intermolecular forces such as non-covalent interactions (Hydrogen bonding, ion-dipole interactions, and π-π interactions) between molecules that can be used to bring molecular entities together to form a supramolecular complex that often exhibit properties that are distinct from their molecular components.to form a new complex.[1] Underneath the overarching theme of supramolecular chemistry, lies multiple conceptual and application areas including molecular self-assembly, molecular recognition, molecular interlocking, catalysis, drug solubilization and delivery[2]. Within the realm of biology, it is clear that many biological functions cellular transport, cell-cell communications and enzymatic functions are driven by high affinity and high selectivity molecular recognition events that are carefully orchestrated in space and time. The main focus of this dissertation is the synthesis and molecular recognition properties of a new class of supramolecular hosts known as cucurbit[n]urils (CB[n]) that also exhibit high binding affinity and high selectivity in aqueous solution toward hydrophobic ammonium ions. As the target guests we have focused, in part, on those guests that are components of or display interesting biological functions.

Beyond the molecular recognition properties of CB[n]-type hosts lies interest in using supramolecular systems to control catalytic processes of designed systems.[3]

Molecular recognition is the specific association of two or more guests driven by non-covalent interactions including hydrophobic effect, hydrogen bonding, and shape and size complementarity, polarity etc.[4] Enzymes use two mechanisms for molecular recognitions the "lock and key" mechanism and the "induced fit" mechanism[5]. The binding of the substrate to the active site of the enzyme is critical for the efficiency of the enzymatic activity. In the lock and key mechanism, the substrate fits precisely in the enzyme active site through shape and size complementarity. In the induced fit model, the conformation of the substrate and the enzyme changes to simultaneously to complement each other in order to induce the binding. Of major interest to supramolecular chemist is the synthesis of molecular artificial receptors able to mimic the functioning of enzymes in biological conditions.[6] This introduction section discusses molecular hosts and their applications with a focus on cucurbit[n]urils, acyclic cucurbit[n]uril and its derivatives.

1.2 Introduction to Macrocyclic Hosts

Macrocyclic receptors are host molecules that are able to bind to and sequester smaller molecule typically within a central cavity. Such macrocyclic receptors are often referred to as molecular container compounds because they are able to hold onto their guests in much the same way that real-world containers hold onto other objects. The encapsulation of guest molecules within these molecular containers results in new entities known as host•guest complexes that can display properties that are different from those of the components. For example, host•guest complexes may enhance the solubility of poorly soluble guests, can prolong the lifetime of guests that are prone to decomposition reactions, can suppress the vapor pressure of guests that

are malodorous, and can even influence the *in vitro* and *in vivo* activity of biological active guests.[7] Of course, the successful creation of such functional systems requires the availability of high affinity host systems to effectively sequester the guests. Below, I present examples of other popular host systems that are used in these and related applications, along with some of the guiding principles in the creation or discovery of high affinity host systems.

The 1987 Nobel Prize in Chemistry was awarded in part to Professor Donald J. Cram for his elucidation of the principle of preorganization,[8-10] which is one route to enables the formation of stable host-guest complexes. The principle of preorganization states that the closer the geometry and solvation of the uncomplexed host and uncomplexed guest resemble their host•guest complex the more stable their host•guest complex will be.[10] Accordingly, a key question in the field of supramolecular chemistry and more specifically molecular container chemistry is how to generate a preorganized host? Host•guest complexes generally feature a smaller guest molecule that is more or less surrounded by the larger host molecule (Figure I-1).

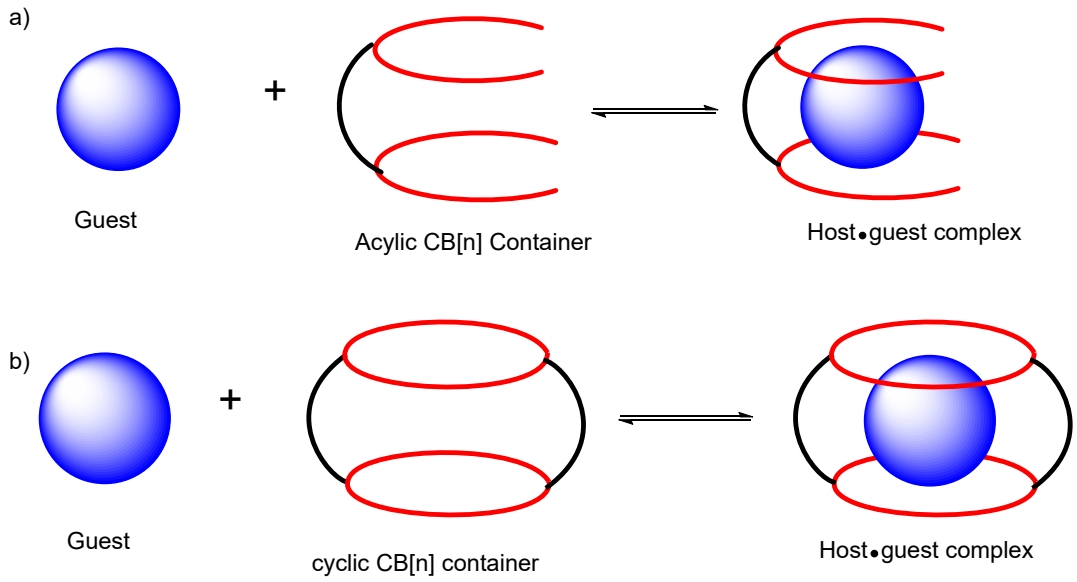

Figure I-1. Illustration of host• guest complexation. a) complexation between a C-shaped container and a guest. b) complexation between a cyclic shaped container and a guest

For example, Figure I-1a shows the geometry of the hypothetic complex formed between a roughly spherical guest and an acyclic C-shaped host. In order to assume the C-shaped conformation required for binding the hypothetical acyclic hosts typically must restrict many rotational degrees of freedom (e.g. $(CH_2)_n$ linkers) which is energetically costly and thereby reduces the observed free energy of complexation. Accordingly, one way to reduce the energetic penalty incurred upon host•guest complexation is simply to pay the energetic price of conformational restriction during the synthesis by the formation of a macrocyclic host that has fewer conformational degrees of freedom.

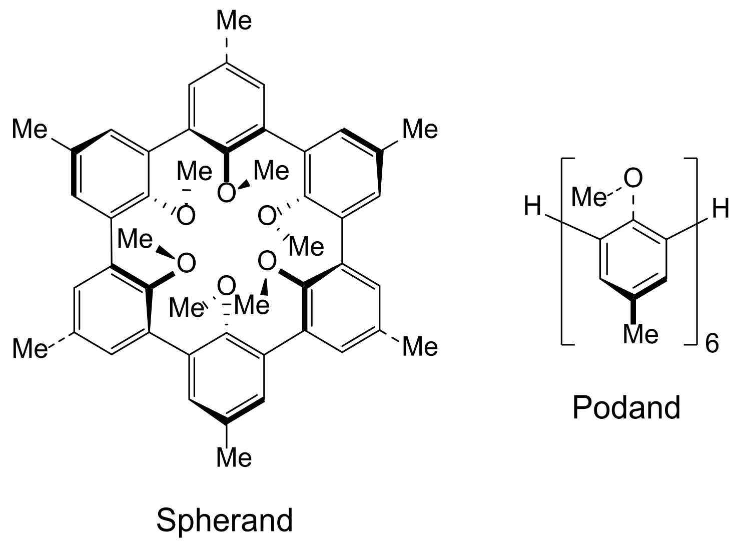

Figure I-2. Chemical structure of Spherand and Podand.

A seminal example of the power of preorganization comes from the work of Cram who studied the binding of spherand and its acyclic analogue toward Li^+ and observed a >17 kcal mol^{-1} decrease in affinity due to the cleavage of a single carbon-carbon bond (Figure I-2). Popular examples of macrocyclic host systems also include CB[n], cyclodextrins, 4-sulfo-calix[4]arene (Figure I-3). However, acyclic systems are also capable of exhibiting variable degrees of preorganization. For example, in 1978 Whitlock, the term "Molecular Tweezers" to refer to a class of acyclic molecular receptors with two flat arms, generally aromatic, separated by a more or less rigid spacer, that converge on one another and define a pocket for guest inclusion.[11] The group of Professor Steven Zimmerman has made large contributions toward the development of the field of molecular tweezers. Of more direct relevance to the work described in this dissertation is the work of Prof. Roeland Nolte and Prof. Frank-Gerrit Klaerner on the glycoluril derived molecular clips and benzonorbornene derived molecular tweezers, respectively (Figure I-3). Klaerner's phosphorylated

molecular tweezers are water soluble, exhibit high binding affinities, and selectivity toward arginine and lysine peptide residues up to 10^4 M^{-1}.[12-14] It was further demonstrated that they are able to function as inhibitors of amyloid plaque formation due to their specific interaction to the lysine residue of the amyloid β protein.[13, 15] Prof. Roeland Nolte's group developed molecular clips composed of one central diphenyl glycoluril ring and two aromatic *o*-xylylene rings.[16] By virtue of the conformational preferences of the seven-membered rings connecting the central bicyclic glycoluril unit to the aromatic sidewalls, these molecular clips feature a binding cleft. Nolte's molecular clips are pre-organized despite the lack of a macrocycle, relying instead on the conformational preferences of the fused polycyclic ring system.

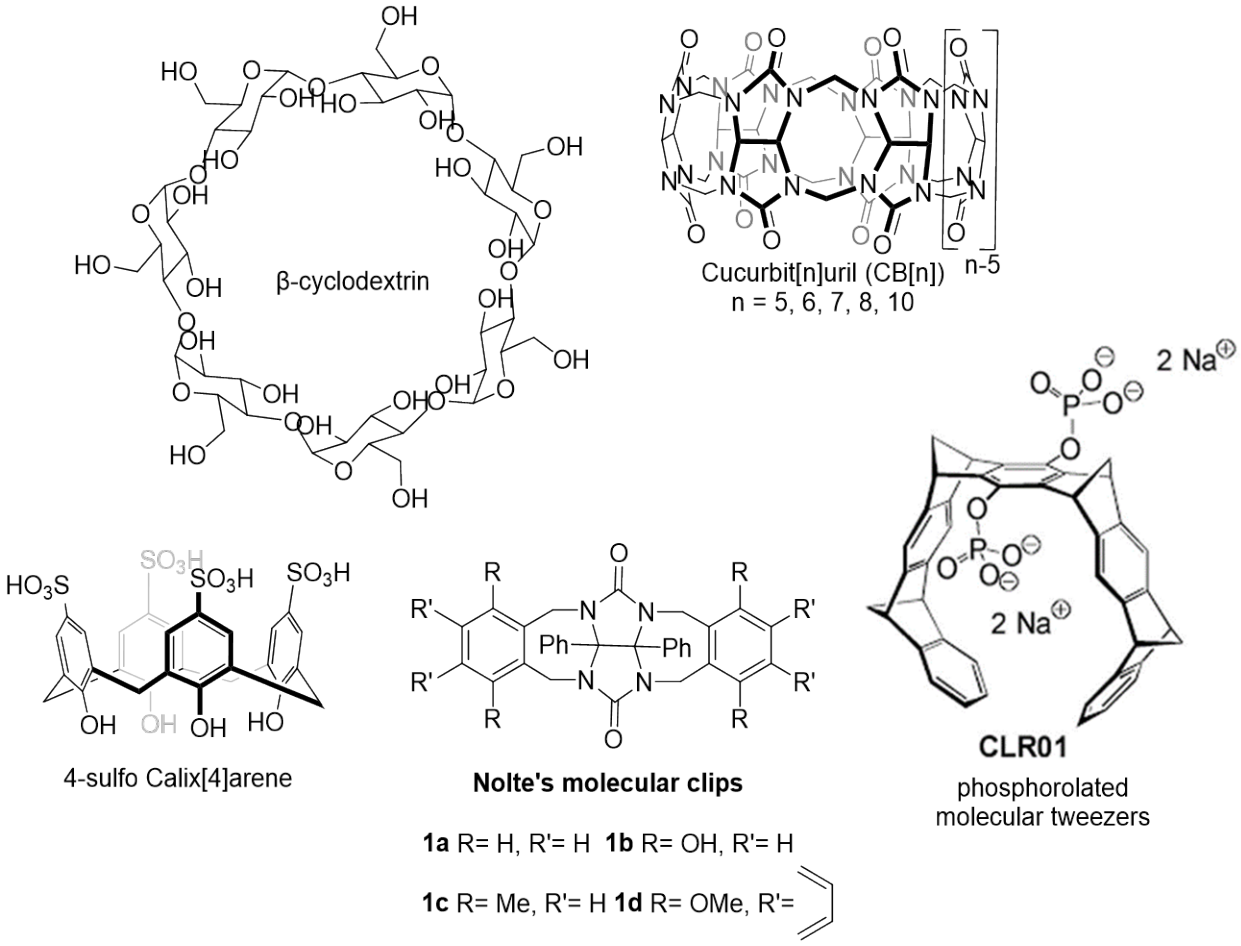

Figure I-3. Chemical structures of selected molecular container molecules including β-Cyclodextrins, CB[n], 4-sulfo Calix [4] arene, and Klaerners phosphorylated molecular tweezers and Nolte's molecular clips.

A brief description of the structures and binding properties of calixarenes, cyclodextrins, and various cyclophanes are given below to serve as an introduction to the broader field of molecular containers. Calixarenes are composed of n aromatic rings (n = 4 – 8 mainly) – typically phenols – linked in the 2,6-positions (e.g. meta linkages) by methylene bridges.[17, 18] The synthetic chemistry of calixarenes is particularly well developed which allows the preparation of numerous variants for

molecular recognition of cations, anions, and molecular species in organic solvents and in water.[19, 20] Calixarenes are commercially available and have shown applications as ionophores for membrane transport, extractants, stationary phases, electrode ionophores and in optical, electrochemical, biological and chemical sensors.[21] Calixarenes can exist in four different conformational forms, namely the cone, partial cone, 1,2-alternate, and 1,3-alternate conformers. Of highest relevance to molecular recognition of molecular guests is the cone conformation which features a bowl-shaped hydrophobic cavity. Of highest relevance to the research described in this dissertation is the molecular recognition properties of sulfo calix[4]arene (Figure I-3) that displays high solubility in water. Sulfo calix[4]arene is able to bind to hydrophobic molecules in water and particularly hydrophobic cations that benefit from ion-ion interactions and the hydrophobic effect upon complexation. The binding affinity of sulfo calix[4]arene toward such hydrophobic cations in water is typically in the range of $10^4 – 10^5$ M^{-1} which relatively low selectivity.[22] Despite this low affinity and selectivity, sulfo calix[4]arene has a variety of biological applications including as an in vivo reversal agents for the toxicity of methyl viologen.[23, 24]

Cyclodextrins are another type of widely used and commercially available molecular hosts. Cyclodextrins are macrocyclic oligomers composed of n glucose rings (α- n = 6, β- n = 7, γ- n= 8) connected by α-1,4-glycosidic bonds. Cyclodextrins are cheap, commercially available, nicely soluble in water, and non-toxic. Cyclodextrins exhibit molecular recognition properties toward hydrophobic cations, anions, and neutral molecules with K_a values up to $\approx 10^4$ M^{-1}. Cyclodextrins have been used for a variety of academic purposes including supramolecular

catalysis,[25, 26] chemical sensors,[27] stationary phases for chiral separations,[28] and supramolecular polymers and materials.[29] Cyclodextrins also have a variety of more practical everyday uses. For example hydroxypropyl-β-CD (HP-β-CD) is the active ingredient in the household product Febreze™ where the cyclodextrin serves to release a fragrance molecule and take up odorant molecules when sprayed in the air.[30] Cyclodextrins also have a variety of applications in pharmaceutical science. For example, HP-b-CD and sulfobutyl ether b-CD (SBE-CD, Captisol™) are used to increase the solubility and thereby formulate for human delivery > $5 billion per year of various active pharmaceutical ingredients.[31] Precise molecular engineering of γ-cyclodextrin allowed the creation of Sugammadex (figure I-4) which exhibits 10^7 M^{-1} affinity toward the clinically important neuromuscular blocking agents rocuronium and vecuronium.[32] Sugammadex is a billion dollar per year drug that is marketed by Merck under the trade name Bridion™ and is used as a reversal agent for these neuromuscular blockers post-surgically.

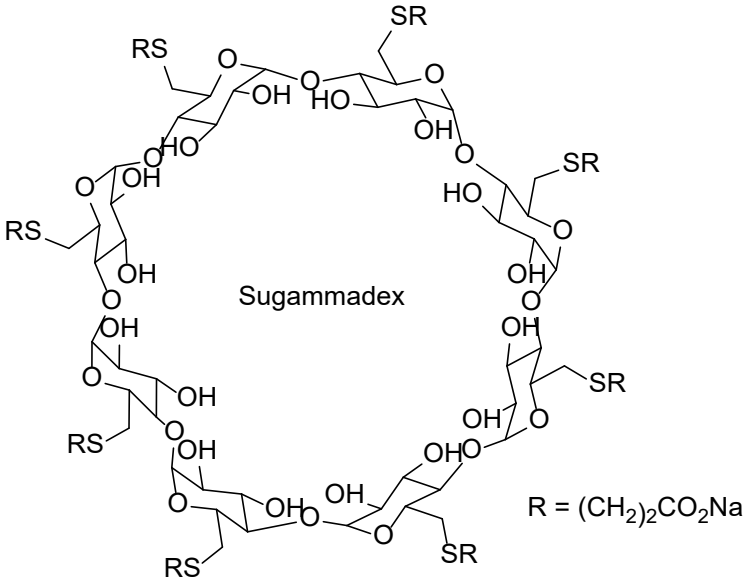

Figure I-4. Chemical structure of Sugammadex

The other most popular class of molecular container compounds are the cyclophanes which are macrocycles composed of aromatic building blocks and come in a variety of sizes and shapes. A complete description of all the different types of cyclophanes are beyond the scope of this introduction; the reader is referred to several reviews of aspects of this area.[33-38] An increasingly popular class of cyclophanes are the pillar[n]arenes (Figure I-5) which are composed of n phenylene or arylene units which are linked by methylene bridges in the para positions. The synthetic chemistry of pillararenes has rapidly developed in the past decade and pillararenes soluble in both organic solvents and water are available. Pillararenes have been used for a wide variety of applications including the purification of gases, membrane transport, supramolecular polymers, chemical sensors, and an increasing number of biomedical applications.[39, 40] Another class of cyclophanes that have drawn intense interest and ultimately garnered the 2016 Nobel Prize in Chemistry for the development of molecular machines for Professor Fraser Stoddart is the cationic cyclophane known as the blue box (Figure I-5).[41] By virtue of its cationic viologen walls, the cavity of the blue box is highly electron deficient and constitutes a binding site for electron ring aromatic rings. Furthermore, the viologen units are electrochemically active and can form the radical cations upon electrochemical reduction. This change in the electronic properties of the aromatic walls changes its molecular recognition properties and allows the construction of a variety of molecular devices like molecular switches, shuttles, elevators, and the like.[42-44] Most recently the Stoddart

group has greatly expanded the potential of this system by expanding the aromatic sidewalls and going into the third dimension to create cage systems.[41, 43]

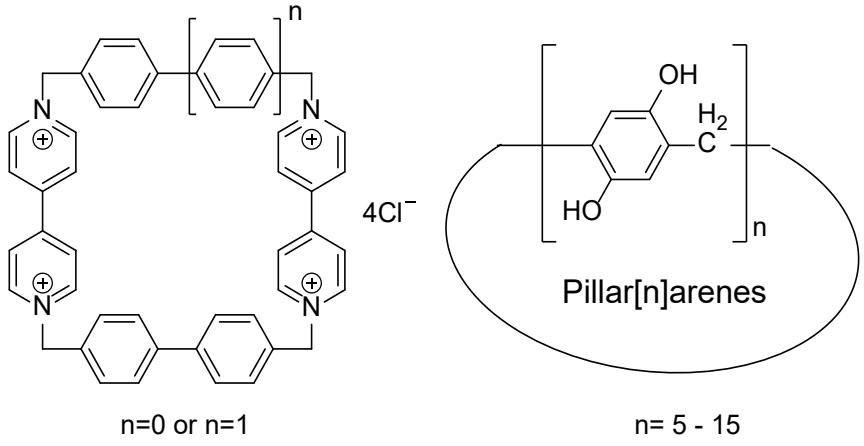

Figure I-5. Chemical structure of Blue box and general structure Pillar[n]arenes

1.3 The Cucurbit[n]uril Family of Molecular Containers

The molecular containers described above (e.g. calixarenes, cyclodextrins, cyclophanes) were constructed from aromatic or sugar building blocks. An alternative building block known as glycoluril (**1,** Scheme I-1**)** has also become popular in supramolecular chemistry. Because glycoluril is a bicyclic ring system and because it is concave its incorporation into molecular hosts facilitates the curvature needed for macrocyclization to cucurbiturils, for the preparation of C-shaped compounds that form dimeric assemblies by H-bond driven self-assembly,[45] and for the creation of molecular clips.[46] In 1905 Prof. Robert Behrend reported the condensation reaction of glycoluril with formaldehyde (2 equivalents) in concentrated HCl followed by recrystallization from conc. H_2SO_4 yielded a crystalline substance whose structure was not elucidated, but which possessed the ability to form

complexes with inorganic salts and dye stuffs (Scheme I-1).[47] The structural elucidation of the product of Behrend's reaction would need to wait until 1981 when Mock and co-workers structurally characterized it and dubbed it cucurbituril due to its resemblance to the segmented geometry of pumpkins which are members of the cucurbitaceae family of plants. Subsequently, cucurbituril has been referred to as cucurbit[6]uril (CB[6]) because it is composed of six glycoluril units. When the groups of Kim and co-workers and Day and co-workers conducted the cucurbituril forming reaction under milder conditions there were able to form and isolate the key members of the cucurbit[n]uril (n = 5, 6, 7, 8) family of molecular containers.[47-52]

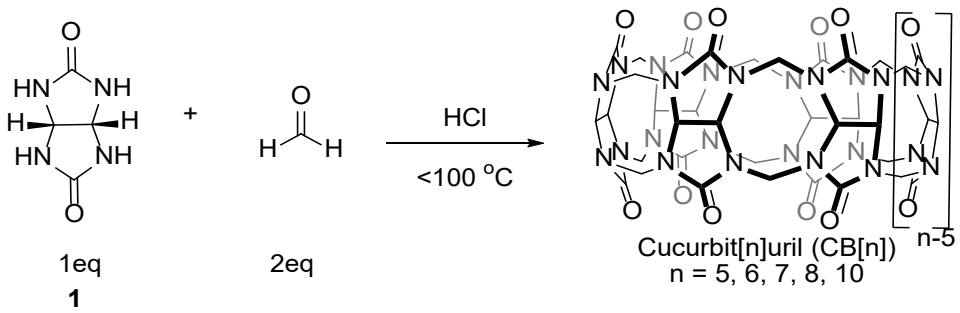

Scheme I-1. Synthesis of CB[n].

The structure of CB[n] molecular containers feature glycoluril monomers linked by pairs of methylene bridges. CB[n] molecular containers are structurally rigid, highly symmetric (D_{nh}), and contain a hydrophobic cavity surrounded by two electrostatically negative ureidyl carbonyl portals. The height of each CB[n] homologue is generally 9.1Å however, the volume of the cavity varies with the number of glycoluril repeat units. CB[5], the smallest homologue, has a volume of 68Å^3 making it optimal for inclusion of small gases such as N_2. CB[6] has a volume

of 142Å^3 and CB[7] has a large volume of 242Å^3 and CB[8] has an even larger volume of 367Å^3. The even numbered homologues (CB[6] and CB[8]) have low solubility in water (< 100 μM) whereas the odd numbered homologues (CB[5] and CB[7]) display higher (> 10 mM) solubility in water. The synthesis, molecular recognition properties, and applications of macrocyclic CB[n] hosts have been the subject of more than 2000 publications to date and the reader is referred to various authoritative reviews on the subject.[47, 49, 53-55] The most unique feature of the molecular recognition properties of CB[n] molecular containers is that they exhibit remarkably high binding affinities (K_a routinely 10^6 M^{-1}, often 10^9 M^{-1}, and even up to 10^{17} M^{-1} in special cases)[55, 56] hydrophobic (di)cations in water (Figure I-6). This remarkably tight binding is attributed to a combination of the ion-dipole interactions at each portal and the hydrophobic effect which is enhanced due to the presence of high energy waters in the cavity of the uncomplexed CB[n] hosts.[55, 57-60] Equally importantly, because CB[n] are such selective hosts they often display large changes in binding affinity due to changes in pH as well as electrochemical, photochemical, or chemical stimuli.[50] These unique properties of CB[n] have been harnessed to create CB[n] derived functional systems including drug delivery, supramolecular catalysts, chemical sensing, and drug solubilization.[7, 61-64] Somewhat outside the scope of this introduction is the recognition behavior of CB[8] which is large enough to encapsulate two aromatic rings simultaneously which has been used by the Kim Scherman, and Urbach groups extensively to create molecular machines, for the

recognition of amino acids, peptides and proteins, and for supramolecular materials chemistry.[4, 63, 65-69]

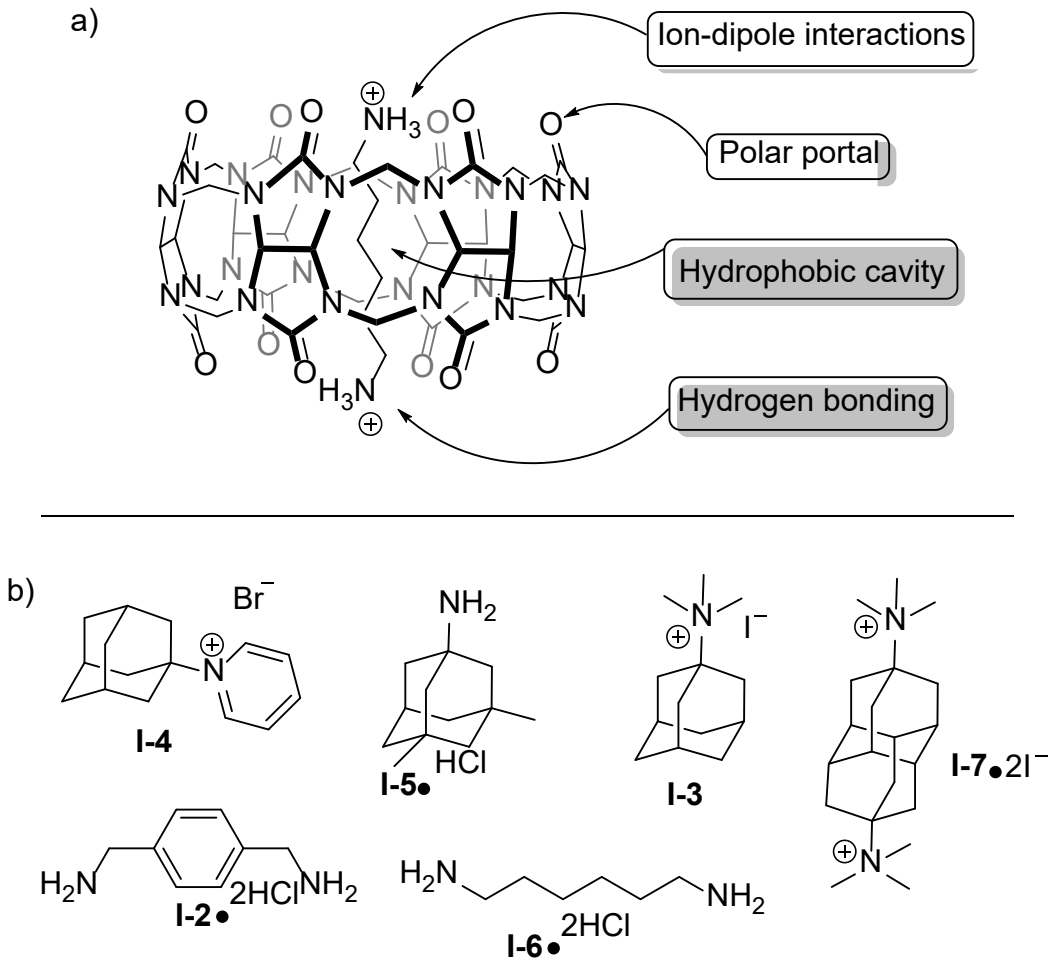

Figure I-6. a) Recognition properties of CB[n]. b) Typical alkyl ammonium guests for CB[n]

1.3.1 Molecular recognition of cucurbit[n]uril (CB[n]) towards amino acids

Buschman et al. were the first to perform binding studies of CB[6] with amino acids and amino alcohols using isothermal titration calorimetry (ITC) (Table I-1).[70, 71] The study was performed in 50% (v/v) aqueous formic acid at 25˚C with select amino acids including Glycine (Gly), Alanine (Ala), Valine (Val), and phenylalanine (Phe).

There was little change in binding strength despite the difference in size and hydrophobicity of the amino acids. It is believed that the amino acids formed exclusion complexes at the ureidyl carbonyl portal of CB[6] instead of going inside its hydrophobic cavity. However, this study opened the door for further investigations of CB[n]s with amino acids.

Table I-1. Thermodynamic parameters for the complexes CB[6] with amino acids.[71]

Amino acids	K_a (M^{-1})	ΔH (kcal•mol^{-1})	$T\Delta S$ (kcal•mol^{-1})
Gly	4.7×10^3	-3.1	1.9
Ala	1.0×10^3	-1.7	2.4
Val	1.4×10^3	-1.0	3.2
Phe	1.4×10^3	-1.6	2.7

Kim et al. demonstrated that CB[8] could simultaneously bind two guests, namely methyl viologen (MV) and 2,6-dihydroxynaphthalene (HN).[72] Subsequently, they also showed that the CB[8]•MV complex was able to bind with the amino acids tryptophan (Trp) and tyrosine (Tyr) by the insertion of the aromatic sidechain into the remaining cavity to form the CB[8]•MV•amino acid ternary complexes.[73] A complete study of the binding of CB[8]•MV toward all 20 amino acids was subsequently performed by the Urbach group, which revealed the selectivity of CB[8]•MV toward Trp, Phe, and Tyr. No binding was observed for the remaining amino acids.[74-76] Urbach and co-workers also studied the influence of overall guest charge on their ability to successfully form CB[8]•MV•amino acids complexes (Figure I-7).[77] Postively charged guests **1** and **2** bind more strongly than zwitterionic free amino acid Trp, which in turn binds more strongly than negatively charged guests **3** and **4** by at least one order of magnitude.[77] The enhancement of binding is due to the fact that the

ureidyl C=O portal of CB[n] is electrostatically negative and therefore a cation binding site; conversely the ureidyl C=O portals of CB[n] reject guests that place additional negative charge at the portal.[48, 78, 79] Other studies demonstrated that DPT or MBBI could be used instead of MV to form a complex with CB[8] which display similar binding to Trp but with enhanced optical outputs.[61, 80] These studies of CB[8] heteroternary complex formation has been most useful in the context of sensing applications and electrochemical molecular machines. In a separate line of inquiry, Prof. Kim and Inoue found that CB[8] could bind two equivalents of Trp or Phe on their own with binding constants of 6.9×10^7 and 1.1×10^8 M^{-1} respectively which has subsequently been used to promote peptide and protein dimerization as described below.[74] An elongated CB[6] derivative was able to bind the aromatic amino acids including His and the (±)-bis-nor-seco-cucurbit[6]uril host studied in the Isaacs lab was found to bind Phe with a XX:1 diastereoselectivity.[81, 82] The binding of CB[7] toward amino acids was performed by the Kim and Urbach group,[59, 83] which revealed analogous binding preferences with higher binding affinities.

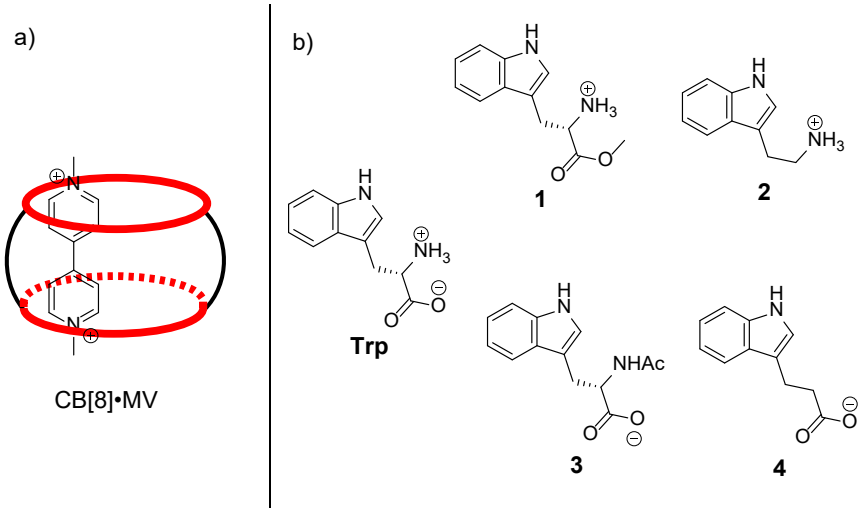

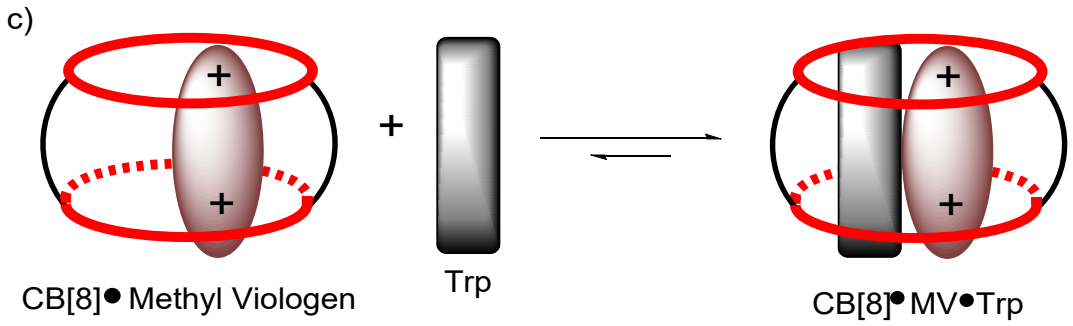

Figure I-7. a) Illustration of CB[8]•MV complex. b) Chemical structures of tryptophan (Trp) and Trp derivatives.[77] c) CB[8] promoted dimerization of Trp and Methyl Viologen.[4]

1.3.2 Molecular recognition of cucurbit[n]urils toward peptides

Since peptides consist of multiple amino acid residues, molecular recognition of peptides adds another layer of challenges and complexity. Peptide contain an oligoamide backbone, which can have different structures based on the amino residue sequence and have multiple sidechains and charges. Binding studies were performed with CB[6] and various dipeptides and tripeptides.[70, 71, 84] The binding constants ranged from 3.7×10^2 to 1.5×10^3 M^{-1} concluding the peptides formed exclusion complexes with CB[6].[84, 85] As previously mentioned, CB[8]•MV forms a stronger binding complex with positively charged Trp derivatives. Based on this information it was hypothesized that CB[8]•MV would selectively bind to N-terminal Trp in peptides due to a combination of N-terminal NH_3^+•••O=C ion-dipole interactions and the hydrophobic effect. A binding study of CB[8]•MV toward a series of tripeptides containing Trp residues at the N-terminus, internal position, and C-terminus were used to prove this hypothesis.[77] The results showed the application of CB[8] as a

synthetic receptor which is capable of sequence specific peptide recognition.[77] CB[8] has been used in multiple applications such as self-assembled multivalent receptors for peptides,[86] peptide dimerization,[87] and selective capture and release of N-terminal Trp peptide.[69]

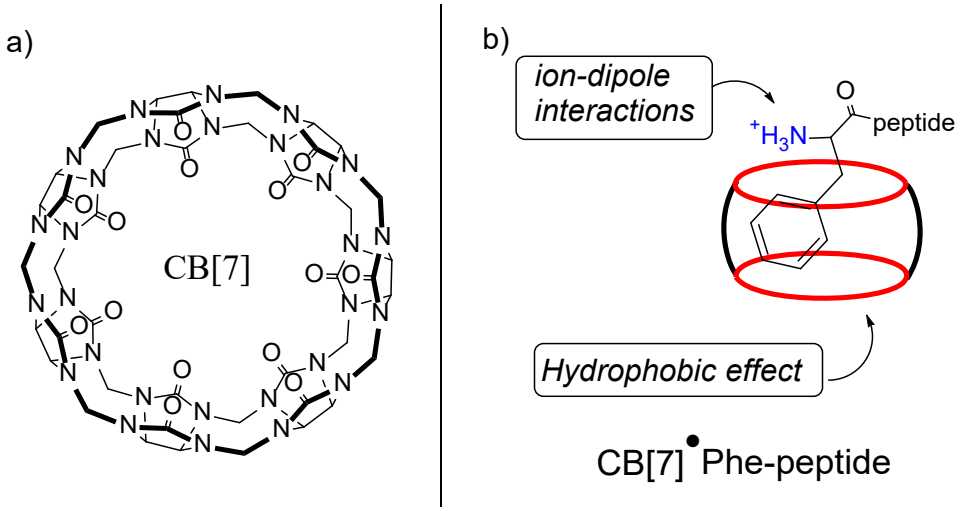

Figure I-8. a) Structures of CB[7] and b) Illustration of non-covalent interactions (ion-dipole interactions and hydrophobic effect) governing the complexation of CB[7] and N-terminal phenylalanine.[88]

In 2006, *Kim et al*. reported that CB[7] was able to selectively recognize N-terminal Phe in the context of dipeptides (Figure I-8).[88] This study focused on the ability of CB[7] to discriminate between different zwitterionic peptides and cationic peptides compared to their sequence diastereomers.[67, 88] *Kim et al*., also demonstrated that CB[7] had selective binding towards other N-terminal aromatic peptides.[88]

1.3.3 Molecular recognition of cucurbit[n]urils toward proteins

The information obtained from the previously mentioned studies demonstrates the potential use of CB[n]s for the molecular recognition of proteins. Multiple

research groups have taken steps toward this goal including the Wang research group, that use CB[8] to mediate the binding of a photodynamic therapy sensitizer to bovine serum albumin (BSA)[89] and Nau and coworkers, that use CB[7] to enhance the fluorescence and binding of a dye (Brilliant Green) to BSA.[90] Most importantly, however, the Urbach research group has shown that CB[7] exhibits a high, selective binding affinity (K_a = 1.5 x 10^6 M^{-1}) toward the N-terminal phenylalanine residue of Insulin (Figure I-6).[63] Interestingly, the x-ray crystallographic results show that the N-terminus needs to unravel slightly to accommodate the CB[7] unit. By virtue of this ability to unwind, Urbach asserts that the N-terminus of proteins constitutes a privileged recognition domain. Subsequently, a collaboration between Urbach and Isaacs should that immobilized CB[7] could be used to perform affinity purification of proteins (insulin and human growth hormone) from within complex mixtures by a catch and release process.[63] This preceding sections have shown that CB[n] possess a variety of interesting molecular recognition properties and can be used in a variety of application areas. However, CB[n] do possess some limitations including their low water solubility and the difficulty of modifying them. Chapter 2 of this dissertation details the molecular recognition properties of two prototypical acyclic CB[n]-type receptors toward amino acids, peptides, and the protein insulin.

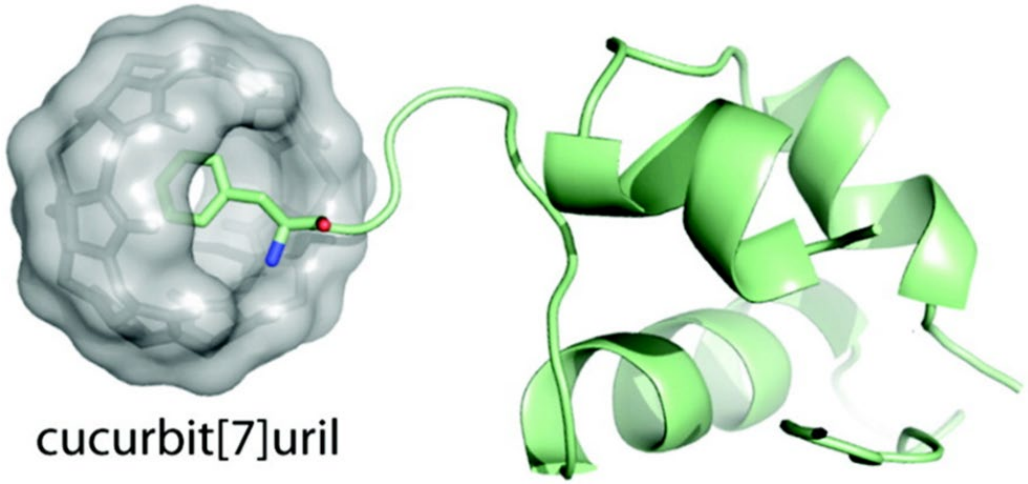

Figure I-9. Illustration of N- terminal residue of phenylalanine of insulin binding to CB[7].[63]

1. 4 Acyclic cucurbit[n]urils

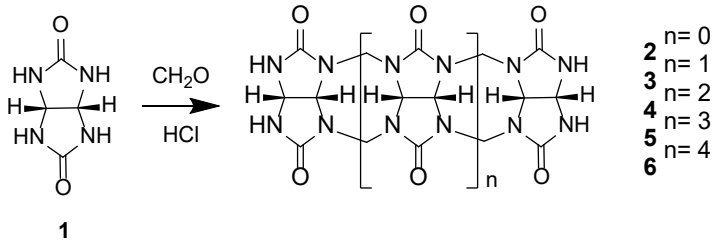

Figure I-10. Synthesis of C-shaped glycoluril oligomers **2-6**.

The research theme of the Isaacs group is centered around developing an understanding of the mechanism of CB[n] formation and using that knowledge to create new CB[n]-type receptors with enhanced functions. As part of these mechanistic studies, the Isaacs group isolated methylene bridged glycoluril dimer – hexamer (**2** – **6**) and studied their molecular recognition properties toward hydrophobic dications (Figure I-10).[91, 92] They found that the acyclic hexamer still

bound quite nicely to the hydrophobic dications with a loss of only about 100-fold in binding affinity relative to macrocyclic CB[6]. Based on this result, the Isaacs group realized that acyclic CB[n]-type receptors would retain the essential recognition elements of macrocyclic CB[n], but unfortunately, hexamer is not very soluble and can undergo decomposition reactions. Accordingly, the Isaacs groups saw the opportunity to create acyclic CB[n]-type receptors to address issues of solubility and enable more straightforward functionalization.

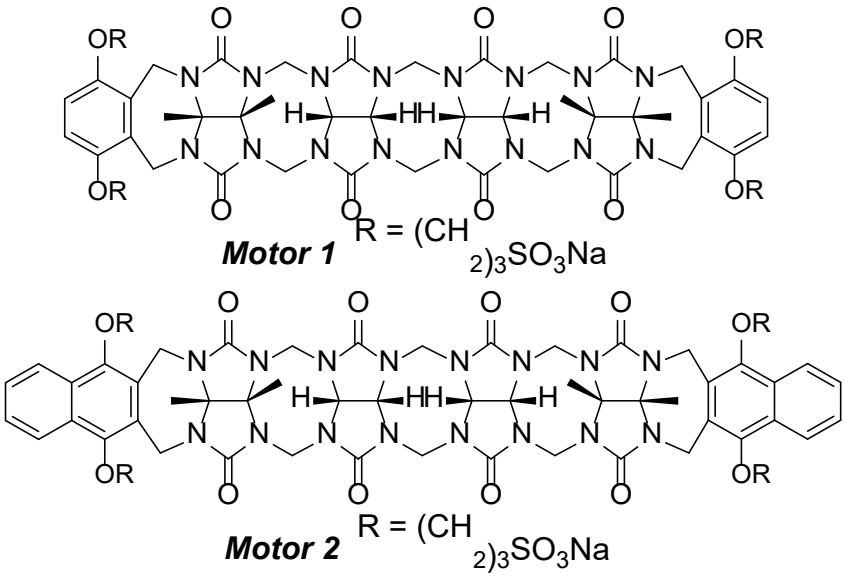

Figure I-11. Chemical structures of Calabadion **1** and **2** also known as **M1** and **M2**

Figure I-11 shows that structure of the two prototypical acyclic CB[n]-type receptors (**M1** and **M2**) studied extensively by the Isaacs group over the past decade for use in biomedical applications.[7] The structure of **M1** and **M2** feature a central glycoluril tetramer which gives the molecular an overall C-shape and the ability to bind to hydrophobic cations, two terminal aromatic walls which allow it to engage in π–π interactions with guests that contain aromatic rings in their structure, and four

sodium sulfonate groups which dramatically enhance their solubility in water and electrostatic interactions with positively charged guests.[93, 94] Compared to macrocyclic CB[n], **M1** (356 mM) and **M2** (18 mM) are much more soluble in pure water.

Scheme I-2 shows the convergent building block based synthetic route used to prepare the Motor1 host on scales up to 50 grams. Methylene bridged glycoluril dimer is obtained by the condensation of glycoluril with formaldehyde (1 equiv.) in HCl. Subsequently, **2** is allows to undergo controlled condensation with glycoluril bis(cyclic ether) in $MeSO_3H$ to give glycoluril tetramer **7** as a key glycoluril oligomer building block. Subsequently, **7** reacts with aromatic wall **8** by a double electrophilic aromatic substitution process in acidic conditions (Scheme I-2) to yield Motor1.[7] A related route can be used to synthetize **M2** simply by changing the aromatic wall building block in the final step. **M1** and **M2** can be easily synthesized on large scale making them a good candidate for industrial applications.

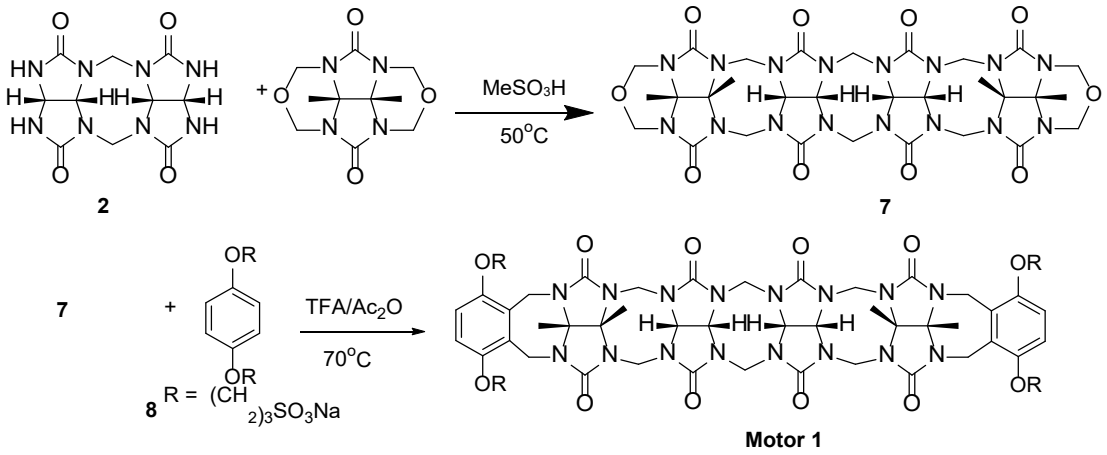

Scheme I-2. Synthesis of Acyclic CB[n] (**M 1**).

Due to their high binding affinity, high water solubility, and ease of synthesis, **M1** and **M2** have been used for a multiple applications including as solubilizing agents for insoluble drugs, hydrocarbons and carbon nanotubes, reversal agents for neuromuscular blocking agents, reversal agents for rat intoxication with Methamphetamine, and components of sensor arrays.[95-98] Not only do acyclic CB[n]s show multiple applications, when compared to other already commercialized host molecules they show higher efficiency. Take for example Sugammadex, a type of cyclodextrin currently used clinically as a post-surgical reversal agent for rocuronium and vecuronium. **M2** binds to Rocuronium and Vecuronium a 100-fold stronger than Sugammadex and maintains a high level of discrimination against acetylcholine.[97] In vivo studies with rats were conducted with **M2** confirming their efficiency and effectiveness.[98]

1.5 Acyclic cucurbit[n]uril derivatives

As described above, the synthesis of **M1** and **M2** proceeds by a building block approach using glycoluril oligomer and aromatic wall building blocks. The Isaacs group is in the process of performing a medicinal chemistry type structure-binding affinity optimization of the properties of acyclic CB[n]-type receptors. Modifications to **M1** and **M2** have been made with the goal of improving binding affinity, water solubility, binding selectivity, glycoluril backbone, enhancing aromatic walls π-π interactions, and even introduction new properties such as fluorescence.[95, 99] The following section will focus on four type of modifications made to acyclic CB[n]. First analogs with different solubilizing groups attached to the aromatic wall. Second,

analogs with different length alkyl linker to sulfonate groups. Third, modifications were made using different type of aromatic arms. Fourth, analogs with different length glycoluril backbone, notably a trimer glycoluril backbone.

1.5.1. Modification of the solubilizing groups.

One of the key structural features of the structure of **M1** and **M2** are the $(CH_2)_3SO_3^-$ arms which function in part as solubilizing groups. In order to assess the scope of functional groups that would confer high solubility in water of acyclic CB[n]-type receptors while maintaining high binding affinity, the Isaacs group designed and studied new acyclic CB[n] featuring anionic (SO_3^-), neutral (OH), and cationic (NH_4^-)[100] (Figure I-12) solubilizing groups.

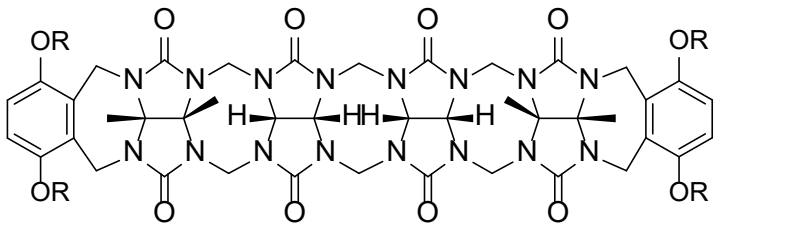

9 R = $(CH_2)_2SO_3Na$, **10** R = $(CH_2)_2NH_3Cl$, **11** R = $(CH_2)_2OH$

10

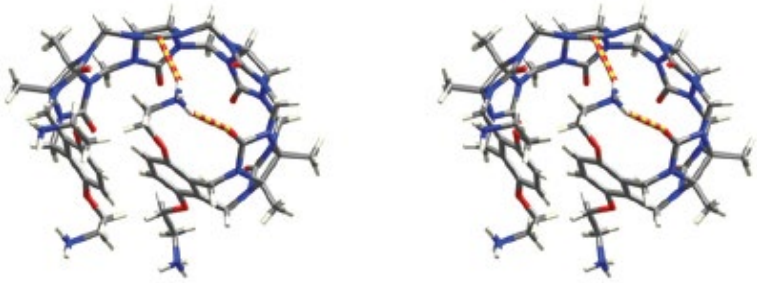

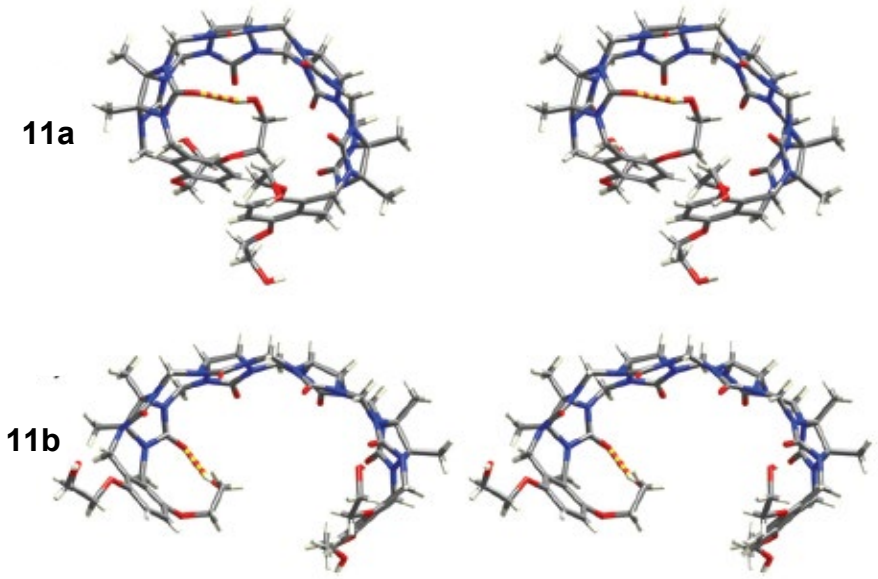

Figure I-12. Chemical structures of acyclic CB[n] derivatives with different solubilizing groups; **9** (SO_3Na), **10** (NH_3Cl), and **11** (OH). X-ray crystal structure of **10** and **11** in self-complexation form and open form.

It was determined that **9** (346 mM) and **10** (250 mM) displayed high solubility in water but that **11** (<2.00 mM) with its OH groups displayed insufficient water solubility to be considered for use as a solubilizing excipient for insoluble drugs.[100, 101] According to x-ray crystallography all three analogs (**9** – **11**) assume an overall C-shape featuring CH-π and π-π interactions between their aromatic walls. Similar geometric features were seen previously for **M1** and **M2**. In contrast to the behavior of Motor1, however, the ammonium solubilizing groups of **10** were found to undergo self-complexation with its own C=O portals driven by intramolecular ion-dipole interactions ($-NH_3^+$•••O=C). This self-folding of the arms of **10** results in a smaller cavity and reduces the binding affinity of **10** toward its guests. In the context of the

potential use of **10** as a solubilizing agent for insoluble drugs, this lower binding affinity dramatically reduces its utility.[100] Compound **11** with its OH solubilizing groups also displayed self-complexation between the hydroxyl group and the carbonyl portal (OH•••O=C) which also reduced guest binding affinity, but not so significantly as that of **10**. Interestingly, the x-ray crystal structure of **11** shows two different conformations of **10** in the crystal that differ in the degree of curvature of the glycoluril oligomer backbone which provides direct evidence of the ability of acyclic CB[n] to adapt their shape to accommodate different sized guests.[101] The binding properties of **9** – **11** toward hydrophobic ammonium ions and three insoluble drugs (tamoxifen, 17α-ethynylestradiol, and indomethacin) were determined by ^{1}H NMR, UV/vis spectroscopy, and phase solubility diagrams. It was found that tetra-anionic host **9** was the superior host for cationic guests compared to the neutral host **11** or the cationic host **10** which can be understood based on electrostatic interactions and the presence of self-folded conformations for **10** and **11** that feature intramolecular H-bonds or ion-dipole interactions. The Isaacs group concluded that the SO_3^- groups are not merely solubilizing groups but also enhance the affinity of acyclic CB[n]-type receptors toward cationic guests electrostatically. Chapter 4 describes a modification to the solubilizing arms that further enhances binding affinity in particular toward dicationic guests.

1.5.2 Modifications of aromatic arms

The aromatic walls of acyclic CB[n]-type hosts represent one of the key synthetic building blocks used in their synthesis. Over the years, the Isaacs group has

studied a number of different aromatic sidewalls including the benzene and naphthalene walls of **M1** and **M2**, an isomer of **M2** known as Zhang1 (**12**), and methylated and cyclohexane fused versions.[102] These ability of these hosts to function as solubilizing excipients for insoluble drug molecules was tested by constructing phase solubility diagrams. From this work, the Isaacs group concluded that **M1** with its high solubility and very good binding affinity is the most general purpose host whereas **M2** displays highest affinity toward its guests. By virtue of their aromatic sidewalls, acyclic CB[n] have excellent potential to construct fluorescence sensors arrays.[103-107] A collaboration between the Isaacs Lab and Prof. Anzenbacher showed that a mixture of **12** and a naphthyl derivative of CB[6] function as a supramolecular sensing array for cancer associated nitrosamines, over-the-counter drugs, and opiates and their metabolites.[106] In this study, the naphthalene substituted cucurbit[6]uril has high affinity and selectivity toward small guests whereas acyclic cucurbit[n]uril derivative **12** with its flexible methylene bridged glycoluril backbone functions a cross-reactive component of the sensor array. [105] Because of the stimuli responsive properties of (acyclic) CB[n] hosts, this sensing array is sensitive to the presence of metal ions such as Eu^{3+}, because of its interaction with the carbonyl portals. When a guest reduced or removes this interaction between the metal ion and the carbonyl portal, a change in fluorescence is observed which further enhances the sensitivity of the assay.[105, 106] Significantly, such sensors are able to quantify the presence of drugs within the urine of with a single fluorescence reading.[106]

More recently, inspired by the work of Swager and others,[108] the Isaacs research group synthesized the triptycene walled acyclic CB[n] host **13**.[109] Triptycene

have been used as building blocks for polymeric material and fluorescent sensor applications.[109-112] Host **13** features a central glycoluril tetramer unit and $O(CH_2)_3SO_3Na$ solubilizing groups which are identical to those of **M1** and **M2** (Figure I-13). Host **13** has good water solubility (3.00 mM) due to the sulfonate groups. However, the triptycene walls each possess two benzene rings that help define the cavity which in theory makes **13** a host that has eight subunits (e.g. 4 glycolurils and 4 benzene rings) and may create a more voluminous cavity akin to CB[8]. Unfortunately, the x-ray crystal structure of **13** showed the presence of π–π interactions between the blades of the opposing triptycene walls in a self-complexed geometry which reduced overall cavity volume. Quite interestingly, however, the researchers found that **13** could bind to large guests such as the Fujita square and Stoddarts blue box. However, in these cases the intertwined structures of the complexes blurred the lines between what molecules constituted the host and which constituted the guest. Host **13** also displays changes in fluorescence upon **13•**guest complexation presumably due to changes in orientation between triptycene walls and undergoes complete quenching in the presence of electron deficient pyridinium guests.[108] The triptycene walled acyclic CB[n] is just one example of the interesting features and properties that can be observed when modifications are made to the original acyclic CB[n]. In Chapter 3 of this thesis I present my work on the synthesis and molecular recognition properties of a triptycene walled glycoluril trimer that we hoped would circumvent the issue of cavity self-inclusion and π–π stacking between the opposing triptycene walls.

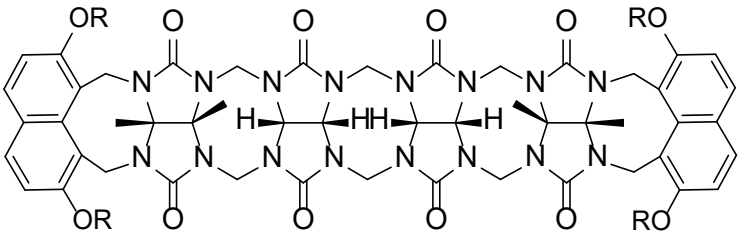

12 R= $(CH_2)_3SO_3Na$

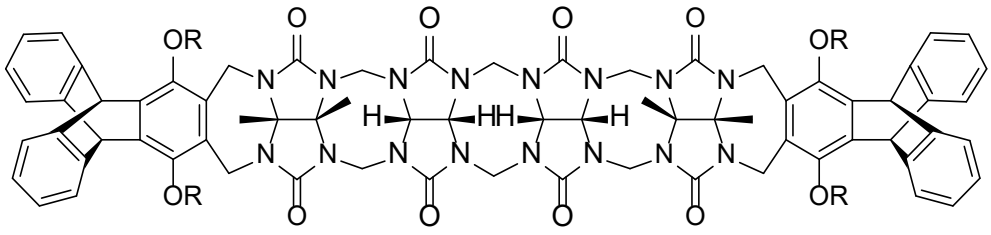

13 R= $(CH_2)_3SO_3Na$

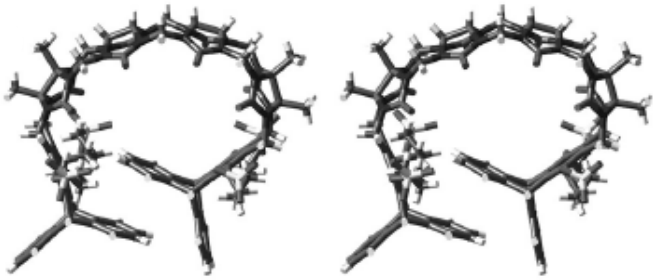

13

Figure I-13. Chemical structure of Zhang 1 **12** and triptycene walled acyclic cucurbit[n]uril **13**.

1.5.3 Modifications of glycoluril backbone

Whereas supramolecular hosts containing glycoluril monomer[46] or methylene bridged glycoluril dimer[113] have been known for many years, systems based on glycoluril trimer are uncommon. Accordingly, a collaboration between the groups of Profs. Vladimir Sindelar and Lyle Isaacs sought to study the influence of glycoluril

oligomer length on the hosts ability to act as solubilizing excipients for insoluble drugs.[114] Dr. Laura Gilberg created glycoluril trimer hosts (Trimer Host 1 and Trimer Host 2, Figure I-14) analogous to Motor1 and Motor2 using our building block approach. For this purpose, she first condensed glycoluril with dimethyl glycoluril bis(cyclic ether) to give methylene bridged glycoluril trimer building block (**2**, Scheme III-1). Subsequently, a double electrophilic aromatic substitution reaction between (**2**, Scheme III-1) and the appropriate aromatic wall was performed which delivered Trimer Host 1 (48%) and Trimer Host 2 (59%) in good yields.[114] Trimer host **1** and Trimer Host **2** possess good water solubility (102 and 336 mM) but possess smaller cavities than the **M1** and **M2**. The Isaacs group studied the ability of Trimer Host 1 and Trimer Host 2 as solubilizing excipients for the insoluble drugs camptothecin, ziprasidone, PBS-1086, and b-estradiol by means of phase solubility diagrams. The researchers found that the glycoluril trimers host performed better than analogous hosts based on glycoluril monomer or dimer but less well than **M1** or **M2**.[114] Trimer Host 1 and Trimer Host 2 display lower binding affinity that **M1** and **M2** toward a common guest presumably due to the smaller cavity volume and the presence of fewer high energy waters[78] in the cavity of the trimer derived hosts.

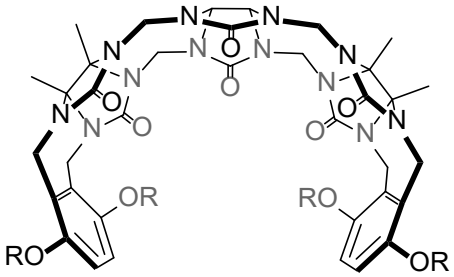

Trimer host 1

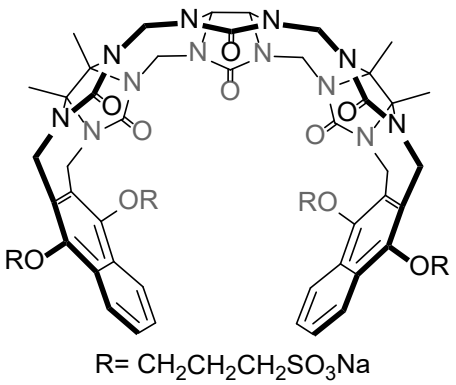

Trimer host 2

Figure I-14. Chemical structures Trimer acyclic CB[n] host **1** and **2**

1.5.4 Modifications of alkyl linker on aromatic arms

A final structural variable of acyclic CB[n] that has been considered by the Isaacs lab is the length of the $O(CH_2)_nSO_3Na$ linking group. Two acyclic CB[n] were made, **M2C2** and **M2C4** with $(CH_2)_n$ (n=2 and n=4 respectively) and studied in comparison to **M2** (n = 3) itself (Figure I-14).[115] Just like **M2** the hydrophobic cavity and carbonyl portal of **M2C2** and **M2C4** allow for the encapsulation of hydrophobic cations as good guests. Compared to **M2** (water solubility 14 mM), **M2C2** and **M2C4** have higher water solubility (68 mM or 196 mM, respectively). It is however, worth noting, that **M2C4** become a viscous solution as concentration increases. After investigation, it was determined that **M2C4** forms a gel in the presence of insoluble drugs, however, **M2C2** was determined increase water solubility of insoluble drugs. The slopes of the phase solubility diagrams show that the binding strength of the three hosts toward a panel of 15 insoluble drugs generally follows the order: Motor2 > **M2C2** > **M2C4**. Therefore, **M2C2** with its higher aqueous solubility has untapped potential as a potential solubilizing excipient. In Chapter 4 of this dissertation I present the synthesis and molecular recognition properties of an analogue of **M1** where the $O(CH_2)_nSO_3Na$ alkylene linker has been completed removed and becomes OSO_3Na groups instead.

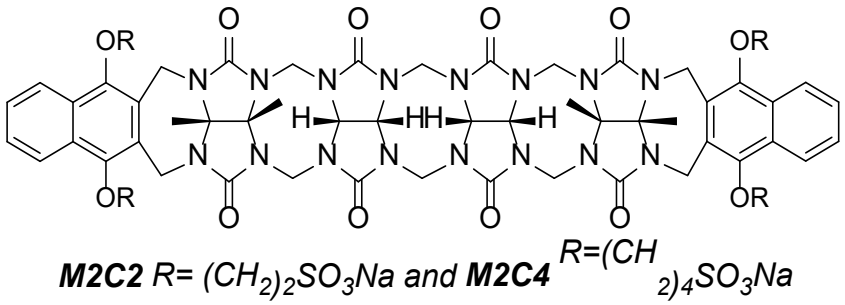

Figure I-15. General structure of acyclic CB[n] with 2 or 4 carbon chain alkyl linkers

1.6 conclusion

This introductory chapter has presented some of the background of the field of molecular recognition using molecular containers compounds (e.g. cyclodextrins, calixarenes, pillararenes, cyclophanes). These macrocyclic molecular containers are preorganized for binding and therefore display high binding affinity at selectivity. In this thesis, I focus on the molecular recognition properties of molecular containers that are acyclic – acyclic CB[n]-type receptors – which have limited degrees of freedom and are therefore preorganized and display very good levels of binding affinity and selectivity. The influence of different structural variables (e.g. aromatic wall, glycoluril oligomer length, solubilizing group, linker length) on the recognition properties of acyclic CB[n]-type receptors conducted prior to my work was reviewed. In the three research chapters of this dissertation I study the: 1) molecular recognition properties of Motor 1 and Motor2 toward amino acids, peptides, and insulin in comparison to CB[n], 2) the molecular recognition properties of a triptycene walled glycoluril trimer, and 3) an analog of Motor 1 whose $(CH_2)_3$ linking groups have been removed to create sulfate functional groups.

Chapter 2: Molecular Recognition Properties of Acyclic Cucurbit[*n*]urils Toward Amino Acids, Peptides, and a Protein

The work presented in this chapter was take from Zebaze Ndendjio, S.; and Isaacs, L. Molecular recognition properties of acyclic cucurbiturils toward amino acids, peptides, and a protein. *Supramol. Chem*. **2019**. This work was entirely done by me.

2. 1 Introduction.

The synthetic and supramolecular chemistry of the CB[n] family has played a leading role in the field since the preparation of cucurbit[n]uril homologues example, the K_a for CB[7]•guest complexes routinely exceed 10^6 M^{-1}, often exceed 10^9 M^{-1}, and in special cases (e.g. cationic adamantanes and diamantanes) can even exceed 10^{12} M^{-1} in water due to the combined effects of ion–dipole interactions and the hydrophobic (CB[n], Figure II-1) at the turn of the millennium.[52, 78]

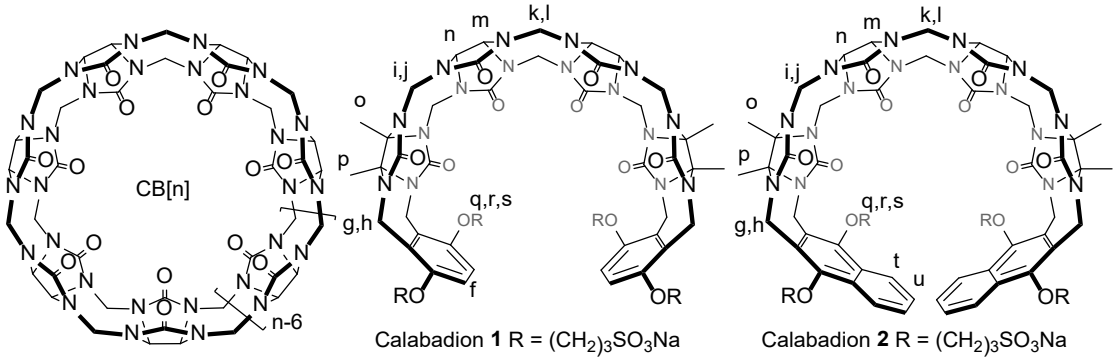

Figure II-1. Chemical structures of CB[n] and Calabadions **1** and **2**.

CB[n] compounds are powerful receptors for hydrophobic (di)cations in aqueous solution due to their two-symmetry equivalent ureidyl carbonyl-lined portals

which guard entry to a hydrophobic cavity[58]. For example, the K_a for CB[7]•guest complexes routinely exceed 10^6 M^{-1}, often exceed 10^9 M^{-1}, and in special cases (e.g. cationic adamantanes and diamantanes) can even exceed 10^{12} M^{-1} in water due to the combined effects of ion–dipole interactions and the hydrophobic effect. [57, 58] In addition to high-affinity binding, CB[n]•guest complexes also display high stimuli responsiveness (e.g. pH, electrochemistry, photochemistry, competing guest) which allows for the use of CB[n] in a variety of applications.[50, 53] For example, CB[7]•guest binary complexes and CB[8]•guest1•guest2 ternary complexes are used to construct molecular switches and machines[116], as supramolecular catalysts[54, 117], to solubilize, protect, sequester, and even create targeted pharmaceuticals[118], as components of chemical sensors[119, 120], and to promote the assembly of supramolecular polymers, materials, and frameworks[121]. CB[n] have also found wide applicability in peptide and protein chemistry. For example, in pioneering work, the Urbach group showed that CB[8] promotes the cooperative dimerisation of the Phe-Gly-Gly peptide in water via formation of the CB[8]•$(Phe\text{-}Gly\text{-}Gly)_2$ complex with K_a=1.5 x 10^{11} M^{-2} [4]. This motif has been capitalized upon by Brunsveld and Liu to promote the dimerisation of proteins tagged with N-terminal FGG units and thereby control biological functions.[122] For example, Brunsveld engineered a split luciferase[123] that could be reconstituted by addition of CB[8], and similarly CB[8] was found to promote the dimerisation of monomeric caspase-9 into the active dimer.[124] Scherman has used the FGG motif to promote hydrogel formation.[68]

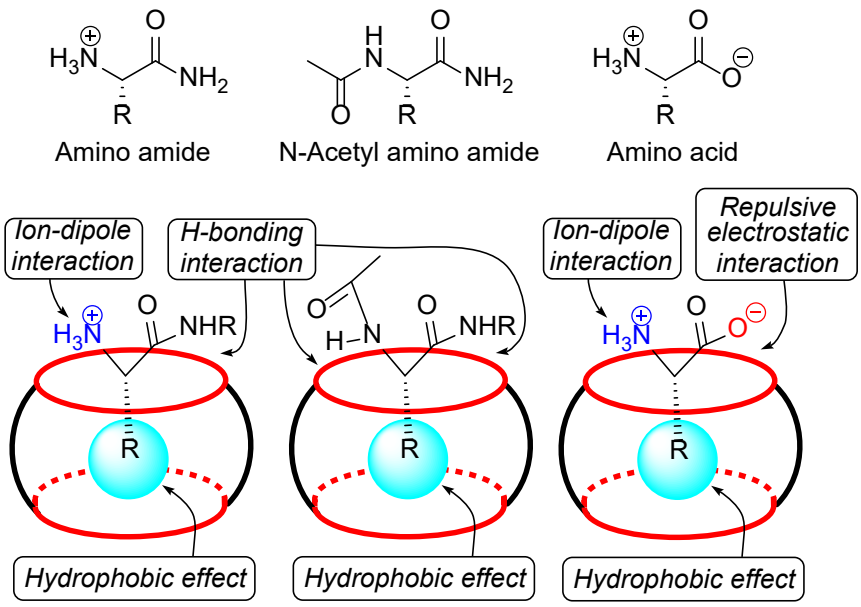

Figure II-2. Chemical structure of amino acids, amino amides, and N-acetyl amino amides used as guests in this study and illustration of the geometries and driving forces involved in their complexation with macrocyclic CB[n].

In a lovely series of papers, Urbach and collaborators demonstrated that the N-terminus of peptides and proteins is a privileged site for host complexation due to simultaneous ammonium ion and side chain binding (Figure II-2). In particular, they found that CB[7] displays a selectivity toward N-terminal Phe over other N-terminal residues presumably because they display suboptimal fit for the CB[7] cavity (e.g. other aromatic or hydrophobic amino acids may not fully release cavity waters of solvation) or because they cannot sterically accommodate N-terminus and cationic side chain binding (e.g. Lys, His, Arg). The CB[7]•N-terminal Phe motif was used to recognize Insulin in solution and on resin, to determine protease substrate selectivity, to impose sequence-specific inhibition on a non-specific protease, and for supramolecular enhancement of protein analysis.[125] Recently, Langer, Anderson, and

Isaacs used a monofunctionalised CB[7] derivative to non-covalently PEGylate the N-terminal Phe residue of Insulin and thereby prolong its in vivo function.[126]

In recent years, the Isaacs group has synthesized and investigated the molecular recognition properties of acyclic CB[n]-type receptors that feature a central glycoluril oligomer, two terminal aromatic walls, and four sulphonate solubilising groups.[95] Two prototypical acyclic CB[n] (Calabadion **1** and Calabadion **2**) are shown in Figure 1 although numerous variants are known.[102] The Calabadions retain the essential molecular recognition features of CB[n], but because they are acyclic, they are able to flex their methylene bridged glycoluril oligomer backbone to accommodate more voluminous guests. Additionally, the acyclic structure of the Calabadions may allow guest substituents to protrude through the side of the host•guest complex rather than through the portals as required for macrocyclic CB[n]. The Calabadions have several important biomedical applications including the solubilization of insoluble anticancer drugs for in vivo application[127, 128], as agents to reverse neuromuscular block in vivo[62], and most recently to modulate the hyper locomotor activity of rats treated with methamphetamine.[98] Recently the Ma group has been using acyclic CB[n] for acid-sensitive controlled release and bioimaging applications.[129] By virtue of their aromatic walls, Calabadions undergo changes in their UV/Vis and fluorescence properties upon guest binding and have therefore been use as sensors for nitrosamines, over-the counter drugs, amino acids, and opioids.[105, 107] Given the ability of CB[7] and CB[8] to interact with peptide N-termini and internal residues, protein N-termini, and to promote dimerization and the fact that Calabadions retain the essential recognition properties of macrocyclic CB[n] we

hypothesized that **1** and **2** would perform well in peptide and protein recognition perhaps with selectivity that is complementary to that observed for CB[n].

2.2 Results and discussion

This results and discussion section is organized as follows. First, we lay out the goals and the hypotheses to be tested in this study. Next, we describe ^{1}H NMR investigations of the binding properties of **1** and **2** toward 19 amino acid amides to confirm the 1:1 binding stoichiometry and shed light on the geometrical features of the complexes. Next, we present the energetics (ΔG, ΔH, ΔS) of binding of 1 and 2 toward the various amino amides by isothermal titration calorimetry. Subsequently, we detail the influence of electrostatics on the energetics of host•guest binding as probed through mutation of amino acid to amino acid amide to N-acetyl amino acid amide. Next, we present the binding of 1 and 2 toward selected tripeptides to delineate the influence of neighboring residues. Finally, we present the results of binding of 1 and 2 toward insulin compared to CB[7].

2.2.1 Goals of the study

Macrocyclic CB[7] selectively recognizes peptides that feature an N-terminal hydrophobic aromatic residue like Phe or Trp due to a combination of ion–dipole interactions and the hydrophobic effect and discriminates against residues containing hydrophobic aliphatic side chains, polar neutral side chains, acidic (anionic) side chains, and even basic (cationic) side chains.[4, 67, 130] The discrimination of CB[7] against the residues with cationic side chains (e.g. Lys and Arg) is due to the fact that the side chain cannot thread through the cavity to form ion–dipole interactions at both

portals without creating steric interactions between the wall of CB[7] and the adjacent CONHR group. We hypothesized that acyclic CB[n] 1 and 2 – with their acyclic structure – would display higher affinity toward Lys and Arg and because the steric constraints of these amino acids might be better accommodated.[131] Accordingly, a primary goal of the work is the measurement of the binding affinity of 1 and 2 toward the amino acid amides which mimics the context of the amino acid in a longer peptide. Within this realm, we also sought to compare the peptide recognition properties of **1** and **2** which differ in the nature of their aromatic walls, cavity size, and presumably their selectivity toward aromatic amino acids in particular. Given the ability of CB[8] to bind two residues simultaneously[4, 68], we were aware of the possibility of similar behavior with 2 (or 1) and were careful to verify the binding stoichiometry. Given that 1 and 2 are tetra-anionic in pH 7.4 water whereas CB[7] is neutral at this pH we sought, as a secondary goal, to understand the role of electrostatics on the molecular recognition properties of 1 and 2 toward amino amides, N-acetyl amino amides, and amino acids themselves. Finally, we wanted to examine the recognition properties of 1 or 2 toward N-terminal amino acid in the context of a protein (insulin).

2.3 ^{1}H NMR investigations of calabadion•guest binding

First, we investigated the binding interactions between 1 and 2 toward amino acid amides by ^{1}H NMR spectroscopy. We performed these experiments in biologically relevant 20mM sodium phosphate buffered D_2O at pD7.4 to ensure that the N-terminus of each amino acid amide is present as its NH_3^+ form which provides a primary binding site for hosts **1** and **2**. As documented in the Supporting

Information for 19 amino acid amides (excluding cysteine), we measured ^{1}H NMR spectra at different host:guest ratios (generally 1:2, 1:1.5, 1:1, and 1:0.5). We monitored the change in guest chemical shifts upon complexation to provide crude information on host•guest stoichiometry and to determine whether the kinetics of guest exchange is in the fast, intermediate, or slow exchange regime on the ^{1}H NMR timescale. Rather than discuss the precise changes for each host•guest complex, we discuss here some general trends that are observed in the chemical shifts of both host and guest upon complexation. For example, Figure II-3 shows the ^{1}H NMR spectra recorded for mixtures of 1 and H-Phe-NH_2. A comparison of Figure II-3(a,d) shows that the protons on the aromatic ring of H-Phe-NH_2 (H_c – H_e) and the adjacent benzylic CH_2 group (H_b) undergo a substantial upfield change in chemical shift upon complexation (H_c – H_e; 1–1.5 ppm; $H_b \approx 0.8$ ppm) which strongly suggests that the Arring and benzylic CH_2 of H-Phe-NH_2 is bound within the cavity of **1** within the **1**•H-Phe-NH_2 complex. Conversely, the α-proton Ha of H-Phe-NH_2 undergoes a slight downfield shift (≈ 0.2 ppm) upon complex formation which indicates that H_a is located nearby the deshielding region defined by the ureidyl C = O groups of the host. When an excess of H-Phe-NH_2 is present (e.g. 1:2, Figure II-3(b)) the resonances for H_c – H_e shift back toward the position observed for uncomplexed H-Phe-NH_2 and broaden which indicates that this complex displays intermediate exchange kinetics on the ^{1}H NMR timescale and likely has 1:1 stoichiometry. In accord with this data and based on the known binding preferences of CB[n] and acyclic CB[n], we formulate the geometry of the 1•H-Phe-NH_2 complex as illustrated in Figure II-4(a).

We believe that the amide (C = O)NH_2 group of H-Phe-NH_2 is hydrogen bonded to the ureidyl C=O group of host 1 in the complex.[87]

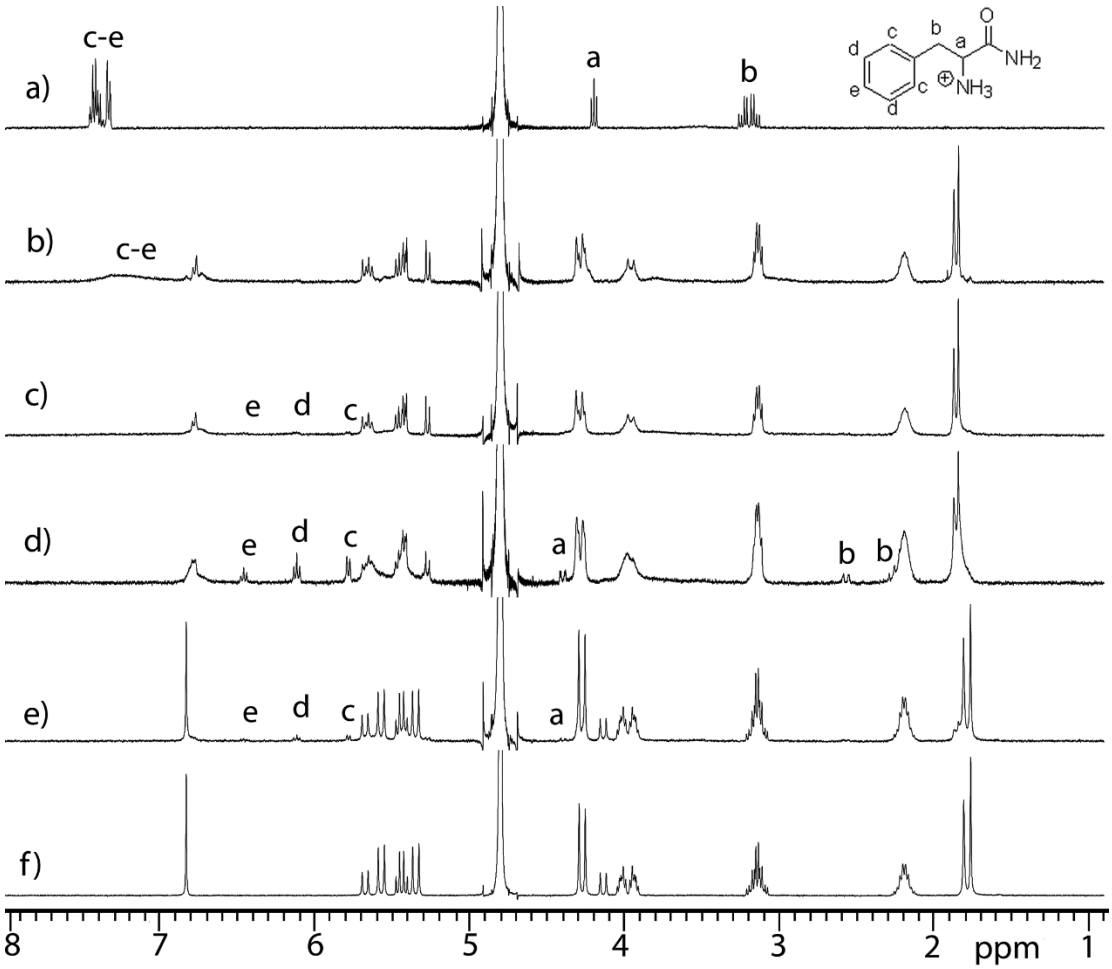

Figure II-3. ^{1}H NMR spectra recorded (400 MHz, RT, 20 mM NaH_2PO_4 buffered D_2O , pD 7.40) for: a) H-Phe-NH_2 (5 mM), (b) **1** (1 mM) and H-Phe-NH_2 (2 mM), c) **1** (1 mM) and H-Phe-NH_2 (1.5 mM), (d) **1** (1 mM) and H-Phe-NH_2 (1 mM), e) **1** (1 mM) and H-Phe-NH_2 (0.5 mM), (f) **1** (2 mM).

Related changes are observed during the complexation of the hydrophobic amino acid amides (Appendix 1) indicating that side chain cavity inclusion and NH_3^+ portal binding is the dominant geometry. Changes are also observed in the ^{1}H NMR

resonance for host 1 in the 1•H-Phe-NH_2 complex. For example, the H_f protons in C_{2v}-symmetric 1 are symmetry equivalent and display a sharp singlet (Figure II-3(f)) but become broadened and split upon formation of the C_1- symmetric (e.g. no symmetry) 1•H-Phe-NH_2 complex. This observation can be explained by the fact that the chiral host•guest complex renders all four Hf atoms diastereotopic. In the case of fast kinetics of exchange, typified beautifully by the 1•H-Leu-NH_2 complex, two doublets are observed for H_f (Appendix 1, Figure S83). Related observations are observed with host **2**. None of the complexes between **1** or **2** and the amino acid amides displayed slow kinetics of exchange on the ^{1}H NMR timescale. Interestingly, for complexes between 1 (2) and the hydrophobic non-aromatic amino acid amides, we typically observe a small downfield shift for host aromatic sidewall resonance H_f, H_t, H_u (1: up to 0.3 ppm; 2: up to 0.5 ppm).

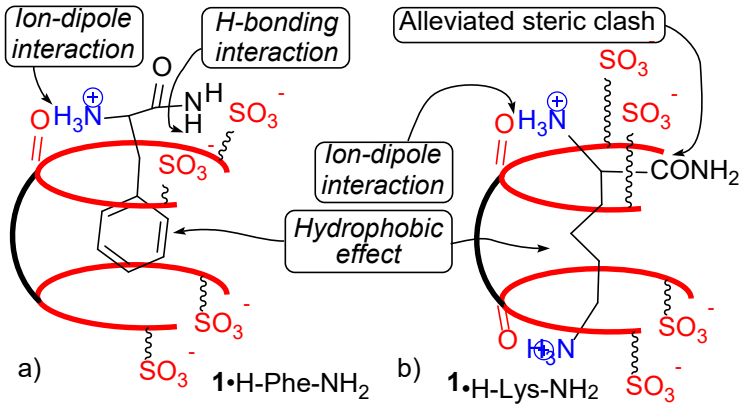

Figure II-4. (Color online) Schematic illustrations of the geometry of (a) **1**•H-Phe-NH_2 and (b) **1**•H-Lys-NH_2 complexes.

As described previously in related systems, we believe this is due to a conformational change that hosts **1** and **2** undergo upon complexation that removes edge-to-face C-H•••π interactions that occur in the uncomplexed host that result in

upfield shifting.[95] In contrast, for the aromatic amino acid amides (e.g. H-Trp-NH_2, H-Tyr-NH_2, H-Phe-NH_2) only very small changes in chemical shift are observed for H_f which we believe reflects a balance between the expected downfield shift due to conformational change and upfield shift due to the shielding effect of the aromatic ring of the guest. Interestingly, we found no evidence by ^{1}H NMR of binding of 1 or 2 (at mM concentrations) toward Asp and Glu which contain CO_2H groups in their side chains that are expected to be present in their anionic CO_2^- form at pD 7.4. This result is in accord with previous observations from CB[n] molecular recognition that the electrostatically negative ureidyl C = O portals do not tolerate the presence of guest negative charge at the portals.[59, 132] Furthermore, the presence of the SO_3^- solubilizing groups on 1 and 2 would be expected to electrostatically destabilize complexes with Asp and Glu. Finally, for H-Gly-NH_2, H-Ala-NH_2, and H-Ser-NH_2 which have no, small, or hydrophilic side chains we observe only small changes (e.g. $\Delta\delta$ and broadening) in the ^{1}H NMR which probably indicates very weak binding or non-inclusion binding (e.g. portal binding) or a combination thereof. In the ^{1}H NMR experiments, we often observed substantial upfield shifts for guest resonances at 1:1 host:guest stoichiometry which moved back toward the position for complexed guest at 1:2 host:guest ratios which suggested the formation of 1:1 complexes. We constructed Job plots[133] to further established the 1:1 host:guest stoichiometry in select cases where the resonances were sharp enough to be easily monitored. For example, Figure II-5 shows a Job plot constructed for mixtures of **1** and H-Lys-NH_2 at a constant total concentration of 1 mM in phosphate buffered D_2O (pD 7.40). The chemical shift of H_f of the host was monitored. As can readily be seen, the Job plot

displays a maximum at a mole fraction of 0.5 which firmly establishes the 1:1 absolute stoichiometry of the 1•H-Lys- NH_2 complex. A related Job plot was constructed to confirm the 1:1 stoichiometry of the 1•H-Arg-NH_2 complex.

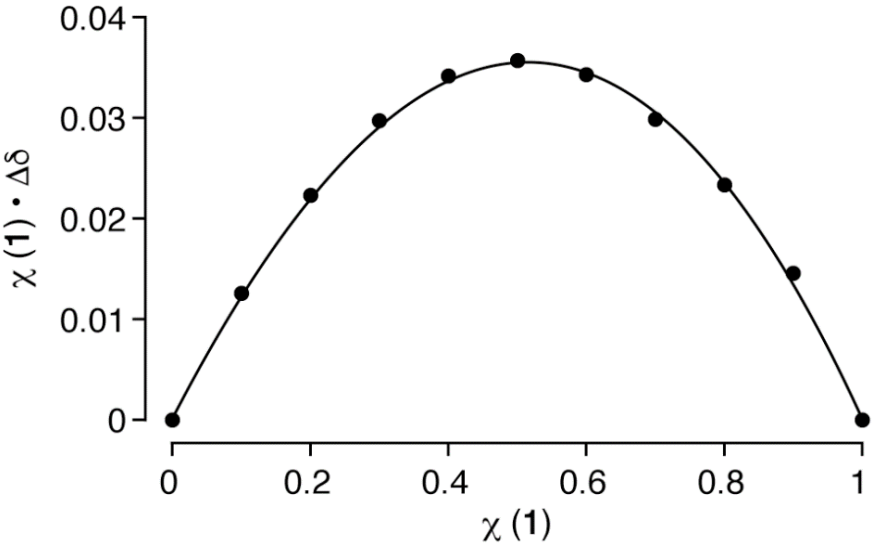

Figure II-5. Job plot constructed for the interaction of 1 with H-Lys-NH_2 ([1] + [H-Lys-NH_2] = 1 mM) monitoring the chemical shift of H_f on 1 by ^1H NMR spectroscopy (600 MHz, RT, 20 mM NaH_2PO_4 buffered D_2O, pD 7.40). The solid line serves as a guide for the eye.

2.4 Isothermal titration calorimetry (ITC) determination of host•guest energetics

The substantial broadening and intermediate exchange kinetics observed in the ^1H NMR spectra of the complexes of **1** and **2** with amino acid amide guests complicates the use of NMR to determine binding constants. Accordingly, we turned to ITC to determine the thermodynamic parameters for binding. Figure II-6(a) shows a representative ITC Thermogram recorded for the titration of **1** (100 μM) in the ITC cell with a solution of H-Phe-NH_2 (1 mM) in the ITC syringe and the fitting of the data to a 1:1 binding model using the PEAQ ITC analysis software (Figure II-6(b)). In this manner, we were able to extract $K_a = 2.62 \times 10^6\ M^{-1}$ and $\Delta H = -17.1$ kcal mol$^-$

[1] for the 1•H-Phe-NH_2 complex. Analogous ITC titrations were performed for the complexation between hosts **1** and **2** and the remainder of the amino acid amides, amino acids, and N-acetyl amino acid amides (Appendix 1), and the results are presented in Table 1.

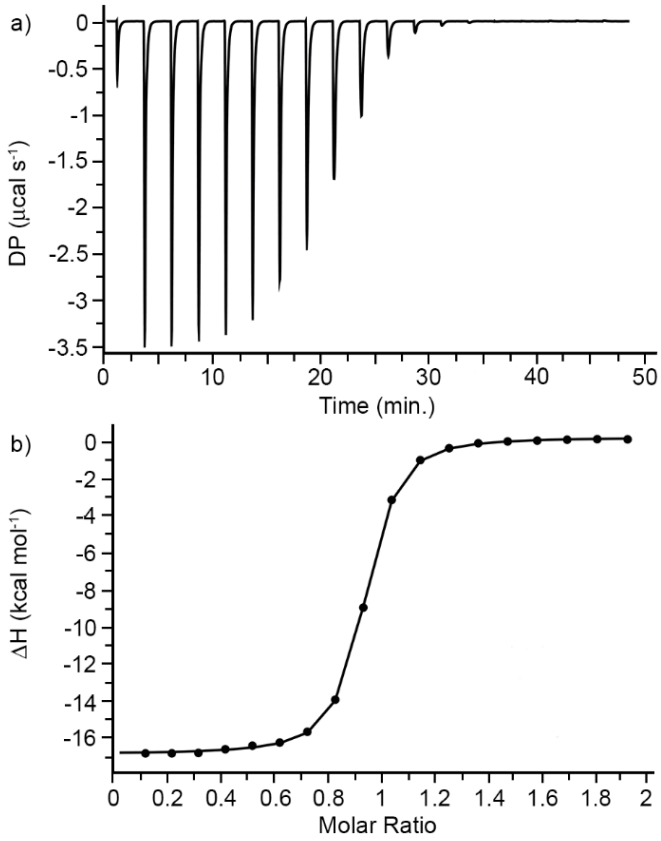

Figure II-6. (a) Thermogram obtained during the titration of **1** (100 µM) in the cell with H-Phe-NH_2 (1 mM) in the syringe (298.0 K, 20 mM sodium phosphate buffered H_2O, pH 7.4) and (b) fitting of the data to a 1:1 binding model with K_a = 2.62 x 10^6 M^{-1} and $\Delta H = -17.1$ kcal mol^{-1}.

2.4.1 Discussion of trends in the thermodynamic parameters

The dynamic range of binding constants presented in Table 1 spans the range from10^2 M^{-1} to above 10^6 M^{-1}. Given the constraints of this relatively narrow range, we have been able to discern some trends in the thermodynamic parameters and

present them here grouped according to the chemical nature of the amino acid amide side chain (e.g. anionic, cationic, aromatic, hydrophobic aliphatic, polar).

Table II-1. Thermodynamic parameters obtained by ITC for the interaction of **1** and **2** with the amino acid amides, N-acetyl amino amides, and amino acids.

	Host 1				**Host 2**			
Guest	K_a / M^{-1}	ΔG^o kcal mol^{-1}	ΔH^o kcal mol^{-1}	$-T\Delta S^o$ kcal mol^{-1}	K_a / M^{-1}	ΔG^o kcal mol^{-1}	ΔH^o kcal mol^{-1}	$-T\Delta S^o$ kcal mol^{-1}
Aromatic Sidechain								
H-Phe-NH_2	2.62×10^6	-8.76	-17.1 ± 0.04	8.36	3.24×10^6	-8.88	-17.3 ± 0.07	8.45
H-Phe-CO_2^-	7.87×10^4	-6.68	-12.5 ± 0.153	5.83	9.61×10^4	-6.80	-7.23 ± 0.074	0.432
Ac-Phe-NH_2	4.17×10^3	-4.94	-8.95 ± 0.448	4.01	2.99×10^4	-6.11	-10.1 ± 0.239	4.04
H-Trp-NH_2	2.56×10^5	-7.38	-14.8 ± 0.064	7.43	3.98×10^6	-9.00	-17.7 ± 0.07	8.68
H-Trp-CO_2^-	1.06×10^4	-5.50	-7.41 ± 0.132	1.91	1.14×10^5	-6.90	-6.93 ± 0.026	0.026
AcTrp-NH_2	8.40×10^2	-3.99	-10.4 ± 0.854	6.43	3.56×10^4	-6.21	-5.38 ± 0.30	-0.828
H-Tyr-NH_2	1.01×10^6	-8.19	-15.1 ± 0.03	6.89	9.52×10^5	-8.16	-15.6 ± 0.03	7.40
H-Tyr-CO_2^-	1.01×10^4	-5.46	-8.60 ± 0.226	3.14	2.03×10^4	-5.88	-8.76 ± 0.111	2.88
AcTyr-NH_2	1.26×10^3	-4.23	-9.36 ± 0.371	5.12	3.06×10^3	-4.76	-8.21 ± 0.079	3.45
H-His-NH_2	2.35×10^4	-5.97	-9.72 ± 0.128	3.75	2.61×10^4	-6.03	-7.18 ± 0.104	1.15
Cationic Sidechains								
H-Lys-NH_2	7.43×10^5	-8.01	-10.9 ± 0.02	2.90	1.41×10^5	-7.03	-9.02 ± 0.12	1.99
H-Lys-CO_2^-	3.33×10^2	-3.44	-11.6 ± 5.02	8.18	497	-3.68	-2.19 ± 0.036	-1.49

Ac-Lys-NH_2	9.80 × 10^3	-5.45	-7.13 ± 0.220	1.68	8.06 × 10^3	-5.33	-2.84 ± 0.078	-2.49
H-Arg-NH_2	7.09 × 10^5	-7.98	-11.6 ± 0.02	3.57	8.26 × 10^4	-6.71	-8.84 ± 0.058	2.13
H-Arg-CO_2^-	1.51 × 10^3	-4.34	-3.93 ± 0.099	-0.416	2.39 × 10^3	-4.61	-9.82 ± 0.386	5.21
AcArg-NH_2	8.13 × 10^3	-5.34	-6.84 ± 0.178	1.50	7.87 × 10^3	-5.32	-5.44 ± 0.248	0.119
Non-aromatic polar sidechains								
H-Gln-NH_2	1.47 × 10^4	-5.69	-5.71 ± 0.213	0.02	7.25 × 10^3	-5.27	-2.82 ± 0.69	-2.44
H-Ser-NH_2	1.25 × 10^4	-5.59	-0.867 ± 0.007	-4.73	1.90 × 10^3	-4.47	0.944 ±0.185	-5.42
H-Thr-NH_2	8.33 × 10^3	-5.35	-0.546 ± 0.112	-4.80	n.b	n.b	n.b	n.b
H-Asn-NH_2	1.44 × 10^3	-4.31	1.42 ± 1.22	-5.73	1.35 × 10^3	-4.27	-1.62 ± 0.012	-2.66
H-Met-NH_2	1.32 × 10^5	-6.99	-13.1 ± 0.04	6.08	8.85 × 10^4	-6.75	-11.7 ± 0.04	4.97
Hydrophobic aliphatic sidechains								
H-Ile-NH_2	9.43 × 10^4	-6.79	-10.8 ± 0.04	4.02	1.68 × 10^5	-7.13	-9.18 ± 0.085	2.05
H-Val-NH_2	1.40 × 10^4	-5.66	-10.1 ± 0.085	4.40	2.15 × 10^4	-5.91	-4.66 ± 0.142	-1.26
H-Leu-NH_2	2.85 × 10^5	-7.44	-9.80 ± 0.027	2.35	2.29 × 10^5	-7.31	-8.20 ± 0.43	0.891
H-Pro-NH_2	5.75 × 10^3	-5.13	-5.43 ± 0.149	0.299	1.70 × 10^4	-5.77	-5.26 ± 0.146	-0.510
H-Ala-NH_2	408	-3.56	-5.32 ± 0.545	1.76	515	-3.70	-2.77 ± 0.130	-0.930
H-Gly-NH_2	80.6	-2.60	-3.88 ± 0.742	1.28	115	-2.81	-1.36 ± 0.125	-1.46

Firstly, in agreement with our ^{1}H NMR measurements, no heat is evolved during the titration of **1** or **2** with the H-Asp-NH_2 and H-Glu-NH_2 and we therefore conclude that no binding occurs with these amino acid amides that contain anionic side chains. This result is in accord with the well-known preference of the CB[n]

cavity for hydrophobic and neutral binding epitopes over hydrophilic and anionic groups.[58, 132] Second, we find that the aromatic amino acid amides (H-Phe-NH_2, H-Trp-NH_2, H-Tyr-NH_2 form the tightest complexes with **1** and **2** with K_a values that exceed 10^6 M^{-1} and with large enthalpic driving forces in the range of −15 – −18 kcal mol^{-1}. This trend is not so surprising in light of the hydrophobicity of the aromatic rings of the amino acid amides, the ability of aromatic walls of **1** and **2** to engage in π-π interactions with the guest, and of course the precedent from the work of Kim, Inoue, Nau and Urbach that showed that peptides with aromatic side chains at the N-terminus are bound selectively by CB[7].[4, 67, 88, 130] Macrocyclic CB[7] has been reported to bind Phe-Gly-Gly (K_a = 2.8 x 10^6 M^{-1}), Phe-Gly (K_a = 3 x 10^7 M^{-1}), Tyr-Gly (K_a = 3.6 x 10^6 M^{-1}), and Trp-Gly (K_a = 5.6 x 10^5 M^{-1}) with affinities that are comparable to those observed for 1 and 2.[4, 88] For H-Phe-NH_2 and H-Trp-NH_2, the larger host 2 binds stronger than 1 as expected based on its larger cavity size.[62, 102] H-His-NH_2 with its hydrophilic and charged aromatic side chain is bound significantly weaker to both 1 and 2 ($K_a \approx 10^4$ M^{-1}) and with significantly lower enthalpic driving force. Third, H-Lys-NH_2 and H-Arg-NH_2 which are dicationic at neutral pH and contain 4–5 C-atoms between cationic N-atoms bind toward 1 with affinities ($K_a \approx 7 \times 10^5$ M^{-1}) that are only slightly lower that the aromatic amino acid amides. They do not reach the very high affinity typically observed for diammonium ion complexes with cucurbiturils presumably because of the presence of the $CONH_2$ group. Host 1 displays higher affinity than **2** toward H-Lys-NH_2 (5.3-fold) and H-Arg-NH_2 (8.6-fold) because the cavity of 1 is smaller than 2 and prefers narrower (e.g. alkylene) guests as observed previously.[95] Fourth, among the amino acid amides with polar side

chains, we find that H-Met-NH_2 binds most strongly to 1 (K_a = 1.32 x 10^5 M^{-1}) and 2 (K_a = 8.85 x 10^4 M^{-1}) with substantial enthalpic driving forces. This is not surprising given that methionine has both the largest side chain surface area and the least favorable free energy of transfer from cyclohexane to water which enhances the hydrophobic driving force for complexation.[4] The remaining polar amino acid amides (H-Gln-NH_2, H-Asn-NH_2, H-Thr-NH_2, H-Ser-NH_2) bind more weakly with K_a in the 10^2 –10^4 M^{-1} range which reflects the need to desolvate the side chains polar OH and $CONH_2$ functional groups as they enter the host cavity. As expected, a comparison of the binding constant of 1 toward H-Gln-NH_2 versus H-Asn-NH_2 and H-Thr-NH_2 versus H-Ser-NH_2 reveals that the compound with the additional CH_2-group in the side chain is the stronger binder.[58] Finally, the amino acid amides with hydrophobic aliphatic side chains (H-Ile-NH_2, H-Val-NH_2, H-Leu-NH_2, H-Pro-NH_2) bind to 1 and 2 with K_a values in the 6 × 10^3 to 3 × 10^5 M^{-1} range and ΔH values in the−5 to−7.5 $kcalmol^{-1}$ range with; host 2 is generally the tighter binder. The order of binding affinity toward 1 and 2 follows the order H-Pro-NH_2<H-Val-NH_2 < H-Ile-NH_2 < H-Leu-NH_2. As expected, H-Pro-NH_2 and H-Val-NH_2 which have fewer C-atoms in the side chain relative to H-Ile-NH_2 and H-Leu-NH_2 (e.g. 3 versus 4) bind more weakly. We speculate that the pyrrolidine ring of H-Pro-NH_2 displays reduced affinity because the preferences of ion–dipole and hydrophobic effect cannot be fully satisfied simultaneously. Finally, H-Gly-NH_2 and H-Ala-NH_2 with no or minimal side chains exhibit low binding affinity toward 1 and 2 ($K_a \leq 10^3$ M^{-1}) probably due to weak electrostatic effects.

2.4.2 Influence of N-acetylation and C-amidation

We measured the binding of 1 and 2 toward the unmodified amino acid and N-acetyl amino acid forms of phenylalanine, tryptophan, tyrosine, lysine, and arginine (Table II-1). We hypothesized that the amino acid amides would bind more strongly than the amino acids themselves due to the absence of unfavorable CO_2^- to SO_3^- and/or C=O portal interactions. Similarly, we expected that the amino acid amides would bind more strongly than the N-acetyl amino acid amides due to the loss of NH_3^+ to O=C ion–dipole in the later. These interactions are presented schematically in Figure II-7. For 1•H-Phe-NH_2 (2•H-Phe-NH_2) the loss of NH_3^+•••O=C ion–dipole interactions costs 3.8 kcal mol^{-1} (2.8 kcal mol^{-1}) whereas the introduction of unfavorable CO_2^- electrostatic interactions costs 2.1 kcal mol^{-1} (2.1 kcal mol^{-1}). Related losses of free energy were observed for the complexes of 1 (2) toward H-Trp-NH_2 (1: 3.4 and 1.9 kcal mol^{-1} ; 2: 2.8 and 2.1 kcal mol^{-1}) and H-Tyr-NH_2 (1: 3.96 and 2.7 kcal mol^{-1}; 2: 3.4 and 2.3 kcal mol^{-1}) upon acylation of the N-terminus and introduction of a C-terminal CO_2^- group. In contrast, for the dicationic amino acids H-Lys-NH_2 (1: 2.6 and 4.6 kcal mol^{-1} ; 2: 1.7 and 3.4 kcal mol^{-1}) and H-Arg-NH_2 (1: 2.6 and 3.6 kcal mol^{-1}; 2: 1.4 and 2.1 kcal mol^{-1}) the introduction of the CO_2^- group is energetically more costly than removal of the NH_3^+•••O=C ion–dipole interactions. We rationalize this observation based on the fact that for Lys and Arg the diammonium spans the two C=O portals which conformationally fixes the CO_2^- group within the cavity near the electrostatically negative C=O portals of 1 or 2. Accordingly, we conclude that ion–dipole interactions play a primary role in determining the strength of complexes between tetra-anionic 1 (2) and amino acid

amides but that secondary electrostatic interactions can significantly modulate binding affinity.

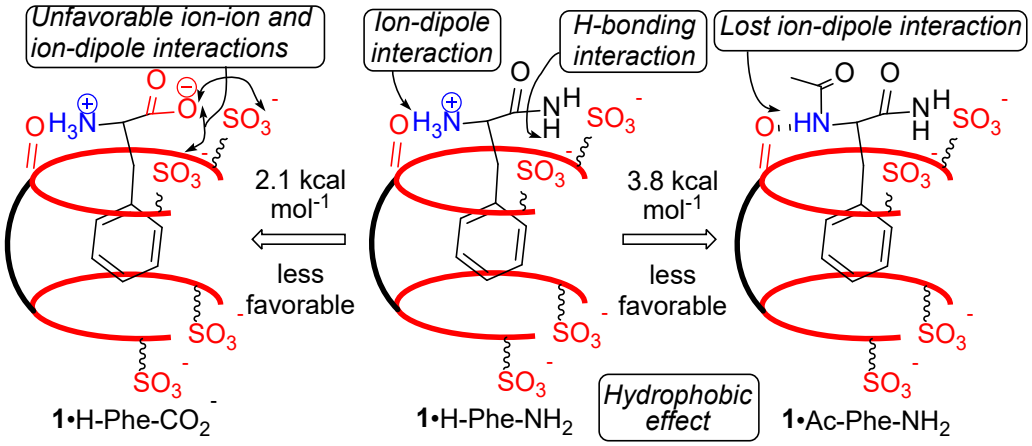

Figure II-7. (Colour online) Schematic illustration of the complexes of **1** with H-Phe-CO_2^-, H-Phe-NH_2, and Ac-Phe-NH_2 along with their driving forces and relative stabilities.

2.5 Influence of neighboring residues

We were inspired by the recent work of Urbach which showed that CB[8] is capable of simultaneously binding two adjacent side chains within the context of a tripeptide with nanomolar affinity.[65] Accordingly, we sought to determine if acyclic cucurbiturils like 1 or 2 could recognize an N-terminal Phe along with an adjacent residues sidechain. We selected FGA as control tripeptide along with six tripeptides (FFA, FLA, FVA, FIA, FPA, FKA) with adjacent aromatic, hydrophobic, or cationic sidechain. ITC experiments were performed for these tripeptides toward 1 and 2 and the results are given in Table II-2. First, we found that the 1•FGA complex (K_a = 1.48 × 10^6 M^{-1} ; $\Delta H = -13.3$ kcal mol^{-1}) is of comparable affinity and enthalpic driving force to the 1•H-Phe-NH_2 complex (K_a = 2.62 × 10^6 M^{-1}; $\Delta H = -17.1$ kcal mol^{-1}). Interestingly, compared to the 1•FGA complex all of the tripeptides with aromatic, hydrophobic, or cationic adjacent residues bind 6 to 22-fold more weakly. The 1•FPA

complex is the weakest with K_a = 6.62 x 10^4 M^{-1} presumably due to the loss of a potential N-H•••O=C H-bond due to the tertiary amide bond at proline. All these results suggest that the cavity of **1** cannot expand to accommodate a second residue and that the second residue experiences unfavourable steric interactions which reduces affinity. The binding of 1 to FVA was of relevance to our planned binding experiments toward insulin since the N-terminus of insulin also has the FV sequence. Unfortunately, the 1•FVA complex has similar affinity to all the other tripeptides tested. The behavior of **2** is more subtle and the affinity toward all the tripeptides cluster around $10^5 M^{-1}$. Despite the previously demonstrated ability of 1 and 2 to expand its cavity to accommodate larger guests with roughly circular cross sections in the form of adamantanes, steroids, and even carbon nanotubes[62, 93], they prefer to bind a single narrower alkyl and phenyl ring when given the option.[102, 114, 134]

Table II-2. Thermodynamic parameters obtained by ITC for the interaction of **1** and **2** with tripeptides.

	Host 1				**Host 2**			
Guest	K_a / M^{-1}	ΔG kcal mol^{-1}	ΔH kcal mol^{-1}	-TΔS kcal mol^{-1}	K_a / M^{-1}	ΔG kcal mol^{-1}	ΔH kcal mol^{-1}	-TΔS kcal mol^{-1}
FGA	1.48 x 10^6	-8.42	-13.3 ± 0.038	4.93	1.20 x 10^5	-6.93	-18.1 ±0.697	11.1
FFA	2.52 x 10^5	-7.37	-13.7 ±0.097	6.37	1.22 x 10^5	-6.94	-12.5 ± 0.27	5.56
FLA	1.57 x 10^5	-7.09	-13.4 ±0.201	6.27	2.59 x 10^5	-7.39	-10.1 ±0.176	2.72
FIA	1.40 x 10^5	-7.02	-13.3 ± 0.121	6.32	2.62 x10^5	-7.39	-10.0 ±0.131	2.62
FVA	3.89 x 10^5	-7.63	-12.7 ± 0.076	5.07	3.84 x 10^5	-7.62	-11.7 ± 0.03	4.13
FPA	6.62 x 10^4	-6.58	-12.4 ±0.169	5.81	1.06 x 10^5	-6.86	-8.16 ±0.207	1.30
FKA	2.34 x 10^5	-7.32	-14.4 ± 0.224	7.03	5.32 x10^4	-6.45	-9.29 ±0.814	2.84

2.6 Molecular recognition of insulin by 1, 2, and CB[7]

Finally, we decided to study the interaction of 1 and 2 with a protein. As the model protein, we selected insulin based on the pioneering work of the Urbach group.[63] Accordingly, we sought to measure the binding affinity of 1 and 2 toward insulin and compare the results to those measured previously with CB[7]. ITC binding studies were performed in our standard 20 mM sodium phosphate buffered water at pH 7.4 containing 4 mM EDTA which sequesters metal ions that promote oligomerization of insulin. Table II-3 shows the results of the ITC studies which indicates that CB[7] binds insulin the strongest followed closely by 2 and then 1. The affinity of the insulin•CB[7] complex (5.59 x 10^5 M^{-1}) is slightly lower than that measured previously by Urbach (K_a = 1.5 x 10^6 M^{-1}) which we attribute to the less competitive 10mM sodium phosphate buffer they used.[63] Satisfyingly, the binding constants measured for 1 and 2 toward insulin are comparable to those measured toward the FVA peptide which indicates that secondary electrostatic interactions between the tetra-anionic hosts and insulin are not energetically costly. In comparison, the K_a values measured for the interaction of H-Phe-NH_2 with 1 and 2 are about 10-fold higher (Table II-1) which confirms the sensitivity of 1 and 2 to the steric bulk at the neighboring amino acid residue.

Table II-3. Thermodynamic parameters obtained by ITC for the interaction of CB [7], **1**, and **2** with Insulin.

HOST	K_a / M^{-1}	ΔG	ΔH	-TΔS
CB[7]	5.59 x 10^5	-7.84	-8.97 ± 0.232	1.13
1	1.32 x 10^5	-6.99	-16.9 ± 0.225	9.91
2	3.47 x 10^5	-7.56	-10.4±0.151	2.86

2.7 Conclusion

In summary, we have delineated the binding properties of acyclic CB[n]-type receptors **1** and **2** toward 19 amino acid amides by a combination of ^{1}H NMR spectroscopy and ITC. The side chains typically undergo cavity inclusion whereas the N-terminus binds at the C=O portal by ion–dipole and ion-SO_3^- interactions. Binding constants range from $<10^2$ (for anionic and small side chains) to $\approx 10^6$ M^{-1} for amino acid amides with aromatic (Phe, Trp, Tyr) and even cationic (Lys and Arg) side chains. The broader range of residues undergoing high-affinity binding by **1** and **2** stands in contrast to that of CB[7] which suggests a broad range of potential applications. Studies of the binding of **1** and **2** toward the N-acetyl amino acid amides and the free amino acids allowed us to quantify the energetic contributions of electrostatics to the binding process. For example, the removal of the NH_3^+•••O=C ion–dipole interactions (e.g. 1•H-Phe-NH_2 versus 1•Ac-Phe-NH_2) costs 3.8 kcal mol^{-1} whereas the introduction of unfavorable CO_2^- electrostatic interactions costs 2.1 kcal mol^{-1}. Given the propensity of acyclic CB[n] to expand their cavity to bind to large guests, we explored the possibility of 1 or 2 simultaneously binding two amino acid side chains but observed no evidence for such phenomena. Finally, we demonstrate that 1 and 2 bind to insulin with affinities similar to CB[7]. Overall, the work demonstrates that acyclic CB[n] have a broad affinity toward aromatic and cationic side chains of N-terminal amino acids which suggests that acyclic CB[n] have a bright future as a component of enzyme assays, sensor arrays, and biotechnology applications.

Chapter 3: Triptycene Walled Glycoluril Trimer: Synthesis and Recognition Properties

The work presented in this chapter was take from Zebaze Ndendjio, S.; Liu, W.; Yvanez, N.; Meng, Z.; Zavalij, P.Y.; Isaacs, L. Triptycene walled glycoluril trimer: synthesis and recognition properties. *New J. Chem*. **2019**. In this work, Liu first developed a synthetic procedure to synthesize impure trimer triptycene glycoluril host. Yvanez then attempted the purification of the trimer host by HPLC but with limited results. After Yvanez departure, I succeeded in the purification of the trimer host by a recrystallization method. After obtaining the pure host I was able to conduct the NMR and ITC studies, most importantly I was fortunate enough to obtain a crystal structure of the trimer triptycene host.

3.1 Introduction

The synthesis and molecular recognition properties of the cucurbit[n]uril (CB[n]) family of molecular container compounds has undergone rapid development since the turn of the millennium[49] Figure III-1 shows the molecular structure of CB[n] which are composed of n glycoluril units connected by 2n methylene bridges that form a barrel shaped macrocycle with two electrostatically negative ureidyl carbonyl fringed portals and a central hydrophobic cavity. Accordingly, macrocyclic CB[n] bind tightly to hydrophobic (di)ammonium ions in water with binding constants typically in the 10^6–10^{12} M^{-1} range, even exceeding 10^{17} M^{-1} in special cases.[58, 135]

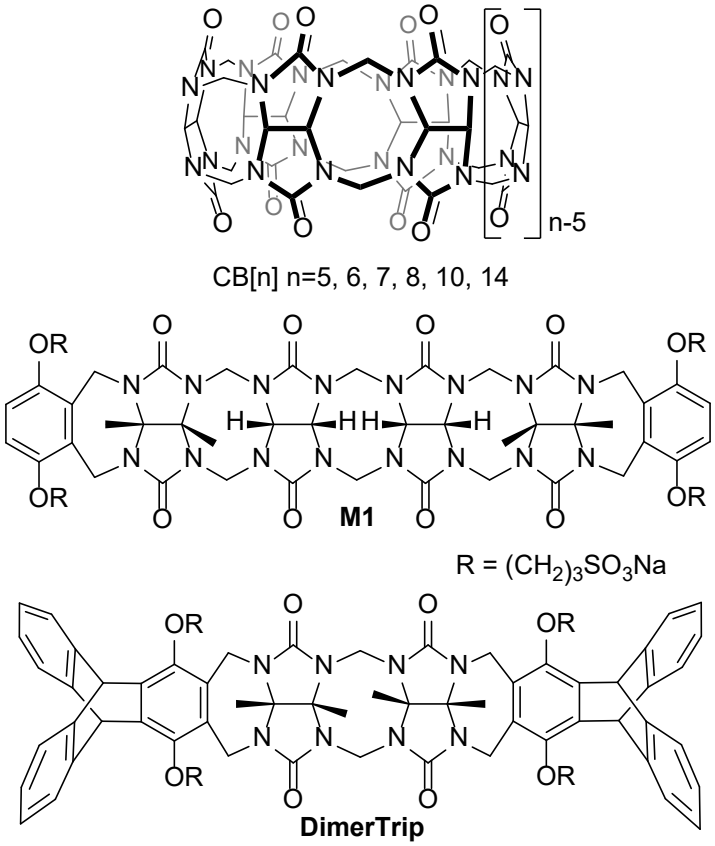

Figure III-1. Structure of CB[n] (n = 5, 6, 7, 8, 10, 14), acyclic CB[n]-type receptor **M1**, and **DimerTrip**.

The very high affinity of CB[n]•guest complex has been traced, in part to the presence of intracavity waters that lack a full complement of H-bonds that are released upon complexation.[79] Accordingly, the K_a values for CB[n]• guest complexes have been featured prominently in a series of blinded challenges (SAMPL and Hydrophobe) that aim to improve computational approaches to free energy calculations in water. CB[n]•guest complexes respond sensitively to appropriate stimuli (e.g. pH, chemical, electrochemical, photochemical)[116] allowing them to be used as a high-fidelity switching element in complex systems. Accordingly, unfunctionalized macrocyclic CB[n] has found numerous uses including as a

component of (bio)sensing ensembles,[119] for drug formulation, delivery and sequestration,[136] to create supramolecular organic frameworks,[137] and to perform supramolecular catalysis.[48, 54] With the development of functionalized CB[n], the range of application has been expanded to include CB[n] based targeted drug delivery and theranostics, materials for protein capture, supramolecular Velcro, and nanoparticle based optical assays.[138]

In recent years, we and others have been studying acyclic CB[n]-type receptors that feature a central glycoluril oligomer (e.g. dimer–tetramer) that is capped by aromatic sidewalls.[95, 139-143] Figure III-1 shows the structure of the prototypical acyclic CB[n] (**M1**) which features a central glycoluril tetramer, o-xylylene sidewalls, and sulfonate solubilizing groups. **M1** shows excellent biocompatibility according to a variety of *in vitro* and *in vivo* assays[97, 144] and is therefore considered for real world applications. For example, **M1** and analogues have been used as solubilizing excipients for insoluble drugs,[102] for pH triggered delivery agents,[145] as in vivo sequestration agents for neuromuscular blockers and drugs of abuse,[62] and as components of sensing arrays.[107] Most recently, we have created chimeric receptors comprising glycoluril monomer, dimer, or tetramer units with triptycene sidewalls with the goal of increasing binding capacity and binding strength and observed interesting behavior like triggered decomposition of vesicles and the ability to wrap around macrocyclic guests.[146] In this paper we prepare acyclic CB[n]-type host 1 derived from glycoluril trimer, investigate its binding properties toward alkylammonium ions to elucidate its basic recognition properties and to serve

as a blinded dataset for the SAMPL7 challenge,[147] and finally to assess its potential as a sequestration agent toward drugs of abuse.

3.2 Results and discussion

This results and discussion section is organized as follows. First, we present the design, synthesis, and characterization of host **1**. Next, we quantify the self-association propensity of **1** and perform qualitative ^{1}H NMR based host•guest complexation studies. Subsequently, we measure the complexation thermodynamic parameters by isothermal titration calorimetry (ITC) and discuss the observed structure binding constant trends

3.2.1 Design, synthesis, and characterization of host 1

The synthesis of host **1** is based on our previously described building block approach[95] involving the electrophilic aromatic substitution reactions between glycoluril bis(cyclic ethers) and activated aromatic rings. Accordingly, we reacted glycoluril trimer 2[114] with triptycene derivative 3[108] under acidic conditions (TFA, Ac_2O) which delivered crude 1 after precipitation with EtOH. Purification of **1** was challenging and required a combination of washing with EtOH and acetone followed by recrystallization from mixtures of EtOH and H_2O to deliver 1 in 4.4% isolated yield. The chemical structure of **1** was fully elucidated by spectroscopic means and was further confirmed by single crystal X-ray diffraction studies (vide infra). The ^{1}H NMR spectrum of **1** in D_2O shows a single resonance for the glycoluril methine protons (H_j), two pairs of resonances for the diastereotopic methylene bridges (H_f,g and $H_{h,i}$), two CH_3-groups (k and l), and two pairs of aromatic protons

($H_{a,b}$ and $H_{c,d}$). The number of resonances is fully consistent with the time-averaged C_{2v}-symmetry depicted in Scheme III-1. However, the resonance for H_b on the tip of the aromatic ring is upfield shifts and appears at 5.7 ppm which suggests that uncomplexed **1** assumes a self-folded conformation in water (vide infra) similar to previously prepared triptycene walled glycoluril tetramer.[108] The ^{13}C NMR spectrum for 1 recorded in DMSO-d_6 displays 22 resonances which is also in agreement with time averaged C_{2v}-symmetry. Finally, the high resolution ESI-MS spectrum of **1** shows a doubly charged ion at m/z 829.20204 which is in accord with the calculated value ($C_{76}H_{75}N_{12}NaO_{22}S_4$, $[M + {}^1H\ 3Na]_2$, calculated 829.19495).

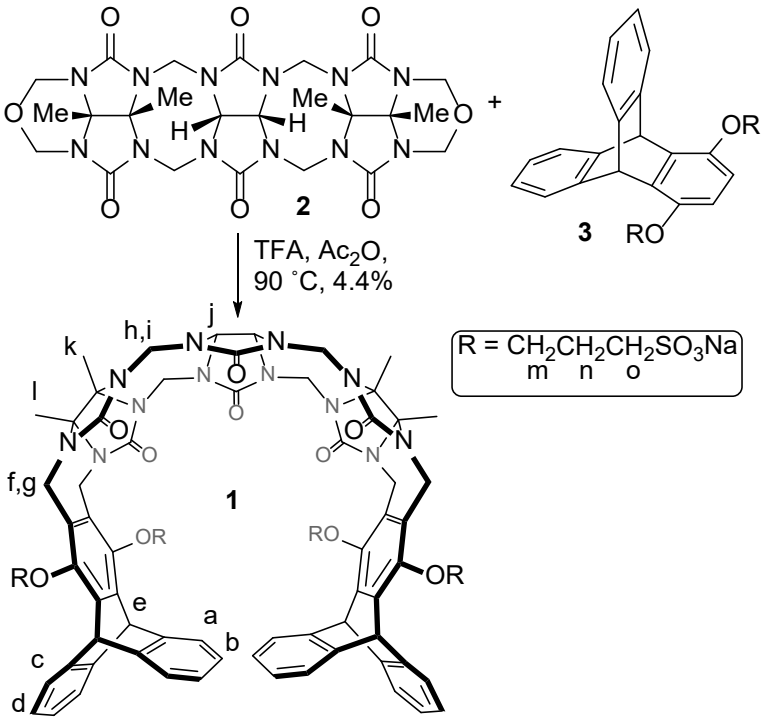

Scheme III-1. Synthesis of host **1**.

*3.2.2 Self-association properties of host **1***

Before proceeding to investigate the host•guest properties of 1 we perform dilution studies to quantify the extent of self-association of 1. Accordingly, we

measured the ^{1}H NMR spectra of a series of solutions of **1** in D_2O from its solubility limit of 3 mM down to 0.05 mM (Appendix 2,Figure S4, ESI†). We observe small changes in chemical shift of many protons including H_b, $H_{k/l}$, and H_f. Figure III-2 shows a plot of the concentration of **1** versus chemical shift of H_b that was fitted to a dimerization model in Scientist^{TM} (ESI†) which allowed us to extract the self-association constant (K_s = 480 ± 81 M^{-1}). The measurement of the thermodynamic parameters of complexation of **1** (vide infra) were measured by ITC at [**1**] = 100 mM where the host remains monomeric.

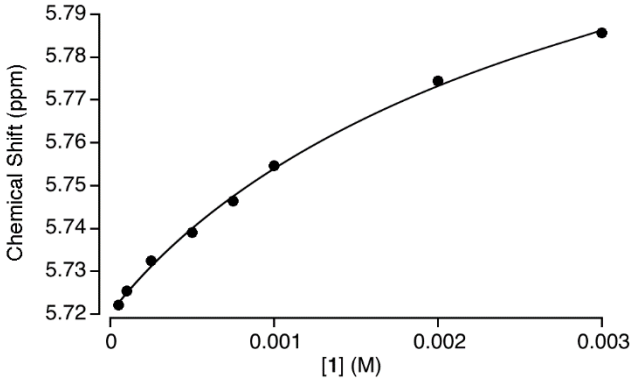

Figure III-2. Plot of chemical shift of Hb versus [**1**] used to determine the self-association constant K_s = 480 ± 81 M^{-1} for **1**.

3.2.3 X-ray crystal structure of 1

We were fortunate to obtain single crystals of 1 by recrystallization from mixtures of EtOH and H_2O and to solve its structure by X-ray crystallography (CCDC-1949769). † Figure III-3a and b show stereoscopic representations of the two independent molecules of **1** in the crystal. The molecule of 1 in Figure III-3a is C_2-symmetric and features an out-of-plane helical distortion that renders it chiral. Similarly, the molecule of **1** in Figure III-3b is skewed out-of-plane and is therefore

chiral; it also includes a solvating CF_3CO_2H molecule. Interestingly, only one sense of handedness is present in the crystal structure of 1 and therefore the crystal is a conglomerate. Figure III-3c shows a stereoview of how these two different molecules of **1** pack next to each other in the crystal. The external face of the triptycene unit of one molecule of 1 embraces the convex face of the glycoluril region of the adjacent molecule of 1 and vice versa. The fact that two different conformations were observed in the crystal and the ^{1}H NMR evidence of a p-stacked conformation presented above highlights the conformational flexibility of the acyclic CB[n] that enables it to bind to a wide variety of guests.[100]

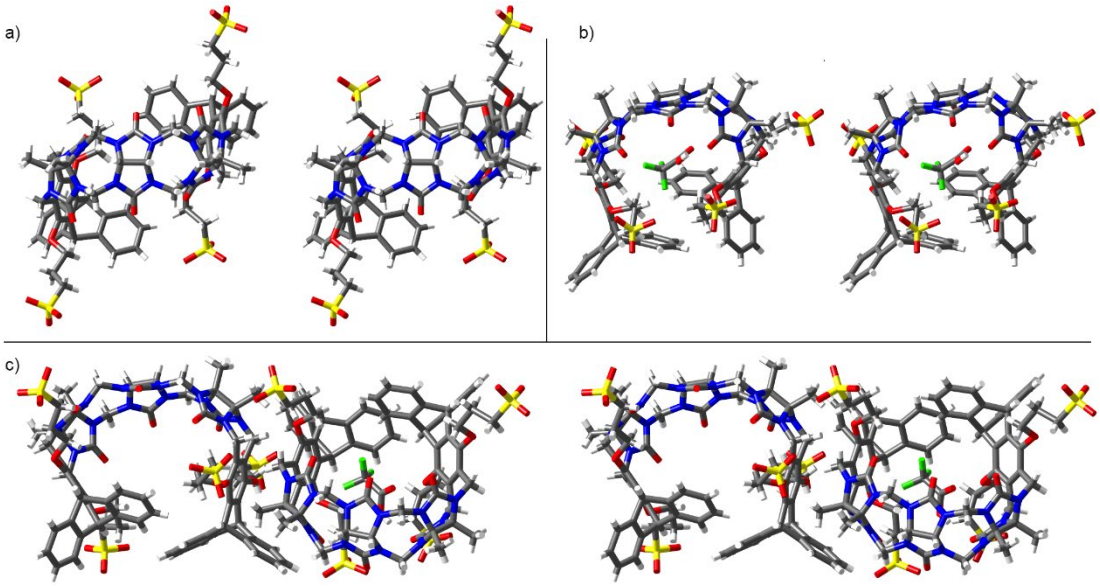

Figure III-3. Cross-eyed stereoviews of the crystal structure of 1. (a and b) Two independent molecules of **1**. (c) Packing of the two independent molecules of 1 into a dimeric unit. Color code: C, grey; H, white; N, blue; O, red; S, yellow; F, green.

3.2.4 Qualitative ^{1}H NMR host guest recognition study

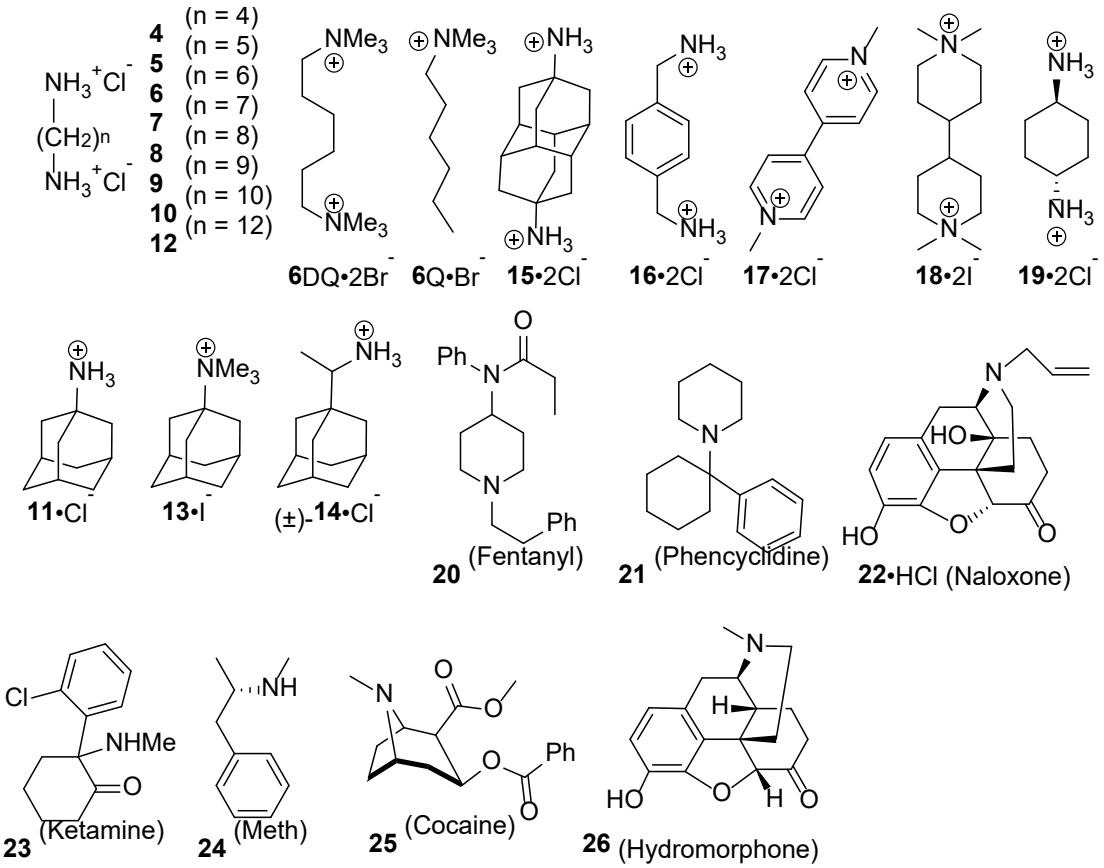

Figure III-4. Structures of guests 4–26 used in this study

Next, we decided to perform a qualitative investigation of host•guest binding of 1 toward guests 4–19 (Figure III-4) by ^{1}H NMR spectroscopy (ESI†). For example**,** Figure III-5a–c shows the ^{1}H NMR spectra recorded for uncomplexed **8**, and 1: 1 and 1 : 2 mixtures of 1 with **8**. As expected, the resonances for guest protons H_r, H_s, and H_t undergo substantial upfield shifts (41.5 ppm) upon formation of the **1•8** complex reflecting the encapsulation of the hydrophobic octylene chain inside the hydrophobic cavity of the host defined by the four aromatic rings of the triptycene sidewalls. The resonance for H_q also shifts significantly upfield (0.95 ppm) probably due to a helical

twisting of **1** in the complex which deepens the cavity and brings H_q into proximity of a triptycene sidewall. The presence of separate resonances for free guest **8** and bound guest **8** (Figure III- 5b) at a 1: 2 (1: 8) stoichiometry reflects the slow kinetics of host•guest exchange on the chemical shift timescale. Host **1** also undergoes significant changes in chemical shift upon formation of the **1•8** complex. For example, the triptycene bridgehead methine resonance (H_e) moves downfield by 0.3 ppm. Most significantly, however, the resonance for H_b undergoes a substantial downfield shift (E1.78 ppm) upon complexation which indicates that guest binding unfolds the self-folded conformation described above. Similar qualitative binding studies were performed for the remainder of the guests. In accord with expectations, we find that the resonances for the hydrophobic regions of guests 4–19 undergo substantial upfield shifts upon complexation due to the shielding effect of the triptycene sidewalls. The complexes of **1** with guests 5–10, 12, 13, 16, 17, and 18 display slow to intermediate exchange kinetics (e.g. two sets of broadened resonances) on the NMR timescale whereas guests 4, 11, 14–15, and 19–26 display intermediate to fast (e.g. one set of broadened resonances) kinetics of exchange.

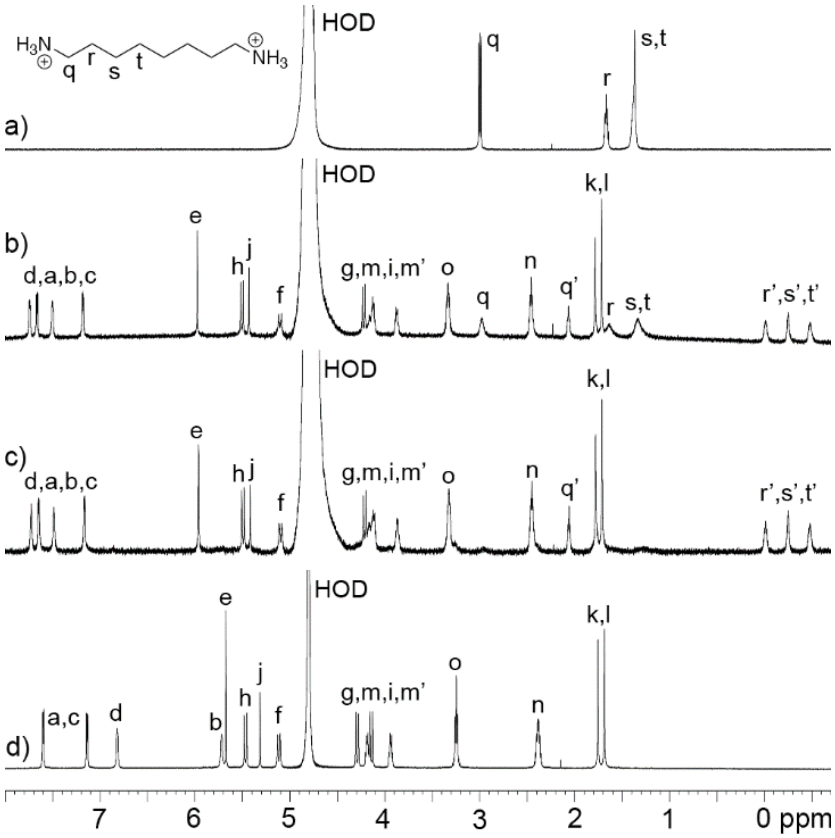

Figure III-5. ^{1}H NMR spectra recorded (600 MHz, RT, 20 mM sodium phosphate buffered D_2O, pH 7.0) for: (a) guest 8 (2 mM), (b) a mixture of 1 (250 mM) and 8 (500 mM), (c) a mixture of 1 (250 mM) and 8 (250 mM), and (d) host 1 (250 mM).

3.3 Measurement and discussion of the thermodynamic parameters of complex formation

After qualitatively assessing the host•guest binding properties of **1** we decided to quantify the binding constants (K_a, M^{-1}). Given that CB[n]•guest binding constants typically exceed the dynamic range of ^{1}H NMR we decided to use ITC to simultaneously measure K_a and DH; ITC experiments were conducted in duplicate. For example, Figure III-6a shows the thermogram recorded when a solution of 1 (100 mM) in the ITC cell was titrated with a solution of pentane diammonium 5 (1 mM) in

the syringe. Figure III-6b shows the fitting of the integrated heat values to a 1: 1 binding model with K_a = 1.33 10^6 M^{-1} and ΔH = 8.58 kcal mol^{-1}. For the 1•guest values with $K_a \leq 4.08 \times 10^6$ M^{-1} reported in Table III-1 we performed similar direct ITC titrations. For complexes with higher K_a values, and therefore c-values that exceed the recommended range,[148] we turned to competitive ITC titrations. In competition ITC, a solution of the host and an excess of a weaker binding guest is titrated with a solution of the tighter binding guest. Using the known concentrations of host, weak guest, and host•weak guest K_a and ΔH as inputs allowed us to fit the thermogram to a competitive binding model in the PEAQ-ITC data analysis software to extract the thermodynamic constants for the tighter host•guest complexes reported in Table III-1 (ESI†).

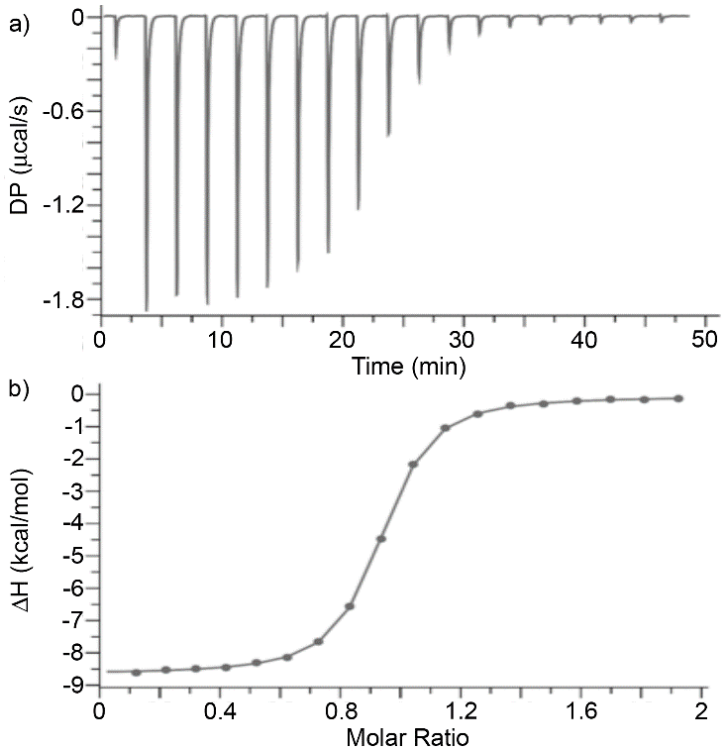

Figure III-6. (a) ITC thermogram recorded during the titration of host **1** (100 mM) in the cell with guest 5 (1.0 mM) in the syringe, (b) fitting of the data to a 1: 1 binding model with $K_a = 1.33\times10^6$ M^{-1}.

3.3.1 Magnitude of binding constants and enthalpies

A perusal of Table III-1 reveals that the K_a values for **1** with guests 4–19 fall in the range of 4670 – 4.55×10^8 M^{-1}; this large dynamic range of K_a values is desirable given their use as the blinded dataset in the upcoming SAMPL7 challenge. The complexes are all driven by favorable enthalpic contributions with ΔH values ranging from 3.98 to 14.7 kcal mol^{-1}. The substantial enthalpic driving forces observed are not unexpected given that cavity bound waters that lack a full complement of H-bonds are known to provide an enthalpic driving force for the complexes of macrocyclic CB[n].[57]

Table III-1. Binding constants (K_a, M^{-1}) and binding enthalpies (ΔH, kcal mol^{-1}) measured for **1**•guest. Binding constants (K_a, M^{-1}) measured for **DimerTrip**•guest, and **M1**•guest complexes (298 K, 20 mM NaH_2PO_4 buffered water, pH 7.4)

G	1	DimerTrip / M1 [f]
4	$(2.92 \pm 0.257) \times 10^{4}$ [a] -6.03 ± 0.260	$(4.47 \pm 0.75) \times 10^{3}$ –
5	$(1.33 \pm 0.0308) \times 10^{6}$ [a] -8.58 ± 0.021	$(1.23 \pm 0.05) \times 10^{5}$ –
6	$(2.29 \pm 0.166) \times 10^{7}$ [c] -10.8 ± 0.044	$(8.81 \pm 0.59) \times 10^{5}$ $(5.05 \pm 0.31) \times 10^{7}$
6DQ	$(5.00 \pm 0.209) \times 10^{7}$ [c] -12.7 ± 0.028	$(1.26 \pm 0.09) \times 10^{6}$ $(8.93 \pm 0.33) \times 10^{7}$
6Q	$(1.20 \pm 0.0329) \times 10^{6}$ [a] -8.54 ± 0.027	$(3.41 \pm 0.5) \times 10^{4}$ $(1.24 \pm 0.06) \times 10^{6}$
7	$(7.24 \pm 0.702) \times 10^{7}$ [c]	$(7.11 \pm 0.32) \times 10^{5}$

	-10.1 ± 0.036	–
8	(1.41 ± 0.195) × 10^{8d} -11.5 ± 0.094	(6.27 ± 0.41) × 10^5 –
9	(2.42 ± 0.334) × 10^{8d} -11.4 ± 0.062	(5.23 ± 0.34) × 10^5 –
10	(2.81 ± 0.507) × 10^{8e} -11.3 ± 0.068	(3.7 ± 0.16) × 10^5 –
12	(4.55 ± 0.943) × 10^{8d} -10.4 ± 0.064	– –
11	(3.57 ± 0.139) × 10^{5a} -4.83 ± 0.036	– (1.73 ± 0.20) × 10^7
13	(1.13 ± 0.109) × 10^{7a} -10.1 ± 0.119	(1.04 ± 0.16) × 10^4 (1.70 ± 0.05) × 10^7
14	(4.08 ± 0.341) × 10^{6a} -7.41 ± 0.084	– –
15	(1.11 ± 0.0743) × $10^{6\,a}$ -5.88 ± 0.049	– –
16	(8.77 ± 0.493) × 10^{6c} -10.5 ± 0.044	(7.1 ± 0.23) × 10^4 (1.67 ± 0.08) × 10^8
17	(5.81 ± 0.443) × 10^{7c} -12.4 ± 0.045	– (4.69 ± 0.22) × 10^8
18	(3.57 ± 0.185) × 10^{8d} -13.7 ± 0.039	– –
19	(5.95 ± 0.222) × 10^{4a} -6.61 ± 0.088	(3.29 ± 0.71) × 10^3 (1.95 ± 0.09) × 10^6
20	(1.33 ± 0.0414) × $10^{7\,c}$ -14.7 ± 0.036	– (1.1± 0.04) × 10^7
21	(9.80 ± 0.317) × 10^{4a} -5.09 ± 0.042	– (4.7 ± 0.5) × 10^4
22	(5.61 ± 0.583) × 10^{4b} -3.98 ± 0.0942	– –
23	(8.47 ± 3.10) × $10^{3\,a}$ -4.95 ± 2.30	– (1.1 ± 0.1) × 10^4
24	(9.43 ± 0.198) × 10^{5a} -9.63 ± 0.025	– (7.5 ± 2.9) × 10^6
25	(3.70 ± 0.111) × 10^{4a} -9.99 ± 0.129	– (6.6 ± 0.4) × 10^5
26	(4.67 ± 0.446) × 10^{3b} -8.92 ± 0.445	– 1.8 × 10^5

3.3.2 Influence of diammonium ion length

CB[6] is known to preferentially bind to diammonium ions whose length (e.g. H_3N^+•••NH_3^+) matches the C=O•••O=C distances of the host; CB[6]•5 and CB[6]•6 display maximal affinity.[58] An examination of Table 1 reveals a very different trend in K_a with the K_a values for increasing steadily from **1•4** (2.92 × 10^4 M^{-1}) to 1•8 (1.41 × 10^8 M^{-1}) and then plateaus at ≈ 10^8 M^{-1} for longer diammonium ions **9**, **10**, and **12**.

Host **1** can accommodate longer diamines because it can flex and expand its cavity and because the $(CH_2)_3SO_3^-$ arms deepen the cavity while providing for new ammonium•••sulfonate interactions. Similar observations have been made previously for a carboxylate analogue of **M1**.[94]

3.3.3 Drugs of abuse

Recently, we have found that acyclic CB[n]-type receptors (e.g. **M1**) bind tightly to neuromuscular blocking agents and function as in vivo reversal agents.[62, 97, 144] More recently, we found that acyclic CB[n] bind strongly to methamphetamine and fentanyl and modulate the hyperlocomotion induced by methamphetamine in vivo (rats).[98] Accordingly, we decided to determine the binding affinities of **1** toward a panel of drugs of abuse (**20** –**26**) by ITC (Table III-1). Most notable is the interaction between **1** and fentanyl with K_d = 75 nM which makes it suitable as a potential in vivo reversal agent. The interactions between **1** and 21–26 are substantially weaker ($K_a < 10^6$ M^{-1}). The data in Table III-1 also allow a comparison between **1** and **M1**. As can be seen, **M1** is often a slightly stronger host than **1**, most notably toward methamphetamine. This trend is not unexpected given that acyclic CB[n] based on glycoluril tetramer have more fully formed ureidyl C=O portals and larger cavities[114].

3.3.4 Influence of guest charge

Compounds 6DQ and 6Q differ in the number of quaternary ammonium ions while maintaining a common hexylene hydrophobic core. Table 1 shows that the complex between **1** and dicationic guest 6DQ ($K_a = 5.00 \times 10^7$ M^{-1}) is 42-fold

stronger than **1**•6Q ($K_a = 1.20 \times 10^6$ M^{-1}). Similar, but more pronounced trends are seen for CB[n]•guest complexes where an additional ion–dipole interaction commonly increases K_a by 10^2 –10^3 M^{-1}.[149, 150]

3.3.5 Influence of the cationic headgroup

Compounds 6 and 6DQ as well as 11 and 13 differ only in the presence of primary ammonium (NH_3^+) or quaternary ammonium (NMe_3^+) ion centers. Table III-1 shows that **1** binds the quaternary guests (6DQ and 13) more tightly by 2.2-fold and 31.7-fold. Related effects have been seen for macrocyclic CB[7] complexes where the magnitude of the effect is dependent on the nature of the hydrophobic moiety.[59, 60, 151]

3.3.6 Influence of guest hydrophobic residue

Macrocyclic CB[n]•guest complexes are very sensitive to the size and shape of the guest because the cavity of these hosts cannot easily expand its size to alleviate steric interactions.[58, 59] For example, CB[7] binds **11** ($K_a = 4.23 \times 10^{12}$ M^{-1}) more that 10^8-fold stronger than 3,5-dimethyladamantaneamine (memantine, $K_a = 25000$ M^{-1}).[59] Consider the following series of guests: **6**, **16**, **17**, **18**, and **15**. Across this series, there is a constant number of C-atoms (6) in between the two ammonium ions centers. However, the total number of C-atoms in the hydrophobic moiety of the guest (6: 6; 16: 8, 17: 10, 18: 10, and 15: 14) and the nature of hydrophobicity of the moiety (e.g. aromatic 16 and 17 versus aliphatic 6, 18, 15) is different. As the number of C-atoms of the guest is increased one would expect larger K_a values due to more favorable desolvation of the larger guests upon complexation. Conversely, as the size and cross-sectional area of the hydrophobic guest moiety is increased beyond an optimum one

might expect decreased K_a values due to energetically costly expansion of the host cavity. Within this series of guests, we observe a maximum K_a value of (3.57 ± 0.185) × 10^8 M^{-1} for 1•18. As expected, the bulky multicyclic guests 21, 22, and 26 are quite poor guests for **1** with K_a in the 10^4–10^5 M^{-1} range.

3.3.7 Comparisons between hosts

Table III-1 also presents the binding constants of two related hosts (**M1** and **DimerTrip**) drawn from the literature.[98, 146, 152] Dimer-Trip is an analogue of 1 that only contains two glycoluril rings. Accordingly, the cavity of Dimer Trip is CB[6] sized and therefore smaller than the cavity of **1**. A comparison of the binding constants given in Table 1 reveals that **1** is a superior host compared to Dimer Trip by 6.5 to 1086-fold. The highest selectivities are seen for bulky guests (13: 1086-fold; 10: 760-fold) which cannot be fully encapsulated inside **Dimer Trip** without substantial energetic penalties for cavity expansion. **M1** differs from **1** by the number of glycolurils (4 versus 3) unit and by the different sidewalls (benzene versus triptycene). A comparison of the K_a values in Table 1 toward a given guest shows that **M1** and **1** are comparable hosts in many cases (e.g. 6, 6DQ, 6Q, 13, 20). Interestingly, host **M1** binds significantly stronger than **1** toward 11 (49-fold), 16 (19-fold), 17 (8-fold), and 24 (8-fold). Guests 16, 17, and 24 all contain aromatic ring binding sites which suggests that the hydrophobic box defined by **M1** is more appropriate for simultaneous edge-to-face and offset p-stacking with guests.[102] We conclude that **1** is a surprisingly good host that is nearly on par with the prototypical acyclic CB[n]-type receptor **M1**.

3.4 Conclusion

In summary, we have reported the synthesis of host 1 which is based on a central glycoluril trimer capped with two triptycene sidewalls. Host **1** is water soluble (3 mM) and does not undergo strong self-association in water (K_s = 480). In solution, **1** displays upfield chemical shifts for H_b of the triptycene sidewall (Figure III-5d) which indicates a self-folded conformation. In contrast, the X-ray crystal structure of **1** displays two more open conformations where the triptycene sidewalls undergo an out-of-plane helical distortion. In combination the ^{1}H NMR and X-ray results highlight the high conformational flexibility of **1** which stands in contrast to macrocyclic CB[n]. The geometries and thermodynamics of complexation between **1** and guests 4–26 were elucidated by ^{1}H NMR induced chemical shifts and measured by ITC. A subset of these K_a values form the blinded dataset for the SAMPL7 challenge.[147] We find that host **1** with its central glycoluril trimer is a superior host compared to previously synthesized host DimerTrip. Host **1** even displays K_a values toward many guests that are very close to those measured for **M1** which is the prototypical acyclic CB[n]-type host. Finally, host **1** is a powerful receptor for fentanyl which suggests its potential application as an in vivo sequestration agent.

Chapter 4: Acyclic Cucurbit[*n*]uril-Type Receptors: Optimization of Electrostatic Interactions for Dicationic Guests

The work presented in this chapter was take from Lu, X.; Zebaze Ndendjio, S.; Zavalij, P.Y.; and Isaacs, L. Acyclic Cucurbit[n]uril-Type Receptors: Optimization of Electrostatic. *Org Lett*. **2020**. In this work, Lu first developed the synthetic procedure of the direct sulfonation of the acyclic CB[n] host. I then repeated the synthesis of the host and conducted extensive NMR and ITC studies with various guest including drugs of abuse and Neuromuscular blocking agents.

4.1 Introduction

The preparation of molecular container compounds and their use in basic science and real world applications has been a focal point of research in supramolecular chemistry for several decades.[10, 20, 34, 153] For example, cyclodextrin molecular containers have practical real world use as solubilizing excipients for hydrophobic drugs, as the active ingredient in the household product Febreeze™, and as a sequestration agent for neuromuscular blockers in the form of Sugammadex.[32] cucurbit[n]uril molecular containers have become increasingly popular in the past decade due in part to their high affinity binding toward hydrophobic (di)cations (e.g. K_a commonly 10^6 M^{-1}, often 10^9 M^{-1} and up to 10^{17} M^{-1} in select cases) and their stimuli responsive host•guest binding properties.[20] CB[n] hosts are thereby well suited as components of functional systems (e.g. sensing ensembles, drug delivery systems, and supramolecular materials).[10, 20] In recent years, we and others, have been exploring the synthesis and molecular recognition properties of acyclic CB[n]-

type receptors (e.g. **M1**, Scheme IV-1) which retain the essential binding properties of macrocyclic CB[n] but are more easily functionalized.[95, 145] For example, **M1** has been used as a solubilizing excipient for insoluble drugs and as in vivo sequestration agents for neuromuscular blockers (rocuronium, vecuronium, and cisatracurium) and drugs of abuse (e.g. methamphetamine and fentanyl).[98] These applications require hosts with maximal binding affinities to allow them to outcompete the cognate biological receptors.[32] Herein, we report the synthesis of host **1** whose anionic sulfate groups are positioned at the ureidyl C=O portals to complement cationic guests.

Previously, we studied the influence of the alkylene (e.g. $(CH_2)_n$) linker length between the aromatic walls of acyclic CB[n] and the sulfonate solubilizing groups on their binding affinity toward guests but did not observe large differences for n = 2, 3, 4.[115] We reasoned that these alkylene linkers result in the anionic sulfonate groups being positioned away from the ureidyl carbonyl portal of **M1**, for example, and thereby reduce the electrostatic driving force toward guest complexation. Accordingly, we hypothesized that complete removal of the linker would position the negatively charged group closer to the cation binding site at the ureidyl carbonyl portal and thereby increase binding affinity toward cationic guests.

4.2 Synthesis and characterization

Synthetically, we allowed our key glycoluril tetramer building block (**2**)[94] to react with hydroquinone (**3**) in TFA at room temperature to deliver hydroxylated host **4** in 99% yield on a 20-gram scale. Subsequently, **4** was allowed to react with pyridine-SO_3 complex in pyridine at 90 ˚C to deliver host **1** in 60% yield on a 0.5-gram scale after purification by gel permeation chromatography. Host **1** was fully

characterized by spectroscopic means, but its structure was also confirmed by x-ray crystallographic measurements of its host•guest complexes (vide infra). For example, the ^{1}H NMR spectrum of **1** shows six resonances for the diastereotopic methylene groups on the glycoluril oligomer backbone in the expected 4:4:4:4:2:2 ratio (H_b, H_c, H_d, H_e, H_f, H_g) along with a singlet for the aromatic H-atoms (H_a), two Me resonances (j and k), and two glycoluril methine resonances (H_h, H_i) which is consistent with the depicted C_{2v}-symmetric structure of **1**.

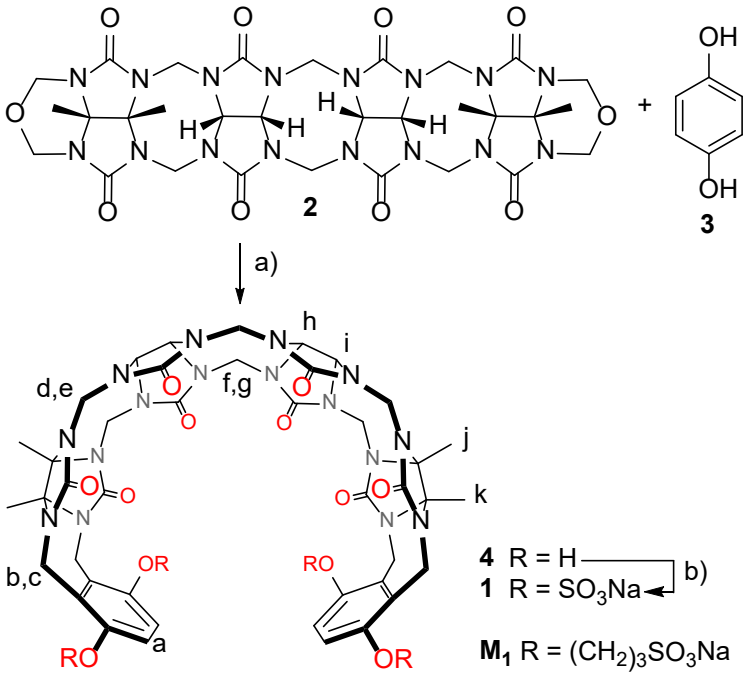

Scheme IV-1. Synthesis of host **1**. Conditions: a) TFA, 25 ˚C, N_2, 16 h; b) pyridine sulfur trioxide, pyridine, 90 ˚C, N_2, 18 h.

In the ^{13}C NMR we observe all 14 resonances expected on the basis of the C_{2v}-symmetric structure depicted for **1**. Finally, the electrospray ionization mass spectrum for **1** as its complex with guest 6d exhibits a doubly charged ion at m/z 787.1679 ($[M + 6d\text{-}2Cl\text{-}]^{2+}$), calculated for $C_{54}H_{70}N_{18}O_{24}Na_{42}^{+}$ 787.1642. Host **1**

exhibits very good solubility in water (>40 mM). Before proceeding to investigate the host•guest properties of **1** we investigated its self-association properties to ensure that self-association does not impinge upon the planned binding constant measurements.[34] Accordingly, we measured the ^{1}H NMR spectrum for aqueous solutions of **1** upon dilution from 40 mM to 1 mM. We did not observe any significant changes in chemical shifts ($\Delta\delta < 0.02$ ppm) over this concentration range and therefore conclude that host **1** is monomeric in aqueous solution (Appendix 3).

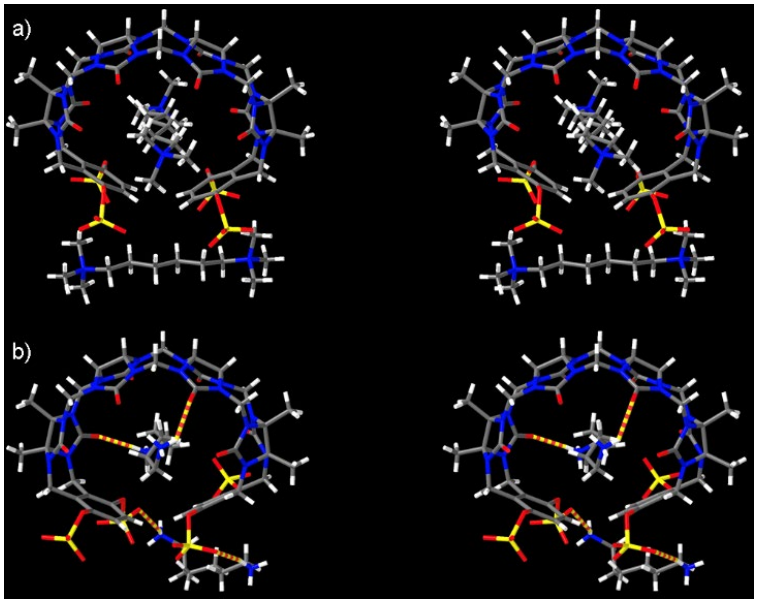

Figure IV-1. Cross eyed stereoviews of the x-ray crystal structures of a) 1•6d, and b) 1•6a. Color code: C, gray; H, white; N, blue; O, red; H-bonds red-yellow striped.

We were fortunate to obtain the x-ray crystal structures of the 1•6d and 1•6a complexes (Figure IV-1). Figure IV-1a shows the 1•6d complex adopts a geometry that optimizes Me_3N^+•••O=C electrostatic interactions at both portals and displays only small out-of-plane skewing of the terminal aromatic rings. The geometry of 1•6d is reminiscent of those of CB[n]•guest complexes where the Me_3N^+•••O=C

distances cluster in the 3.810 – 4.690 Å range to spread the positive charge to the carbonyl portals.[60] Quite interestingly, a second molecule of di-cationic guest 6d fits nicely into a cleft created by the aromatic sidewalls and the outward pointing OSO_3^- groups to balance the overall 4- charges of host **1**. These OSO_3^- groups also engage in electrostatic interactions with 6d with the Me_3N^+•••O-S shortest distances in the 3.808 – 4.722 Å range. The crystal structure of 1•6a (Figure IV-1) also shows one intracavity and one extra cavity molecule of 6a but displays significant out-of-plane twisting of the aromatic termini. Interestingly, one of the four OSO_3^- groups turns inward toward the ammonium ion guest which establishes that this group can directly participate in the guest recognition process.

4.3 ^{1}H NMR spectrum investigation

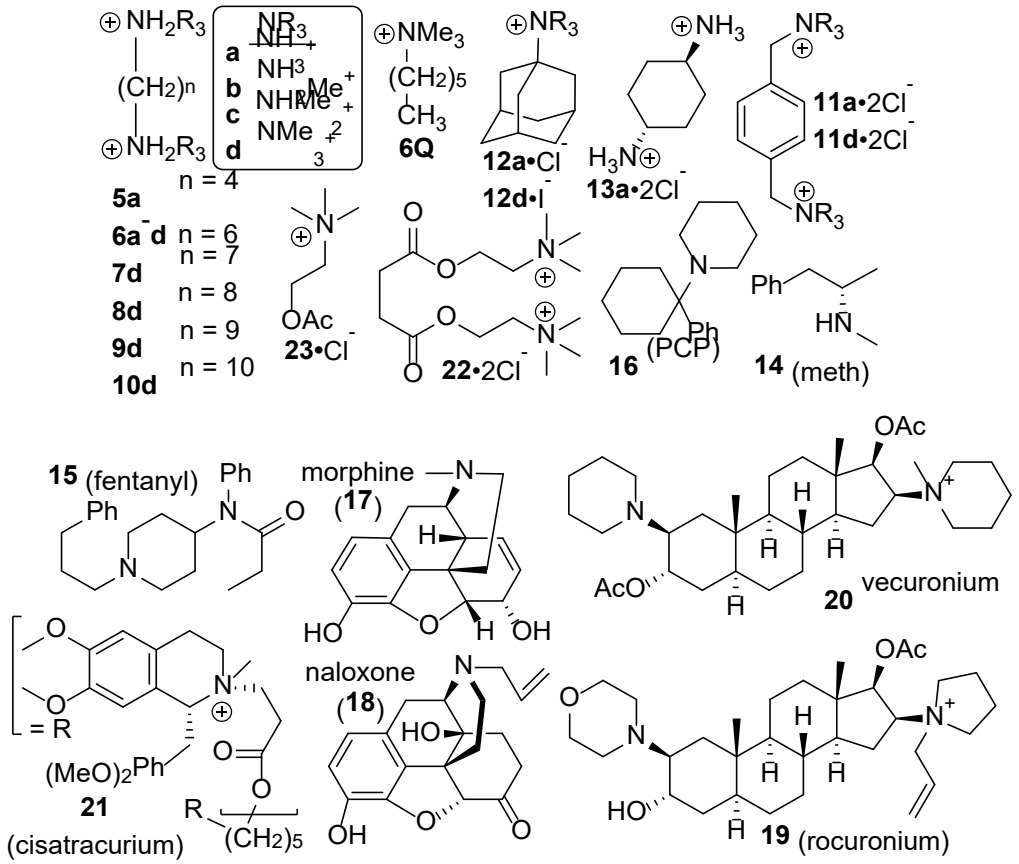

Figure IV-2. Structures of guests 5 – 23 used in this study.

Next, we performed qualitative host•guest binding studies of 1 with guests 5-13 (Figure IV-2, Appendix 3) as monitored by ^{1}H NMR spectroscopy. Figure IV-3 shows the ^{1}H NMR spectra recorded for 1, 6d, and 1:1 and 1:2 mixtures of 1:6d. As expected the methylene resonances for guest 6d (H_m, H_n, H_o) within the 1•6d complex (Figure IV-3b) experience a sizable upfield shift upon complexation due to the anisotropic shielding effects of the aromatic walls and the glycoluril concavity.[45, 58] At a 1:2 1:6d ratio, resonances are observed for both free 6d and 1•6d which indicates slow exchange on the ^{1}H NMR chemical shift time scale which is usually observed only for tight host•guest complexes. Similar ^{1}H NMR measurements were made for

the remainder of the guests (Appendix 3). We find that the narrow guests (e.g. 11a, d and 6a-d) display slow exchange kinetics whereas the bulkier guests 12a,d display intermediate to fast ex-change on the chemical shift timescale. We attribute this to their lower binding constants (vide infra) as a result of the expansion of the cavity of **1** required to accommodate the larger adamantane framework

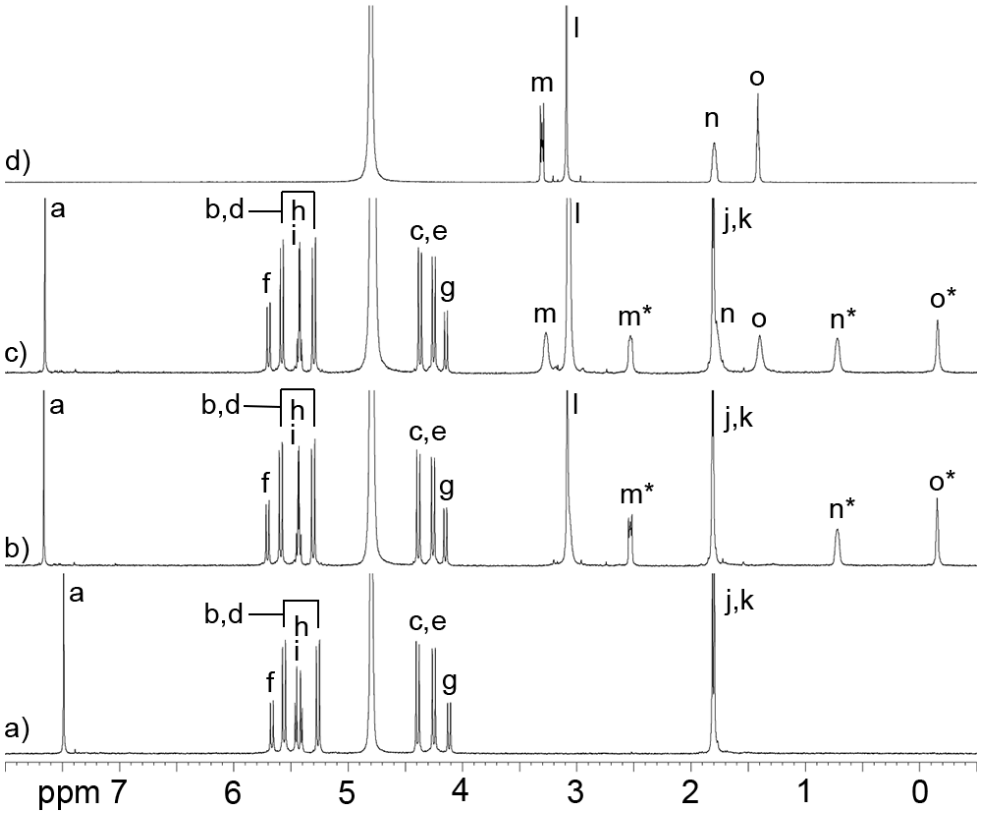

Figure IV-3. ^{1}H NMR spectra (D_2O, 600 MHz) recorded for: a) 1 (1 mM), b) a mixture of 1 (1 mM) and 6d (1 mM), c) a mixture of 1 (1 mM) and 6d (2 mM), and d) 6d (1 mM). Resonances for bound guests as marked with an asterisk (*).

4.4 Isothermal Titration Calorimetry

Given the high binding constants typically observed for host•guest complexes of CB[n] and acyclic CB[n]-type receptors,[95, 154] we elected to use isothermal titration calorimetry (ITC) to measure the K_a values between host **1** and guests 5 – 23. For the weaker binding complexes ($K_a \leq 10^7$ M^{-1}), we performed the direct titration of host 1 in the ITC cell with a solution of guest in the syringe and fitted the data to a 1:1 binding model implemented by the PEAQ ITC software to obtain K_a and ΔH values (kcal mol^{-1}). Table IV-1 reports the thermodynamic data for 1•5, 1•6Q, 1•12a, 1•13a, 1•14 – 1•18, and 1•21 – 1•23 that were obtained by direct ITC titrations (Appendix 3). Complexes with K_a values that exceed 10^7 M^{-1} cannot be measured accurately by direct titrations, so we turned to ITC competitive titrations.[155] In competitive titrations, a solution of host and an excess of a weak guest of known ΔH and K_a is titrated with a solution of a tighter binding guest. Fitting of the heat released during the displacement process is analyzed by a competitive binding model in the PEAQ ITC data analysis software which delivers ΔH and K_a for the tighter binding complex**.** Figure IV-4a shows the thermogram recorded when a mixture of **1** and 13 was titrated with 6d and Figure IV-4b shows the fitting of the integrated heats to a competitive binding model to determine $K_a = 6.79 \times 10^9$ M^{-1} and ΔH = -12.1 kcal mol^{-1}. Table IV-1 reports K_a and ΔH values for the remaining 1•guest complexes obtained in an analogous manner (Appendix 3).

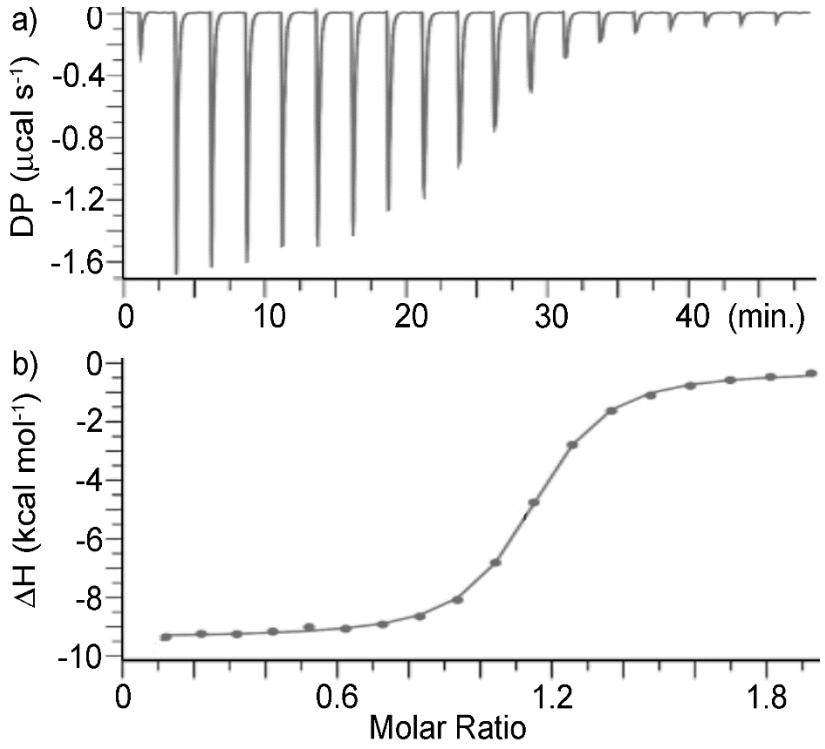

Figure IV-4. a) Thermogram recorded during the titration of a mixture of 1 (100 µM) and 13 (2 mM) in the cell with a solution of 6d (1.0 mM) in the syringe, and b) fitting of the data to a competition binding model to extract $K_a = 6.79 \times 10^9$ M^{-1} and ΔH = -12.1 kcal mol^{-1}.

The binding constant data reported in Table IV-1 allows us to draw some conclusions about the molecular recognition preferences of host **1** in comparison to **M1**. As expected, we find that the 1•guest complexes are uniformly driven by favorable enthalpic (ΔH) contributions. In the CB[n] series of hosts these favorable enthalpy values are attributed to the presence of high energy host intracavity water molecules that are released upon guest binding.[57, 79] Host 1 displays high affinity toward hexane diammonium ion guests 6a – 6d with K_d values in the single digit nM to sub-nM range. Host 1 prefers the quaternary ammonium ion guest 6d by ≈10-fold

over the primary – tertiary ammonium ions 6a – 6c. In selected contexts, related preferences have been seen for CB[7][60] where they are attributed to the more efficient spreading of positive charge to the entire ureidyl C=O portal. Host 1 binds quaternary monoammonium ion guest 6Q 890-fold weaker than the corresponding quaternary diammonium 6d; this $\approx 10^3$ M^{-1} difference in affinity is also noted for CB[n]-type receptors.[20] Importantly, we find that 1 binds to guests 6a – 6c 5.6 – 11.9-fold stronger than **M1**, but 75-fold stronger than **M1** toward bis(quaternary) guest 6d. Similar preferences are observed for di-cationic guests 11a and 11d but not for mono-cationic guests 12a and 12d which suggests that the defined separation between OSO_3^- groups in **1** makes it especially complementary to diammonium ion guests. Host 1 also binds with high affinity (single digit nM to sub nM K_d values) toward the longer alkane di-ammonium ions 7d – 10d although 6d is the tightest binder in this series which reflects the ability of acyclic CB[n] to flex their cavity to accommodate larger guests and optimize binding affinity. Related preferences have been seen for **M1** and related receptors toward primary alkane diammonium ion guests previously.[94]

Table IV-1. Binding constants measured by ITC for host•guest complexes of **1**. Comparative data for **M1** are drawn from the literature. Conditions: 20 mM sodium phosphate buffered H_2O, pH 7.4, 25˚C.

	K_a [M^{-1}]; ΔH (kcal mol^{-1})	
	1	**M1**[e]
5	1.68×10^6; -6.76 ± 0.020[a]	–
6a	3.70×10^8; -8.60 ± 0.021[b]	5.05×10^7; -6.23 ± 0.014
6b	5.26×10^8; -9.82 ± 0.038[c]	9.43×10^7; -7.15 ± 0.025
6c	5.74×10^8; -10.5 ± 0.028[c]	4.81×10^7; -7.66 ± 0.073
6d	6.71×10^9; -12.1 ± 0.042[c]	8.93×10^7; -9.35 ± 0.021
6Q	7.57×10^6; -9.68 ± 0.063[a]	1.24×10^6; -5.67 ± 0.033

7d	6.06×10^9; -12.2 ± 0.041[c)]	–
8d	1.75×10^9; -10.5 ± 0.032[c)]	–
9d	7.57×10^8; -10.2 ± 0.030[c)]	–
10d	5.43×10^8; -10.3 ± 0.088[c)]	–
11a	9.71×10^8; -9.69 ± 0.014[b)]	1.67×10^8; -8.09 ± 0.018
11d	1.05×10^9; -12.0 ± 0.030[b)]	1.78×10^8; -11.4 ± 0.022
12a	9.90×10^5; -4.45 ± 0.021[a)]	9.62×10^5; -6.55 ± 0.029
12d	6.66×10^6; -7.36 ± 0.030[d)]	1.70×10^7; -9.09 ± 0.027
13a	3.41×10^6; -2.92 ± 0.019[a)]	1.95×10^6; -5.70 ± 0.027
14	3.02×10^6; -9.28 ± 0.058[a)]	7.5×10^6
15	3.64×10^6; -12.2 ± 0.076[a)]	1.1×10^7
16	1.89×10^5; -6.18 ± 0.069[a)]	4.7×10^4
17	7.69×10^5; -8.03 ± 0.07[a)]	5.3×10^5
18	4.85×10^6; -5.90 ± 0.205[a)]	–
19	6.29×10^8; -12.9 ± 0.056[b)]	8.4×10^6
20	1.00×10^9; -9.62 ± 0.036[c)]	5.8×10^6
21	5.32×10^5; -15.4 ± 0.174[a)]	9.7×10^5
22	2.41×10^4; -5.26 ± 0.372[a)]	–
23	2.31×10^5; -8.54 ± 0.063[a)]	2.4×10^4

– not reported in the literature. a) Direct titration, b) competitive ITC with 5 as competitor, c) competitive ITC with 13a as competitor, d) competitive ITC with 6d as competitor, e) Taken from the literature. 6,12

4.4.1 binding to drug of abuse

Previously, we have shown that **M1** and a naphthalene walled analogue known as M2 function as in vivo sequestration agents for drugs of abuse (e.g. methamphetamine (14)).[156] Accordingly, we decided to measure the binding affinities of some compounds (14 – 18) relevant to counteracting the effects of drugs of abuse. We find that host **1** binds less tightly than **M1** toward 14 and 15. In contrast, host **1** binds somewhat tighter to PCP (16) and morphine (17) than **M1** does, but the single digit μM dissociation constants are unlikely to render 1 an efficient in vivo sequestration agent for 16 and 17. Accordingly, **1** is not an improved lead compound for the sequestration of drugs of abuse (14 – 17). This is perhaps not surprising given that 1 has a distinct preference for bis(quaternary) di-ammonium ions whereas 14 – 17 are secondary and tertiary ammonium ions.

4.4.2 Serving as reversal agents for neuromuscular blocking molecules

In a separate line of inquiry, we have previously shown that **M1** and **M2** act as in vivo reversal agents for neuromuscular block induced by rocuronium (19), vecuronium (20), and cisatracurium (21).[95, 129] Accordingly, we measured the binding constants of **1** toward a panel of compounds relevant to its potential use as an in vivo reversal agent. **Table 1** shows that **1** possesses higher binding affinity toward 19 (75-fold) and 20 (172-fold) than **M1** does. Importantly, **1** binds >2700-fold tighter to 19 or 20 than to acetylcholine (23). Acetylcholine is also present in the neuromuscular junction and must not be sequestered. The affinity of **1**•19 (6.29×10^8 M^{-1}) and **1**•20 (1.00×10^9 M^{-1}) are comparable to those of **M2**•19 (3.4×10^9 M^{-1}) and **M2**•20 (1.6×10^9 M^{-1}) which function very well in vivo.[129] Host **1**, however, possesses superior aqueous solubility (>40 mM) compared to **M2** (18 mM) which might prove advantageous for formulation purposes.

4.5 Conclusion

In summary, we have presented the synthesis of a new acyclic CB[n]-type receptor (**1**) with OSO_3^- groups directly connected to the aromatic walls. Host **1** has excellent aqueous solubility (40 mM), does not undergo self-association, and binds more tightly to quaternary diammonium ions than analogue **M1** that features propylene linking chains. The X-ray crystal structures of 1•6a and 1•6d show the usual cavity encapsulation of the diammonium guest but also show an external diammonium ion that balances the overall charge of the tetra-anionic host **1**. In conclusion, we find that the negatively charged OSO_3^- groups do not merely function as solubilizing group, but rather than their close proximity to the ureidyl C=O portals

of **1** results in enhanced binding affinity toward quaternary diammonium ions including important neuromuscular blocking agents (19 and 20). This suggests that **1** should be considered alongside **M1** and **M2** as in vivo reversal agents for neuromuscular blockers.

Chapter 5: Conclusion

Section 5.1 Summary

Supramolecular concepts have been applied for molecular recognition, catalysis, drug delivery and reversal, solubilization, spectroscopic sensor probes, carbon nanotubes and more. The development of molecular containers has played a major role in this expansion. Molecular containers such as β-cyclodextrins are already used commercially for pharmaceutical purposes and industrial uses such as in Febreeze™. The discovery of glycoluril based molecular containers such as cucurbit[n]urils and acyclic cucurbit[n]urls opened the door for more innovations. In particular, acyclic cucurbit[n]urils which display higher water solubility due to the sulfonate groups on its aromatic walls, it has a flexible backbone to encapsulate a wider variety of guests. The Isaacs research group did a tremendous work in studying and reporting the applications of acylic cucurbit[n]uril, **M1** and **M2**, in solubilizing drugs, drug reversal toward neuromuscular blocking agents such as Rocuronium and Vecuronium, and recently, reversal of drugs such as Methamphetamine and Fentanyl.

Chapter 2 described the yet another property of acyclic Cucubit[n]uril which is recognition properties toward amino acids, peptides and Insulin. It was found that acyclic CB[n] has high binding affinity toward amino acid amides due to ion-dipole interactions and hydrophobic effect. **M1** and **M2** show preferential binding affinity toward di-cationic and aromatic amino acid amides particularly phenylalanine amide. A deeper analysis shows the energetic cost or benefit in the formation of the complexation of acyclic CB[n] with amino acids or amino acid amides or amino acetyl amides can be linked to ion-dipole and ion-ion interactions between host and

guest. Like cucurbit[n]urils, the acyclic CB[n] can also bind to peptides however they are unable to encapsulate two amino acid residues at once. Finally, **M1** and **M2** show recognition ability toward Insulin in physiological conditions.

In chapter 3, a new acyclic CB[n] host – sulfonated trimer triptycene – was synthesized, characterized by spectroscopic methods, and its molecular recognition properties examined. An X-ray crystal structure of the host revealed its helical structure and an intriguing packing dynamic. This host displayed interesting recognition properties toward alkyl ammonium guests. It was found that the binding affinity increases as the length of the alkyl ammonium guest increases. The determined K_a values served as a blinded experimental dataset for the SAMPL series of challenges for computational chemists looking to improve their methods to calculate binding free energies in water. Finally, the trimer triptycene host shows strong preferential binding affinity toward Fentanyl.

Chapter 4 introduced yet another acyclic CB[n] host, sulfate substituted acyclic CB[n] host. In this new host the alkyl linker connecting the aromatic ring to the sulfonate group is eliminated in order to optimize the binding affinity and selectivity of acyclic CB[n] toward guests. This new host displayed preferential binding affinity toward quaternary ammonium guests. Additionally, the new host demonstrated stronger binding affinity toward Rocuronium and Vecuronium than **M1**. This indicates its potential application as an in vivo reversal agent for neuromuscular blocking agents.

Section 5.2 Future Work

Acyclic cucurbit[n]uril hosts although they were just recently developed have already demonstrated outstanding applications in the field of pharmaceuticals. Although we have shown that **M1** and **M2** bind to a protein (Insulin) there are other proteins that could be targeted by acyclic CB[n]. For example, Klaerner and co-workers have previously shown that benzonorbornene derived molecular tweezers can bind to amyloid protein and prevent aggregation. I suggest that it might be fruitful to perform a similar study with acyclic CB[n]s to evaluate their ability to binding to amyloid protein and their impact on aggregation in physiological conditions. Amyloid proteins are pertinent in the development of Alzheimer's disease which according to the National Institute of Health (NIH) affects over 5.5 million Americans over the age of 65,[157] so this has potentially high impact on human health.

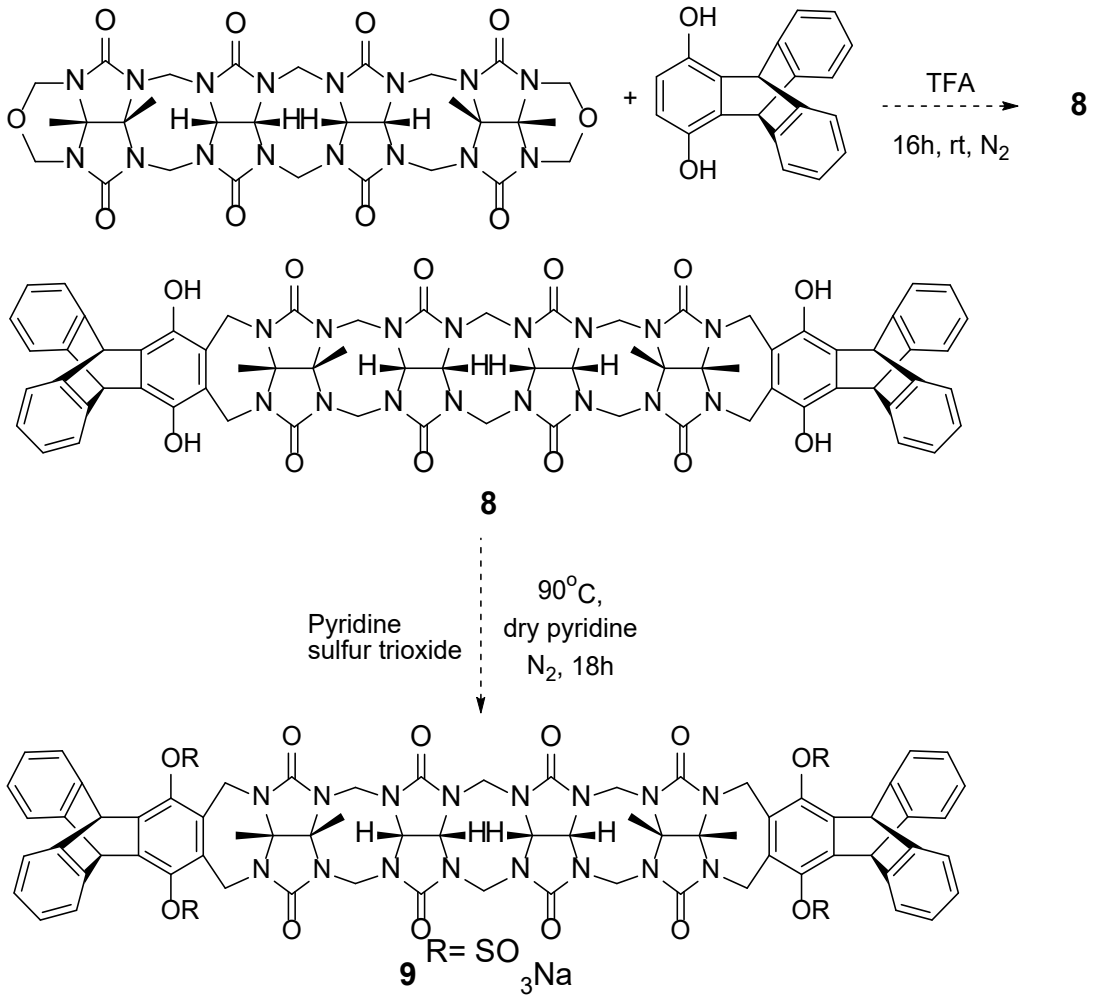

Scheme V-I. Proposed synthesis of a new acyclic CB[n] **8** which would lead to **9.**

Another project to focus on for future work, is the synthesis of a new acyclic host which combined strong binding and selectivity toward quaternary guests and fluorescent sensing properties. To achieve this goal, host **8** can be obtained by reacting dihydroxy triptycene with glycoluril tetramer by double electrophilic aromatic substitution. Once **8** is obtained it can be transformed into **9** by reaction with pyridine sulfur trioxide under dry conditions.

Finally, a series of new sulfate hosts can be produced in order to complete the study of the impact of glycoluril backbone on the molecular recognition properties toward dicationic guests. Now that it is established that the sulfate substituted host with a glycoluril tetramer backbone has a strong binding affinity and selectivity toward quaternary ammonium guests. The new sulfate host **11** and **12** would have smaller cavities and would be selective toward smaller quaternary guests. Host **10** with its trimer glycoluril backbone would most likely feature a helical structure which would allow it to bind to longer quaternary ammonium guests. Accordingly, by creation of a library of acyclic CB[n] we should be able to optimize their binding affinity toward a wide variety of chemically and biologically relevant guests.

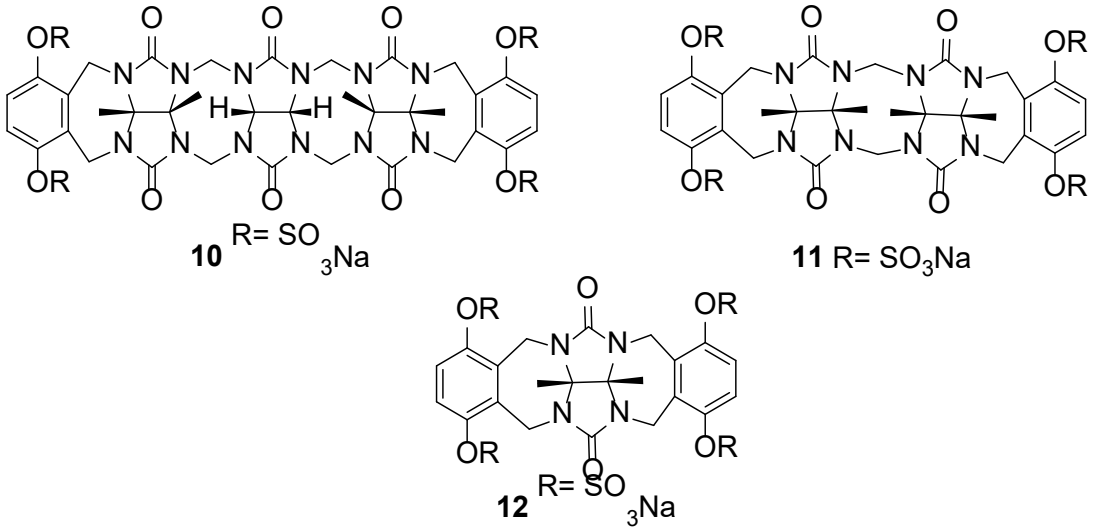

Figure V-1. Series of sulfate hosts composed of trimer sulfate host **10**, dimer sulfate host **11**, monomer sulfate host **12**

Appendix I

Molecular Recognition Properties of Acyclic Cucurbiturils Toward Amino Acids, Peptides, and a Protein

Supporting Information

By Sandra A. Zebaze Ndendjio, and Lyle Isaacs
Department of Chemistry and Biochemistry, University of Maryland, College Park, College Park, MD 20742, USA

Table of Contents **Pages**

General experimental details. The amino acid amides, amino acids, and acetyl amino amides were commercially available and obtained from Bachem, Chem-Impex, Alfa Aeser, and Acros Organic. The acyclic CB[*n*] were synthesized, purified and characterized as described in a previous publication from the Isaacs group[62]. The tripeptides were commercially available and obtained from peptide2go and native human insulin recombinant from *Saccharomyces cerevisiae* (SAFC Biosciences). Calorimetric Titration using microcal PEAQ-ITC from Malvern were performed to obtain stability constants and reaction thermodynamics information for the formation of the complex between acyclic CB[*n*] and amino acid amides, amino acids and acetyl amino amides. Binding studies were also performed using 400 MHz ^{1}H NMR at room temperature in 20 mM sodium phosphate (NaH_2PO_4) buffered D_2O at pD 7.40 with 64 scans.

Details for Isothermal Titration Calorimetry (ITC) measurements. All measurements were performed in High Performance Liquid Chromatography (HPLC) NaH_2PO_4 buffered water at pH 7.40. The Isothermal Titration Calorimetry (ITC) instrument were set at 19 injections with a volume of 2.00 µl per injections, 298.0 K temperature, with a reference power of 5.00 µcal/sec, stir speed of 750 rpm and the feedback was set on high. The measurements for Insulin and the three hosts were done in 20mM sodium phosphate buffered water (NaH_2PO_4) at pH 7.40, 4mM EDTA at room temperature.

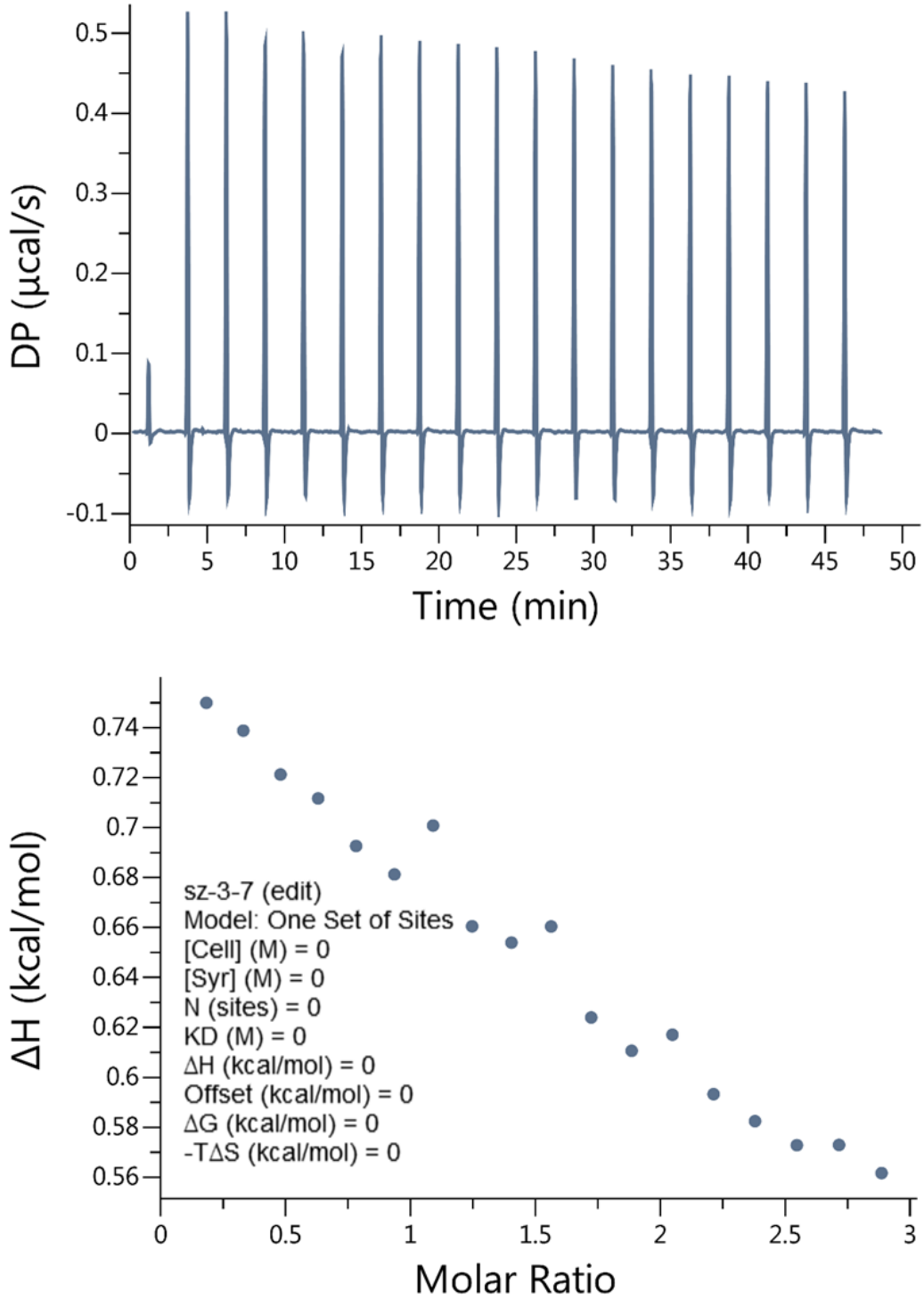

Figure II-S1. Isothermal Titration Calorimetry (ITC) curve obtained when a solution of Motor 2 (100 µM) in the cell was titrated with Threonine amide (1.50 mM) in the syringe at 298.0 K in 20 mM sodium phosphate buffered water at pH 7.4. K_a= No binding

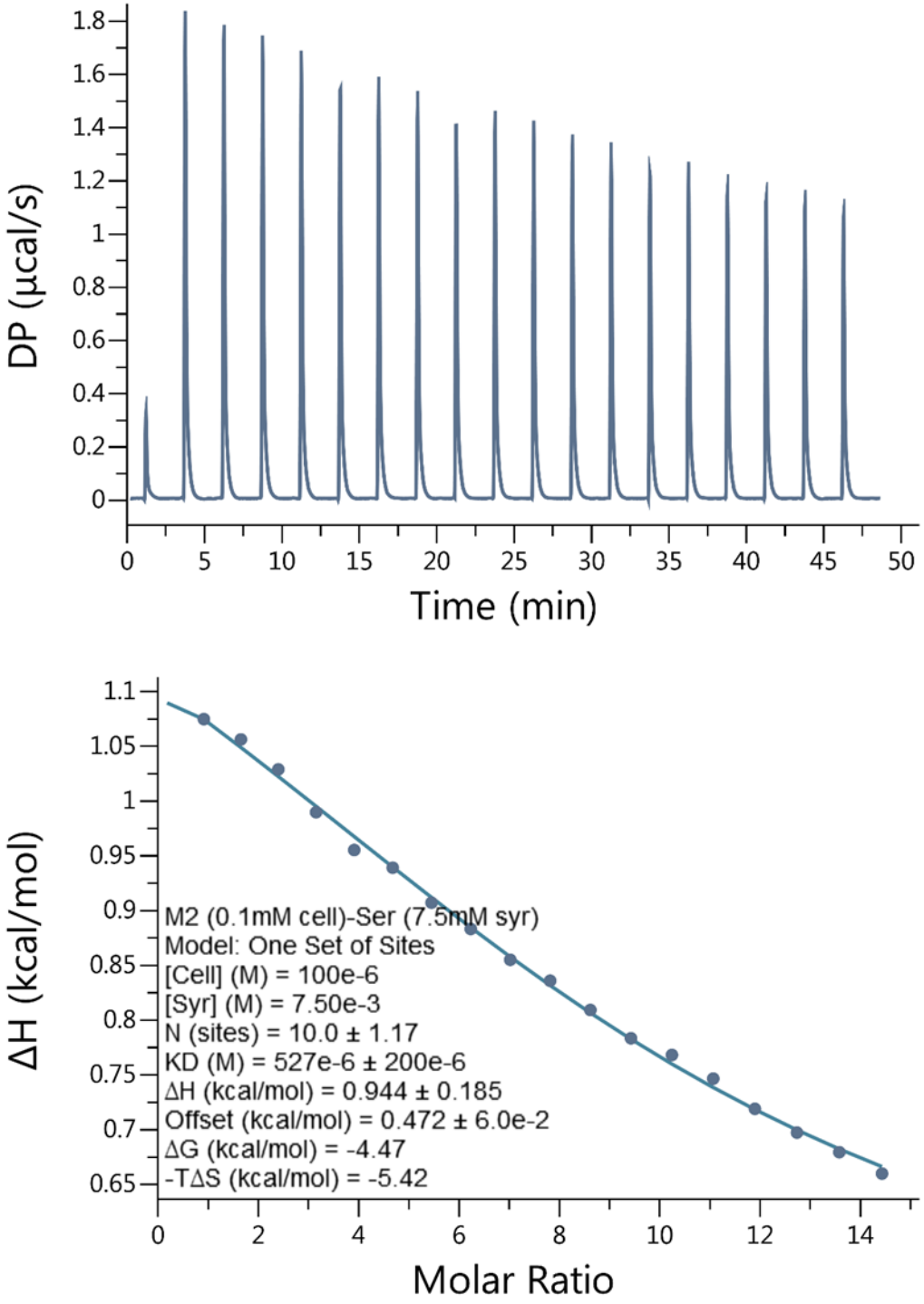

Figure II-S2. Isothermal Titration Calorimetry (ITC) curve obtained when a solution of Motor 2 (100 µM) in the cell was titrated with Serine amide (7.50 mM) in the syringe at 298.0 K in 20 mM sodium phosphate buffered water at pH 7.4. K_a= 1897.5 M^{-1}

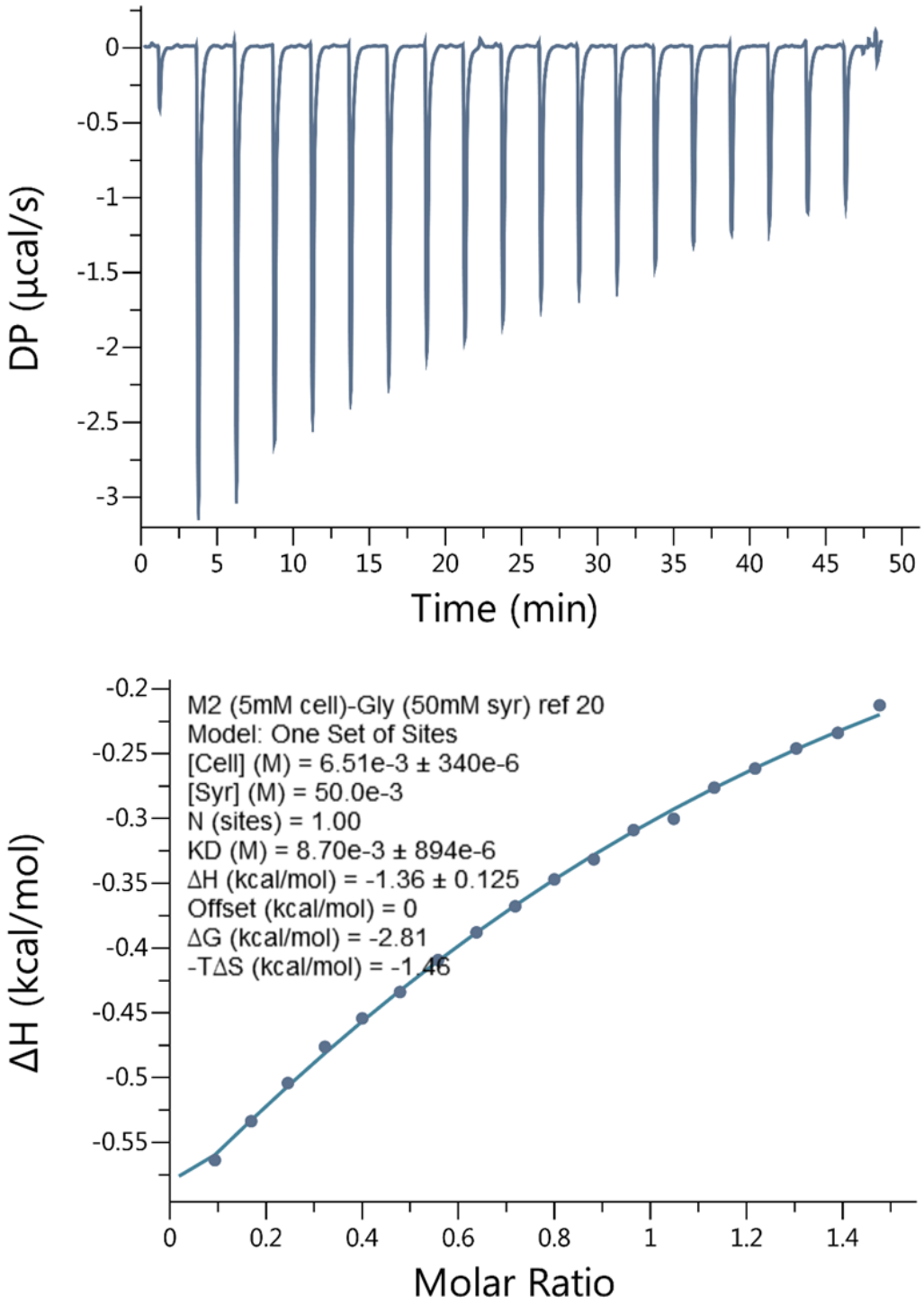

Figure II-S3. Isothermal Titration Calorimetry (ITC) curve obtained when a solution of Motor 2 (5.00 mM) in the cell was titrated with Glycine amide (50.0 mM) in the syringe at 298.0 K in 20 mM sodium phosphate buffered water at pH 7.4. K_a= 115.0 M^{-1}

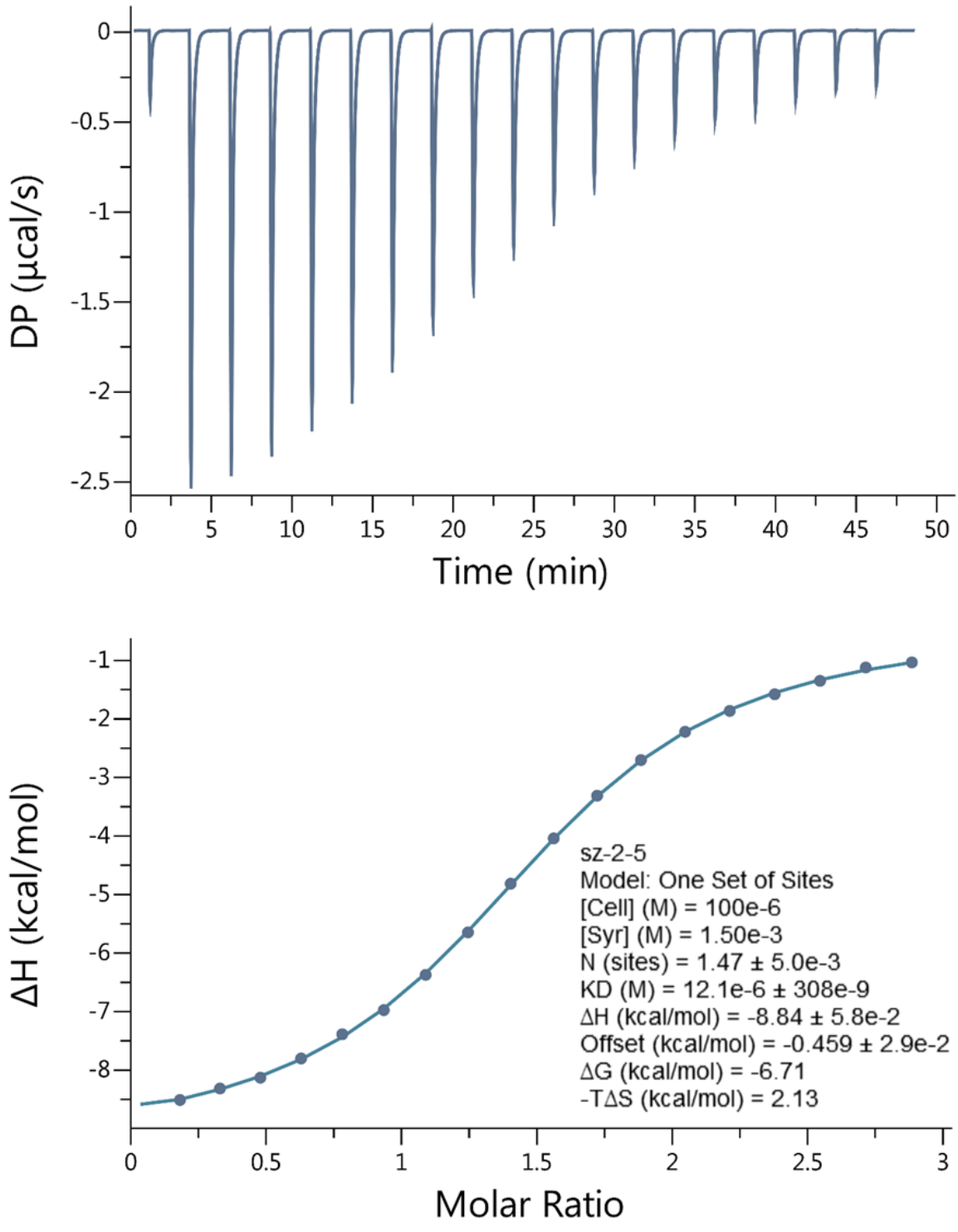

Figure II-S4. Isothermal Titration Calorimetry (ITC) curve obtained when a solution of Motor 2 (100 µM) in the cell was titrated with Arginine amide (1.50 mM) in the syringe at 298.0 K in 20 mM sodium phosphate buffered water at pH 7.4. $K_a = 8.26 \times 10^4\ M^{-1}$

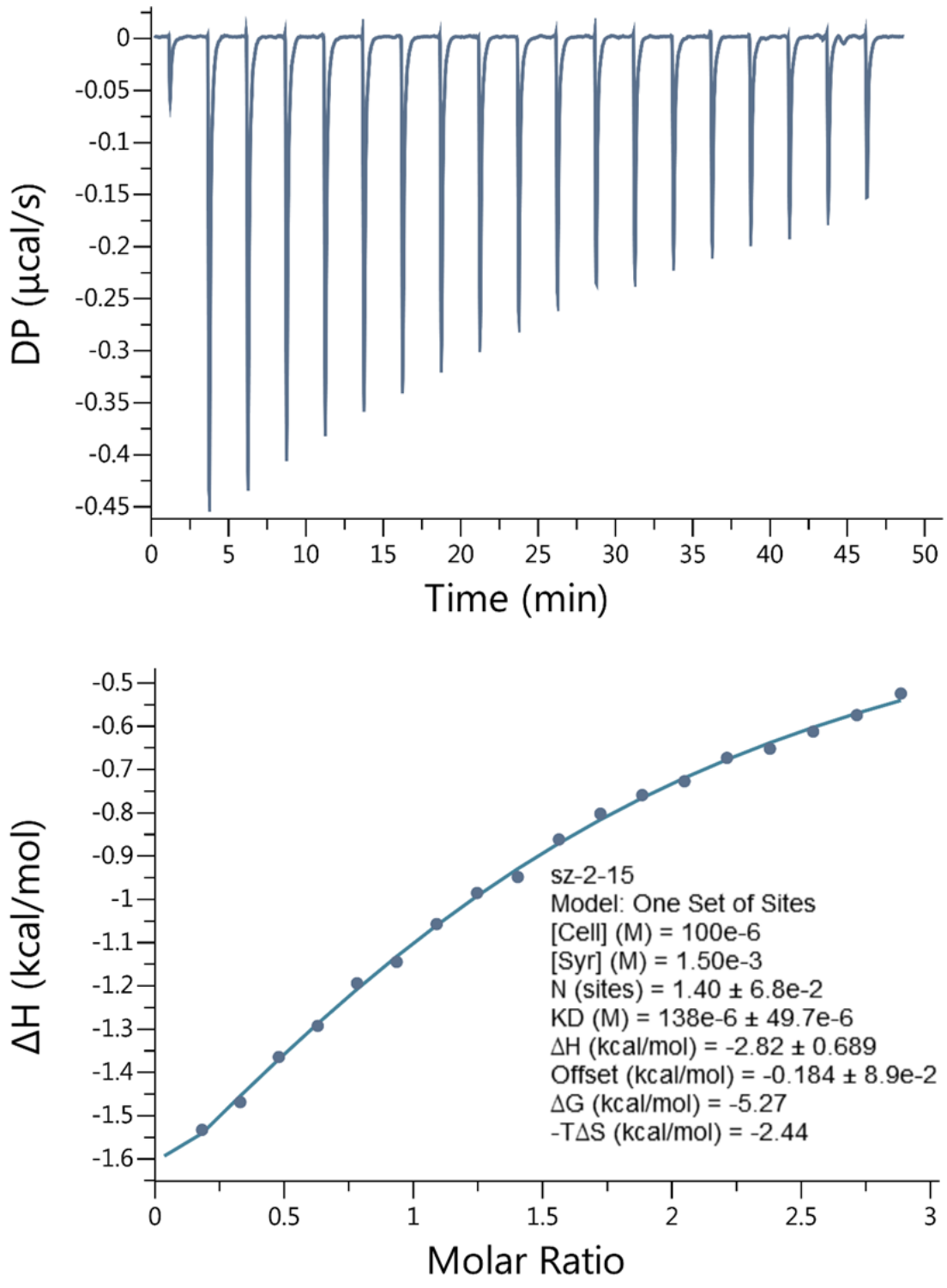

Figure II-S5. Isothermal Titration Calorimetry (ITC) curve obtained when a solution of Motor 2 (100 µM) in the cell was titrated with Glutamine amide (1.50 mM) in the syringe at 298.0 K in 20 mM sodium phosphate buffered water at pH 7.4. $K_a = 7.25 \times 10^3\ M^{-1}$

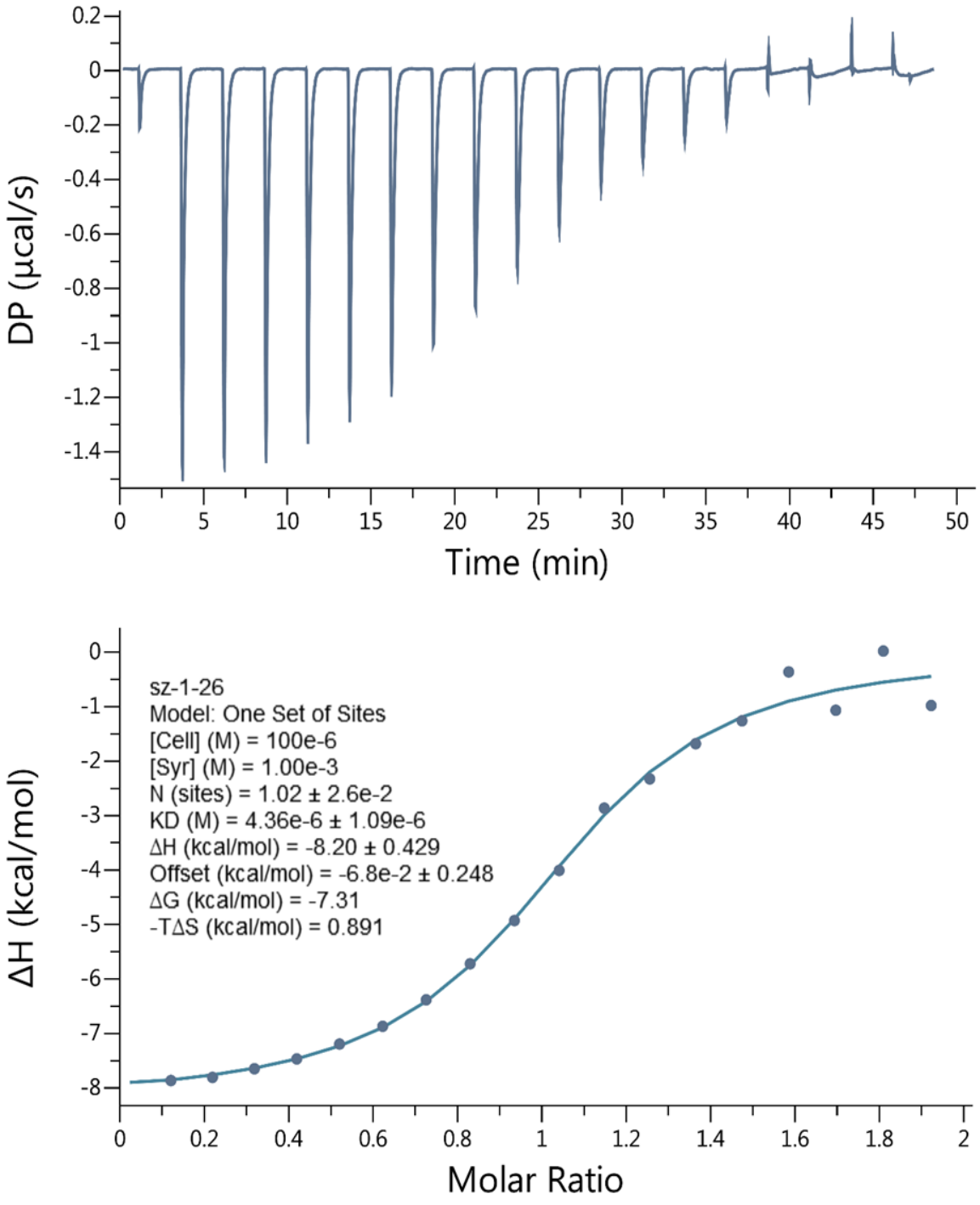

Figure II-S6. Isothermal Titration Calorimetry (ITC) curve obtained when a solution of Motor 2 (100 µM) in the cell was titrated with Leucine amide (1.00 mM) in the syringe at 298.0 K in 20 mM sodium phosphate buffered water at pH 7.4. $K_a = 2.29 \times 10^5\ M^{-1}$

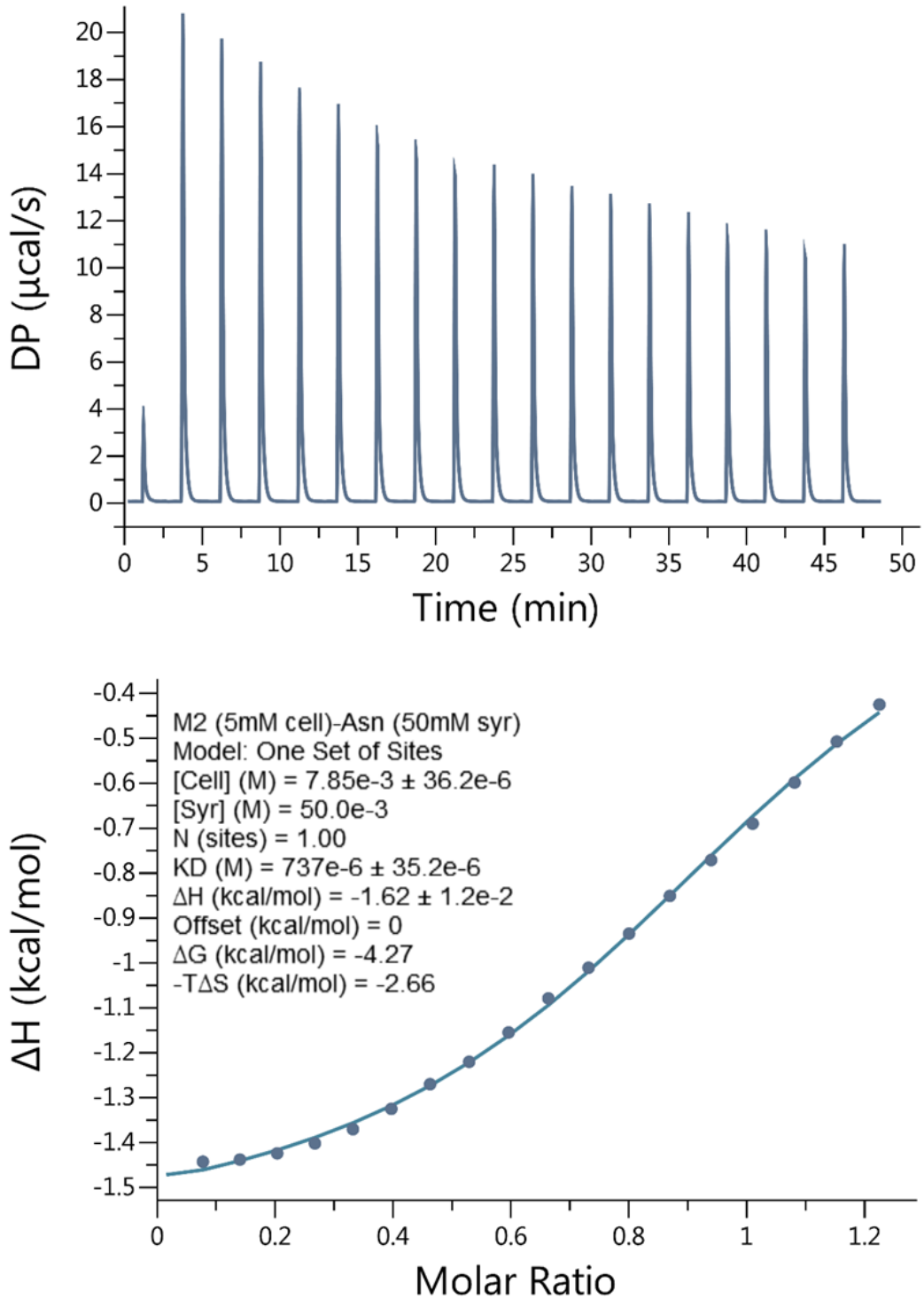

Figure II-S7. Isothermal Titration Calorimetry (ITC) curve obtained when a solution of Motor 2 (5.00 mM) in the cell was titrated with Asparagine amide (50.0 mM) in the syringe at 298.0 K in 20 mM sodium phosphate buffered water at pH 7.4. $K_a = 1.35 \times 10^3\ M^{-1}$

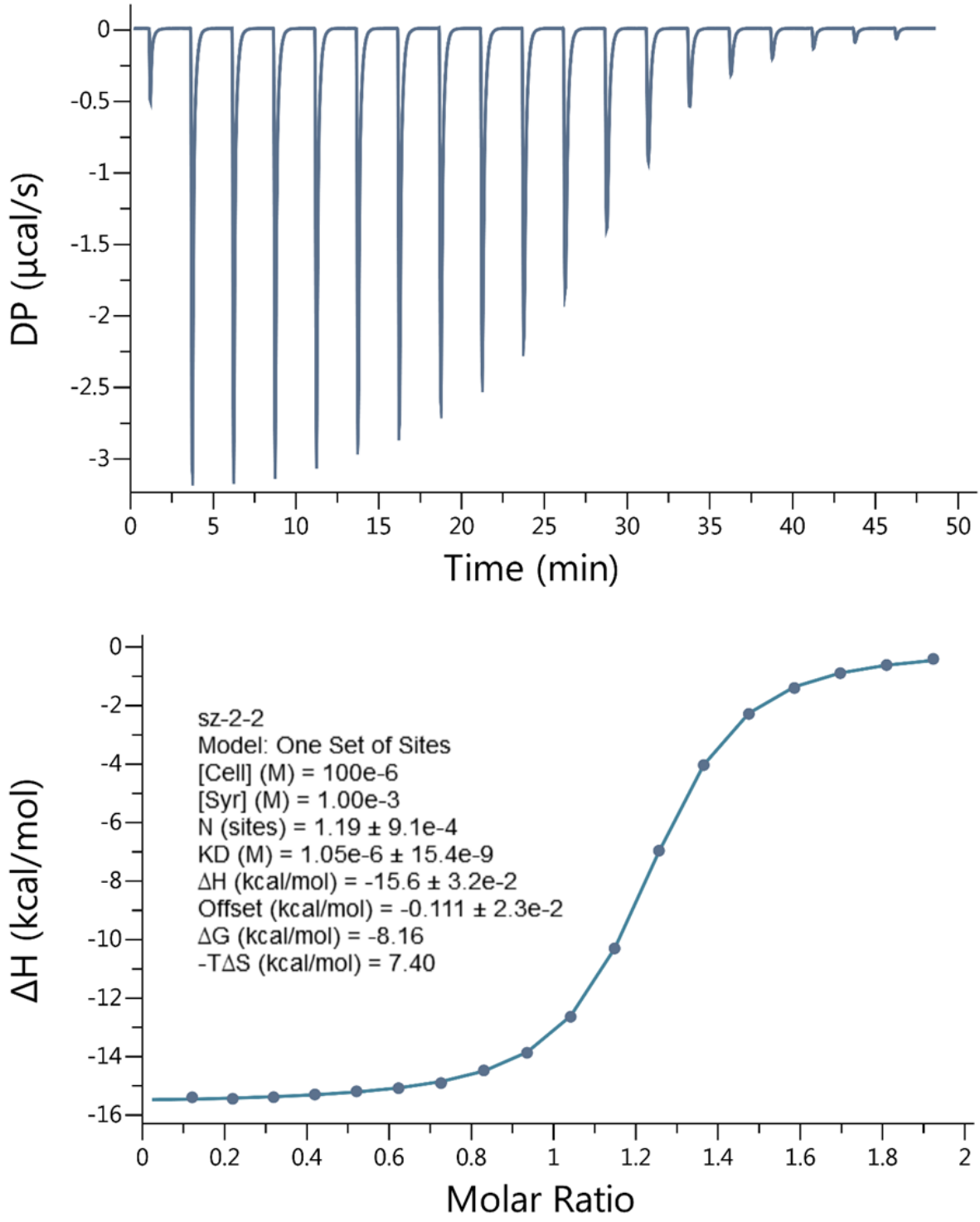

Figure II-S8. Isothermal Titration Calorimetry (ITC) curve obtained when a solution of Motor 2 (100 µM) in the cell was titrated with Tyrosine amide (1.00 mM) in the syringe at 298.0 K in 20 mM sodium phosphate buffered water at pH 7.4. $K_a = 9.52 \times 10^5\ M^{-1}$

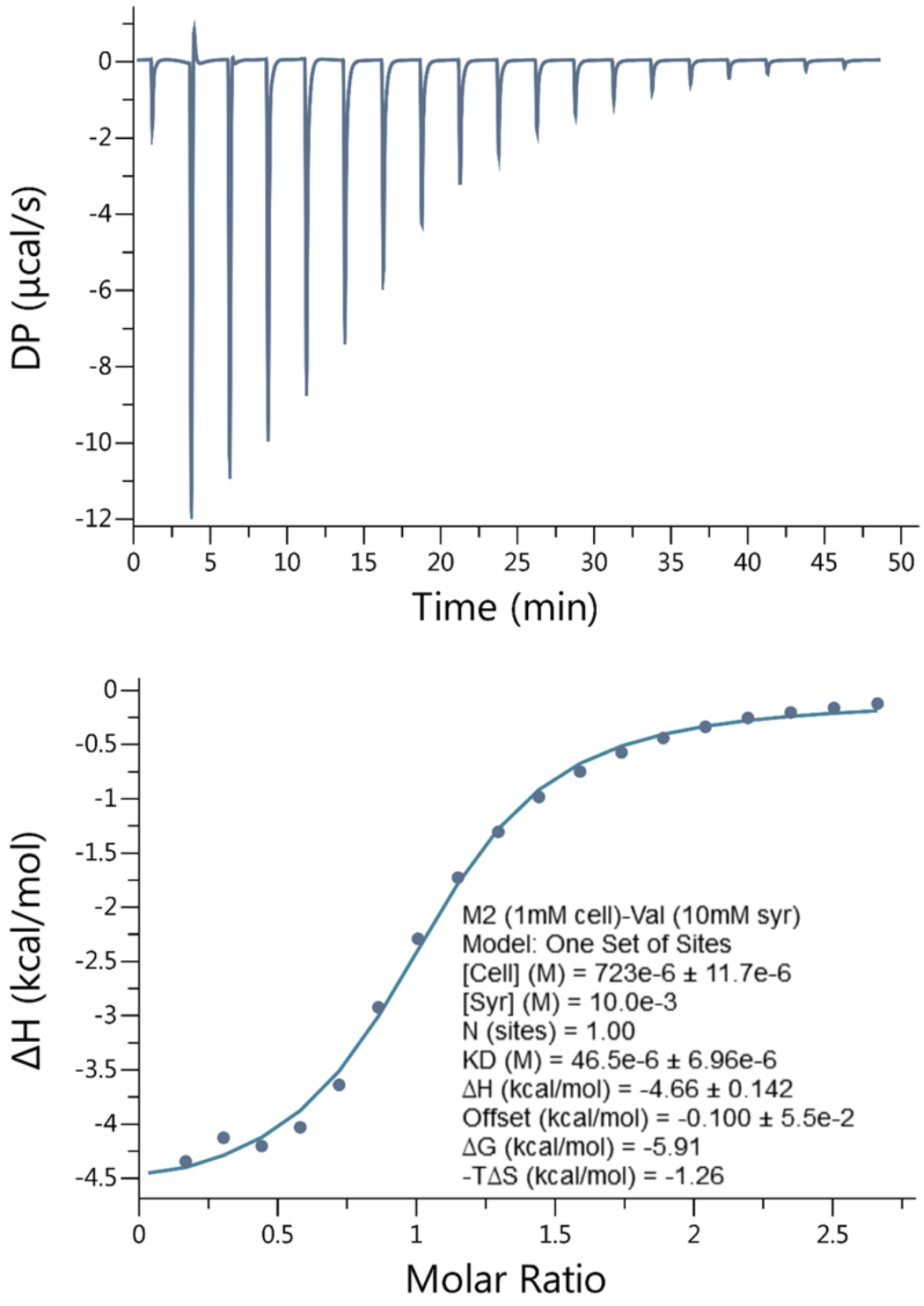

Figure II-S9. Isothermal Titration Calorimetry (ITC) curve obtained when a solution of Motor 2 (1.00 mM) in the cell was titrated with Valine amide (10.0 mM) in the syringe at 298.0 K in 20 mM sodium phosphate buffered water at pH 7.4. $K_a = 2.15 \times 10^4\ M^{-1}$

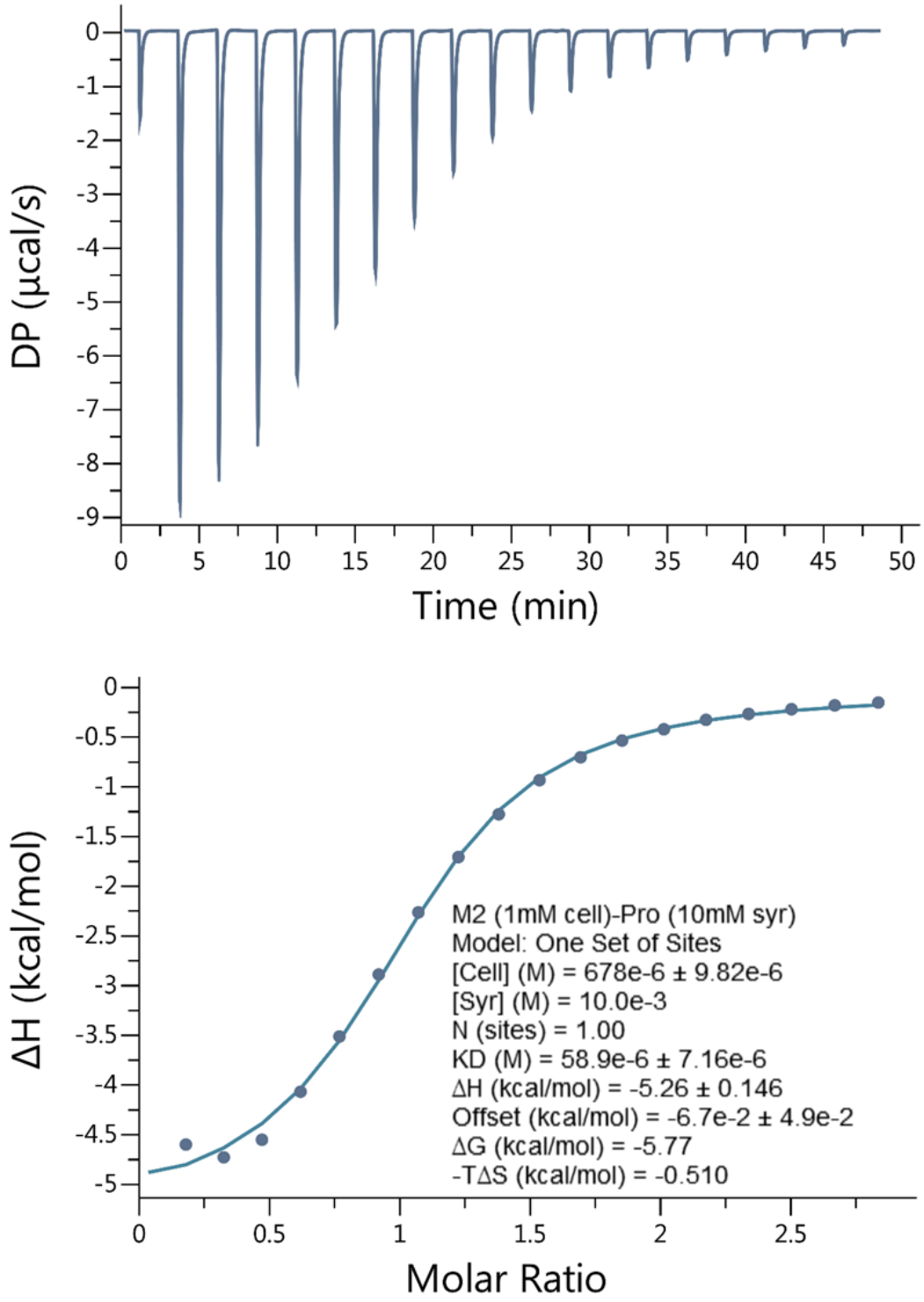

Figure II-S10. Isothermal Titration Calorimetry (ITC) curve obtained when a solution of Motor 2 (1.00 mM) in the cell was titrated with Proline amide (10.0 mM) in the syringe at 298.0 K in 20 mM sodium phosphate buffered water at pH 7.4. K_a= 1.70×10^4 M^{-1}

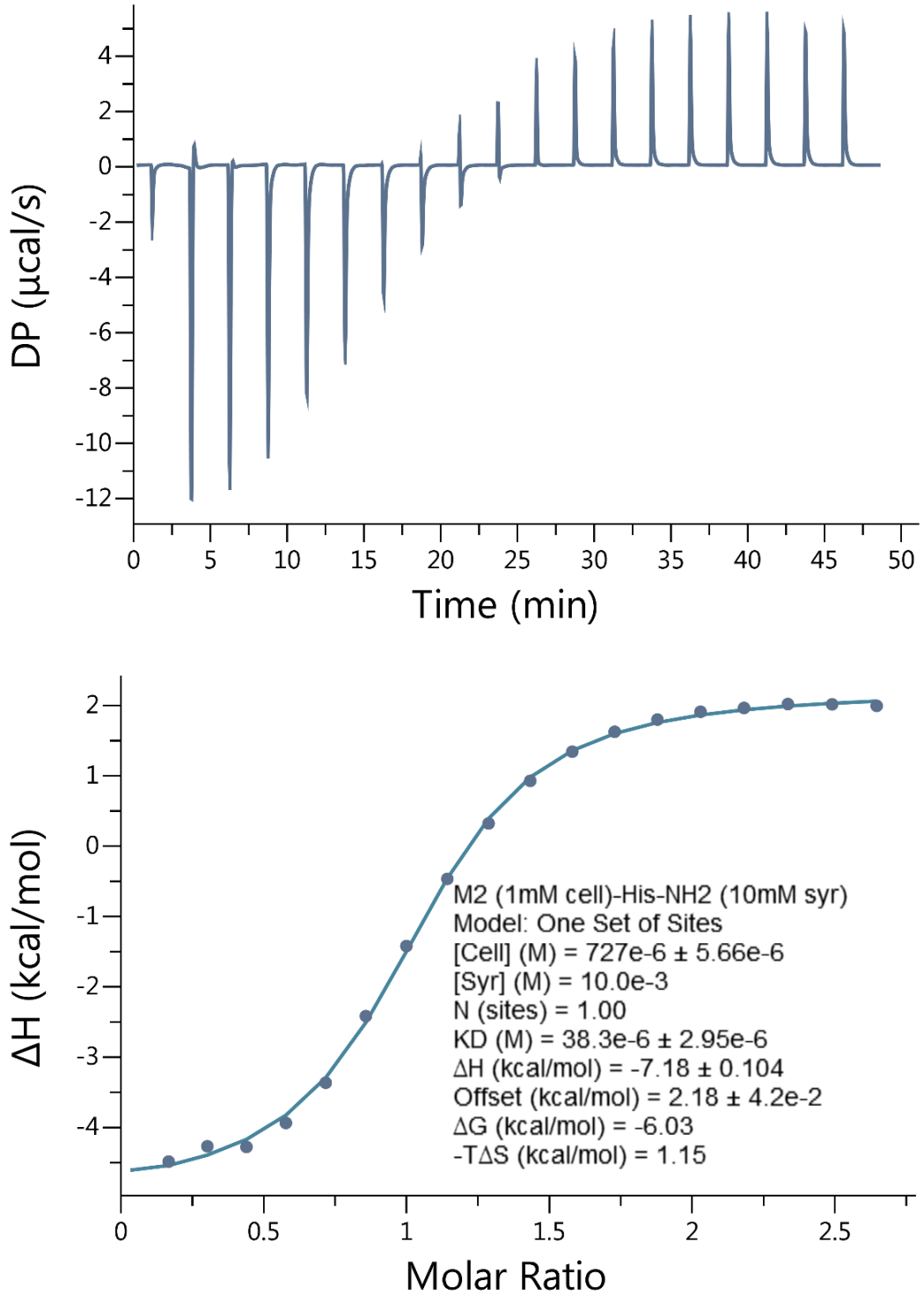

Figure II-S11. Isothermal Titration Calorimetry (ITC) curve obtained when a solution of Motor 2 (1.00 mM) in the cell was titrated with Histidine amide (10.0 mM) in the syringe at 298.0 K in 20 mM sodium phosphate buffered water at pH 7.4. $K_a = 2.61 \times 10^4\ M^{-1}$

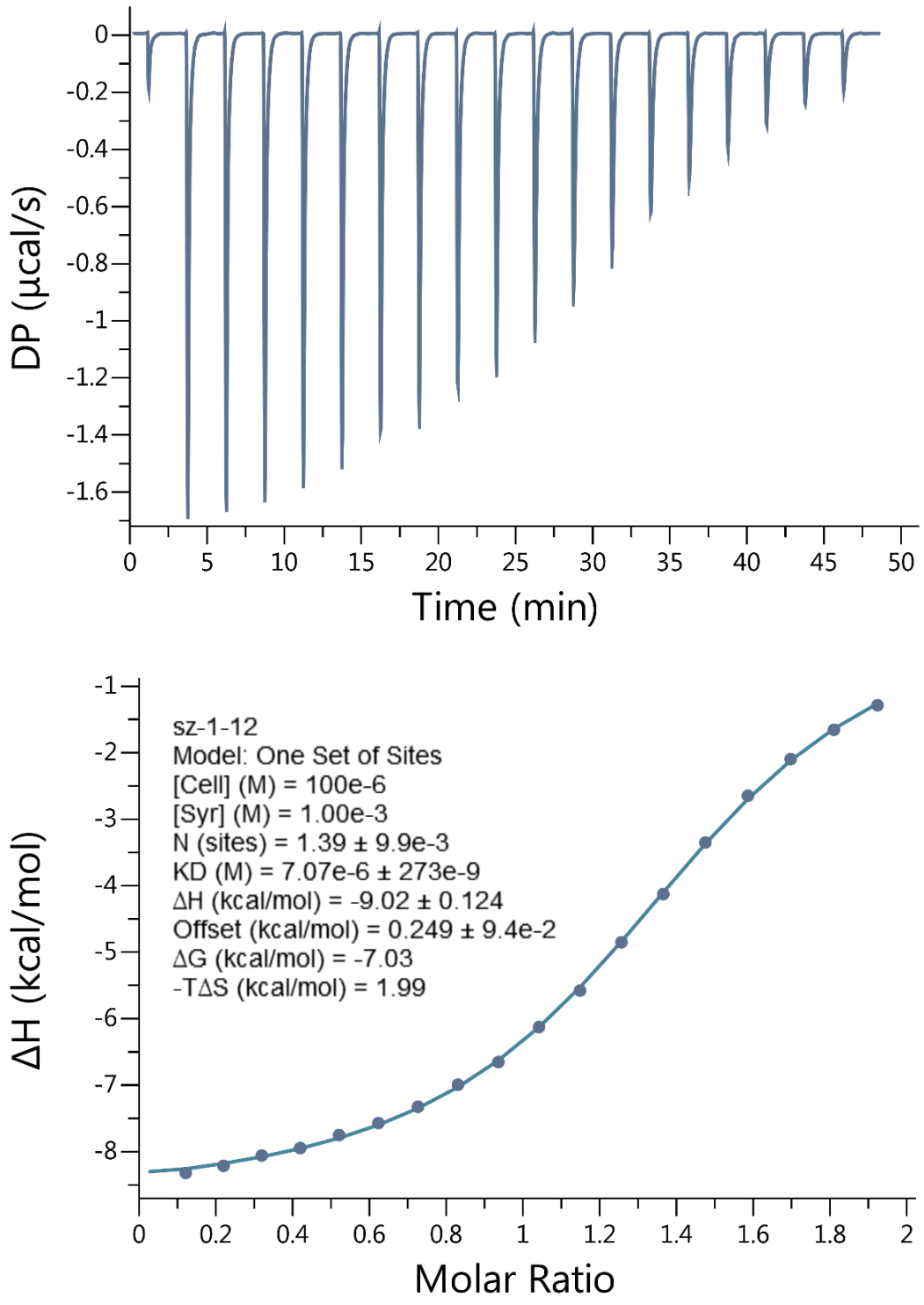

Figure II-S12. Isothermal Titration Calorimetry (ITC) curve obtained when a solution of Motor 2 (100 µM) in the cell was titrated with Lysine amide (1.00 mM) in the syringe at 298.0 K in 20 mM sodium phosphate buffered water at pH 7.4. K_a= 1.41×10^5 M^{-1}

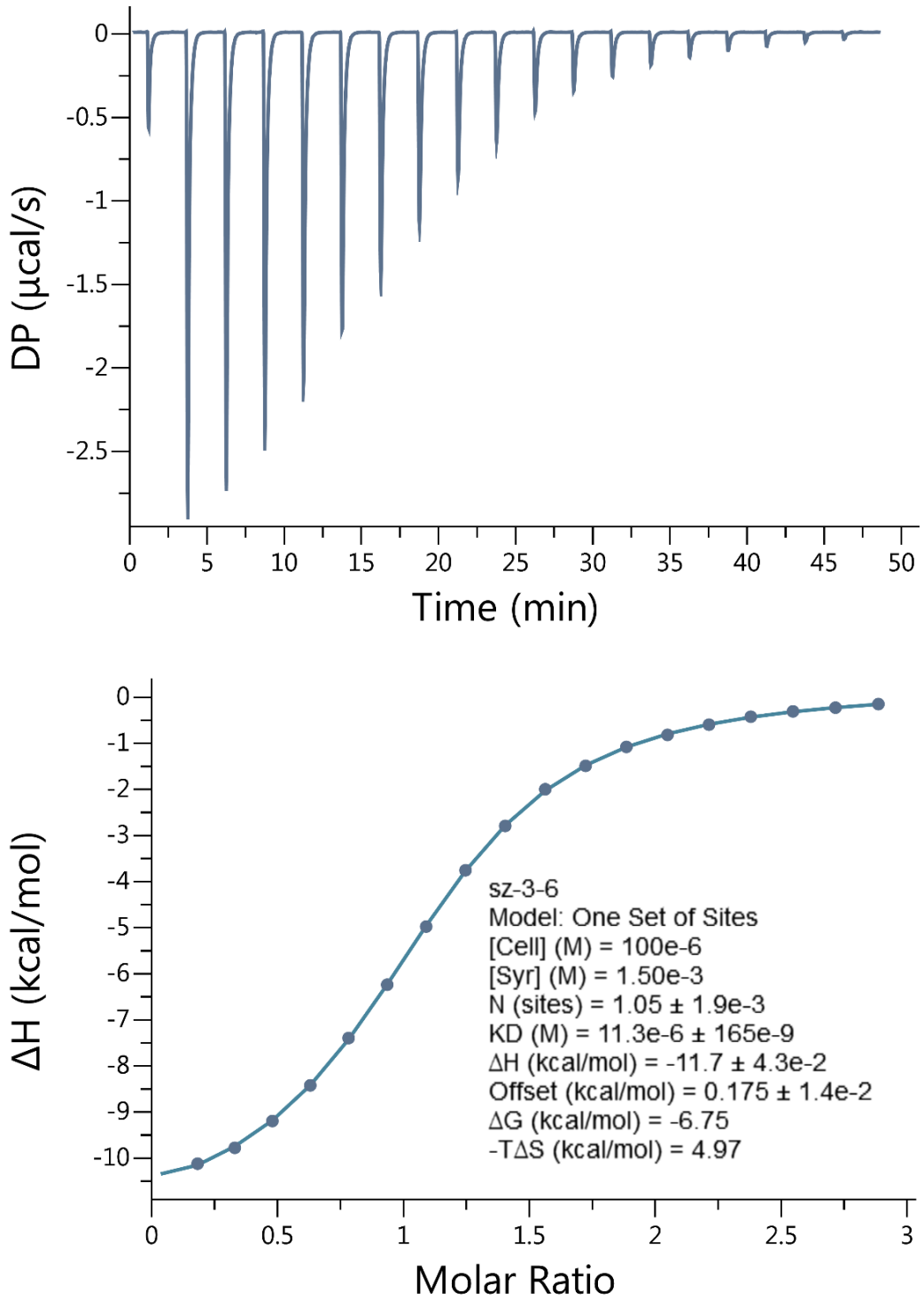

Figure II-S13. Isothermal Titration Calorimetry (ITC) curve obtained when a solution of Motor 2 (100 µM) in the cell was titrated with Methionine amide (1.50 mM) in the syringe at 298.0 K in 20 mM sodium phosphate buffered water at pH 7.4. $K_a = 8.85 \times 10^4\ M^{-1}$

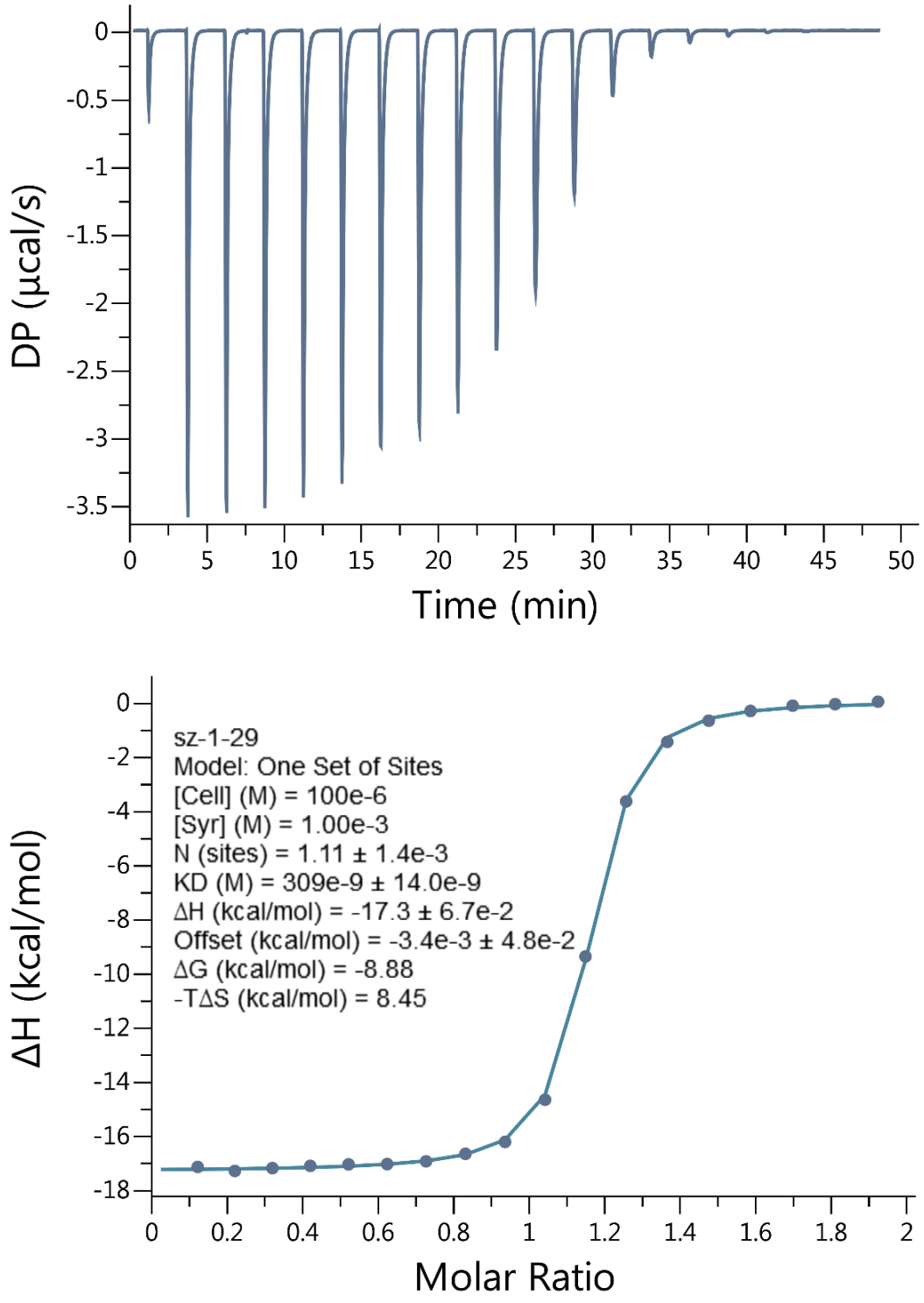

Figure II-S14. Isothermal Titration Calorimetry (ITC) curve obtained when a solution of Motor 2 (100 µM) in the cell was titrated with Phenylalanine amide (1.00 mM) in the syringe at 298.0 K in 20 mM sodium phosphate buffered water at pH 7.4. $K_a = 3.24 \times 10^6\ M^{-1}$

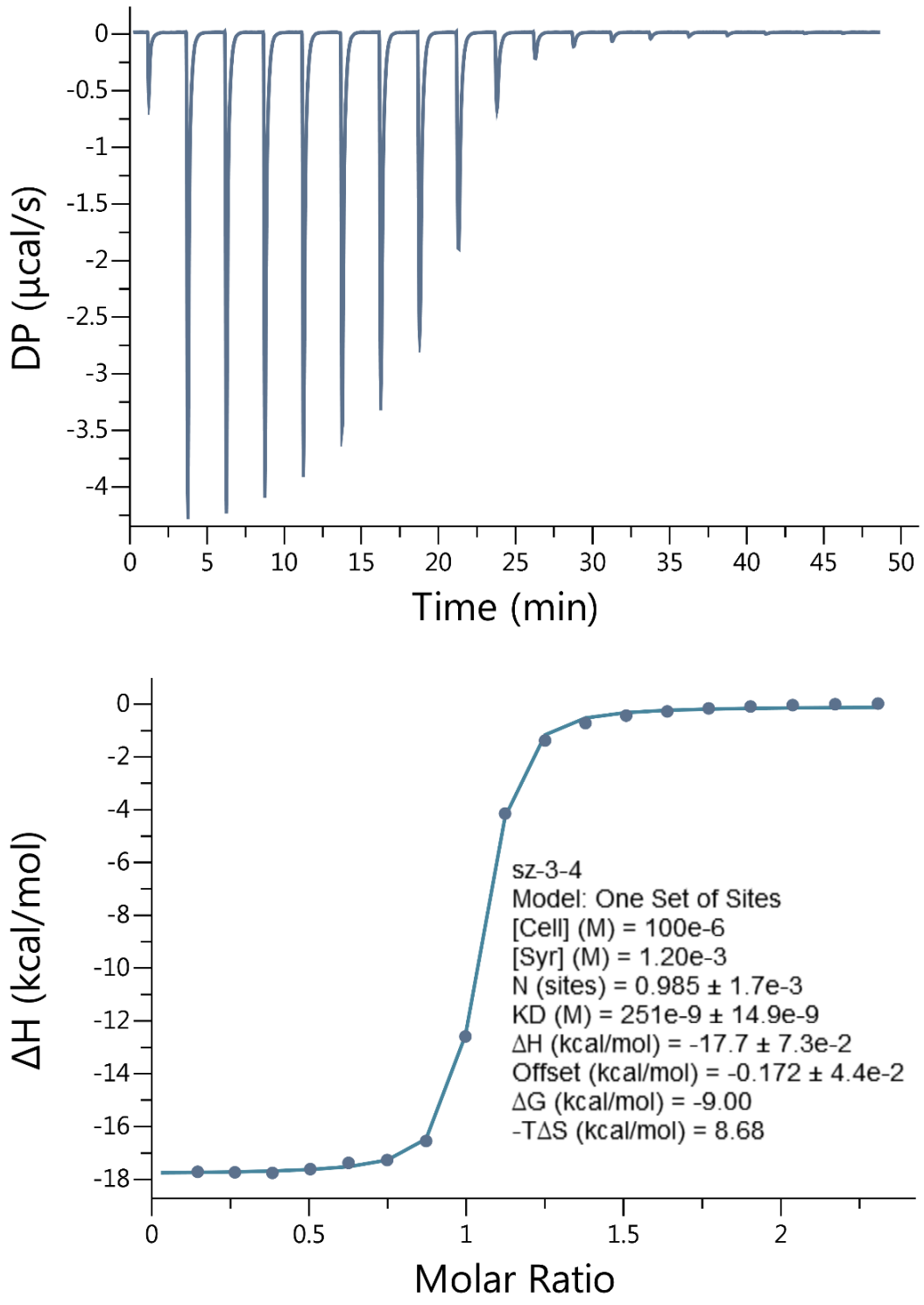

Figure II-S15. Isothermal Titration Calorimetry (ITC) curve obtained when a solution of Motor 2 (100 µM) in the cell was titrated with Tryptophan amide (1.20 mM) in the syringe at 298.0 K in 20 mM sodium phosphate buffered water at pH 7.4. $K_a = 3.98 \times 10^6\ M^{-1}$

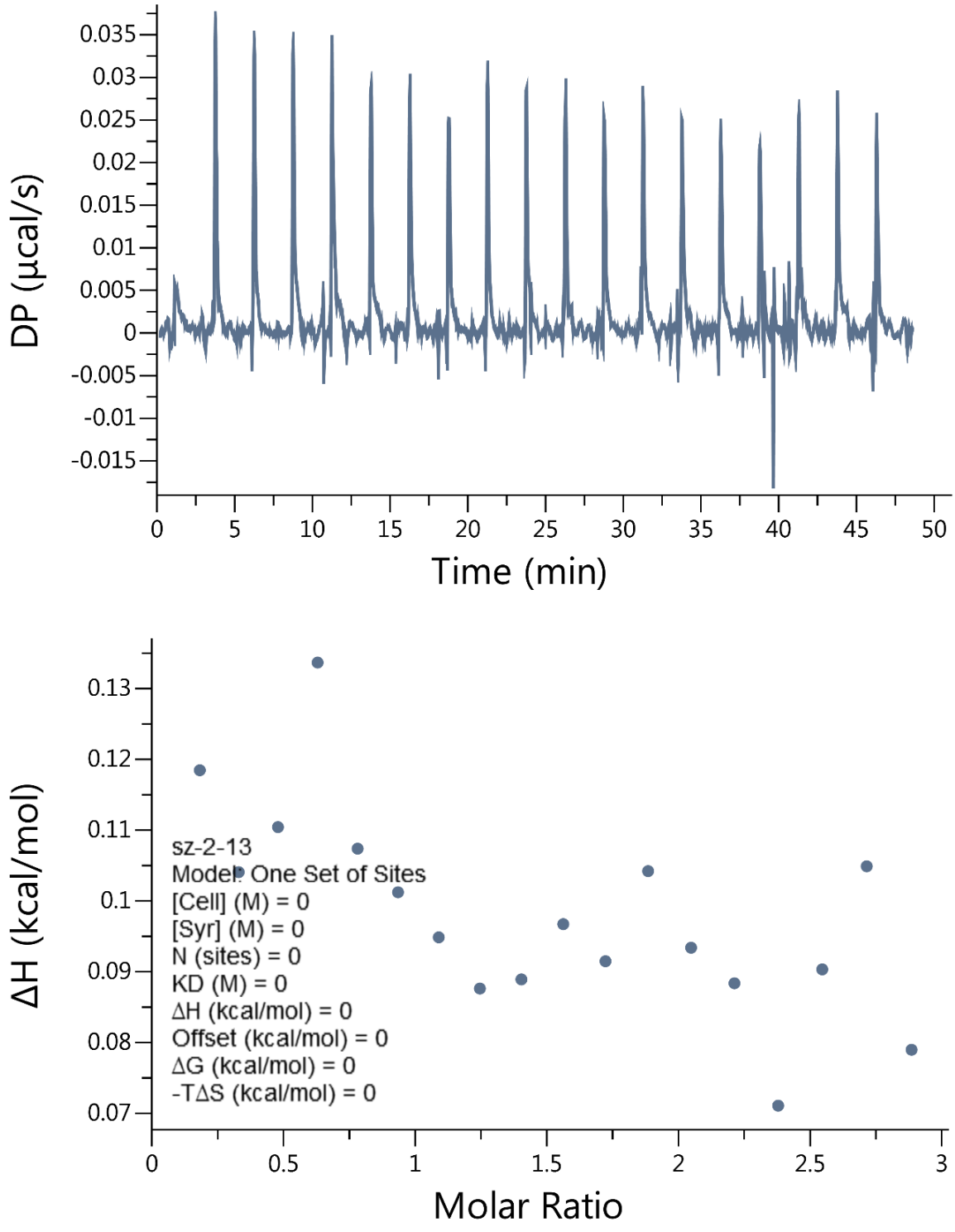

Figure II-S16. Isothermal Titration Calorimetry (ITC) curve obtained when a solution of Motor 2 (100 µM) in the cell was titrated with Aspartic acid amide (1.50 mM) in the syringe at 298.0 K in 20 mM sodium phosphate buffered water at pH 7.4. K_a= No binding

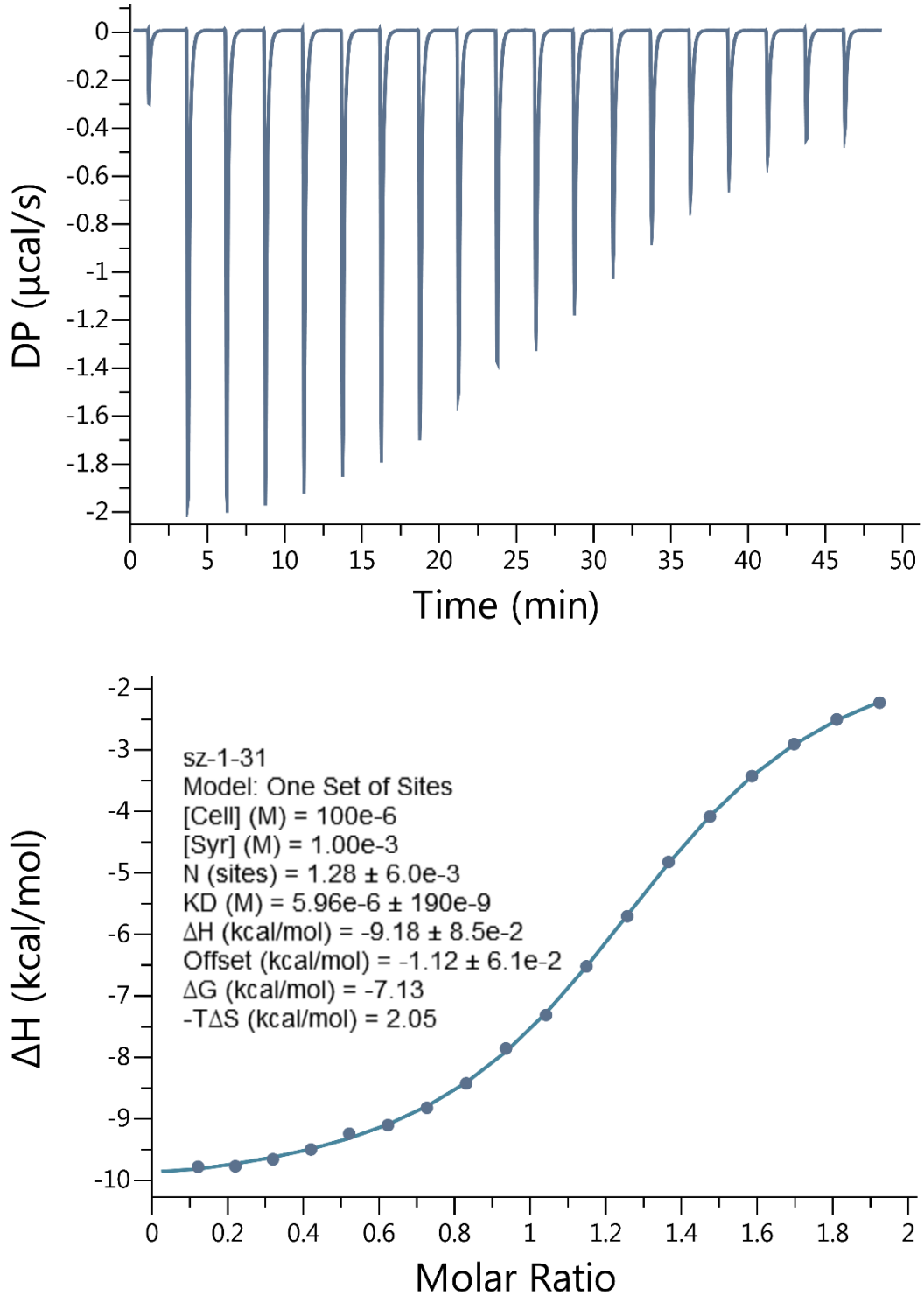

Figure II-S17. Isothermal Titration Calorimetry (ITC) curve obtained when a solution of Motor 2 (100 µM) in the cell was titrated with Isoleucine amide (1.00 mM) in the syringe at 298.0 K in 20 mM sodium phosphate buffered water at pH 7.4. $K_a = 1.68 \times 10^5\ M^{-1}$

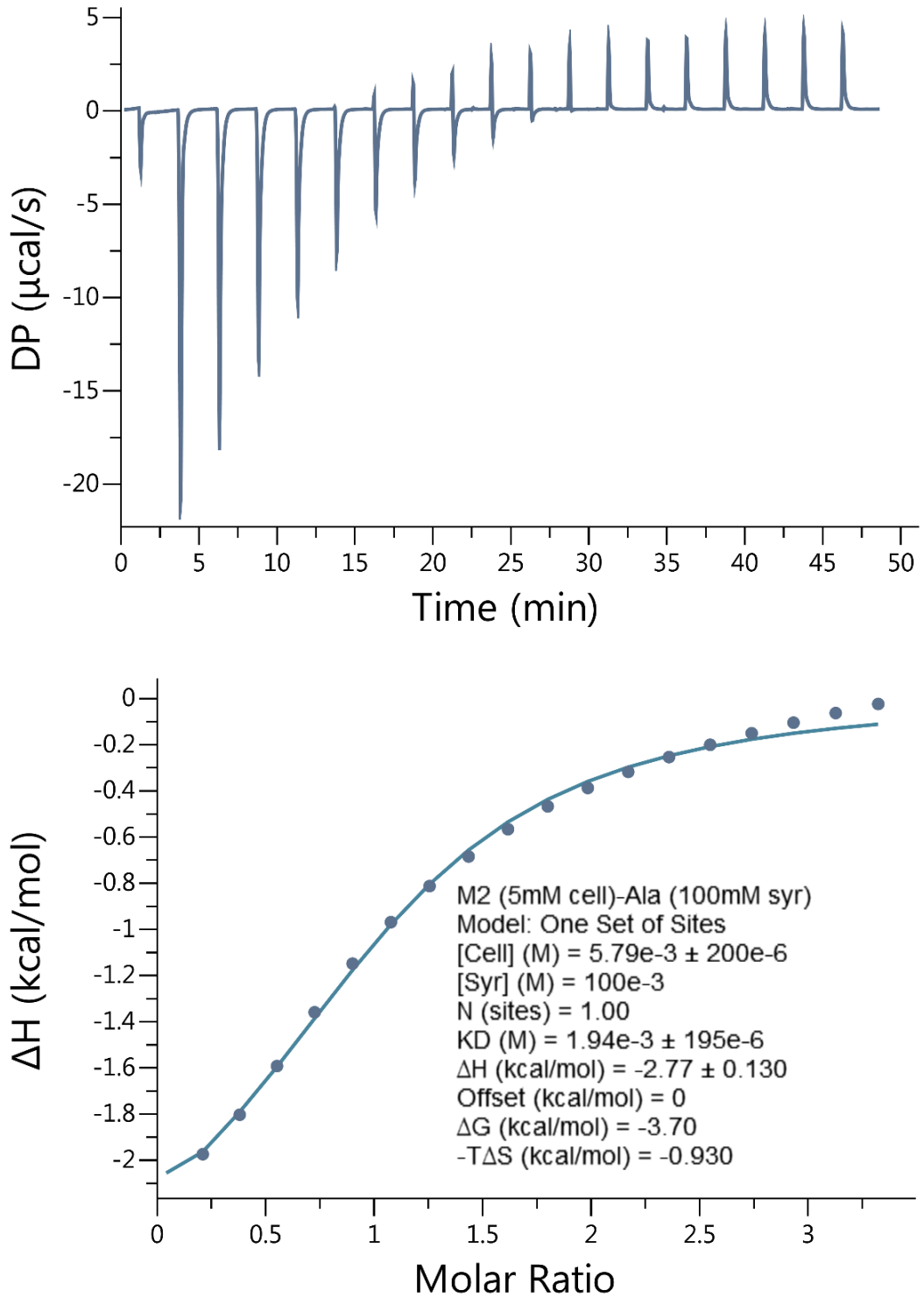

Figure II-S18. Isothermal Titration Calorimetry (ITC) curve obtained when a solution of Motor 2 (5.00 mM) in the cell was titrated with Alanine amide (1.00×10^2 mM) in the syringe at 298.0 K in 20 mM sodium phosphate buffered water at pH 7.4. K_a= 515 M^{-1}

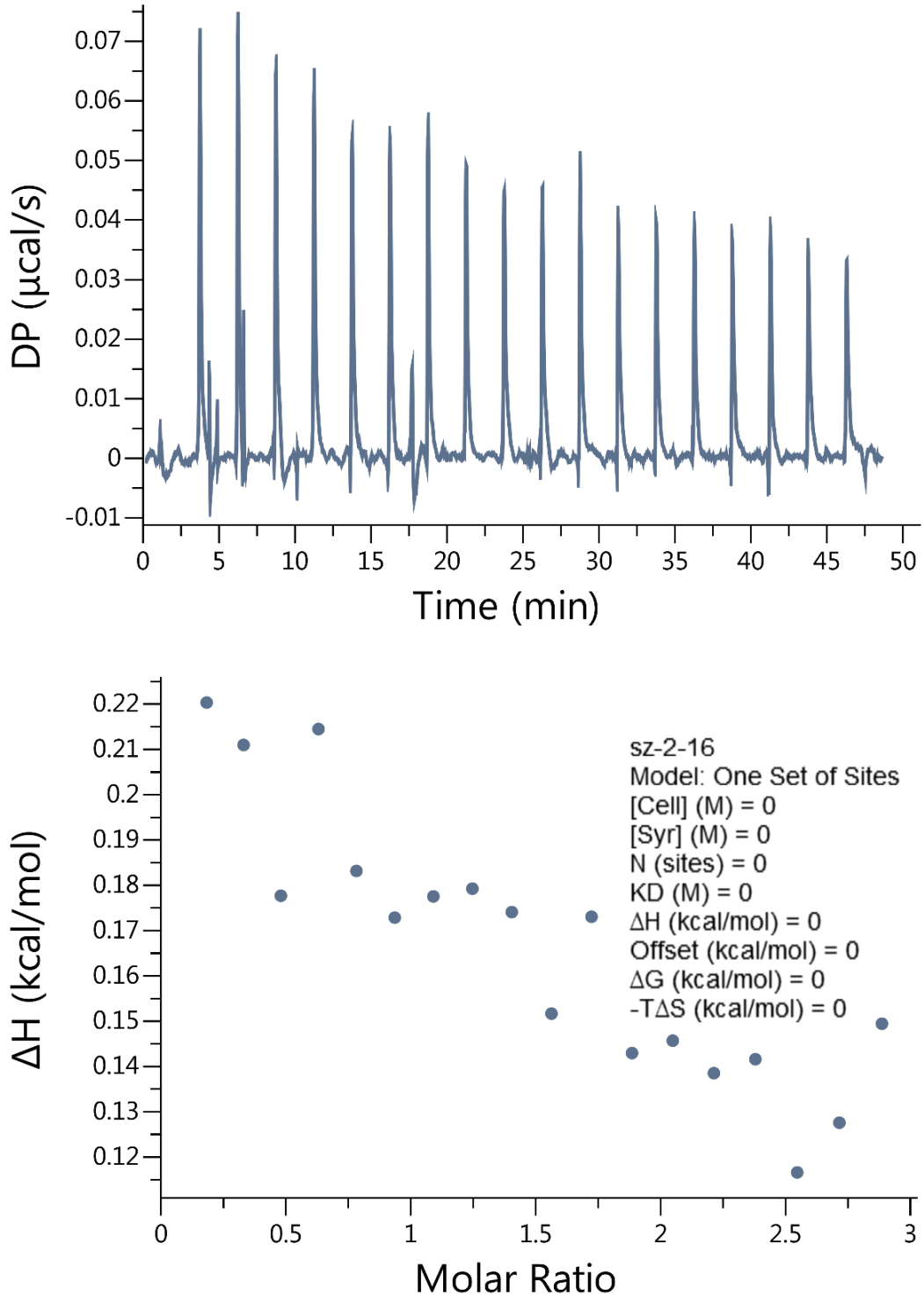

Figure II-S19. Isothermal Titration Calorimetry (ITC) curve obtained when a solution of Motor 2 (100 µM) in the cell was titrated with Glutamic amide (1.50 mM) in the syringe at 298.0 K in 20 mM sodium phosphate buffered water at pH 7.4. K_a= No binding

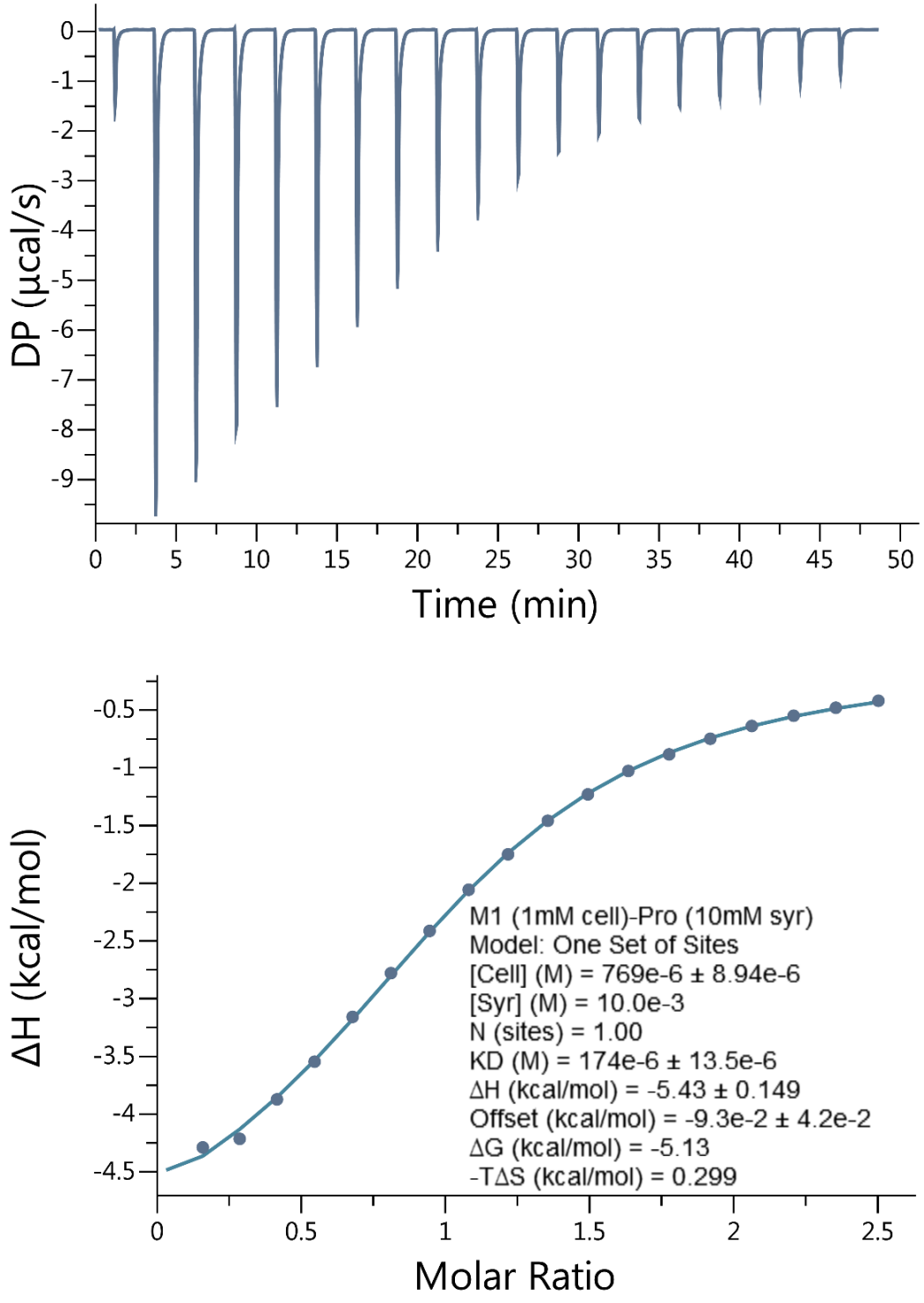

Figure II-S20. Isothermal Titration Calorimetry (ITC) curve obtained when a solution of Motor 1 (1.00 mM) in the cell was titrated with Proline amide (10.0 mM) in the syringe at 298.0 K in 20 mM sodium phosphate buffered water at pH 7.4. $K_a = 5.75 \times 10^3\ M^{-1}$

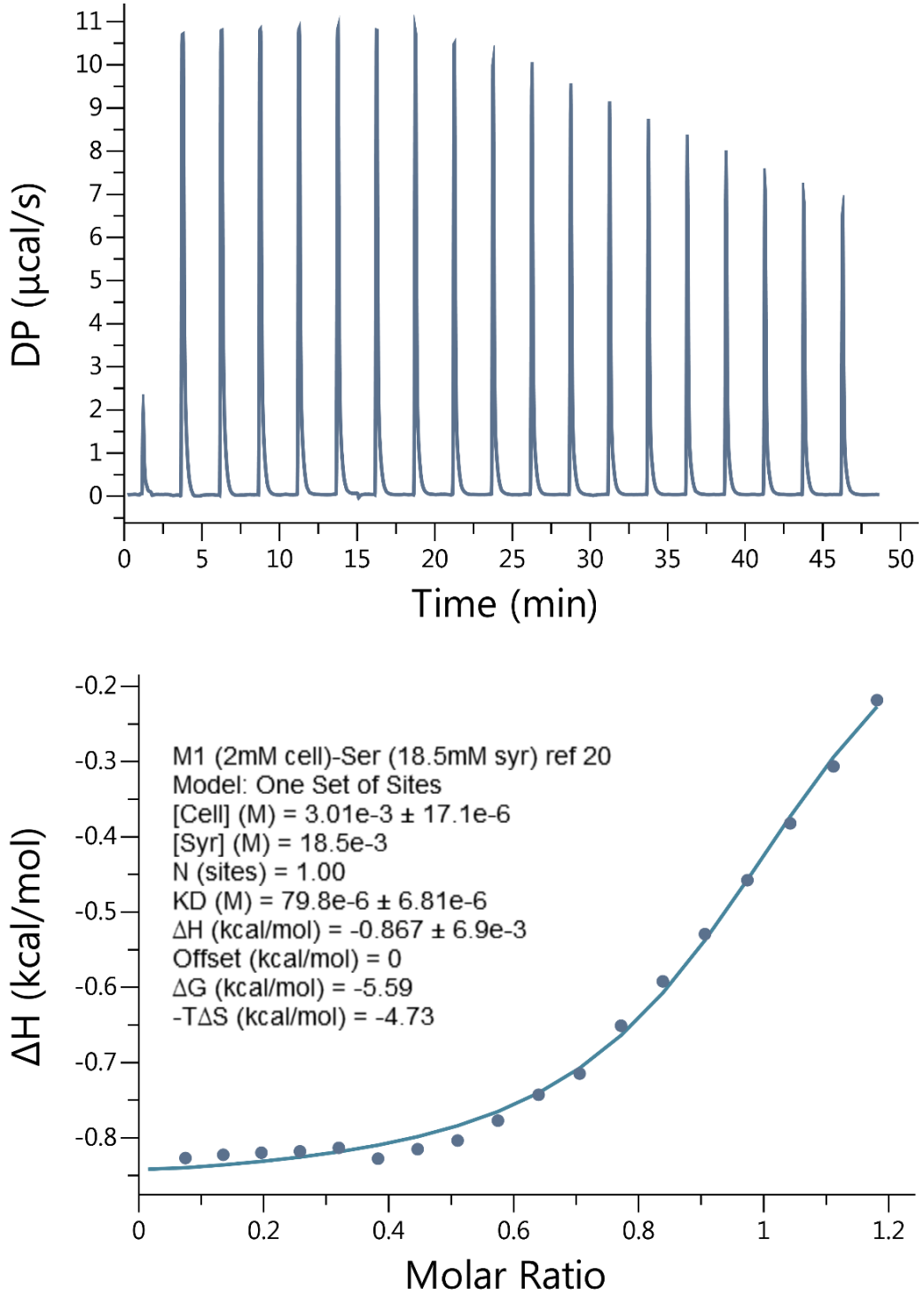

Figure II-S21. Isothermal Titration Calorimetry (ITC) curve obtained when a solution of Motor 1 (2.00 mM) in the cell was titrated with Serine amide (18.5 mM) in the syringe at 298.0 K in 20 mM sodium phosphate buffered water at pH 7.4. K_a= 1.25×10^4 M^{-1}

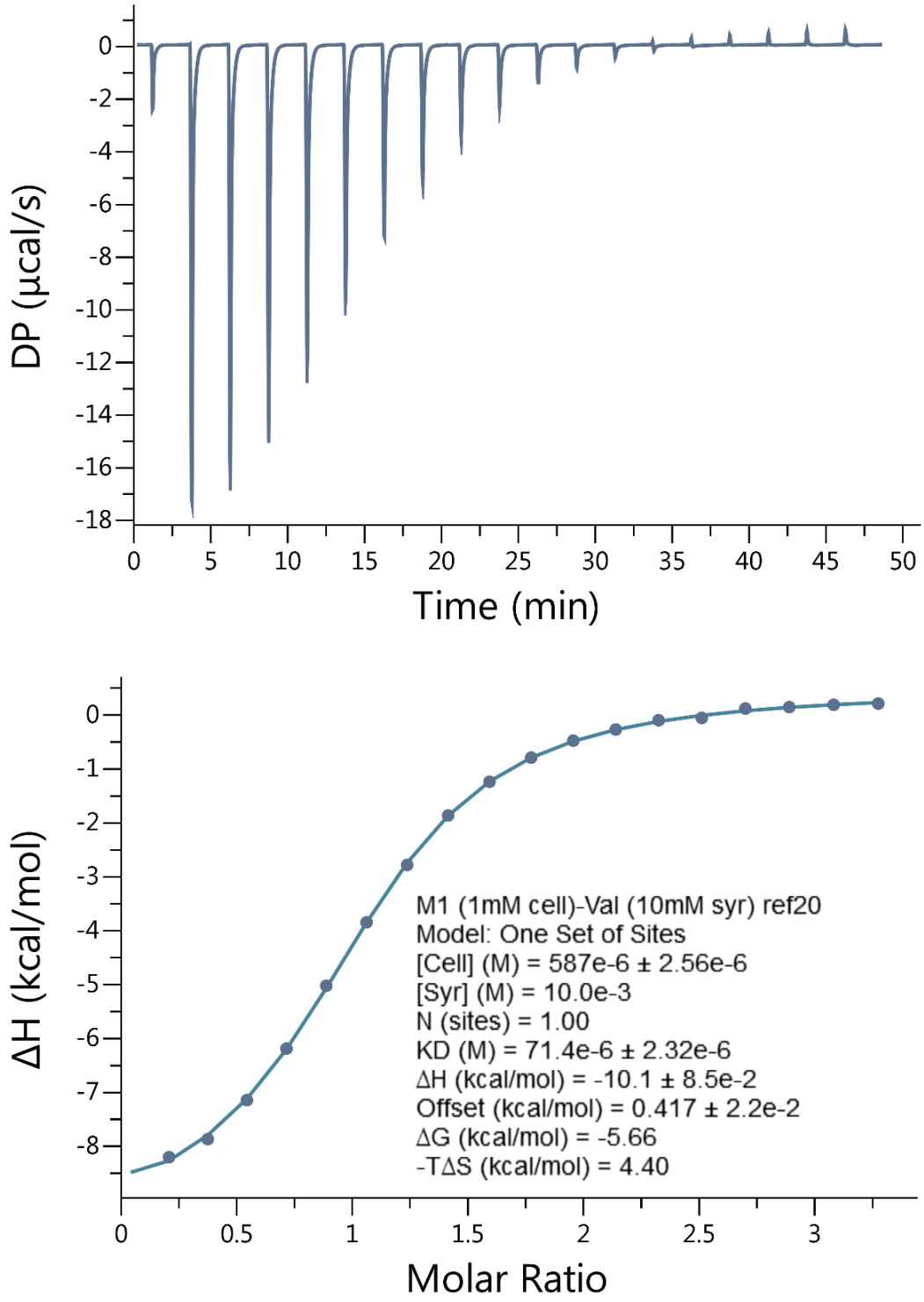

Figure II-S22. Isothermal Titration Calorimetry (ITC) curve obtained when a solution of Motor 1 (1.00 mM) in the cell was titrated with Valine amide (10.0 mM) in the syringe at 298.0 K in 20 mM sodium phosphate buffered water at pH 7.4. K_a= 1.40×10^4 M^{-1}

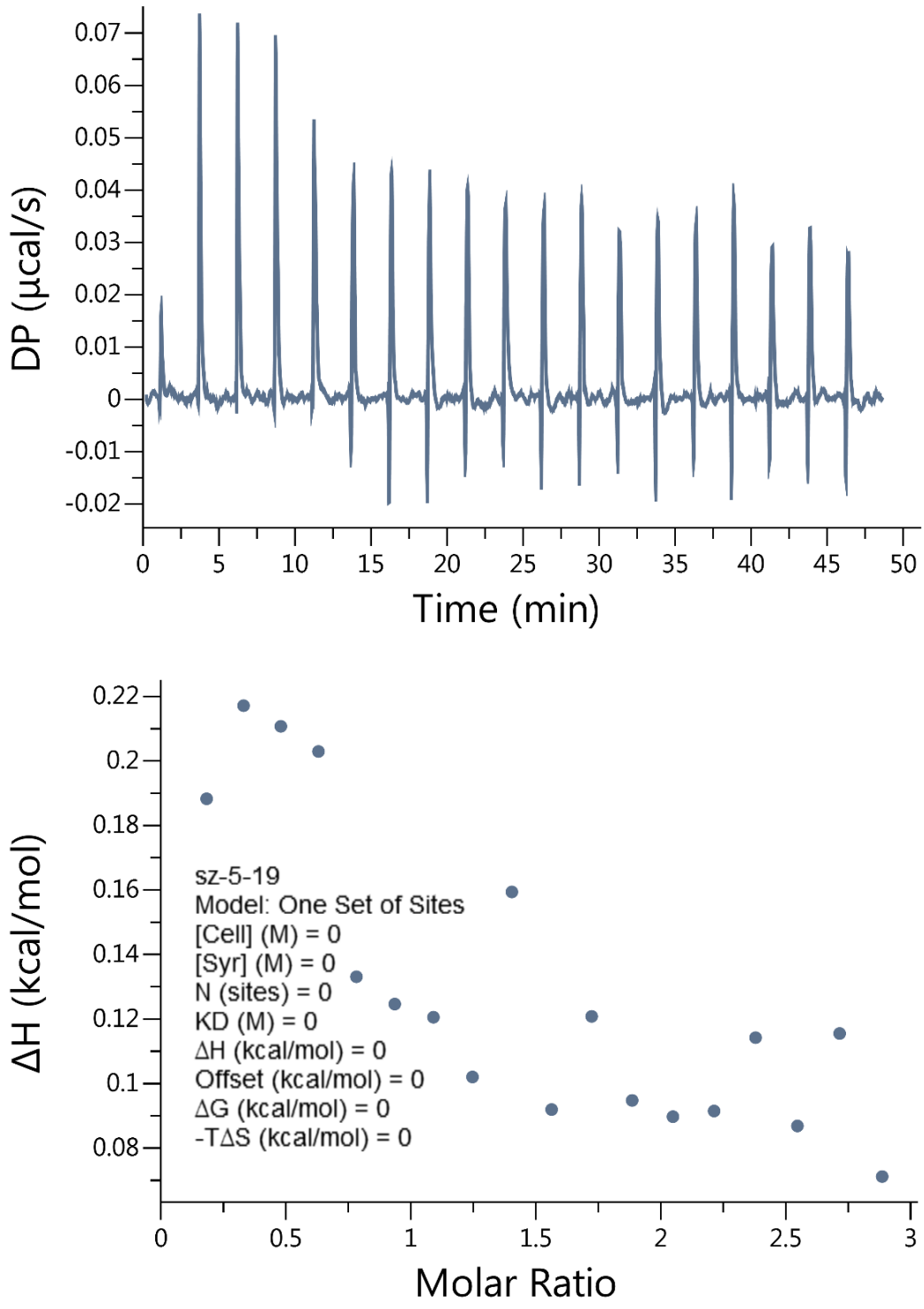

Figure II-S23. Isothermal Titration Calorimetry (ITC) curve obtained when a solution of Motor 1 (100 µM) in the cell was titrated with Glutamic amide (1.50 mM) in the syringe at 298.0 K in 20 mM sodium phosphate buffered water at pH 7.4. K_a= No binding

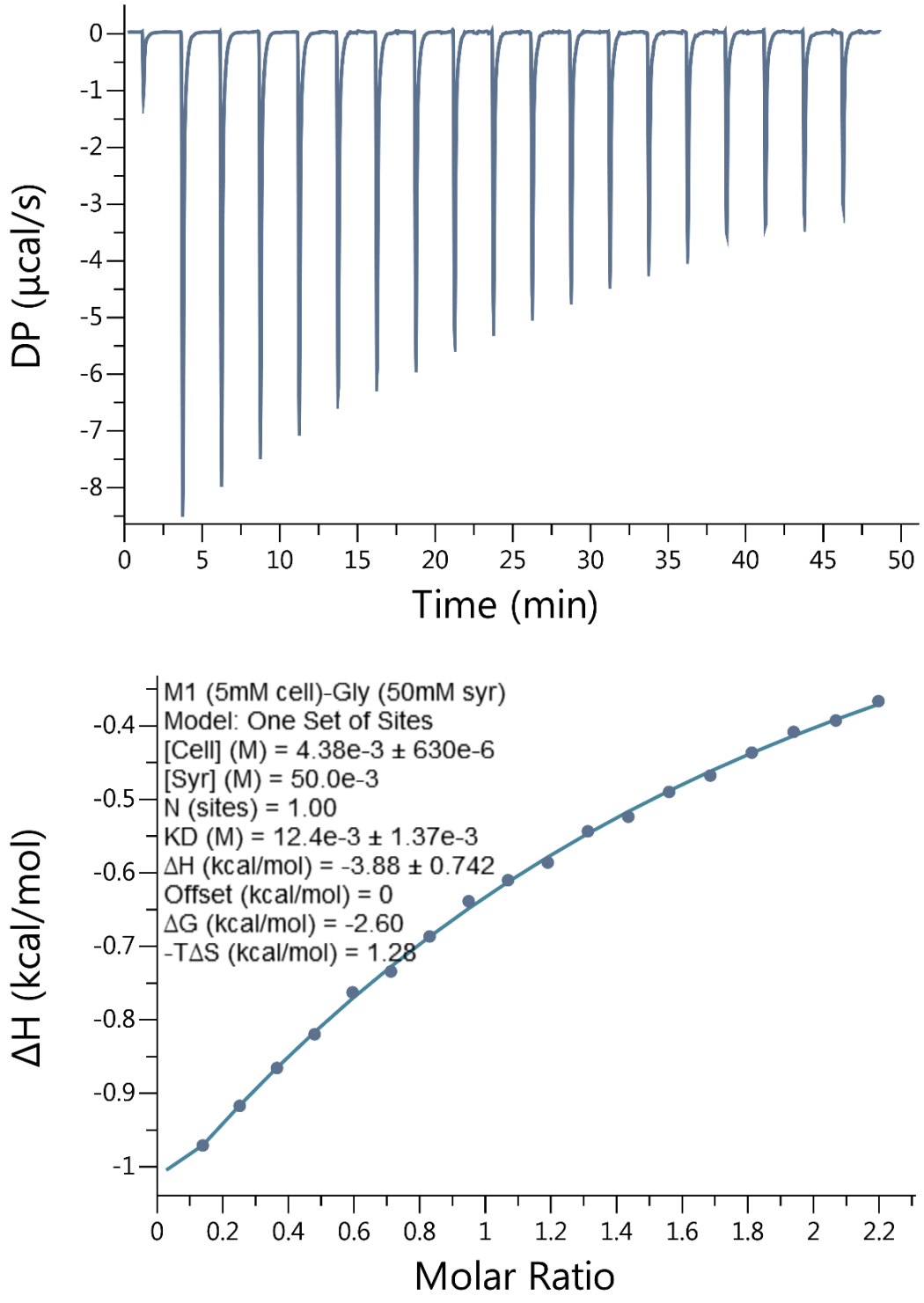

Figure II-S24. Isothermal Titration Calorimetry (ITC) curve obtained when a solution of Motor 1 (5.00 mM) in the cell was titrated with Glycine amide (50.0 mM) in the syringe at 298.0 K in 20 mM sodium phosphate buffered water at pH 7.4. K_a= 80.6 M^{-1}

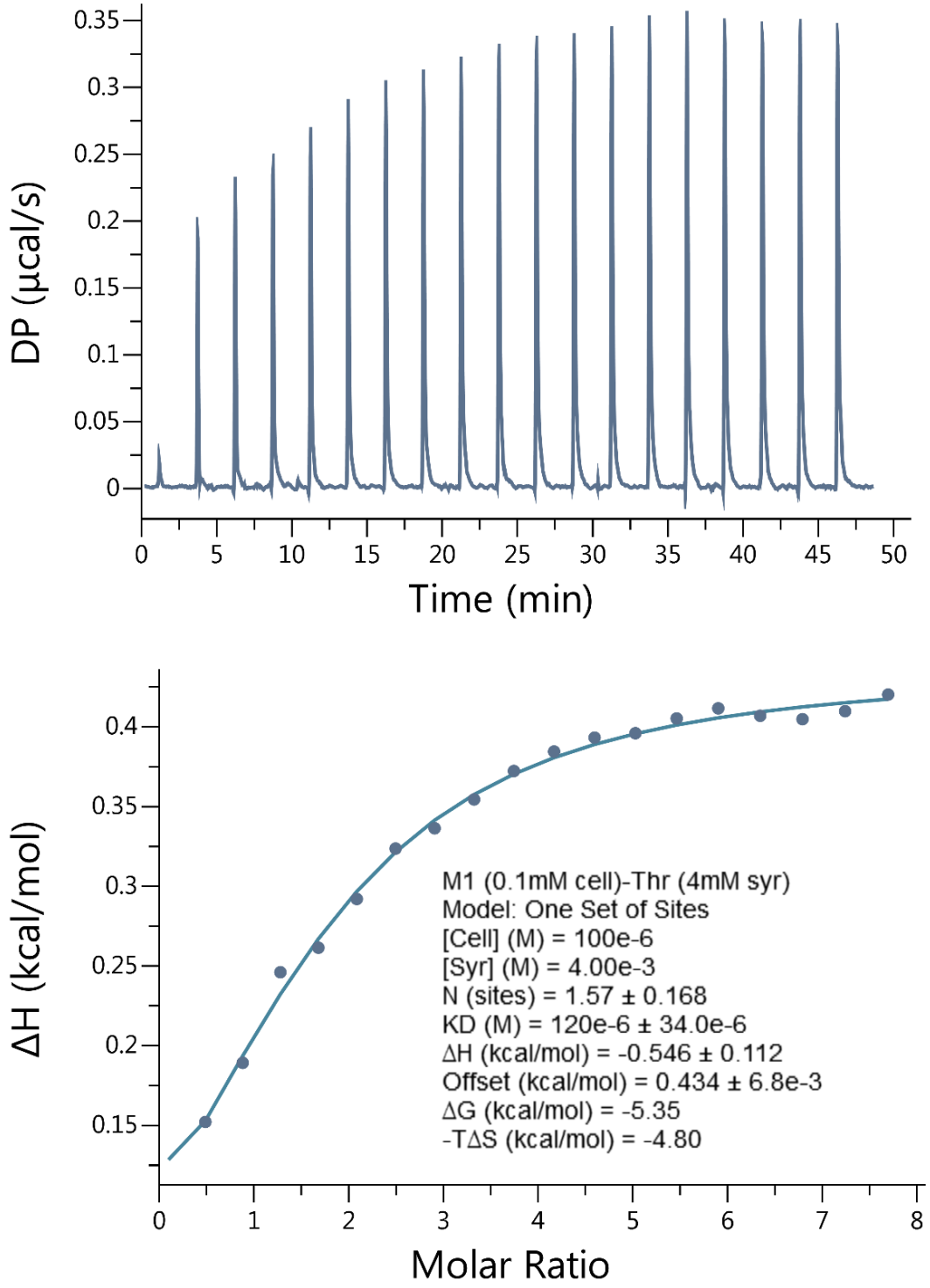

Figure II-S25. Isothermal Titration Calorimetry (ITC) curve obtained when a solution of Motor 1 (100 µM) in the cell was titrated with Threonine amide (4 mM) in the syringe at 298.0 K in 20 mM sodium phosphate buffered water at pH 7.4. K_a= 8333.3 M^{-1}

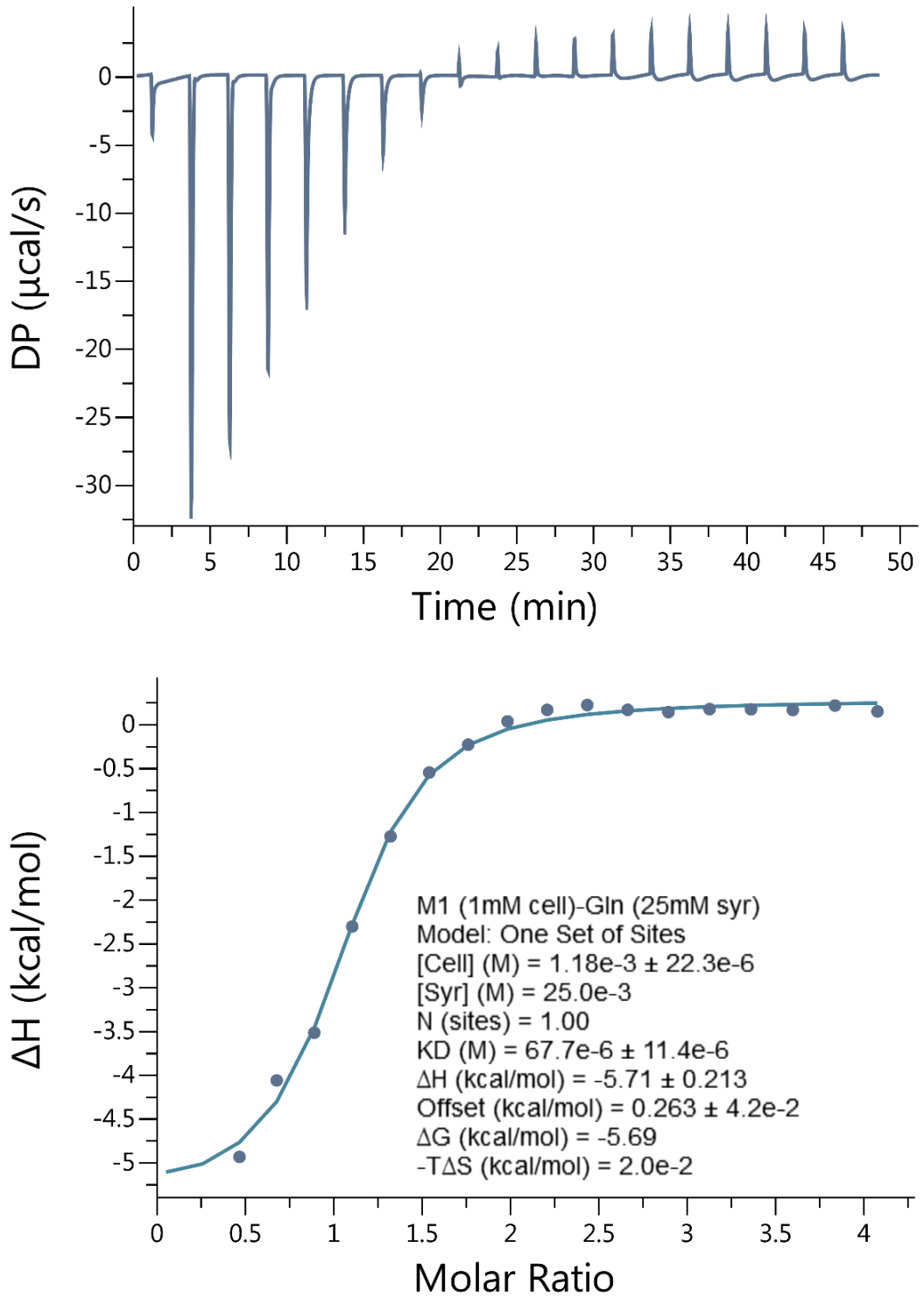

Figure II-S26. Isothermal Titration Calorimetry (ITC) curve obtained when a solution of Motor 1 (1.00 mM) in the cell was titrated with Glutamine amide (25.0 mM) in the syringe at 298.0 K in 20 mM sodium phosphate buffered water at pH 7.4. $K_a = 1.47 \times 10^4\ M^{-1}$

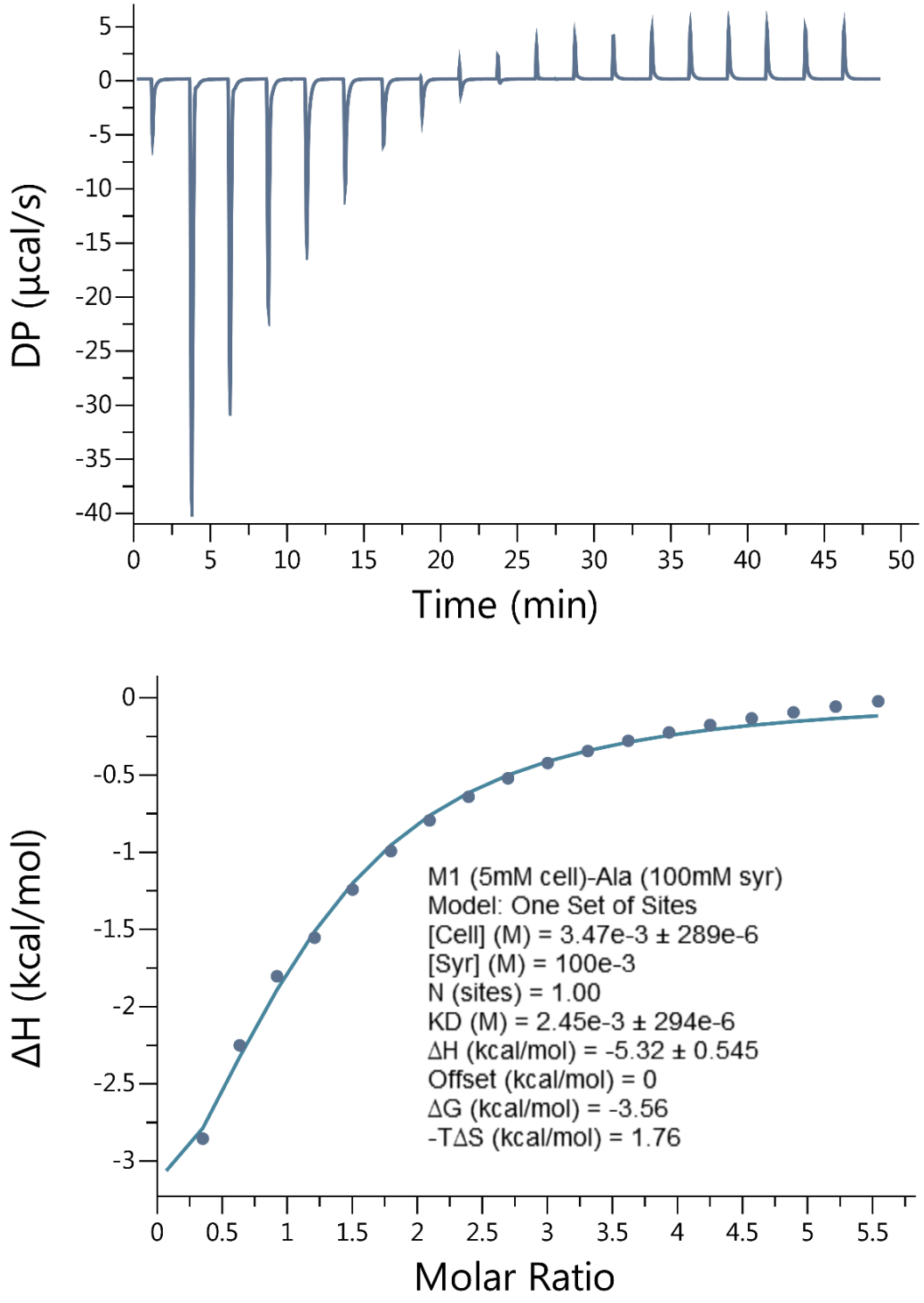

Figure II-S27. Isothermal Titration Calorimetry (ITC) curve obtained when a solution of Motor 1 (5.00 mM) in the cell was titrated with Alanine amide (1.00×10^2 mM) in the syringe at 298.0 K in 20 mM sodium phosphate buffered water at pH 7.4. $K_a = 4.08 \times 10^2\ M^{-1}$

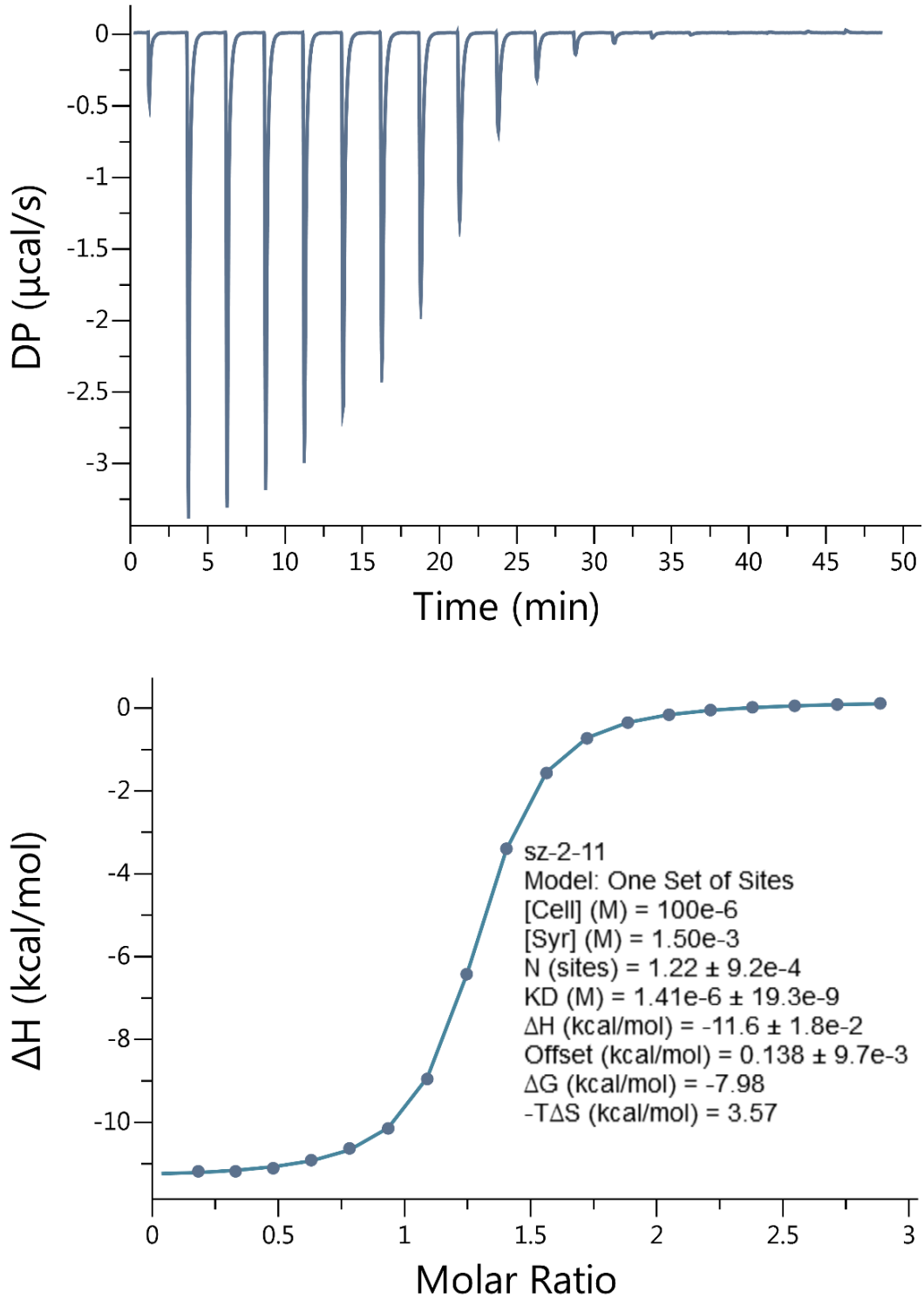

Figure II-S28. Isothermal Titration Calorimetry (ITC) curve obtained when a solution of Motor 1 (100 µM) in the cell was titrated with Arginine amide (1.50 mM) in the syringe at 298.0 K in 20 mM sodium phosphate buffered water at pH 7.4. K_a= 7.09×10^5 M^{-1}

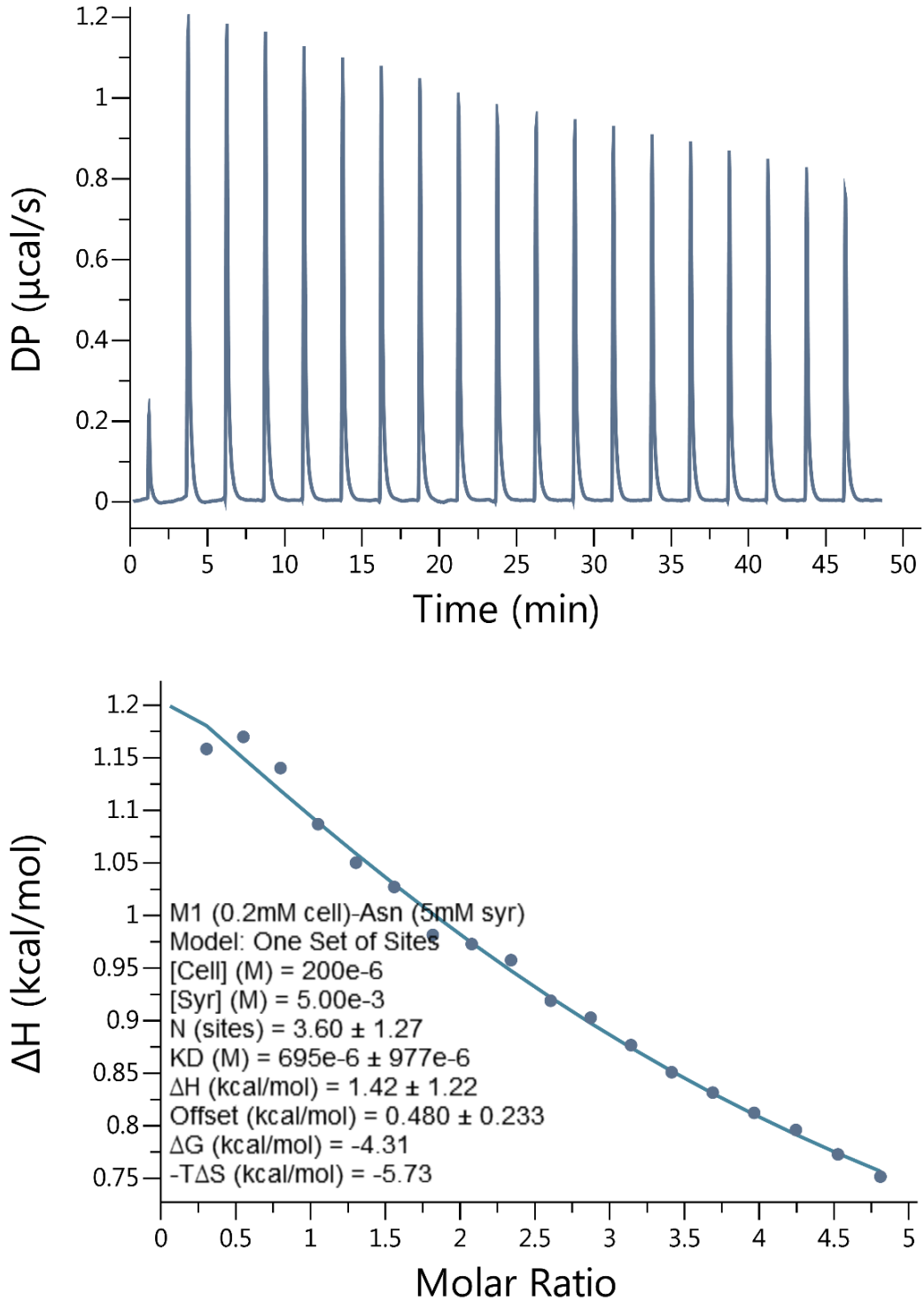

Figure II-S29. Isothermal Titration Calorimetry (ITC) curve obtained when a solution of Motor 1 (200 µM) in the cell was titrated with Asparagine amide (5 mM) in the syringe at 298.0 K in 20 mM sodium phosphate buffered water at pH 7.4. K_a= 1.44×10^3 M^{-1}

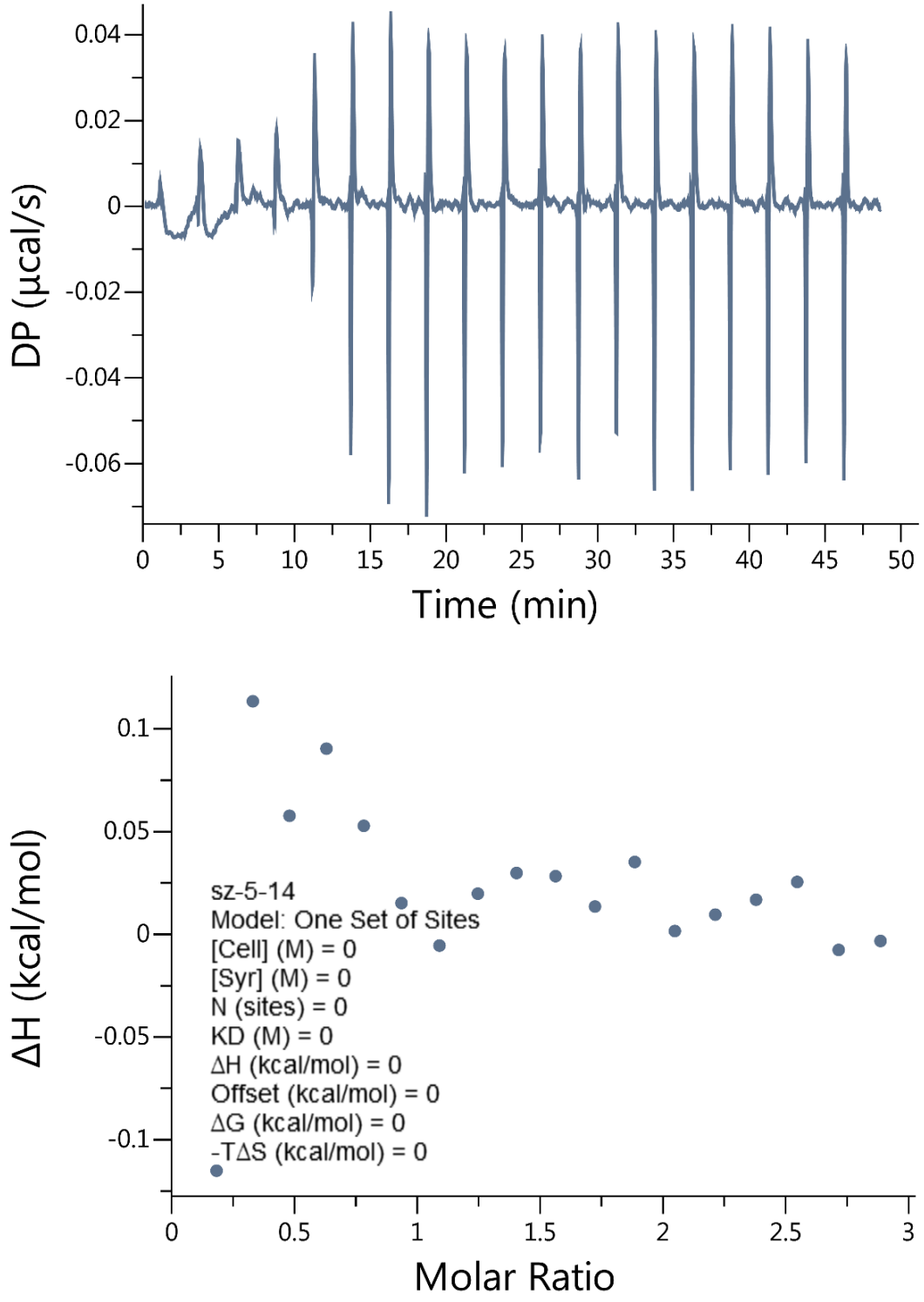

Figure II-S30. Isothermal Titration Calorimetry (ITC) curve obtained when a solution of Motor 1 (100 µM) in the cell was titrated with Aspartic acid amide (1.50 mM) in the syringe at 298.0 K in 20 mM sodium phosphate buffered water at pH 7.4. K_a= No binding

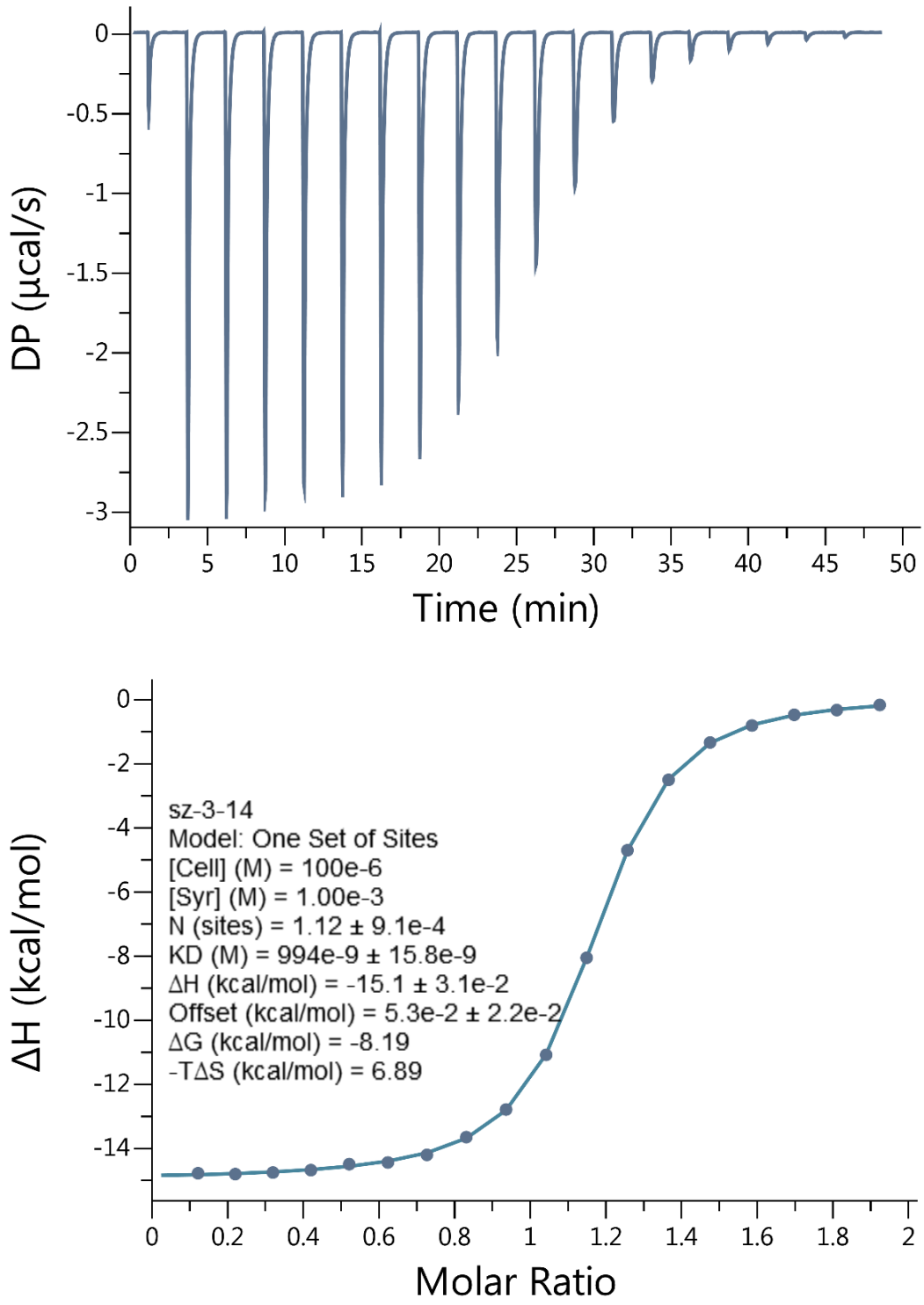

Figure II-S31. Isothermal Titration Calorimetry (ITC) curve obtained when a solution of Motor 1 (100 µM) in the cell was titrated with Tyrosine amide (1.00 mM) in the syringe at 298.0 K in 20 mM sodium phosphate buffered water at pH 7.4. K_a= $1.01 \times 10^6\ M^{-1}$

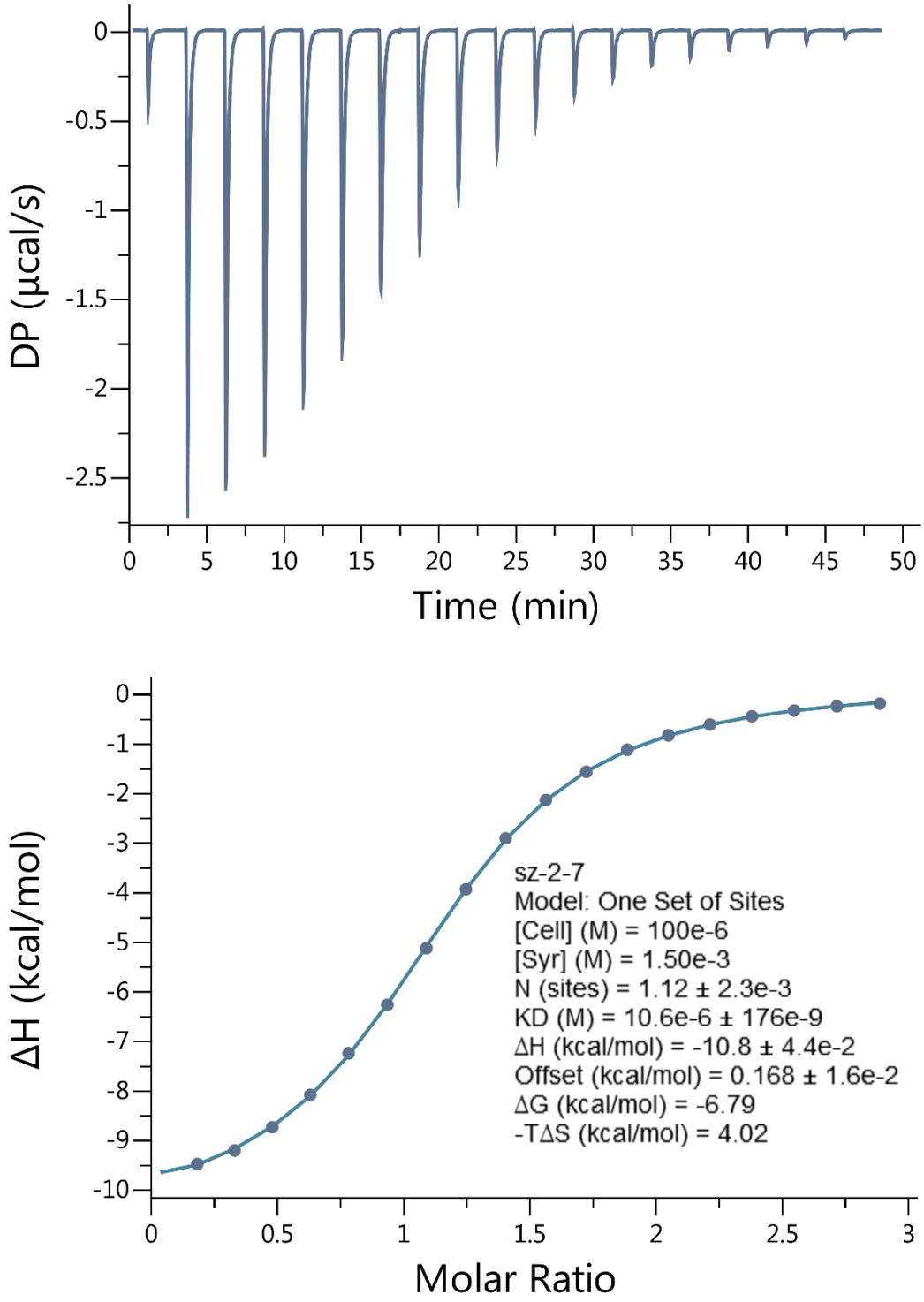

Figure II-S32. Isothermal Titration Calorimetry (ITC) curve obtained when a solution of Motor 1 (100 µM) in the cell was titrated with Isoleucine amide (1.50 mM) in the syringe at 298.0 K in 20 mM sodium phosphate buffered water at pH 7.4. $K_a = 9.43 \times 10^4\ M^{-1}$

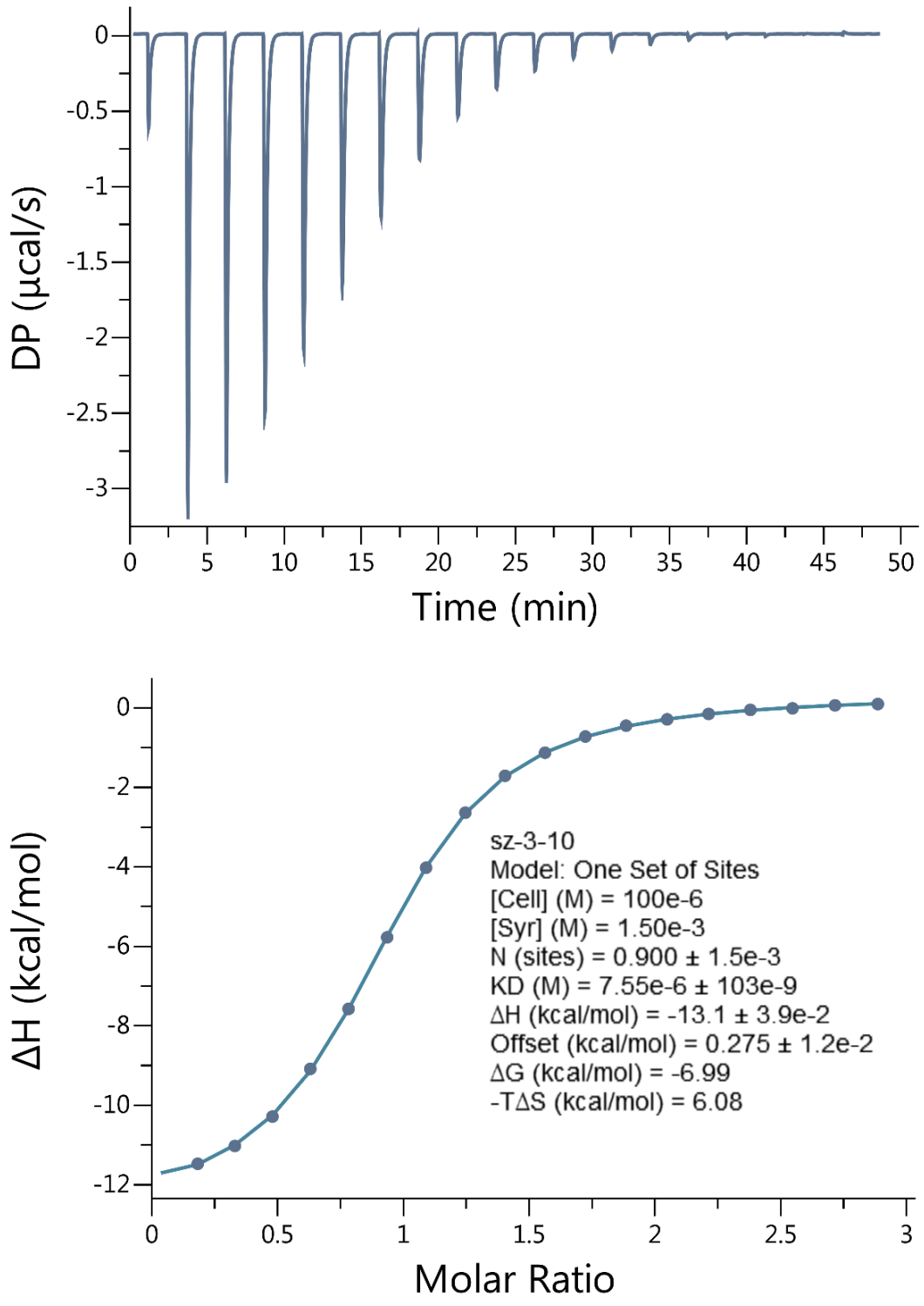

Figure II-S33. Isothermal Titration Calorimetry (ITC) curve obtained when a solution of Motor 1 (100 µM) in the cell was titrated with Methionine amide (1.50 mM) in the syringe at 298.0 K in 20 mM sodium phosphate buffered water at pH 7.4. $K_a = 1.32 \times 10^5\ M^{-1}$

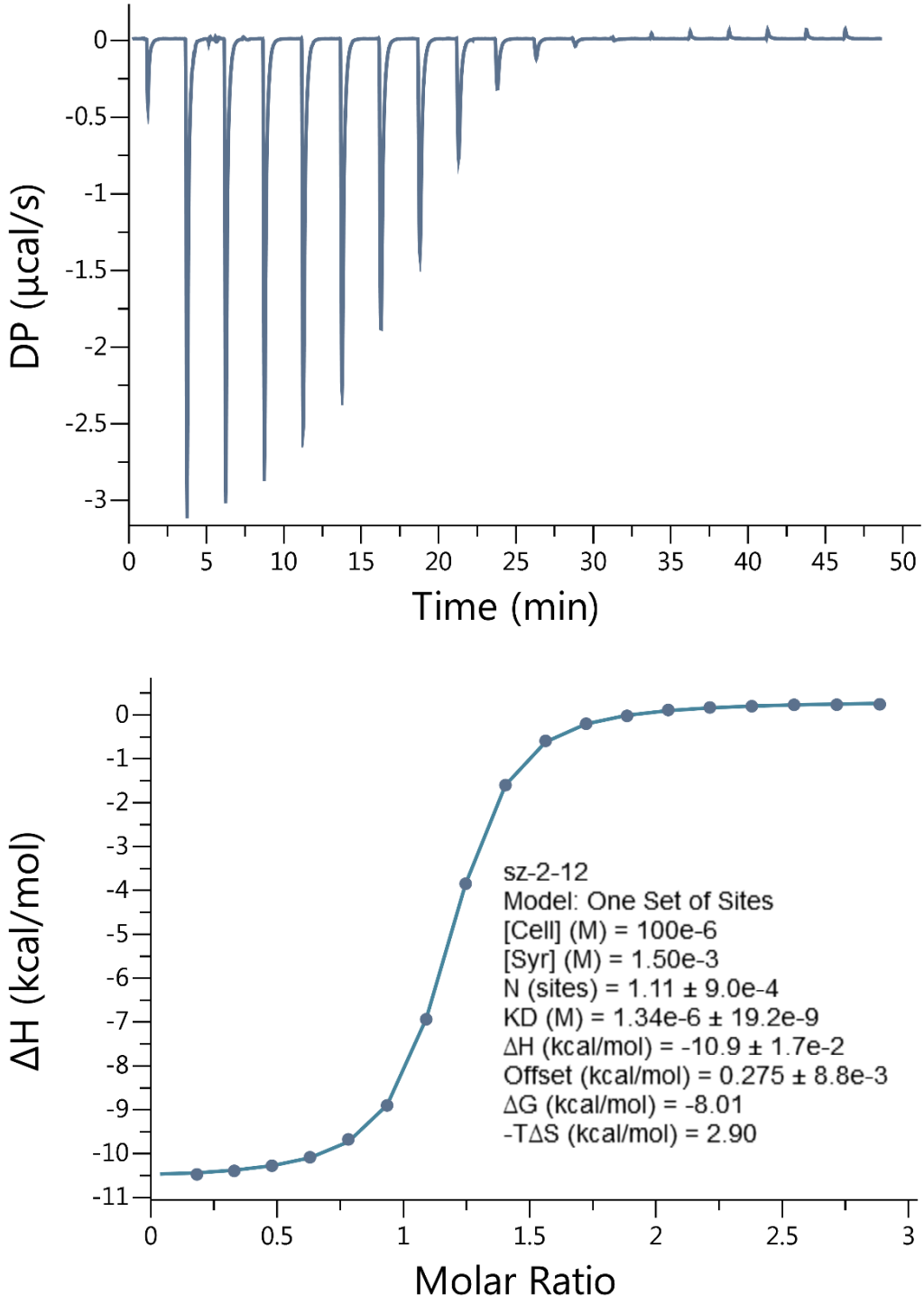

Figure II-S34. Isothermal Titration Calorimetry (ITC) curve obtained when a solution of Motor 1 (100 µM) in the cell was titrated with Lysine amide (1.50 mM) in the syringe at 298.0 K in 20 mM sodium phosphate buffered water at pH 7.4. K_a= 7.46×10^5 M^{-1}

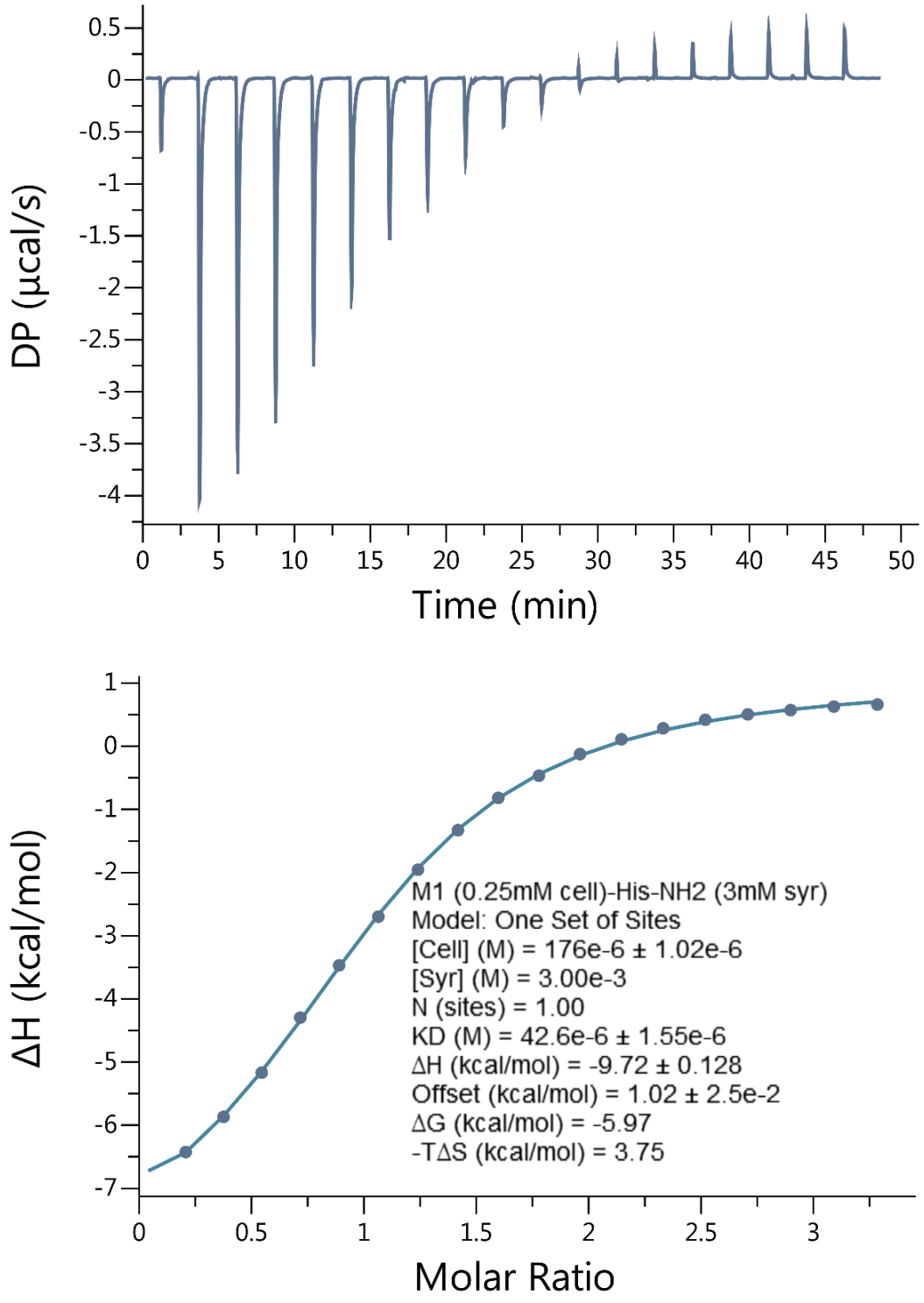

Figure II-S35. Isothermal Titration Calorimetry (ITC) curve obtained when a solution of Motor 1 (250 µM) in the cell was titrated with Histidine amide (3.00 mM) in the syringe at 298.0 K in 20 mM sodium phosphate buffered water at pH 7.4. K_a= 2.35×10^4 M^{-1}

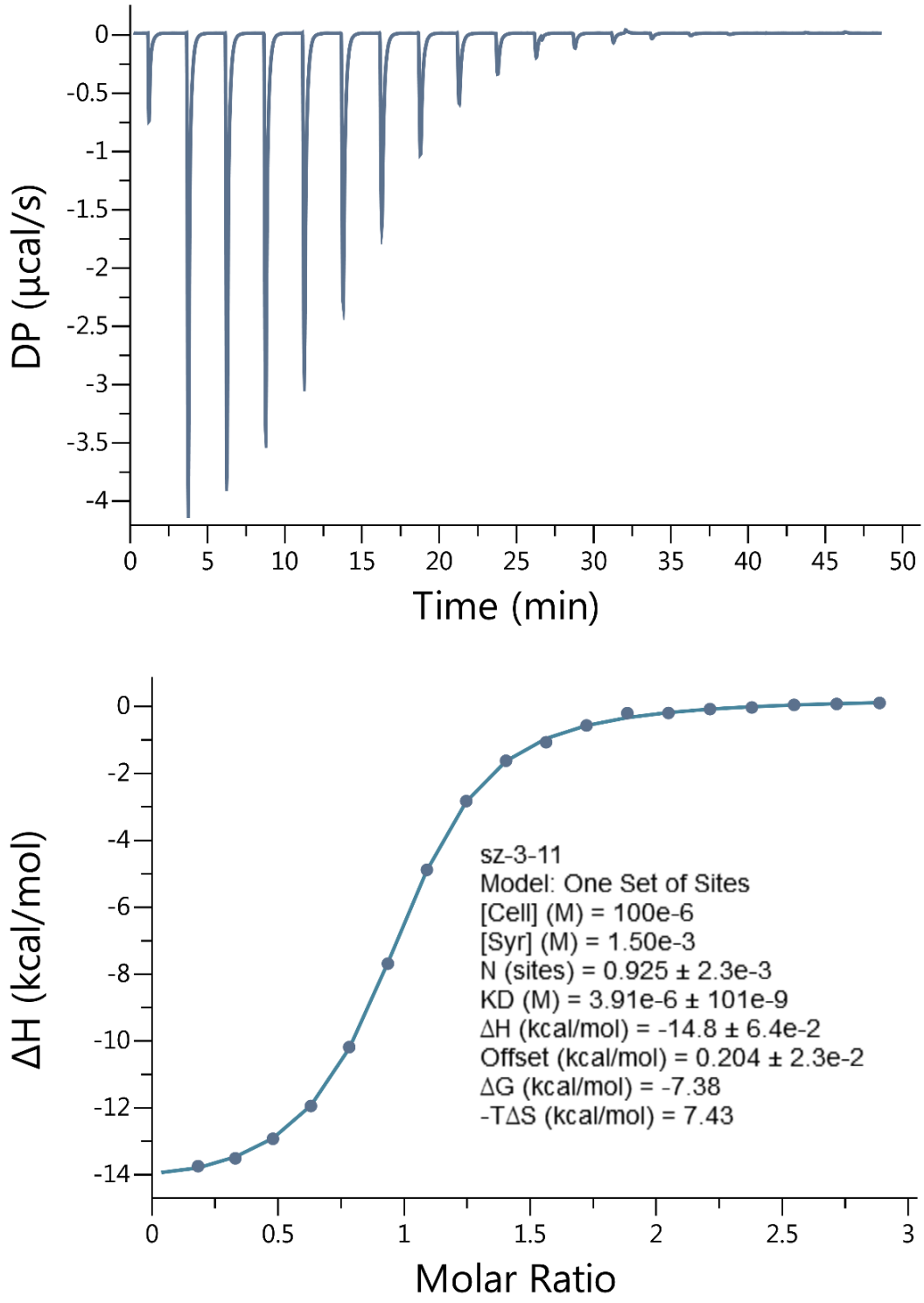

Figure II-S36. Isothermal Titration Calorimetry (ITC) curve obtained when a solution of Motor 1 (100 µM) in the cell was titrated with Tryptophan amide (1.50 mM) in the syringe at 298.0 K in 20 mM sodium phosphate buffered water at pH 7.4. $K_a = 2.56 \times 10^5\ M^{-1}$

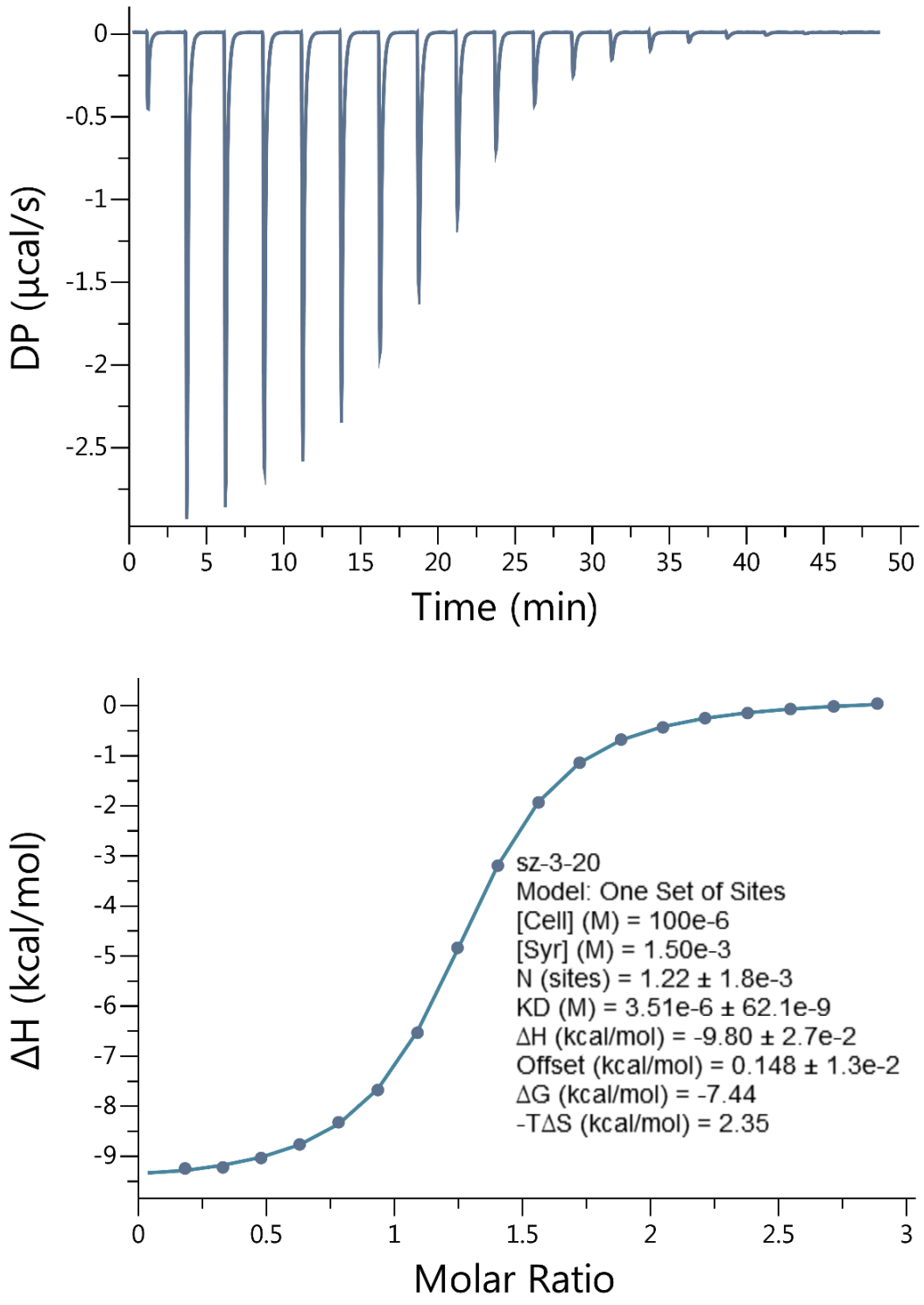

Figure II-S37. Isothermal Titration Calorimetry (ITC) curve obtained when a solution of Motor 1 (100 µM) in the cell was titrated with Leucine amide (1.50 mM) in the syringe at 298.0 K in 20 mM sodium phosphate buffered water at pH 7.4. K_a= 2.85×10^5 M^{-1}

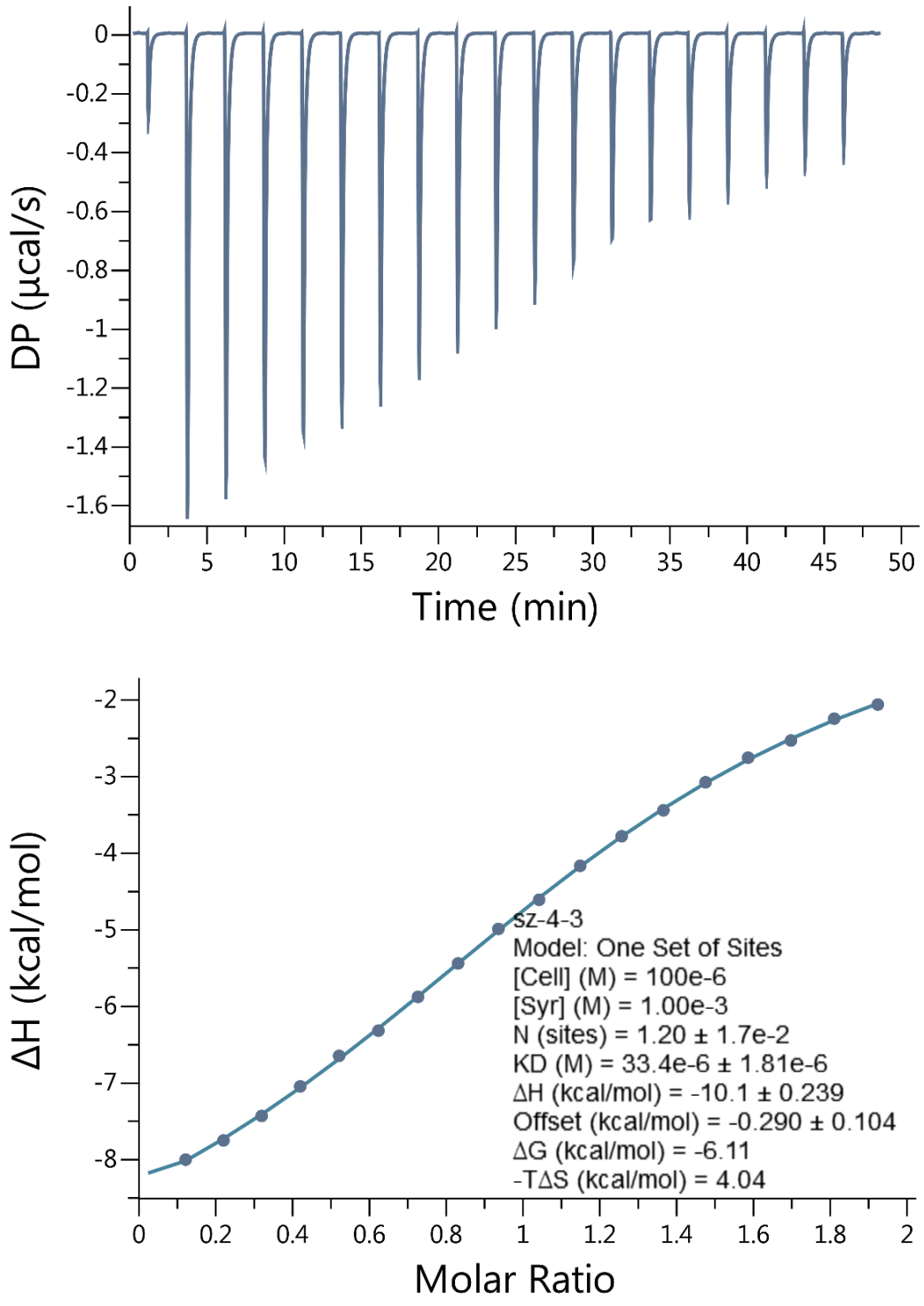

Figure II-S38. Isothermal Titration Calorimetry (ITC) curve obtained when a solution of Motor 2 (100 µM) in the cell was titrated with Acetyl-phenylalanine amide (1.00 mM) in the syringe at 298.0 K in 20 mM sodium phosphate buffered water at pH 7.4. $K_a = 2.99 \times 10^4\ M^{-1}$

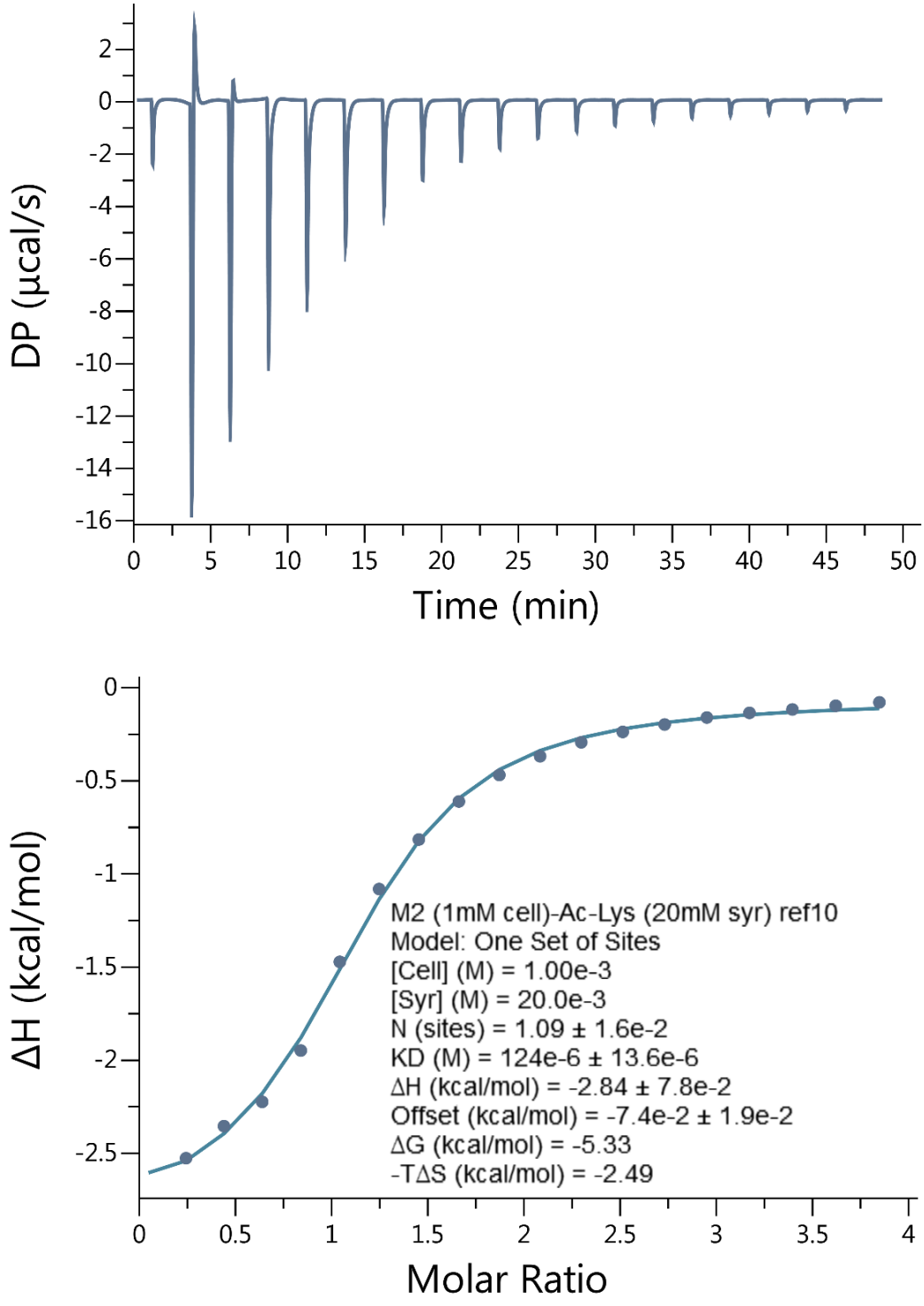

Figure II-S39. Isothermal Titration Calorimetry (ITC) curve obtained when a solution of Motor 2 (1.00 mM) in the cell was titrated with Acetyl-Lysine amide (20.0 mM) in the syringe at 298.0 K in 20 mM sodium phosphate buffered water at pH 7.4. $K_a = 8.06 \times 10^3\ M^{-1}$

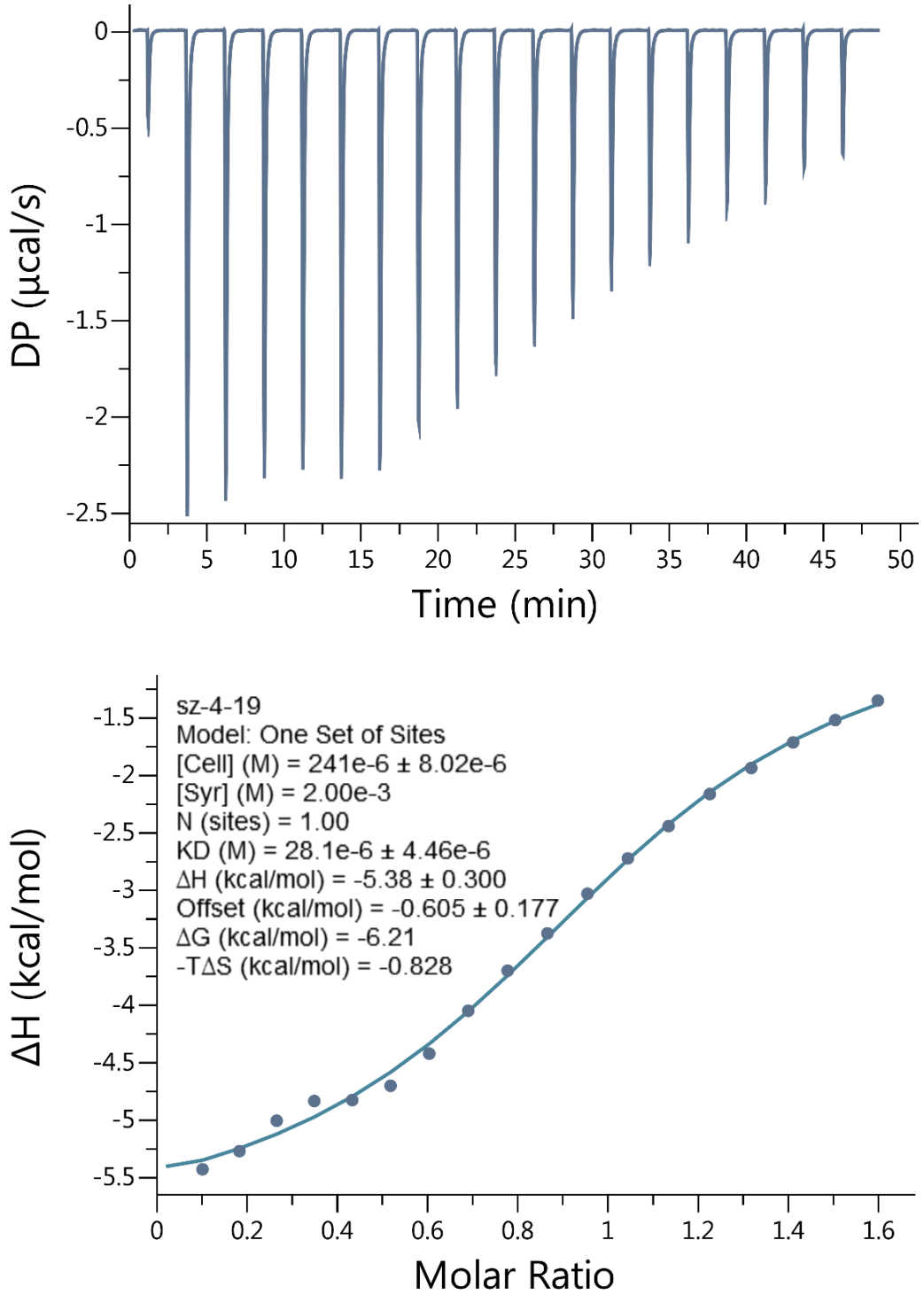

Figure II-S40. Isothermal Titration Calorimetry (ITC) curve obtained when a solution of Motor 2 (100 µM) in the cell was titrated with Acetyl-Tryptophan amide (2.00 mM) in the syringe at 298.0 K in 20 mM sodium phosphate buffered water at pH 7.4. $K_a = 3.56 \times 10^4\ M^{-1}$

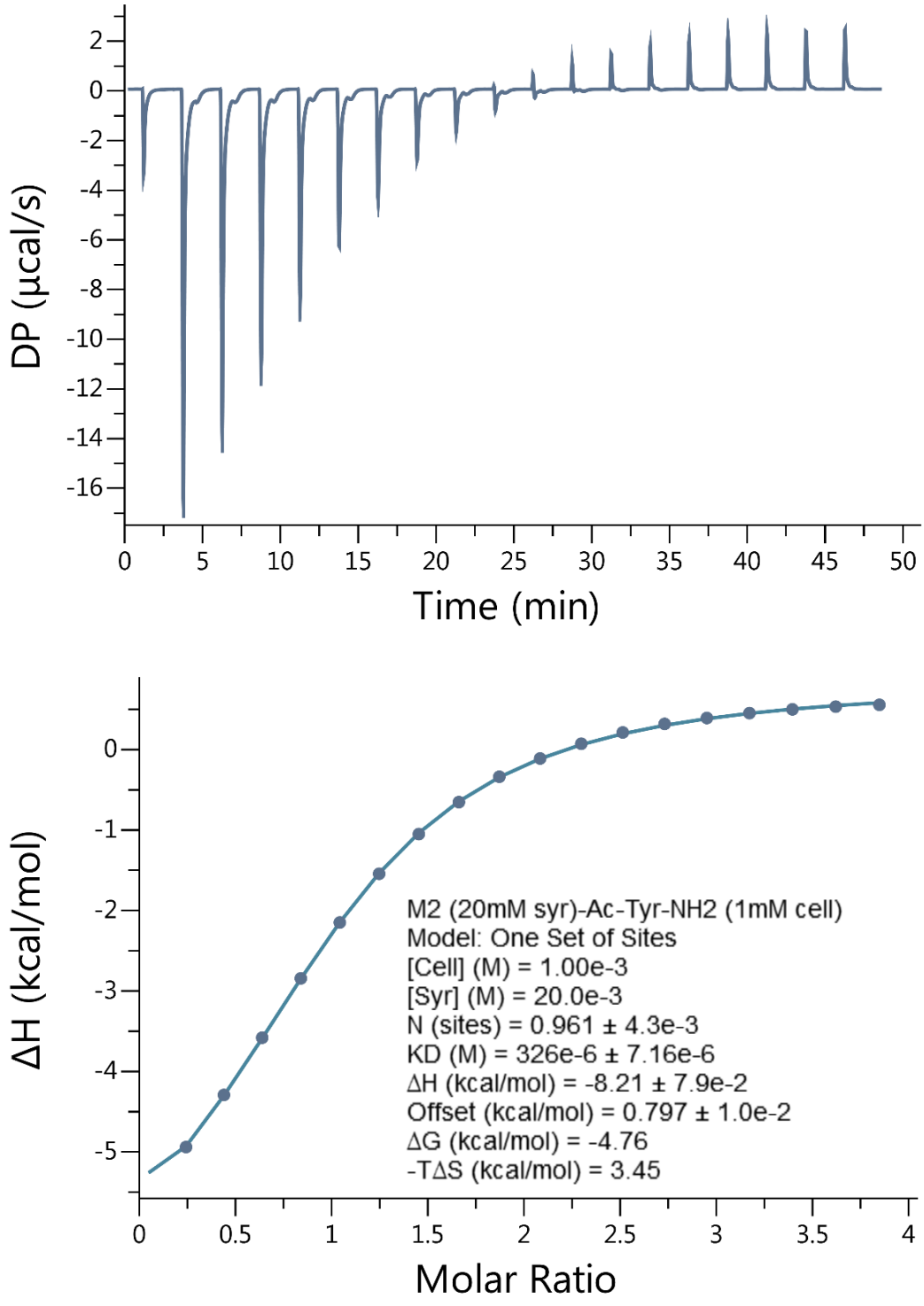

Figure II-S41. Isothermal Titration Calorimetry (ITC) curve obtained when a solution of Acetyl- Tyrosine amide (1.00 mM) in the cell was titrated with Motor 2 (20.0 mM) in the syringe at 298.0 K in 20 mM sodium phosphate buffered water at pH 7.4. $K_a = 3.06 \times 10^3$ M^{-1}

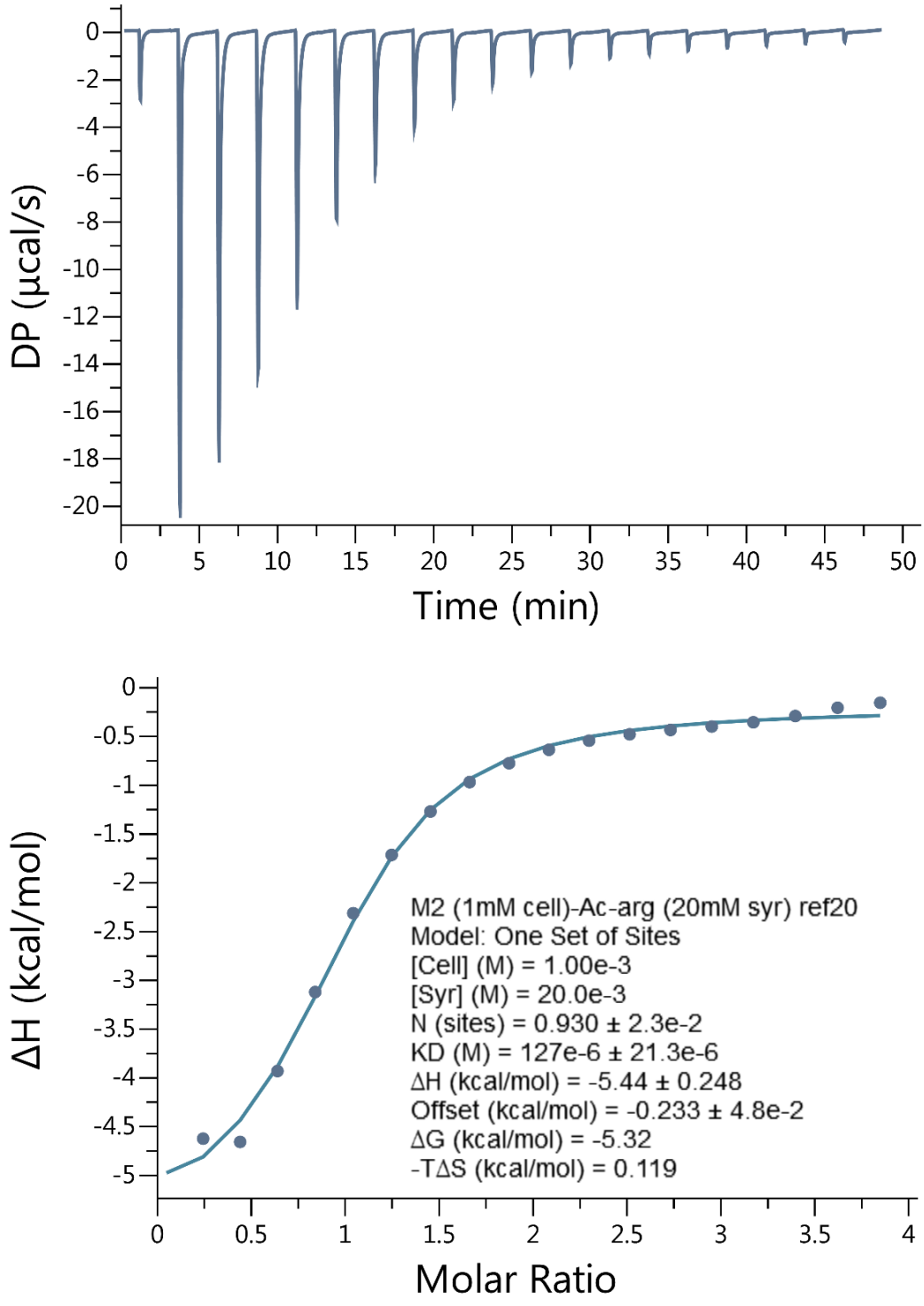

Figure II-S42. Isothermal Titration Calorimetry (ITC) curve obtained when a solution of Motor 2 (1.00 mM) in the cell was titrated with Acetyl-Arginine amide (20.0 mM) in the syringe at 298.0 K in 20 mM sodium phosphate buffered water at pH 7.4. $K_a = 7.87 \times 10^3$ M^{-1}

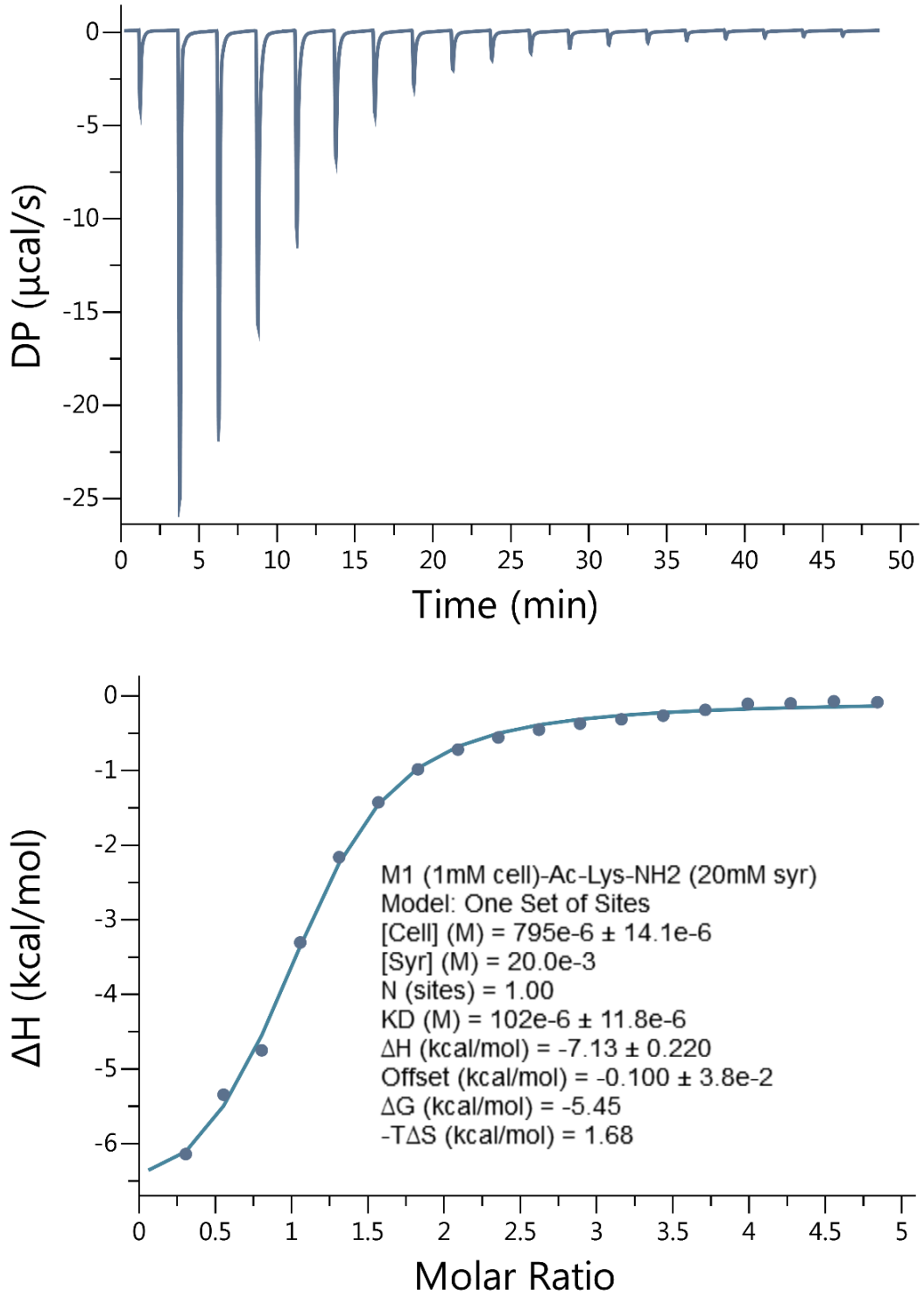

Figure II-S43. Isothermal Titration Calorimetry (ITC) curve obtained when a solution of Motor 1 (1.00 mM) in the cell was titrated with Acetyl-Lysine amide (20.0 mM) in the syringe at 298.0 K in 20 mM sodium phosphate buffered water at pH 7.4. $K_a = 9.80 \times 10^3\ M^{-1}$

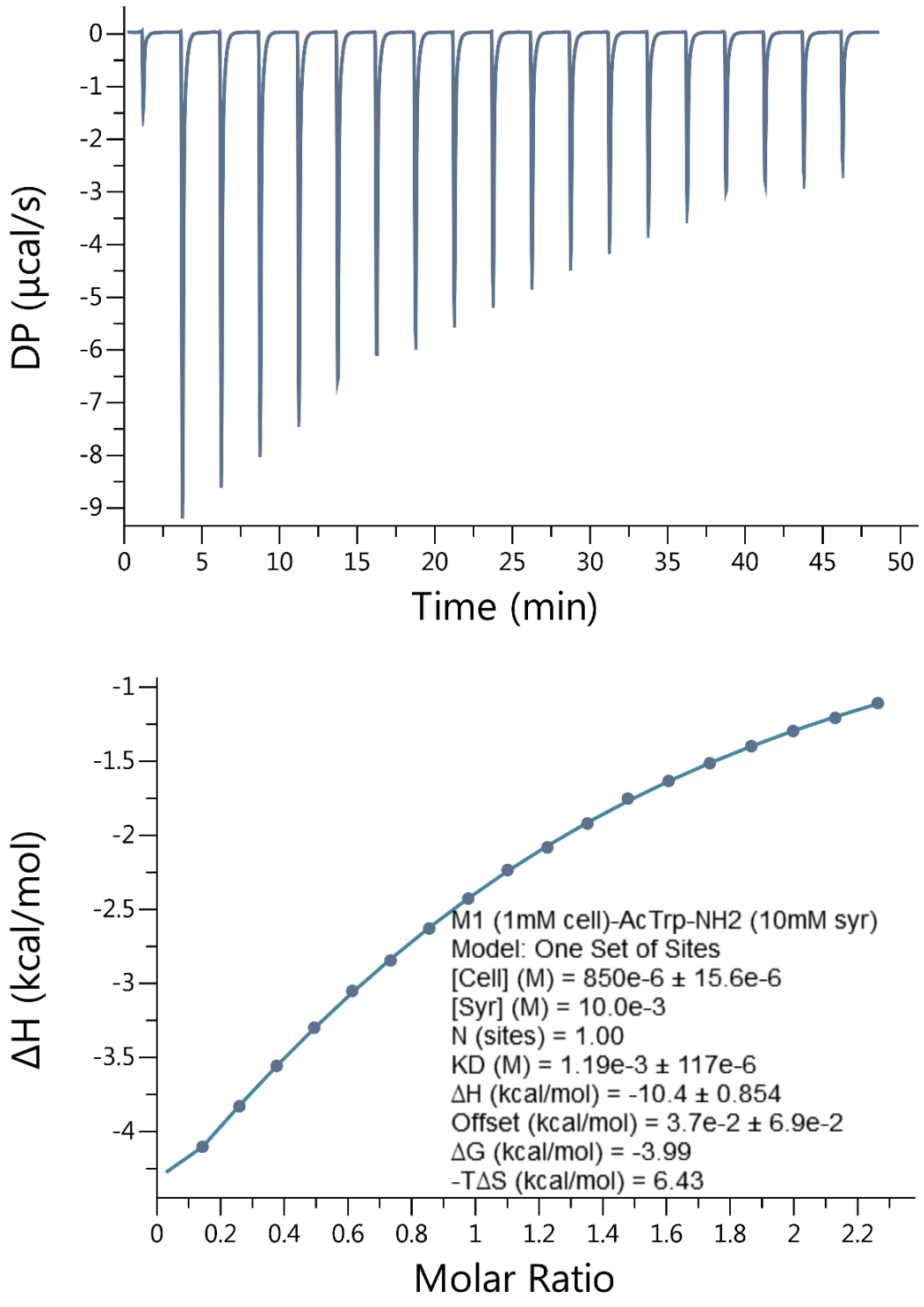

Figure II-S44. Isothermal Titration Calorimetry (ITC) curve obtained when a solution of Motor 1 (1.00 mM) in the cell was titrated with Acetyl-Tryptophan amide (10.0 mM) in the syringe at 298.0 K in 20 mM sodium phosphate buffered water at pH 7.4. $K_a = 8.40 \times 10^2\ M^{-1}$

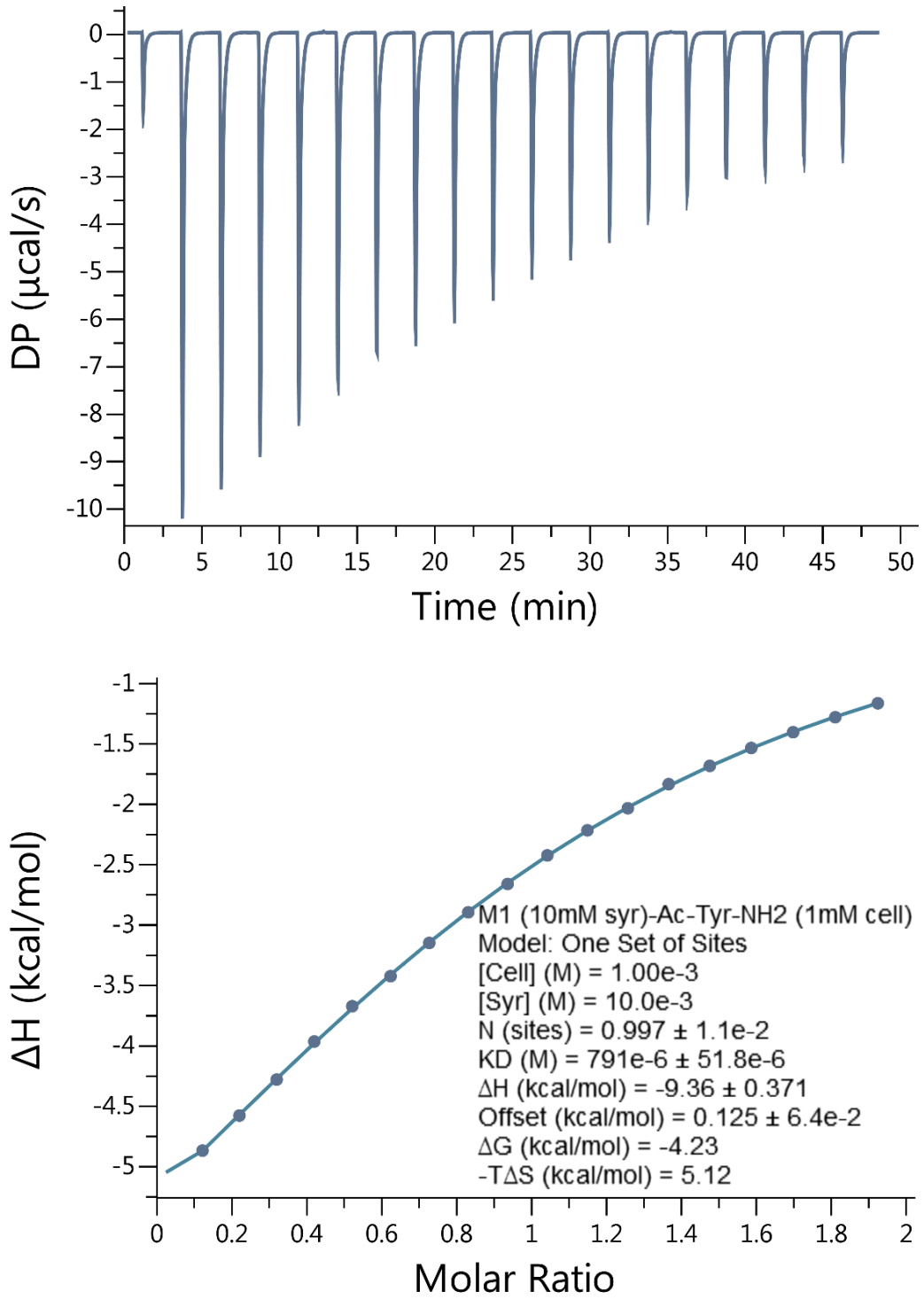

Figure II-S45. Isothermal Titration Calorimetry (ITC) curve obtained when a solution of Acetyl- Tyrosine amide (1.00 mM) in the cell was titrated with Motor 1 (10.0 mM) in the syringe at 298.0 K in 20 mM sodium phosphate buffered water at pH 7.4. $K_a = 1.26 \times 10^3\ M^{-1}$

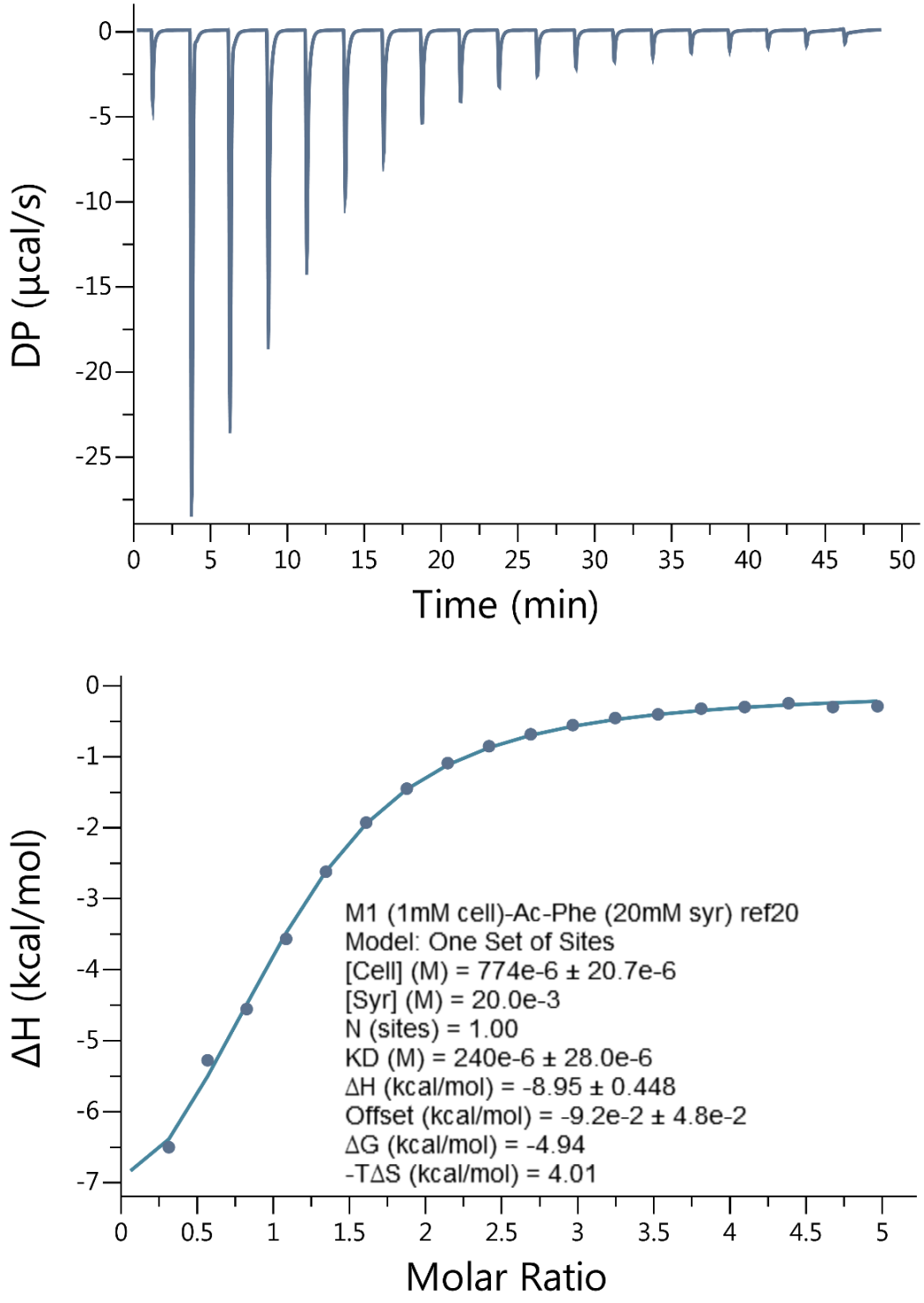

Figure II-S46. Isothermal Titration Calorimetry (ITC) curve obtained when a solution of Motor 1 (1.00 mM) in the cell was titrated with Acetyl-Phenylalanine amide (20.0 mM) in the syringe at 298.0 K in 20 mM sodium phosphate buffered water at pH 7.4. $K_a = 4.17 \times 10^3\ M^{-1}$

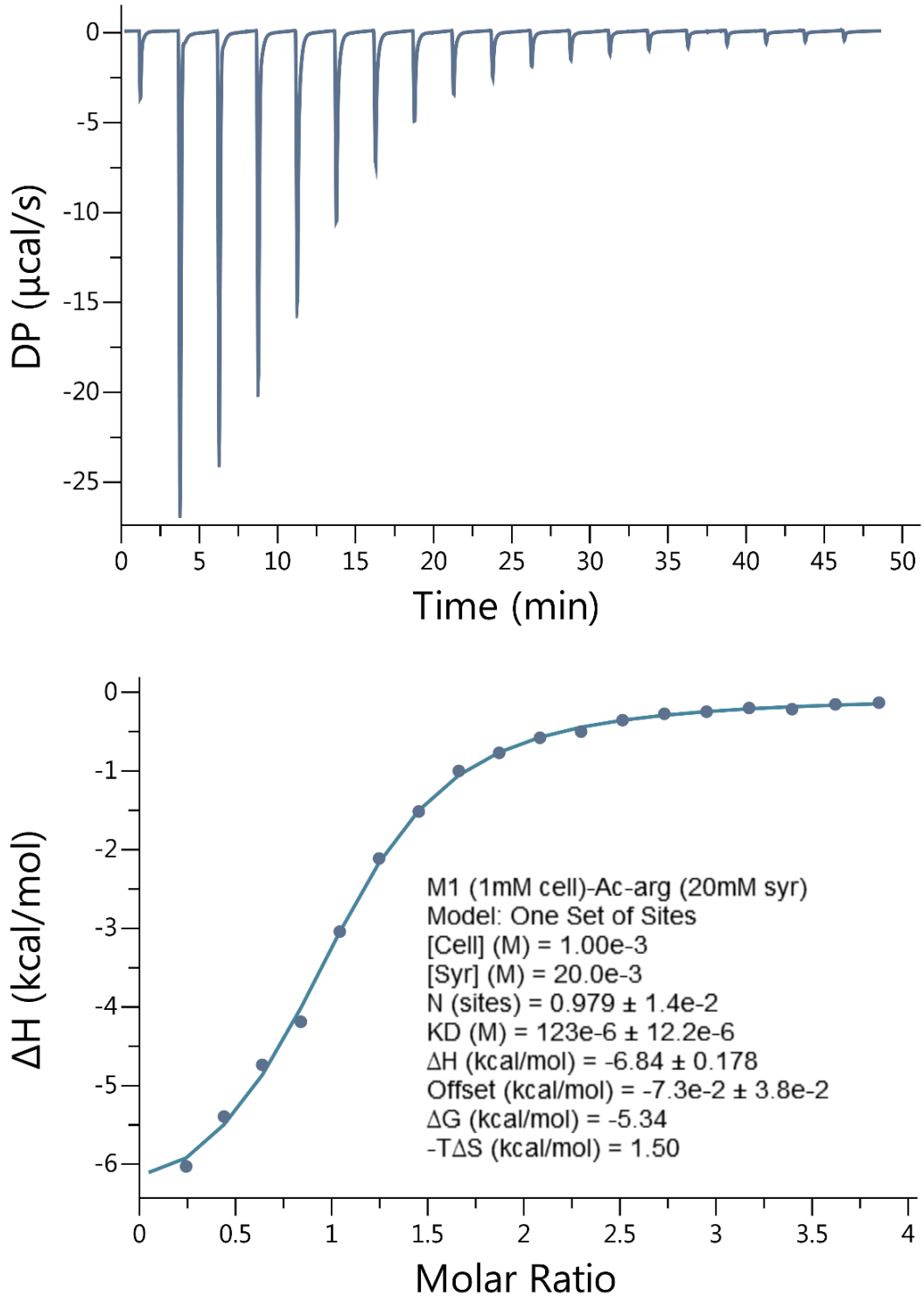

Figure II-S47. Isothermal Titration Calorimetry (ITC) curve obtained when a solution of Motor 1 (1.00 mM) in the cell was titrated with Acetyl-Arginine amide (20.0 mM) in the syringe at 298.0 K in 20 mM sodium phosphate buffered water at pH 7.4. $K_a = 8.13 \times 10^3\ M^{-1}$

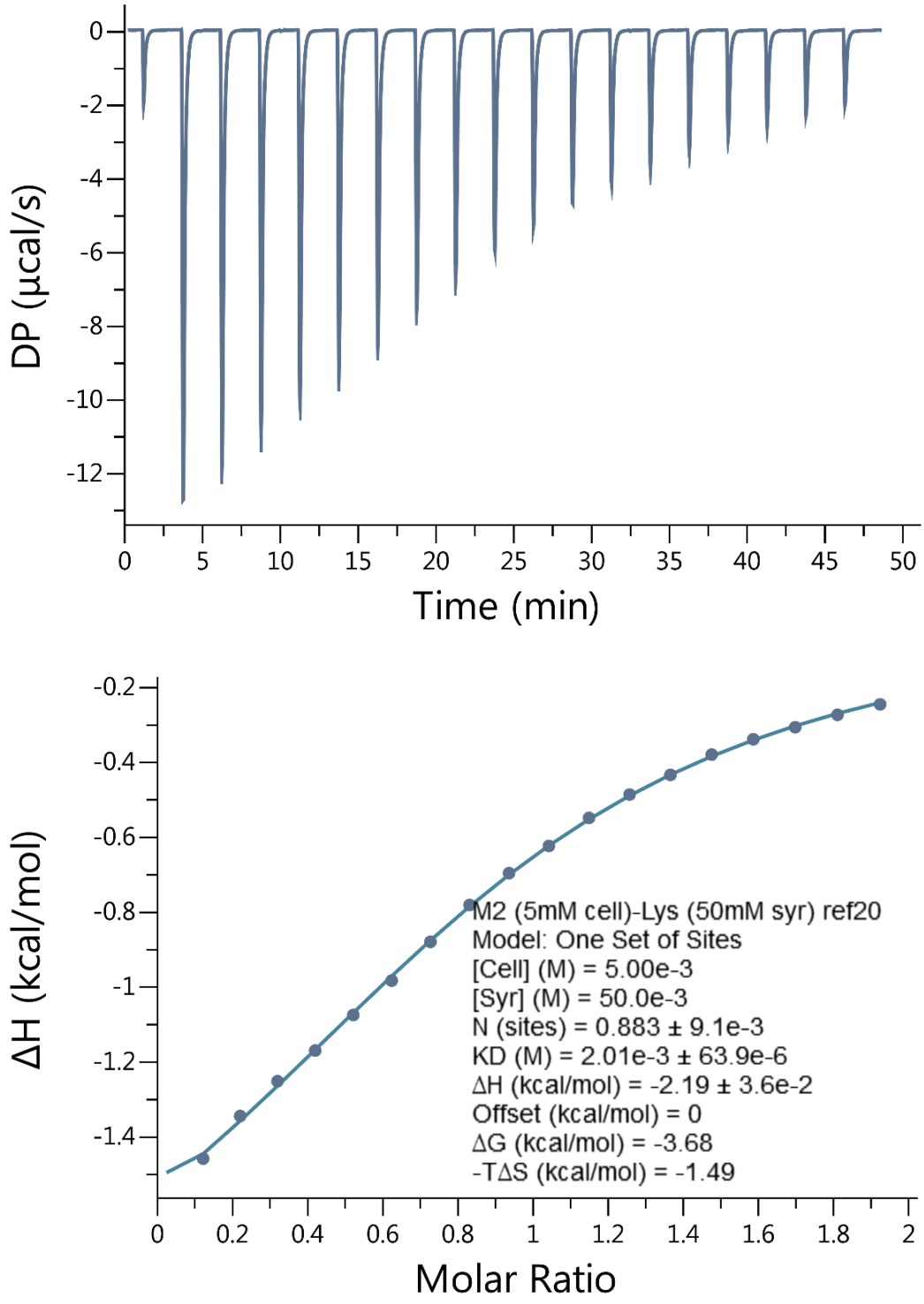

Figure II-S48. Isothermal Titration Calorimetry (ITC) curve obtained when a solution of Motor 2 (5.00 mM) in the cell was titrated with Lysine (50.00 mM) in the syringe at 298.0 K in 20 mM sodium phosphate buffered water at pH 7.4. K_a = 497.5 M^{-1}

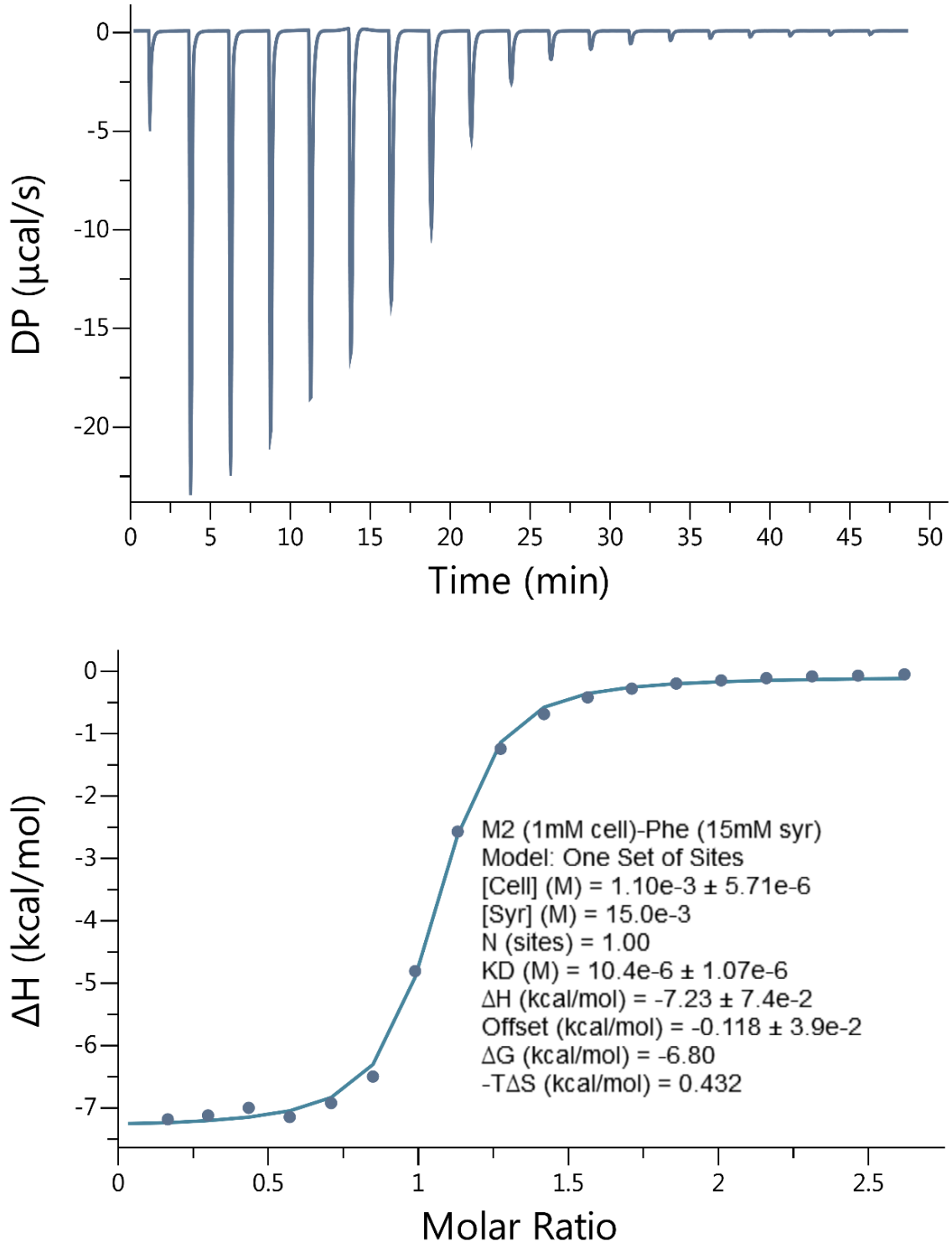

Figure II-S49. Isothermal Titration Calorimetry (ITC) curve obtained when a solution of Motor 2 (1.00 mM) in the cell was titrated with phenylalanine (15.00 mM) in the syringe at 298.0 K in 20 mM sodium phosphate buffered water at pH 7.4. K_a = $9.61 \times 10^4\ M^{-1}$

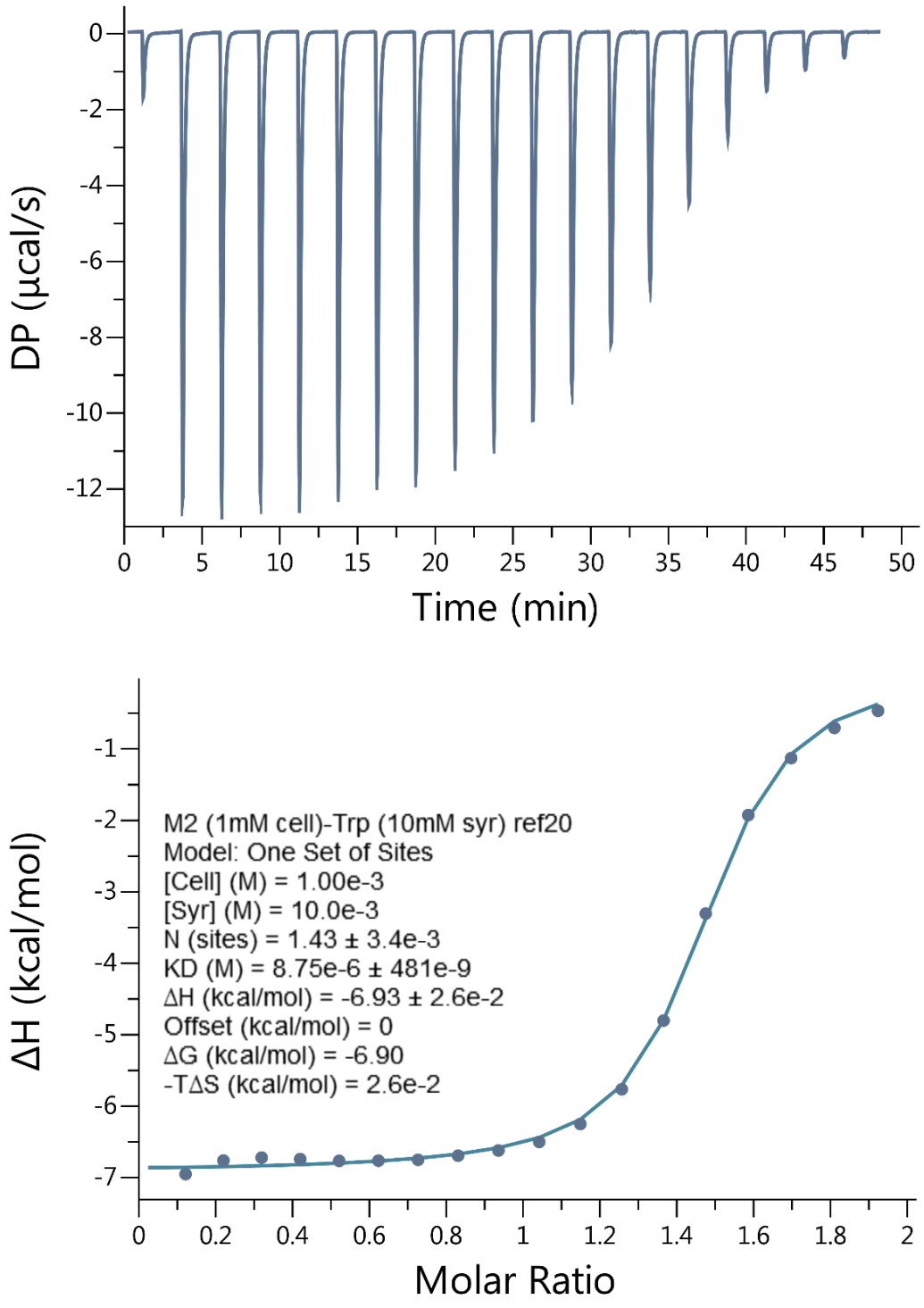

Figure II-S50. Isothermal Titration Calorimetry (ITC) curve obtained when a solution of Motor 2 (1.00 mM) in the cell was titrated with Tryptophan (10.00 mM) in the syringe at 298.0 K in 20 mM sodium phosphate buffered water at pH 7.4. K_a = 1.14×10^5 M^{-1}

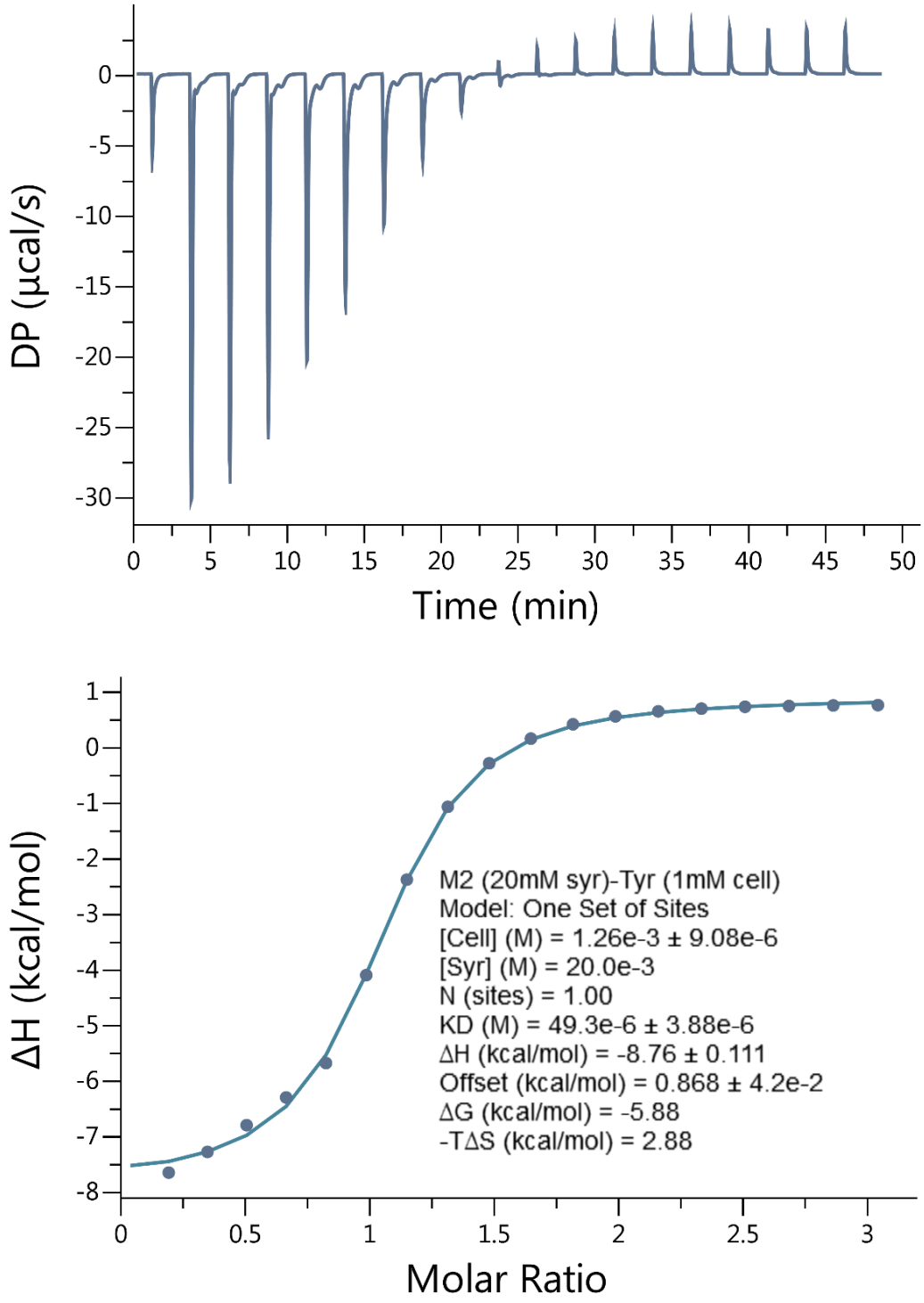

Figure II-S51. Isothermal Titration Calorimetry (ITC) curve obtained when a solution of Tyrosine (1.00 mM) in the cell was titrated with Motor 2 (20.0 mM) in the syringe at 298.0 K in 20 mM sodium phosphate buffered water at pH 7.4. $K_a = 2.03 \times 10^4\ M^{-1}$

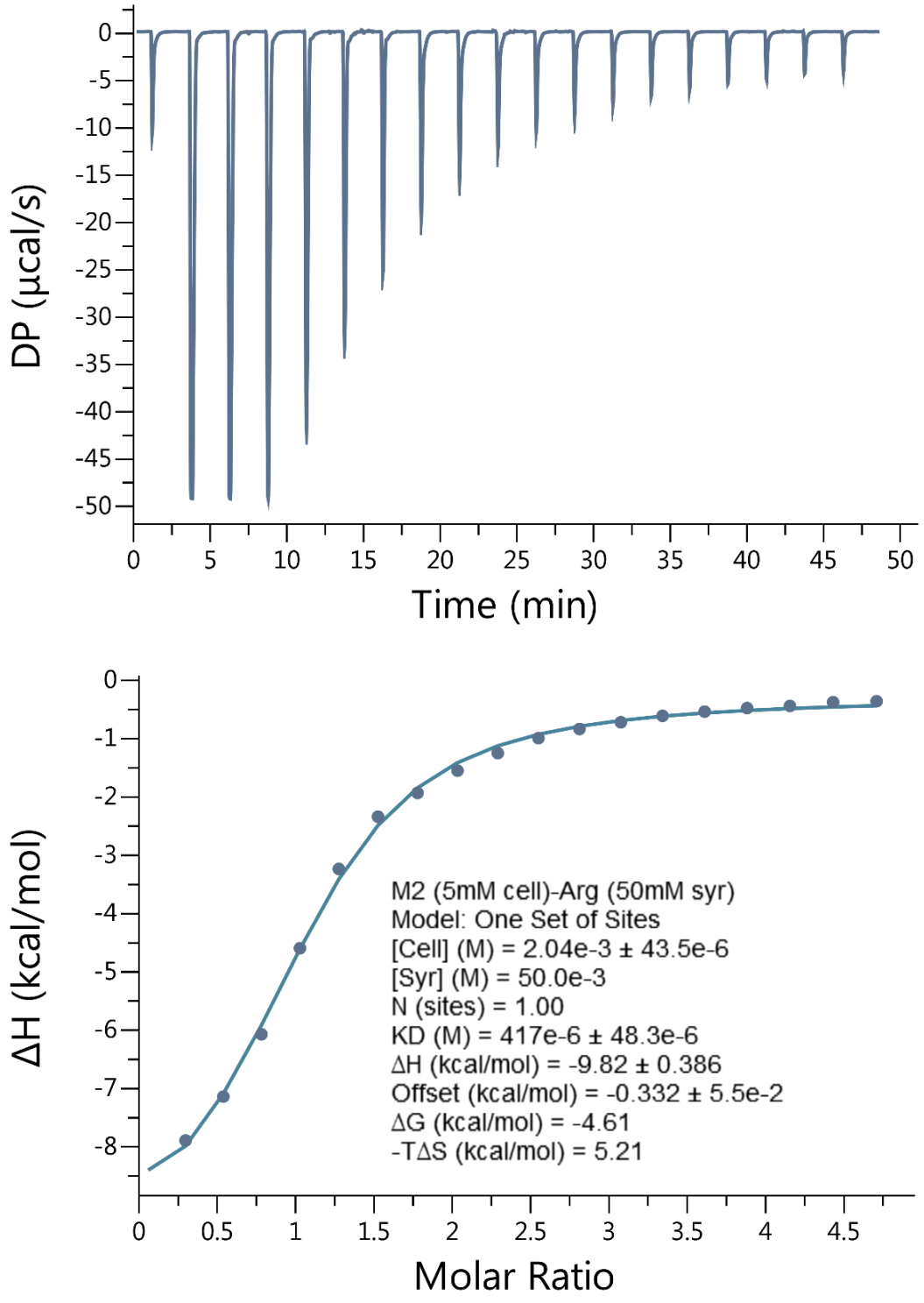

Figure II-S52. Isothermal Titration Calorimetry (ITC) curve obtained when a solution of Motor 2 (5.00 mM) in the cell was titrated with Arginine (50.0 mM) in the syringe at 298.0 K in 20 mM sodium phosphate buffered water at pH 7.4. $K_a = 2.39 \times 10^3\ M^{-1}$

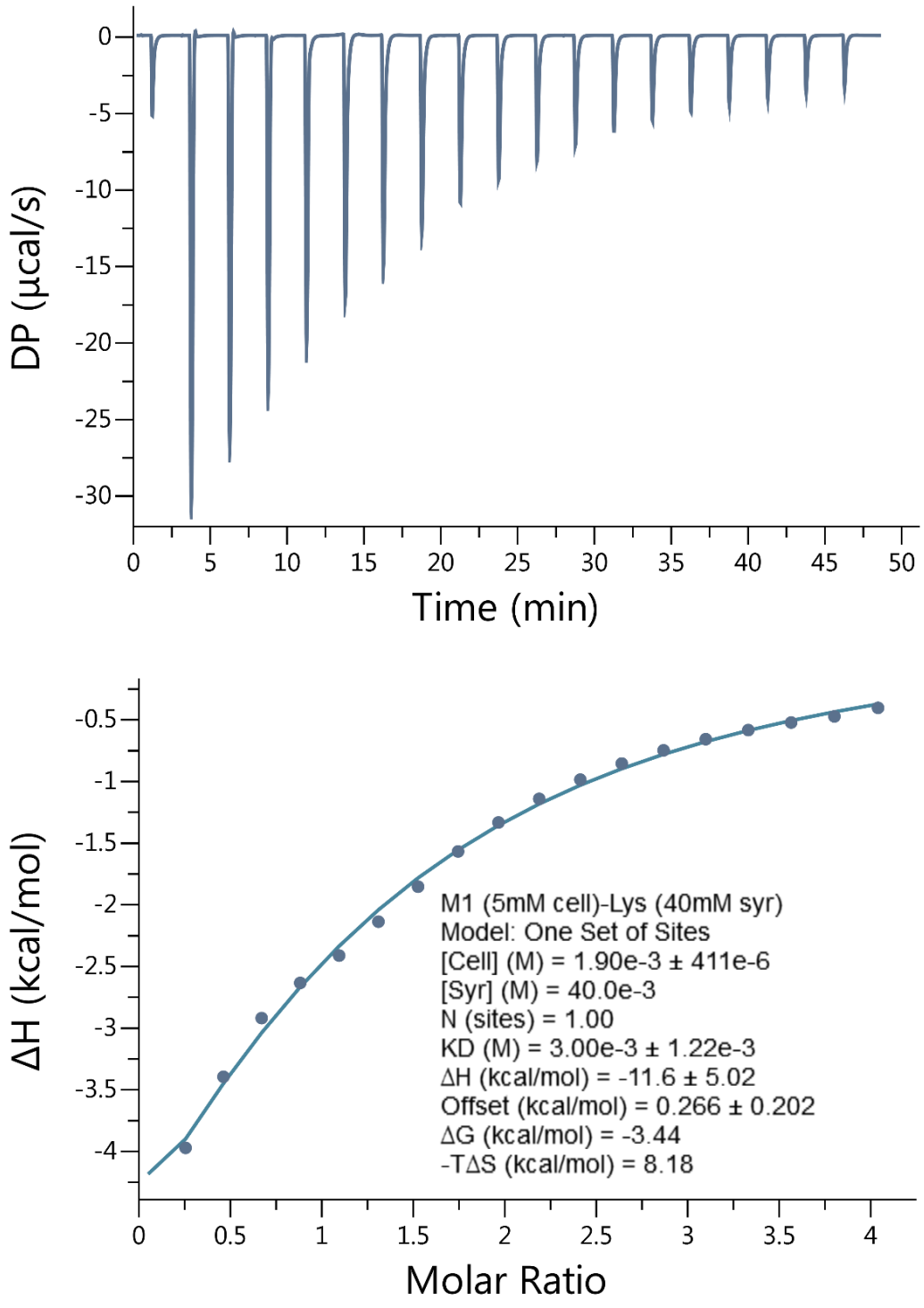

Figure II-S53. Isothermal Titration Calorimetry (ITC) curve obtained when a solution of Motor 1 (5.00 mM) in the cell was titrated with Lysine (40.0 mM) in the syringe at 298.0 K in 20 mM sodium phosphate buffered water at pH 7.4. K_a = 333.3 M^{-1}

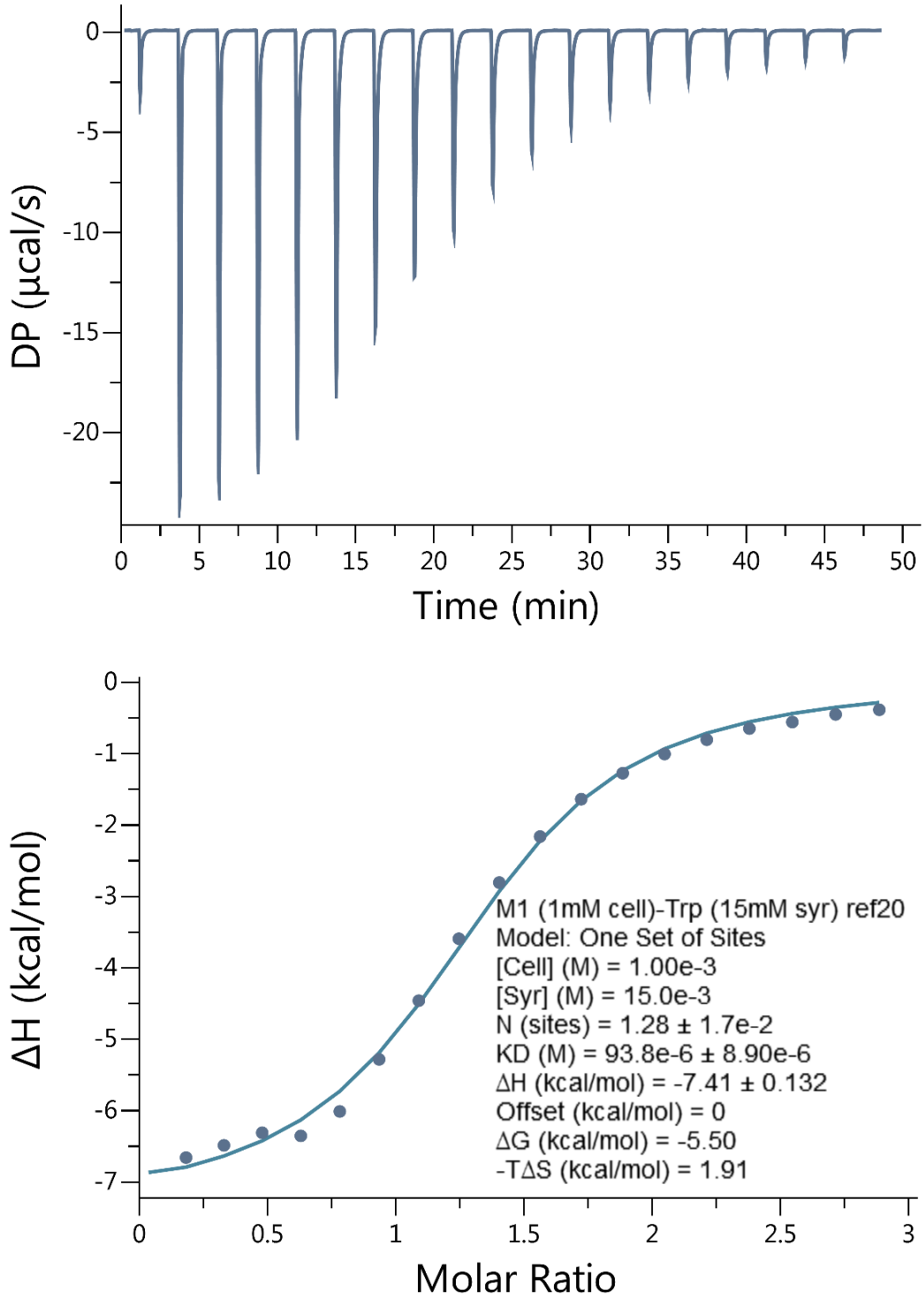

Figure II-S54. Isothermal Titration Calorimetry (ITC) curve obtained when a solution of Motor 1 (1.00 mM) in the cell was titrated with Tryptophan (15.00 mM) in the syringe at 298.0 K in 20 mM sodium phosphate buffered water at pH 7.4. K_a = 1.06×10^4 M^{-1}

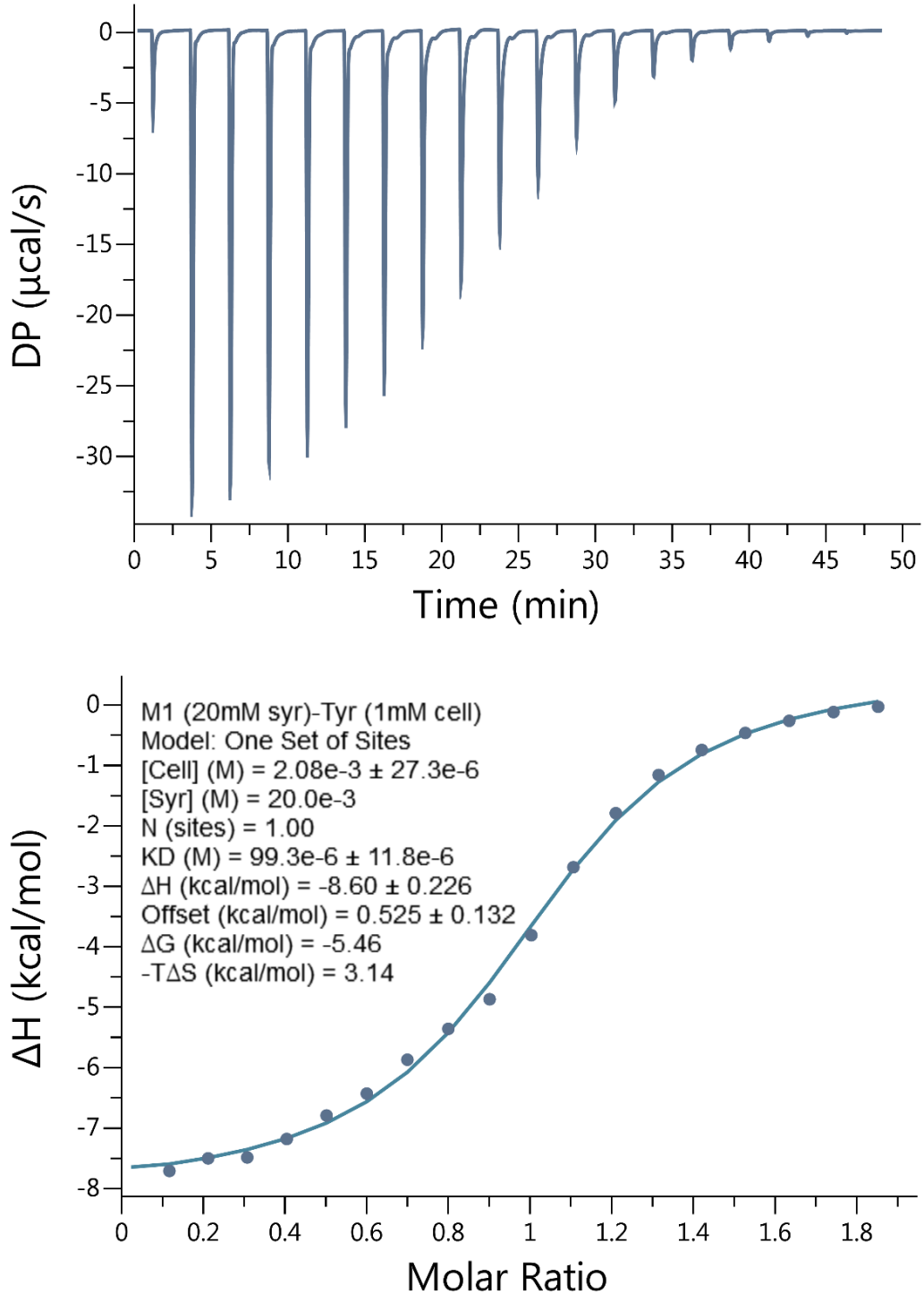

Figure II-S55. Isothermal Titration Calorimetry (ITC) curve obtained when a solution of Tyrosine (1.00 mM) in the cell was titrated with Motor 1 (20.0 mM) in the syringe at 298.0 K in 20 mM sodium phosphate buffered water at pH 7.4. $K_a = 1.01 \times 10^4\ M^{-1}$

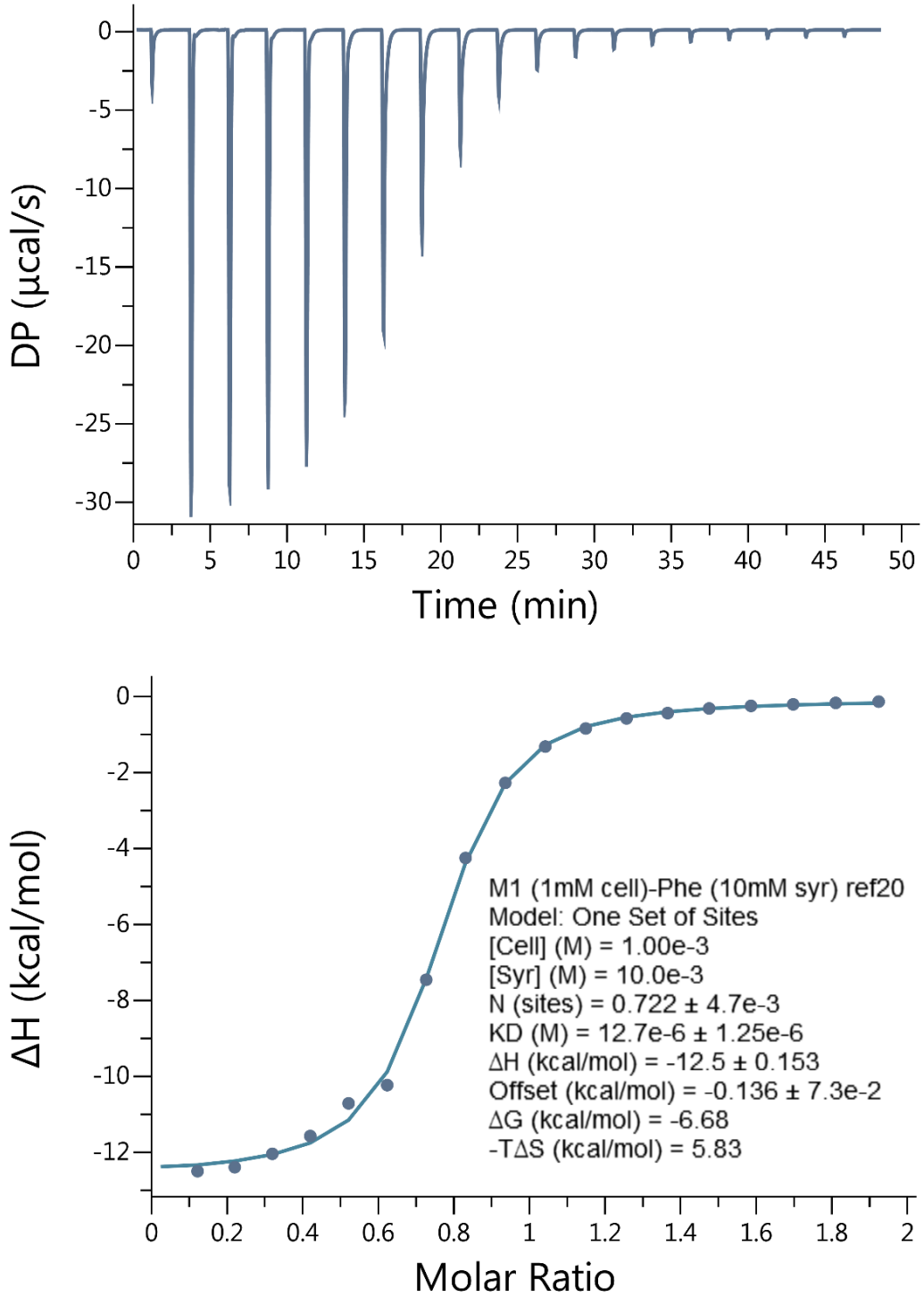

Figure II-S56. Isothermal Titration Calorimetry (ITC) curve obtained when a solution of Motor 1 (1.00 mM) in the cell was titrated with Phenylalanine (10.0 mM) in the syringe at 298.0 K in 20 mM sodium phosphate buffered water at pH 7.4. K_a = 7.87×10^4 M^{-1}

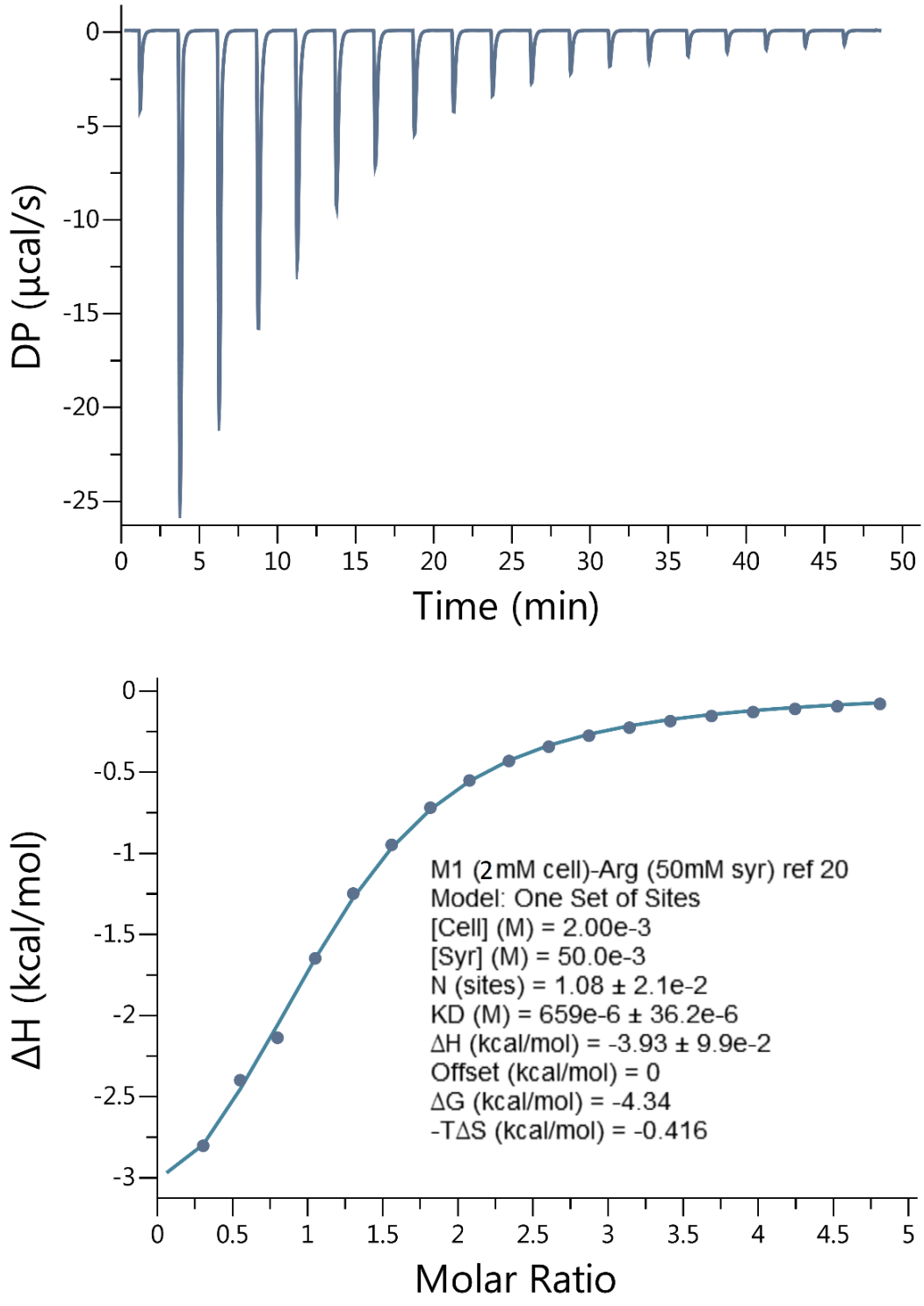

Figure II-S57. Isothermal Titration Calorimetry (ITC) curve obtained when a solution of Motor 1 (2.00 mM) in the cell was titrated with Arginine (50.00 mM) in the syringe at 298.0 K in 20 mM sodium phosphate buffered water at pH 7.4. K_a = 1.51×10^3 M^{-1}

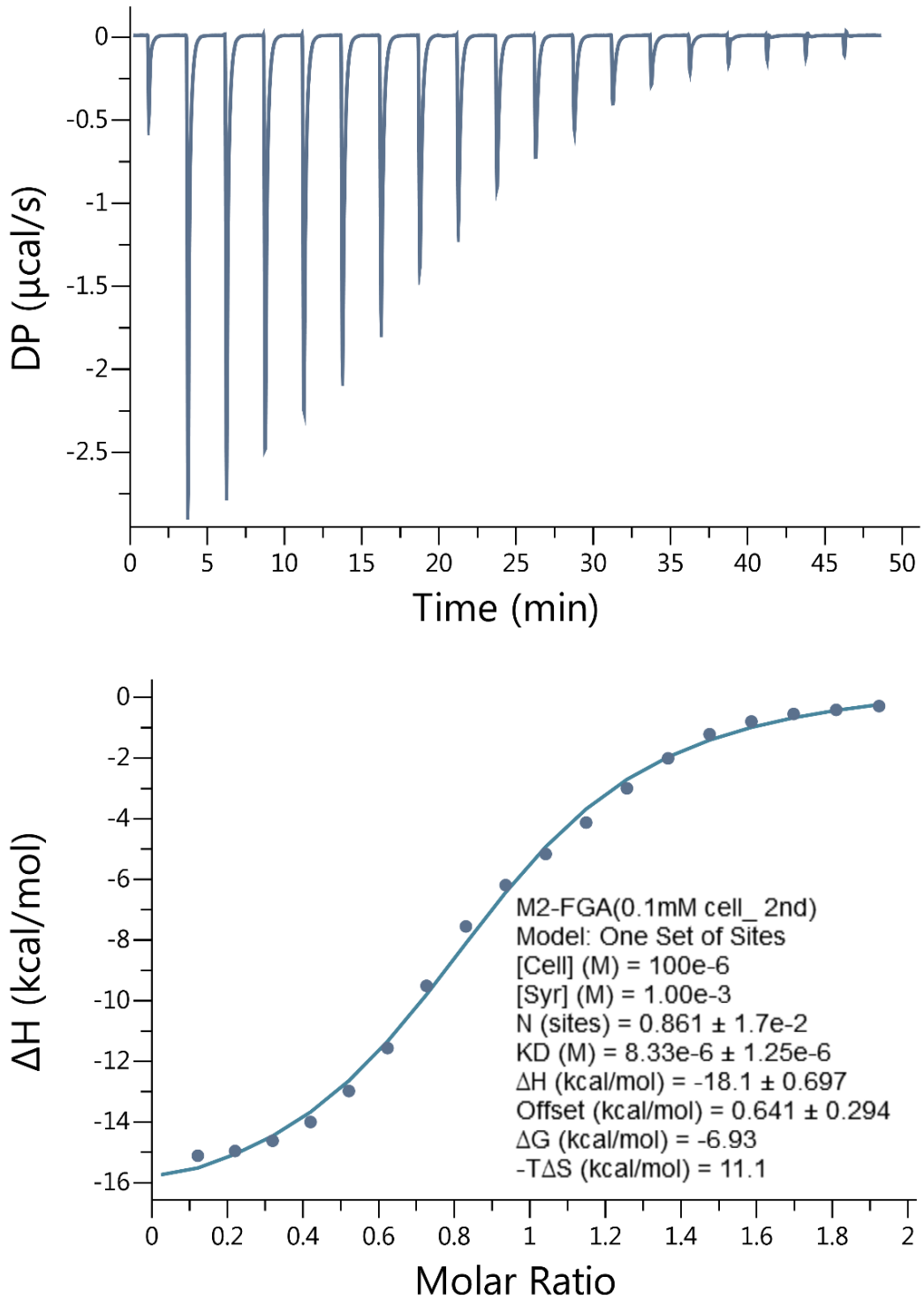

Figure II-S58. Isothermal Titration Calorimetry (ITC) curve obtained when a solution of H-Phe-Gly-Ala-NH_2 (100 µM) in the cell was titrated with Motor 2 (1.00 mM) in the syringe at 298.0 K in 20 mM sodium phosphate buffered water at pH 7.4. $K_a = 1.20 \times 10^5\ M^{-1}$

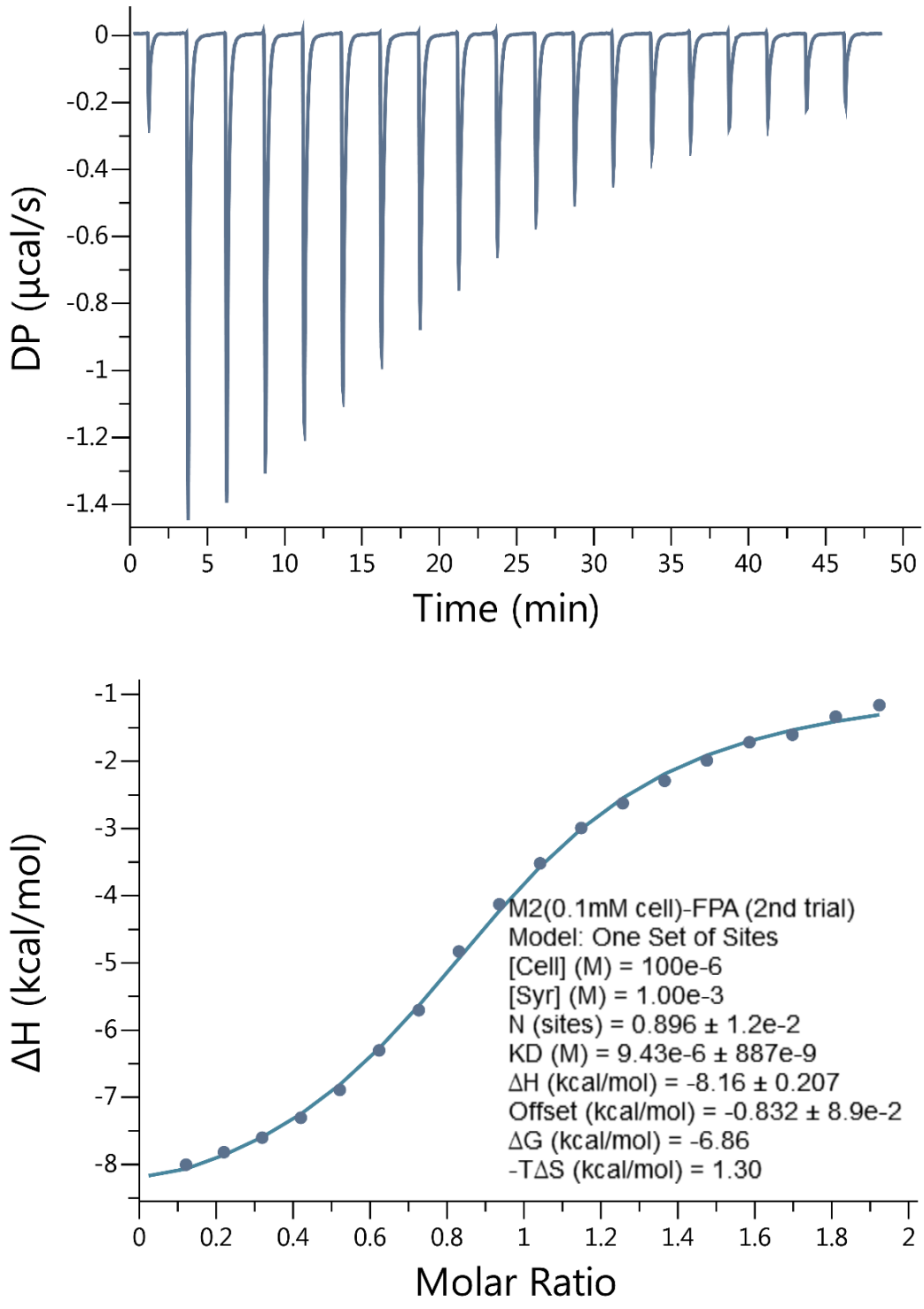

Figure II-S59. Isothermal Titration Calorimetry (ITC) curve obtained when a solution of Motor 2 (100 µM) in the cell was titrated with H-Phe-Pro-Ala-NH_2 (1.00 mM) in the syringe at 298.0 K in 20 mM sodium phosphate buffered water at pH 7.4. $K_a = 1.06 \times 10^5\ M^{-1}$

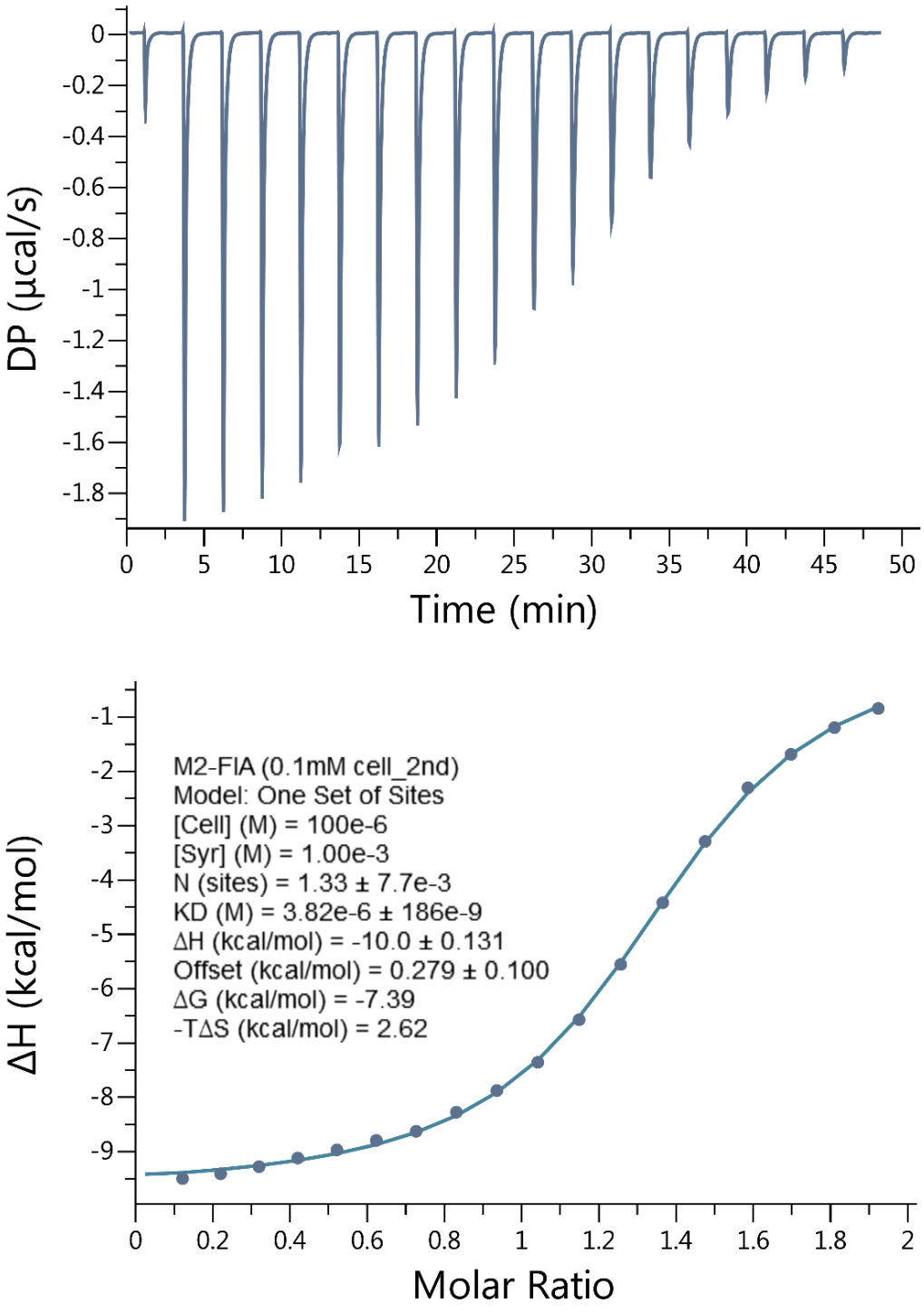

Figure II-S60. Isothermal Titration Calorimetry (ITC) curve obtained when a solution of H-Phe-Ile-Ala-NH_2 (100 µM) in the cell was titrated with Motor 2 (1.00 mM) in the syringe at 298.0 K in 20 mM sodium phosphate buffered water at pH 7.4. $K_a = 2.62 \times 10^5\ M^{-1}$

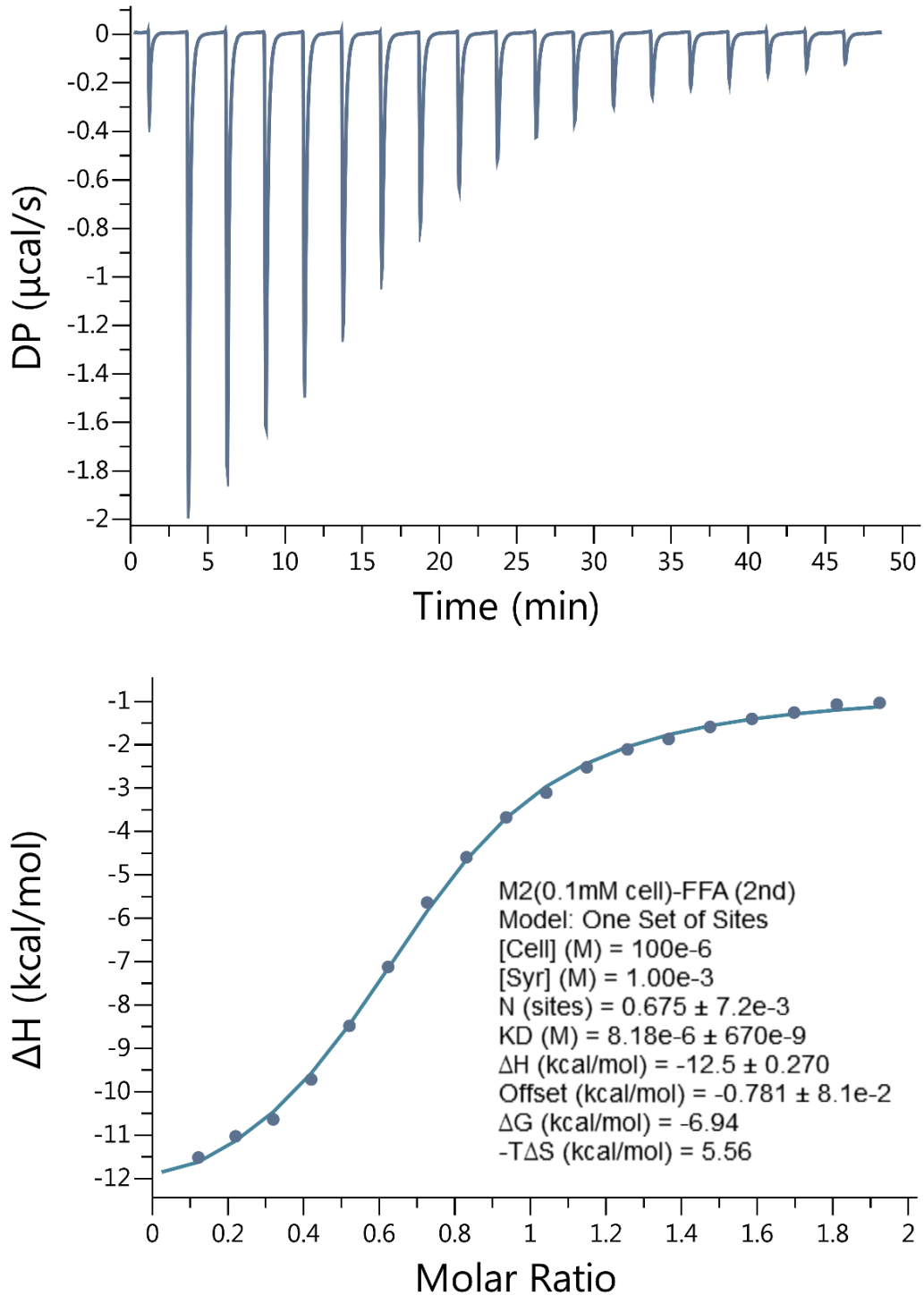

Figure II-S61. Isothermal Titration Calorimetry (ITC) curve obtained when a solution of Motor 2 (100 µM) in the cell was titrated with H-Phe-Phe-Ala-NH_2 (1.00 mM) in the syringe at 298.0 K in 20 mM sodium phosphate buffered water at pH 7.4. $K_a = 1.22 \times 10^5\ M^{-1}$

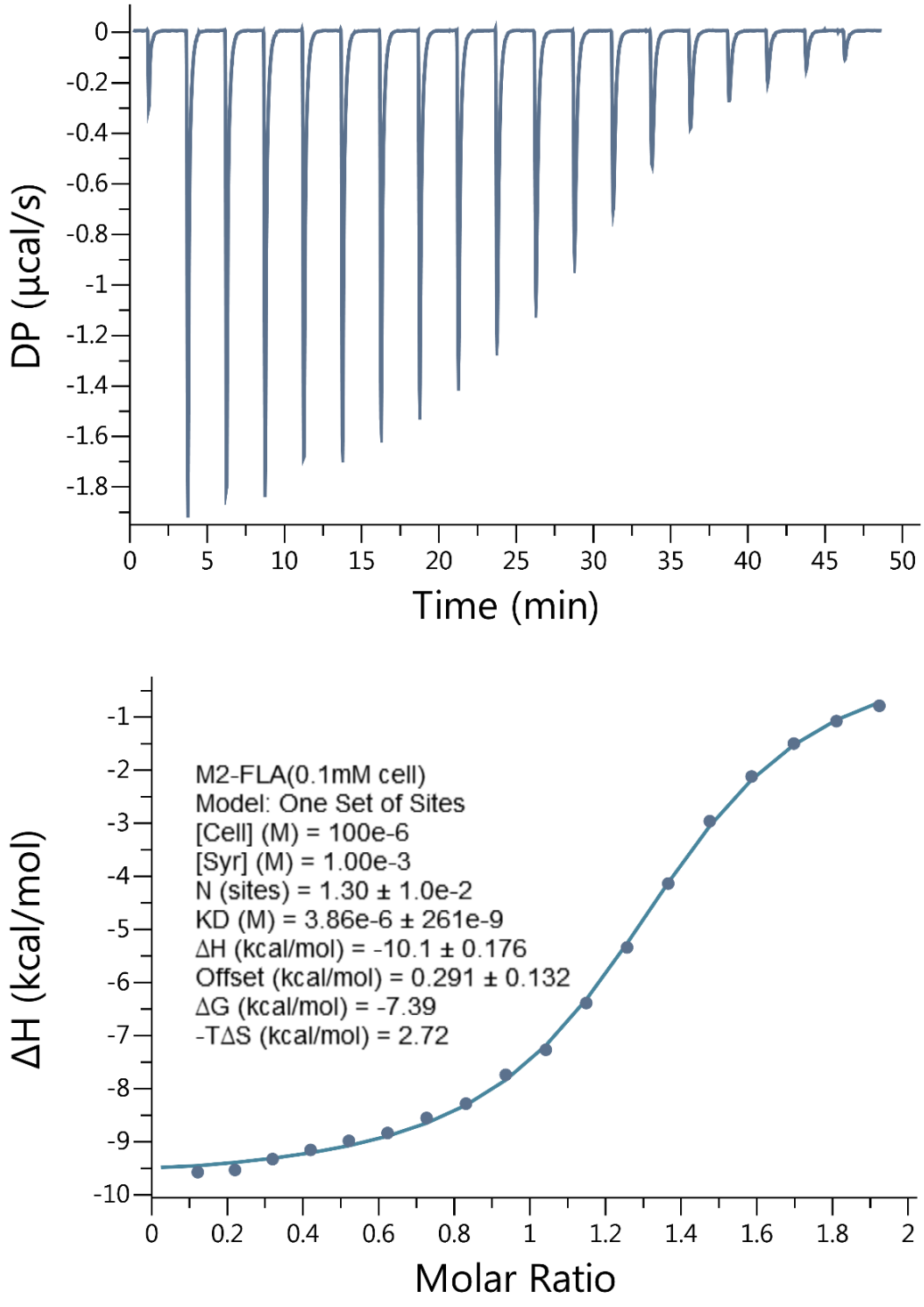

Figure II-S62. Isothermal Titration Calorimetry (ITC) curve obtained when a solution of H-Phe-Leu-Ala-NH_2 (100 µM) in the cell was titrated with Motor 2 (1.00 mM) in the syringe at 298.0 K in 20 mM sodium phosphate buffered water at pH 7.4. $K_a = 2.59 \times 10^5\ M^{-1}$

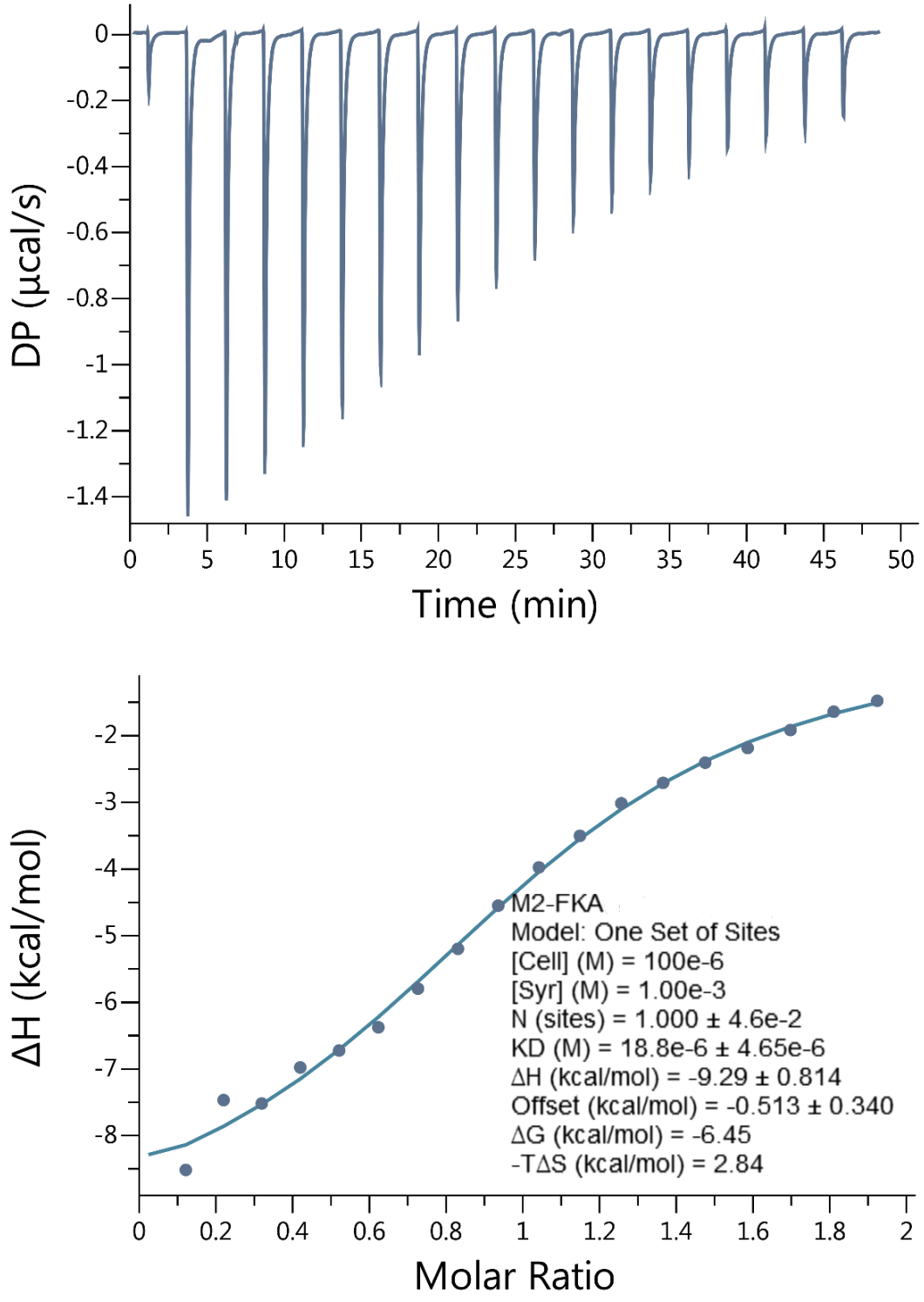

Figure II-S63. Isothermal Titration Calorimetry (ITC) curve obtained when a solution of H-Phe-Lys-Ala-NH_2 (100 µM) in the cell was titrated with Motor 2 (1.00 mM) in the syringe at 298.0 K in 20 mM sodium phosphate buffered water at pH 7.4. $K_a = 5.32 \times 10^4\ M^{-1}$

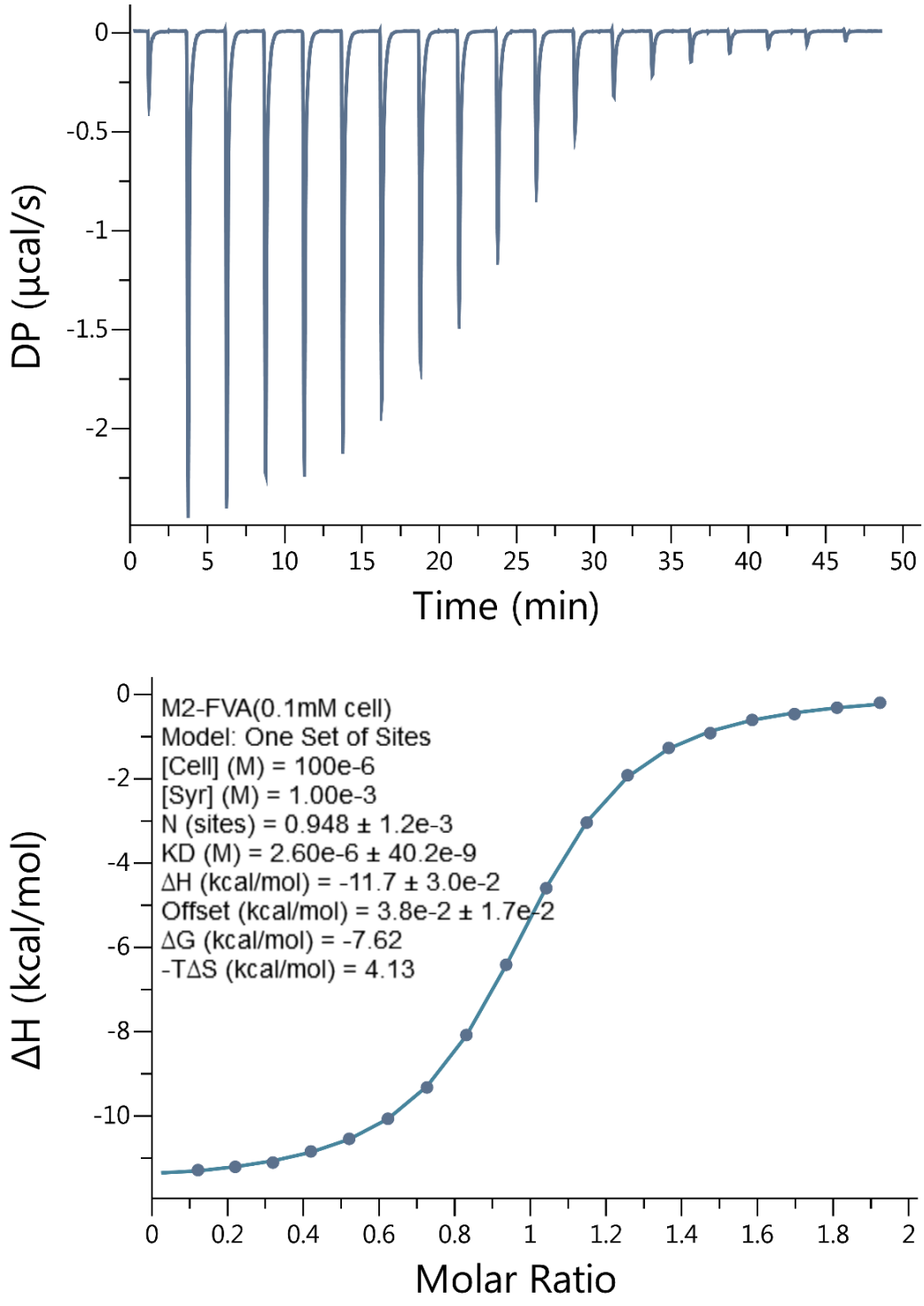

Figure II-S64. Isothermal Titration Calorimetry (ITC) curve obtained when a solution of H-Phe-Val-Ala-NH_2 (100 µM) in the cell was titrated with Motor 2 (1.00 mM) in the syringe at 298.0 K in 20 mM sodium phosphate buffered water at pH 7.4. $K_a = 3.84 \times 10^5\ M^{-1}$

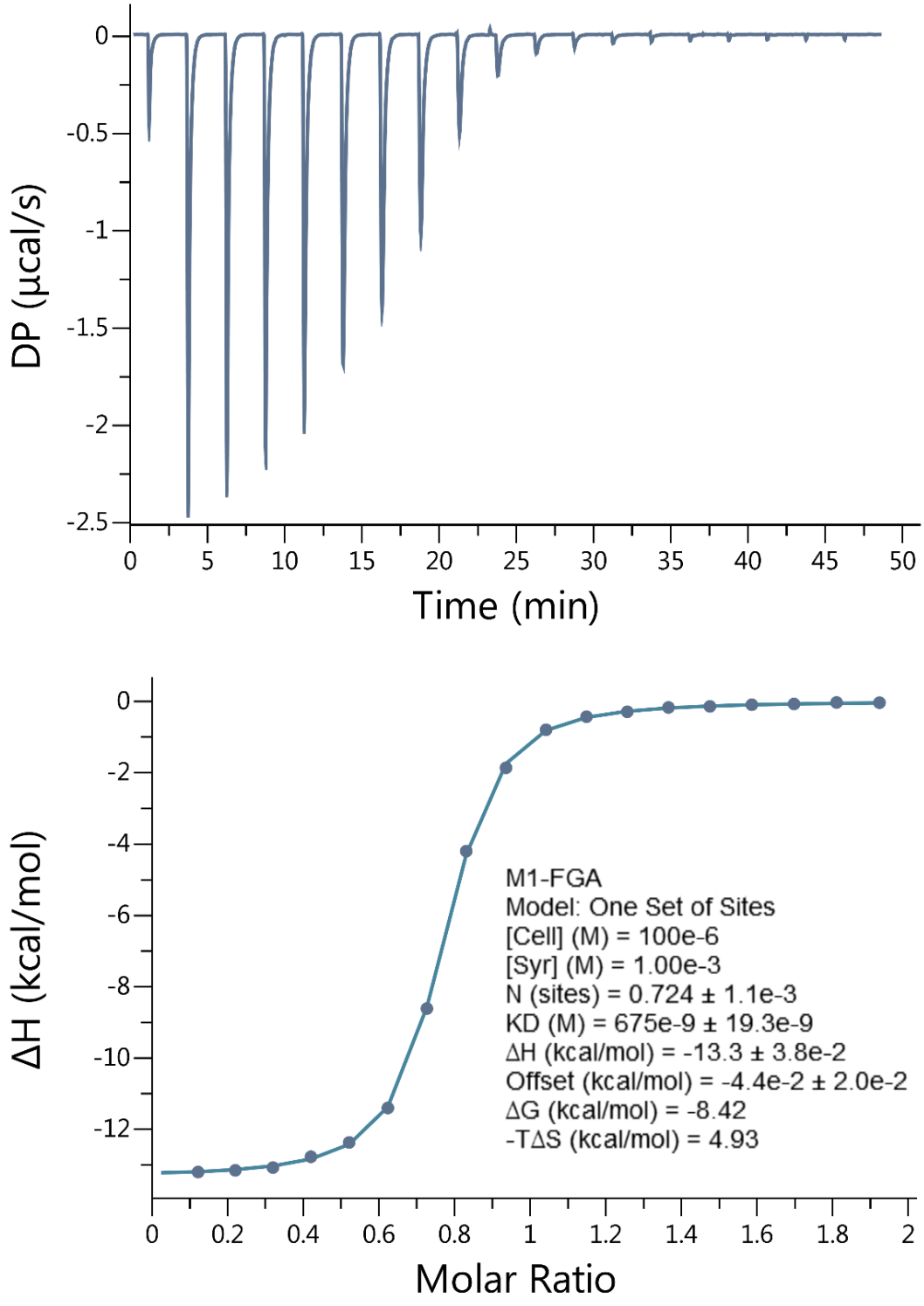

Figure II-S65. Isothermal Titration Calorimetry (ITC) curve obtained when a solution of H-Phe-Gly-Ala-NH_2 (100 µM) in the cell was titrated with Motor 1 (1.00 mM) in the syringe at 298.0 K in 20 mM sodium phosphate buffered water at pH 7.4. $K_a = 1.48 \times 10^6\ M^{-1}$

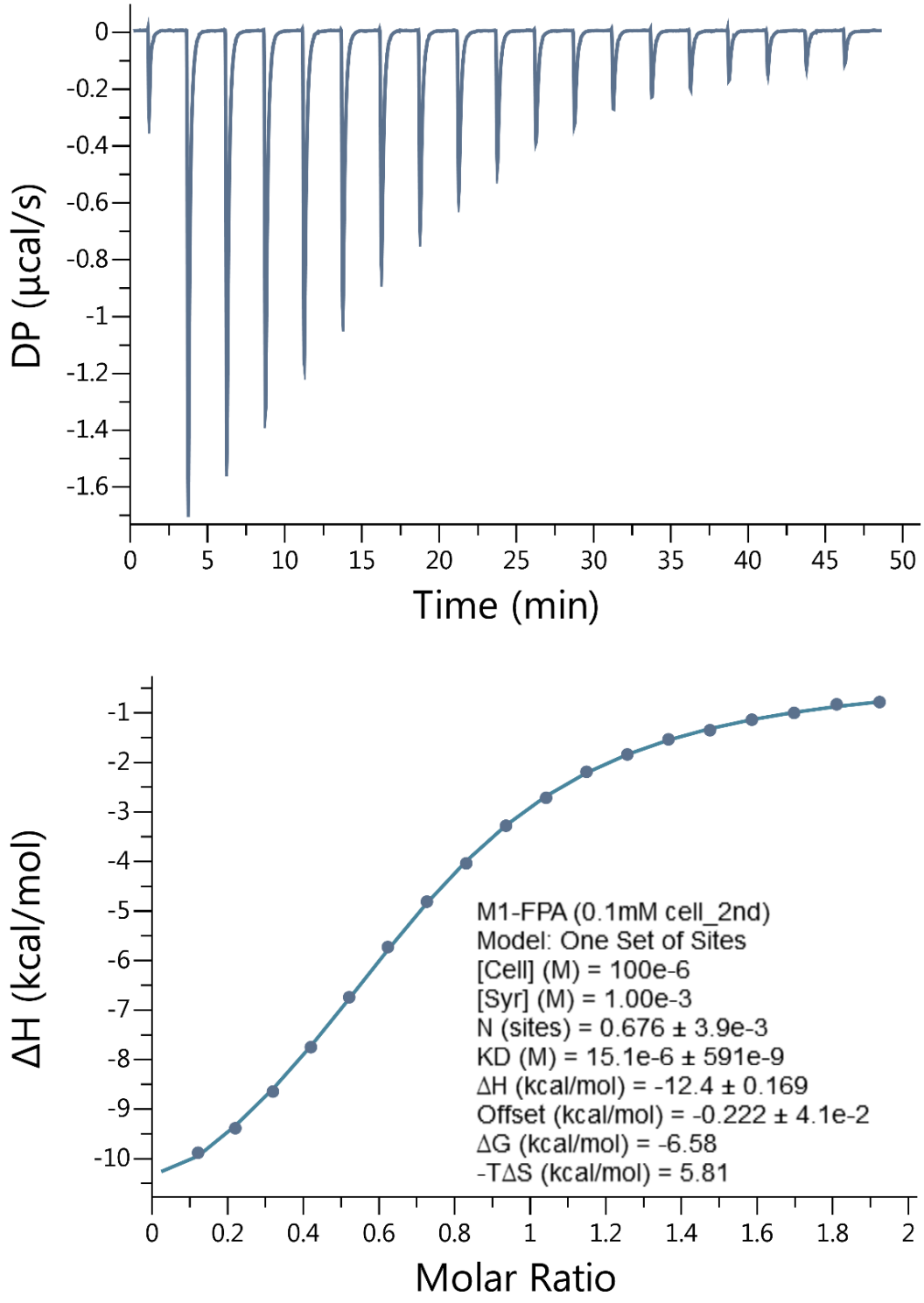

Figure II-S66. Isothermal Titration Calorimetry (ITC) curve obtained when a solution of H-Phe-Pro-Ala-NH_2 (100 µM) in the cell was titrated with Motor 1 (1.00 mM) in the syringe at 298.0 K in 20 mM sodium phosphate buffered water at pH 7.4. $K_a = 6.62 \times 10^4\ M^{-1}$

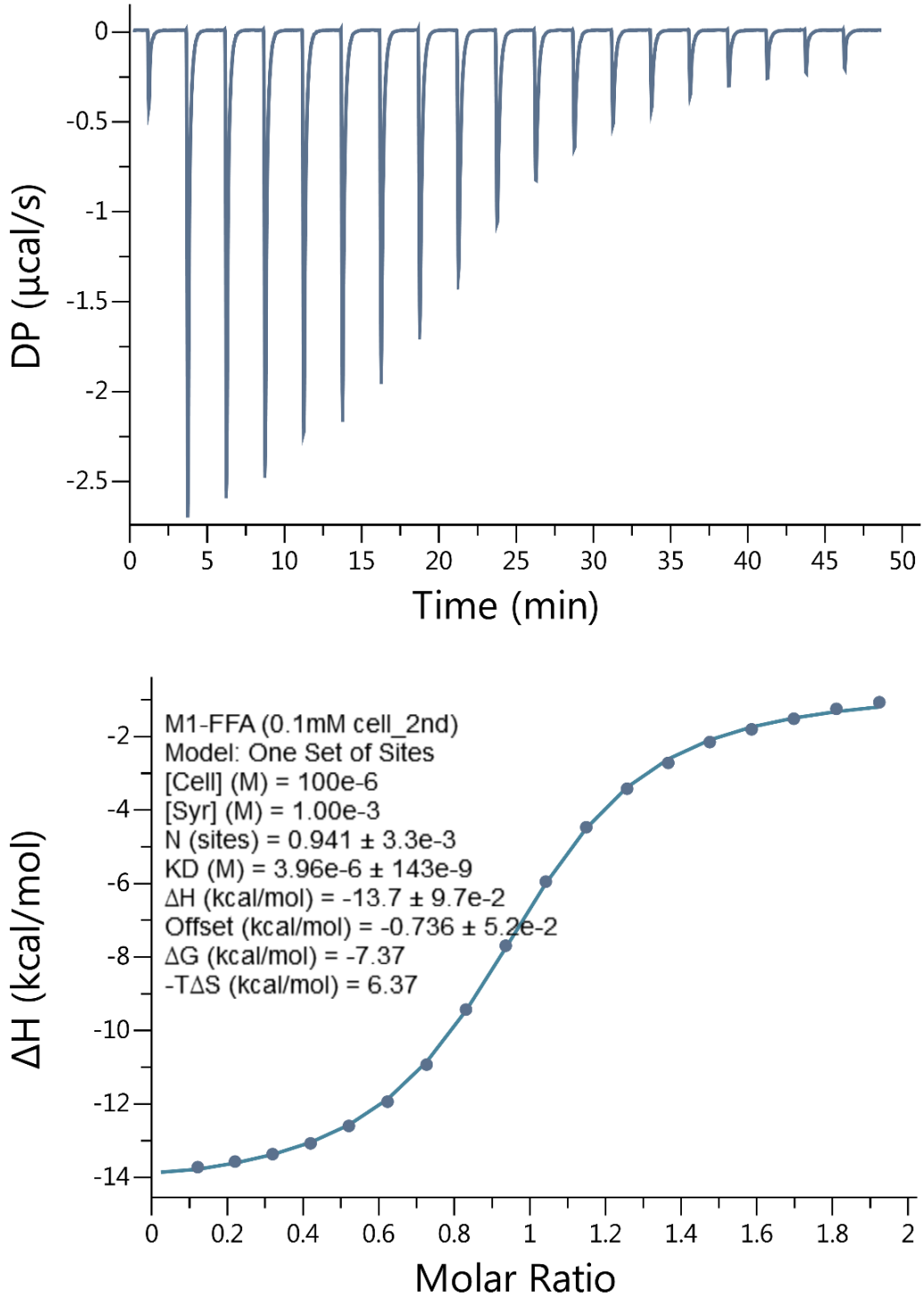

Figure II-S67. Isothermal Titration Calorimetry (ITC) curve obtained when a solution of H-Phe-Phe-Ala-NH_2 (100 µM) in the cell was titrated with Motor 1 (1.00 mM) in the syringe at 298.0 K in 20 mM sodium phosphate buffered water at pH 7.4. $K_a = 2.52 \times 10^5\ M^{-1}$

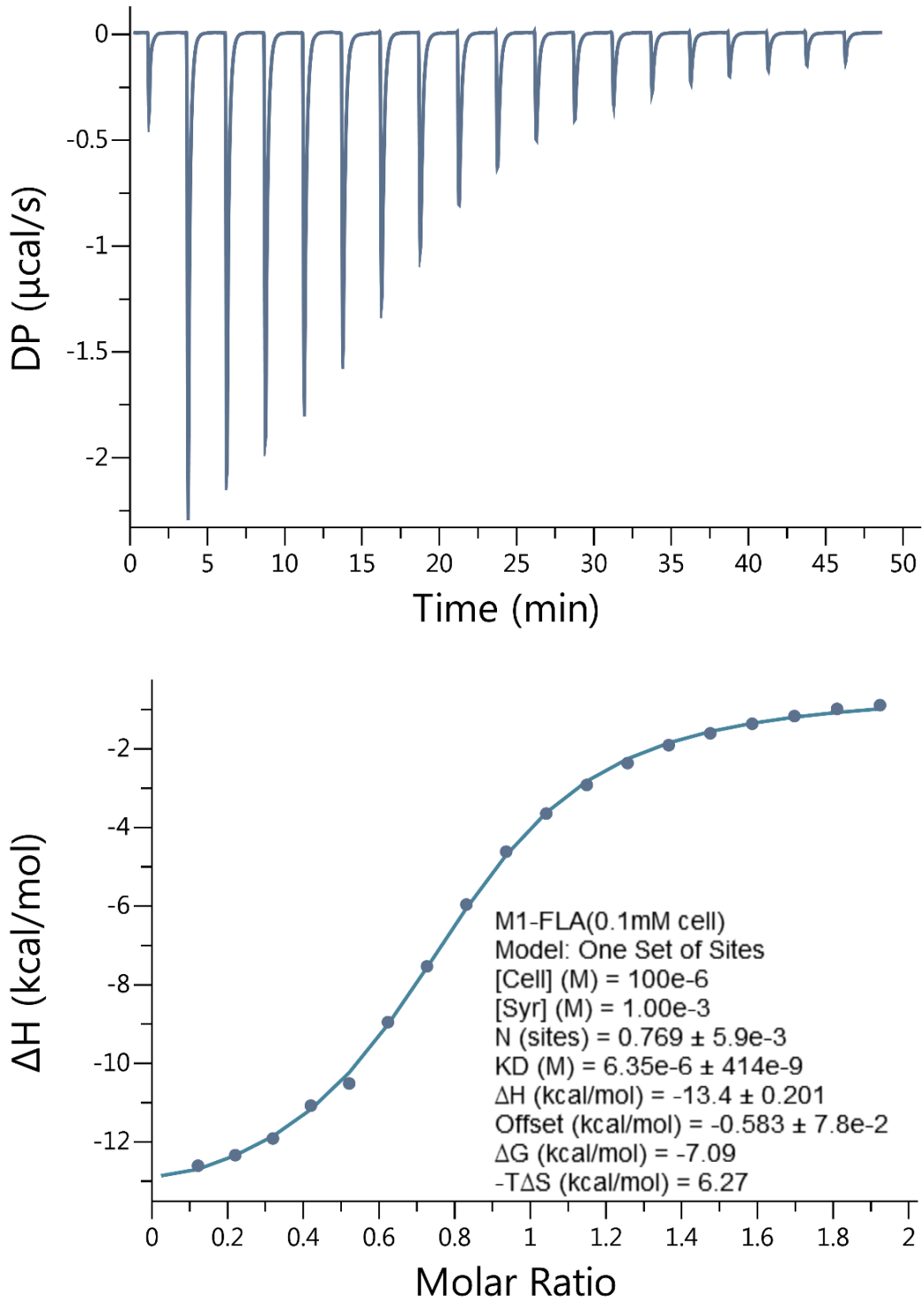

Figure II-S68. Isothermal Titration Calorimetry (ITC) curve obtained when a solution of H-Phe-Leu-Ala-NH_2 (100 µM) in the cell was titrated with Motor 1 (1.00 mM) in the syringe at 298.0 K in 20 mM sodium phosphate buffered water at pH 7.4. $K_a = 1.57 \times 10^5\ M^{-1}$

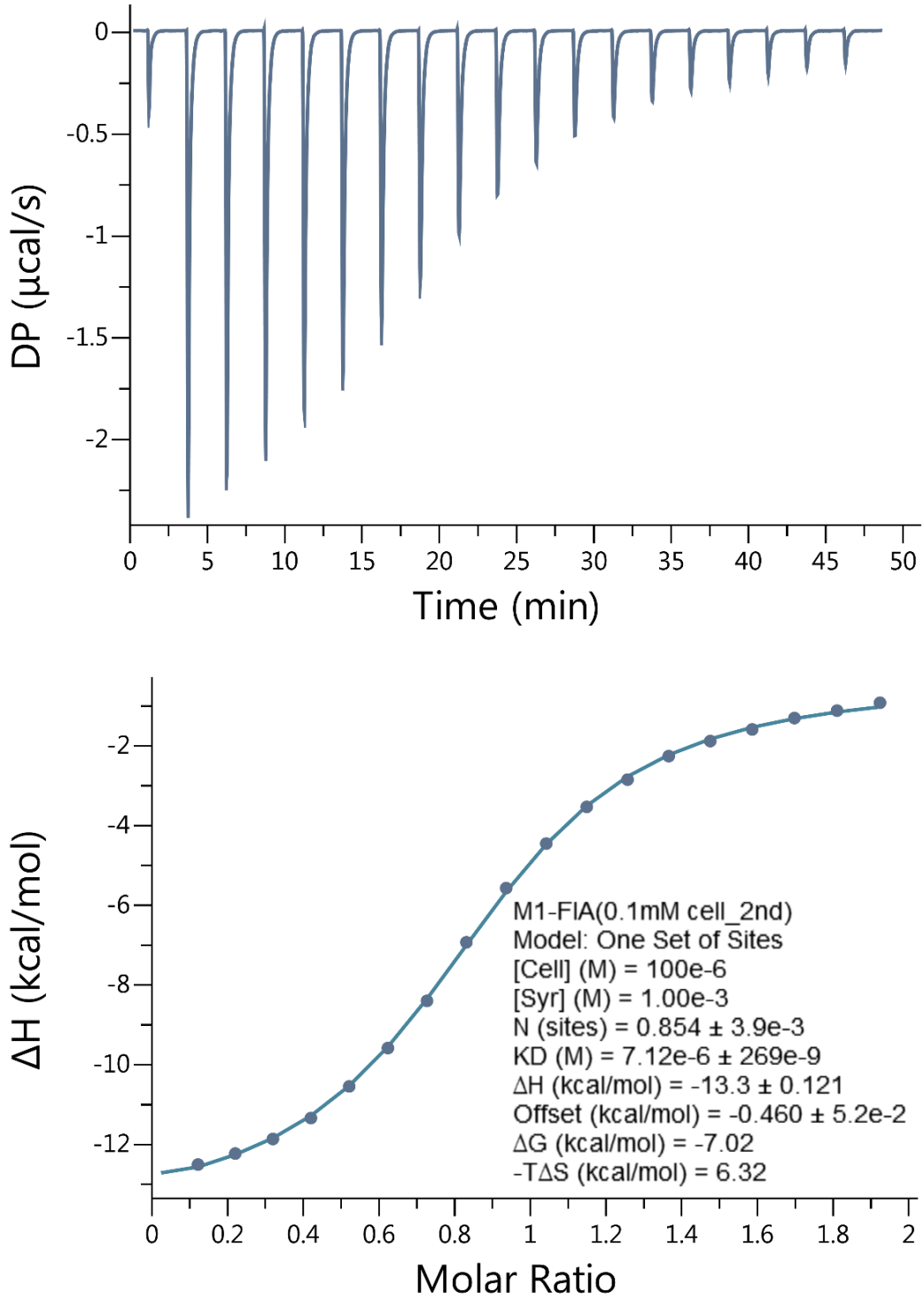

Figure II-S69. Isothermal Titration Calorimetry (ITC) curve obtained when a solution of H-Phe-Ile-Ala-NH_2 (100 µM) in the cell was titrated with Motor 1 (1.00 mM) in the syringe at 298.0 K in 20 mM sodium phosphate buffered water at pH 7.4. $K_a = 1.40 \times 10^5\ M^{-1}$

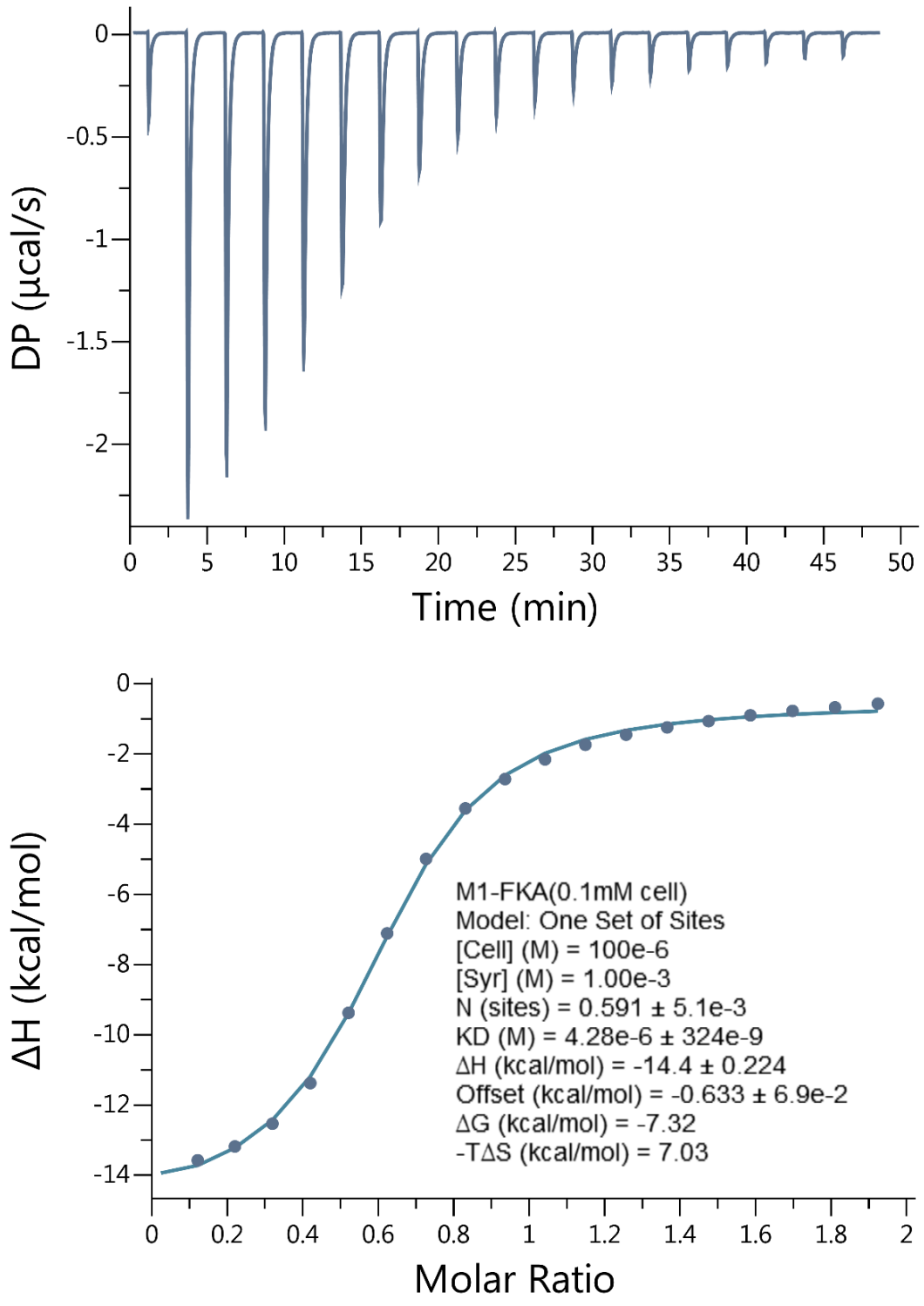

Figure II-S70. Isothermal Titration Calorimetry (ITC) curve obtained when a solution of H-Phe-Lys-Ala-NH_2 (100 µM) in the cell was titrated with Motor 1 (1.00 mM) in the syringe at 298.0 K in 20 mM sodium phosphate buffered water at pH 7.4. $K_a = 2.33 \times 10^5\ M^{-1}$

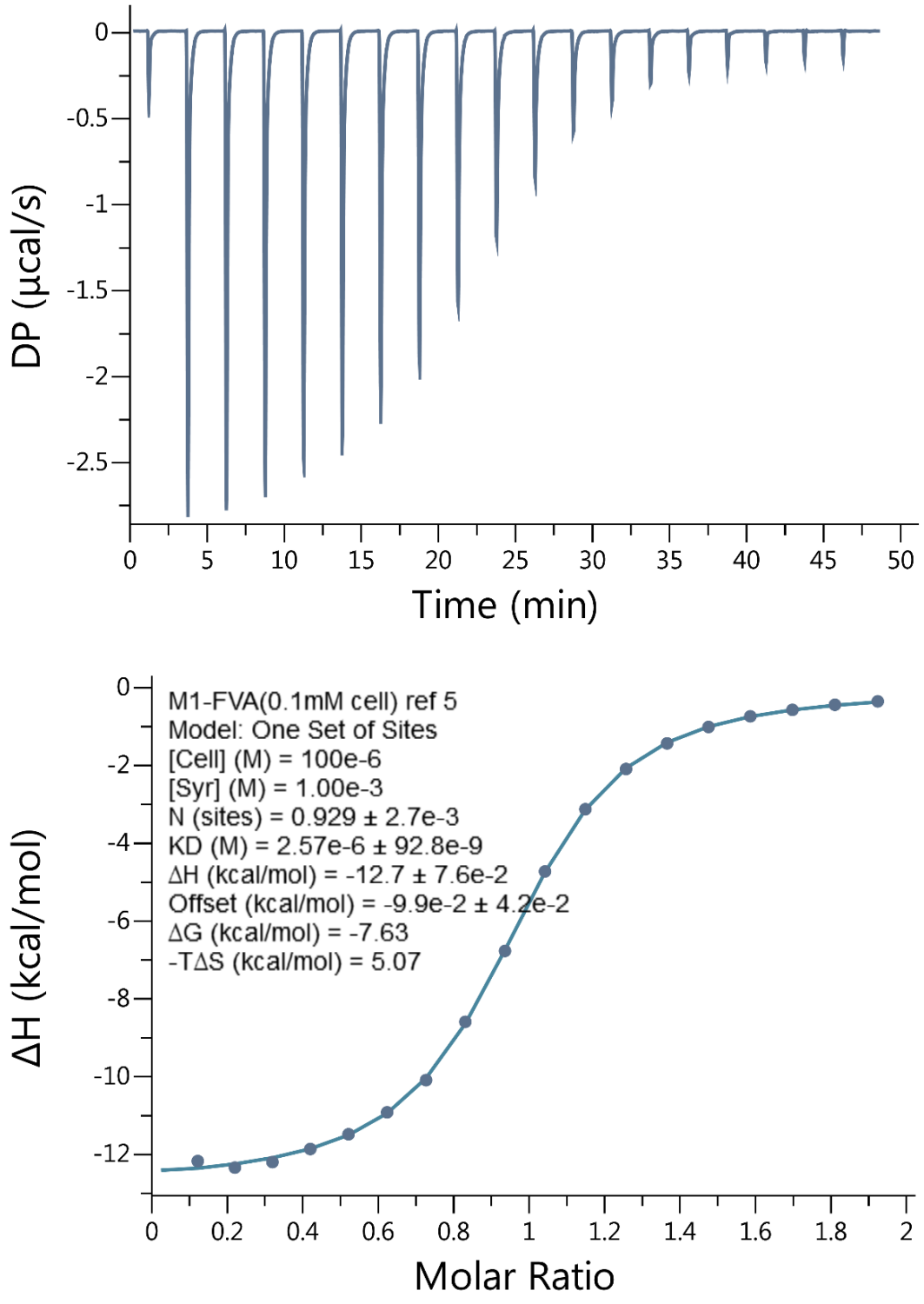

Figure II-S71. Isothermal Titration Calorimetry (ITC) curve obtained when a solution of H-Phe-Val-Ala-NH2 (100 µM) in the cell was titrated with Motor 1 (1.00 mM) in the syringe at 298.0 K in 20 mM sodium phosphate buffered water at pH 7.4. $K_a = 3.89 \times 10^5\ M^{-1}$

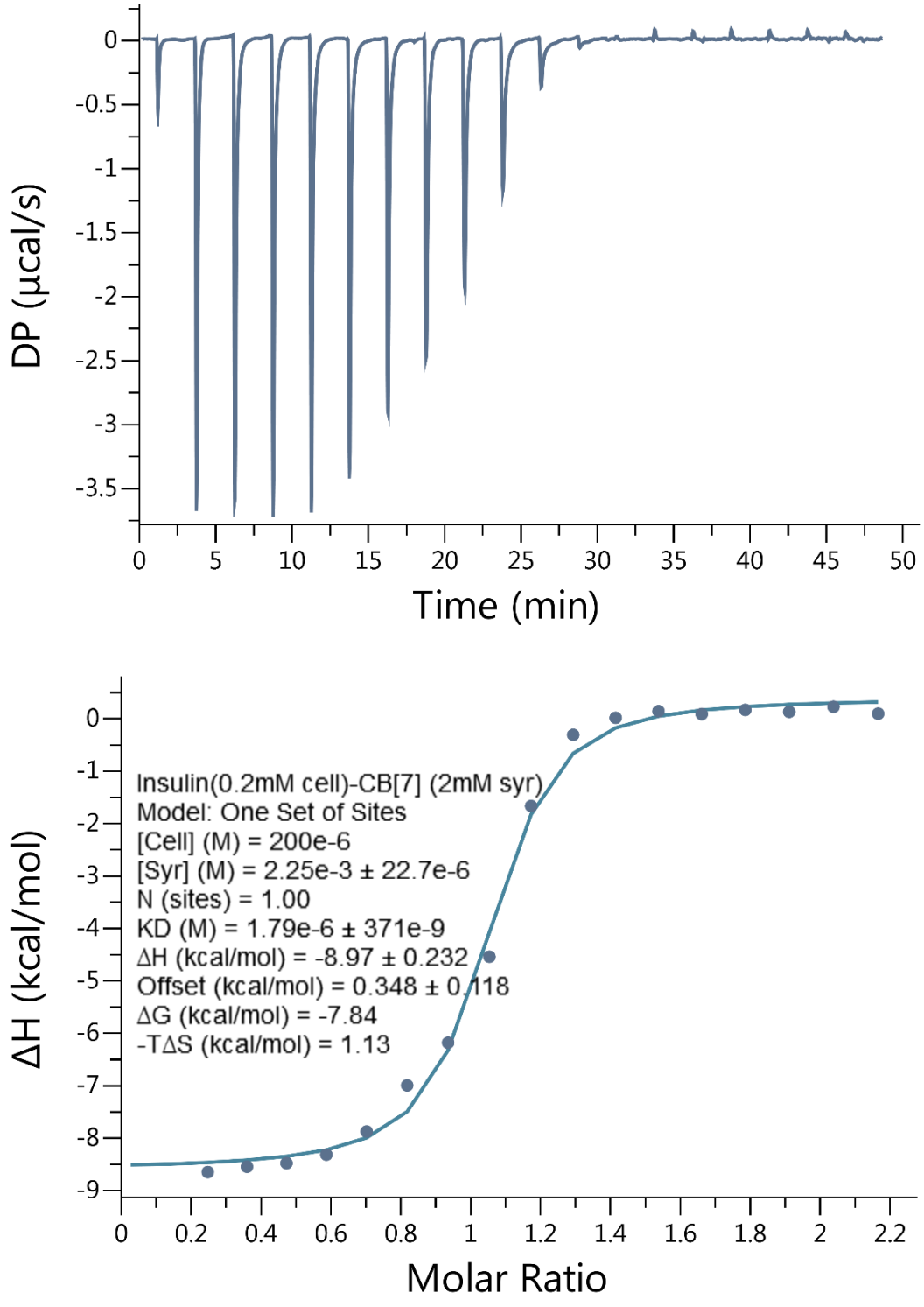

Figure II-S72. Isothermal Titration Calorimetry (ITC) curve obtained when a solution of Insulin (200 µM) in the cell was titrated with CB [7] (2.00 mM) in the syringe at 298.0 K in 20 mM sodium phosphate buffered water at pH 7.4 containing 4 mM EDTA. $K_a = 5.59 \times 10^5\ M^{-1}$

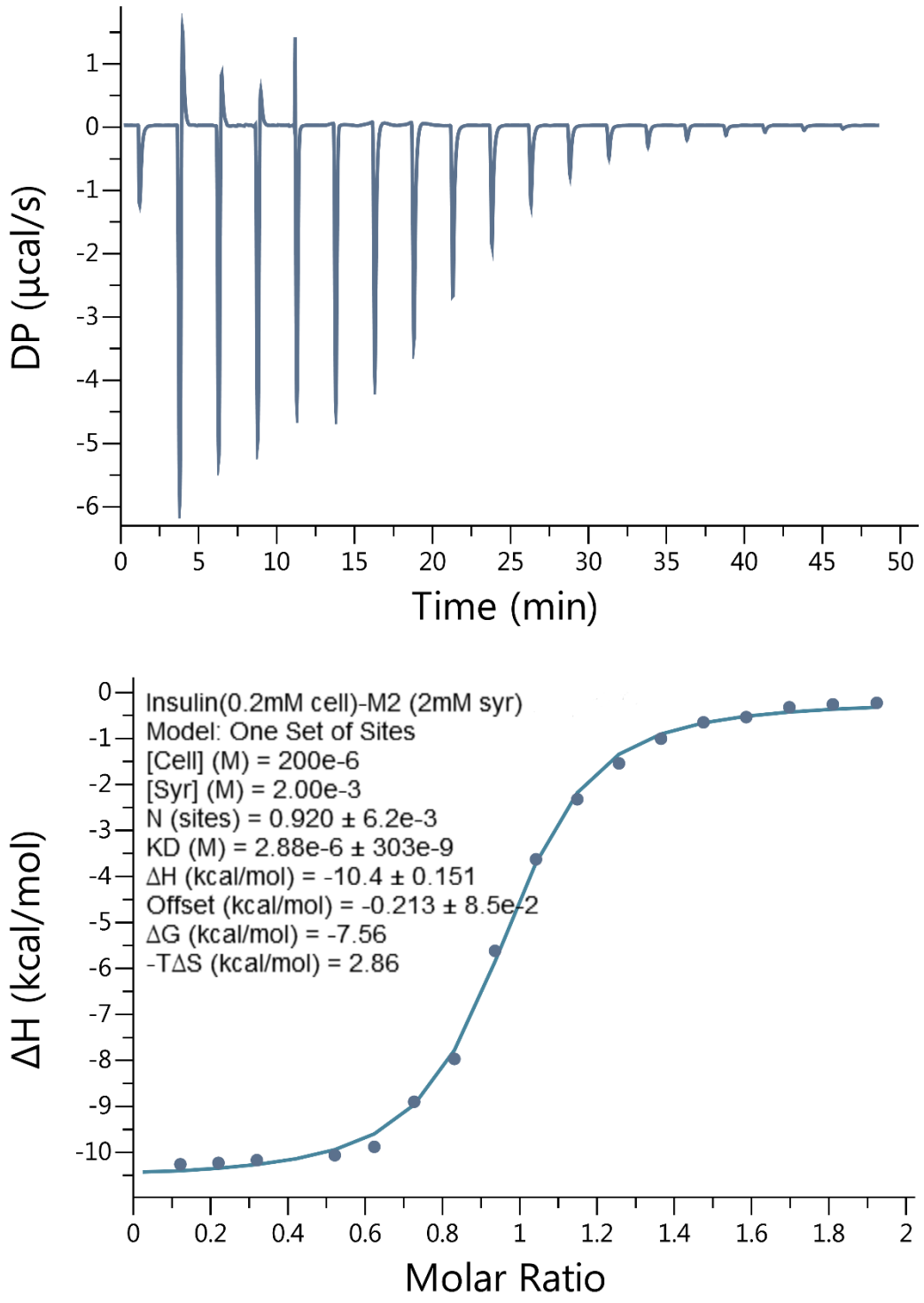

Figure II-S73. Isothermal Titration Calorimetry (ITC) curve obtained when a solution of Insulin (200 µM) in the cell was titrated with Motor 2 (2.00 mM) in the syringe at 298.0 K in 20 mM sodium phosphate buffered water at pH 7.4 containing 4mM EDTA. $K_a = 3.47 \times 10^5\ M^{-1}$

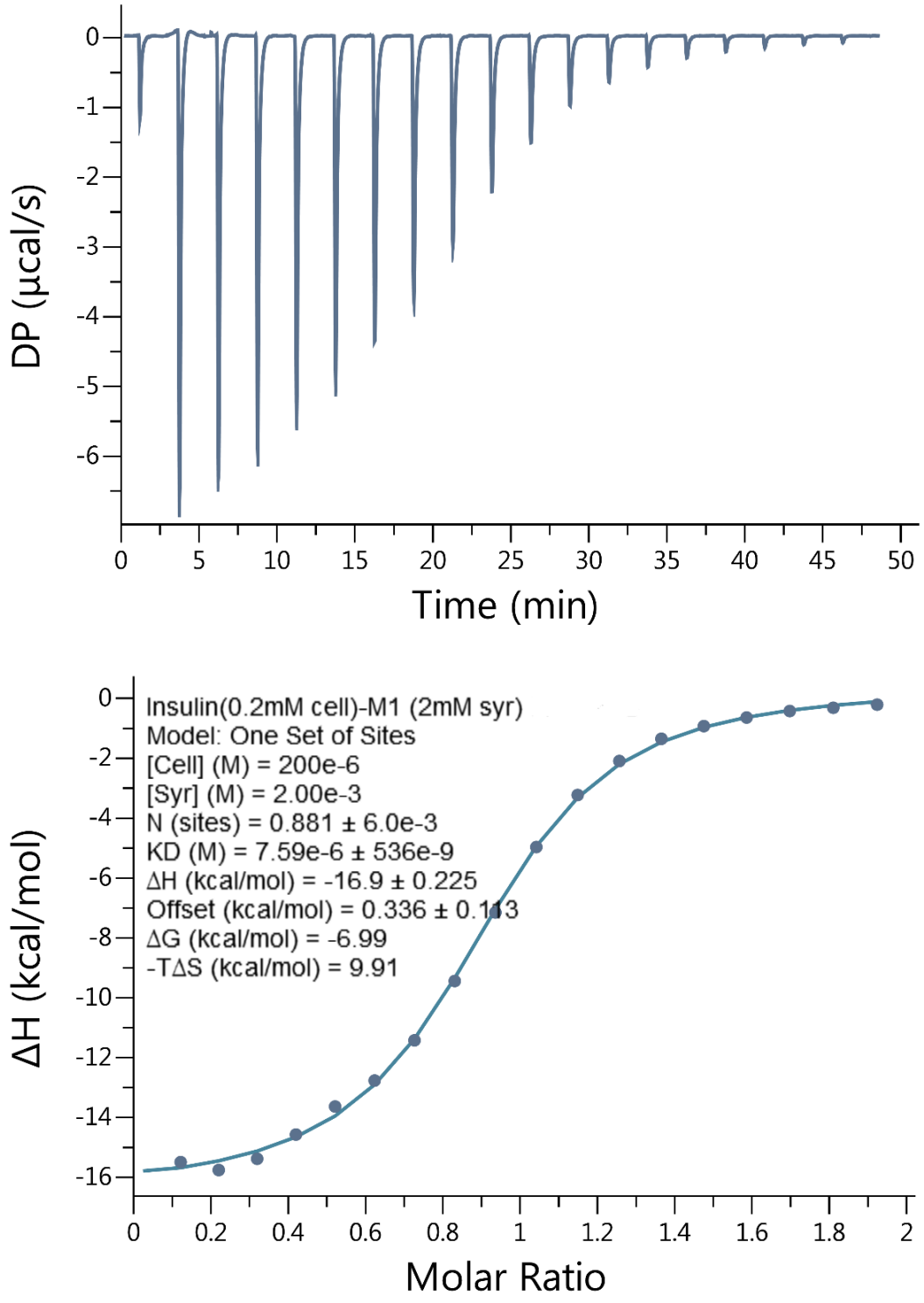

Figure II-S74. Isothermal Titration Calorimetry (ITC) curve obtained when a solution of Insulin (200 µM) in the cell was titrated with Motor 1 (2.00 mM) in the syringe at 298.0 K in 20 mM sodium phosphate buffered water at pH 7.4 containing 4mM EDTA. $K_a = 1.32 \times 10^5\ M^{-1}$

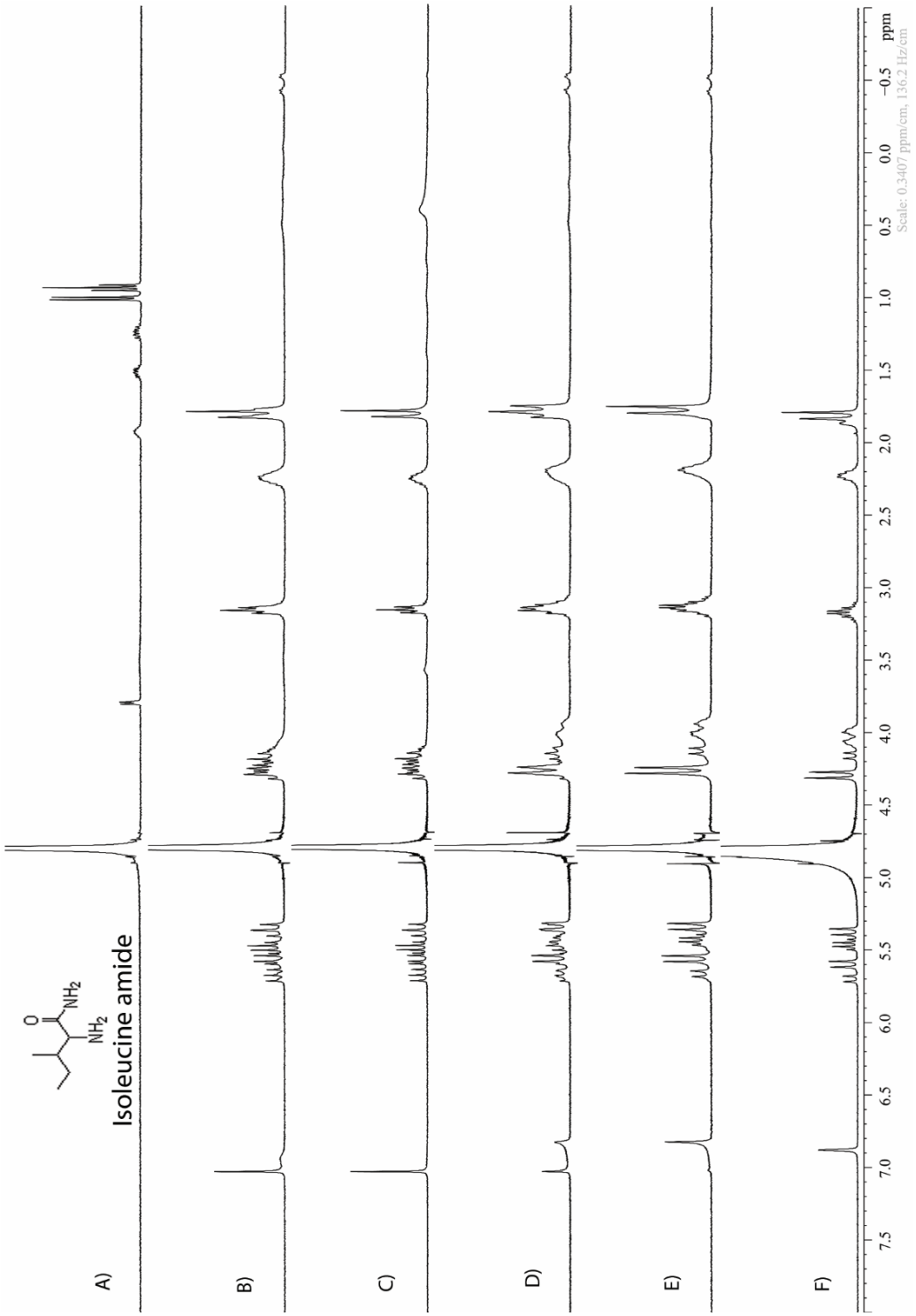

Figure II-S75. ^{1}H NMR spectra recorded (D_2O, 400 MHz, RT) for: a) Isoleucine amide (2 mM), b) a mixture of Motor 1 (1 mM) and Isoleucine amide (2 mM), c) a mixture of Motor 1 (1 mM) and Isoleucine amide (1.5 mM), d) a mixture of Motor 1 (1 mM) and Isoleucine amide (1 mM), e) a mixture of Motor 1 (1 mM) and Isoleucine amide (0.5 mM), f) Motor 1 (1mM).

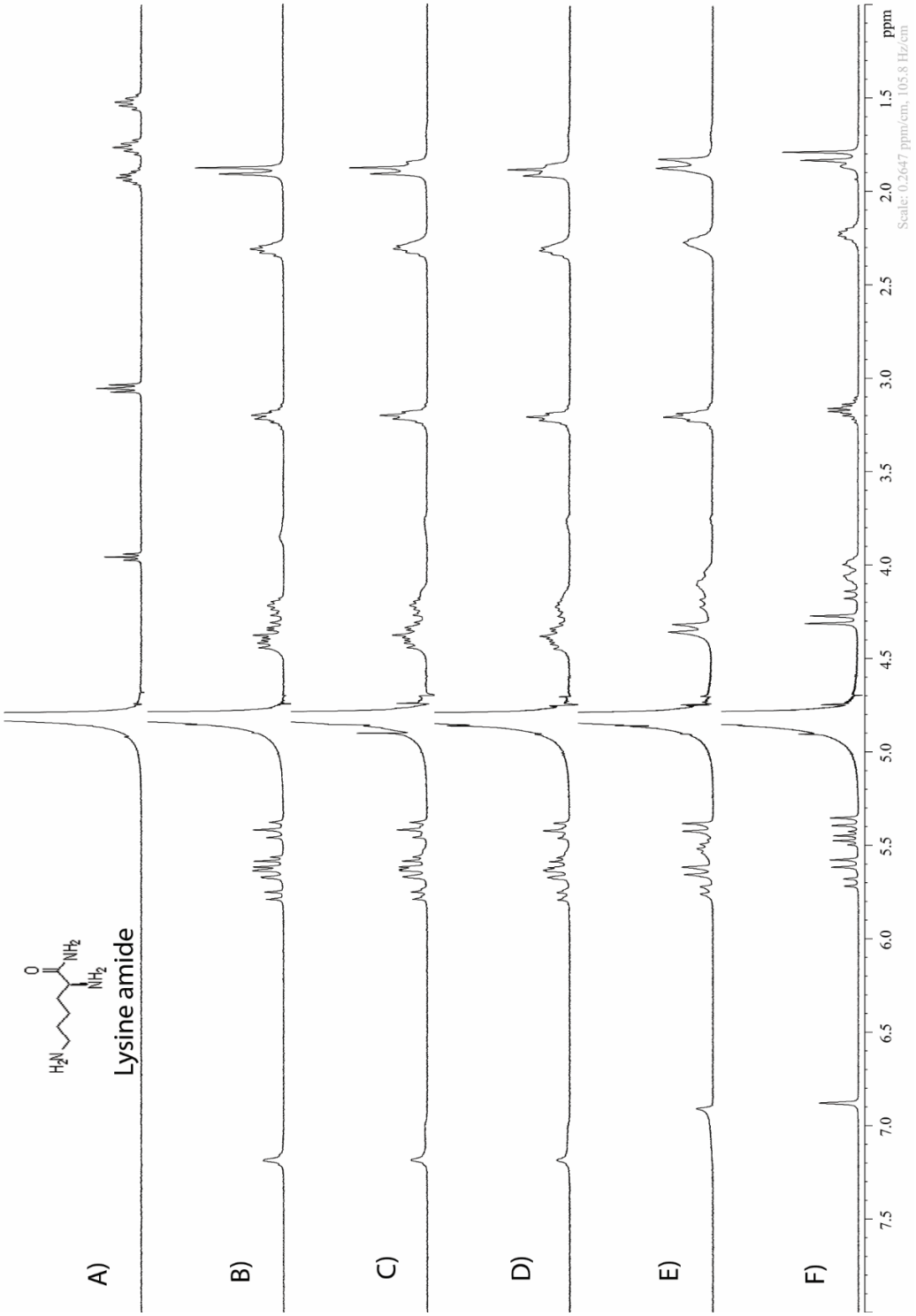

Figure II-S76. ^{1}H NMR spectra recorded (D_2O, 400 MHz, RT) for: a) Lysine amide (2 mM), b) a mixture of Motor 1 (1 mM) and Lysine amide (2 mM), c) a mixture of Motor 1 (1 mM) and Lysine amide (1.5 mM), d) a mixture of Motor 1 (1 mM) and Lysine amide (1 mM), e) a mixture Motor 1 (1 mM) and Lysine amide (0.5 mM), f) Motor 1 (1 mM).

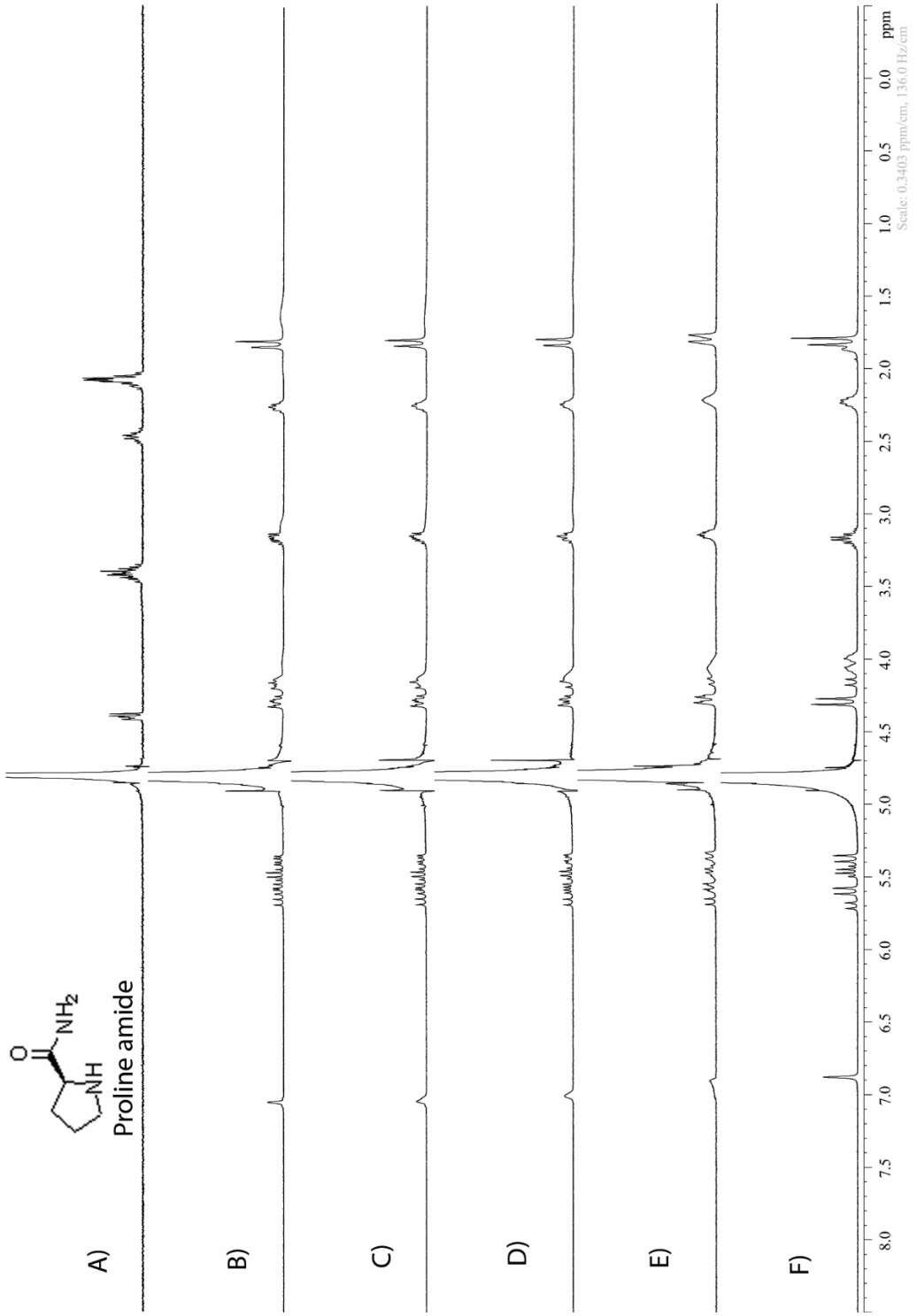

Figure II-S77. ^{1}H NMR spectra recorded (D_2O, 400 MHz, RT) for: a) Proline amide (2 mM), b) a mixture of Motor 1 (1 mM) and Proline amide (2 mM), c) a mixture of Motor 1 (1 mM) and Proline amide (1.5 mM), d) a mixture of Motor 1 (1 mM) and Proline amide (1 mM), e) a mixture Motor 1 (1 mM) and Proline amide (0.5 mM), f) Motor 1 (1 mM).

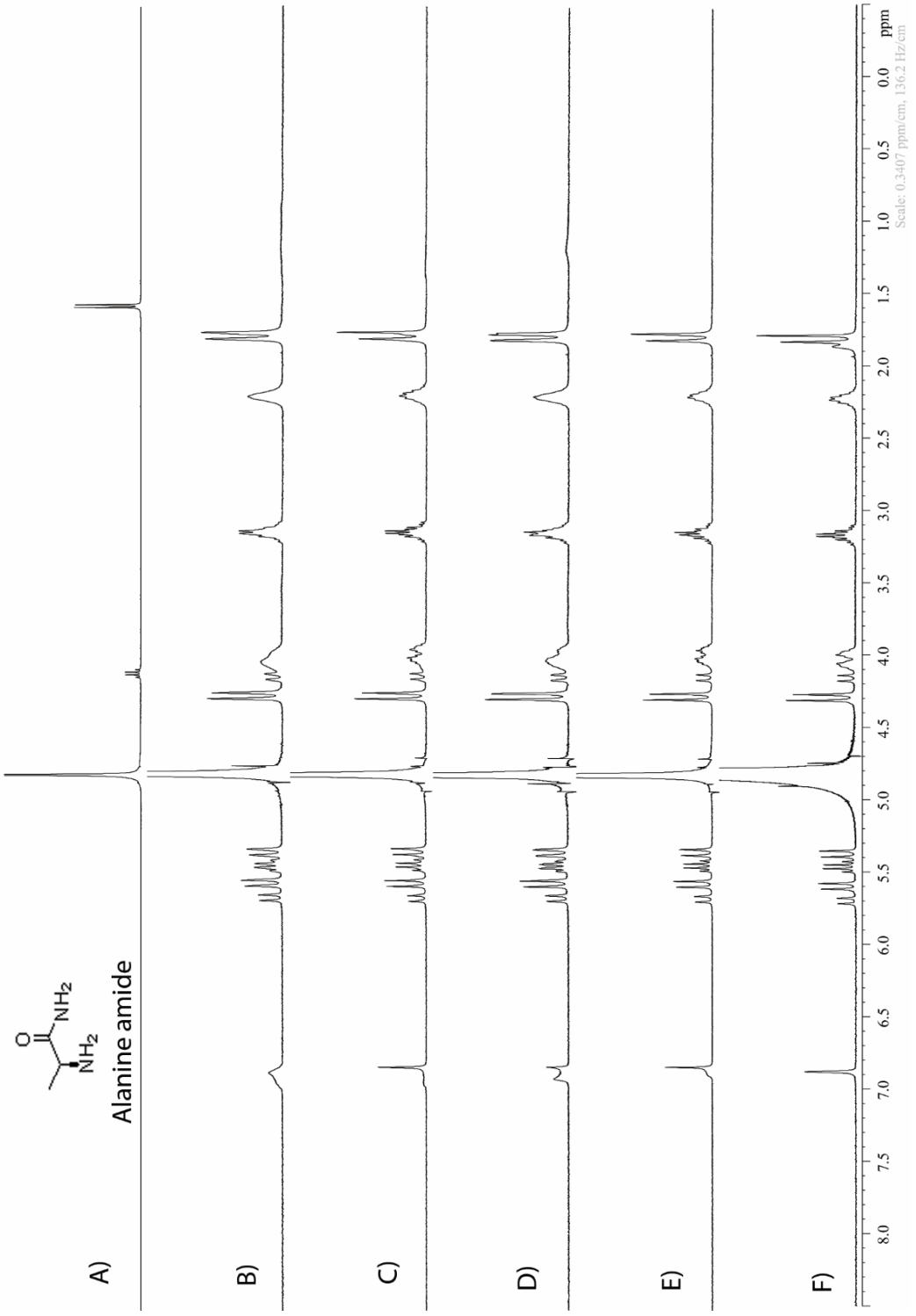

Figure II-S78. ^{1}H NMR spectra recorded (D_2O, 400 MHz, RT) for: a) Alanine amide (2 mM), b) a mixture of Motor 1 (1 mM) and Alanine amide (2 mM), c) a mixture of Motor 1 (1 mM) and Alanine amide (1.5 mM), d) a mixture of Motor 1 (1 mM) and Alanine amide (1 mM), e) a mixture Motor 1 (1 mM) and Alanine amide (0.5 mM), f) Motor 1 (1 mM).

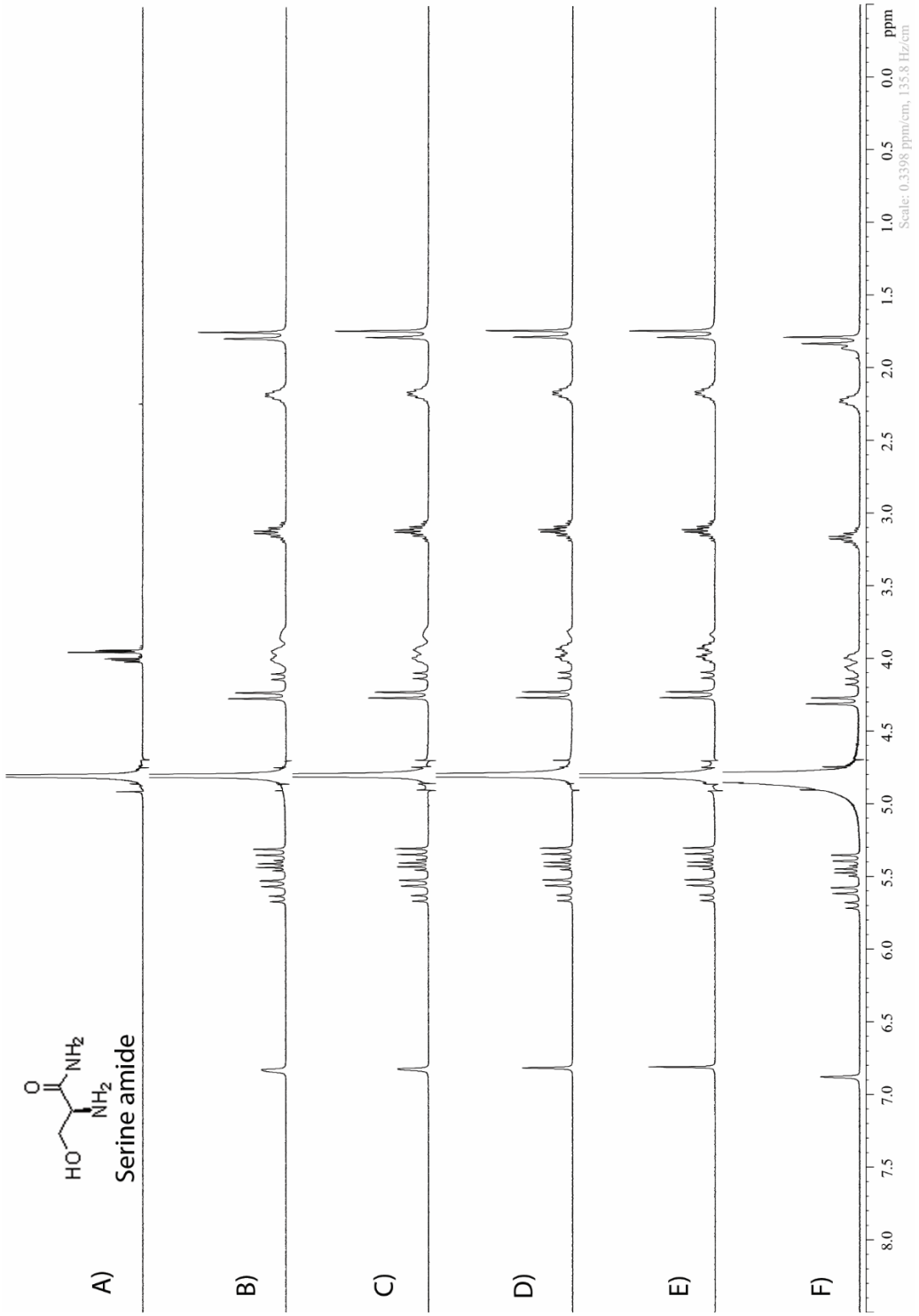

Figure II-S79. ^{1}H NMR spectra recorded (D_2O, 400 MHz, RT) for: a) Serine amide (2 mM), b) a mixture of Motor 1 (1 mM) and Serine amide (2 mM), c) a mixture of Motor 1 (1 mM) and Serine amide (1.5 mM), d) a mixture of Motor 1 (1 mM) and Serine amide (1 mM), e) a mixture of Motor 1 (1 mM) and Serine amide (0.5 mM), f) Motor 1 (1 mM).

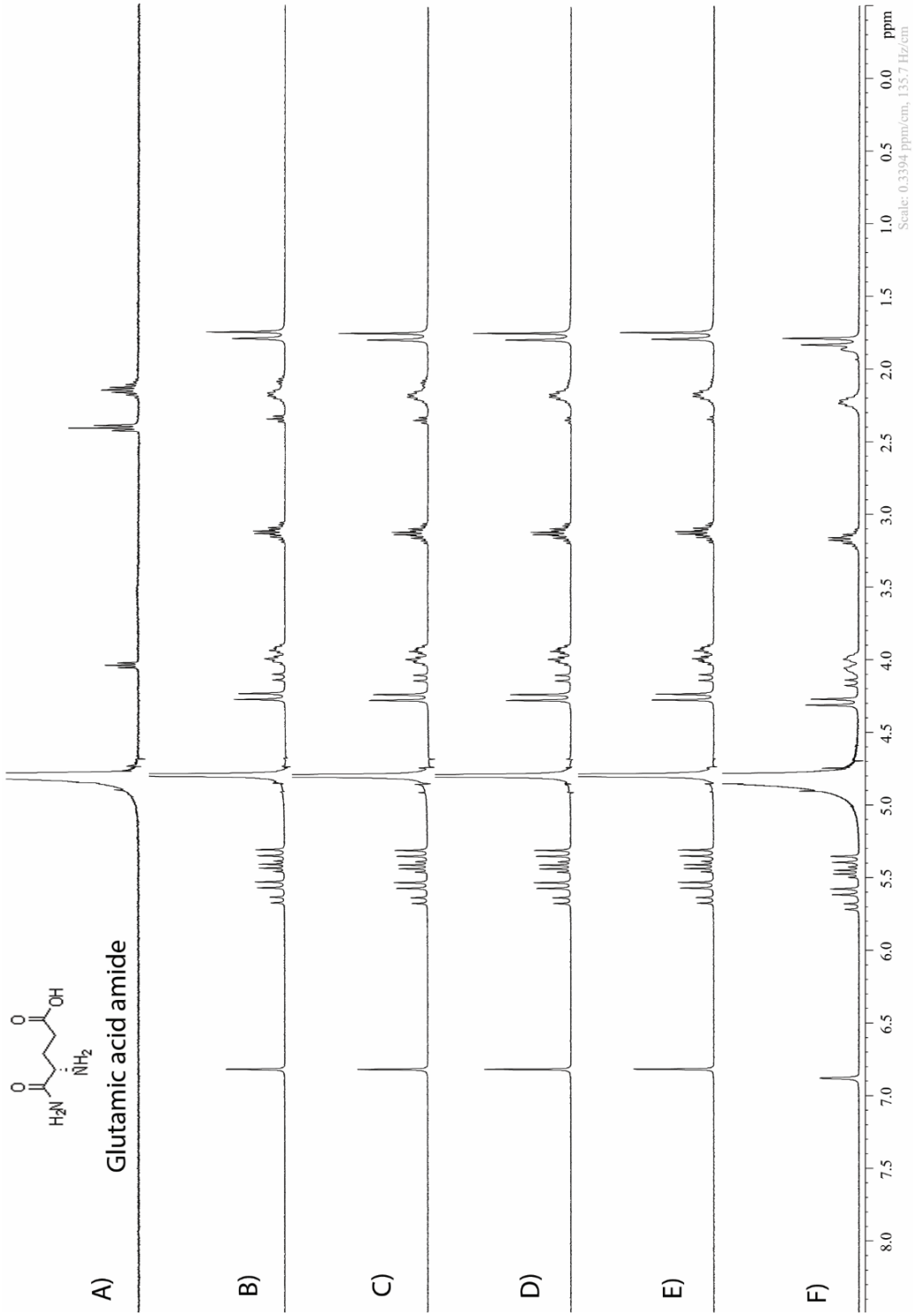

Figure II-S80. ^{1}H NMR spectra recorded (D_2O, 400 MHz, RT) for: a) Glutamic acid amide (2 mM), b) a mixture of Motor 1 (1 mM) and Glutamic acid amide (2 mM), c) a mixture of Motor 1 (1 mM) and Glutamic acid amide (1.5 mM), d) a mixture of Motor 1 (1 mM) and Glutamic acid amide (1 mM), e) a mixture of Motor 1 (1 mM) and Glutamic acid amide (0.5 mM), f) Motor 1 (1 mM).

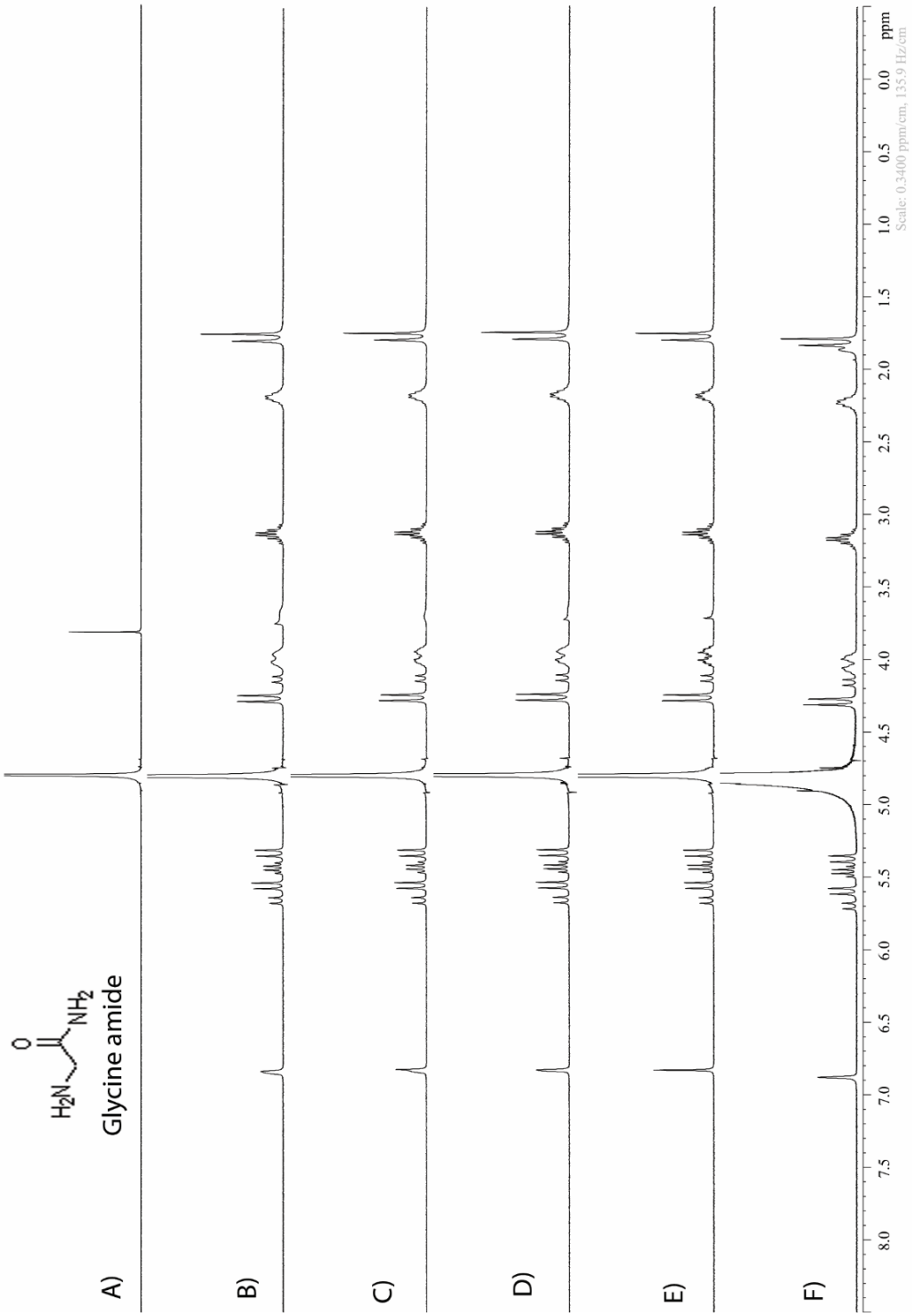

Figure II-S81. ^{1}H NMR spectra recorded (D_2O, 400 MHz, RT) for: a) Glycine amide (3 mM), b) a mixture of Motor 1 (1 mM) and Glycine amide (2 mM), c) a mixture of Motor 1 (1 mM) and Glycine amide (1.5 mM), d) a mixture of Motor 1 (1 mM) and Glycine amide (1 mM), e) a mixture of Motor 1 (1 mM) and Glycine amide (0.5 mM), f) Motor 1 (1 mM).

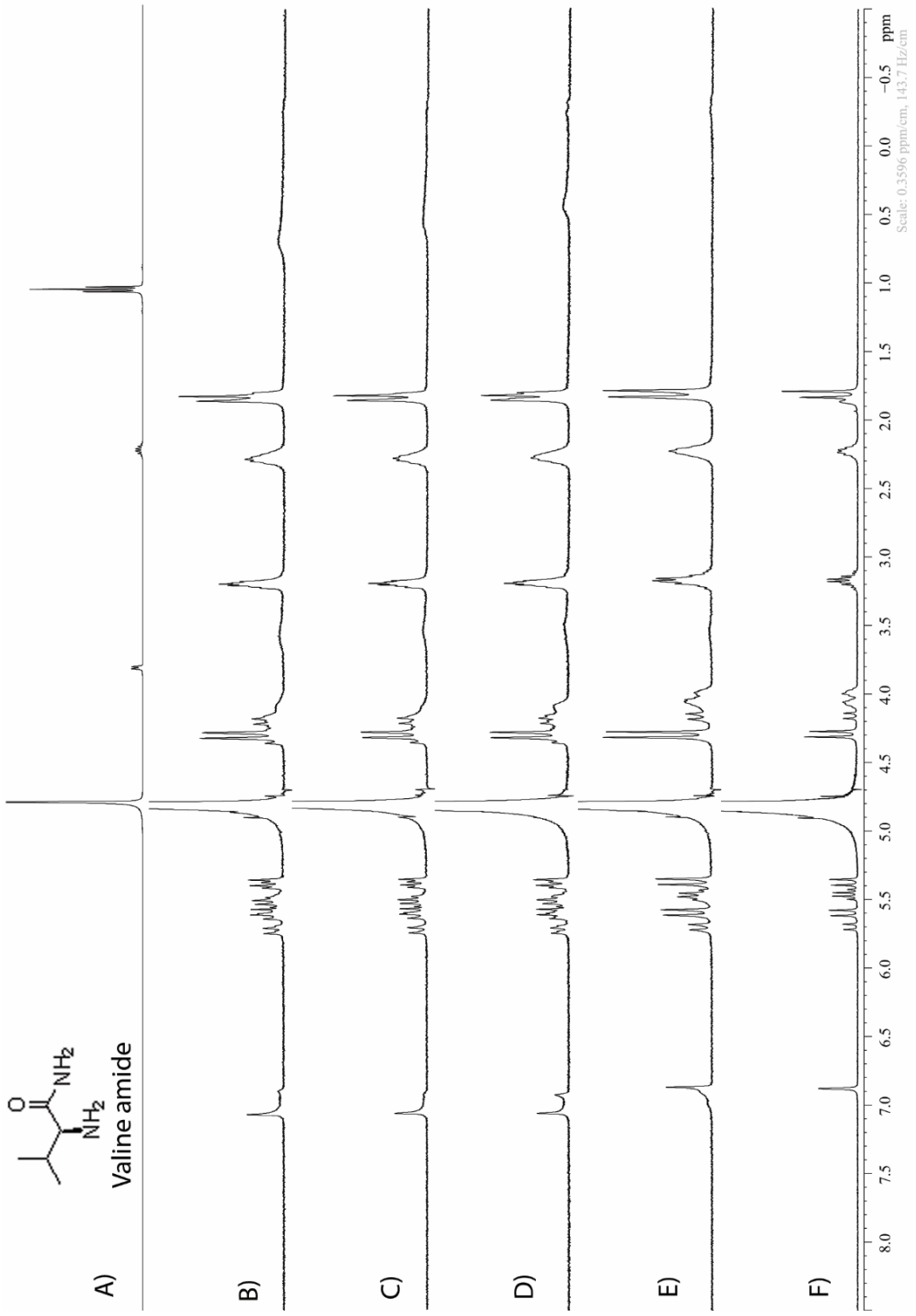

Figure II-S82. ^{1}H NMR spectra recorded (D_2O, 400 MHz, RT) for: a) Valine amide (10 mM), b) a mixture of Motor 1 (1 mM) and Valine amide (2 mM), c) a mixture of Motor 1 (1 mM) and Valine amide (1.5 mM), d) a mixture of Motor 1 (1 mM) and Valine amide (1 mM), e) a mixture of Motor 1 (1 mM) and Valine amide (0.5 mM), f) Motor 1 (1 mM).

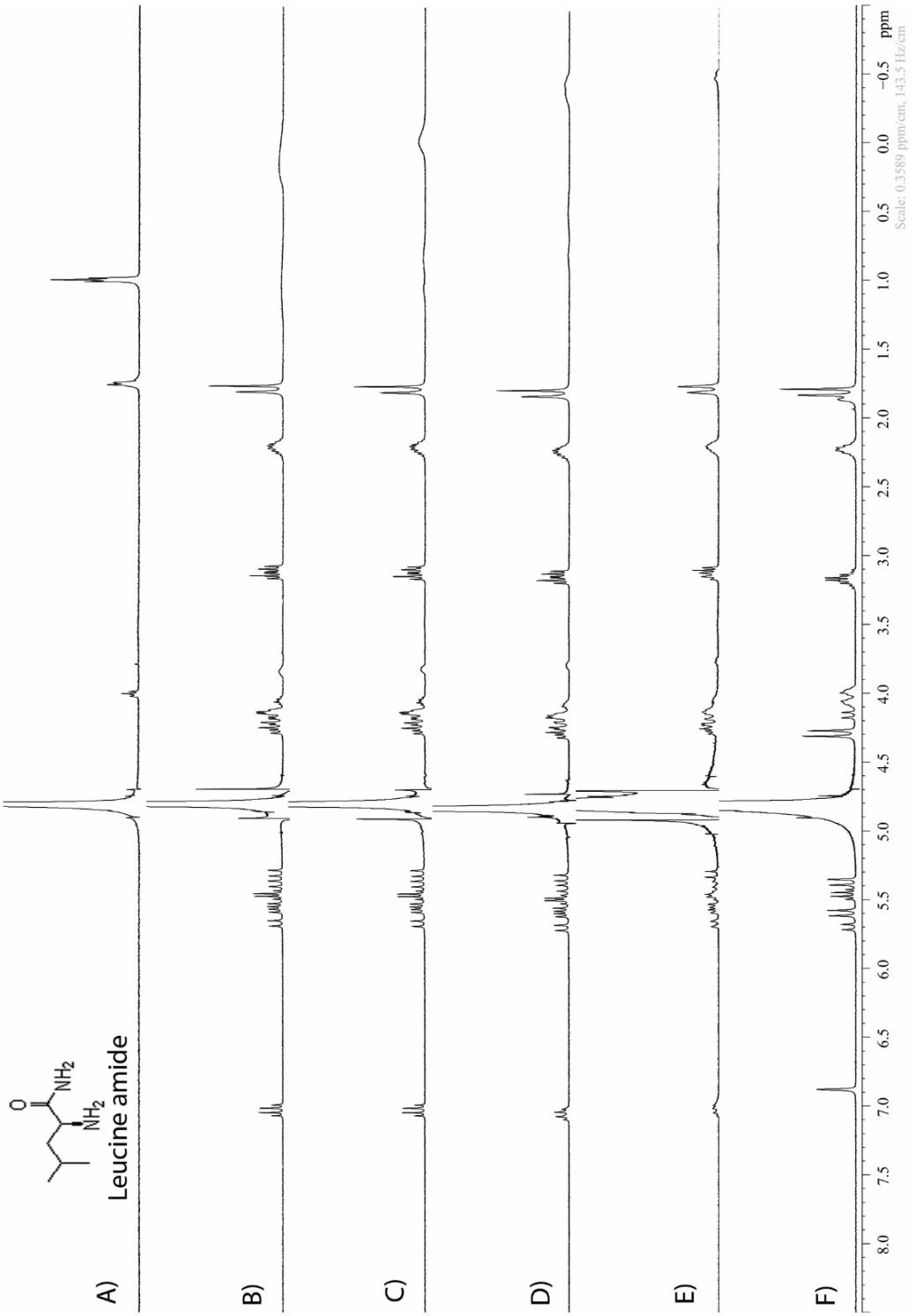

Figure II-S83. ^{1}H NMR spectra recorded (D_2O, 400 MHz, RT) for: a) Leucine amide (2 mM), b) a mixture of Motor 1 (1 mM) and Leucine amide (2 mM), c) a mixture of Motor 1 (1 mM) and Leucine amide (1.5 mM), d) a mixture of Motor 1 (1 mM) and Leucine amide (1 mM), e) a mixture of Motor 1 (1 mM) and Leucine amide (0.5 mM), f) Motor 1 (1 mM).

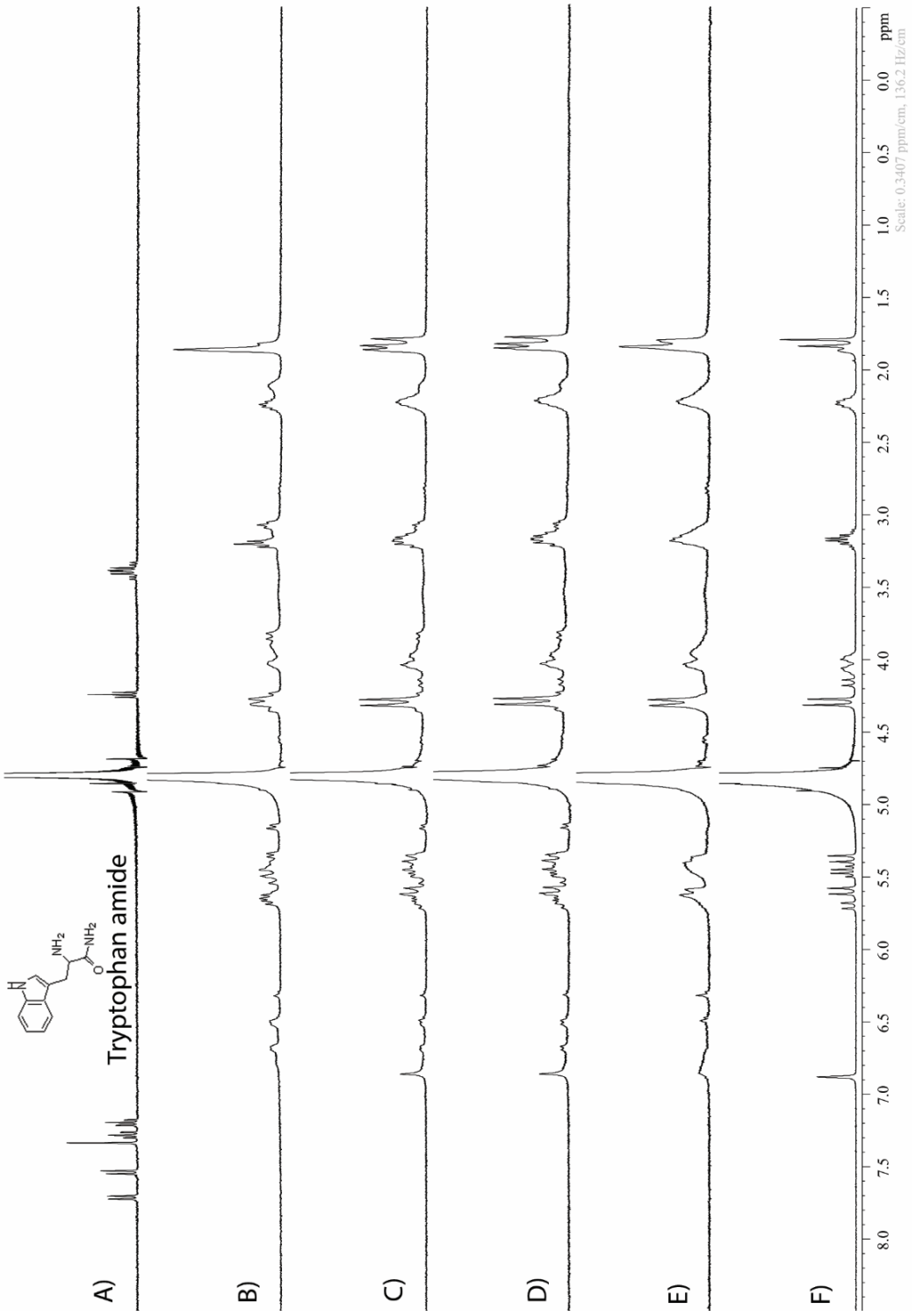

Figure II-S84. ^{1}H NMR spectra recorded (D_2O, 400 MHz, RT) for: a) Tryptophan amide (2 mM), b) a mixture of Motor 1 (1 mM) and Tryptophan amide (2 mM), c) a mixture of Motor 1 (1 mM) and Tryptophan amide (1.5 mM), d) a mixture of Motor 1 (1 mM) and Tryptophan amide (1 mM), e) a mixture of Motor 1 (1 mM) and Tryptophan amide (0.5 mM), f) Motor 1 (1 mM).

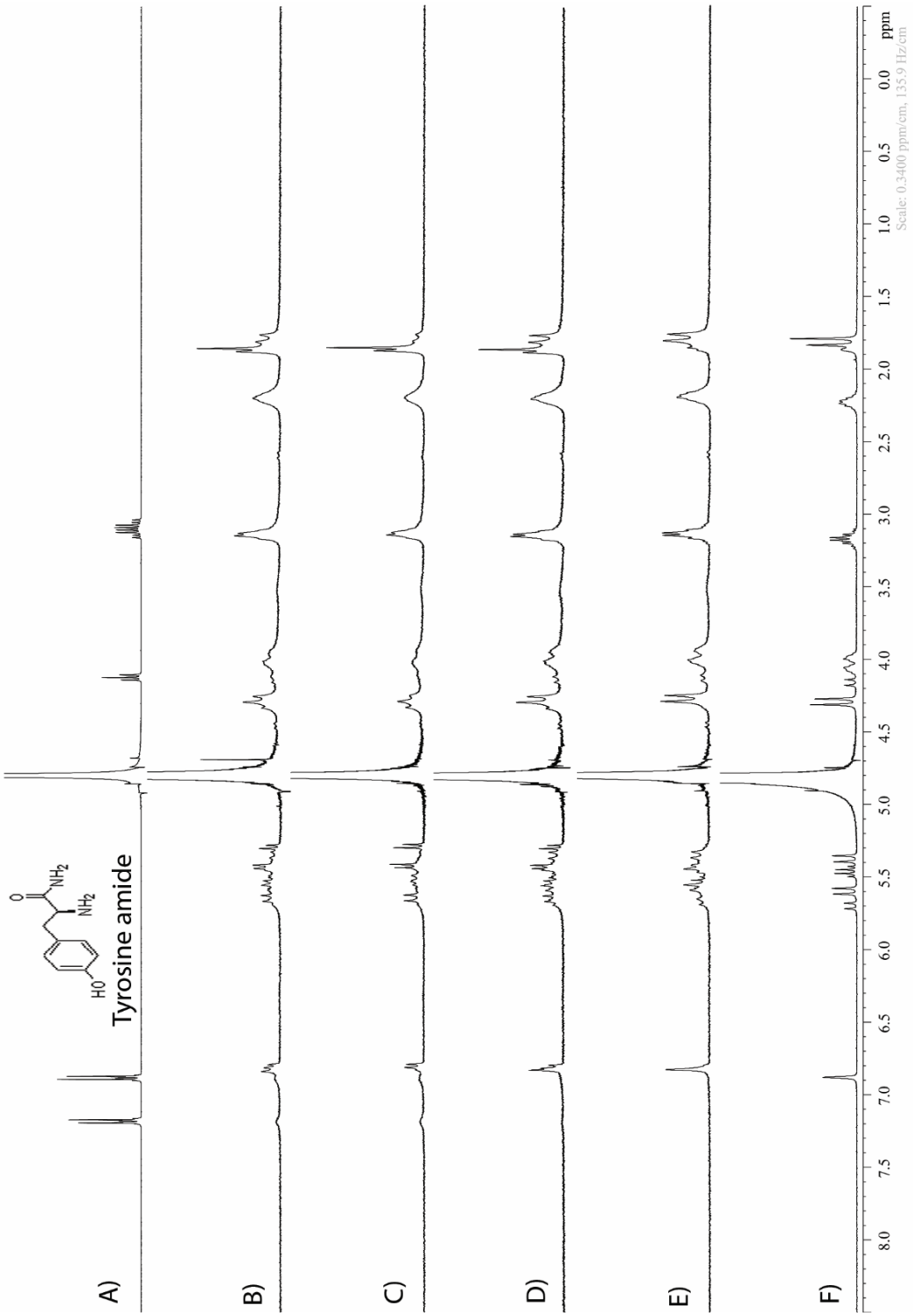

Figure II-S85. ^{1}H NMR spectra recorded (D_2O, 400 MHz, RT) for: a) Tyrosine amide (10 mM), b) a mixture of Motor 1 (1 mM) and Tyrosine amide (2 mM), c) a mixture of Motor 1 (1 mM) and Tyrosine amide (1.5 mM), d) a mixture of Motor 1 (1 mM) and Tyrosine amide (1 mM), e) a mixture of Motor 1 (1 mM) and Tyrosine amide (0.5 mM), f) Motor 1 (1 mM).

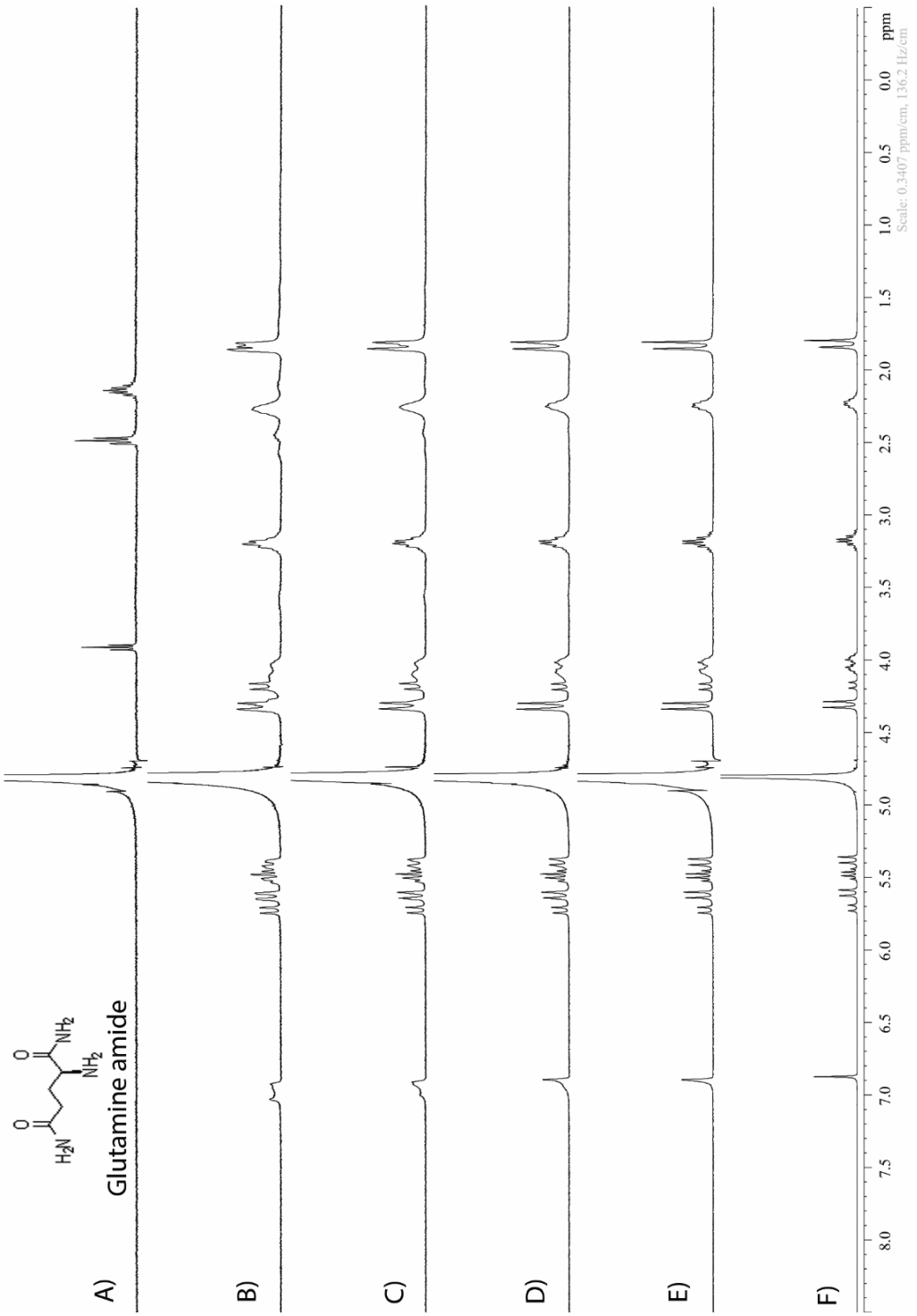

Figure II-S86. ^{1}H NMR spectra recorded (D_2O, 400 MHz, RT) for: a) Glutamine amide (2 mM), b) a mixture of Motor 1 (1 mM) and Glutamine amide (2 mM), c) a mixture of Motor 1 (1 mM) and Glutamine amide (1.5 mM), d) a mixture of Motor 1 (1 mM) and Glutamine amide (1 mM), e) a mixture of Motor 1 (1 mM) and Glutamine amide (0.5 mM), f) Motor 1 (1 mM).

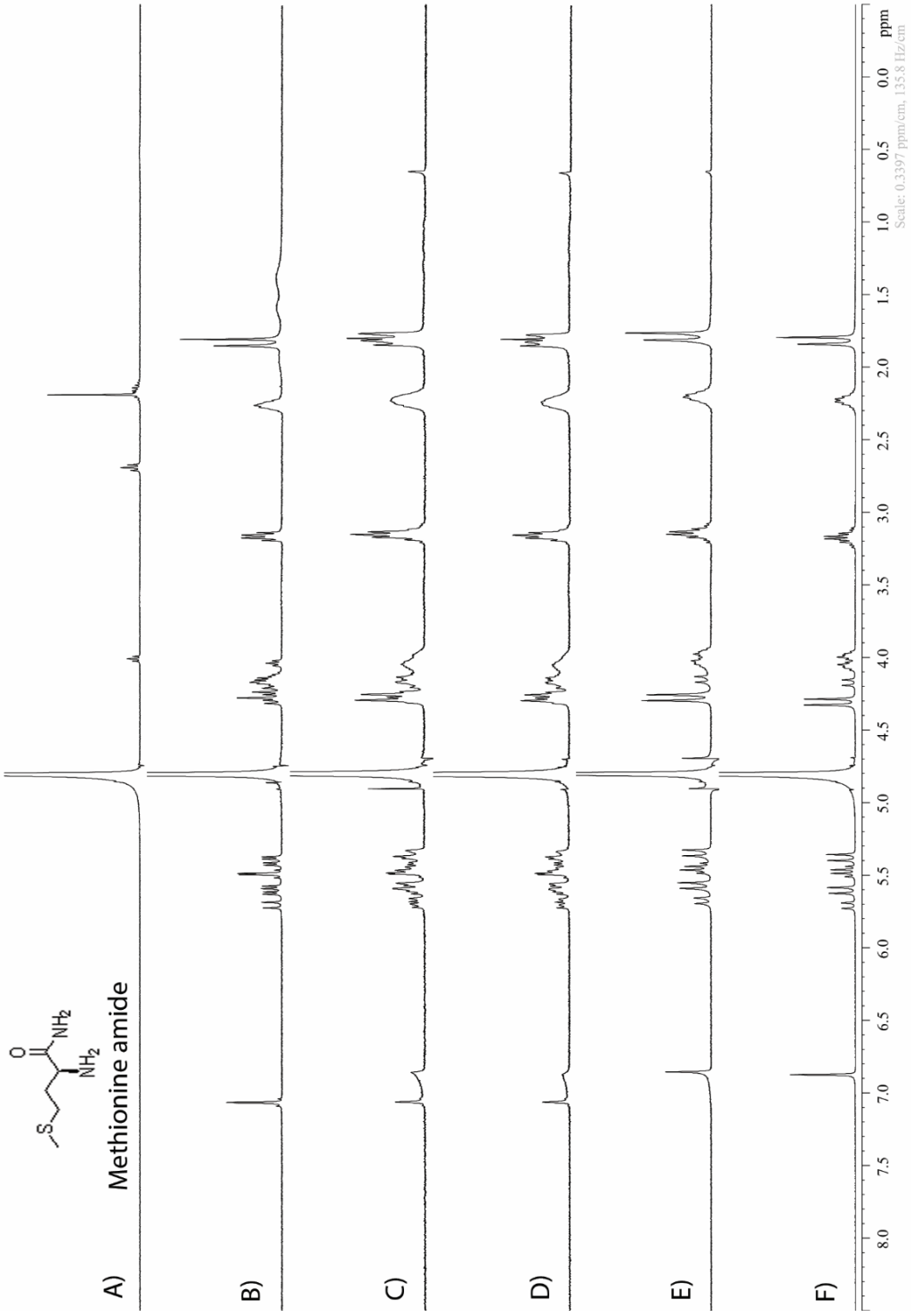

Figure II-S87. ^{1}H NMR spectra recorded (D_2O, 400 MHz, RT) for: a) Methionine amide (2 mM), b) a mixture of Motor 1 (1 mM) and Methionine amide (2 mM), c) a mixture of Motor 1 (1 mM) and Methionine amide (1.5 mM), d) a mixture of Motor 1 (1 mM) and Methionine amide (1 mM), e) a mixture of Motor 1 (1 mM) and Methionine amide (0.5 mM), f) Motor 1 (1 mM).

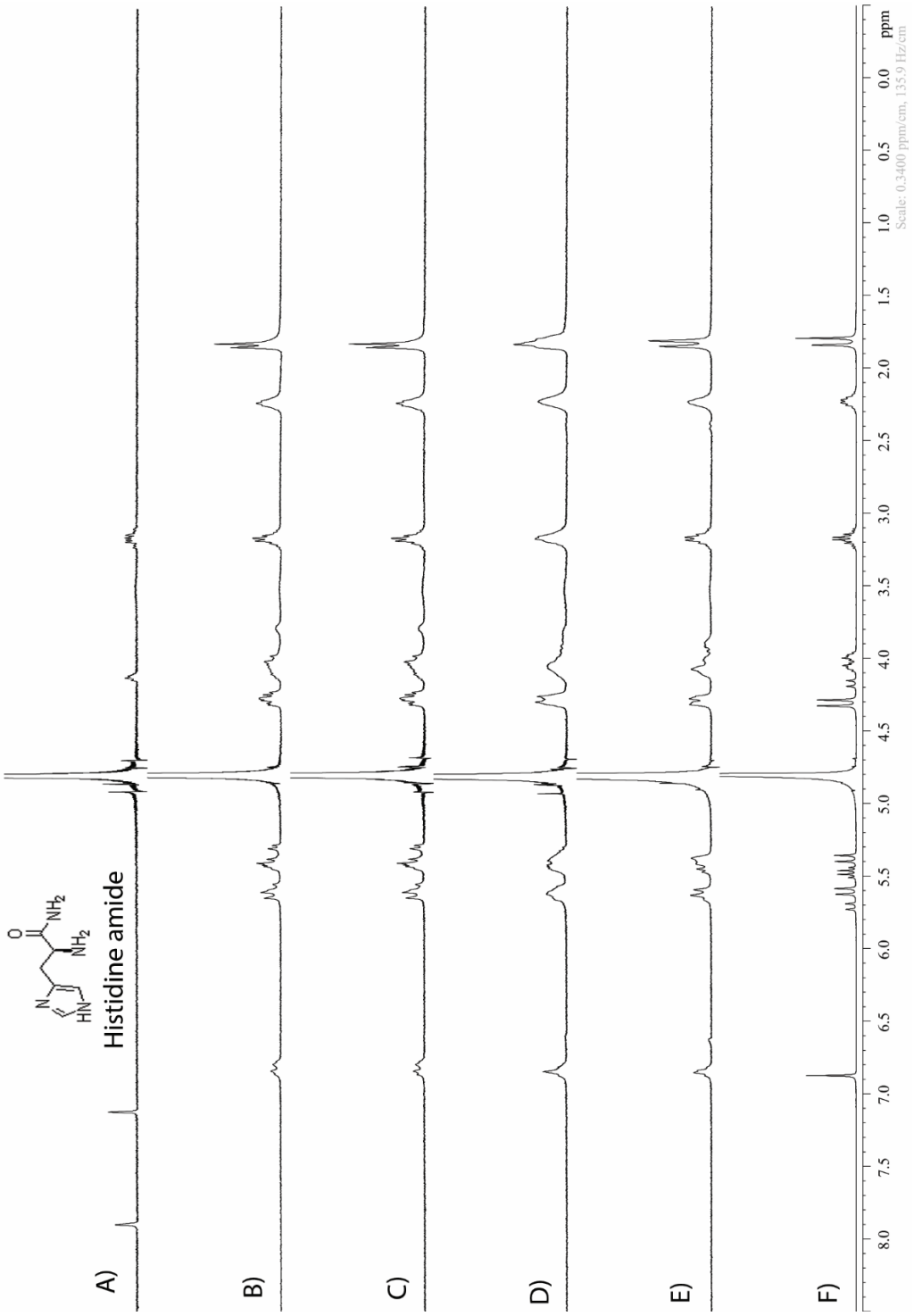

Figure II-S88. ^{1}H NMR spectra recorded (D_2O, 400 MHz, RT) for: a) Histidine amide (2 mM), b) a mixture of Motor 1 (1 mM) and Histidine amide (2 mM), c) a mixture of Motor 1 (1 mM) and Histidine amide (1.5 mM), d) a mixture of Motor 1 (1 mM) and Histidine amide (1 mM), e) a mixture of Motor 1 (1 mM) and Histidine amide (0.5 mM), f) Motor 1 (1 mM).

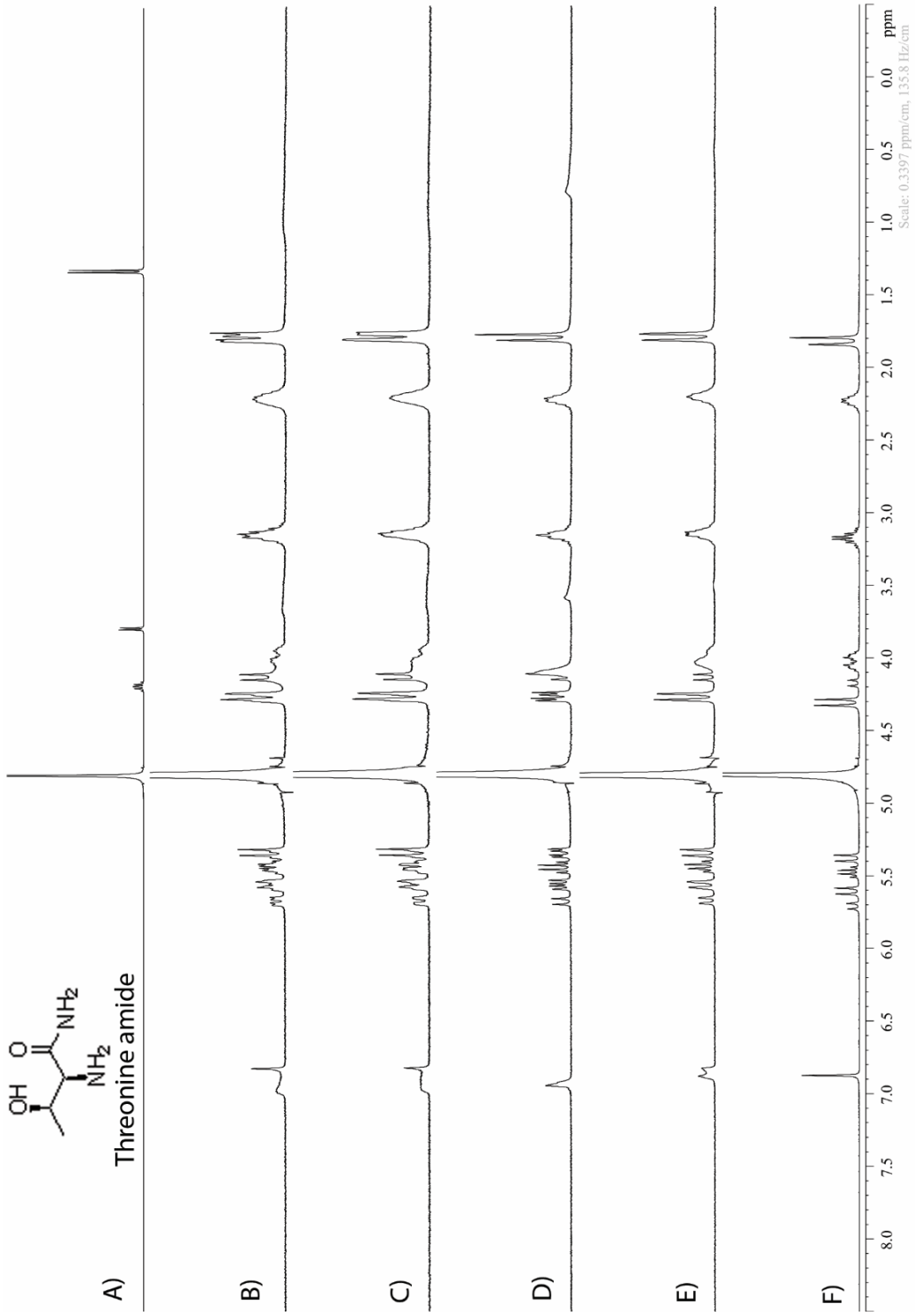

Figure II-S89. ^{1}H NMR spectra recorded (D_2O, 400 MHz, RT) for: a) Threonine amide (2 mM), b) a mixture of Motor 1 (1 mM) and Threonine amide (2 mM), c) a mixture of Motor 1 (1 mM) and Threonine amide (1.5 mM), d) a mixture of Motor 1 (1 mM) and Threonine amide (1 mM), e) a mixture of Motor 1 (1 mM) and Threonine amide (0.5 mM), f) Motor 1 (1 mM).

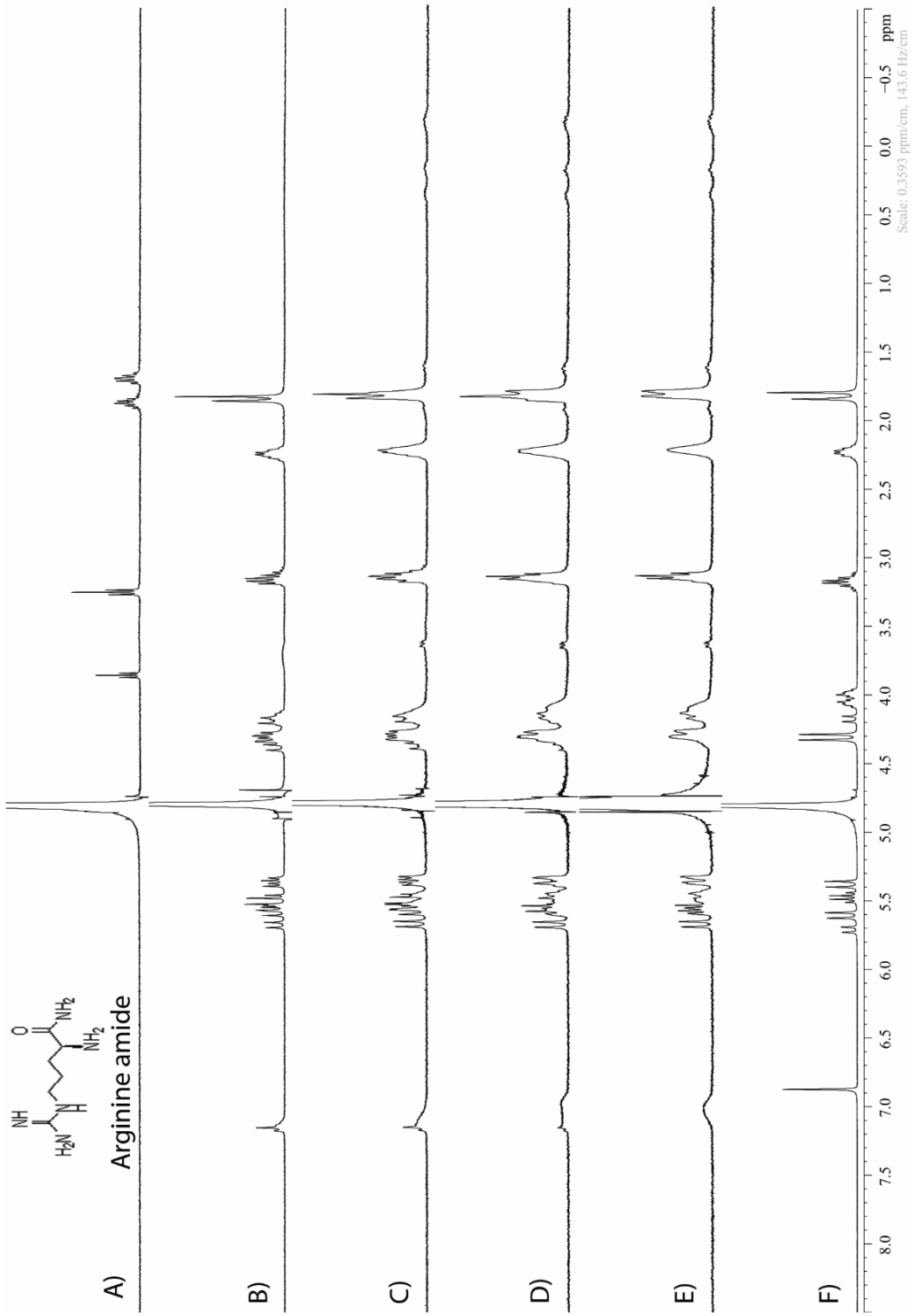

Figure II-S90. ^{1}H NMR spectra recorded (D_2O, 400 MHz, RT) for: a) Aarginine amide (2 mM), b) a mixture of Motor 1 (1 mM) and Arginine amide (2 mM), c) a mixture of Motor 1 (1 mM) and Arginine amide (1.5 mM), d) a mixture of Motor 1 (1 mM) and Arginine amide (1 mM), e) a mixture of Motor 1 (1 mM) and Arginine amide (0.5 mM), f) Motor 1 (1 mM).

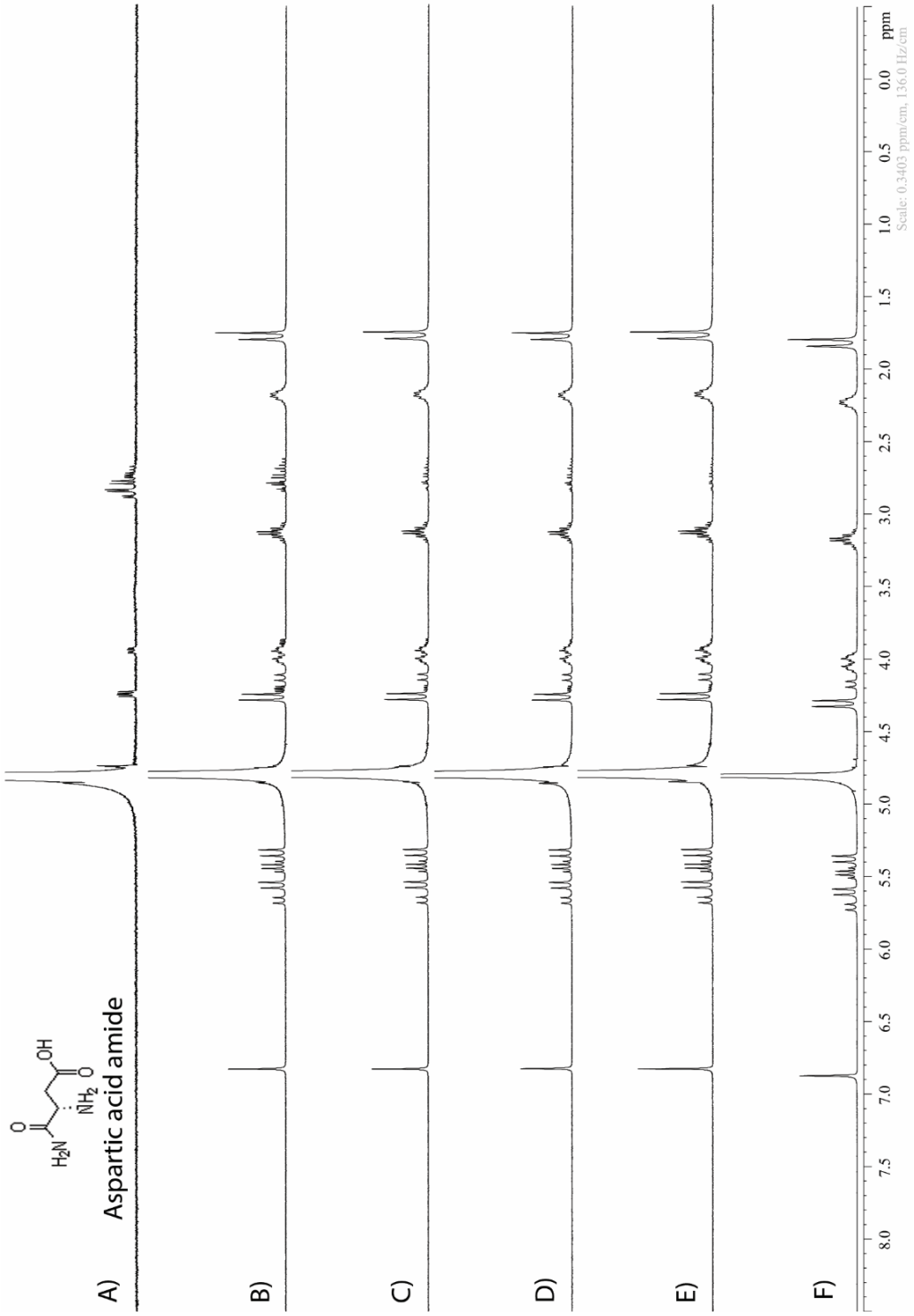

Figure II-S91. ^{1}H NMR spectra recorded (D_2O, 400 MHz, RT) for: a) Aspartic acid amide (2 mM), b) a mixture of Motor 1 (1 mM) and Aspartic acid amide (2 mM), c) a mixture of Motor 1 (1 mM) and Arginine amide (1.5 mM), d) a mixture of Motor 1 (1 mM) and Aspartic acid amide (1 mM), e) a mixture of Motor 1 (1 mM) and Aspartic acid amide (0.5 mM), f) Motor 1 (1 mM).

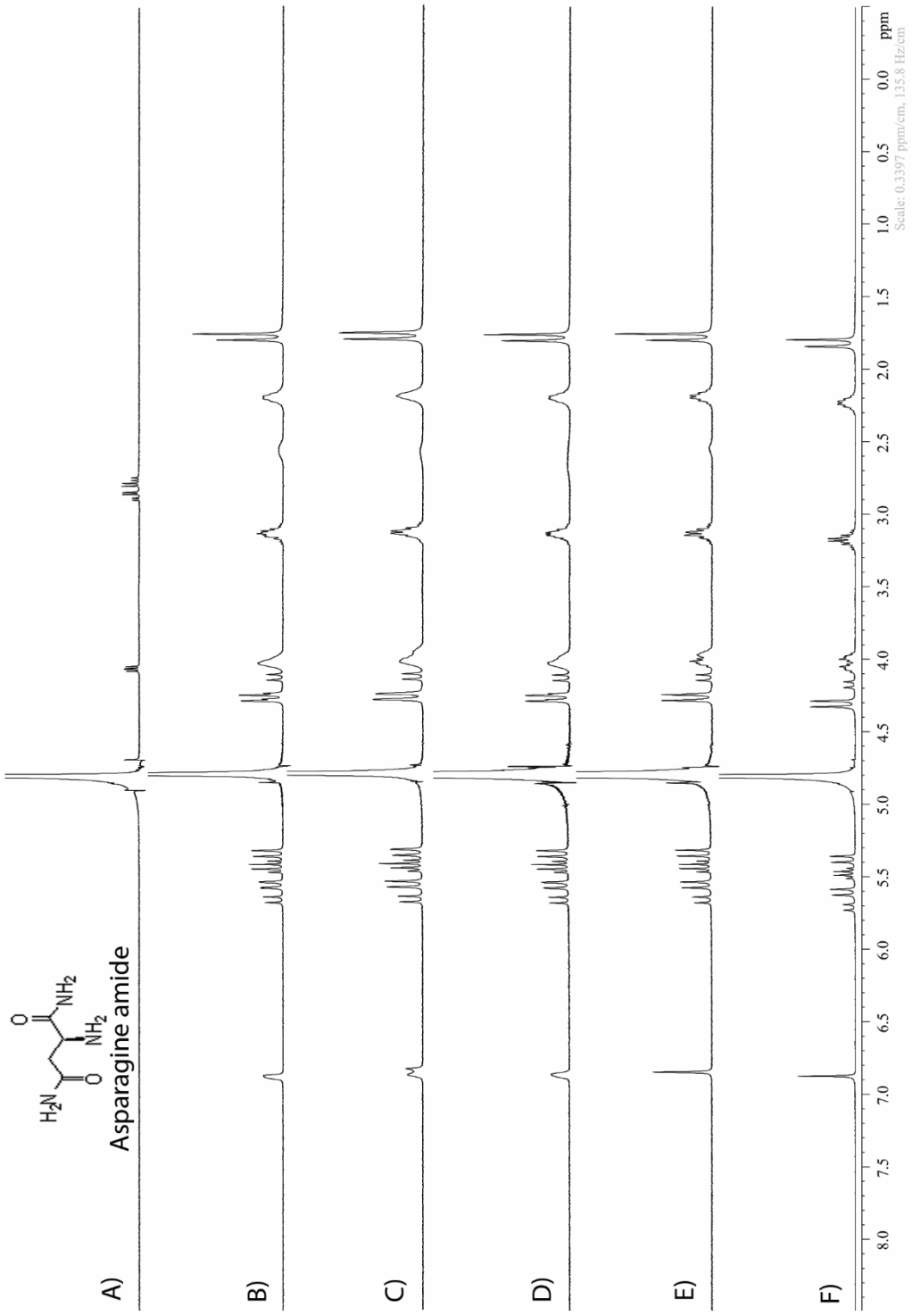

Figure II-S92. ^{1}H NMR spectra recorded (D_2O, 400 MHz, RT) for: a) Asparagine amide (2 mM), b) a mixture of Motor 1 (1 mM) and Asparagine amide (2 mM), c) a mixture of Motor 1 (1 mM) and Asparagine amide (1.5 mM), d) a mixture of Motor 1 (1 mM) and Asparagine amide (1 mM), e) a mixture of Motor 1 (1 mM) and Asparagine amide (0.5 mM), f) Motor 1 (1 mM).

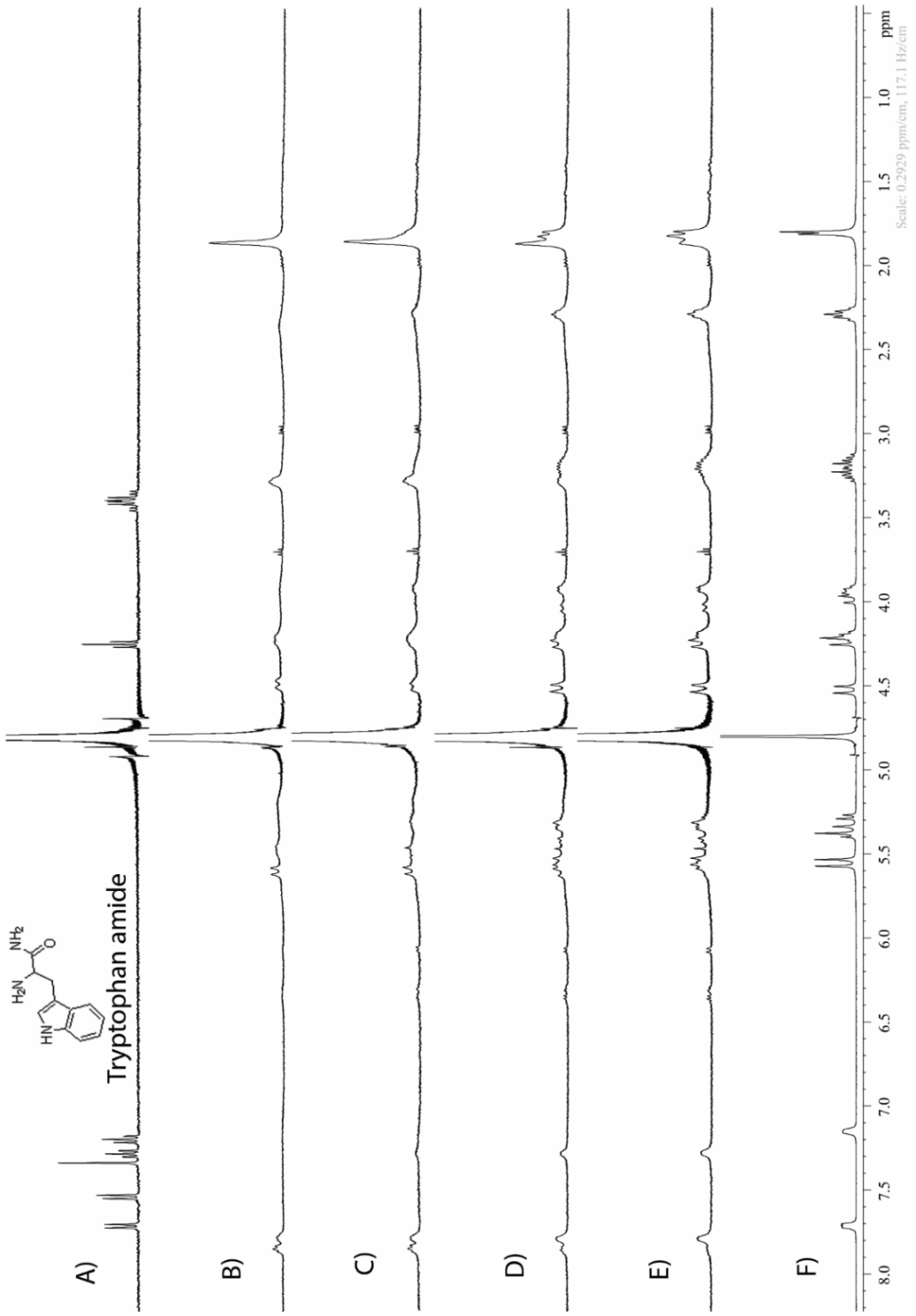

Figure II-S93. ^{1}H NMR spectra recorded (D_2O, 400 MHz, RT) for: a) Tryptophan amide (2 mM), b) a mixture of Motor 2 (1 mM) and Tryptophan amide (2 mM), c) a mixture of Motor 2 (1 mM) and Tryptophan amide (1.5 mM), d) a mixture of Motor 2 (1 mM) and Tryptophan amide (1 mM), e) a mixture of Motor 2 (1 mM) and Tryptophan amide (0.5 mM), f) Motor 2 (5 mM).

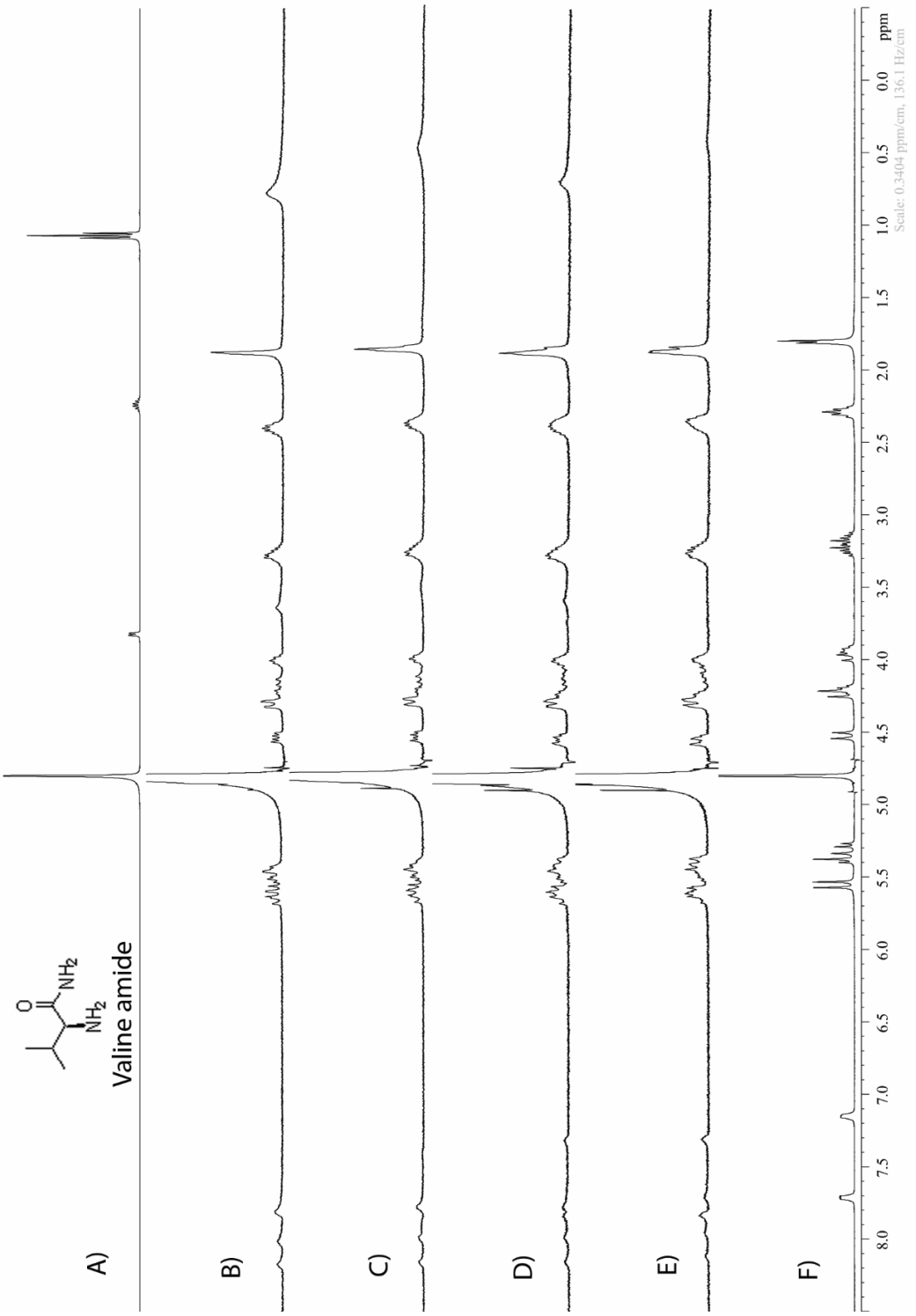

Figure II-S94. ^{1}H NMR spectra recorded (D_2O, 400 MHz, RT) for: a) Valine amide (10 mM), b) a mixture of Motor 2 (1 mM) and Valine amide (2 mM), c) a mixture of Motor 2 (1 mM) and Valine amide (1.5 mM), d) a mixture of Motor 2 (1 mM) and Valine amide (1 mM), e) a mixture of Motor 2 (1 mM) and Valine amide (0.5 mM), f) Motor 2 (5 mM).

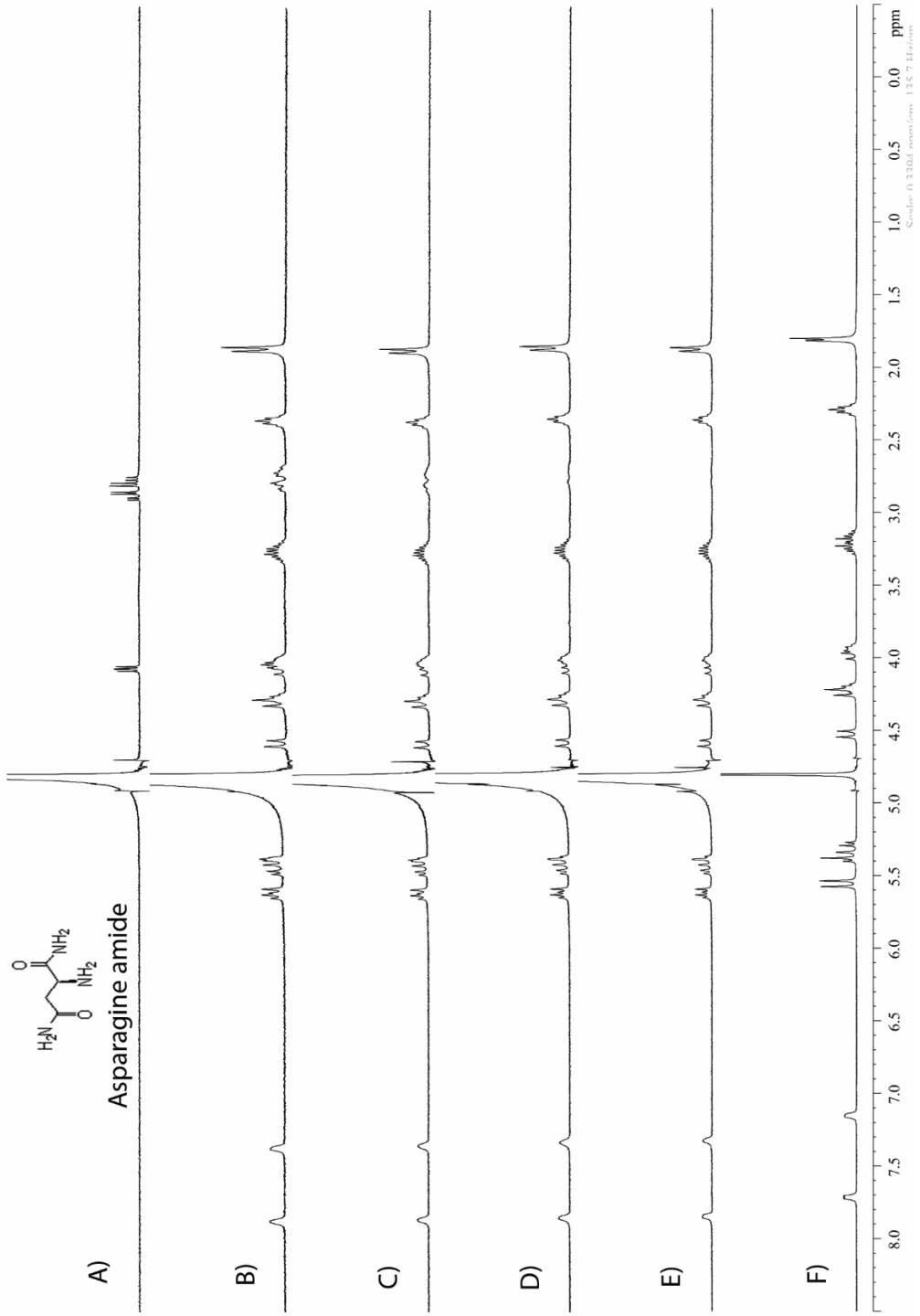

Figure II-S95. ^{1}H NMR spectra recorded (D_2O, 400 MHz, RT) for: a) Asparagine amide (2 mM), b) a mixture of Motor 2 (1 mM) and Asparagine amide (2 mM), c) a mixture of Motor 2 (1 mM) and Asparagine amide (1.5 mM), d) a mixture of Motor 2 (1 mM) and Asparagine amide (1 mM), e) a mixture of Motor 2 (1 mM) and Asparagine amide (0.5 mM), f) Motor 2 (5 mM).

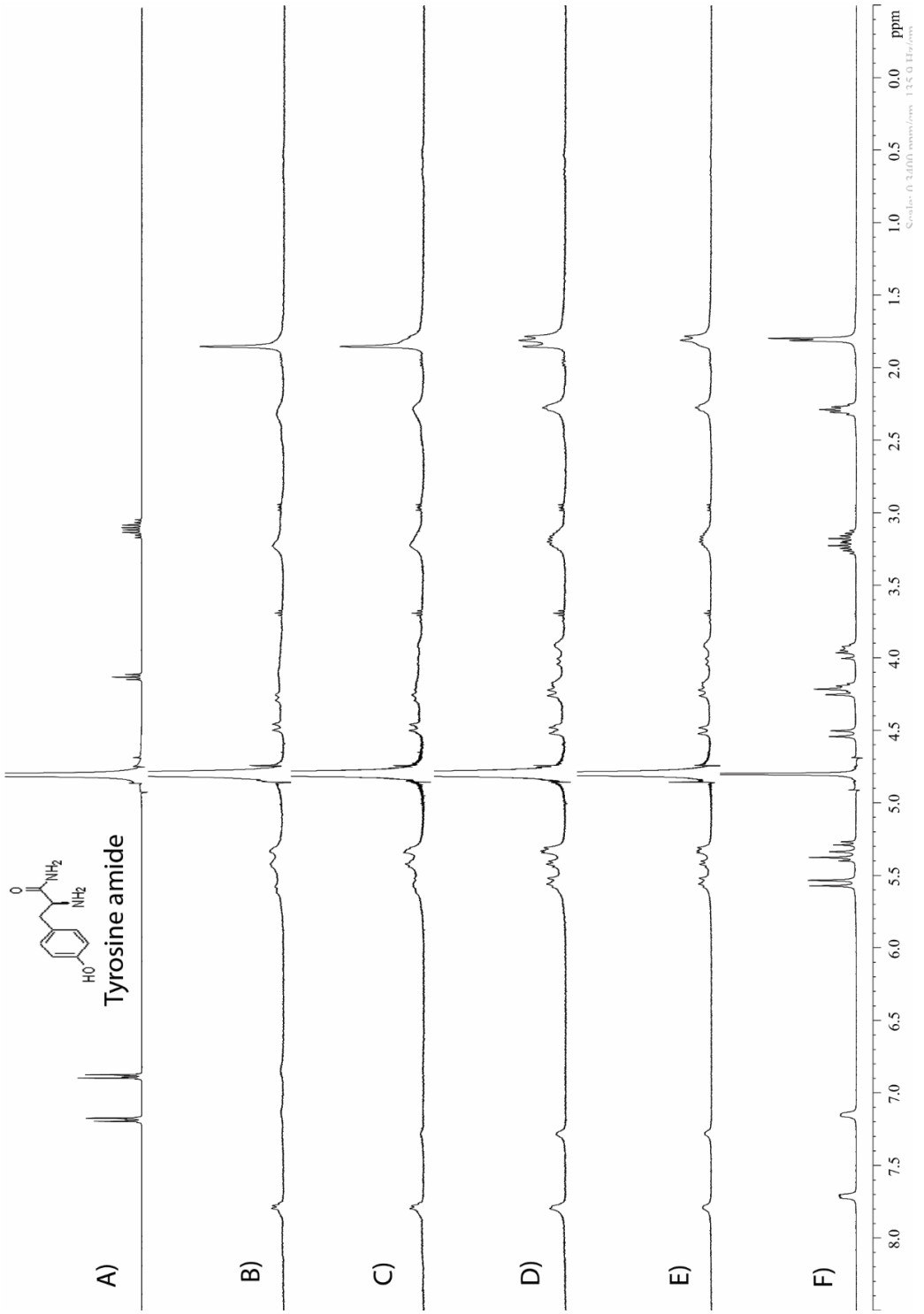

Figure II-S96. ^{1}H NMR spectra recorded (D_2O, 400 MHz, RT) for: a) Tyrosine amide (10 mM), b) a mixture of Motor 2 (1 mM) and Tyrosine amide (2 mM), c) a mixture of Motor 2 (1 mM) and Tyrosine amide (1.5 mM), d) a mixture of Motor 2 (1 mM) and Tyrosine amide (1 mM), e) a mixture of Motor 2 (1 mM) and Tyrosine amide (0.5 mM), f) Motor 2 (5 mM).

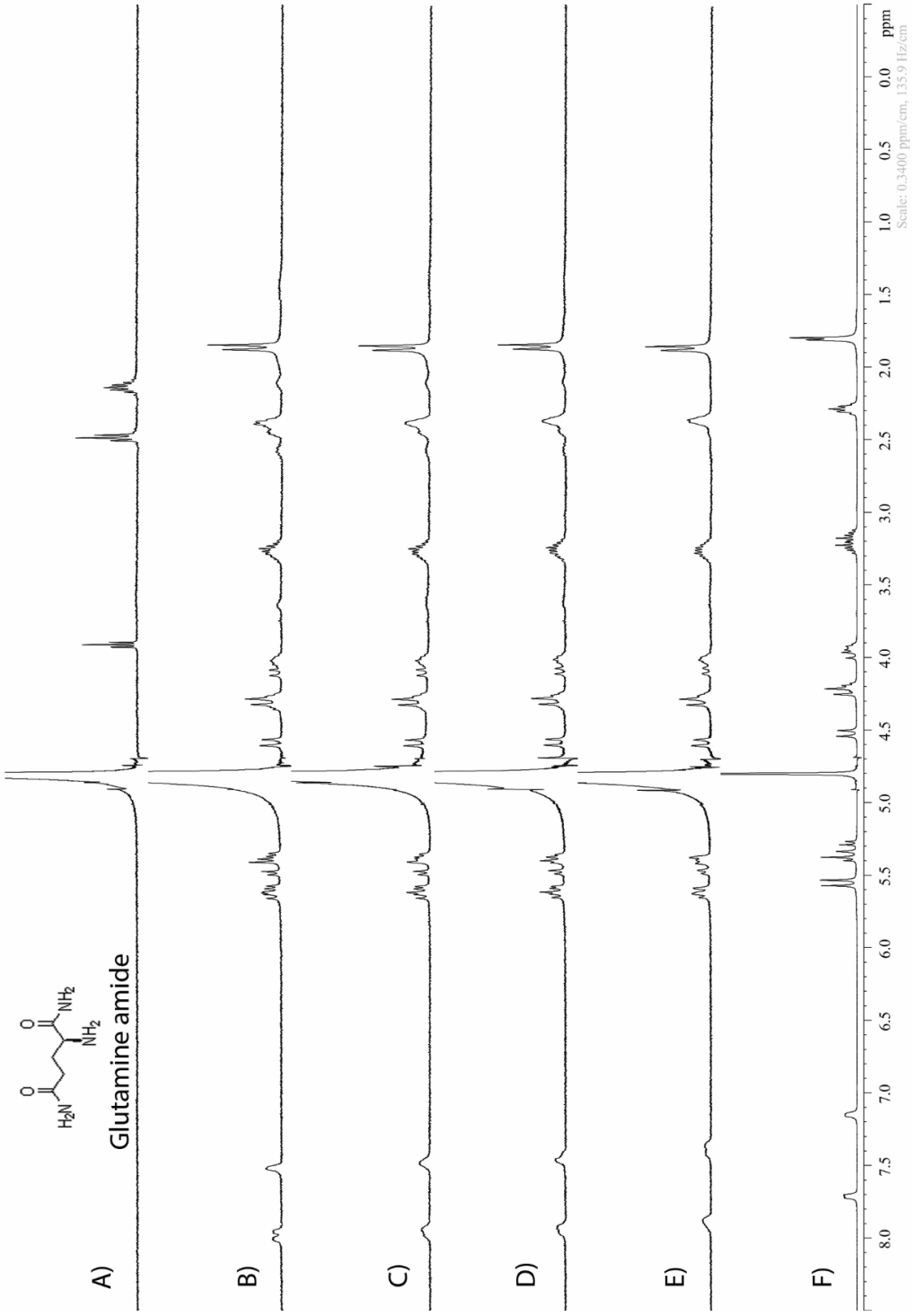

Figure II-S97. ^{1}H NMR spectra recorded (D_2O, 400 MHz, RT) for: a) Glutamine amide (2 mM), b) a mixture of Motor 2 (1 mM) and Glutamine amide (2 mM), c) a mixture of Motor 2 (1 mM) and Glutamine amide (1.5 mM), d) a mixture of Motor 2 (1 mM) and Glutamine amide (1 mM), e) a mixture of Motor 2 (1 mM) and Glutamine amide (0.5 mM), f) Motor 2 (5 mM).

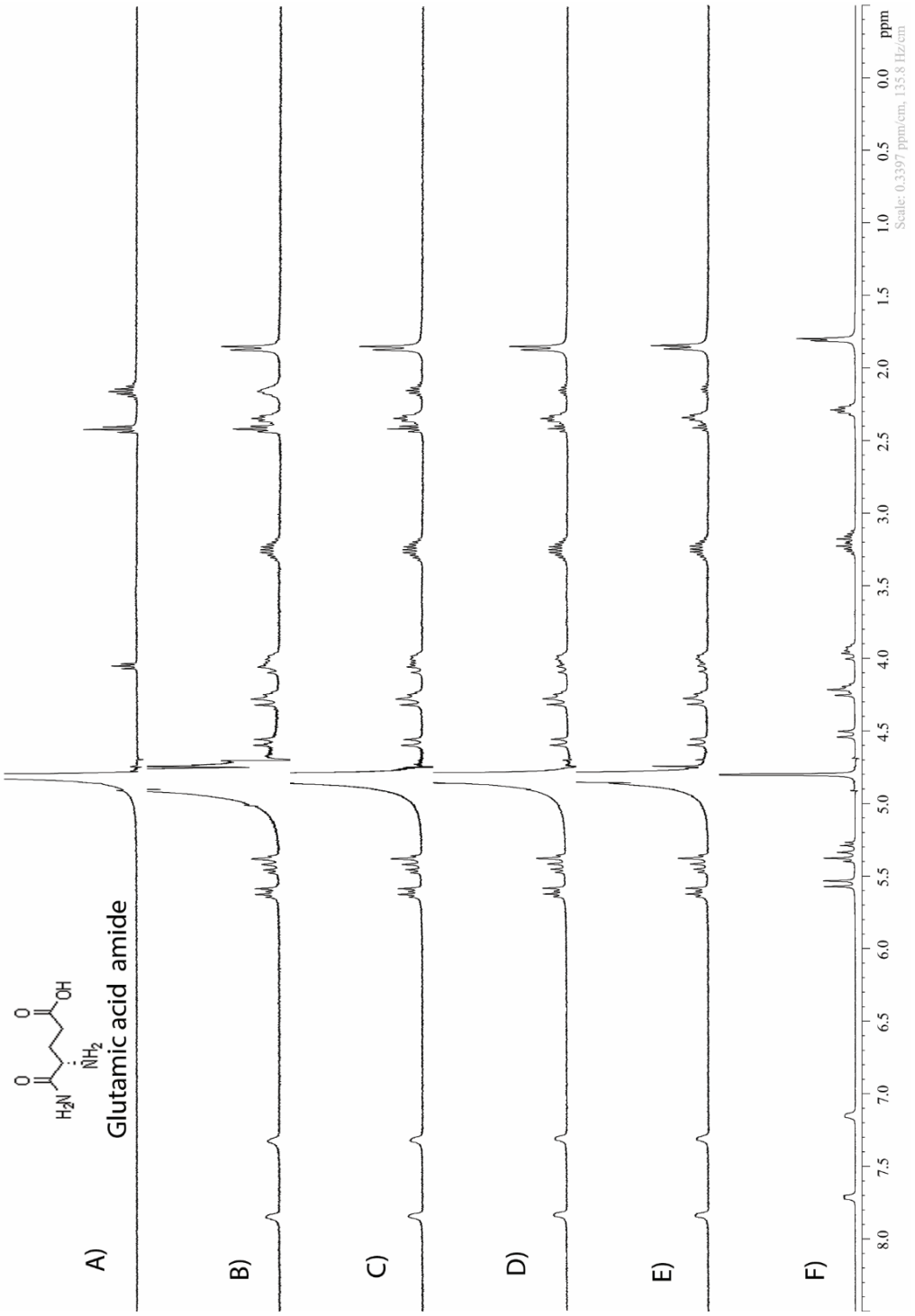

Figure II-S98. ^{1}H NMR spectra recorded (D_2O, 400 MHz, RT) for: a) Glutamic acid amide (2 mM), b) a mixture of Motor 2 (1 mM) and Glutamic acid amide (2 mM), c) a mixture of Motor 2 (1 mM) and Glutamic acid amide (1.5 mM), d) a mixture of Motor 2 (1 mM) and Glutamic acid amide (1 mM), e) a mixture of Motor 2 (1 mM) and Glutamic acid amide (0.5 mM), f) Motor 2 (5 mM).

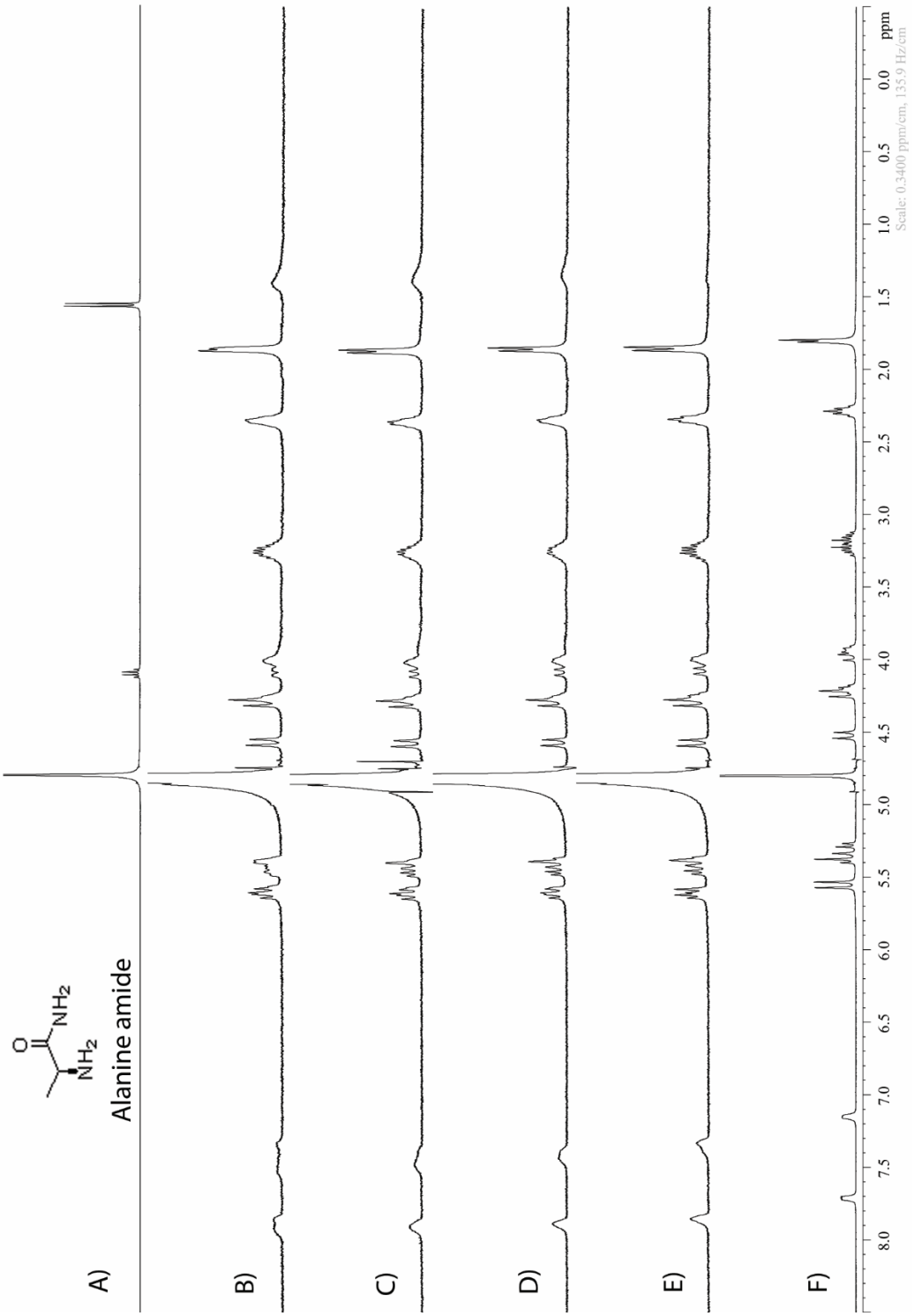

Figure II-S99. ^{1}H NMR spectra recorded (D_2O, 400 MHz, RT) for: a) Alanine amide (2 mM), b) a mixture of Motor 2 (1 mM) and Alanine amide (2 mM), c) a mixture of Motor 2 (1 mM) and Alanine amide (1.5 mM), d) a mixture of Motor 2 (1 mM) and Alanine amide (1 mM), e) a mixture of Motor 2 (1 mM) and Alanine amide (0.5 mM), f) Motor 2 (5 mM).

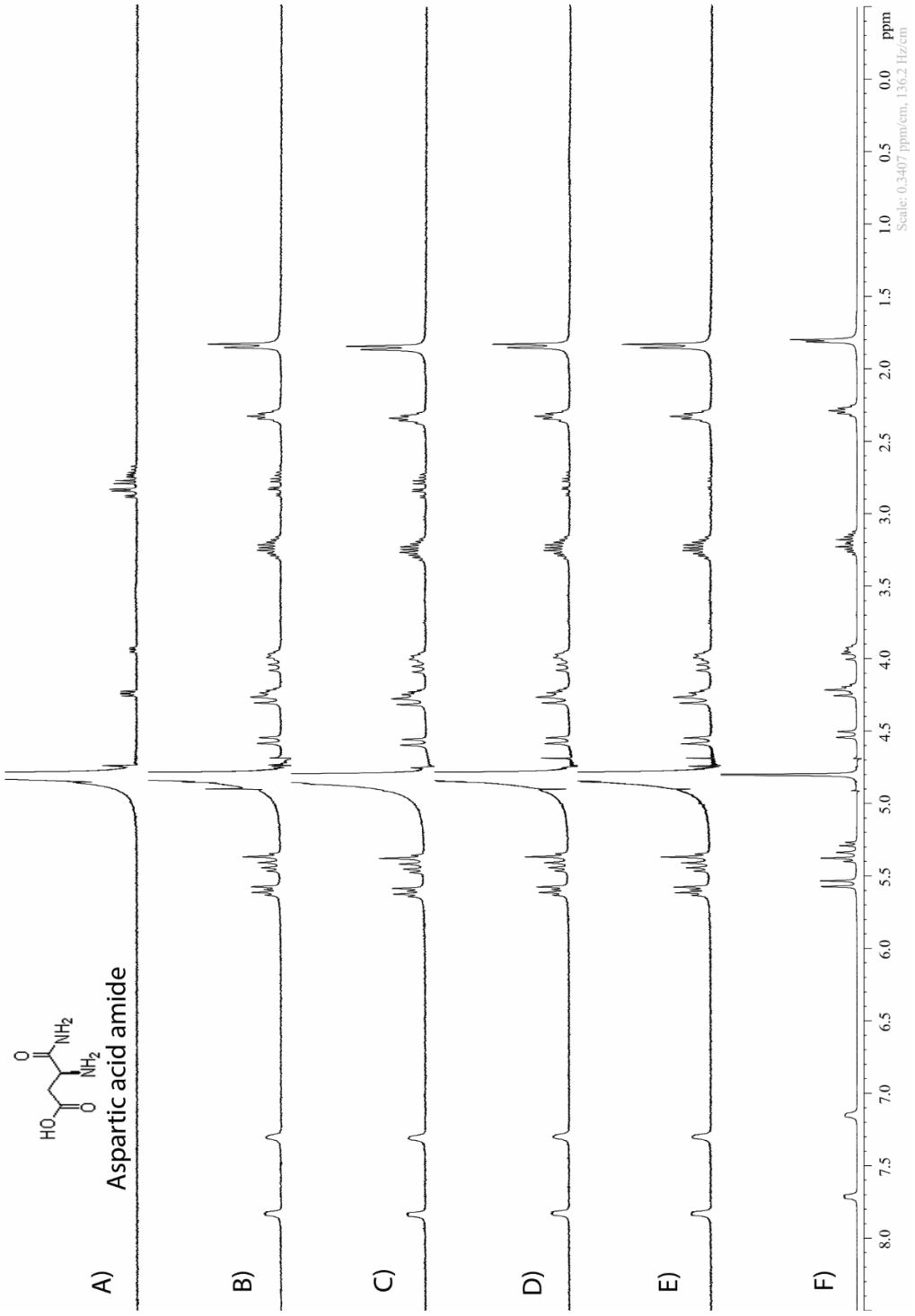

Figure II-S100. ^{1}H NMR spectra recorded (D_2O, 400 MHz, RT) for: a) Aspartic acid amide (2 mM), b) a mixture of Motor 2 (1 mM) and Aspartic acid amide (2 mM), c) a mixture of Motor 2 (1 mM) and Aspartic acid amide (1.5 mM), d) a mixture of Motor 2 (1 mM) and Aspartic acid amide (1 mM), e) a mixture of Motor 2 (1 mM) and Aspartic acid amide (0.5 mM), f) Motor 2 (5 mM).

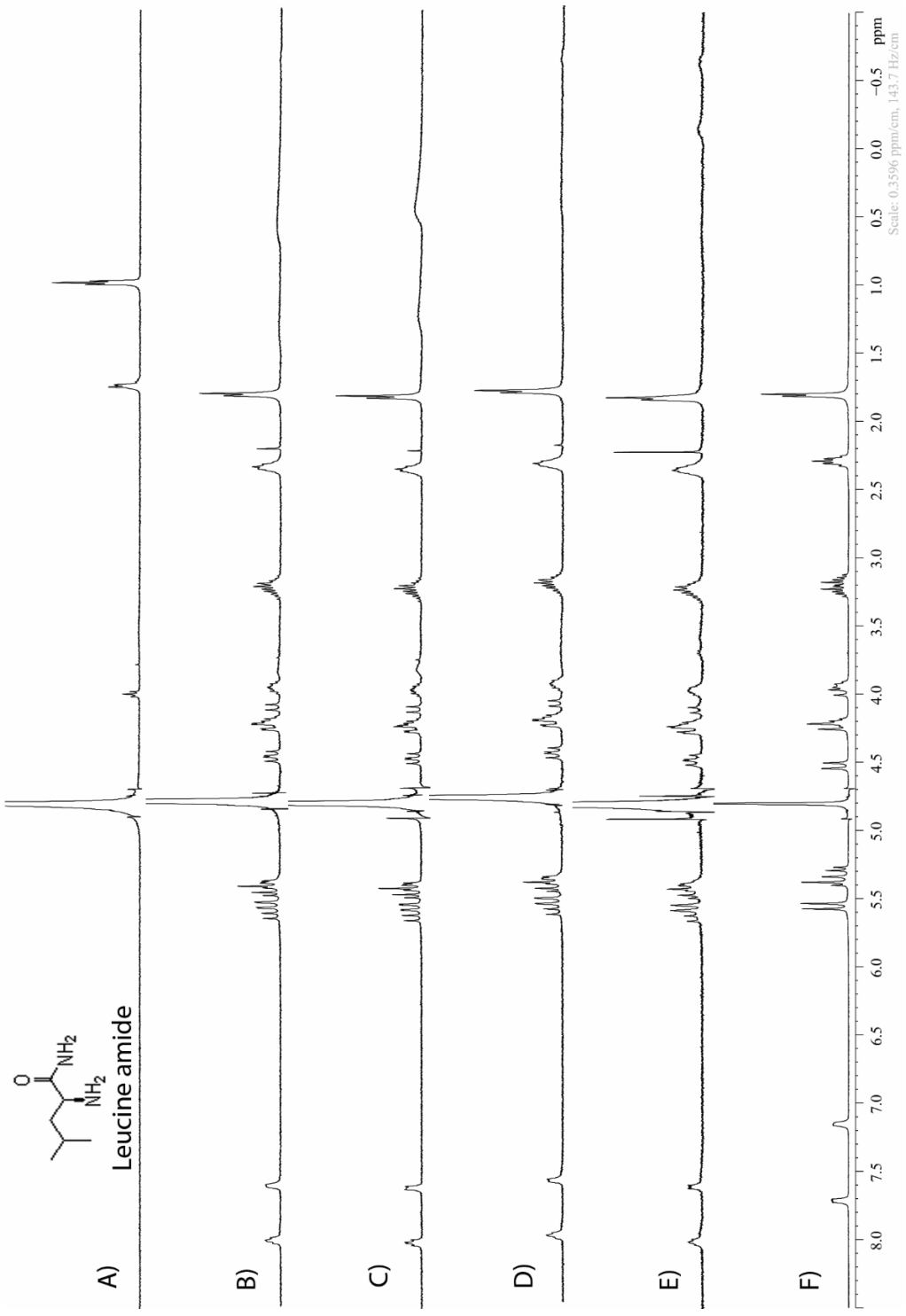

Figure II-S101. ^{1}H NMR spectra recorded (D_2O, 400 MHz, RT) for: a) Leucine amide (2 mM), b) a mixture of Motor 2 (1 mM) and Leucine amide (2 mM), c) a mixture of Motor 2 (1 mM) and Leucine amide (1.5 mM), d) a mixture of Motor 2 (1 mM) and Leucine amide (1 mM), e) a mixture of Motor 2 (1 mM) and Leucine amide (0.5 mM), f) Motor 2 (5 mM).

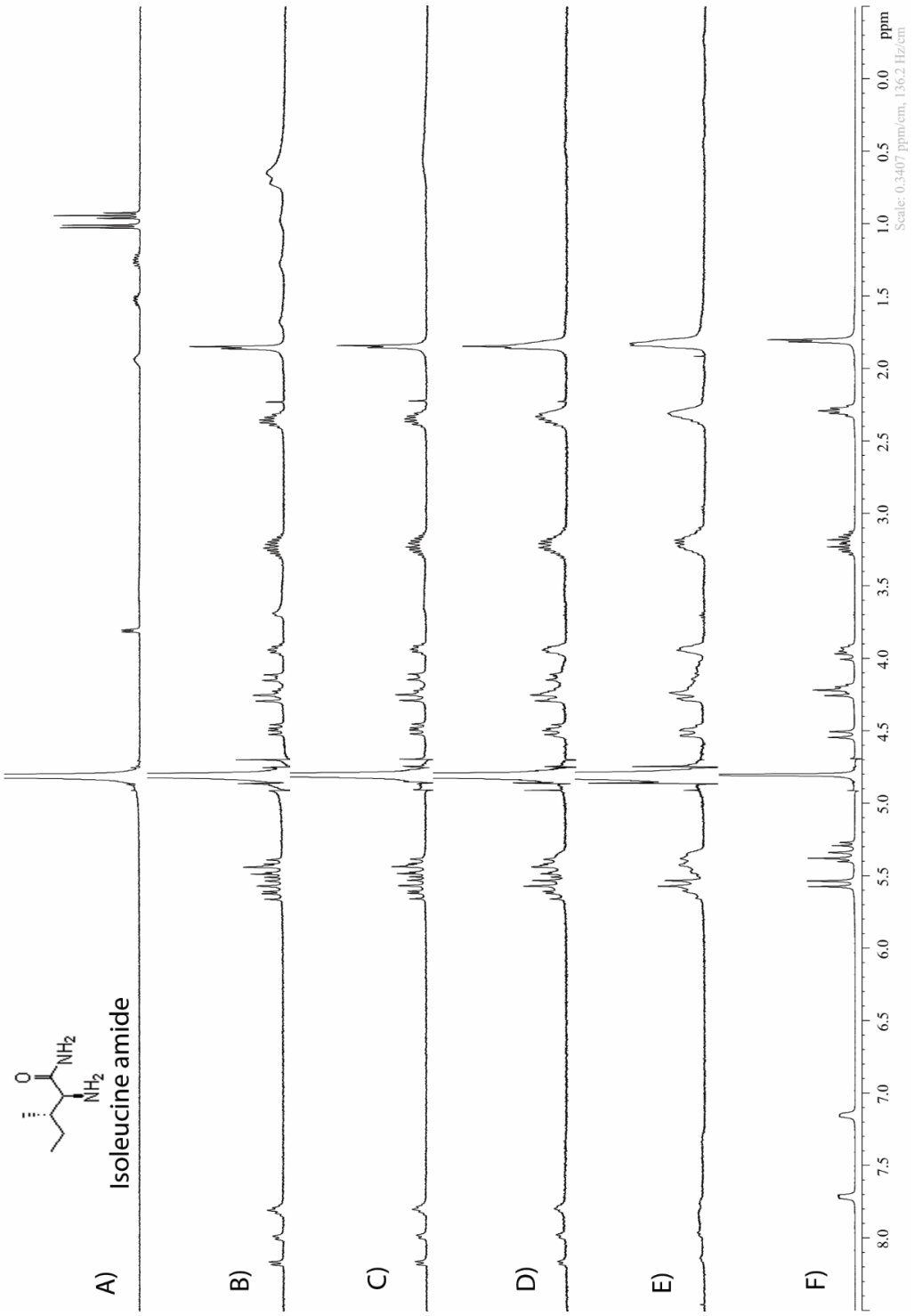

Figure II-S102. ^{1}H NMR spectra recorded (D_2O, 400 MHz, RT) for: a) Isoleucine amide (2 mM), b) a mixture of Motor 2 (1 mM) and Isoleucine amide (2 mM), c) a mixture of Motor 2 (1 mM) and Isoleucine amide (1.5 mM), d) a mixture of Motor 2 (1 mM) and Isoleucine amide (1 mM), e) a mixture of Motor 2 (1 mM) and Isoleucine amide (0.5 mM), f) Motor 2 (5 mM).

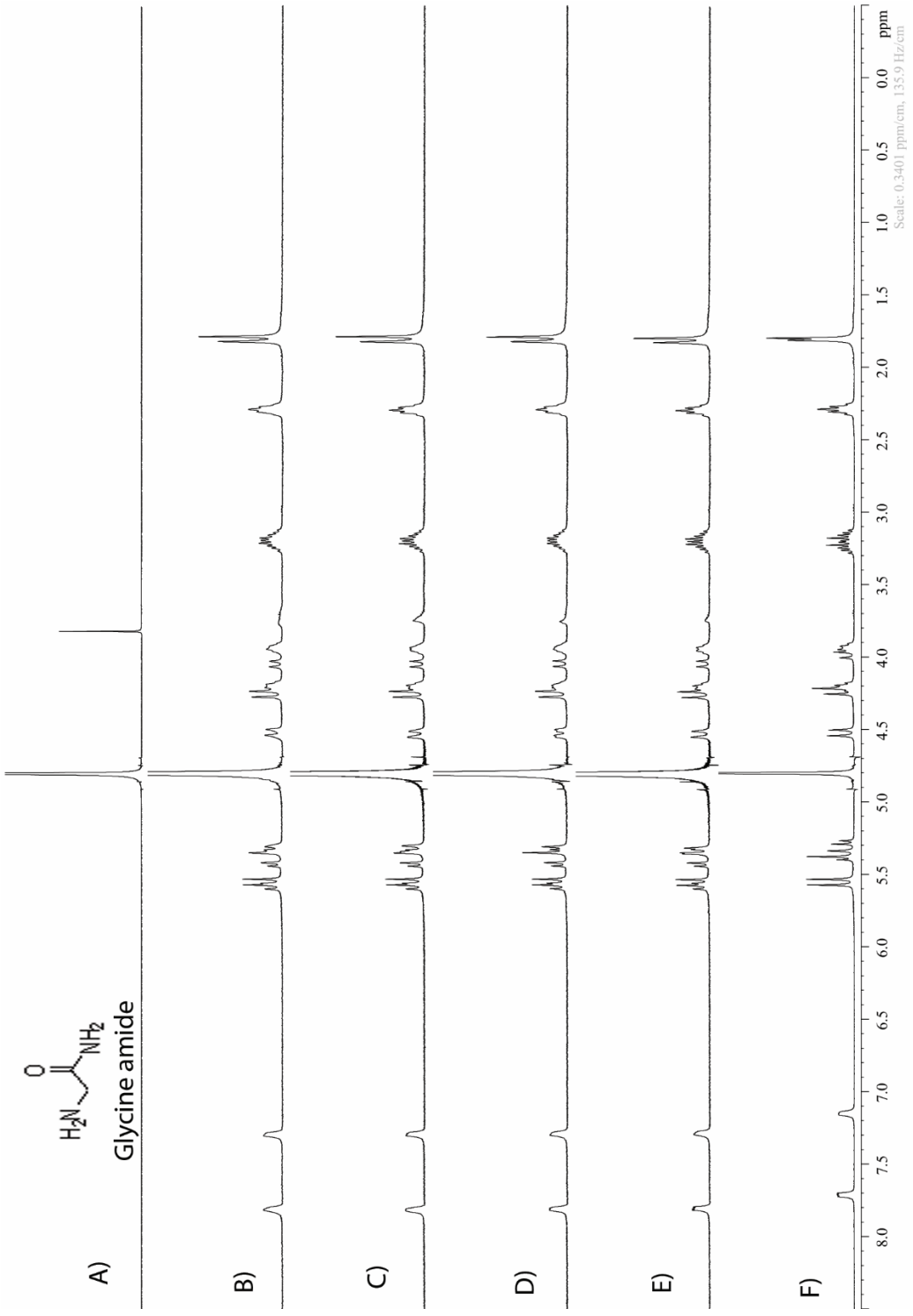

Figure II-S103. ^{1}H NMR spectra recorded (D_2O, 400 MHz, RT) for: a) Glycine amide (3 mM), b) a mixture of Motor 2 (1 mM) and Glycine amide (2 mM), c) a mixture of Motor 2 (1 mM) and Glycine amide (1.5 mM), d) a mixture of Motor 2 (1 mM) and Glycine amide (1 mM), e) a mixture of Motor 2 (1 mM) and Glycine amide (0.5 mM), f) Motor 2 (5 mM).

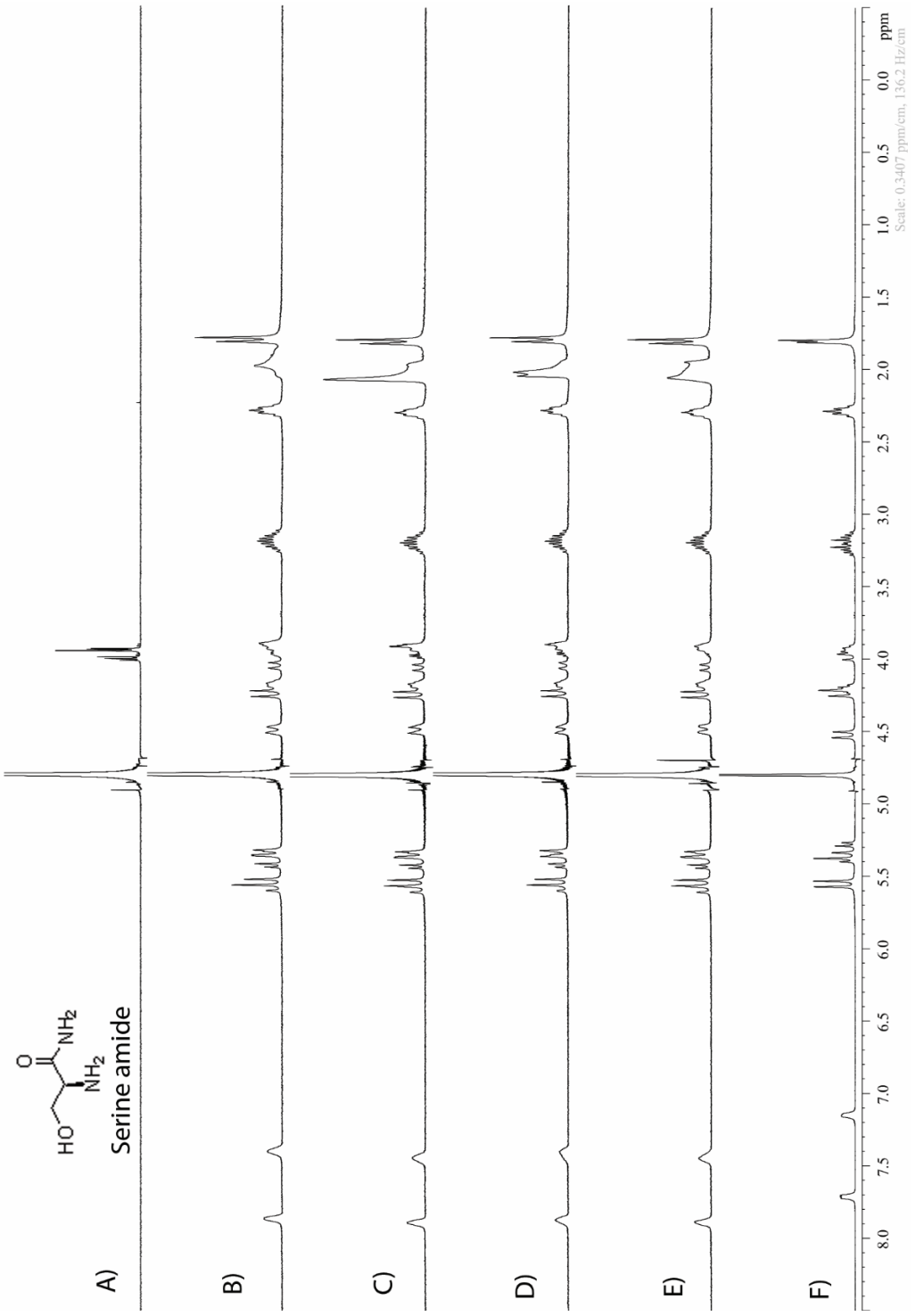

Figure II-S104. ^{1}H NMR spectra recorded (D_2O, 400 MHz, RT) for: a) Serine amide (2 mM), b) a mixture of Motor 2 (1 mM) and Serine amide (2 mM), c) a mixture of Motor 2 (1 mM) and Serine amide (1.5 mM), d) a mixture of Motor 2 (1 mM) and Serine amide (1 mM), e) a mixture of Motor 2 (1 mM) and Serine amide (0.5 mM), f) Motor 2 (5 mM).

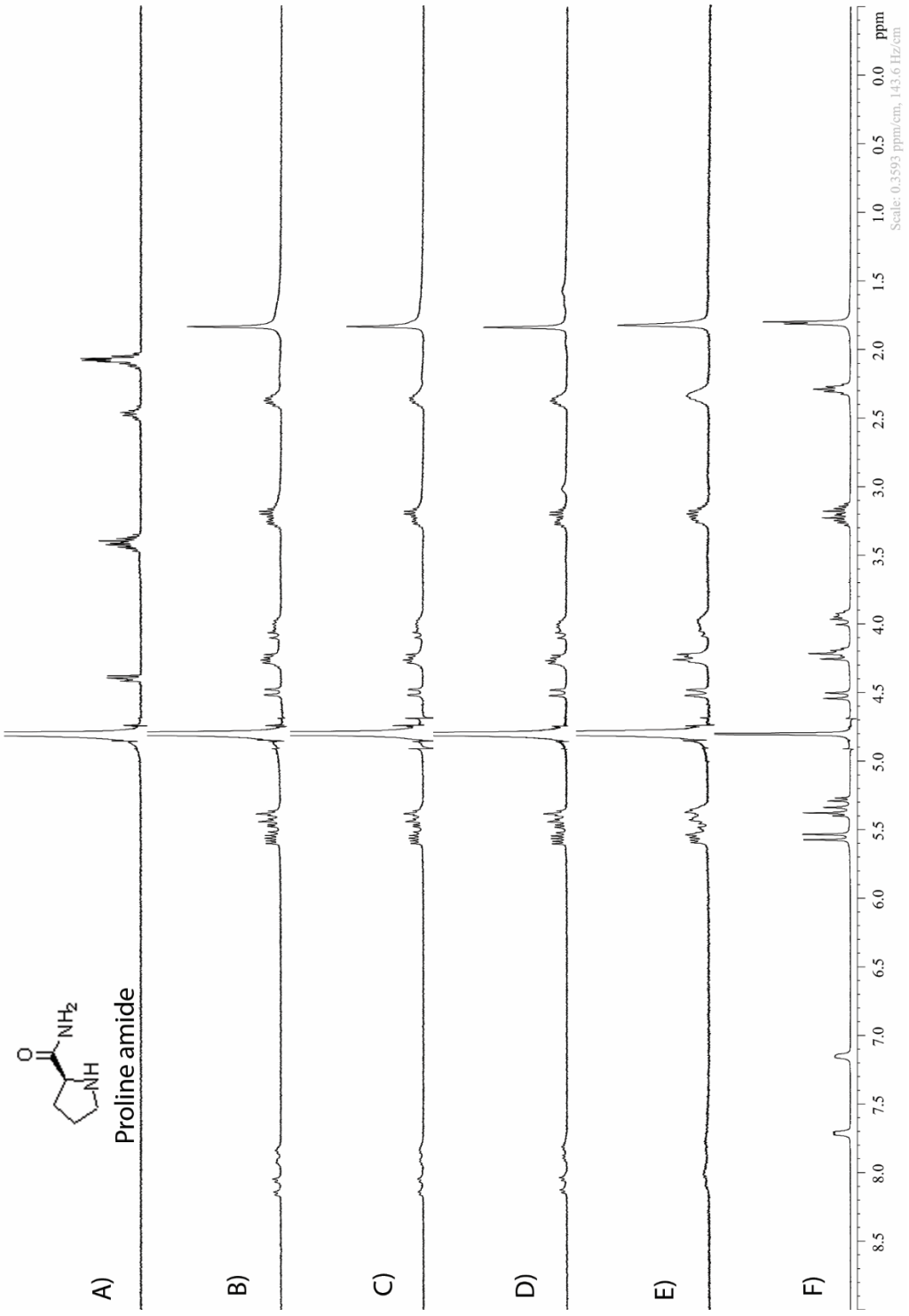

Figure II-S105. ^{1}H NMR spectra recorded (D_2O, 400 MHz, RT) for: a) Proline amide (2 mM), b) a mixture of Motor 2 (1 mM) and Proline amide (2 mM), c) a mixture of Motor 2 (1 mM) and Proline amide (1.5 mM), d) a mixture of Motor 2 (1 mM) and Proline amide (1 mM), e) a mixture of Motor 2 (1 mM) and Proline amide (0.5 mM), f) Motor 2 (5 mM).

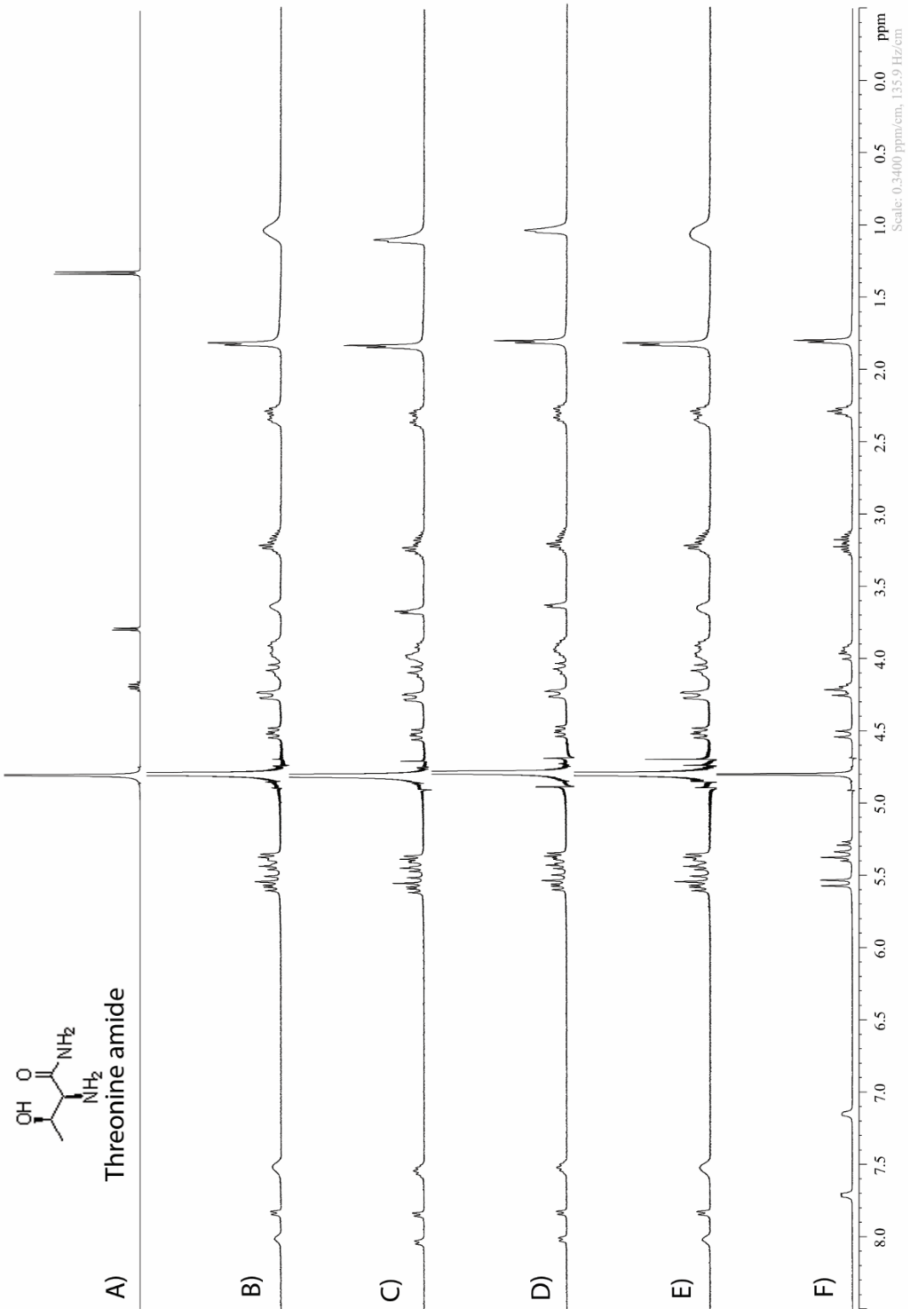

Figure II-S106. ^{1}H NMR spectra recorded (D_2O, 400 MHz, RT) for: a) Threonine amide (2 mM), b) a mixture of Motor 2 (1 mM) and Threonine amide (2 mM), c) a mixture of Motor 2 (1 mM) and Threonine amide (1.5 mM), d) a mixture of Motor 2 (1 mM) and Threonine amide (1 mM), e) a mixture of Motor 2 (1 mM) and Threonine amide (0.5 mM), f) Motor 2 (5 mM).

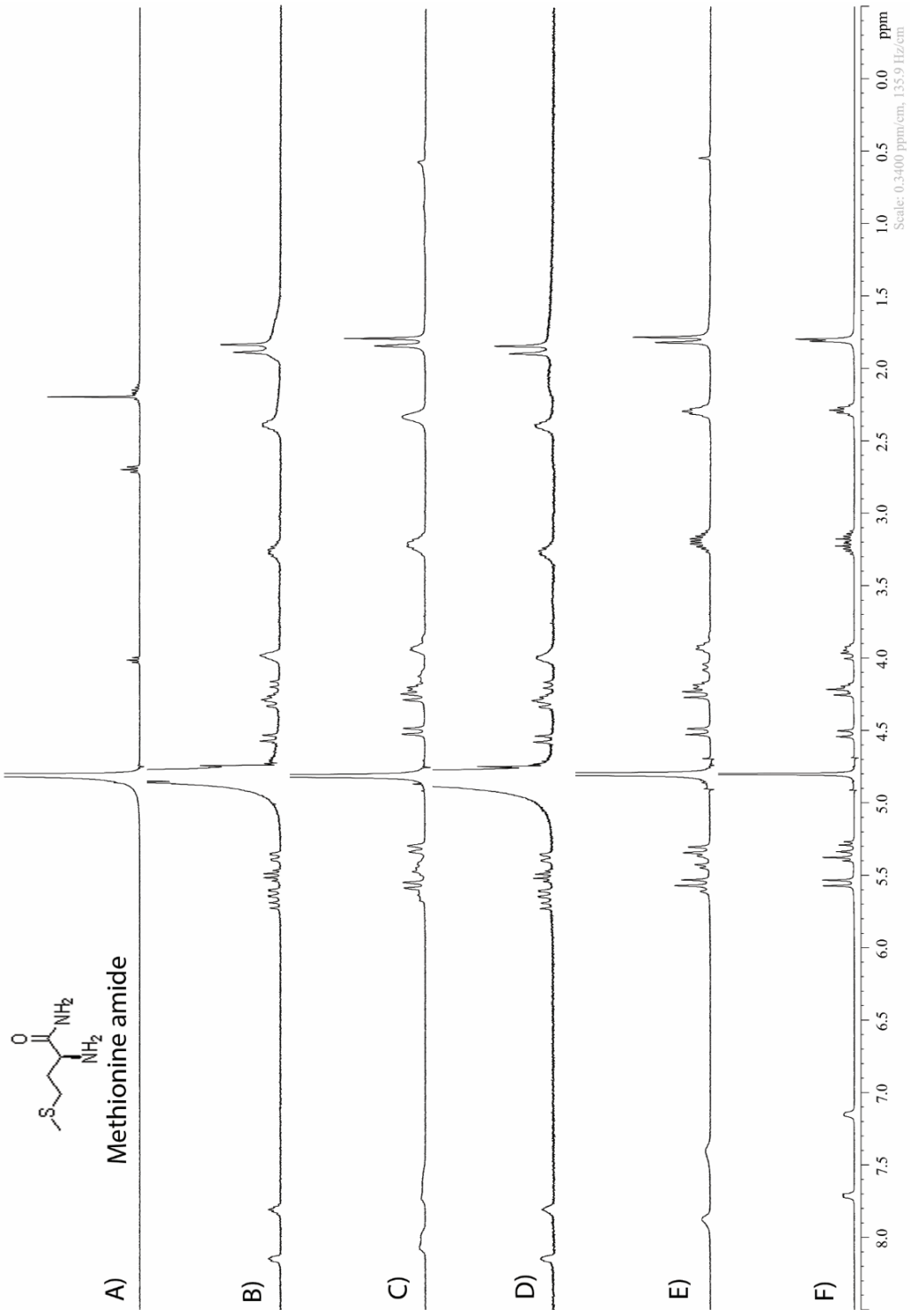

Figure II-S107. ^{1}H NMR spectra recorded (D_2O, 400 MHz, RT) for: a) Methionine amide (2 mM), b) a mixture of Motor 2 (1 mM) and Methionine amide (2 mM), c) a mixture of Motor 2 (1 mM) and Methionine amide (1.5 mM), d) a mixture of Motor 2 (1 mM) and Methionine amide (1 mM), e) a mixture of Motor 2 (1 mM) and Methionine amide (0.5 mM), f) Motor 2 (5 mM).

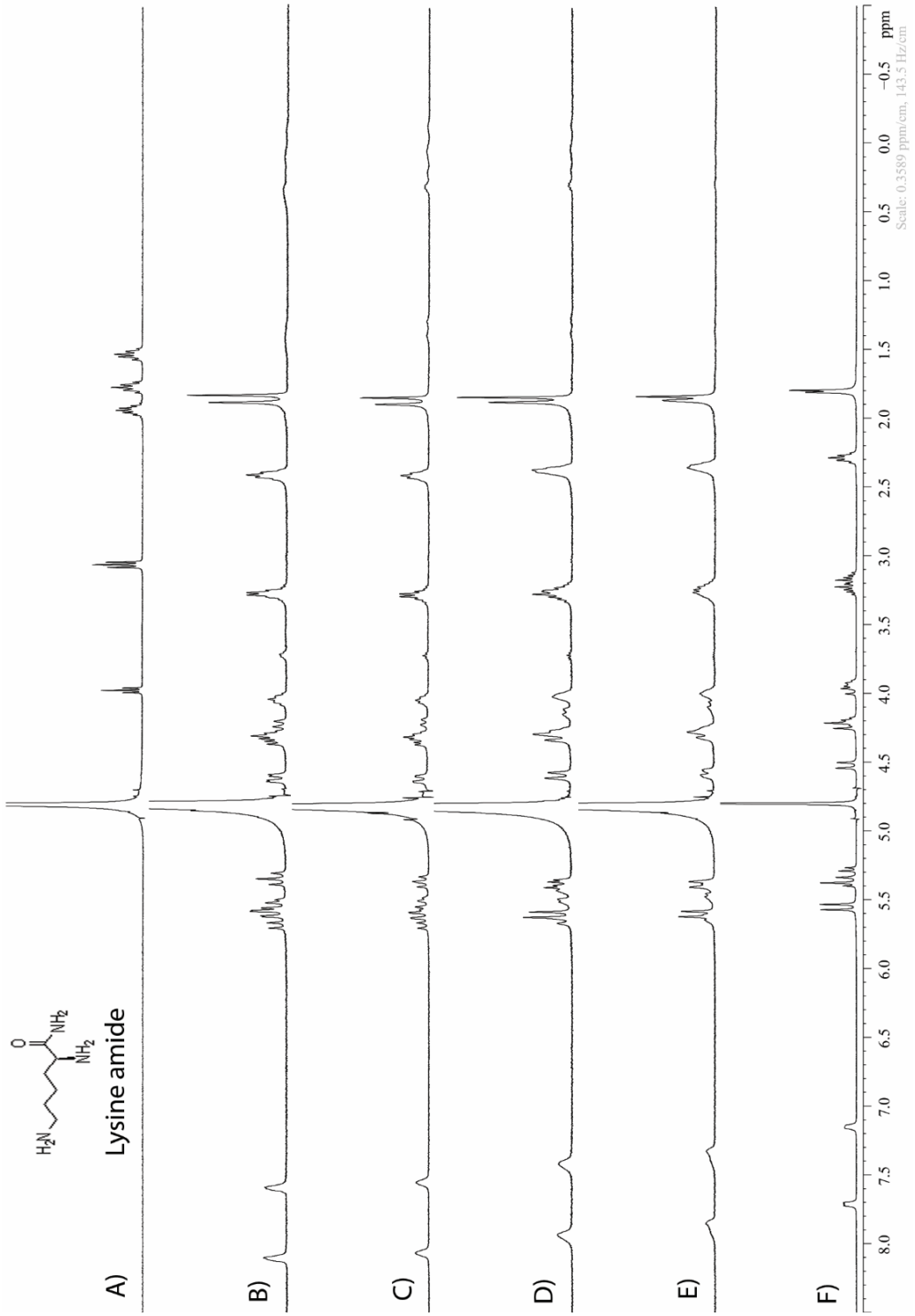

Figure II-S108. ^{1}H NMR spectra recorded (D_2O, 400 MHz, RT) for: a) Lysine amide (2 mM), b) a mixture of Motor 2 (1 mM) and Lysine amide (2 mM), c) a mixture of Motor 2 (1 mM) and Lysine amide (1.5 mM), d) a mixture of Motor 2 (1 mM) and Lysine amide (1 mM), e) a mixture of Motor 2 (1 mM) and Lysine amide (0.5 mM), f) Motor 2 (5 mM).

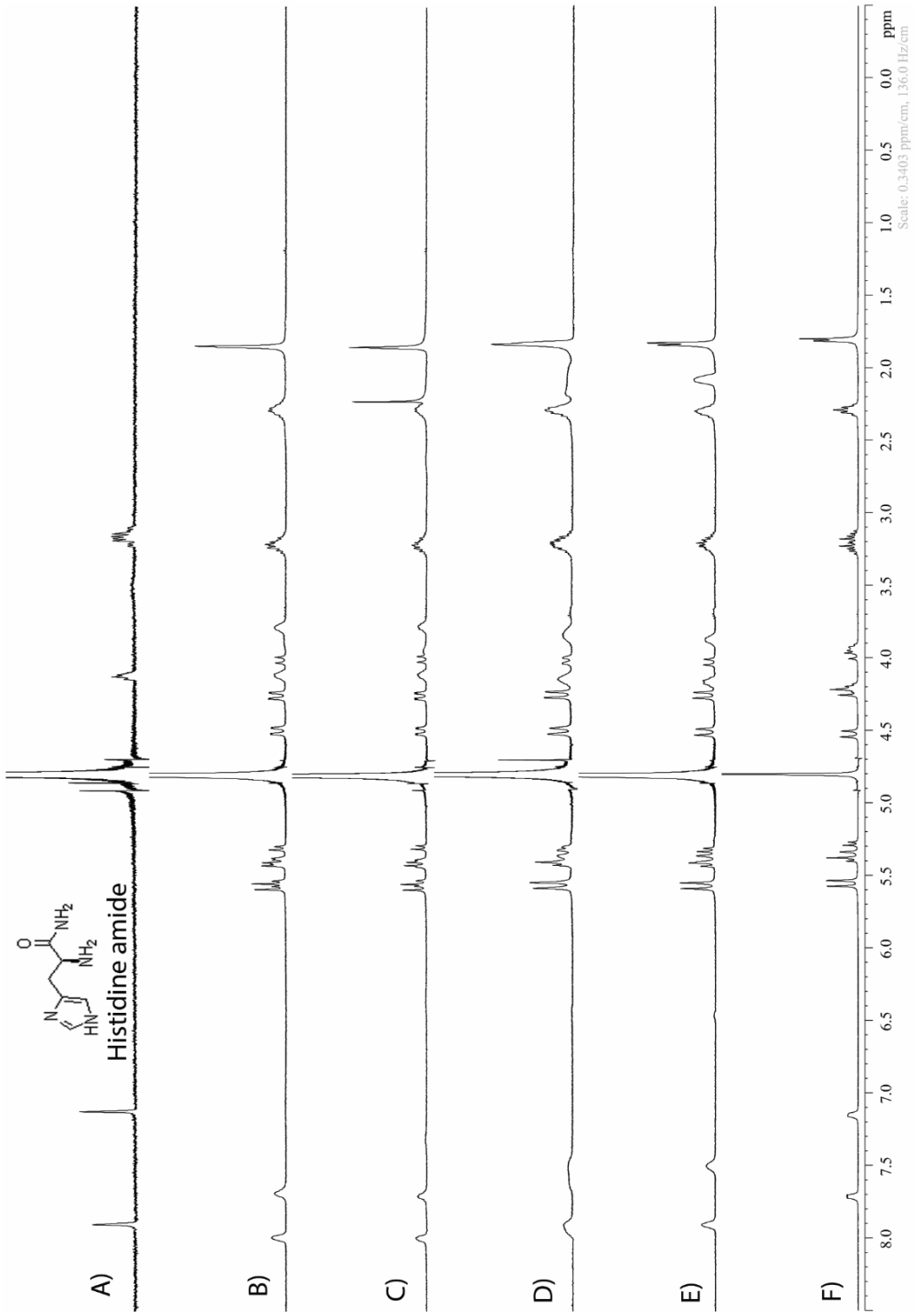

Figure II-S109. ^{1}H NMR spectra recorded (D_2O, 400 MHz, RT) for: a) Histidine amide (2 mM), b) a mixture of Motor 2 (1 mM) and Histidine amide (2 mM), c) a mixture of Motor 2 (1 mM) and Histidine amide (1.5 mM), d) a mixture of Motor 2 (1 mM) and Histidine amide (1 mM), e) a mixture of Motor 2 (1 mM) and Histidine amide (0.5 mM), f) Motor 2 (5 mM).

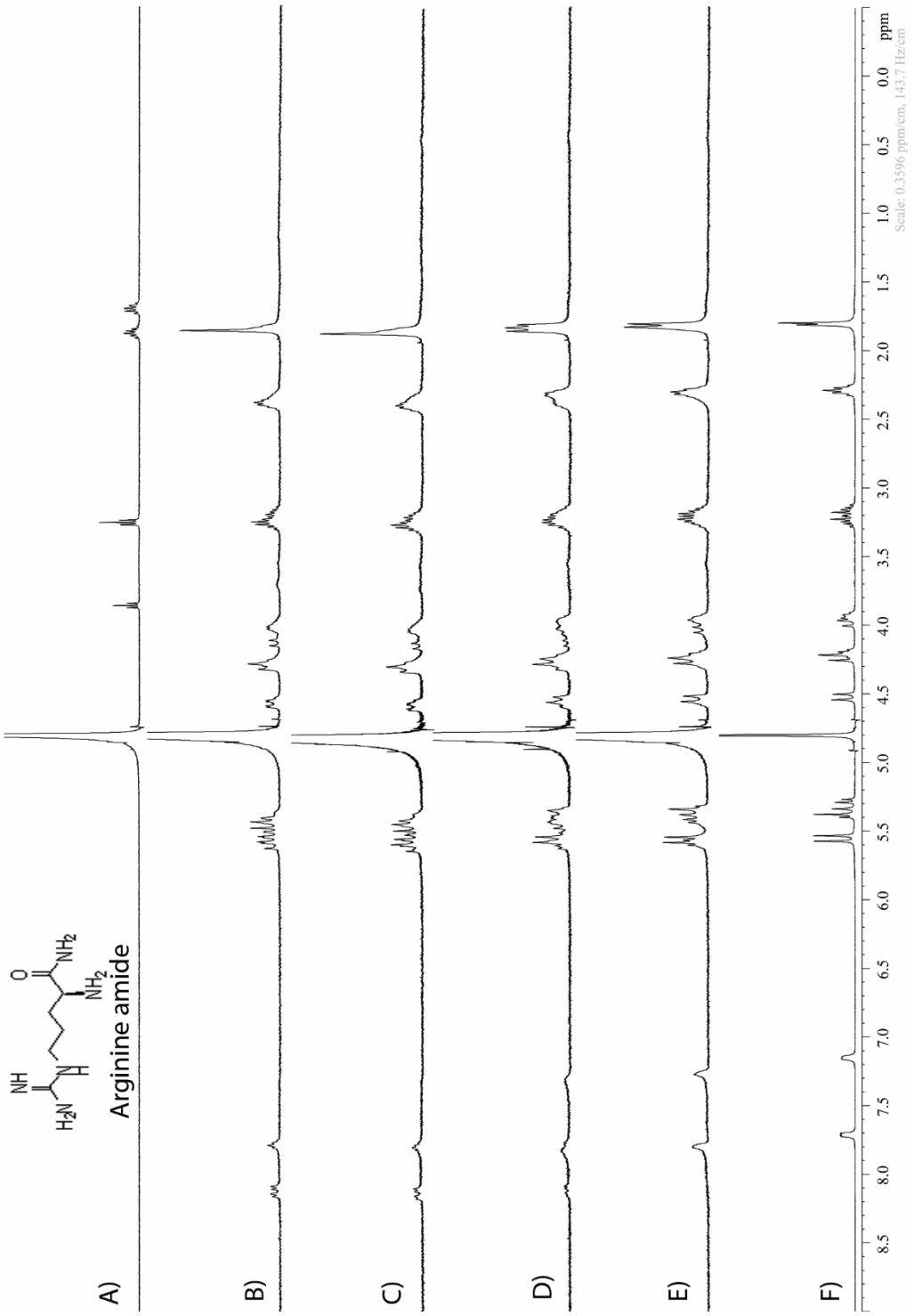

Figure II-S110. ^{1}H NMR spectra recorded (D_2O, 400 MHz, RT) for: a) Arginine amide (2 mM), b) a mixture of Motor 2 (1 mM) and Arginine amide (2 mM), c) a mixture of Motor 2 (1 mM) and Arginine amide (1.5 mM), d) a mixture of Motor 2 (1 mM) and Arginine amide (1 mM), e) a mixture of Motor 2 (1 mM) and Arginine amide (0.5 mM), f) Motor 2 (5 mM).

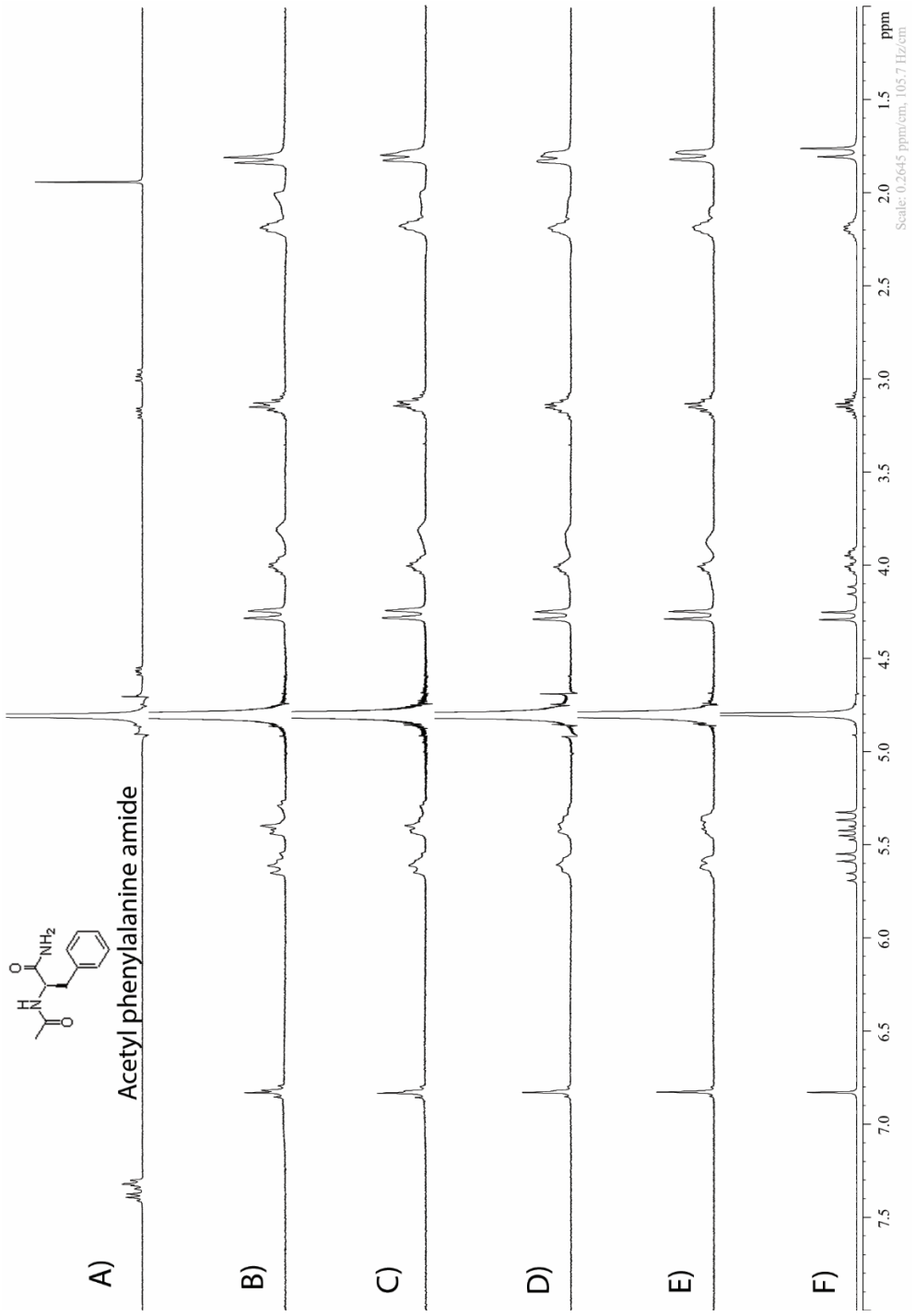

Figure II-S111. ^{1}H NMR spectra recorded (D_2O , 400 MHz, RT) for: a) Acetyl phenylalanine amide (2 mM), b) a mixture of Motor 1 (1 mM) and Acetyl phenylalanine amide (2 mM), c) a mixture of Motor 1 (1 mM) and Acetyl phenylalanine amide (1.5 mM), d) a mixture of Motor 1 (1 mM) and Acetyl phenylalanine amide (1 mM), e) a mixture of Motor 1 (1 mM) and Acetyl phenylalanine amide (0.5 mM), f) Motor 1 (1 mM).

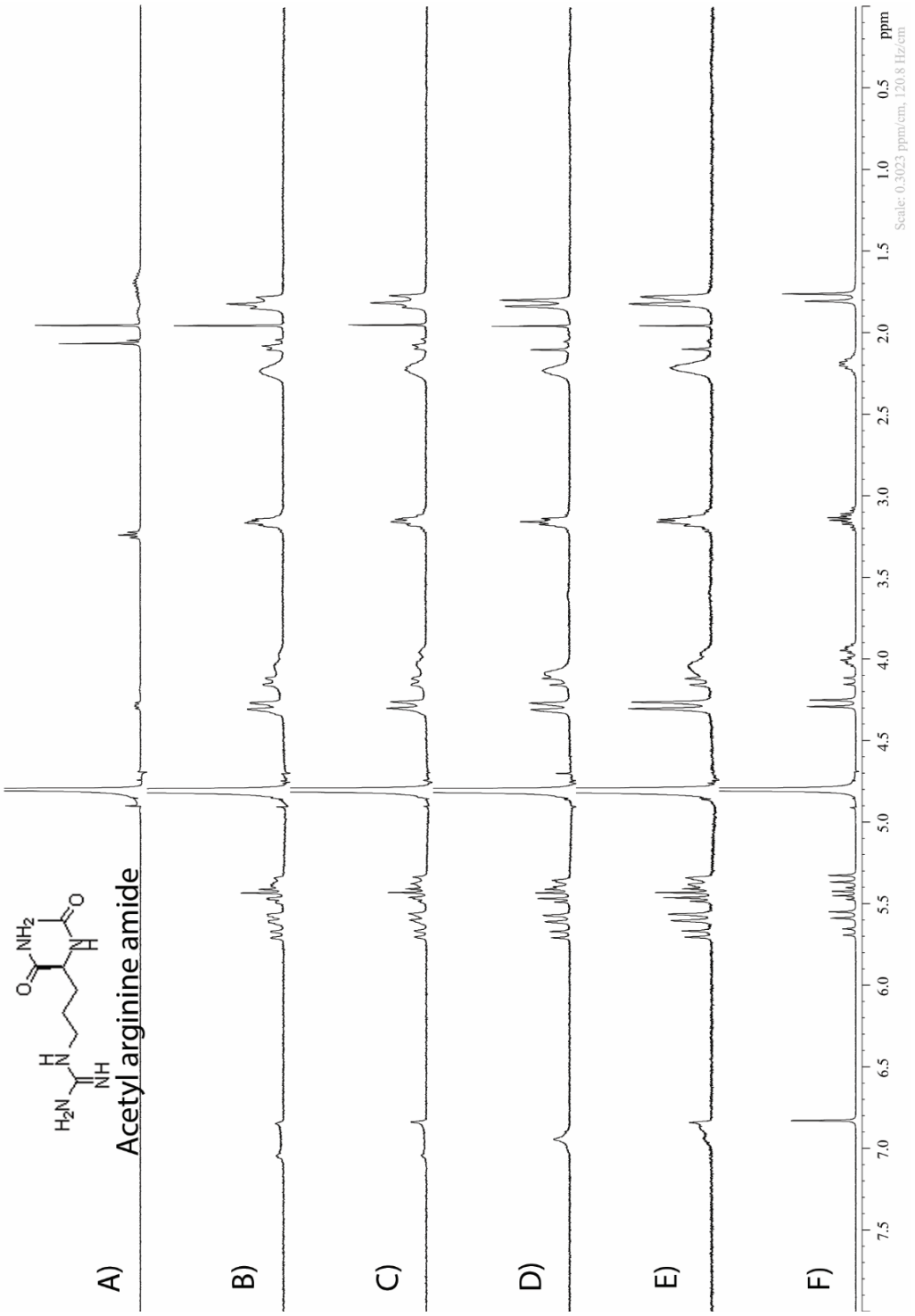

Figure II-S112. ^{1}H NMR spectra recorded (D_2O , 400 MHz, RT) for: a) Acetyl arginine amide (2 mM), b) a mixture of Motor 1 (1 mM) and Acetyl arginine amide (2 mM), c) a mixture of Motor 1 (1 mM) and Acetyl arginine amide (1.5 mM), d) a mixture of Motor 1 (1 mM) and Acetyl arginine amide (1 mM), e) a mixture of Motor 1 (1 mM) and Acetyl arginine amide (0.5 mM), f) Motor 1 (1 mM).

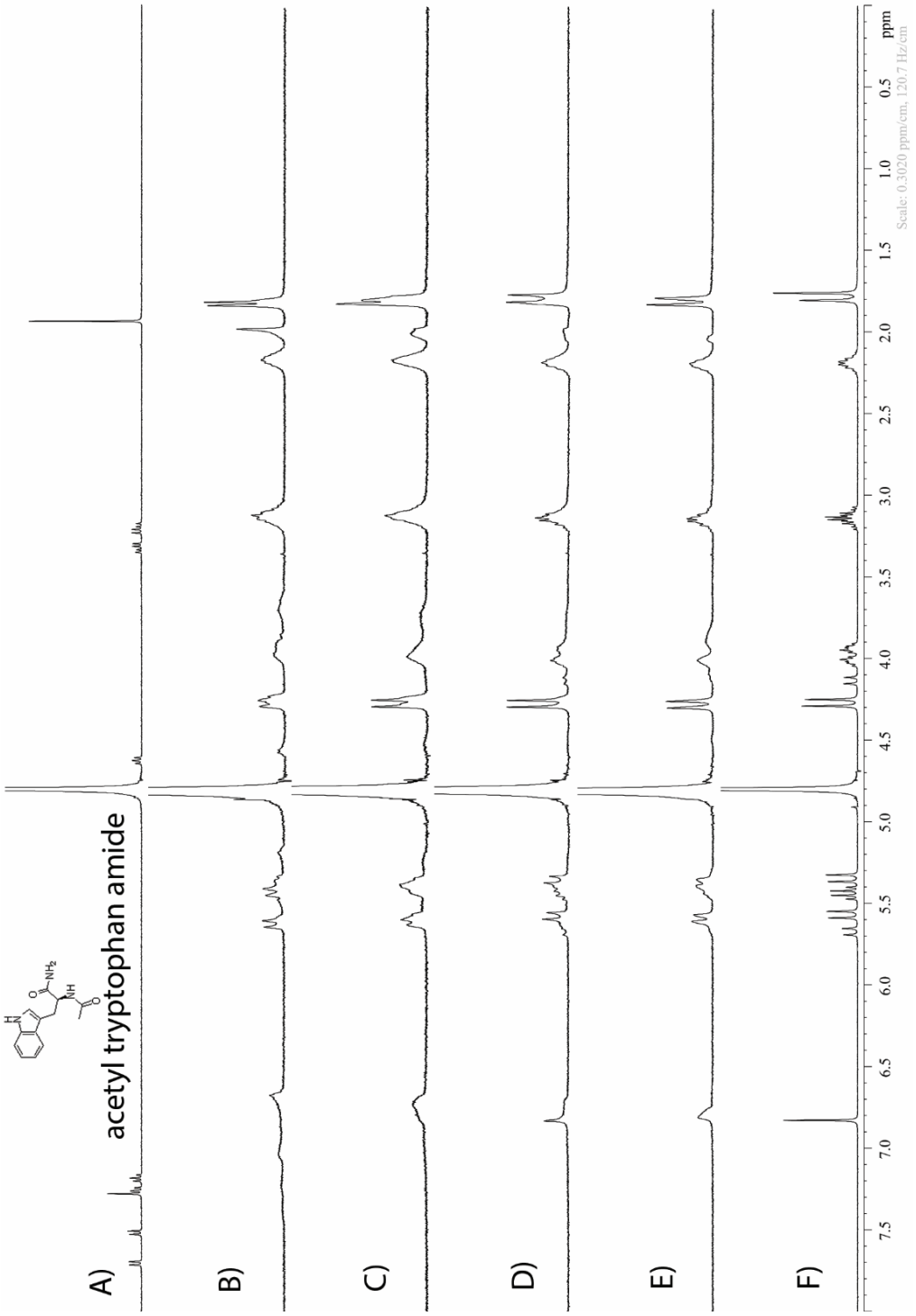

Figure II-S113. ^{1}H NMR spectra recorded (D_2O , 400 MHz, RT) for: a) Acetyl tryptophan amide (2 mM), b) a mixture of Motor 1 (1 mM) and Acetyl tryptophan amide (2 mM), c) a mixture of Motor 1 (1 mM) and Acetyl tryptophan amide (1.5 mM), d) a mixture of Motor 1 (1 mM) and Acetyl tryptophan amide (1 mM), e) a mixture of Motor 1 (1 mM) and Acetyl tryptophan amide (0.5 mM), f) Motor 1 (1 mM).

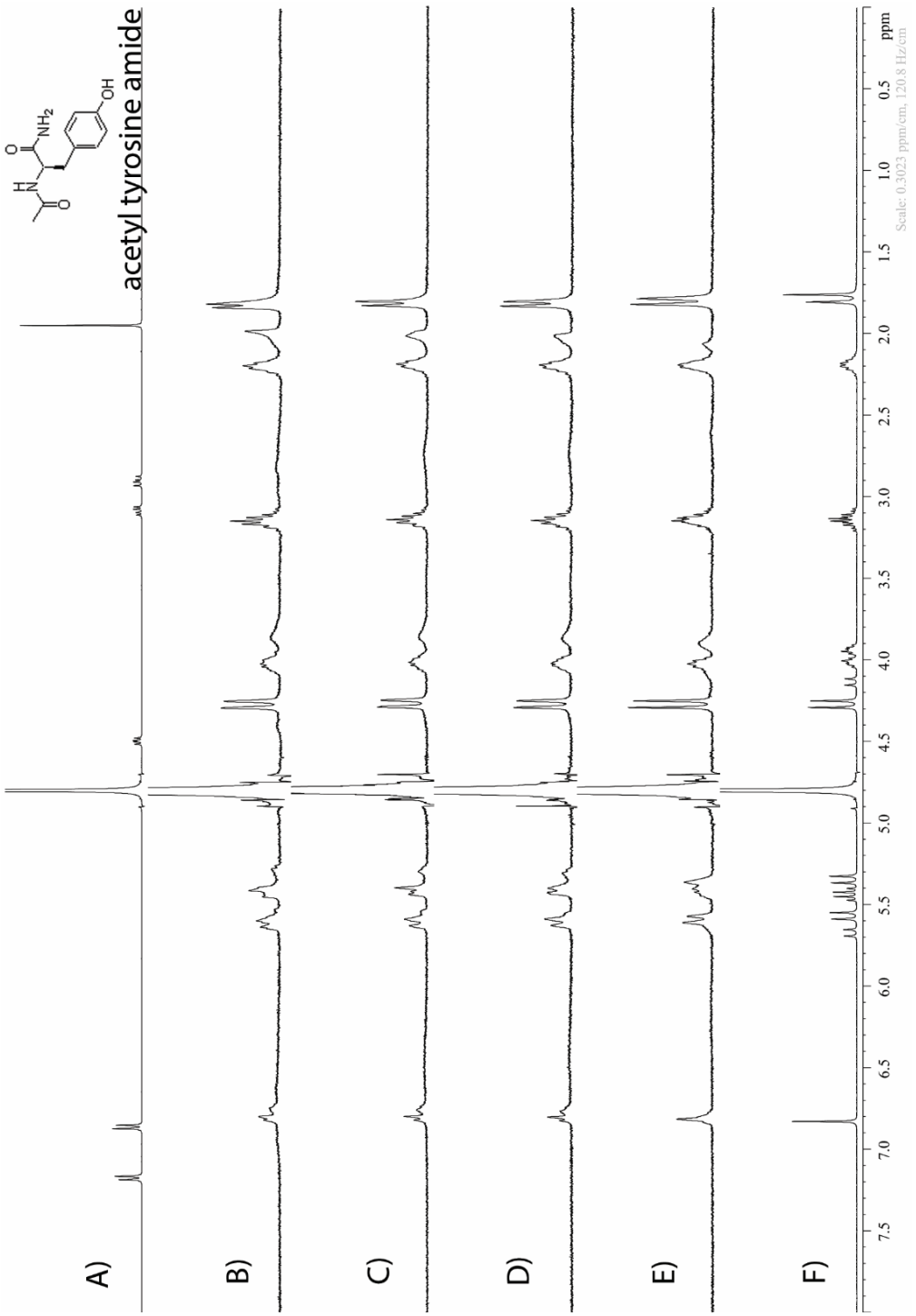

Figure II-S114. ^{1}H NMR spectra recorded (D_2O , 400 MHz, RT) for: a) Acetyl tyrosine amide (2 mM), b) a mixture of Motor 1 (1 mM) and Acetyl tyrosine amide (2 mM), c) a mixture of Motor 1 (1 mM) and Acetyl tyrosine amide (1.5 mM), d) a mixture of Motor 1 (1 mM) and Acetyl tyrosine amide (1 mM), e) a mixture of Motor 1 (1 mM) and Acetyl tyrosine amide (0.5 mM), f) Motor 1 (1 mM).

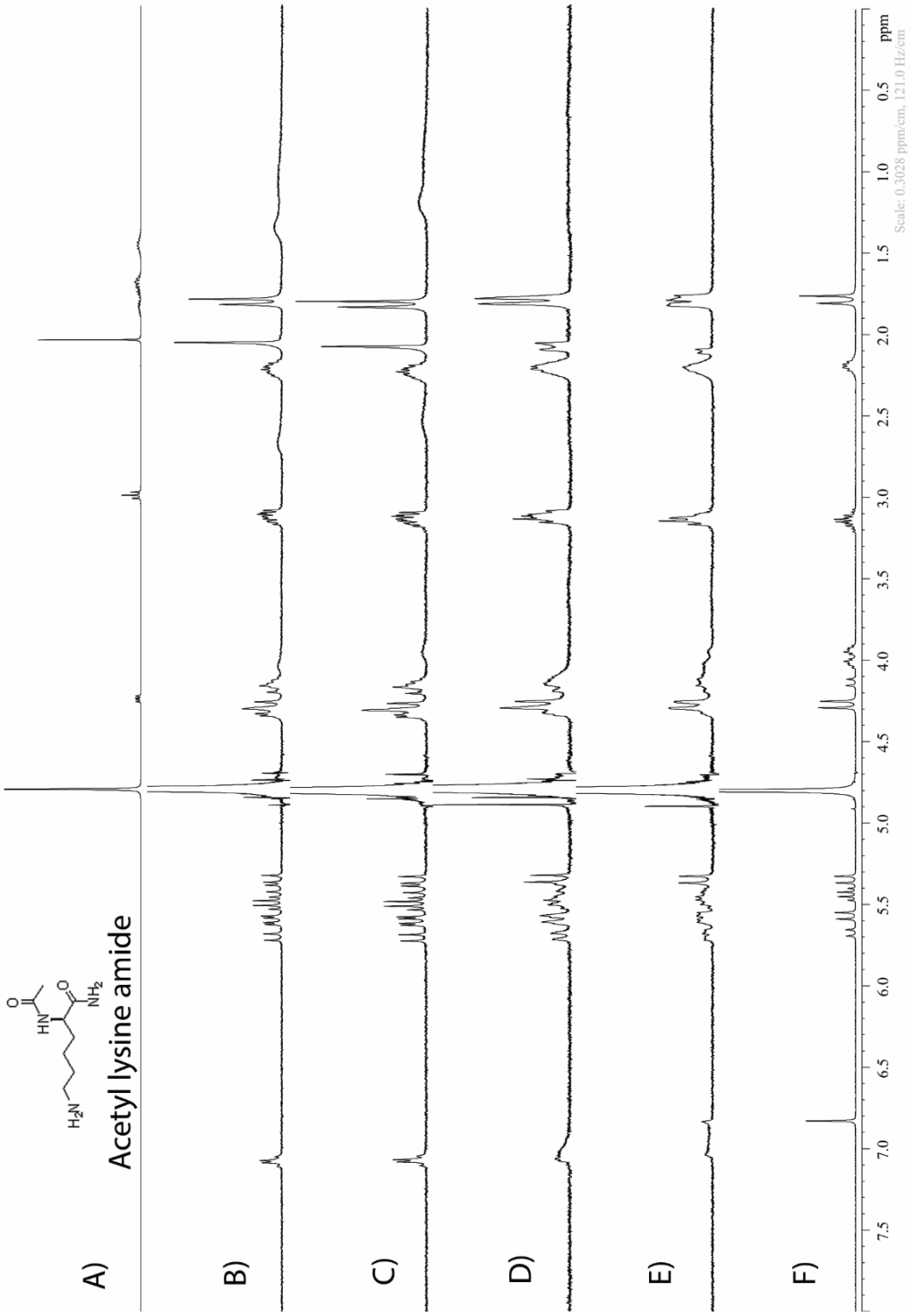

Figure II-S115. ^{1}H NMR spectra recorded (D_2O , 400 MHz, RT) for: a) Acetyl lysine amide (2 mM), b) a mixture of Motor 1 (1 mM) and Acetyl lysine amide (2 mM), c) a mixture of Motor 1 (1 mM) and Acetyl lysine amide (1.5 mM), d) a mixture of Motor 1 (1 mM) and Acetyl lysine amide (1 mM), e) a mixture of Motor 1 (1 mM) and Acetyl lysine amide (0.5 mM), f) Motor 1 (1 mM).

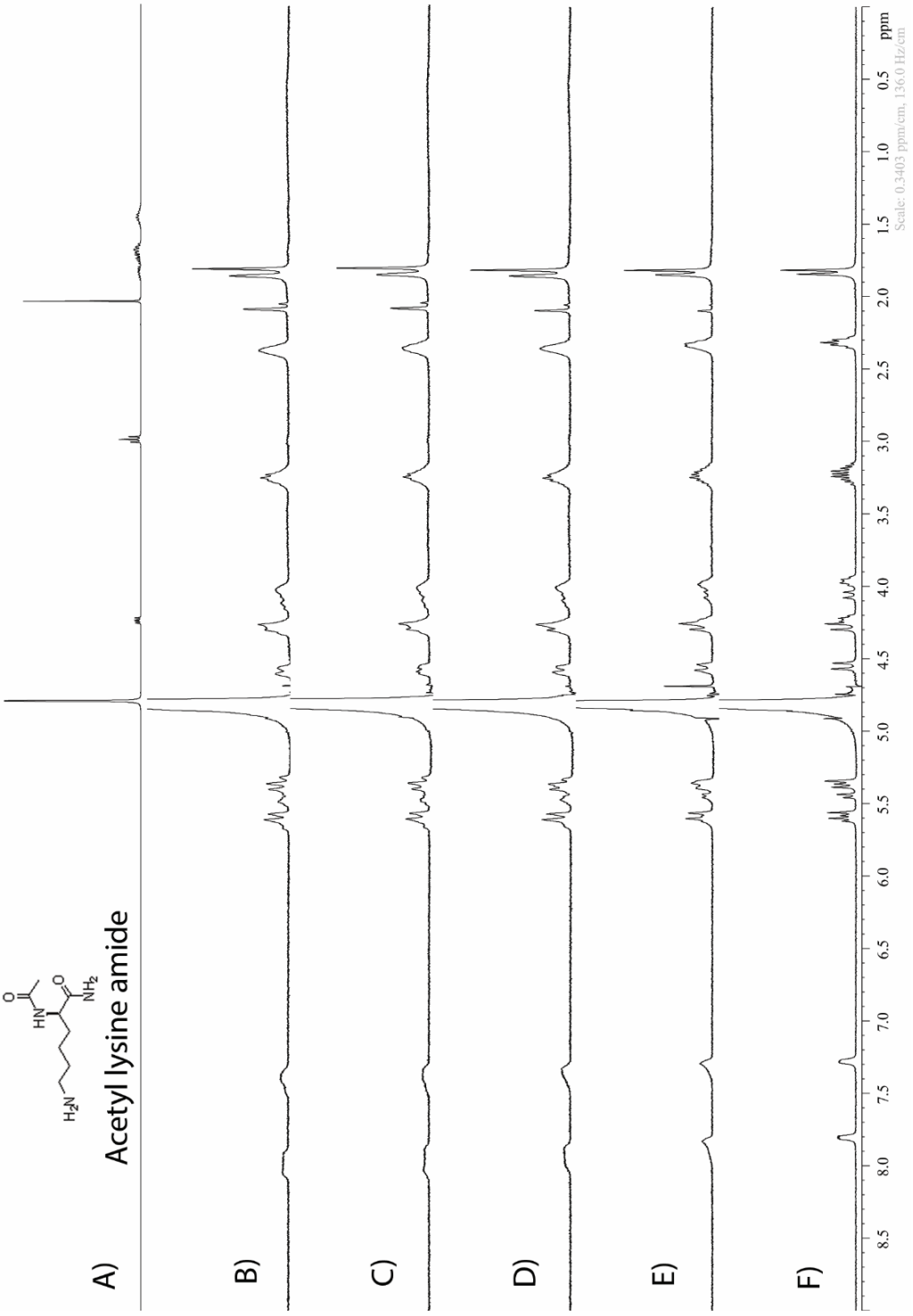

Figure II-S116. ^{1}H NMR spectra recorded (D_2O , 400 MHz, RT) for: a) Acetyl lysine amide (2 mM), b) a mixture of Motor 2 (1 mM) and Acetyl lysine amide (2 mM), c) a mixture of Motor 2 (1 mM) and Acetyl lysine amide (1.5 mM), d) a mixture of Motor 2 (1 mM) and Acetyl lysine amide (1 mM), e) a mixture of Motor 2 (1 mM) and Acetyl lysine amide (0.5 mM), f) Motor 2 (5 mM).

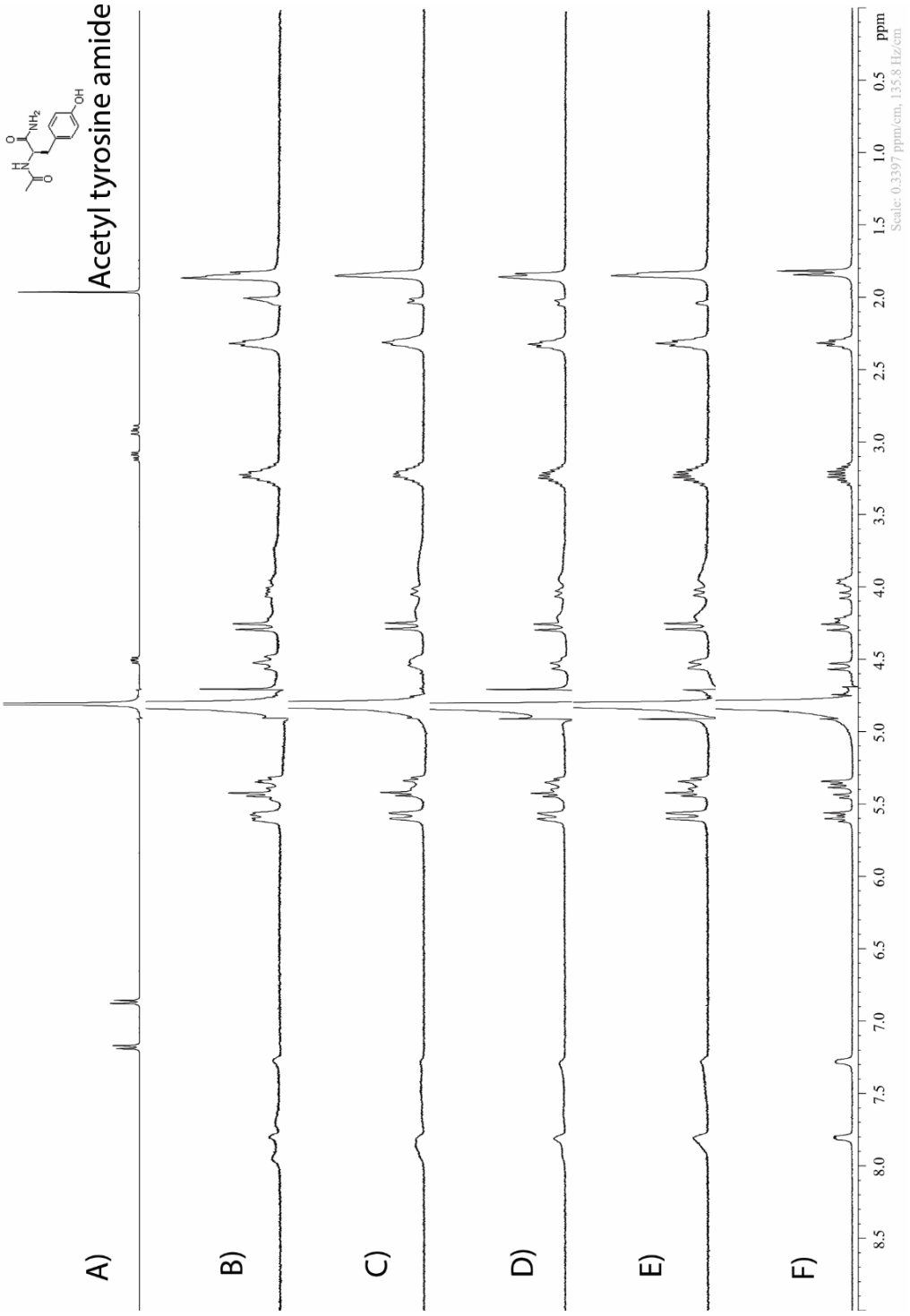

Figure II-S117. ^{1}H NMR spectra recorded (D_2O , 400 MHz, RT) for: a) Acetyl tyrosine amide (2 mM), b) a mixture of Motor 2 (1 mM) and Acetyl tyrosine amide (2 mM), c) a mixture of Motor 2 (1 mM) and Acetyl tyrosine amide (1.5 mM), d) a mixture of Motor 2 (1 mM) and Acetyl tyrosine amide (1 mM), e) a mixture of Motor 2 (1 mM) and Acetyl tyrosine amide (0.5 mM), f) Motor 2 (5 mM).

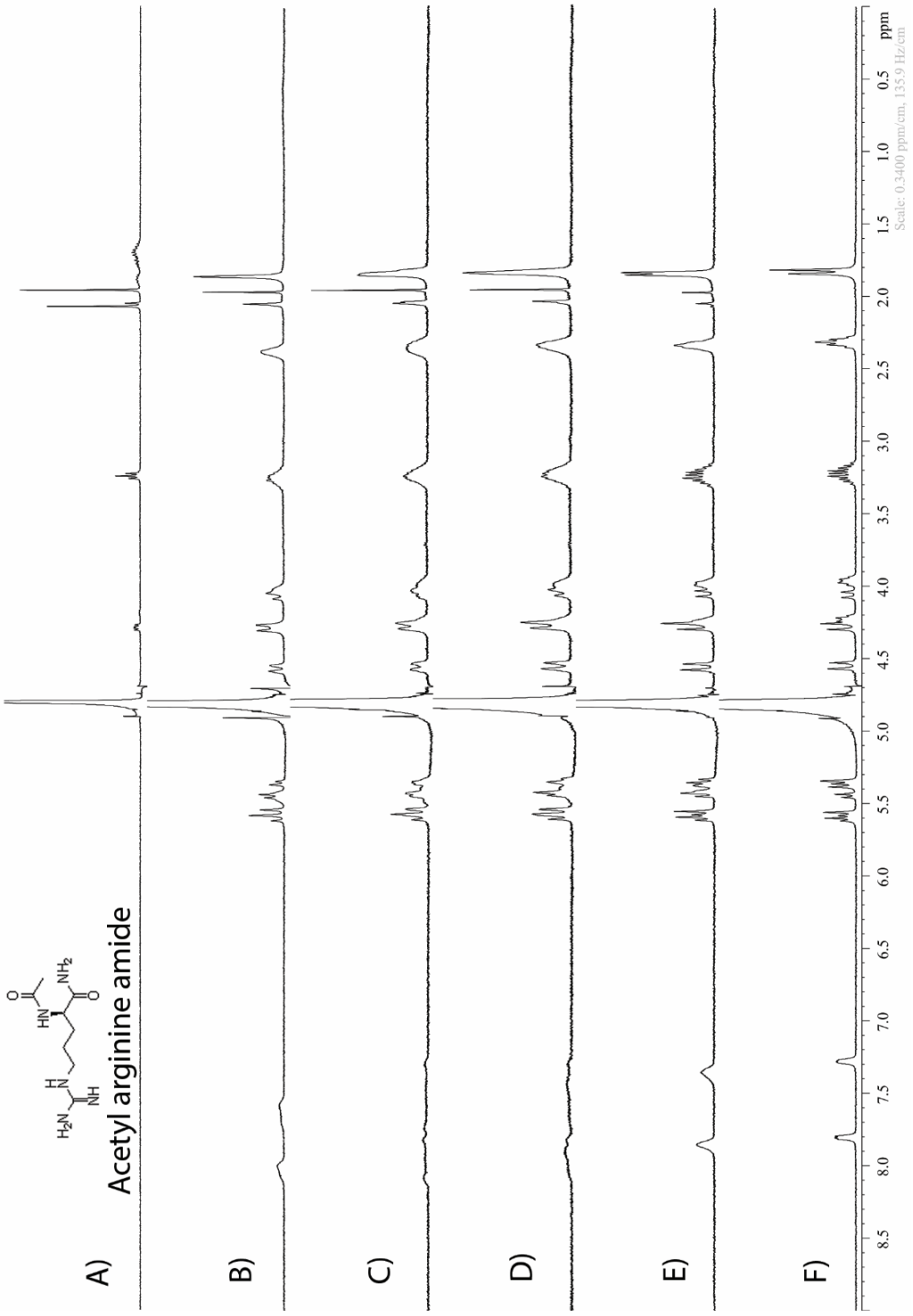

Figure II-S118. ^{1}H NMR spectra recorded (D_2O , 400 MHz, RT) for: a) Acetyl arginine amide (2 mM), b) a mixture of Motor 2 (1 mM) and Acetyl arginine amide (2 mM), c) a mixture of Motor 2 (1 mM) and Acetyl arginine amide (1.5 mM), d) a mixture of Motor 2 (1 mM) and Acetyl arginine amide (1 mM), e) a mixture of Motor 2 (1 mM) and Acetyl arginine amide (0.5 mM), f) Motor 2 (5 mM).

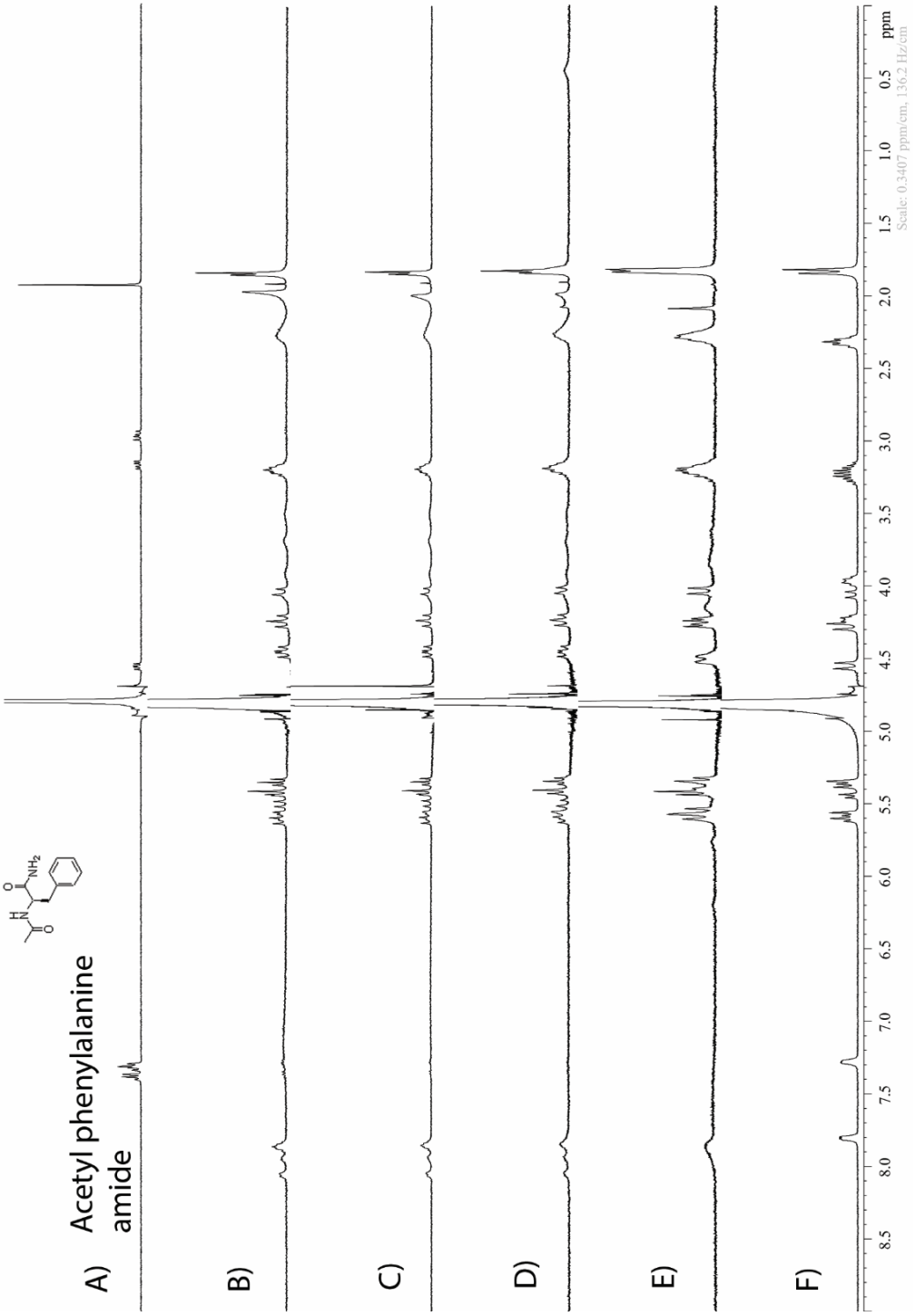

Figure II-S119. ^{1}H NMR spectra recorded (D_2O , 400 MHz, RT) for: a) Acetyl phenylalanine amide (2 mM), b) a mixture of Motor 2 (1 mM) and Acetyl phenylalanine amide (2 mM), c) a mixture of Motor 2 (1 mM) and Acetyl phenylalanine amide (1.5 mM), d) a mixture of Motor 2 (1 mM) and Acetyl phenylalanine amide (1 mM), e) a mixture of Motor 2 (1 mM) and Acetyl phenylalanine amide (0.5 mM), f) Motor 2 (5 mM).

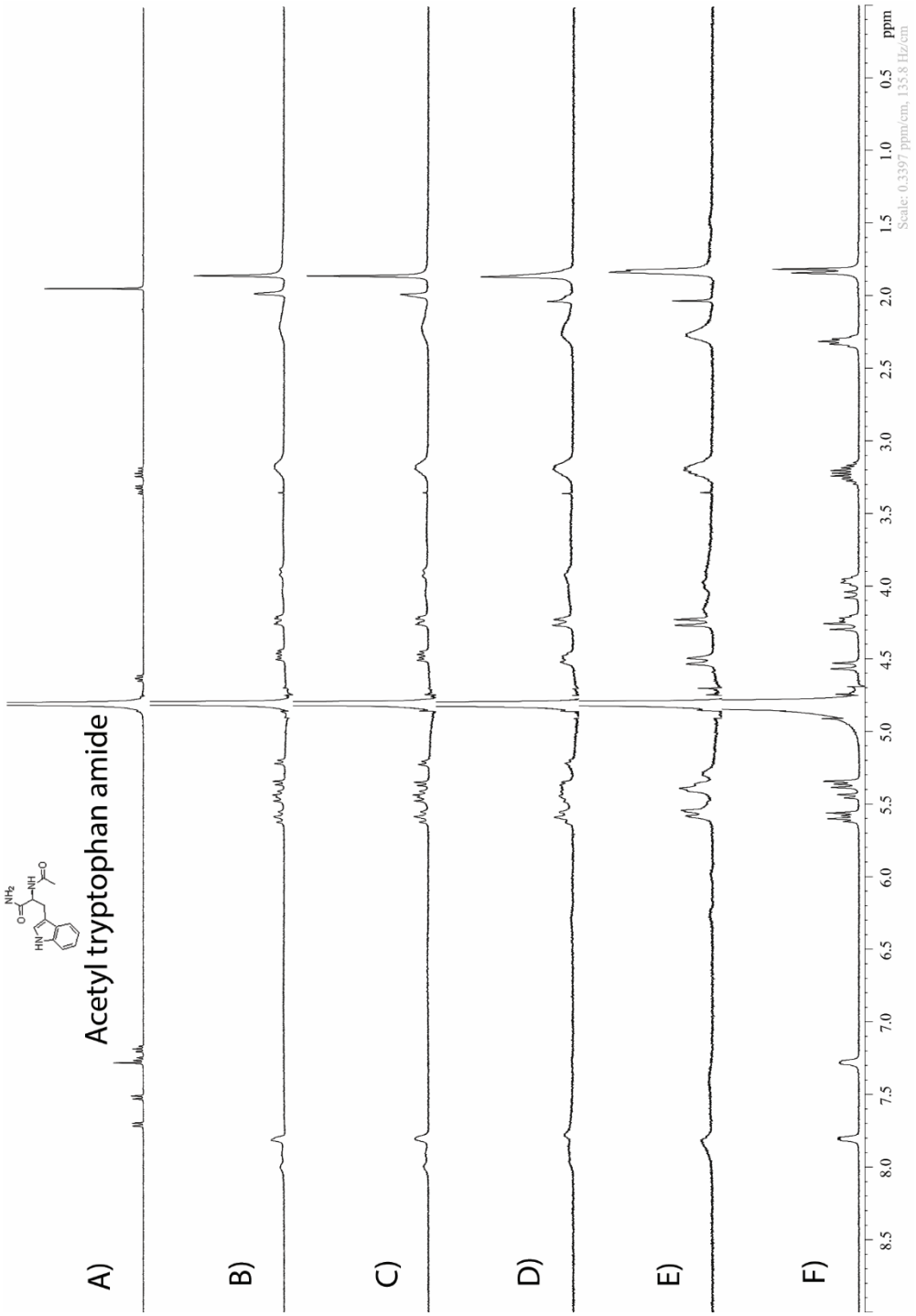

Figure II-S120. ^{1}H NMR spectra recorded (D_2O , 400 MHz, RT) for: a) Acetyl tryptophan amide (2 mM), b) a mixture of Motor 2 (1 mM) and Acetyl tryptophan amide (2 mM), c) a mixture of Motor 2 (1 mM) and Acetyl tryptophan amide (1.5 mM), d) a mixture of Motor 2 (1 mM) and Acetyl tryptophan amide (1 mM), e) a mixture of Motor 2 (1 mM) and Acetyl tryptophan amide (0.5 mM), f) Motor 2 (5 mM).

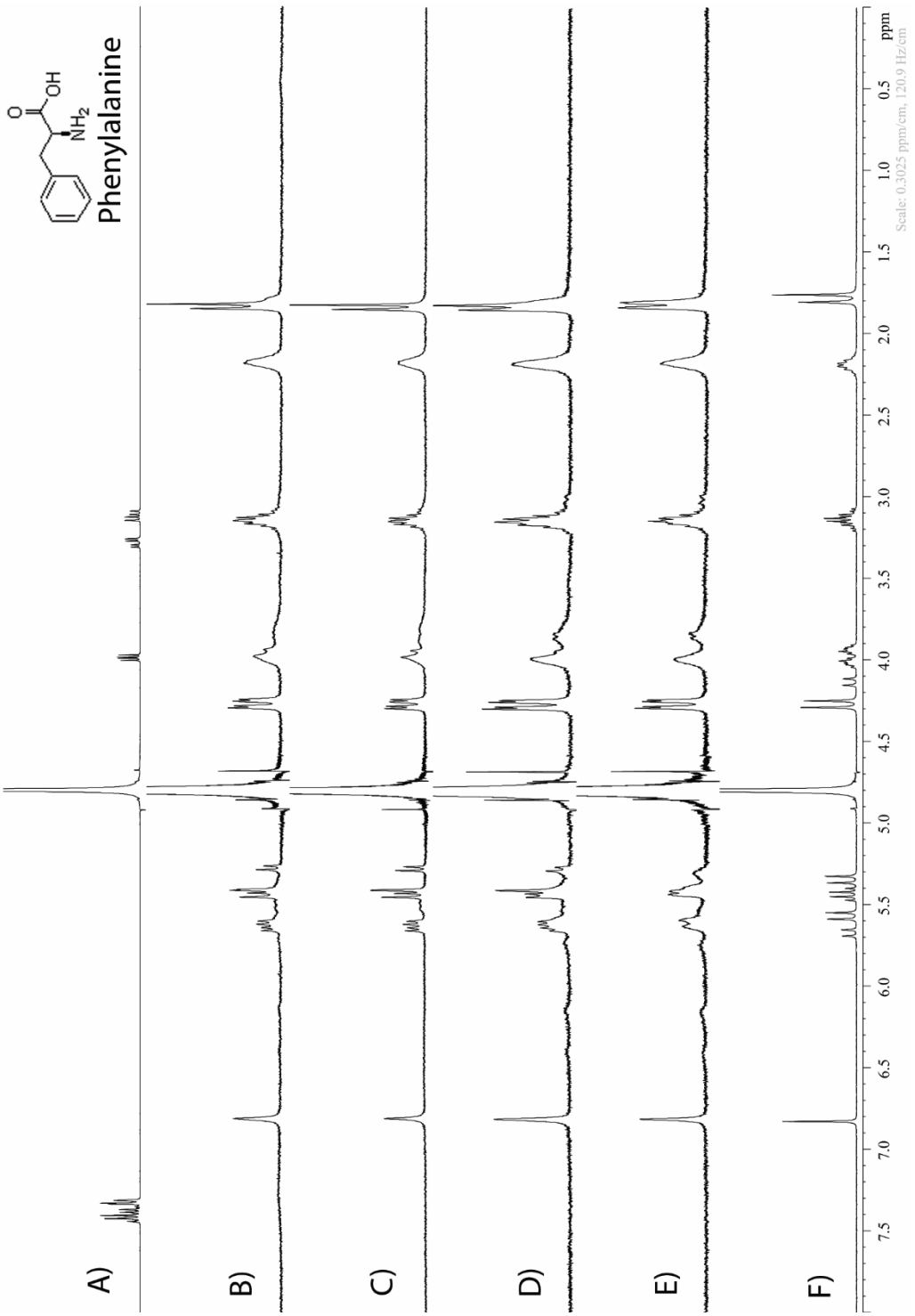

Figure II-S121. ^{1}H NMR spectra recorded (D_2O , 400 MHz, RT) for: a) Phenylalanine (2 mM), b) a mixture of Motor 1 (1 mM) and phenylalanine (2 mM), c) a mixture of Motor 1 (1 mM) and phenylalanine (1.5 mM), d) a mixture of Motor 1 (1 mM) and phenylalanine (1 mM), e) a mixture of Motor 1 (1 mM) and phenylalanine (0.5 mM), f) Motor 1 (1 mM).

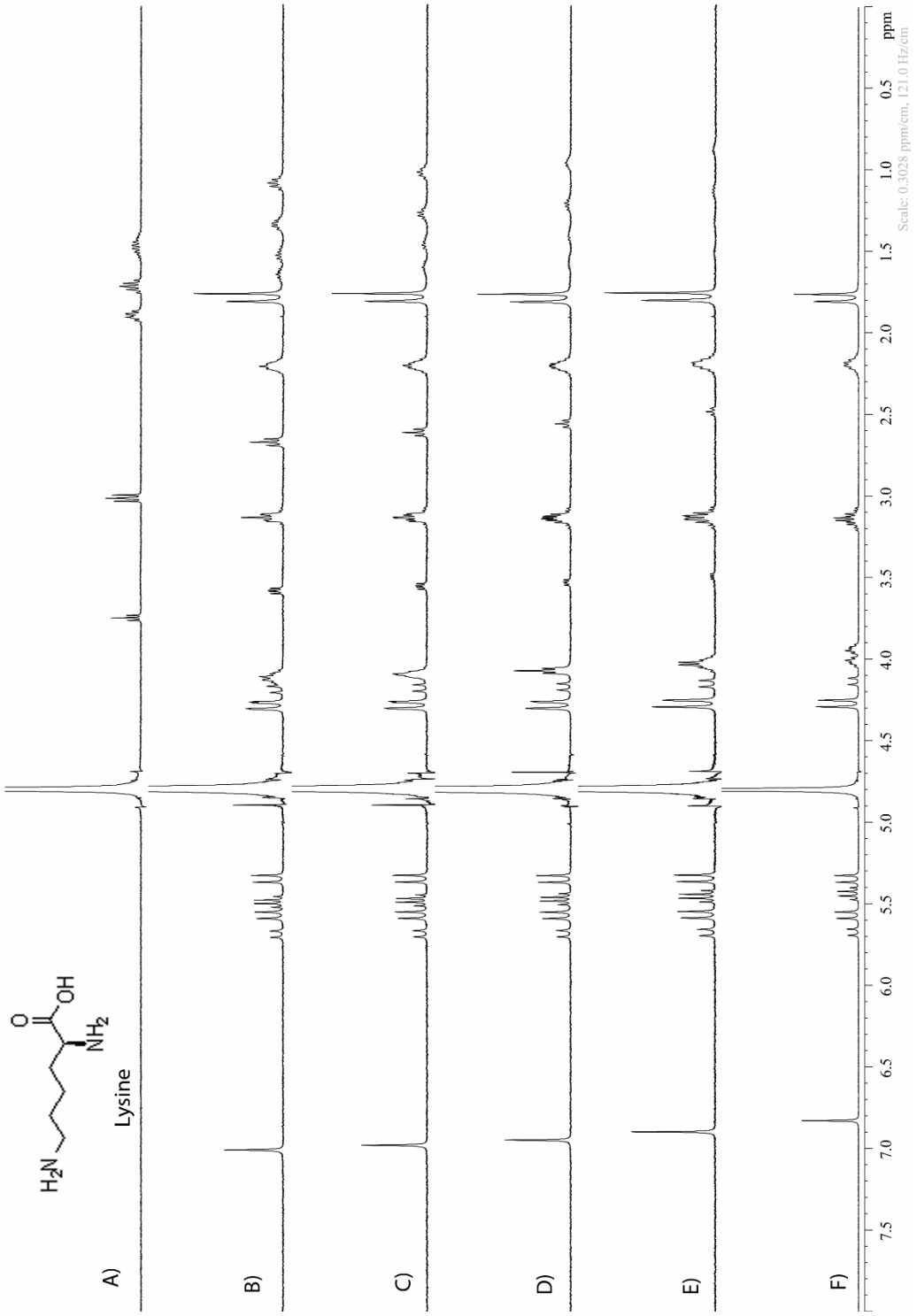

Figure II-S122. ^{1}H NMR spectra recorded (D_2O , 400 MHz, RT) for: a) Lysine (2 mM), b) a mixture of Motor 1 (1 mM) and lysine (2 mM), c) a mixture of Motor 1 (1 mM) and lysine (1.5 mM), d) a mixture of Motor 1 (1 mM) and lysine (1 mM), e) a mixture of Motor 1 (1 mM) and lysine (0.5 mM), f) Motor 1 (1 mM).

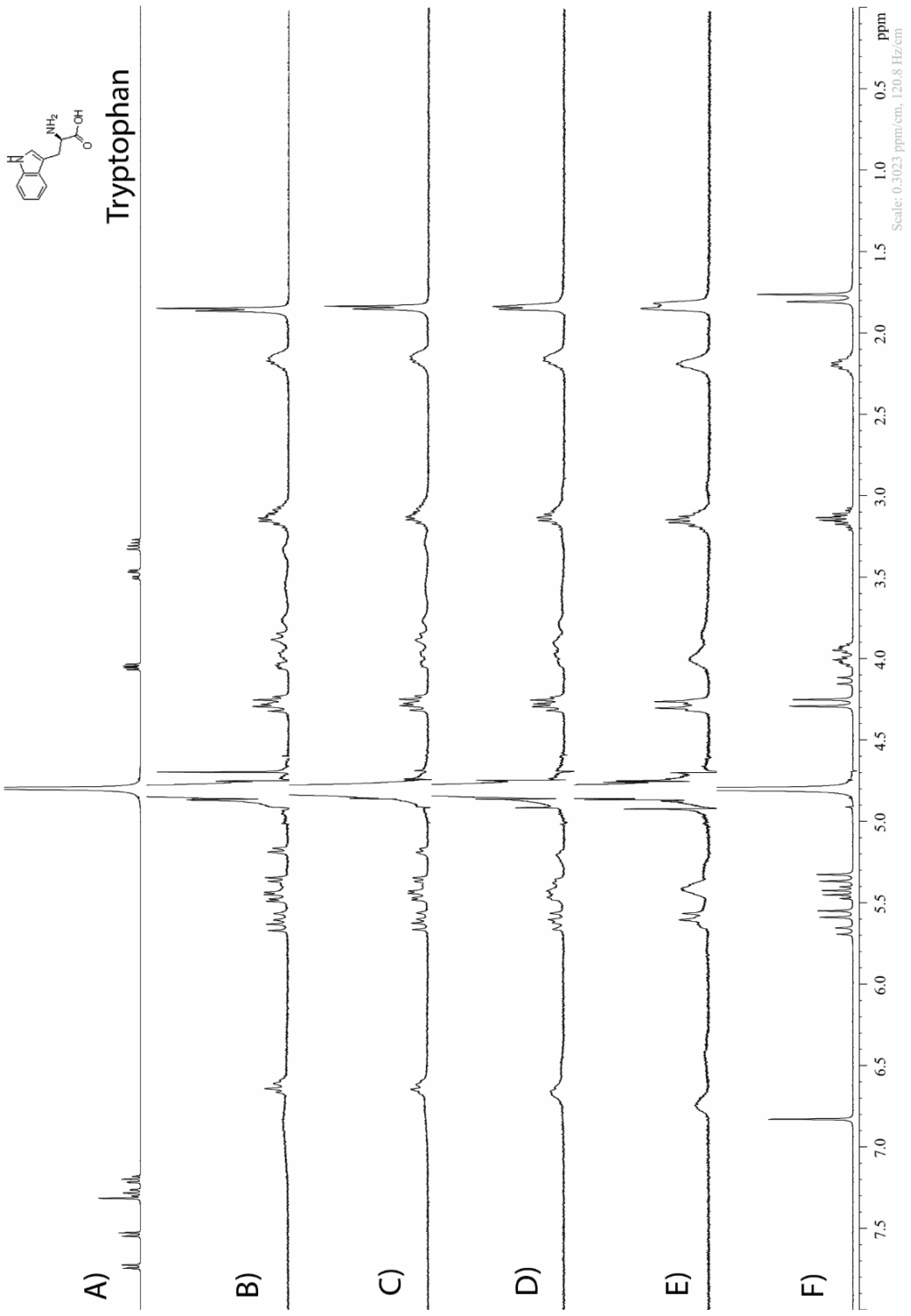

Figure II-S123. ^{1}H NMR spectra recorded (D_2O , 400 MHz, RT) for: a) Tryptophan (2 mM), b) a mixture of Motor 1 (1 mM) and tryptophan (2 mM), c) a mixture of Motor 1 (1 mM) and tryptophan (1.5 mM), d) a mixture of Motor 1 (1 mM) and tryptophan (1 mM), e) a mixture of Motor 1 (1 mM) and tryptophan (0.5 mM), f) Motor 1 (1 mM).

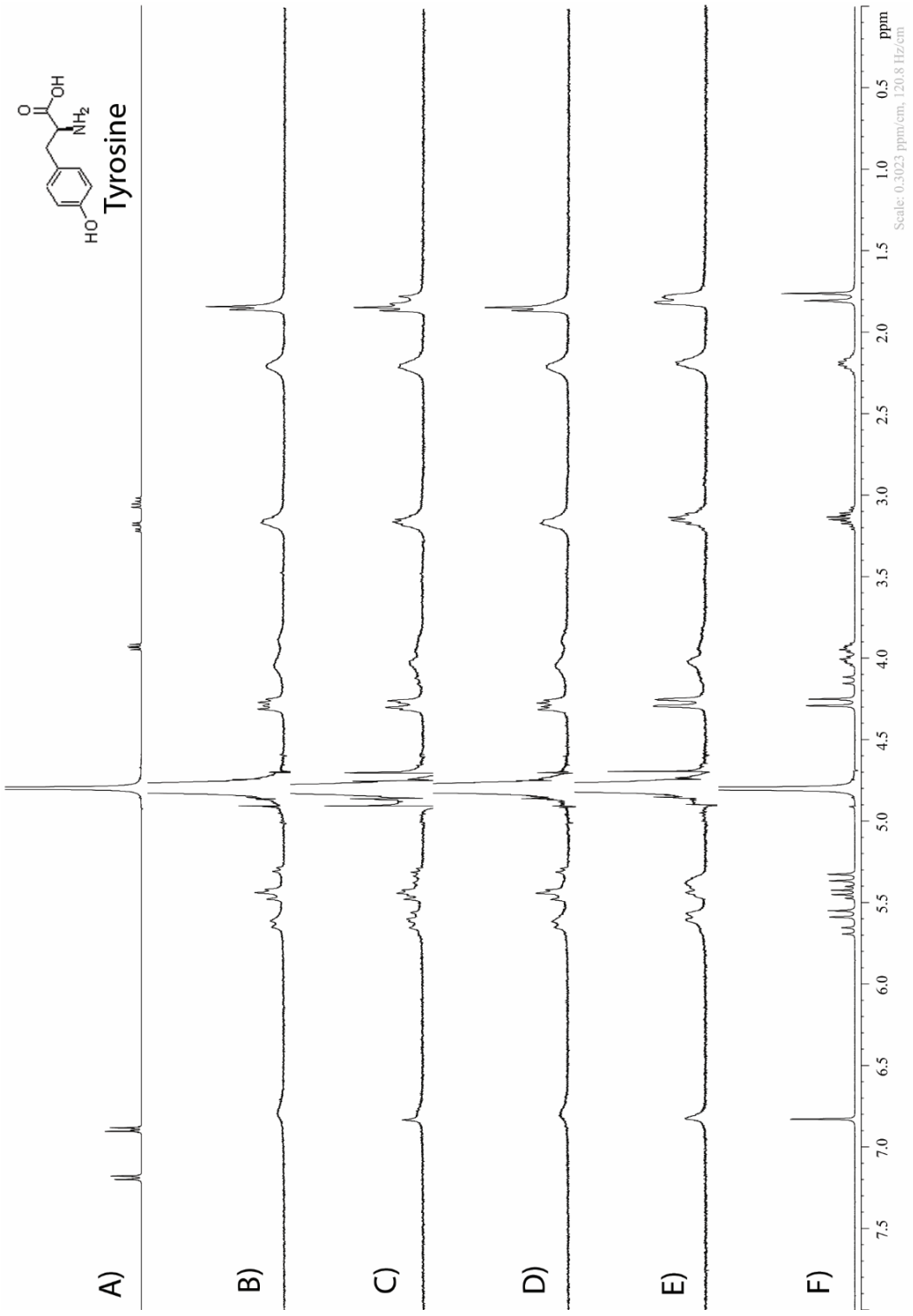

Figure II-S124. ^{1}H NMR spectra recorded (D_2O , 400 MHz, RT) for: a) Tyrosine (2 mM), b) a mixture of Motor 1 (1 mM) and tyrosine (2 mM), c) a mixture of Motor 1 (1 mM) and tyrosine (1.5 mM), d) a mixture of Motor 1 (1 mM) and tyrosine (1 mM), e) a mixture of Motor 1 (1 mM) and tyrosine (0.5 mM), f) Motor 1 (1 mM).

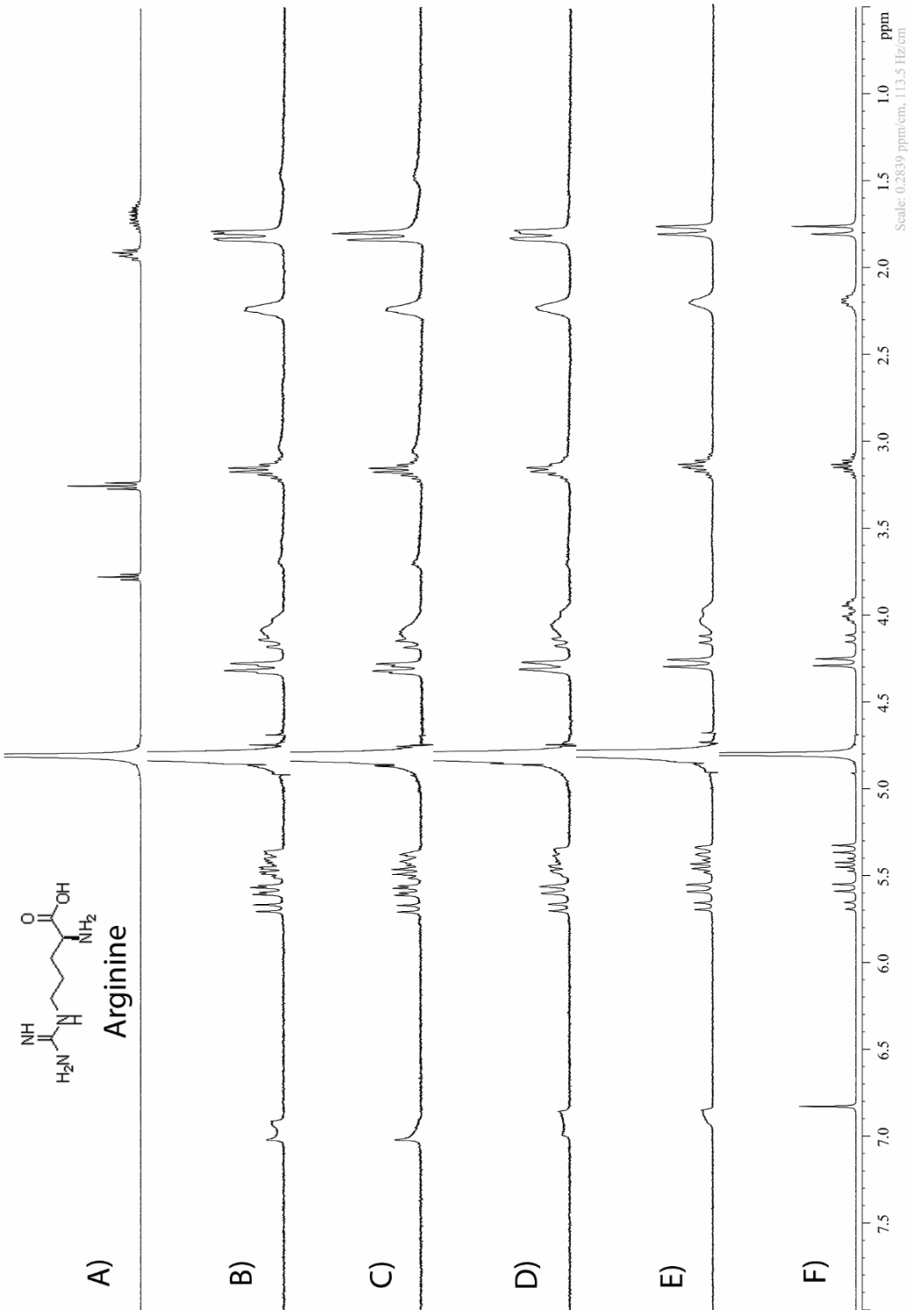

Figure II-S125. ^{1}H NMR spectra recorded (D_2O , 400 MHz, RT) for: a) Arginine (2 mM), b) a mixture of Motor 1 (1 mM) and arginine (2 mM), c) a mixture of Motor 1 (1 mM) and arginine (1.5 mM), d) a mixture of Motor 1 (1 mM) and arginine (1 mM), e) a mixture of Motor 1 (1 mM) and arginine (0.5 mM), f) Motor 1 (1 mM).

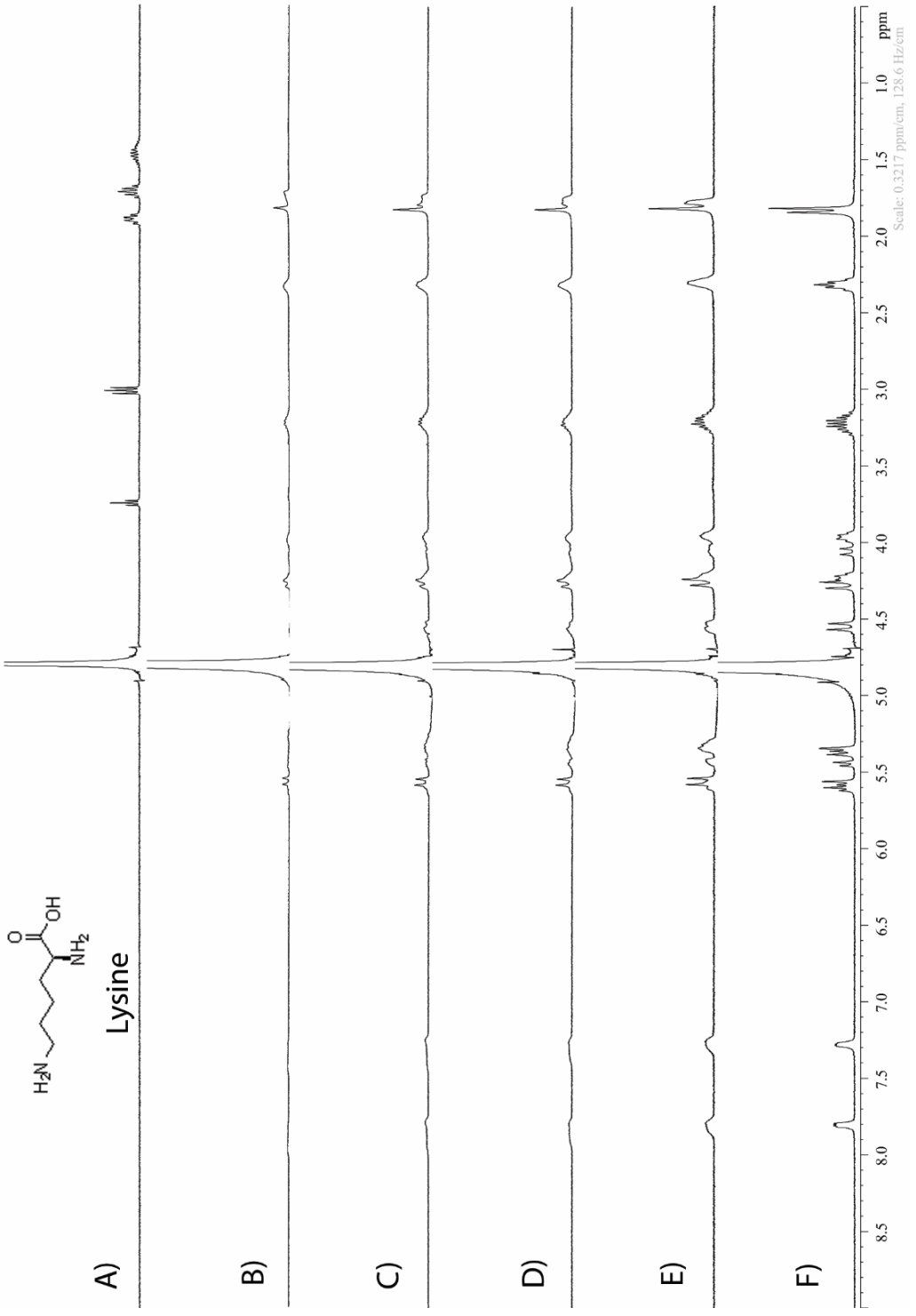

Figure II-S126. ^{1}H NMR spectra recorded (D_2O , 400 MHz, RT) for: a) Lysine (2 mM), b) a mixture of Motor 2 (1 mM) and lysine (2 mM), c) a mixture of Motor 2 (1 mM) and lysine (1.5 mM), d) a mixture of Motor 2 (1 mM) and lysine (1 mM), e) a mixture of Motor 2 (1 mM) and lysine (0.5 mM), f) Motor 2 (5 mM).

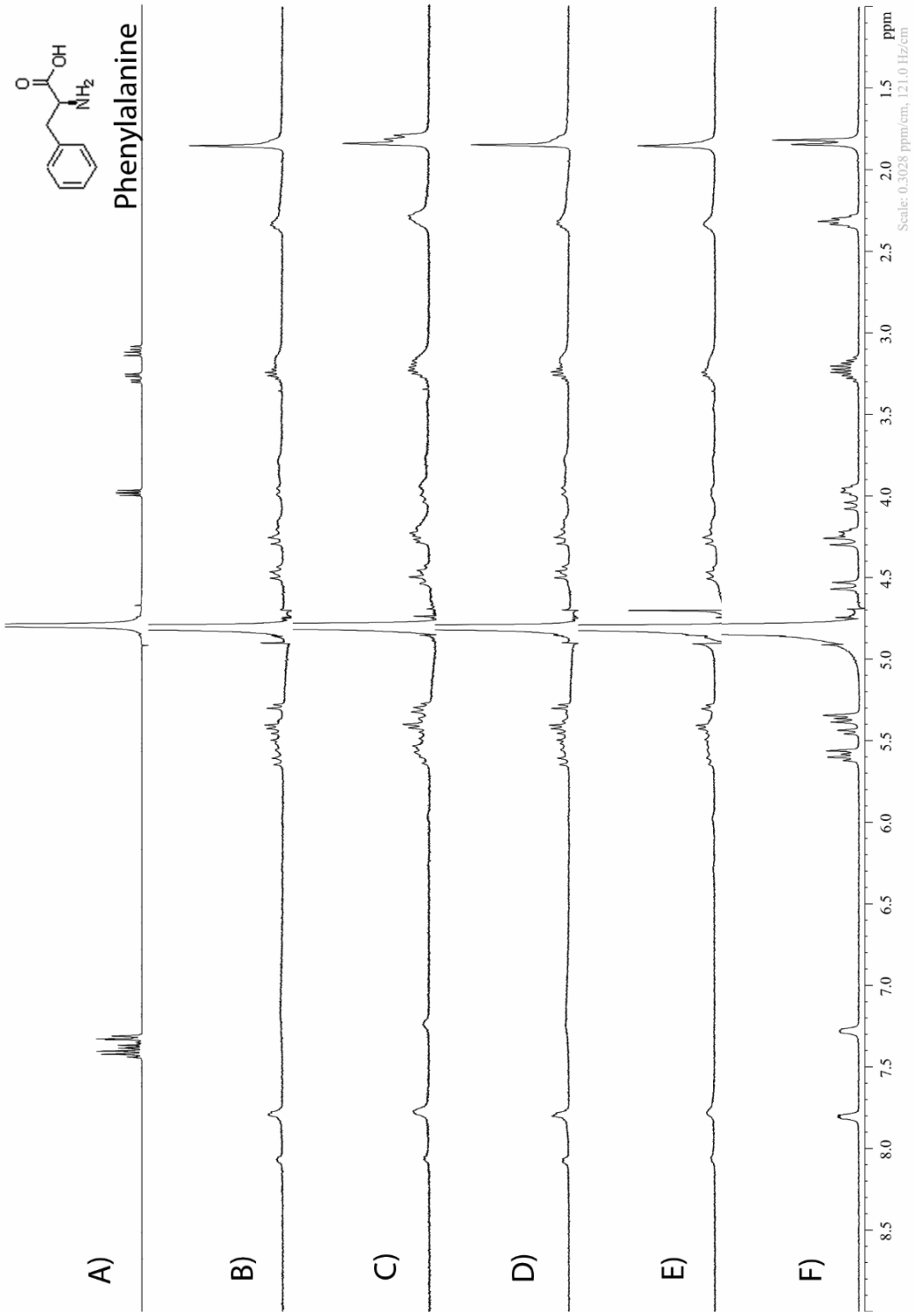

Figure II-S127. ^{1}H NMR spectra recorded (D_2O , 400 MHz, RT) for: a) Phenylalanine (2 mM), b) a mixture of Motor 2 (1 mM) and phenylalanine (2 mM), c) a mixture of Motor 2 (1 mM) and phenylalanine (1.5 mM), d) a mixture of Motor 2 (1 mM) and phenylalanine (1 mM), e) a mixture of Motor 2 (1 mM) and phenylalanine (0.5 mM), f) Motor 2 (5 mM).

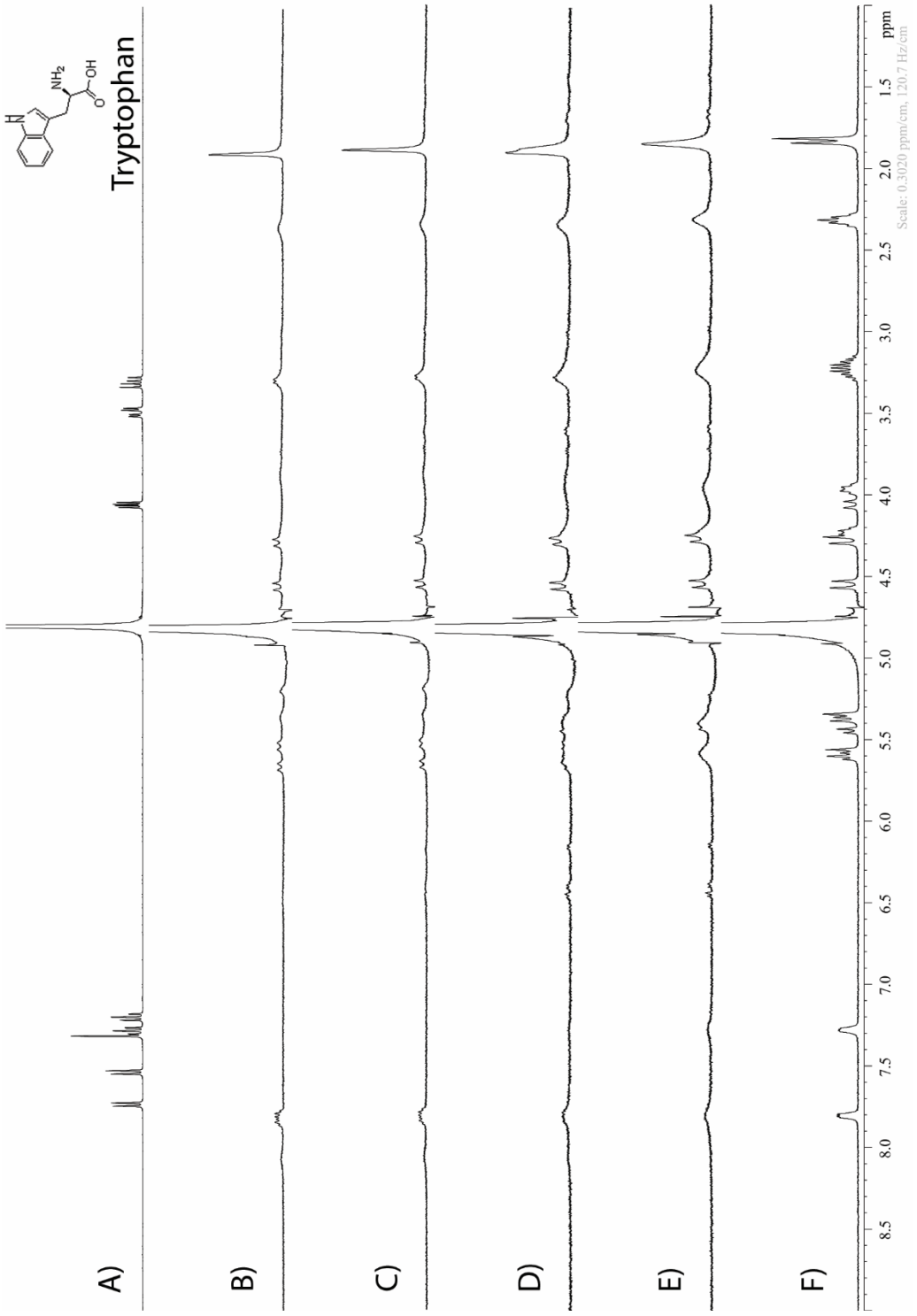

Figure II-S128. ^{1}H NMR spectra recorded (D_2O , 400 MHz, RT) for: a) Tryptophan (2 mM), b) a mixture of Motor 2 (1 mM) and tryptophan (2 mM), c) a mixture of Motor 2 (1 mM) and tryptophan (1.5 mM), d) a mixture of Motor 2 (1 mM) and tryptophan (1 mM), e) a mixture of Motor 2 (1 mM) and tryptophan (0.5 mM), f) Motor 2 (5 mM).

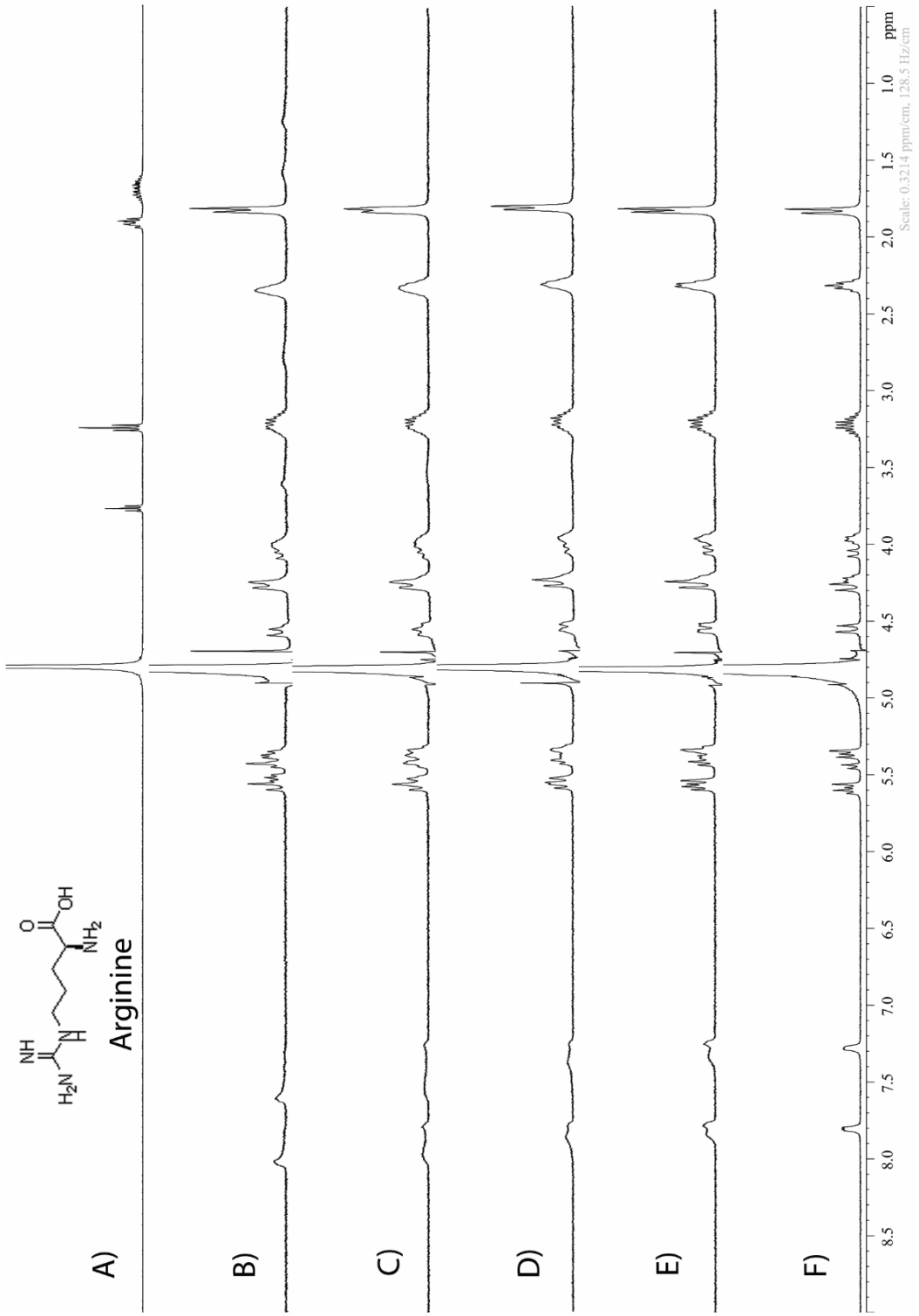

Figure II-S129. ^{1}H NMR spectra recorded (D_2O , 400 MHz, RT) for: a) Arginine (2 mM), b) a mixture of Motor 2 (1 mM) and arginine (2 mM), c) a mixture of Motor 2 (1 mM) and arginine (1.5 mM), d) a mixture of Motor 2 (1 mM) and arginine (1 mM), e) a mixture of Motor 2 (1 mM) and arginine (0.5 mM), f) Motor 2 (5 mM).

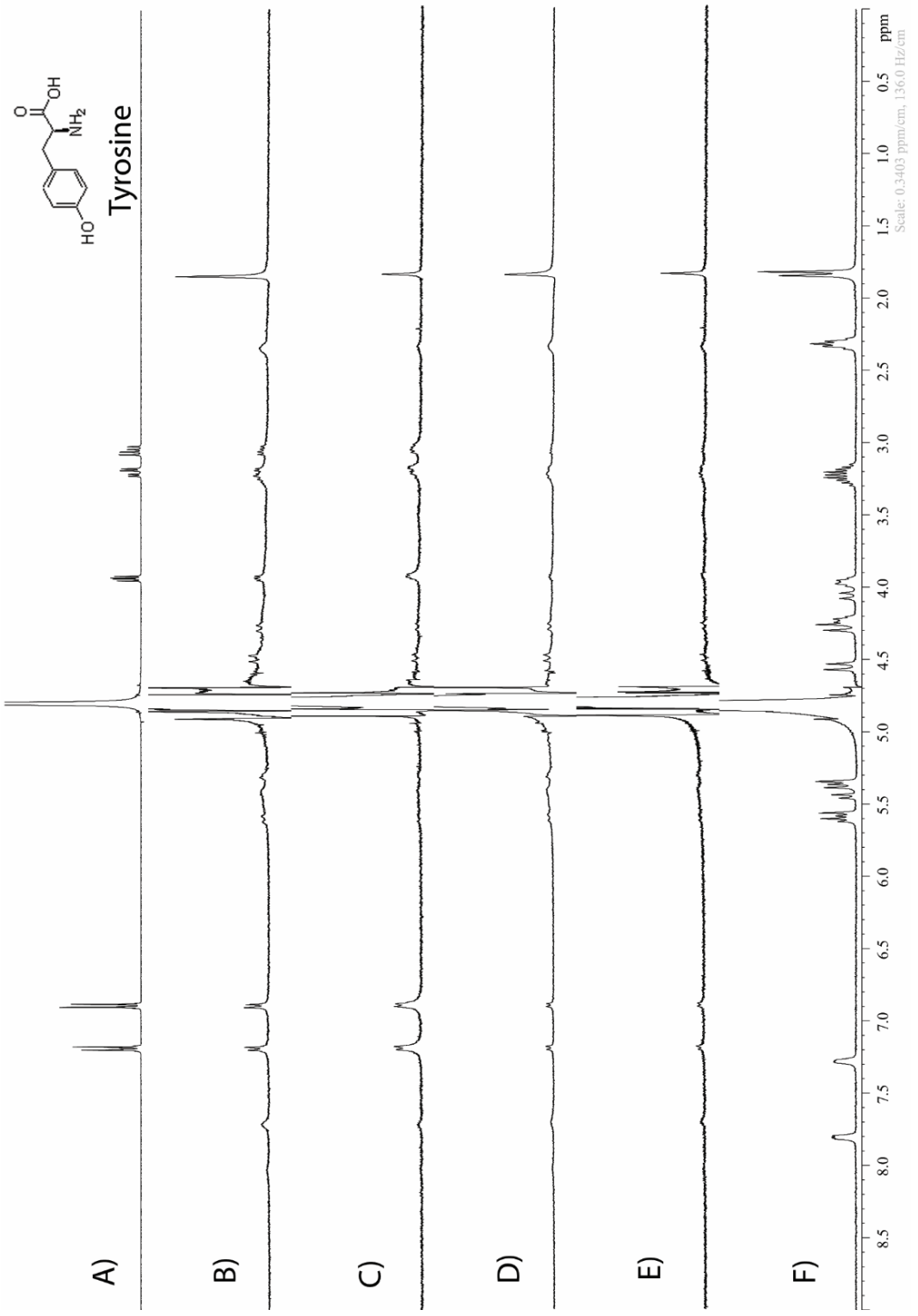

Figure II-S130. ^{1}H NMR spectra recorded (D_2O , 400 MHz, RT) for: a) Tyrosine (2 mM), b) a mixture of Motor 2 (1 mM) and tyrosine (2 mM), c) a mixture of Motor 2 (1 mM) and tyrosine (1.5 mM), d) a mixture of Motor 2 (1 mM) and tyrosine (1 mM), e) a mixture of Motor 2 (1 mM) and tyrosine (0.5 mM), f) Motor 2 (5 mM).

Appendix II

Triptycene Walled Glycoluril Trimer: Synthesis and Recognition Properties

Sandra Zebaze Ndendjio,[a] Wenjin Liu,[a,b] Nicolas Yvanez,[a,c] Zhihui Meng,[b,*] Peter Y. Zavalij,[a] and Lyle Isaacs[a,*]

Supporting Information

[a] Department of Chemistry and Biochemistry, University of Maryland, College Park, Maryland 20742, USA. E-mail: lisaacs@umd.edu
[b] School of Chemistry and Chemical Engineering, Beijing Institute of Technology, 5 South Zhongguancun Street, Beijing 100081, P. R. China
[c] École Nationale Supérieure de Chimie de Paris, 11 rue Pierre et Marie Curie, F75231 Paris cedex 05, France

Table of Contents **Pages**

General experimental

Starting materials were purchased from commercial suppliers and used without further purification or were prepared by literature procedures. Melting points were measured on a Meltemp apparatus in open capillary tubes and are uncorrected. IR spectra were recorded on a JASCO FT/IR 4100 spectrometer and are reported in cm^{-1}. NMR spectra were measured on Bruker spectrometers operating at 400 or 600 MHz for ^{1}H and 100 or 125 MHz for ^{13}C using D_2O, or DMSO-d6 as solvents. Chemical shifts (δ) are referenced relative to the residual resonances for HOD (4.80 ppm) and DMSO-d6 (2.50 ppm for ^{1}H, 39.51 ppm for ^{13}C). Mass spectrometry was performed using a JEOL AccuTOF electrospray instrument (ESI). ITC data was collected on a Malvern Microcal PEAQ-ITC instrument and analyzed using the software provided by the vendor.

^{1}H and ^{13}C NMR spectra of host 1

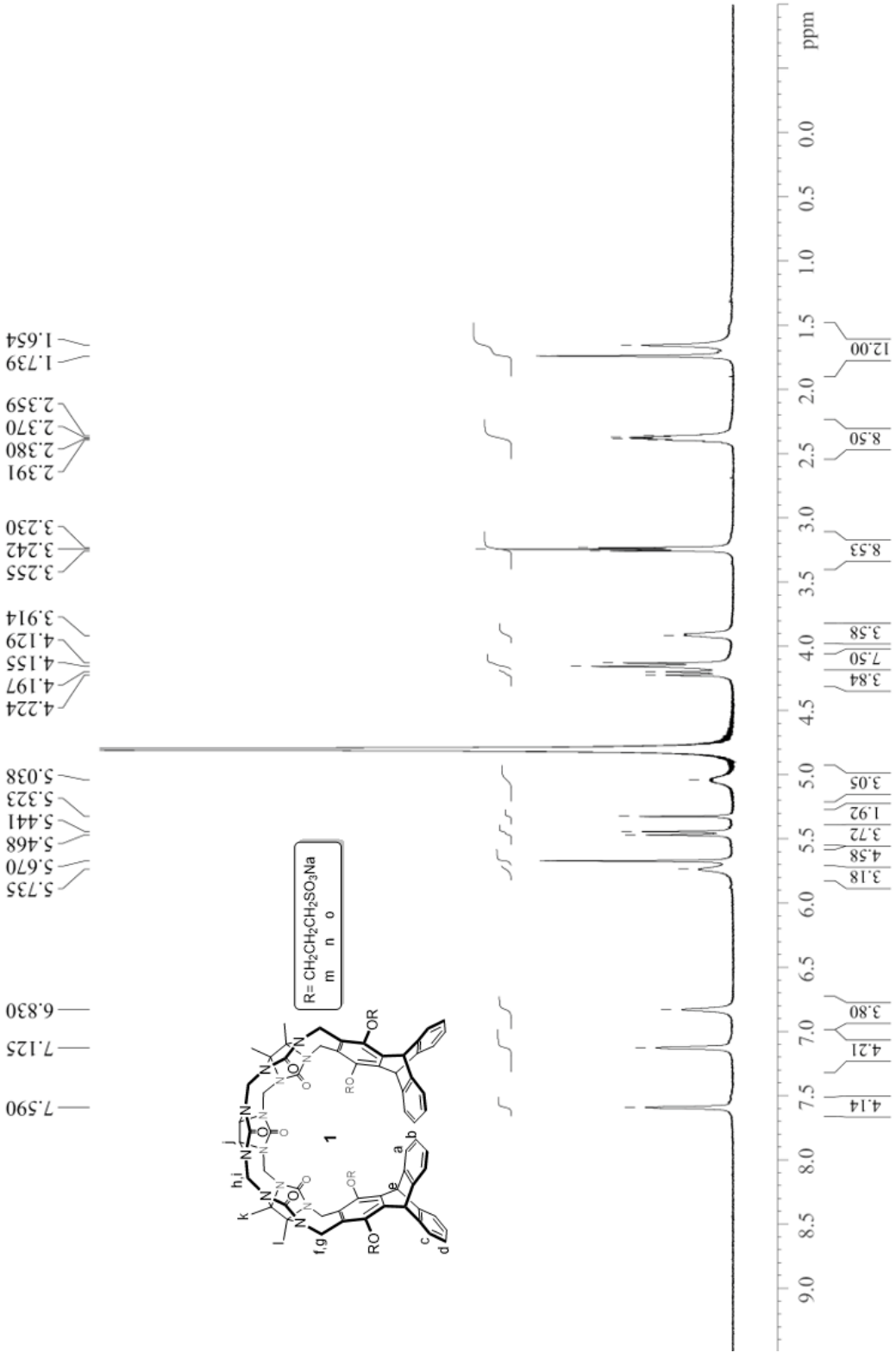

Figure III-S1. ^{1}H NMR spectrum (D_2O, 20 mM sodium phosphate, pD 7.4, 600 MHz, RT) recorded for 1.

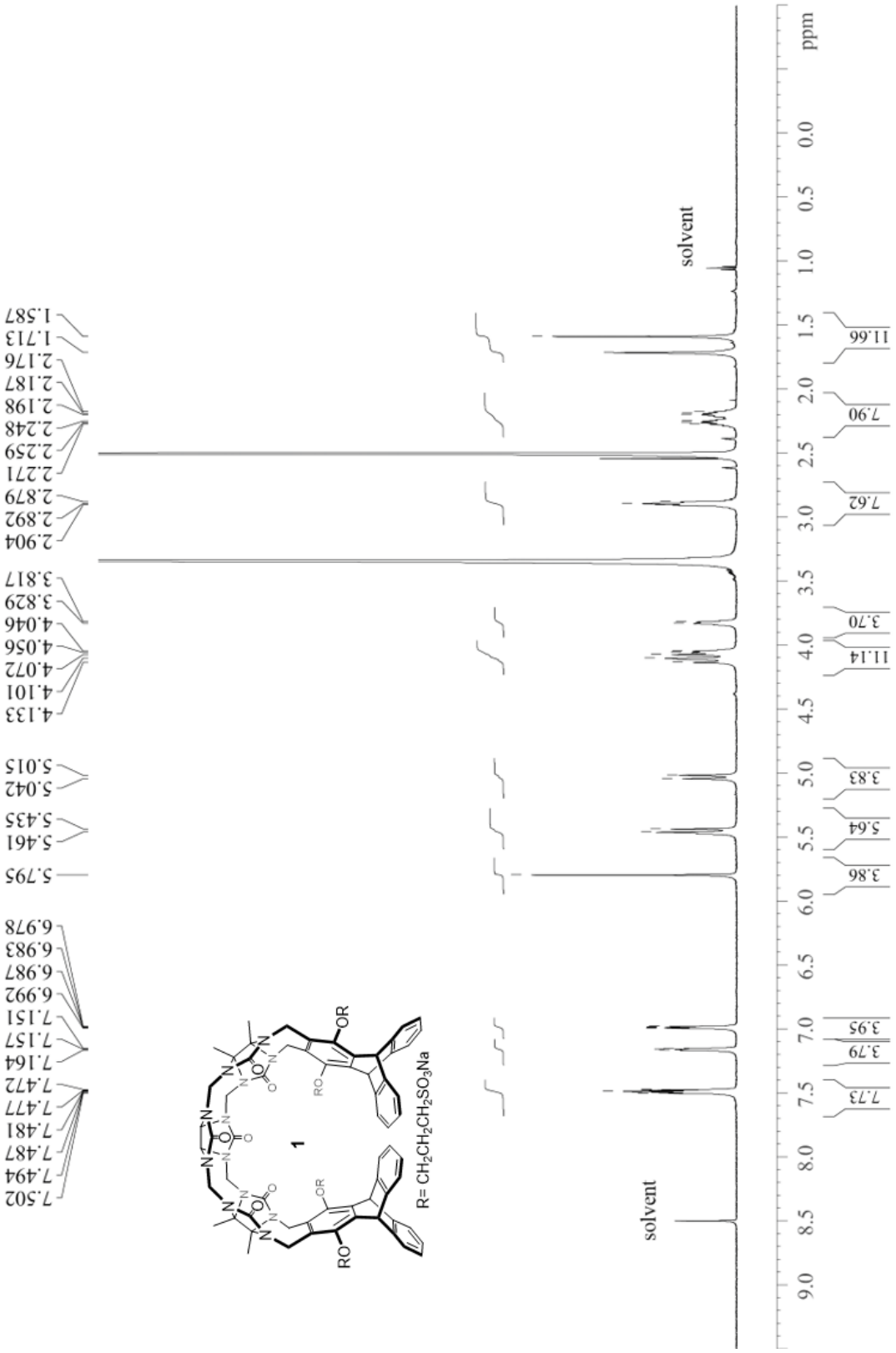

Figure III-S2. ^{1}H NMR spectrum (DMSO-d_6, 600 MHz, RT) recorded for 1.

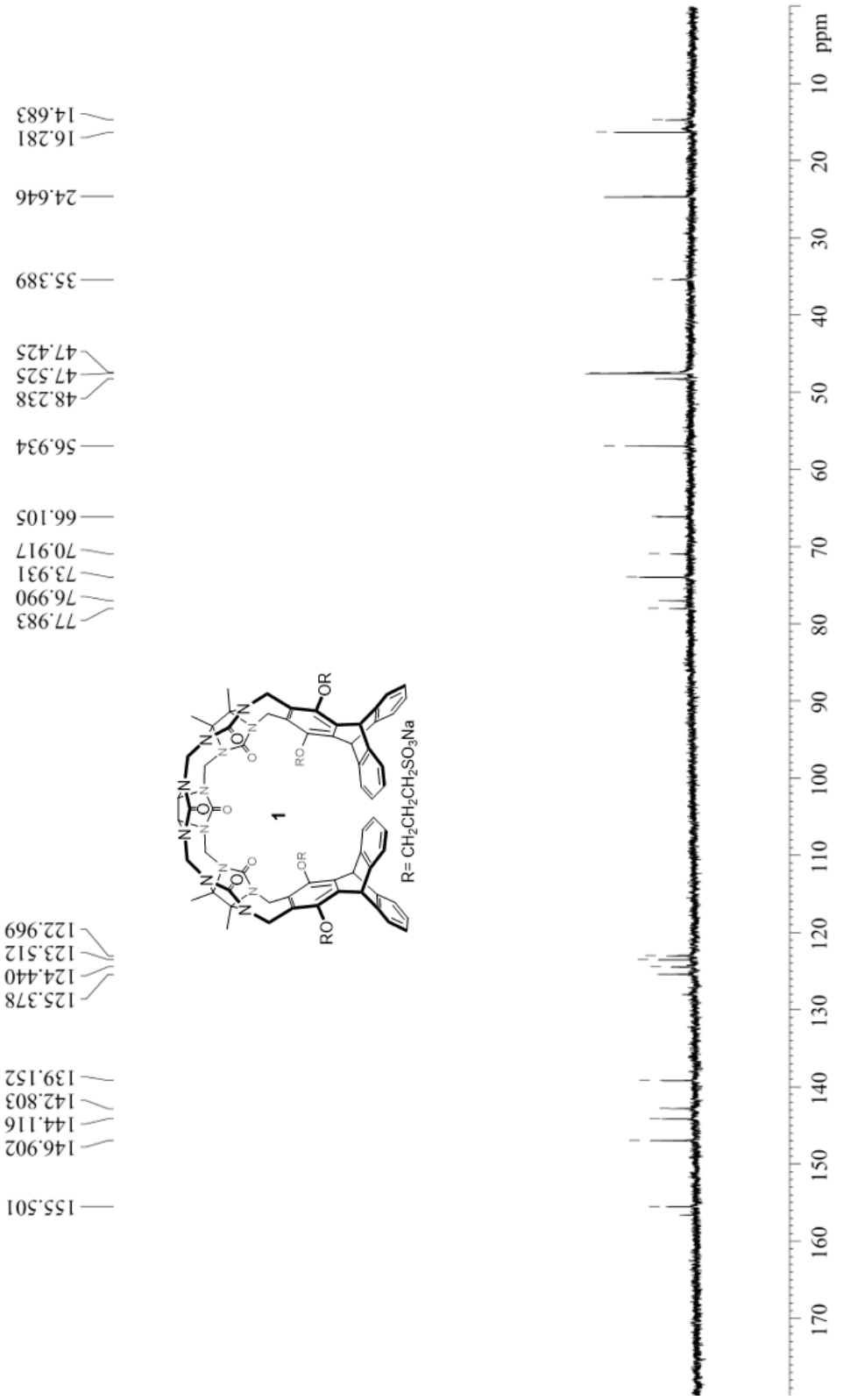

Figure III-S3. ^{13}C NMR spectrum (D_2O, 600 MHz, RT, 1,4-dioxane as internal reference) recorded for 1.

^{1}H NMR Dilution Experiments Performed for host 1

Self-association Binding Model implemented in Scientist™

```
// Micromath Scientist Model File
// self-association model for NMR
IndVars: concTot
DepVars: Deltaobs
Params: Ka, Deltasat, Deltazero
Ka = concBound/(concFree*concFree)
concTot=concFree + concBound/2
Deltaobs = Deltazero + (Deltasat - Deltazero) * (1/2*concBound/concTot)
//Constraints
0 < Ka
0 < concFree < concTot
0 < concBound < concTot
***
```

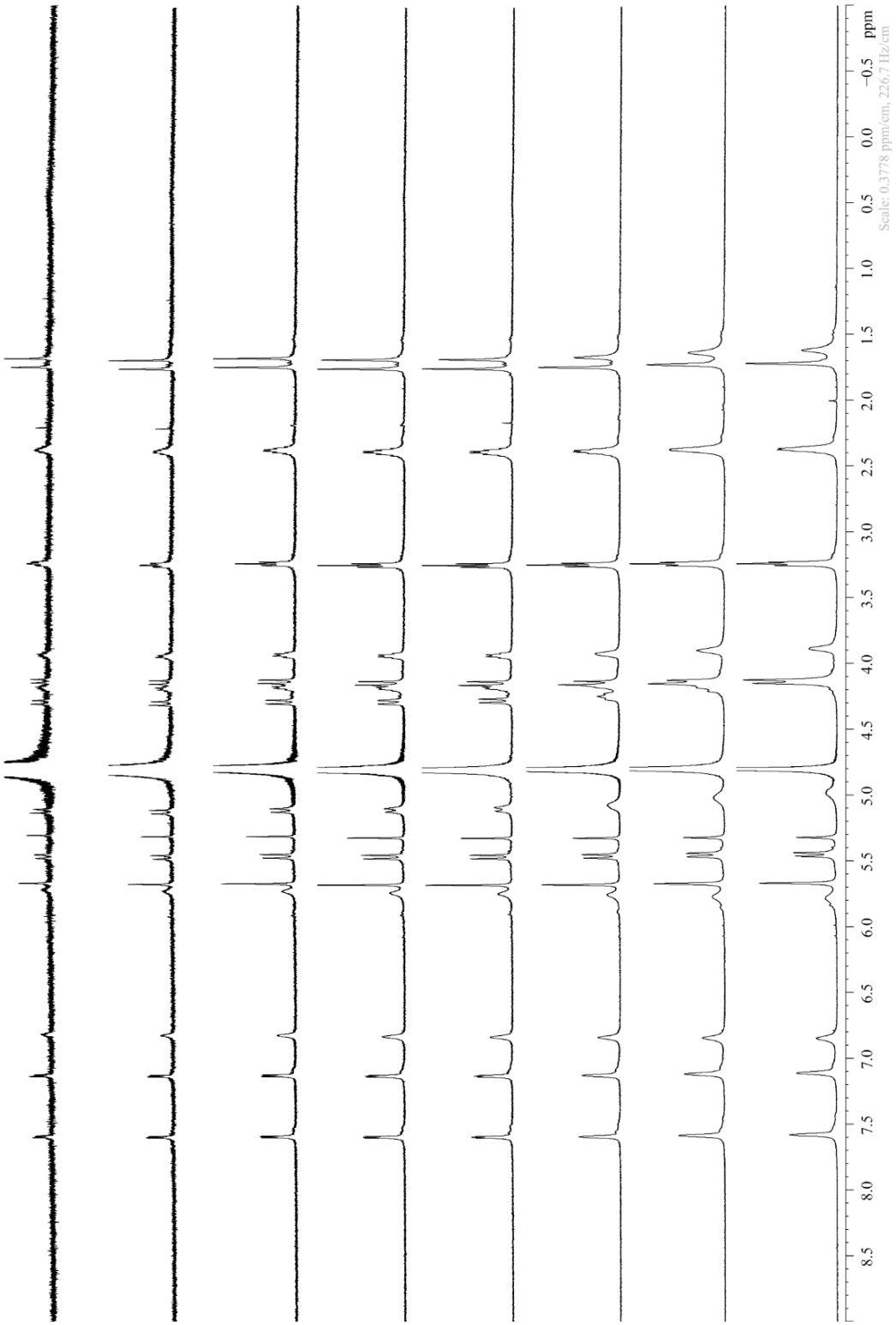

Figure III-S4. ^{1}H NMR spectra recorded (D_2O, 20 mM sodium phosphate, pD 7.40, 600 MHz, RT) for the dilution of host 1 (3 - 0.05 mM). Host 1 weakly self-associates in water ($K_s = 480 \pm 81\ M^{-1}$).

^{1}H NMR spectra of guests (4-26) with host 1

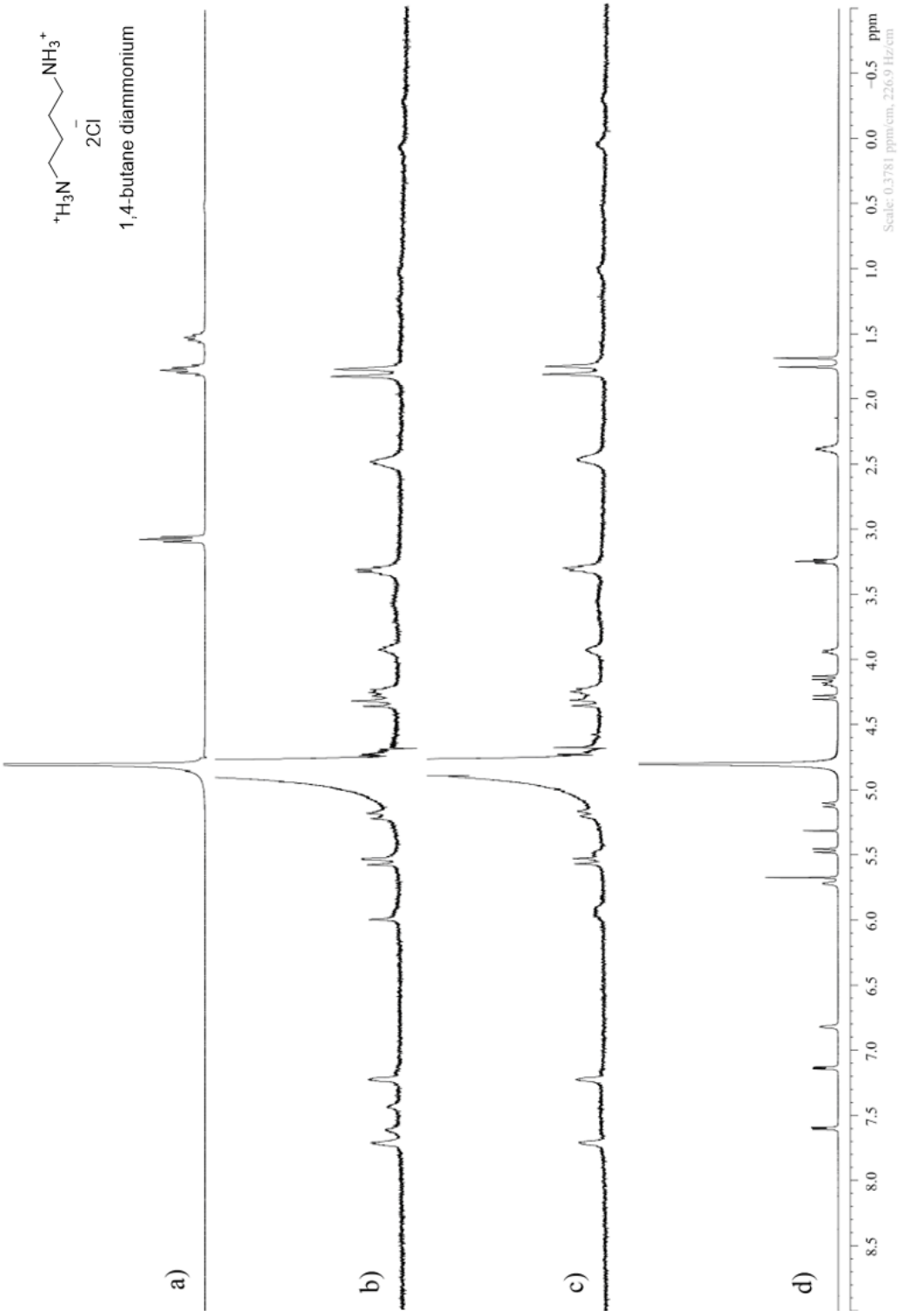

Figure III-S5. ^{1}H NMR spectra recorded (D_2O, 20 mM sodium phosphate, pD 7.40, 400 MHz, RT) for: a) **4** (5 mM), b) a mixture of **1** (125 µM) and **4** (250 µM), c) a mixture of **1** (125 µM) and **4** (125 µM), d) **1** (250 µM).

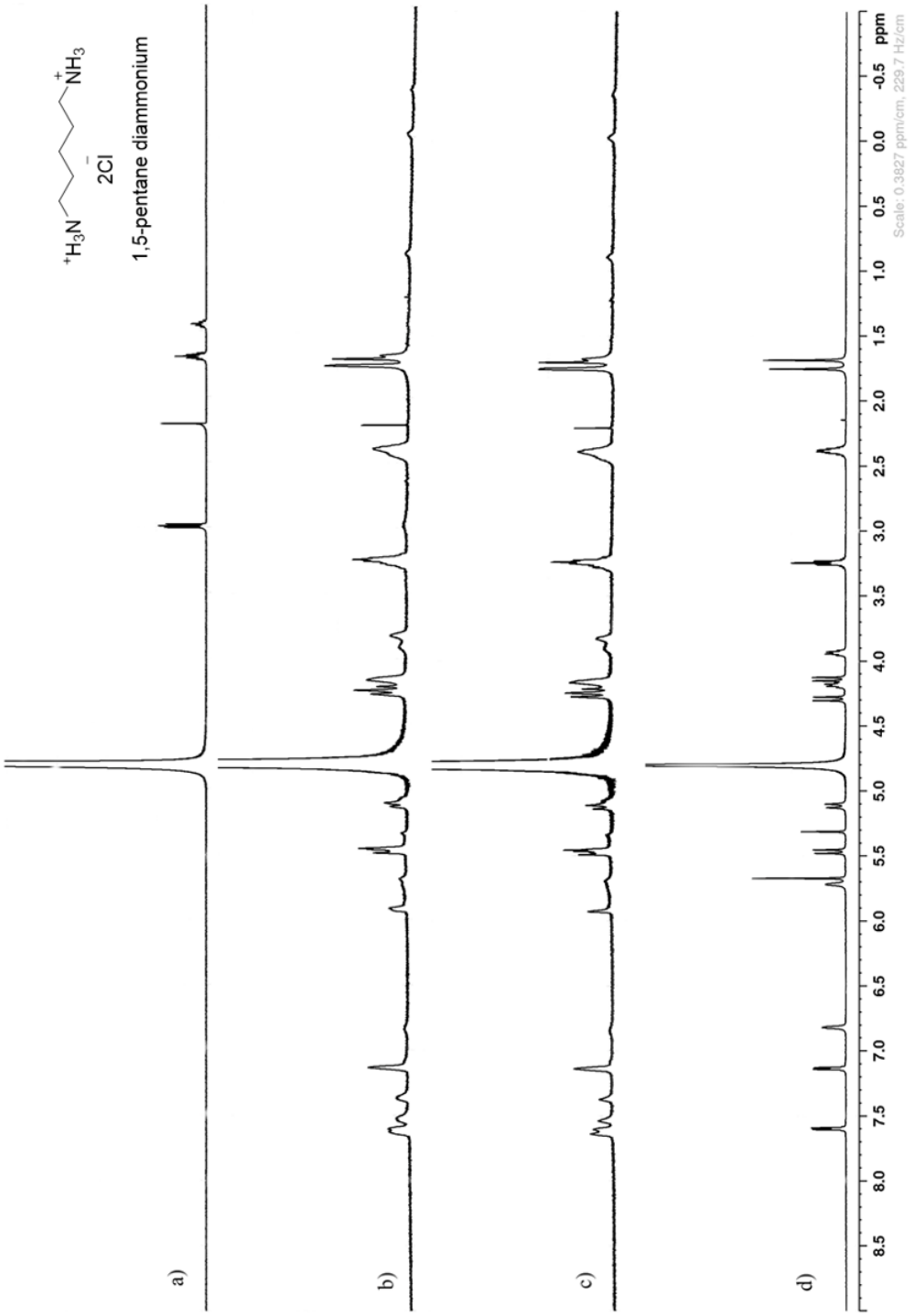

Figure III-S6. ^{1}H NMR spectra recorded (D_2O, 20 mM sodium phosphate, pD 7.40, 600 MHz, RT) for: a) **5** (5 mM), b) a mixture of **1** (250 µM) and **5** (500 µM), c) a mixture of **1** (250 µM) and **5** (250 µM), d) **1** (250 µM).

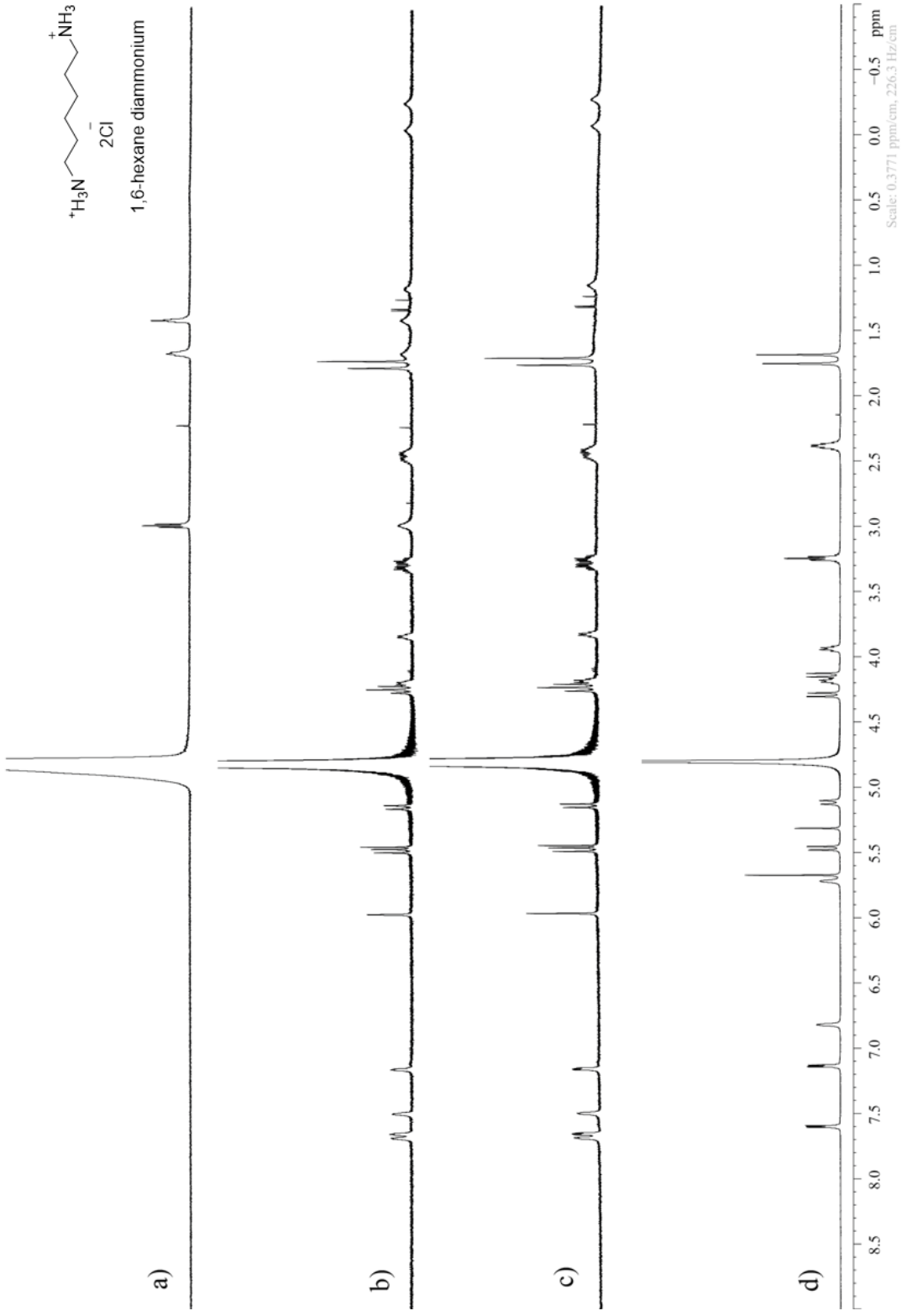

Figure III-S7. ^{1}H NMR spectra recorded (D_2O, 20 mM sodium phosphate, pD 7.40, 600 MHz, RT) for: a) **6** (5 mM), b) a mixture of **1** (250 μM) and **6** (500 μM), c) a mixture of **1** (250 μM) and **6** (250 μM), d) **1** (250 μM).

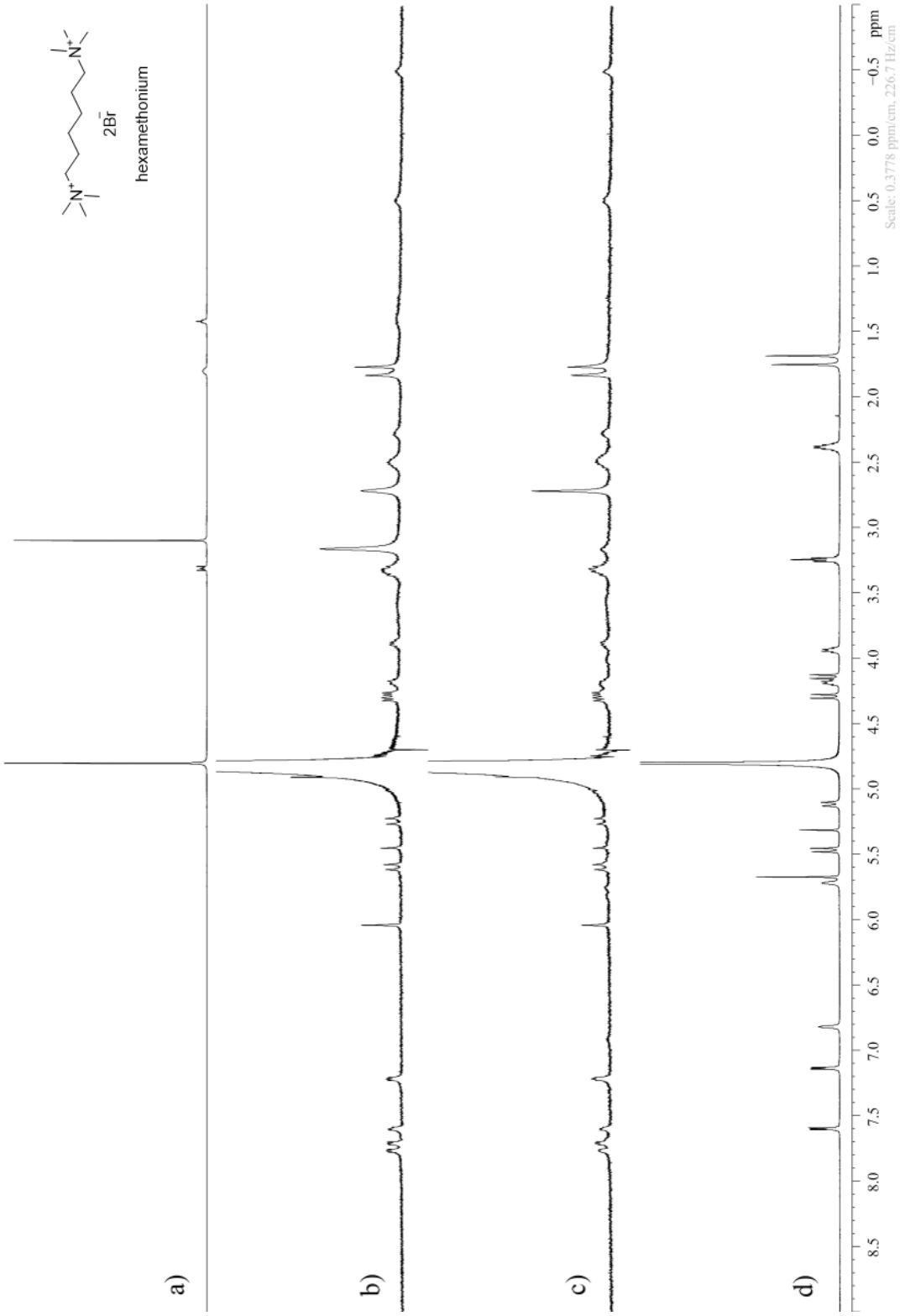

Figure III-S8. ^{1}H NMR spectra recorded (D_2O, 20 mM sodium phosphate, pD 7.40, 600 MHz, RT) for: a) **6DQ•2Br$^-$** (6 mM), b) a mixture of **1** (250 μM) and **6DQ•2Br$^-$** (500 μM), c) a mixture of **1** (250 μM) and **6DQ•2Br$^-$** (250 μM), d) **1** (250 μM).

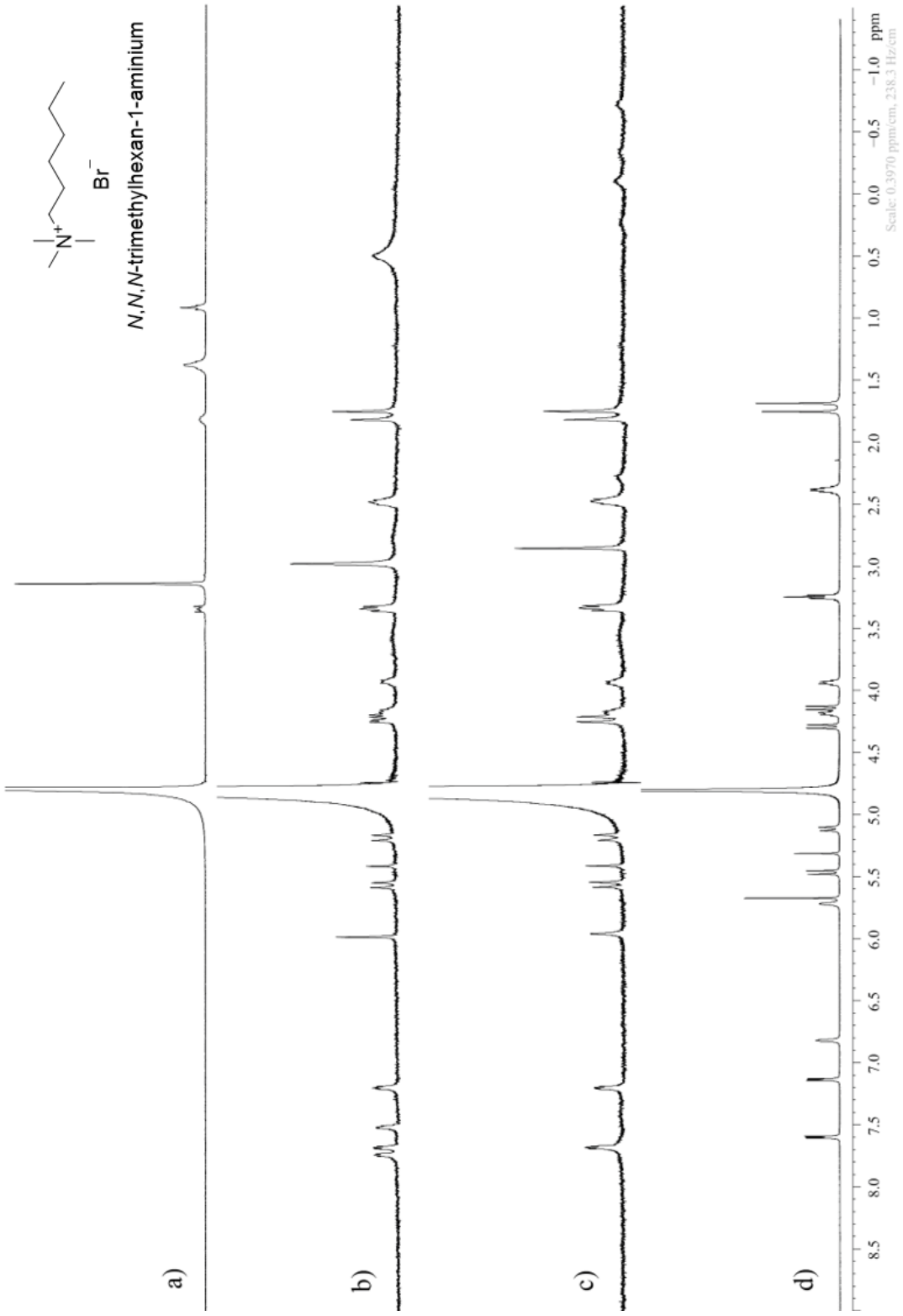

Figure III-S9. ^{1}H NMR spectra recorded (D_2O, 20 mM sodium phosphate, pD 7.40, 400 MHz, RT) for: a) **6Q•Br**$^-$ (4 mM), b) a mixture of **1** (125 μM) and **6Q•Br**$^-$ (250 μM), c) a mixture of **1** (125 μM) and **6Q•Br**$^-$ (125 μM), d) **1** (250 μM).

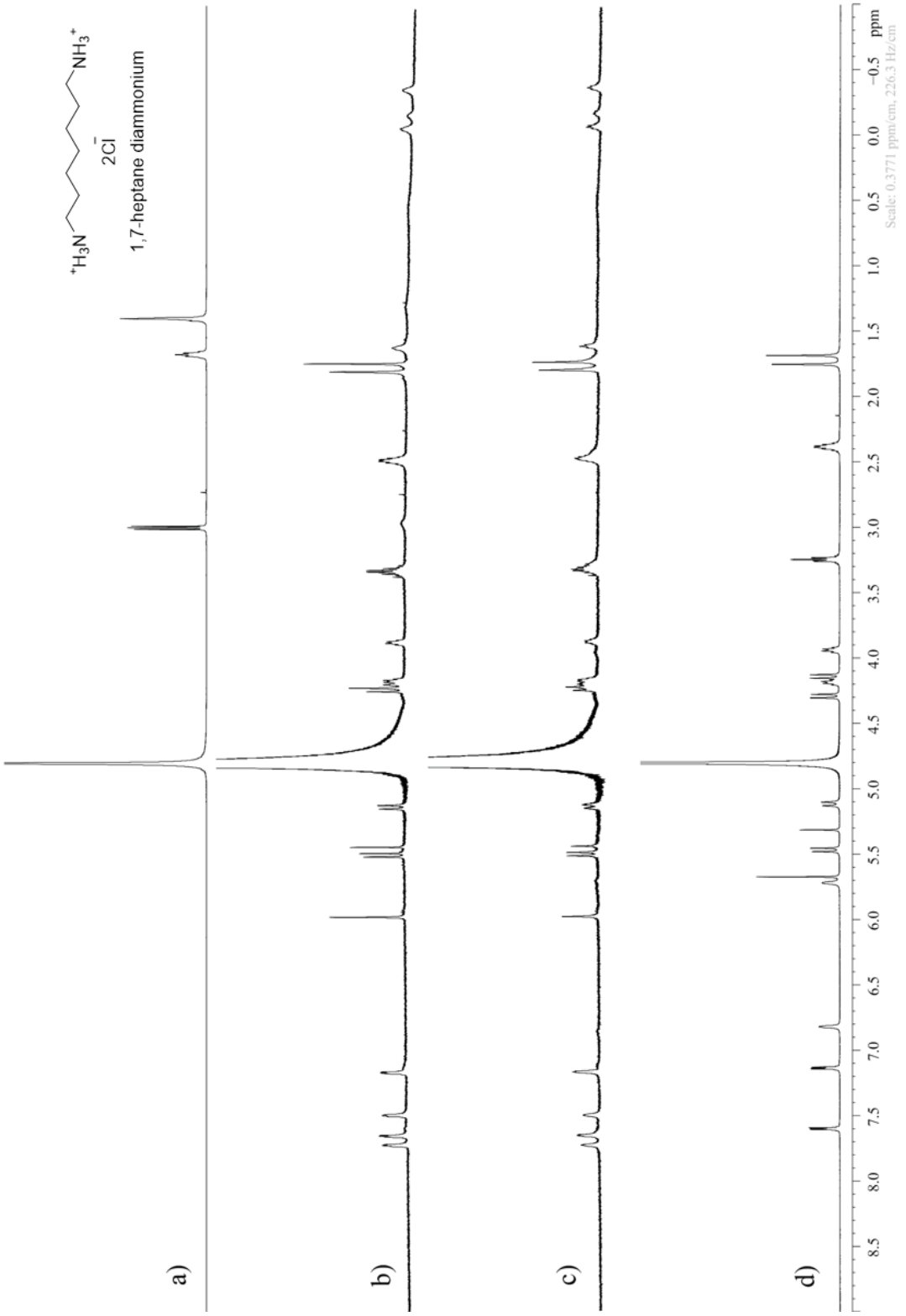

Figure III-S10. ^{1}H NMR spectra recorded (D_2O, 20 mM sodium phosphate, pD 7.40, 600 MHz, RT) for: a) **7** (2 mM), b) a mixture of **1** (125 μM) and **7** (250 μM), c) a mixture of **1** (125 μM) and **7** (125 μM), d) **1** (250 μM).

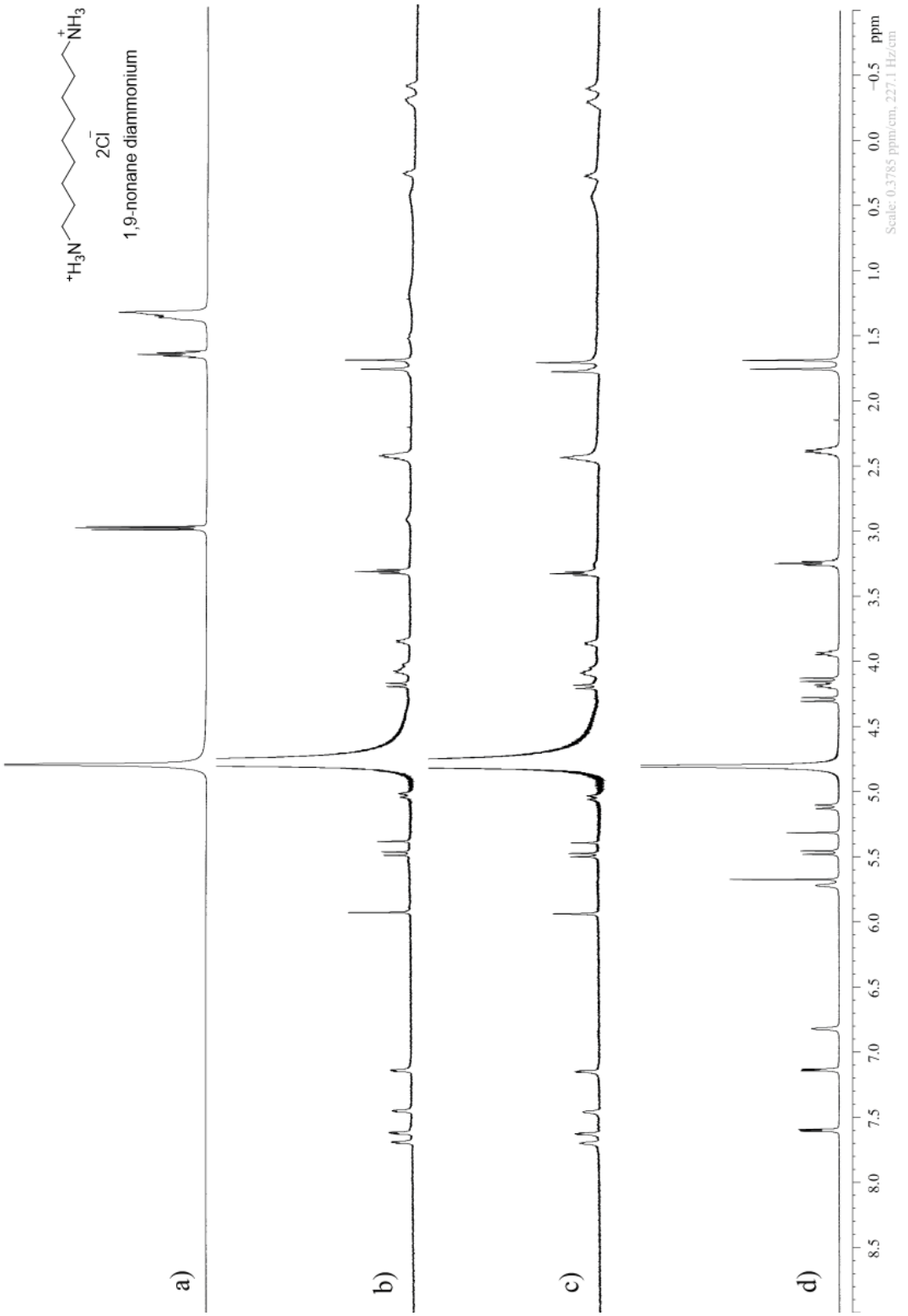

Figure III-S11. ^{1}H NMR spectra recorded (D_2O, 20 mM sodium phosphate, pD 7.40, 600 MHz, RT) for: a) **9** (2 mM), b) a mixture of **1** (125 µM) and **9** (250 µM), c) a mixture of **1** (125 µM) and **9** (125 µM), d) **1** (250 µM).

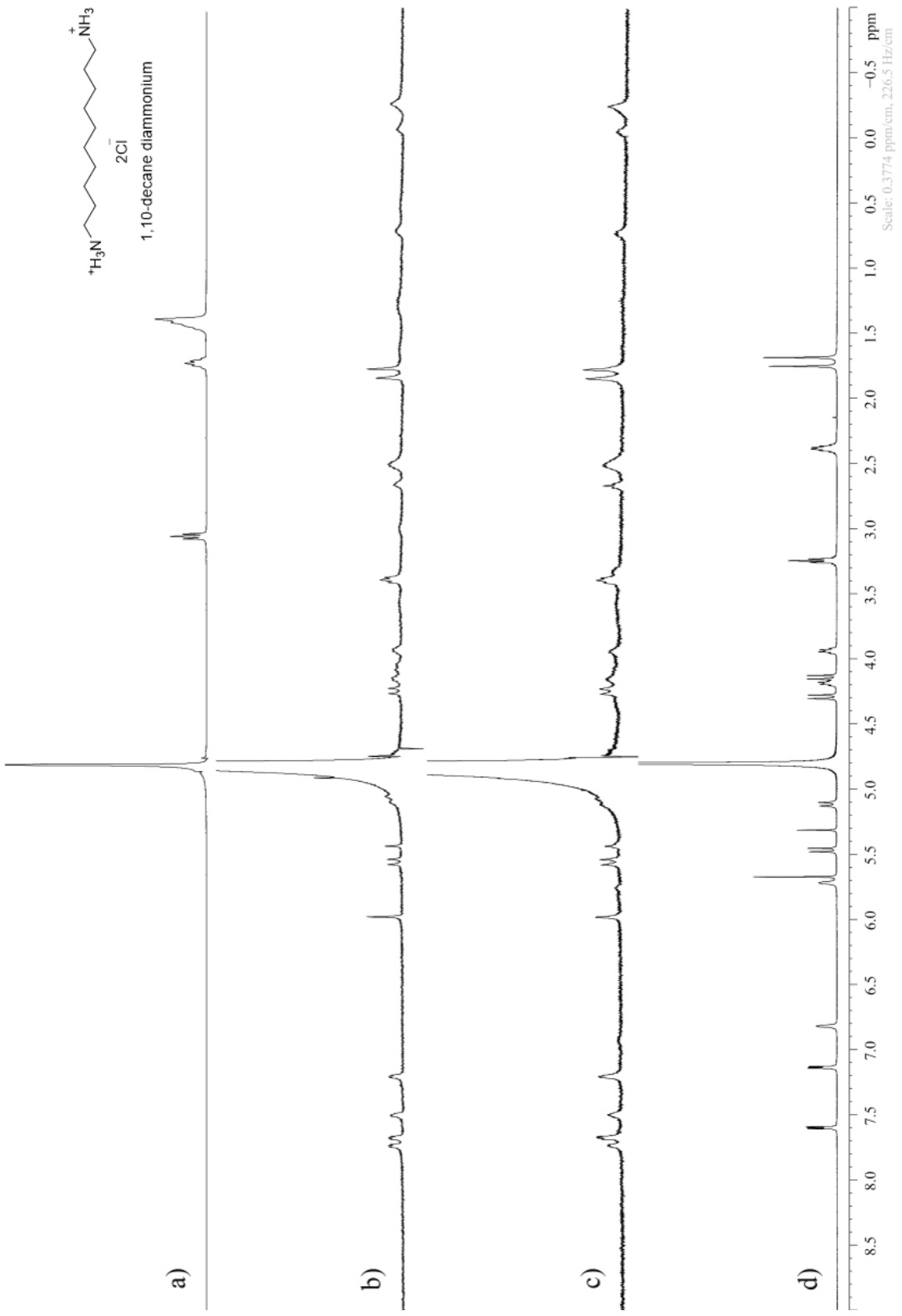

Figure III-S12. ^{1}H NMR spectra recorded (D_2O, 20 mM sodium phosphate, pD 7.40, 600 MHz, RT) for: a) **10** (2 mM), b) a mixture of **1** (125 µM) and **10** (250 µM), c) a mixture of **1** (125 µM) and **10** (125 µM), d) **1** (250 µM).

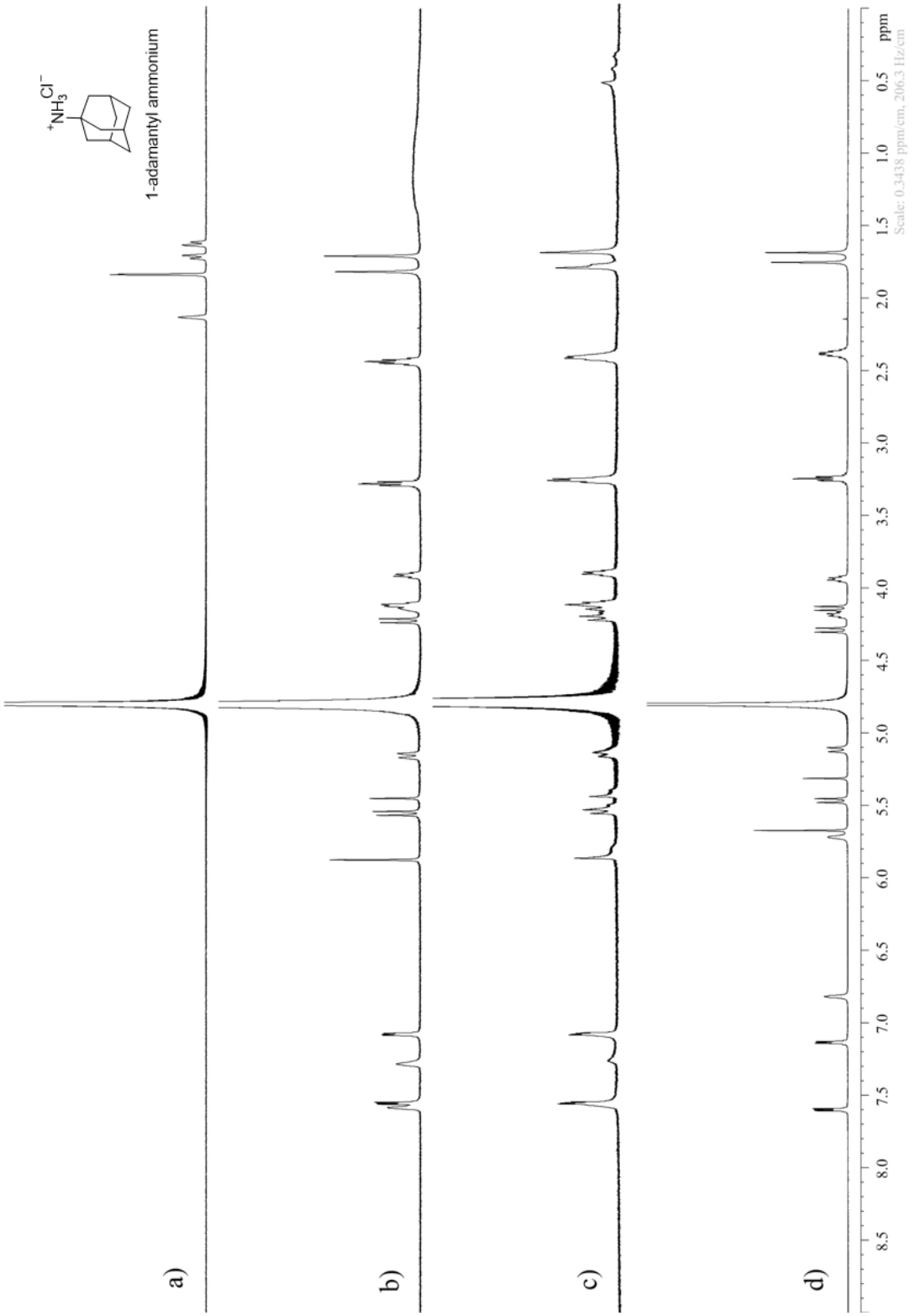

Figure III-S13. ^{1}H NMR spectra recorded (D_2O, 20 mM sodium phosphate, pD 7.40, 600 MHz, RT) for: a) **11** (5 mM), b) a mixture of **1** (250 µM) and **11** (500 µM), c) a mixture of **1** (250 µM) and **11** (250 µM), d) 1 (250 µM).

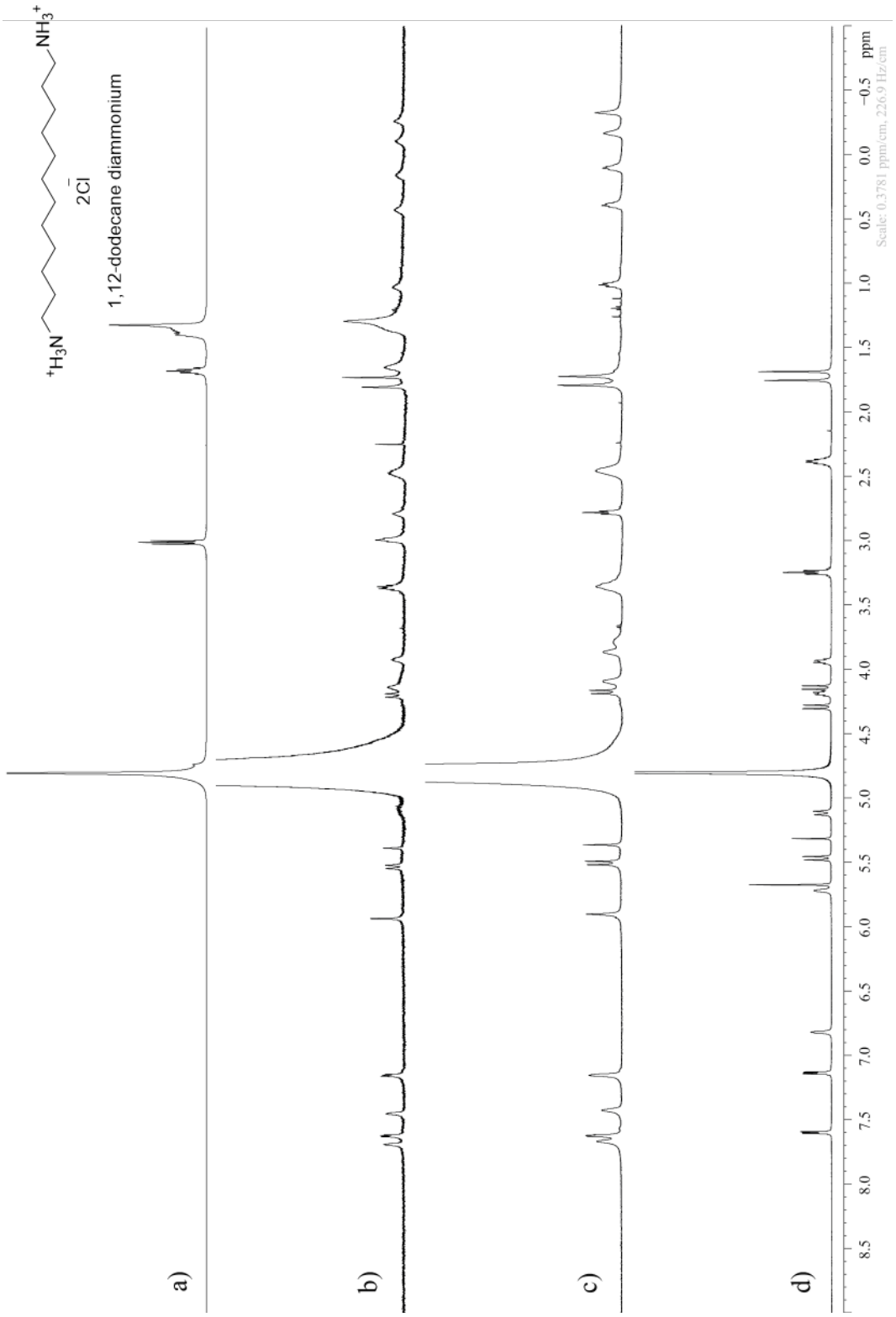

Figure III-S14. ^{1}H NMR spectra recorded (D_2O, 20 mM sodium phosphate, pD 7.40, 400 MHz, RT) for: a) **12** (2 mM), b) a mixture of **1** (125 µM) and **12** (250 µM), c) a mixture of **1** (125 µM) and **12** (125 µM), d) **1** (250 µM).

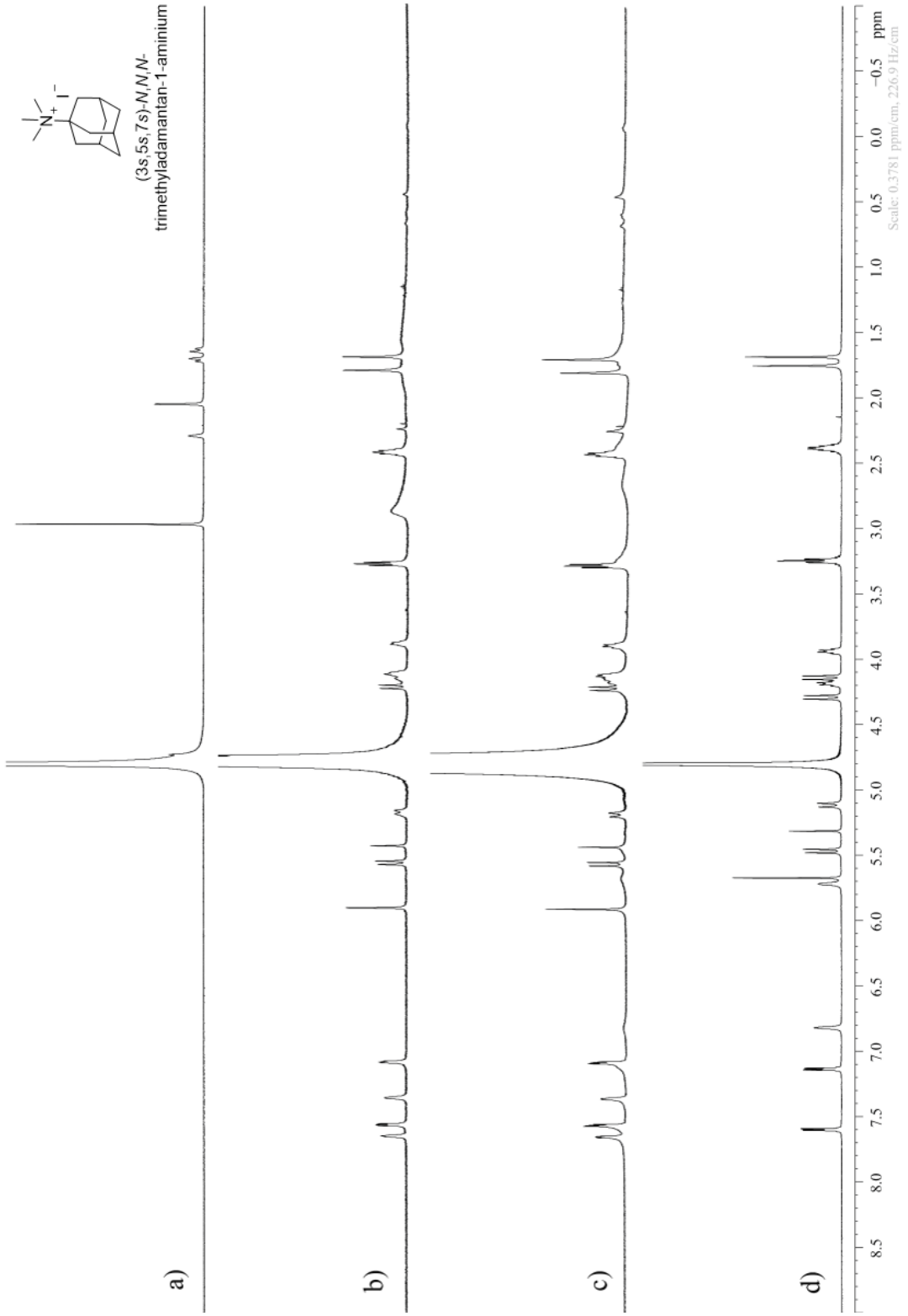

Figure III-S15. ^{1}H NMR spectra recorded (D_2O, 20 mM sodium phosphate, pD 7.40, 600 MHz, RT) for: a) **13** (2 mM), b) a mixture of **1** (125 µM) and **13** (250 µM), c) a mixture of **1** (125 µM) and **13** (125 µM), d) **1** (250 µM).

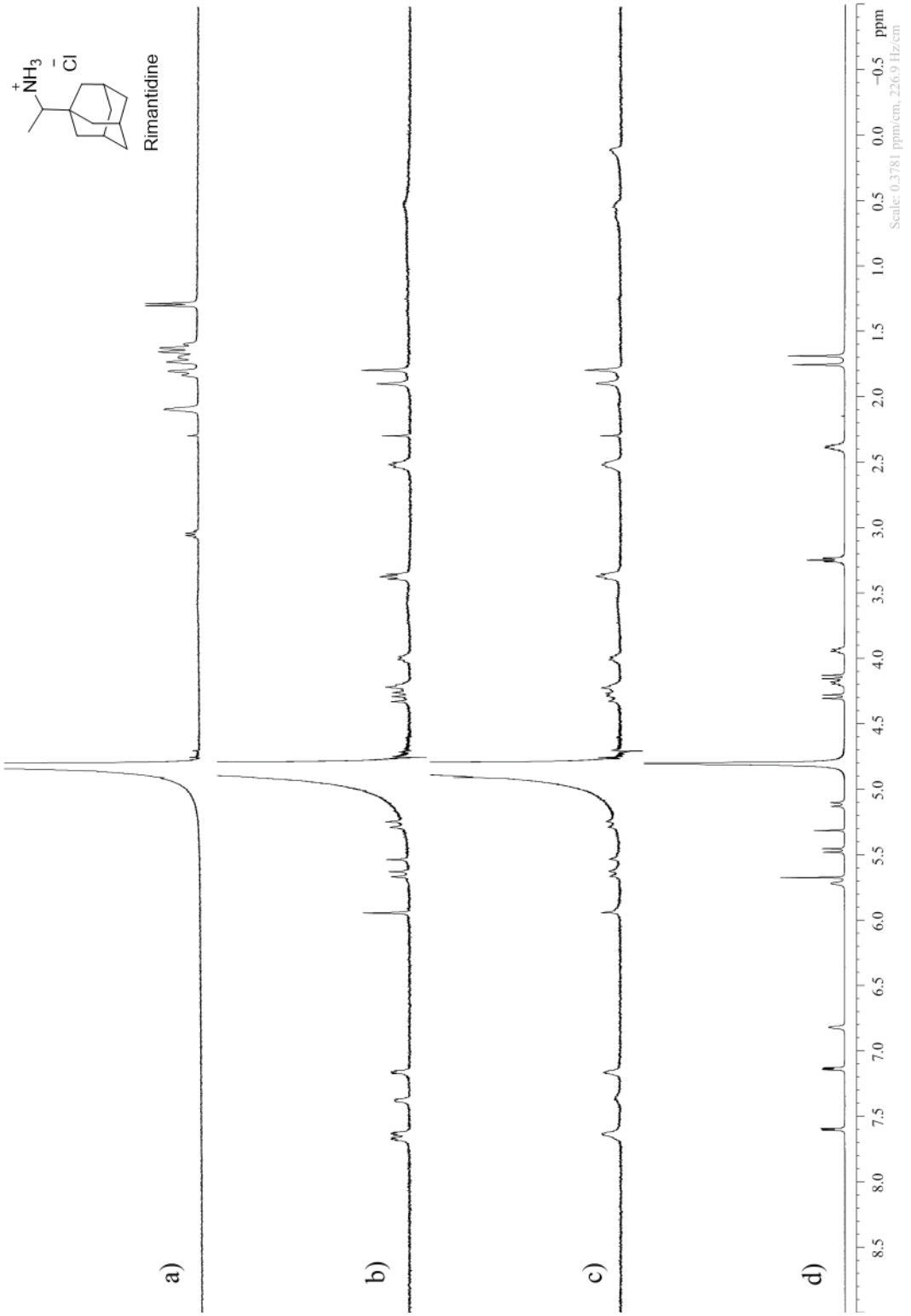

Figure III-S16. ^{1}H NMR spectra recorded (D_2O, 20 mM sodium phosphate, pD 7.40, 600 MHz, RT) for: a) **14** (4 mM), b) a mixture of **1** (125 μM) and **14** (250 μM), c) a mixture of **1** (125 μM) and **14** (125 μM), d) **1** (250 μM).

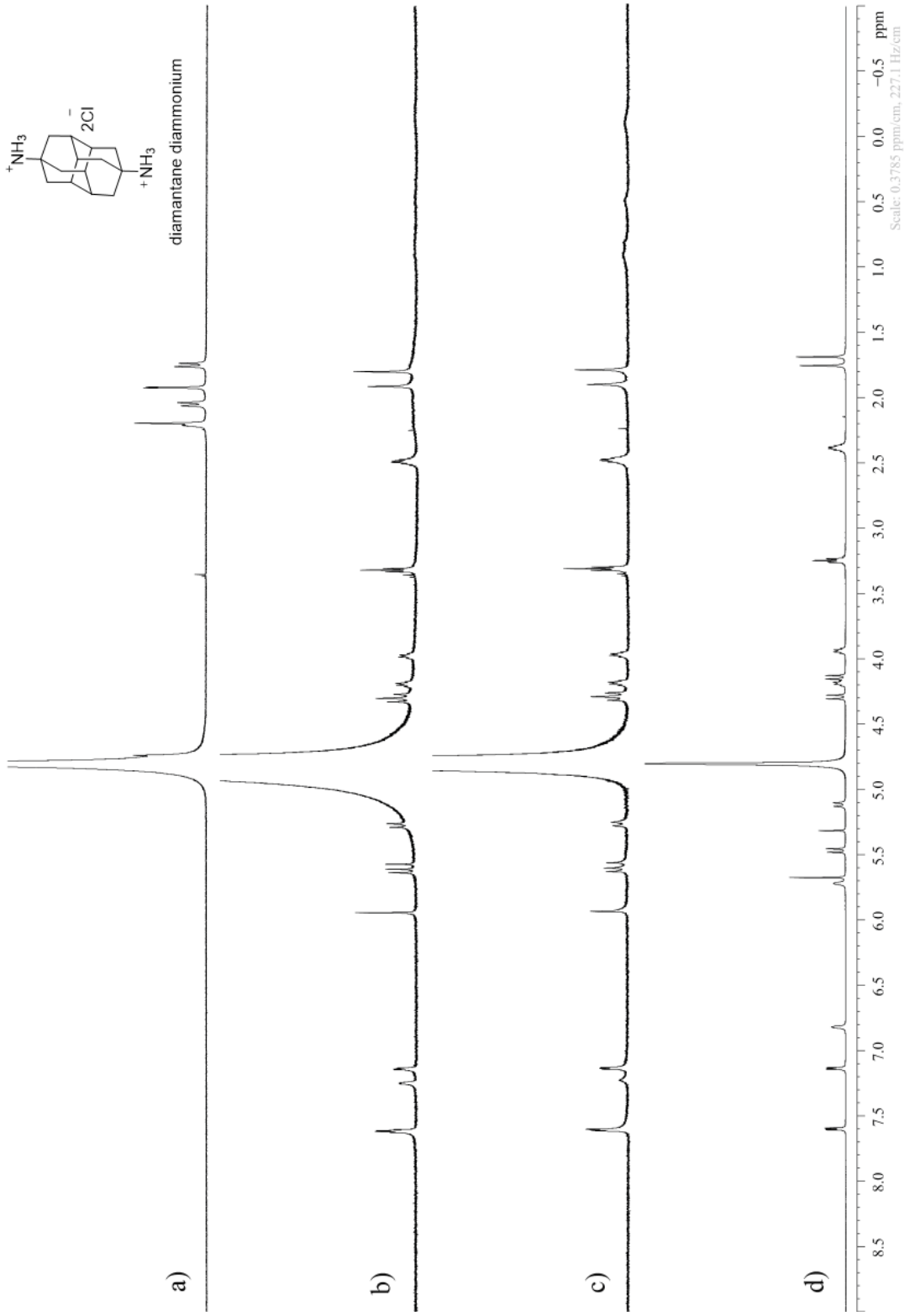

Figure III-S17. ^{1}H NMR spectra recorded (D_2O, 20 mM sodium phosphate, pD 7.40, 600 MHz, RT) for: a) **15** (4 mM), b) a mixture of **1** (250 µM) and **15** (500 µM), c) a mixture of **1** (250 µM) and **15** (250 µM), d) **1** (250 µM).

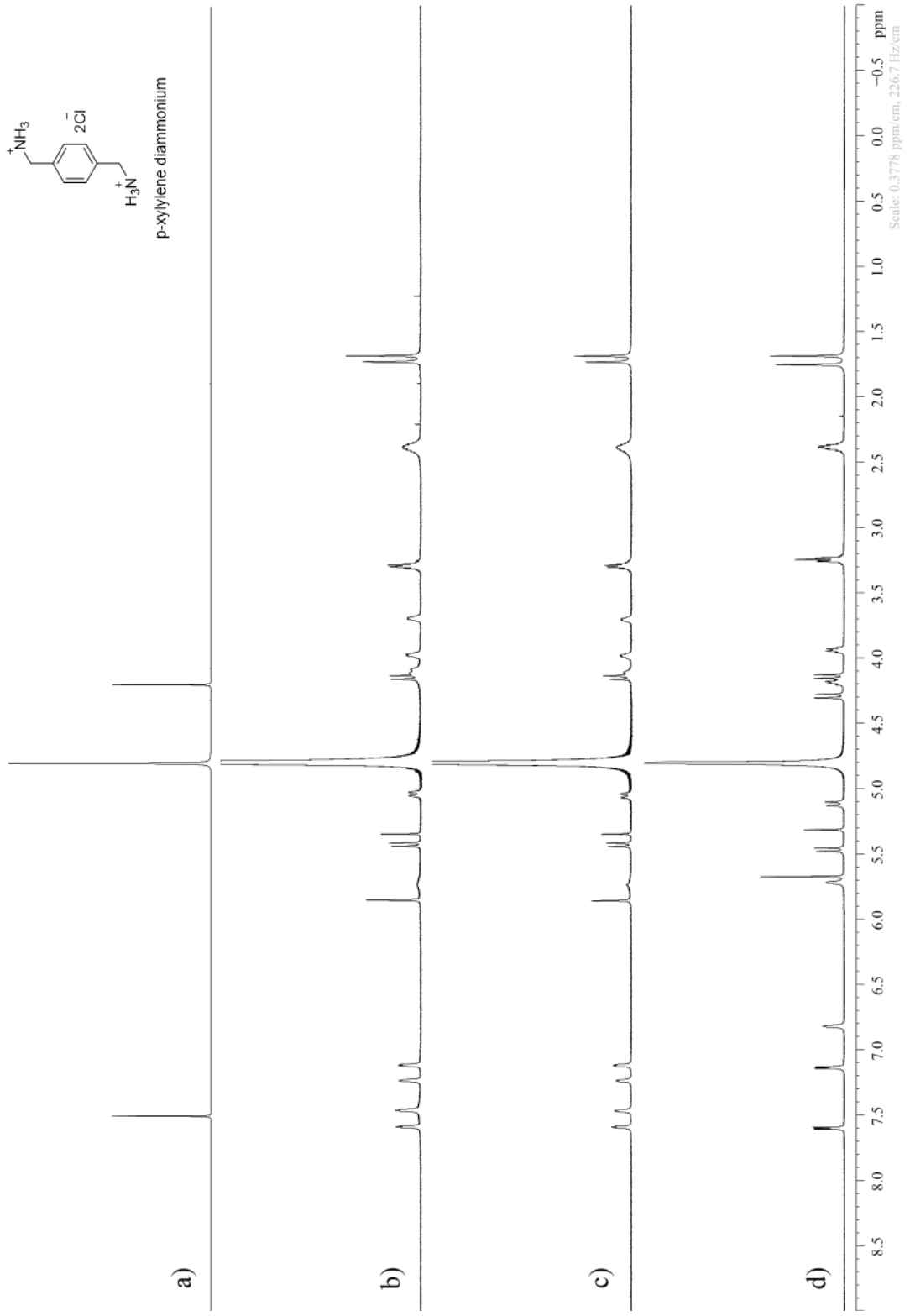

Figure III-S18. ^{1}H NMR spectra recorded (D_2O, 20 mM sodium phosphate, pD 7.40, 600 MHz, RT) for: a) **16** (4 mM), b) a mixture of **1** (250 μM) and **16** (500 μM), c) a mixture of **1** (250 μM) and **16** (250 μM), d) **1** (250 μM).

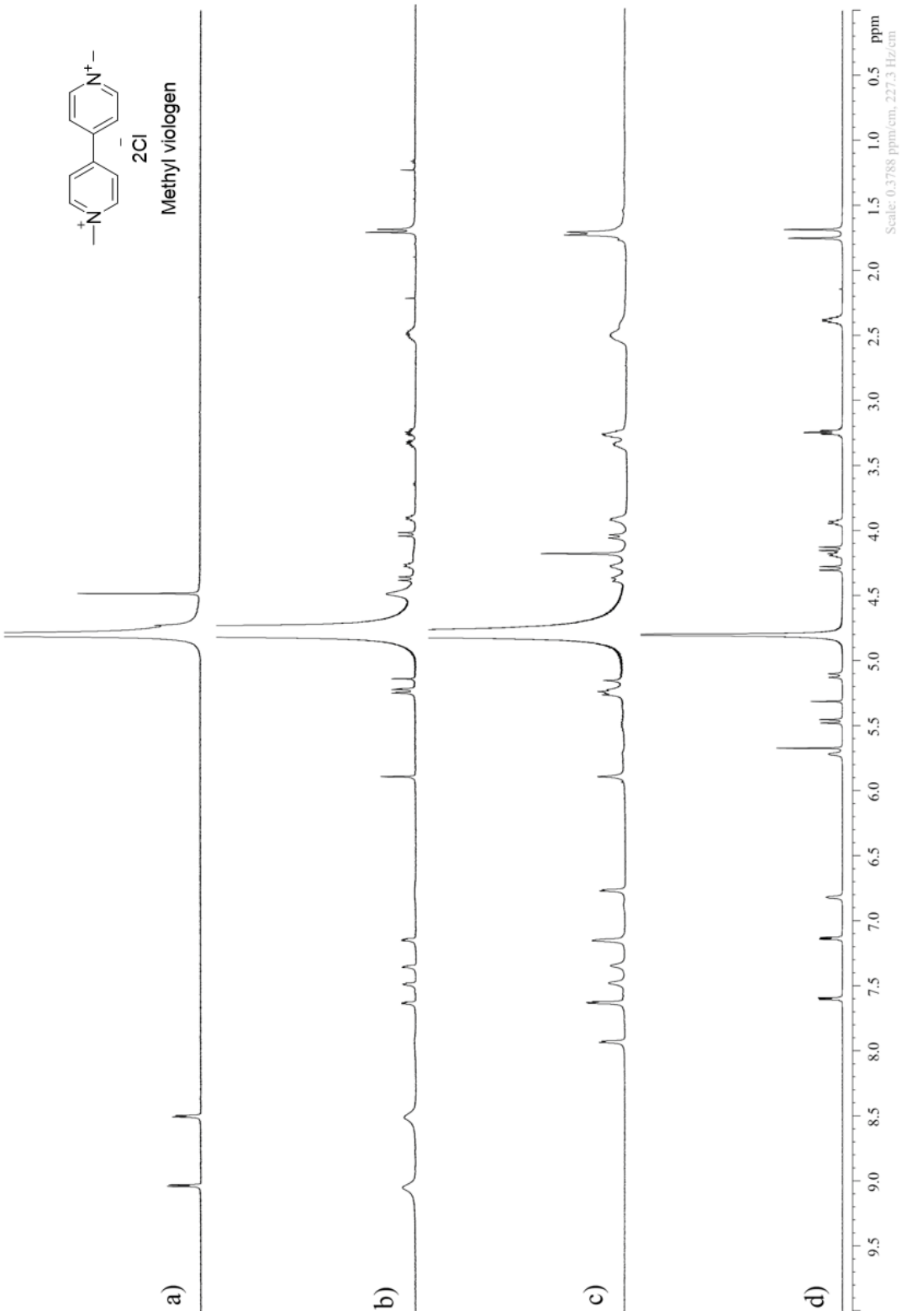

Figure III-S19. ^{1}H NMR spectra recorded (D_2O, 20 mM sodium phosphate, pD 7.40, 600 MHz, RT) for: a) **17** (2 mM), b) a mixture of **1** (250 µM) and **17** (500 µM), c) a mixture of **1** (250 µM) and **17** (250 µM), d) **1** (250 µM).

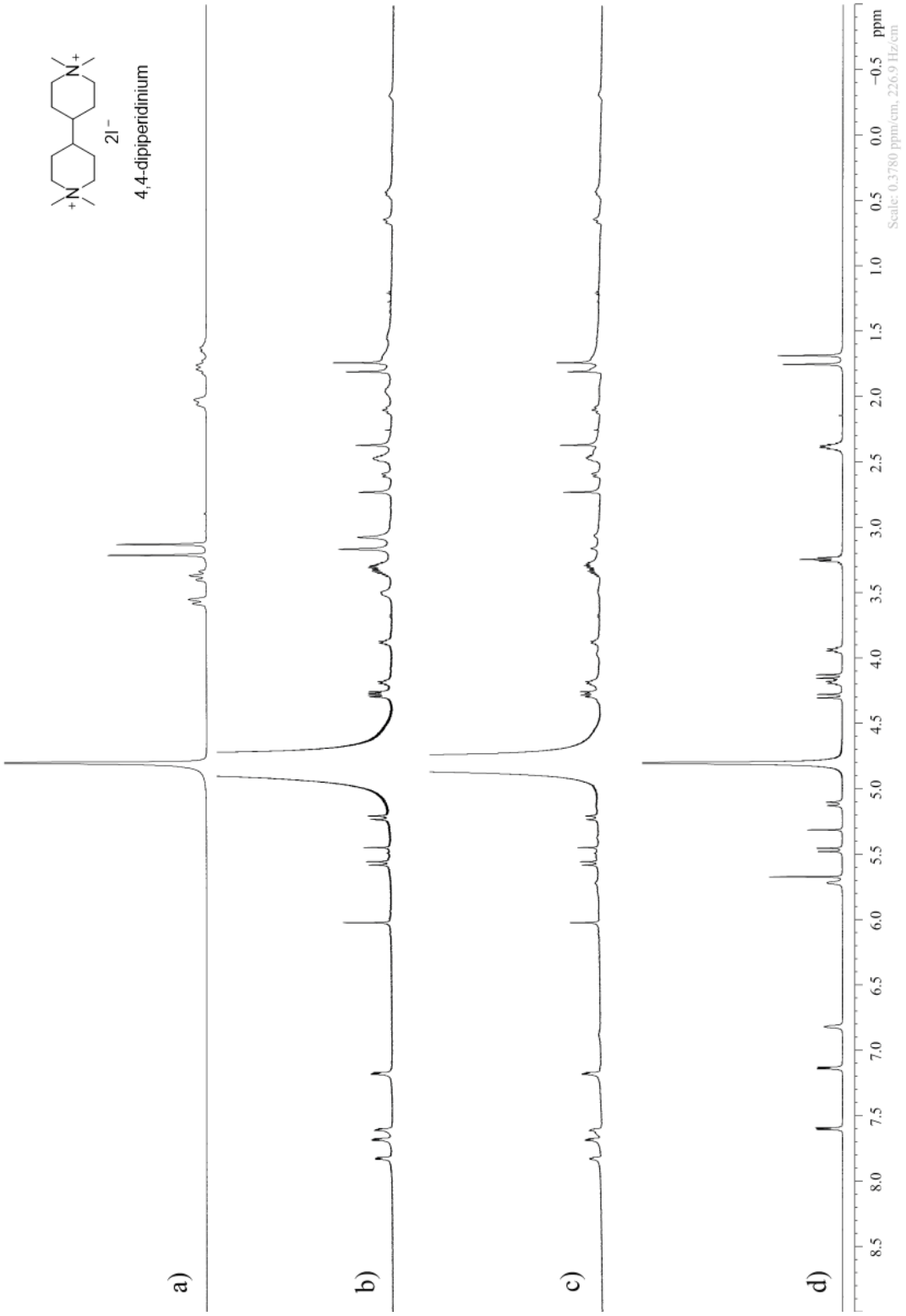

Figure III-S20. ^{1}H NMR spectra recorded (D_2O, 20 mM sodium phosphate, pD 7.40, 600 MHz, RT) for: a) **18** (1 mM), b) a mixture of **1** (125 µM) and **18** (250 µM), c) a mixture of **1** (125 µM) and **18** (125 µM), d) **1** (250 µM).

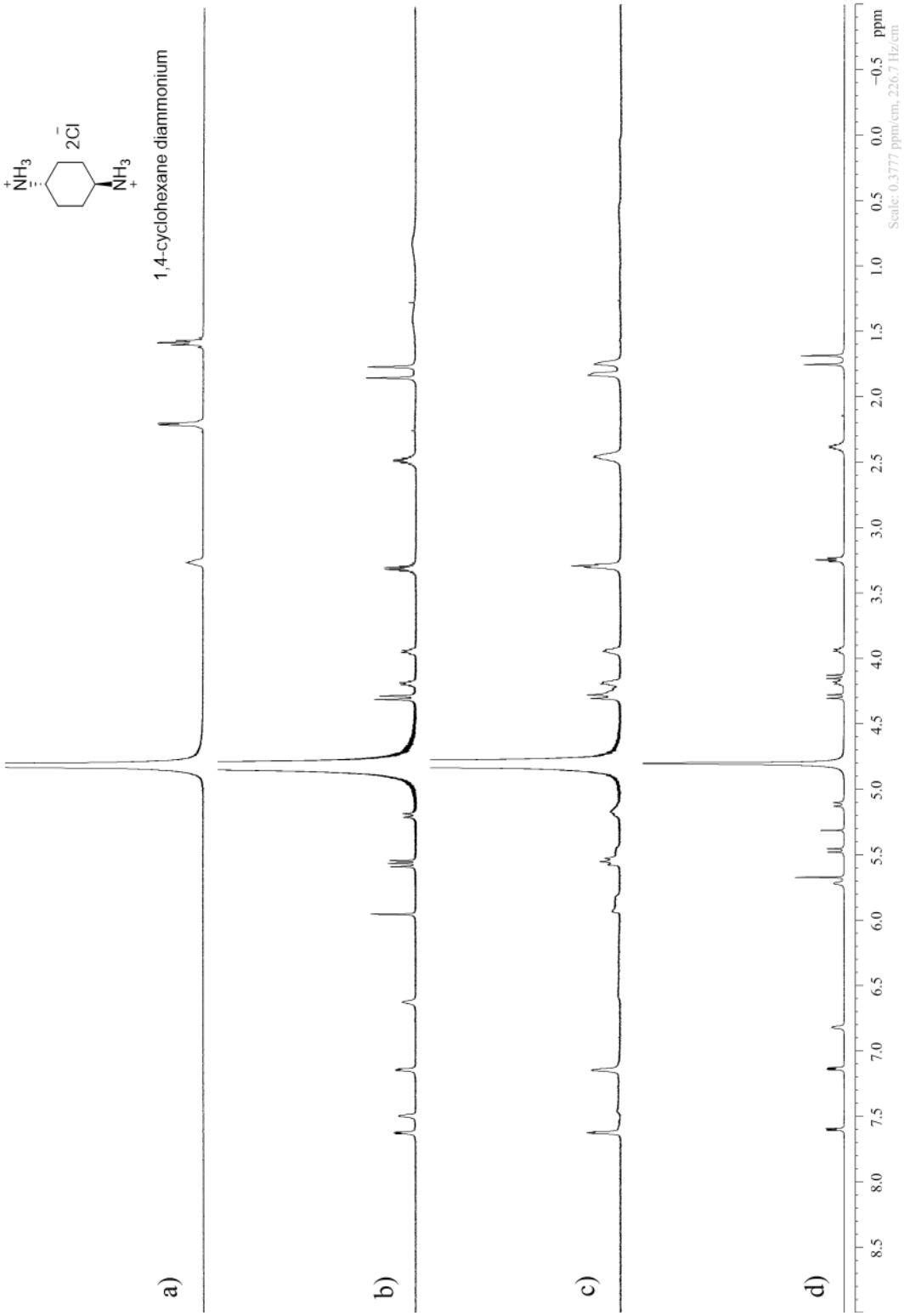

Figure III-S21. ^{1}H NMR spectra recorded (D_2O, 20 mM sodium phosphate, pD 7.40, 600 MHz, RT) for: a) **19** (4 mM), b) a mixture of **1** (250 μM) and **19** (500 μM), c) a mixture of **1** (250 μM) and **19** (250 μM), d) **1** (250 μM).

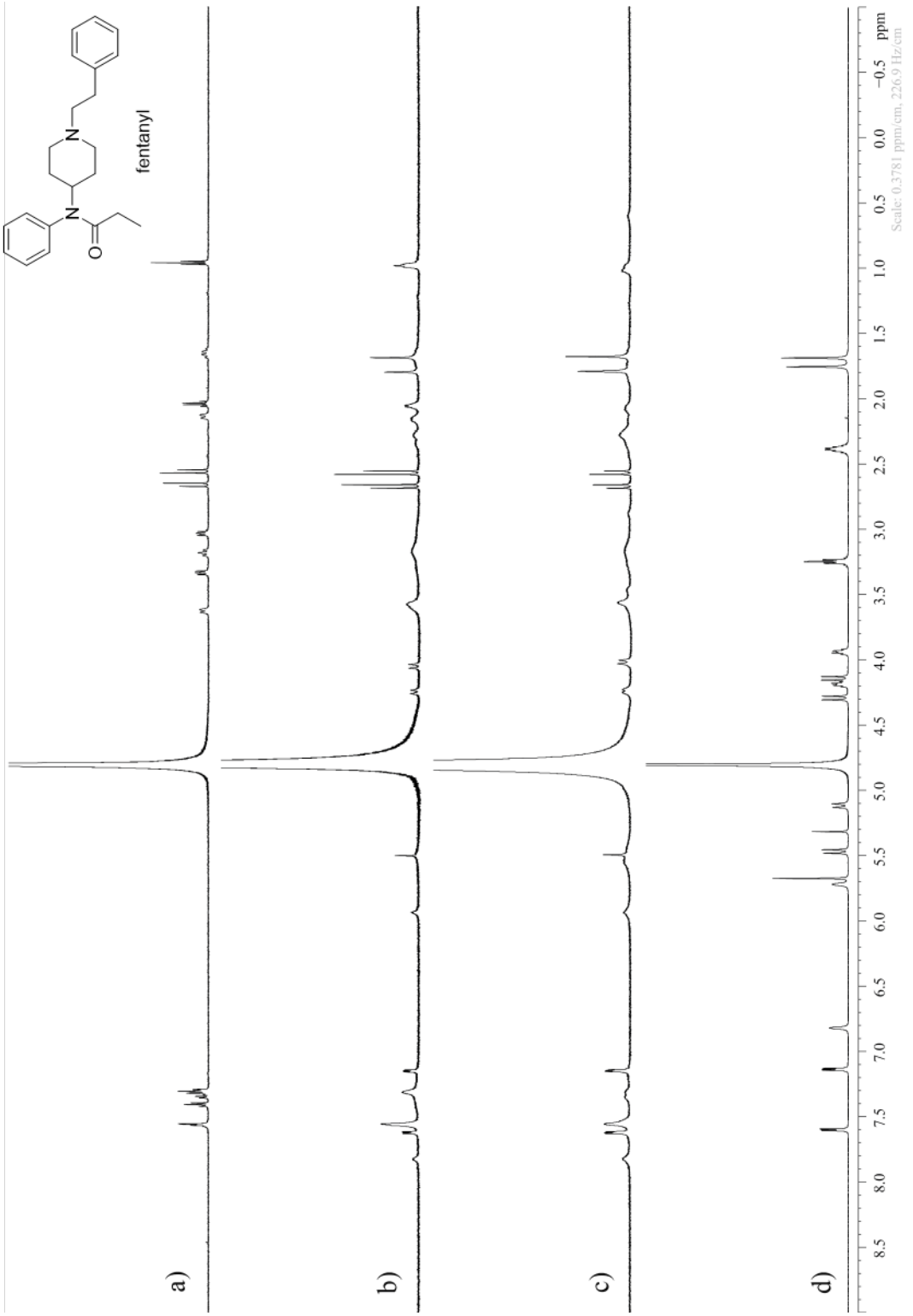

Figure III-S22. ^{1}H NMR spectra recorded (D_2O, 20 mM sodium phosphate, pD 7.40, 600 MHz, RT) for: a) **20** (250 μM), b) a mixture of **1** (125 μM) and **20** (250 μM), c) a mixture of **1** (125 μM) and **20** (125 μM), d) **1** (250 μM).

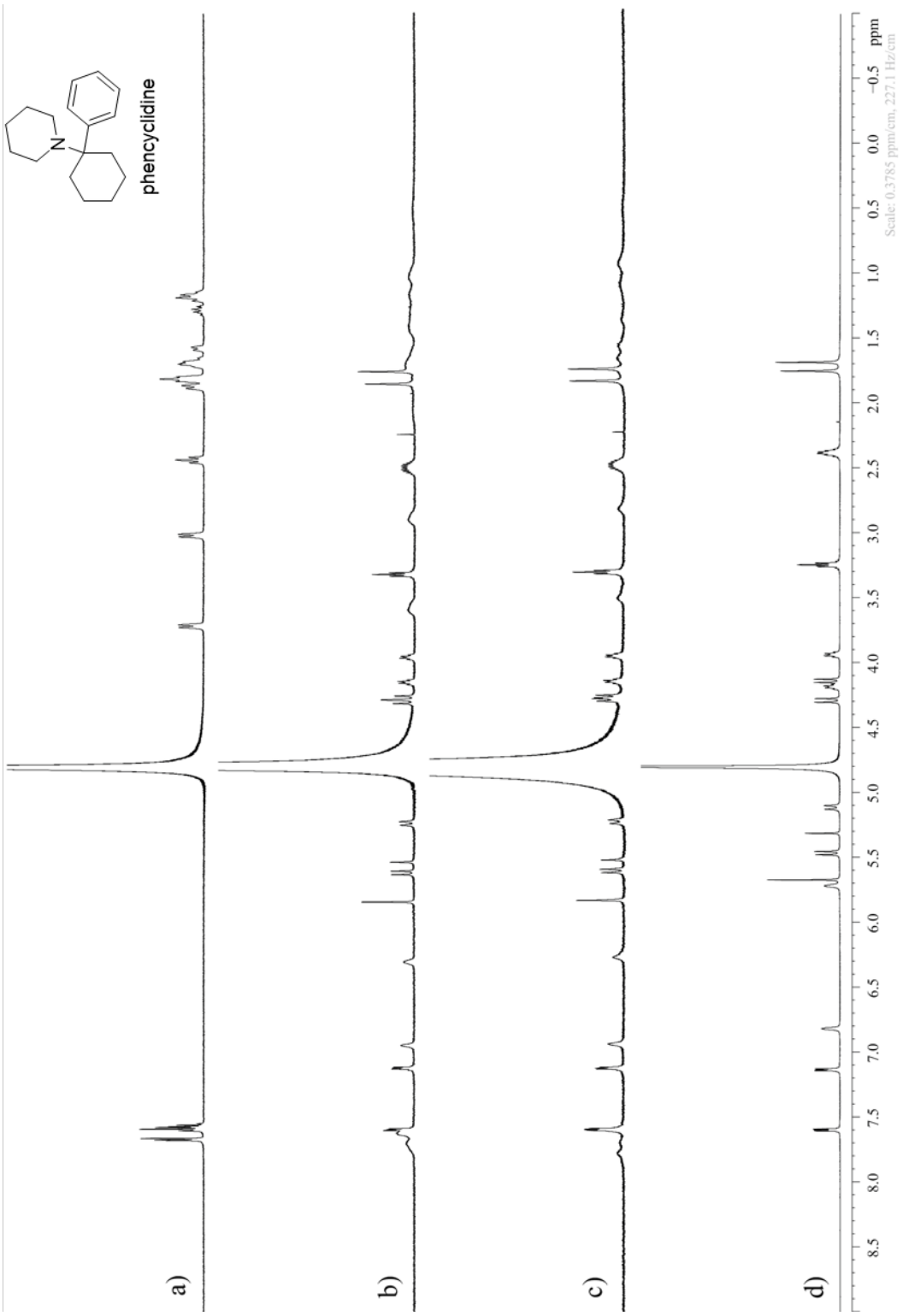

Figure III-S23. ^{1}H NMR spectra recorded (D_2O, 20 mM sodium phosphate, pD 7.40, 600 MHz, RT) for: a) **21** (1 mM), b) a mixture of **1** (125 µM) and **21** (250 µM), c) a mixture of **1** (125 µM) and **21** (125 µM), d) **1** (250 µM).

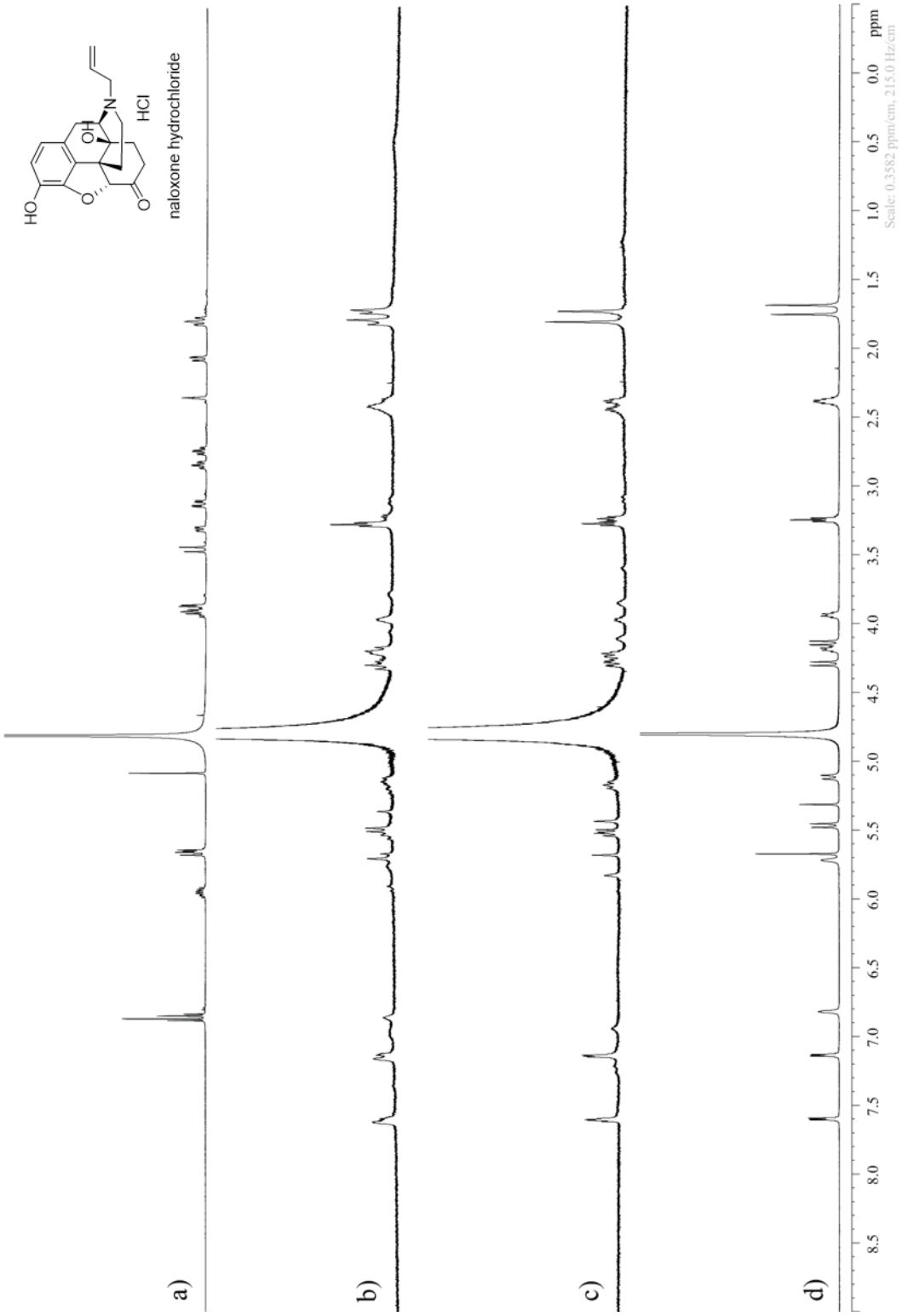

Figure III-S24. ^{1}H NMR spectra recorded (D_2O, 20 mM sodium phosphate, pD 7.40, 600 MHz, RT) for: a) **22** (2 mM), b) a mixture of **1** (125 μM) and **22** (250 μM), c) a mixture of **1** (125 μM) and **22** (125 μM), d) **1** (250 μM).

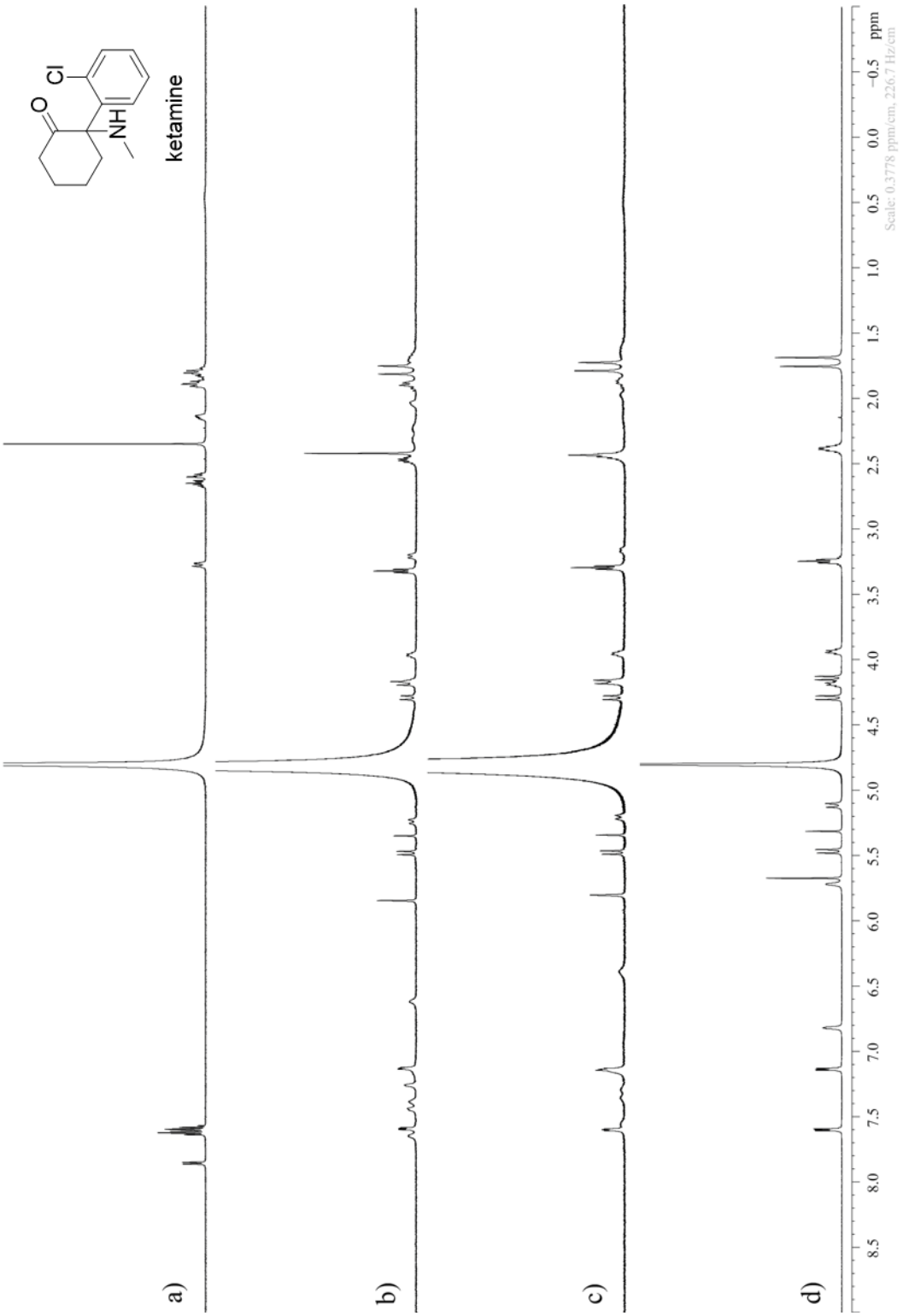

Figure III-S25. ^{1}H NMR spectra recorded (D_2O, 20 mM sodium phosphate, pD 7.40, 600 MHz, RT) for: a) **23** (250 µM), b) a mixture of **1** (125 µM) and **23** (250 µM), c) a mixture of **1** (125 µM) and **23** (125 µM), d) **1** (250 µM).

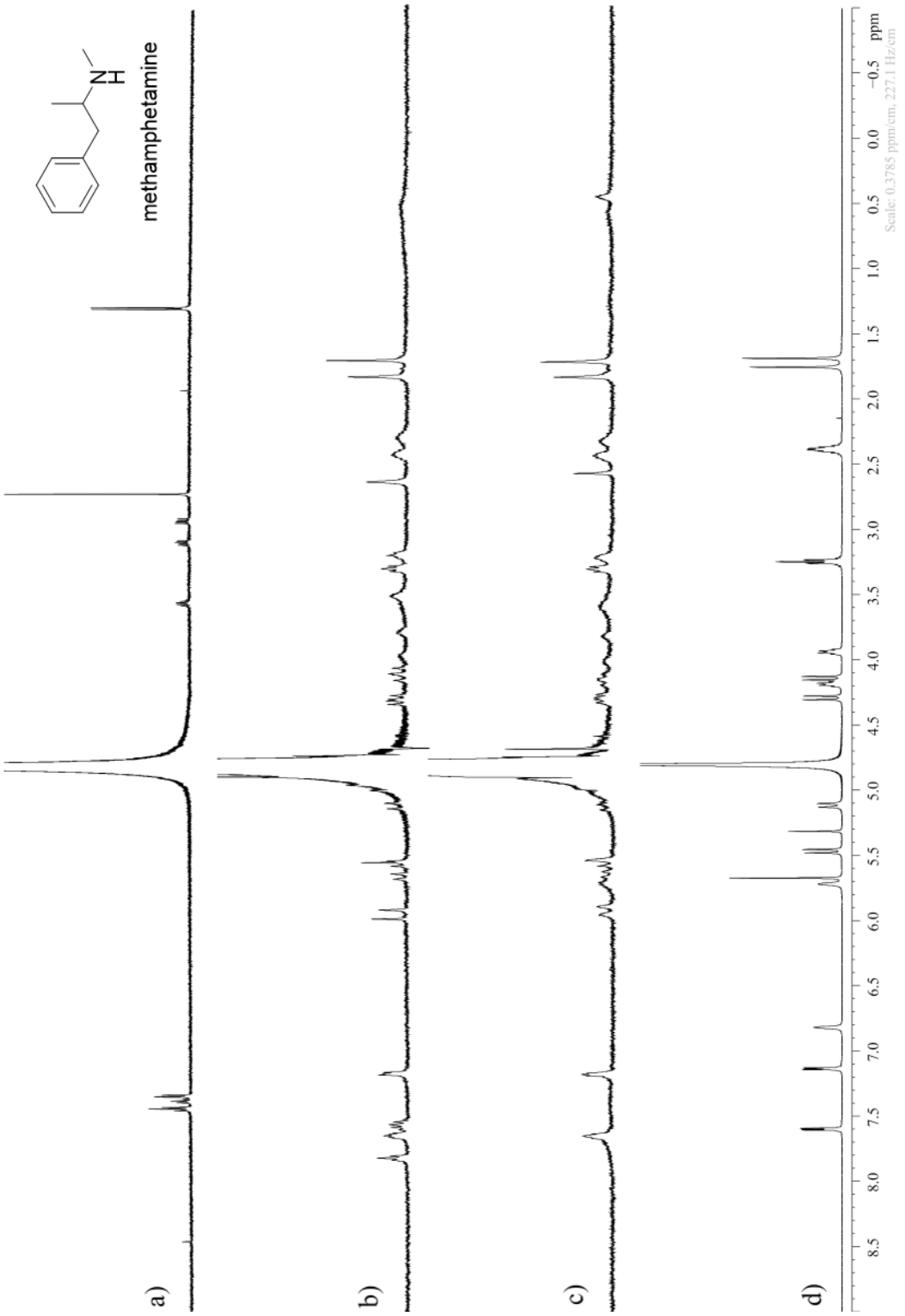

Figure III-S26. ^{1}H NMR spectra recorded (D_2O, 20 mM sodium phosphate, pD 7.40, 400 MHz, RT) for: a) **24** (250 µM), b) a mixture of **1** (125 µM) and **24** (250 µM), c) a mixture of **1** (125 µM) and **24** (125 µM), d) **1** (250 µM).

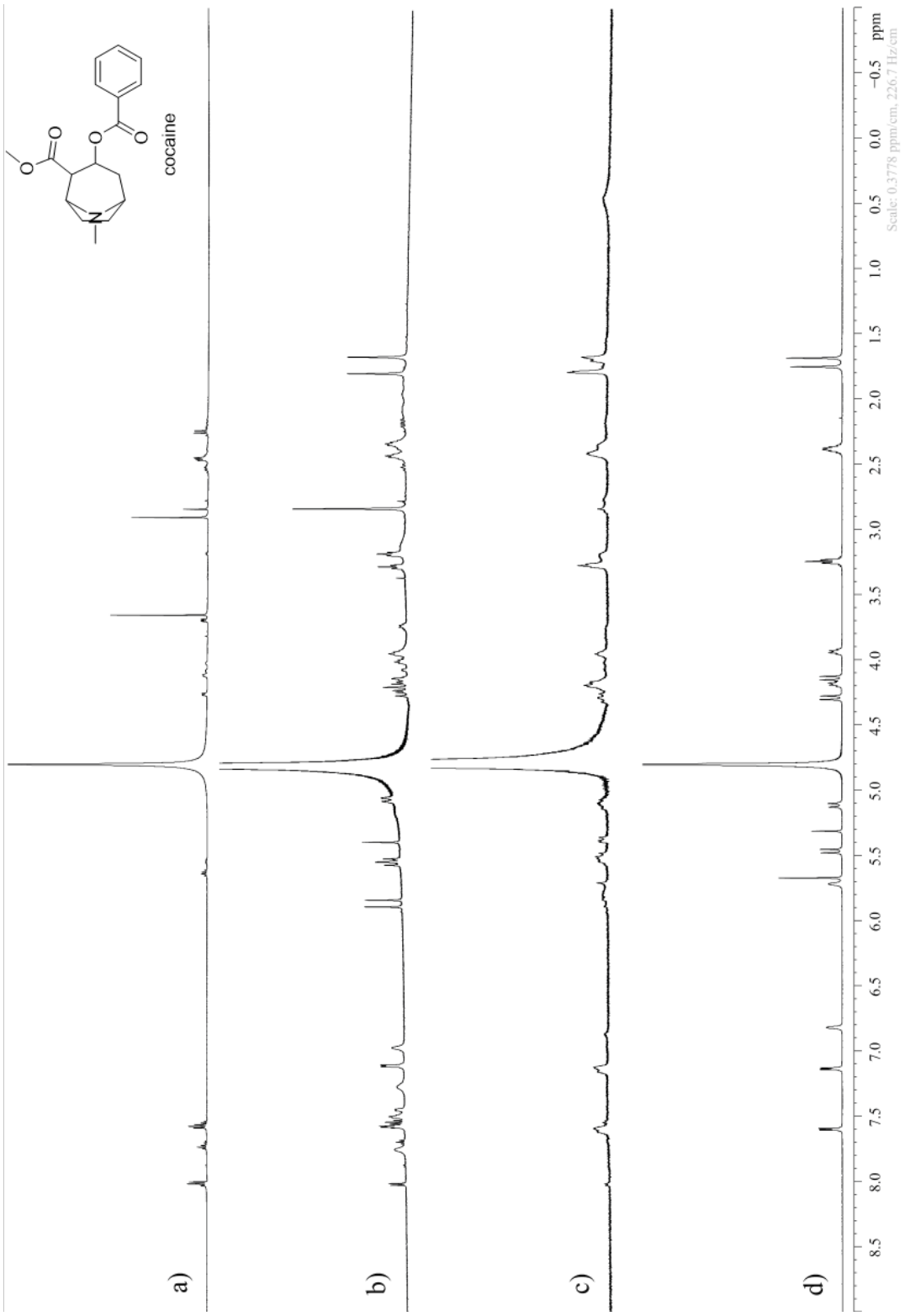

Figure III-S27. ^{1}H NMR spectra recorded (D_2O, 20 mM sodium phosphate, pD 7.40, 600 MHz, RT) for: a) **25** (1 mM), b) a mixture of **1** (125 µM) and **25** (250 µM), c) a mixture of **1** (125 µM) and **25** (125 µM), d) **1** (250 µM).

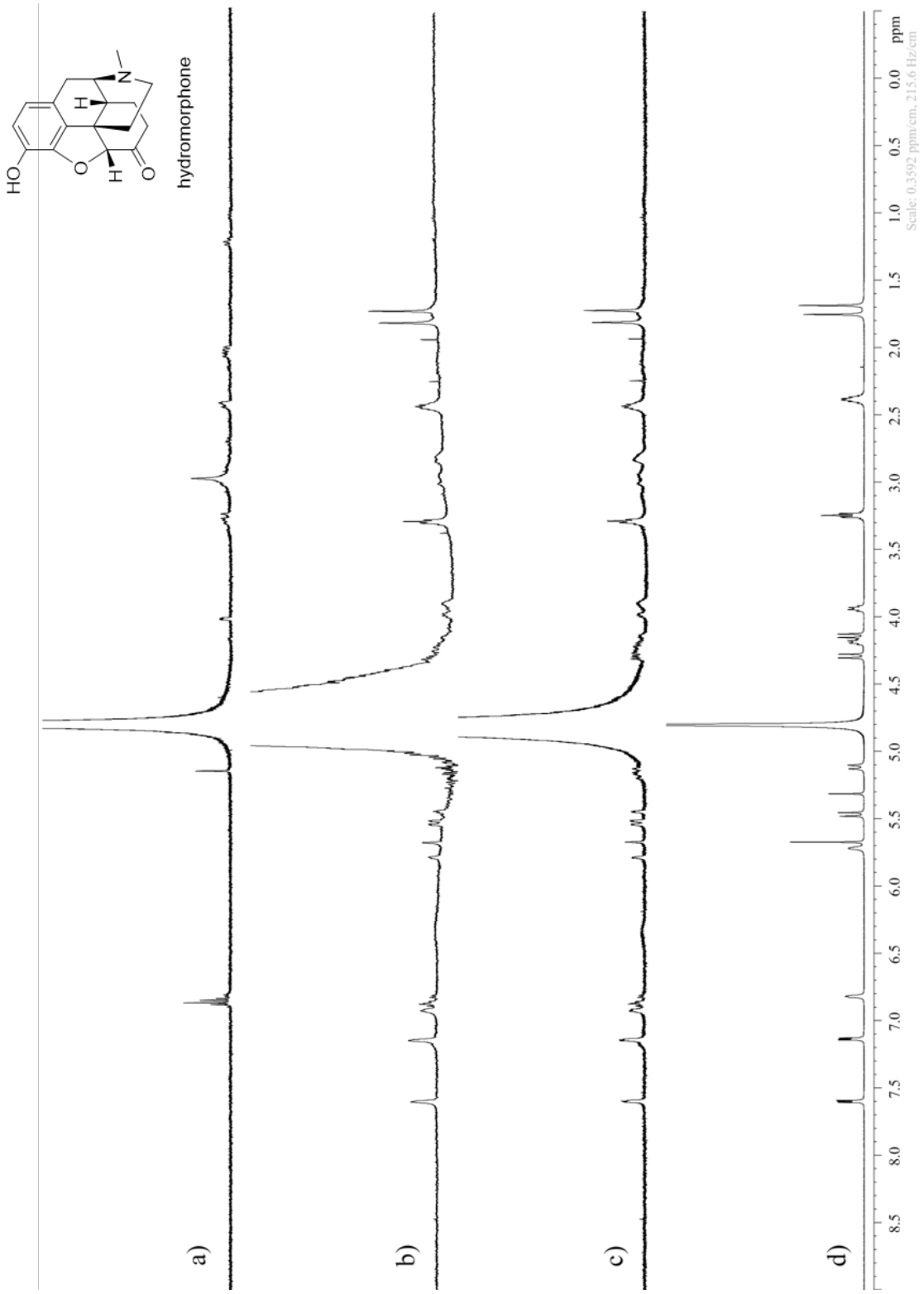

Figure III-S28. ^{1}H NMR spectra recorded (D_2O, 20 mM sodium phosphate, pD 7.40, 600 MHz, RT) for: a) **26** (250 mM), b) a mixture of **1** (62.5 µM) and **26** (125 µM), c) a mixture of **1** (125 µM) and **26** (125 µM), d) **1** (250 µM).

Isotherm of guests (4-26) with host 1

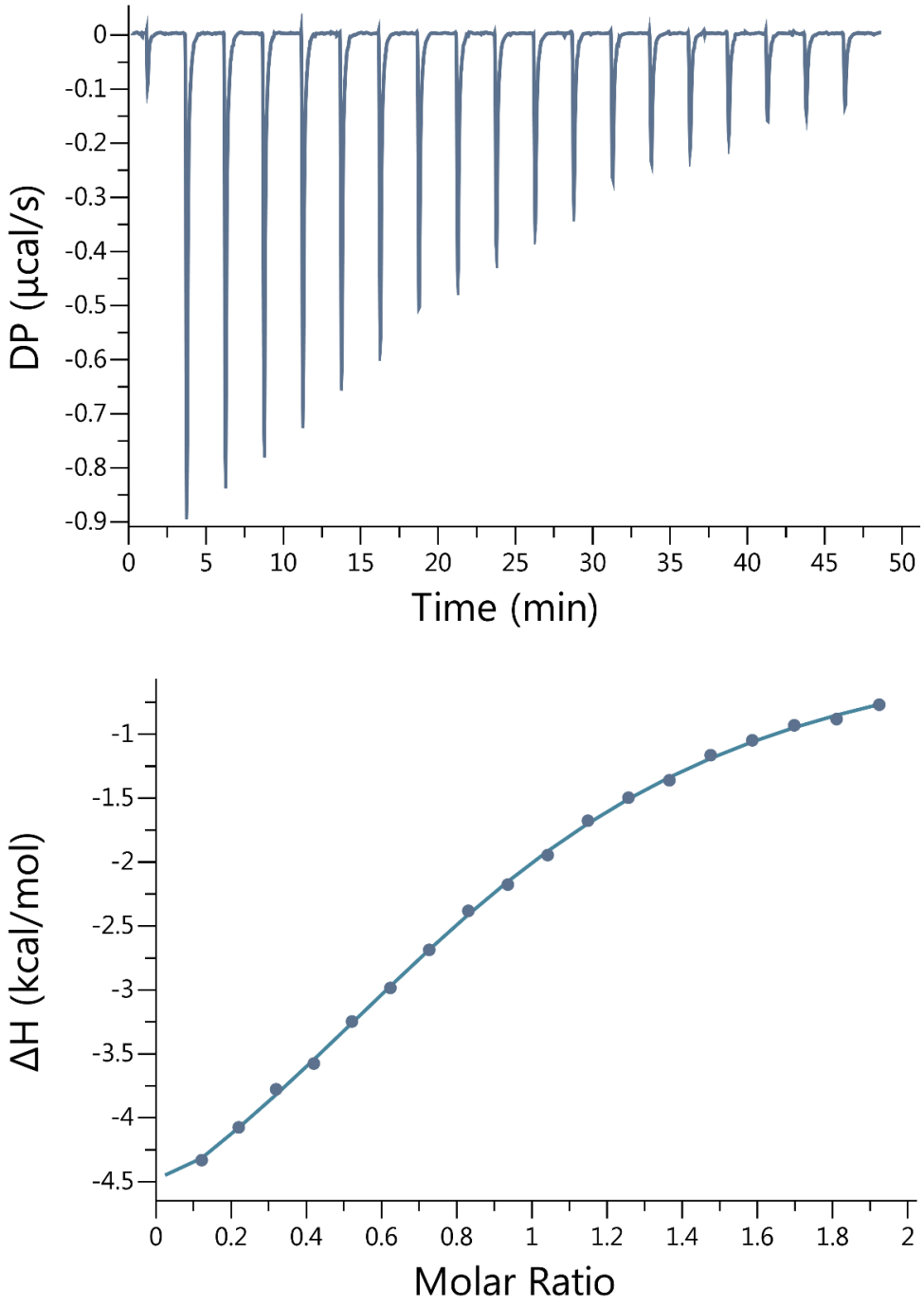

Figure III-S29. Isothermal Titration Calorimetry (ITC) curve obtained when a solution of **1** (100 µM) in the cell was titrated with **4** (1.00 mM) in the syringe at 298.0 K in 20 mM sodium phosphate buffered water at pH 7.4. $K_a = 2.92 \times 10^4\ M^{-1}$ and $\Delta H = -6.03 \pm 0.260$ kcal•mol^{-1}

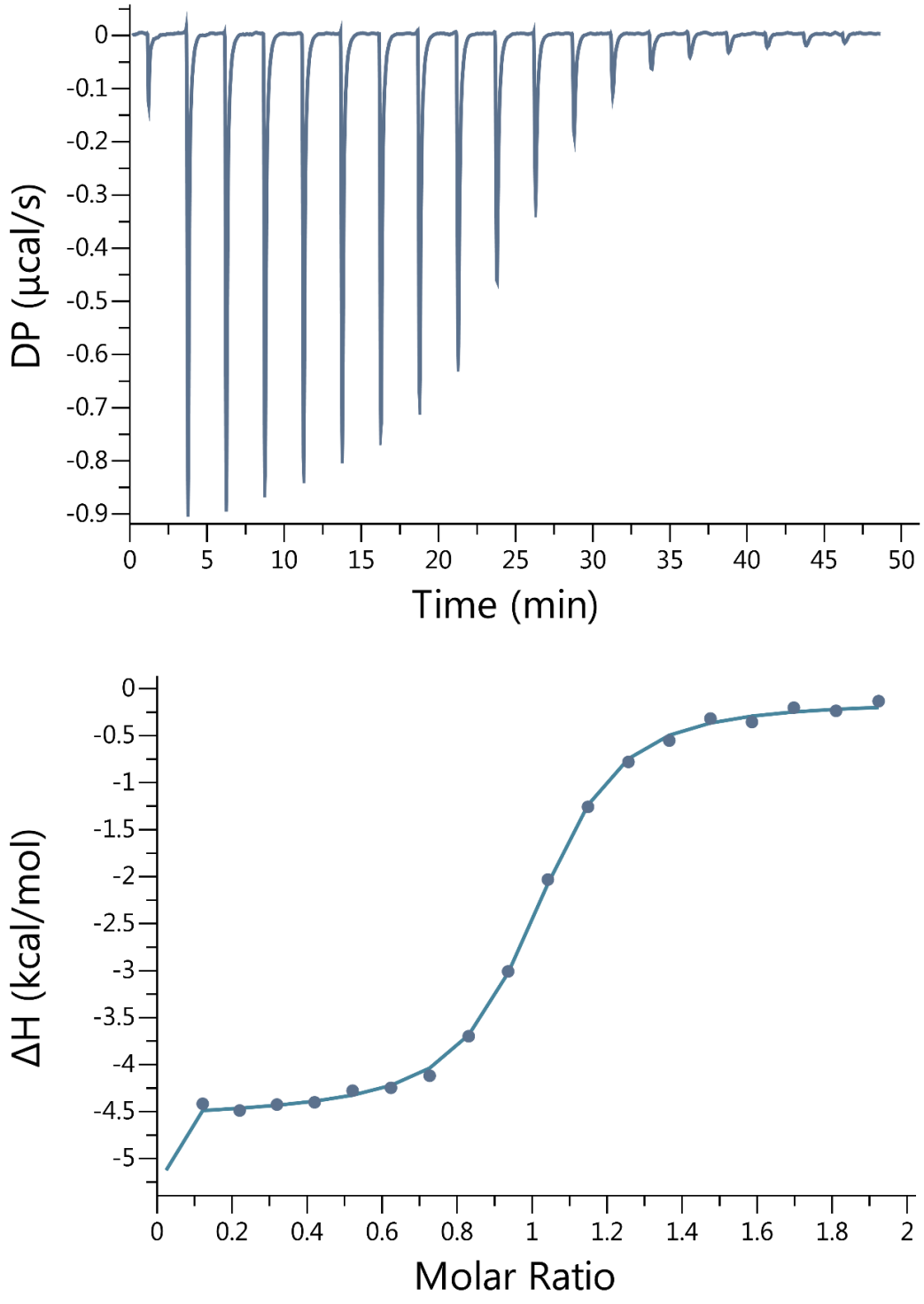

Figure III-S30. Isothermal Titration Calorimetry (ITC) curve obtained through competition binding studies. A solution of **1** (100 µM) and **19** (500 µM) in the cell was titrated with **6** (1.00 mM) in the syringe at 298.0 K in 20 mM sodium phosphate buffered water at pH 7.4. $K_a = 2.30 \times 10^7\ M^{-1}$ and H = -10.8 ± 0.044 kcal•mol^{-1}.

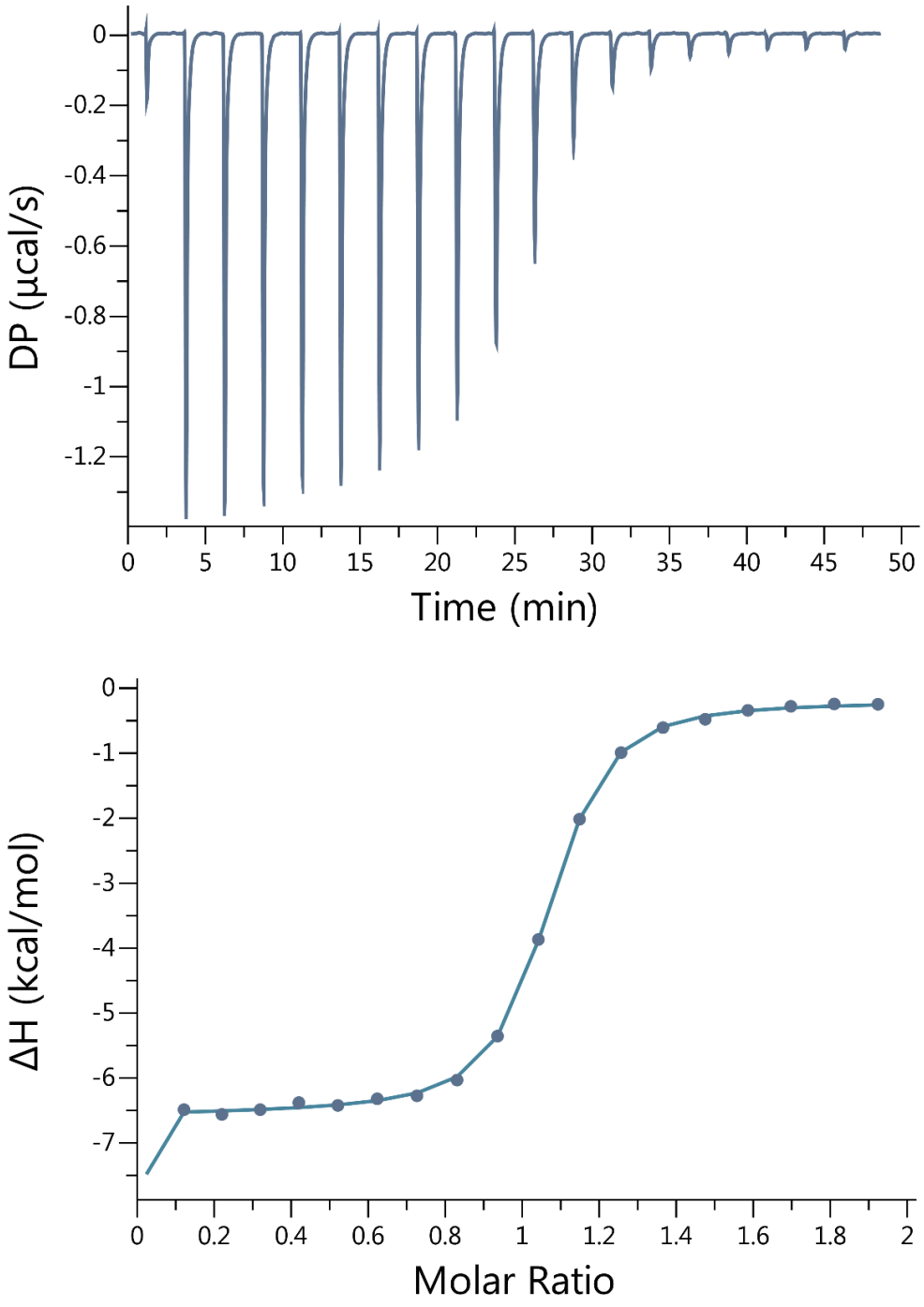

Figure III-S31. Isothermal Titration Calorimetry (ITC) curve obtained through competition binding studies. A solution of **1** (100 µM) and **19** (500 µM) in the cell was titrated with **6DQ** (1.00 mM) in the syringe at 298.0 K in 20 mM sodium phosphate buffered water at pH 7.4. $K_a = 5.00 \times 10^7\ M^{-1}$ and $\Delta H = -12.7 \pm 0.028$ kcal•mol^{-1}

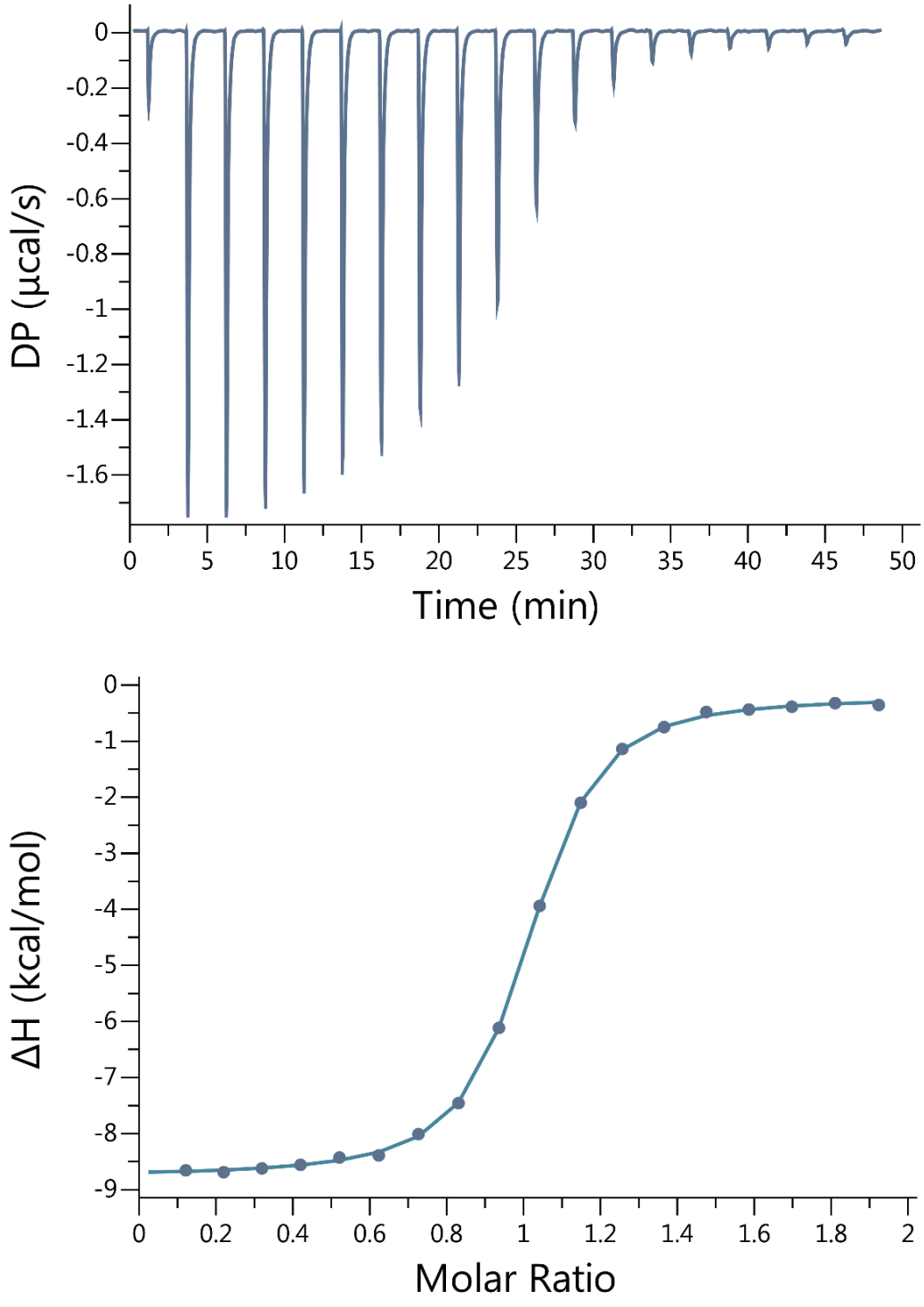

Figure III-S32. Isothermal Titration Calorimetry (ITC) curve obtained when a solution of **1** (100 µM) in the cell was titrated with **6Q** (1.00 mM) in the syringe at 298.0 K in 20 mM sodium phosphate buffered water at pH 7.4. $K_a = 1.20 \times 10^6\ M^{-1}$ and $\Delta H = -8.54 \pm 0.027$ kcal•mol^{-1}.

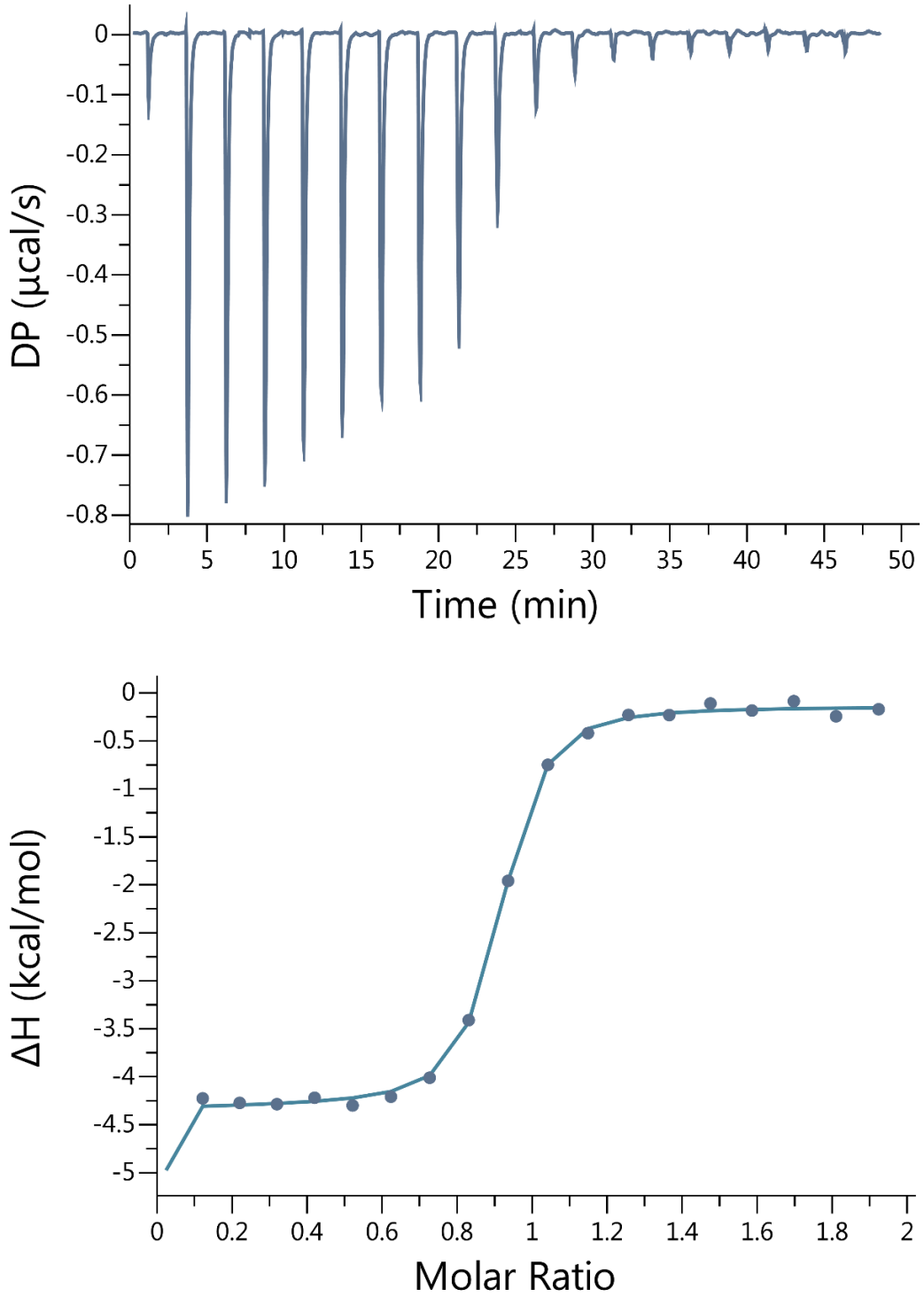

Figure III-S33. Isothermal Titration Calorimetry (ITC) curve obtained through competition binding studies. A solution of **1** (100 µM) and **19** (500 µM) in the cell was titrated with **7** (1.00 mM) in the syringe at 298.0 K in 20 mM sodium phosphate buffered water at pH 7.4. $K_a = 7.24 \times 10^7\ M^{-1}$ and $\Delta H = -10.1 \pm 0.036$ kcal•mol^{-1}.

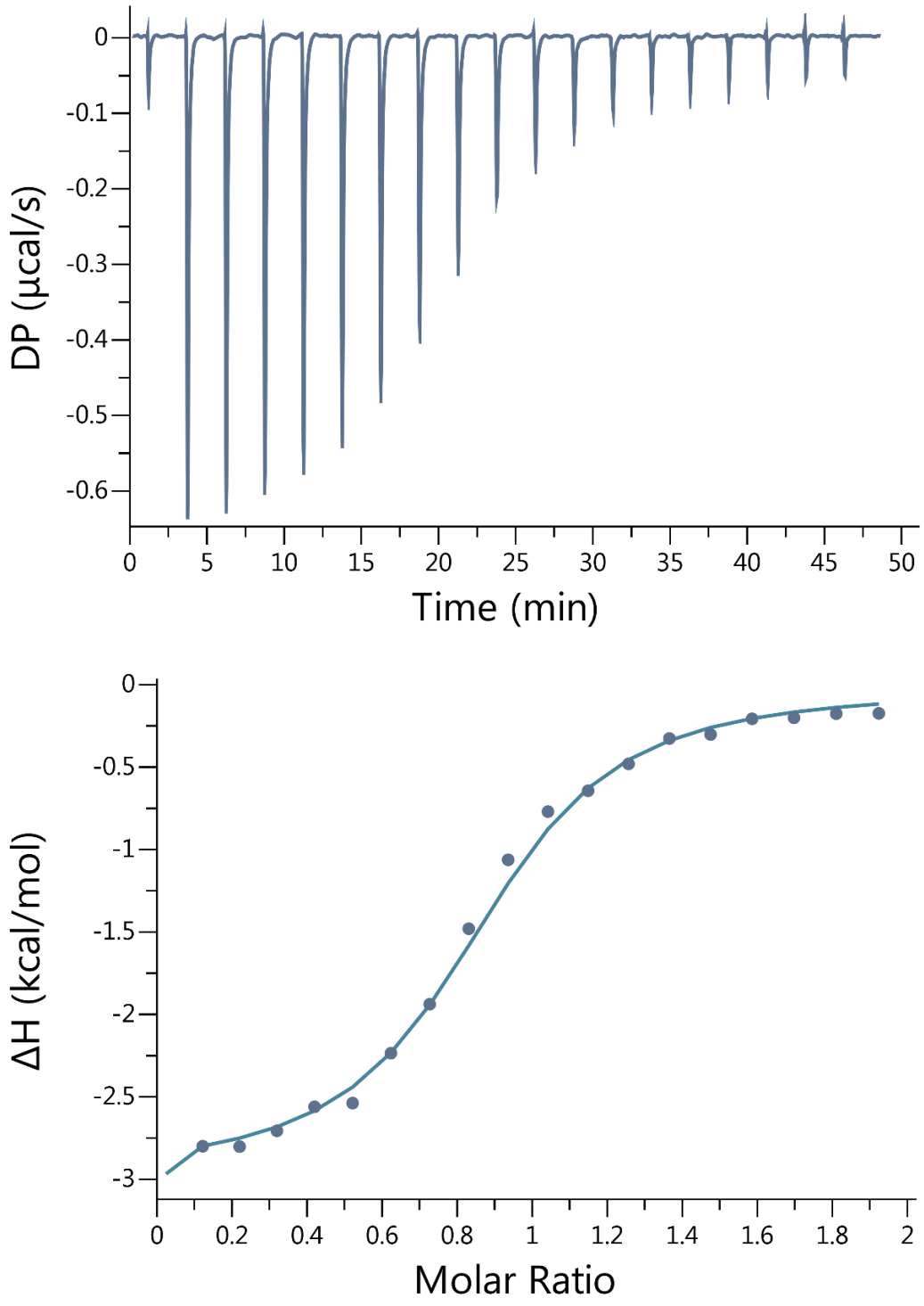

Figure III-S34. Isothermal Titration Calorimetry (ITC) curve obtained through competition binding studies. A solution of **1** (100 µM) and **5** (500 µM) in the cell was titrated with **8** (1.00 mM) in the syringe at 298.0 K in 20 mM sodium phosphate buffered water at pH 7.4. $K_a = 1.41 \times 10^8\ M^{-1}$ and $\Delta H = -11.5 \pm 0.094$ kcal•mol^{-1}.

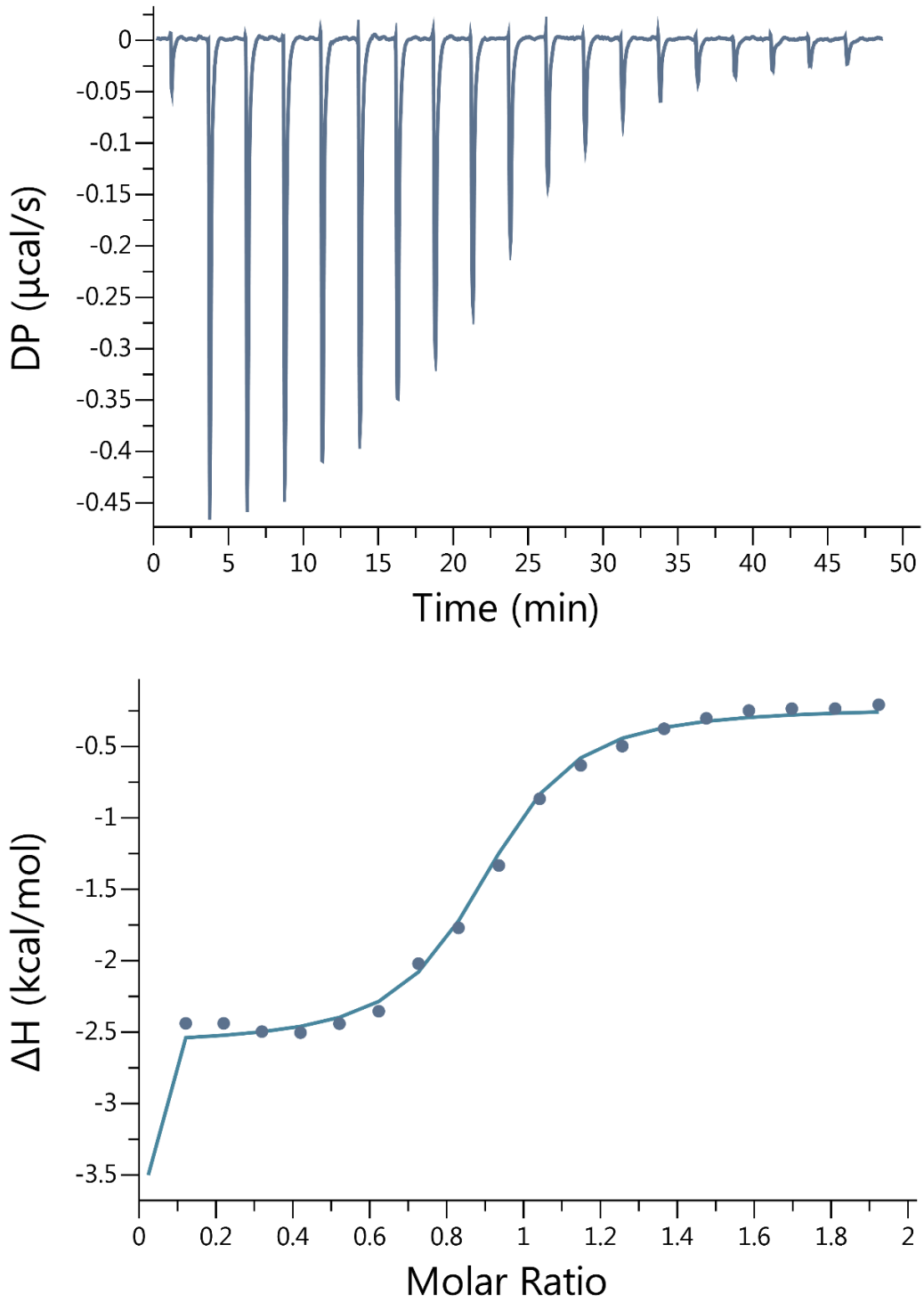

Figure III-S35. Isothermal Titration Calorimetry (ITC) curve obtained through competition binding studies. A solution of **1** (100 µM) and **5** (500 µM) in the cell was titrated with **9** (1.00 mM) in the syringe at 298.0 K in 20 mM sodium phosphate buffered water at pH 7.4. $K_a = 2.42 \times 10^8\ M^{-1}$ and $\Delta H = -11.4 \pm 0.062$ kcal•mol^{-1}.

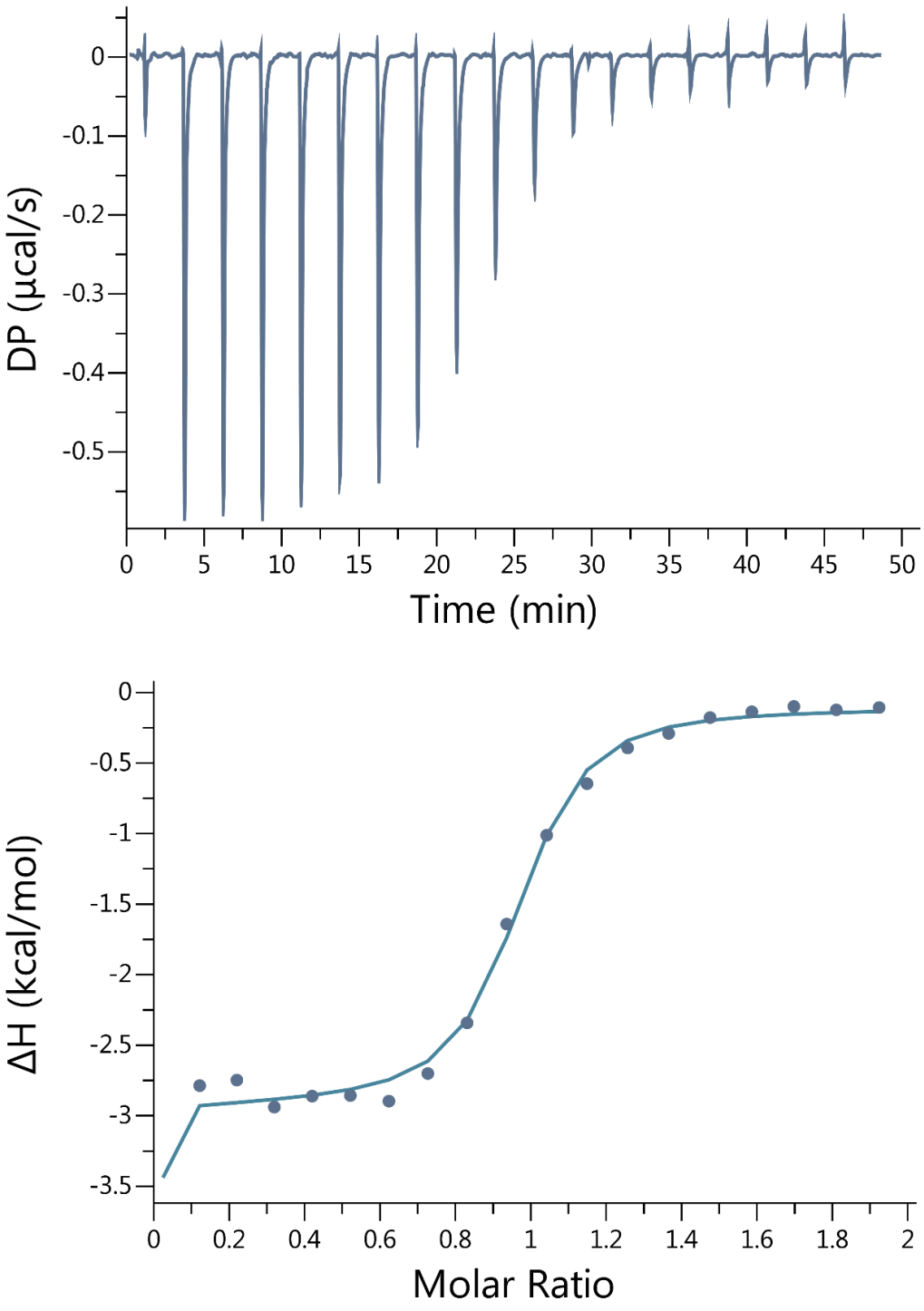

Figure III-S36. Isothermal Titration Calorimetry (ITC) curve obtained through competition binding studies. A solution of **1** (100 µM) and **5** (200 µM) in the cell was titrated with **10** (1.00 mM) in the syringe at 298.0 K in 20 mM sodium phosphate buffered water at pH 7.4. $K_a = 2.81 \times 10^8\ M^{-1}$ and $\Delta H = -11.3 \pm 0.068$ kcal•mol^{-1}.

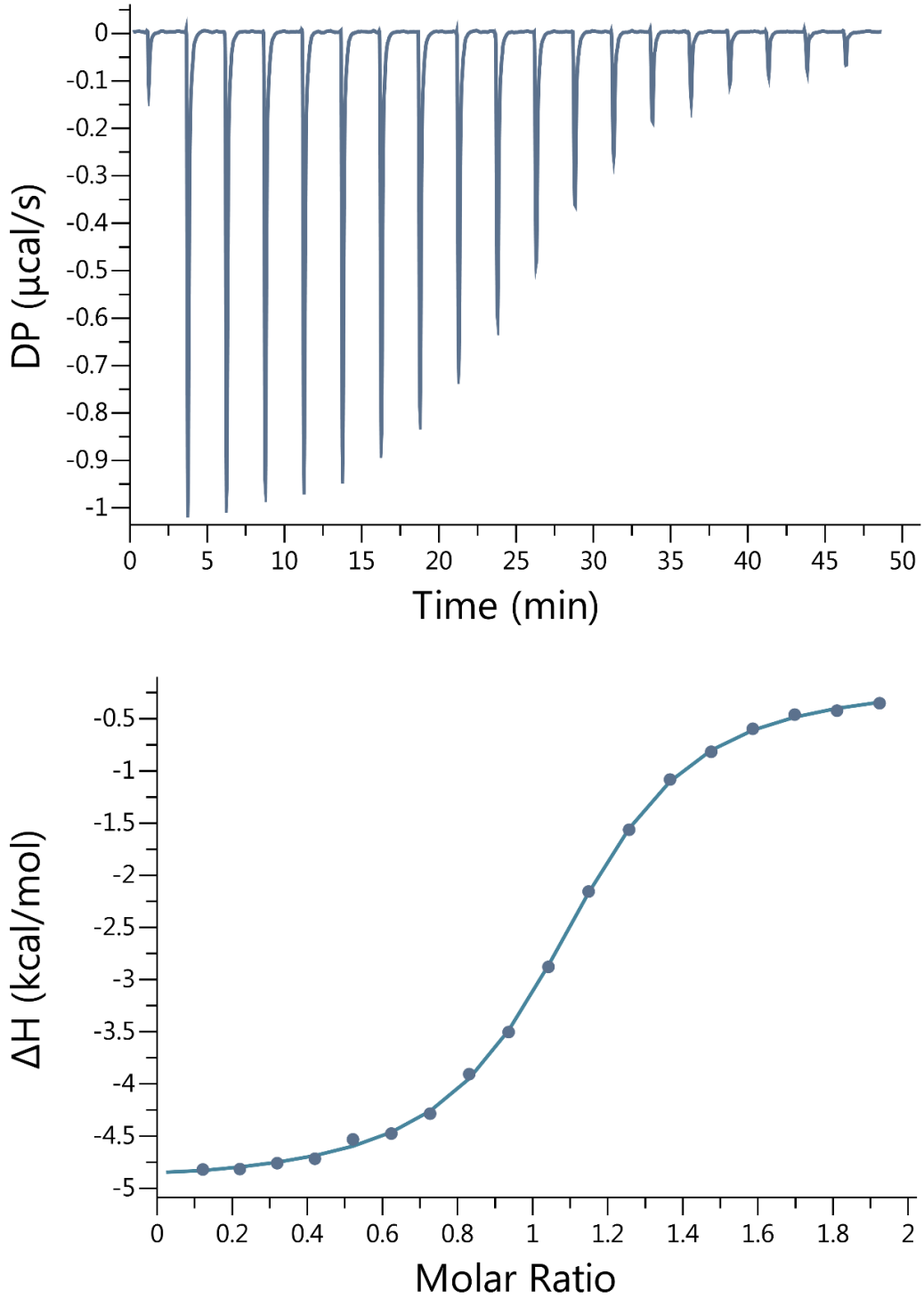

Figure III-S37. Isothermal Titration Calorimetry (ITC) curve obtained when a solution of **1** (100 µM) in the cell was titrated with **11** (1.00 mM) in the syringe at 298.0 K in 20 mM sodium phosphate buffered water at pH 7.4. $K_a = 3.57 \times 10^5$ M^{-1} and $\Delta H = -4.83 \pm 0.036$ kcal•mol^{-1}.

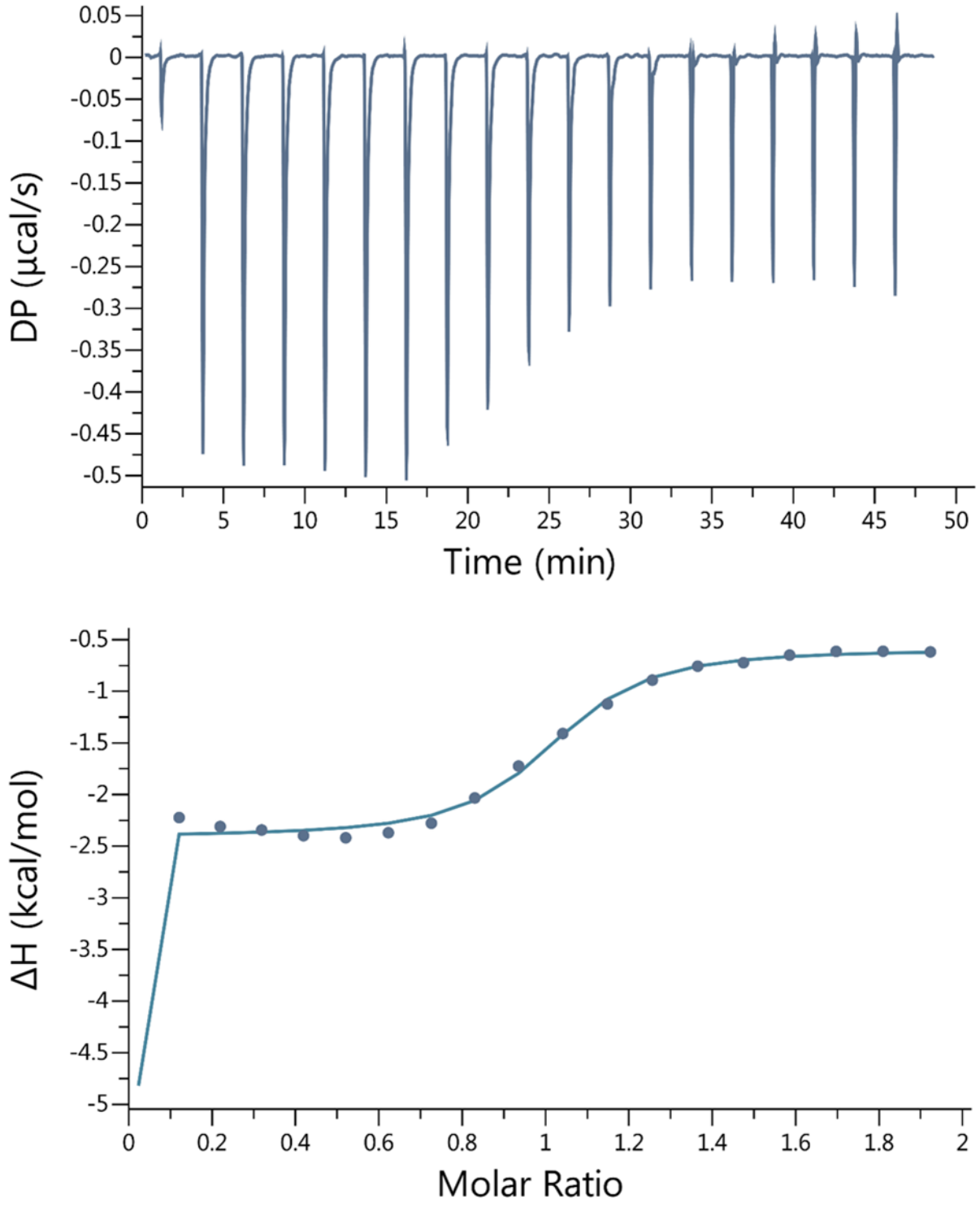

Figure III-S38. Isothermal Titration Calorimetry (ITC) curve obtained through competition binding studies. A solution of **1** (100 µM) and **5** (500 µM) in the cell was titrated with **12** (1.00 mM) in the syringe at 298.0 K in 20 mM sodium phosphate buffered water at pH 7.4. $K_a = 4.55 \times 10^8\ M^{-1}$ and $\Delta H = -10.4 \pm 0.064$ kcal•mol^{-1}.

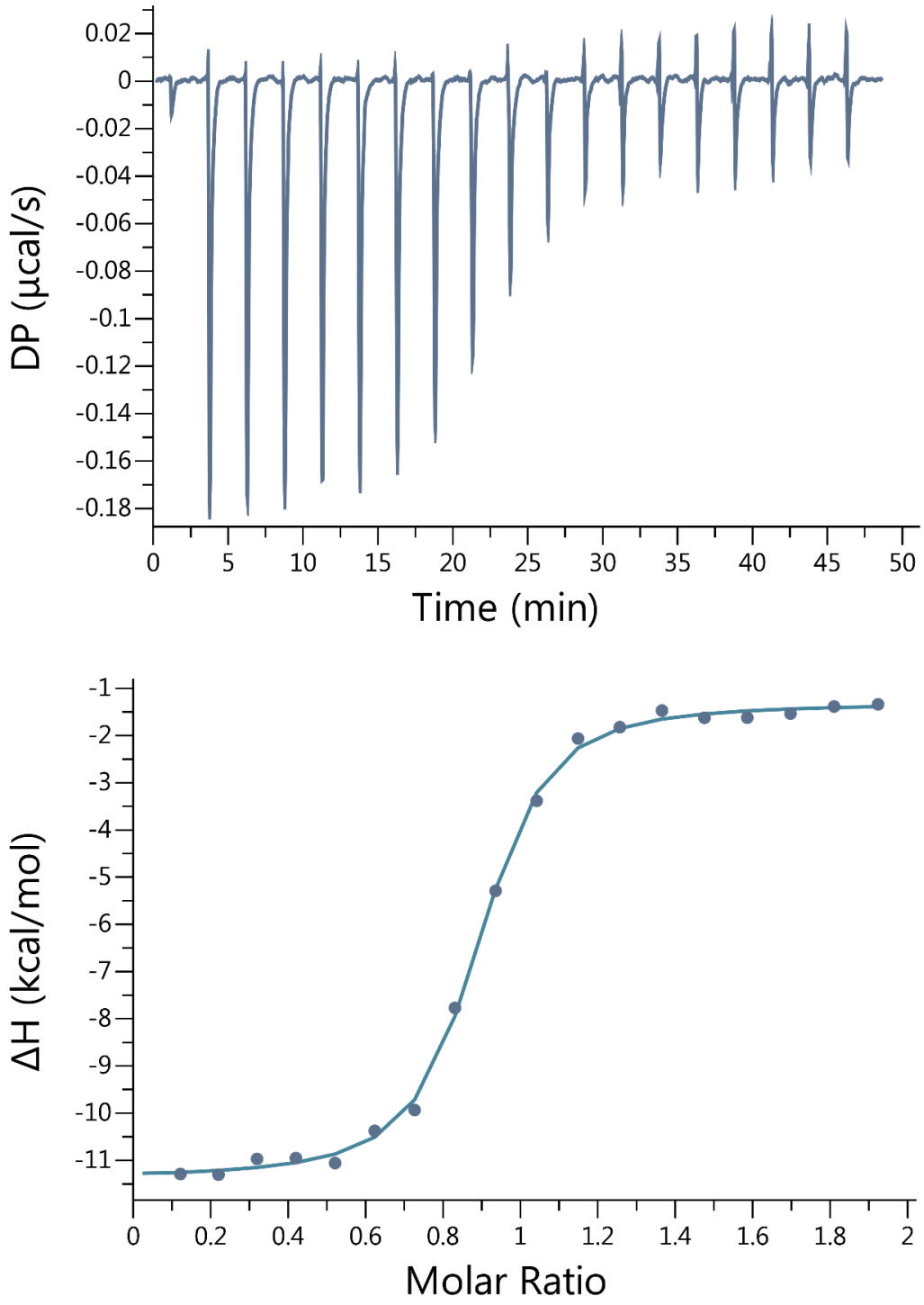

Figure III-S39. Isothermal Titration Calorimetry (ITC) curve obtained when a solution of **1** (10.0 µM) in the cell was titrated with **13** (100 µM) in the syringe at 298.0 K in 20 mM sodium phosphate buffered water at pH 7.4. $K_a = 1.13 \times 10^7\ M^{-1}$ and $\Delta H = -10.1 \pm 0.119$ kcal•mol^{-1}.

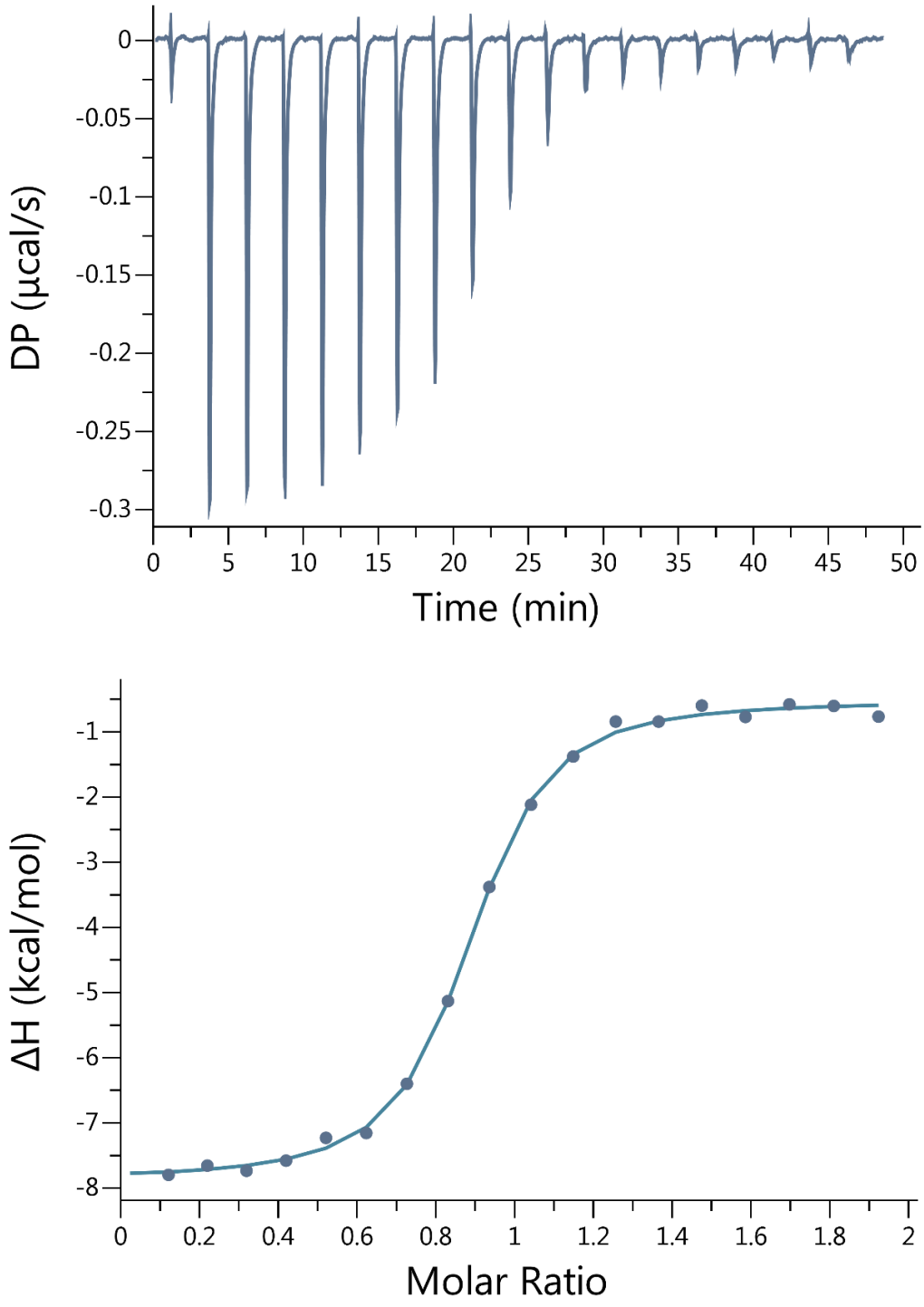

Figure III-S40. Isothermal Titration Calorimetry (ITC) curve obtained when a solution of **1** (20.0 µM) in the cell was titrated with **14** (200 µM) in the syringe at 298.0 K in 20 mM sodium phosphate buffered water at pH 7.4. $K_a = 4.08 \times 10^6\ M^{-1}$ and $\Delta H = -7.41 \pm 0.084$ kcal•mol^{-1}.

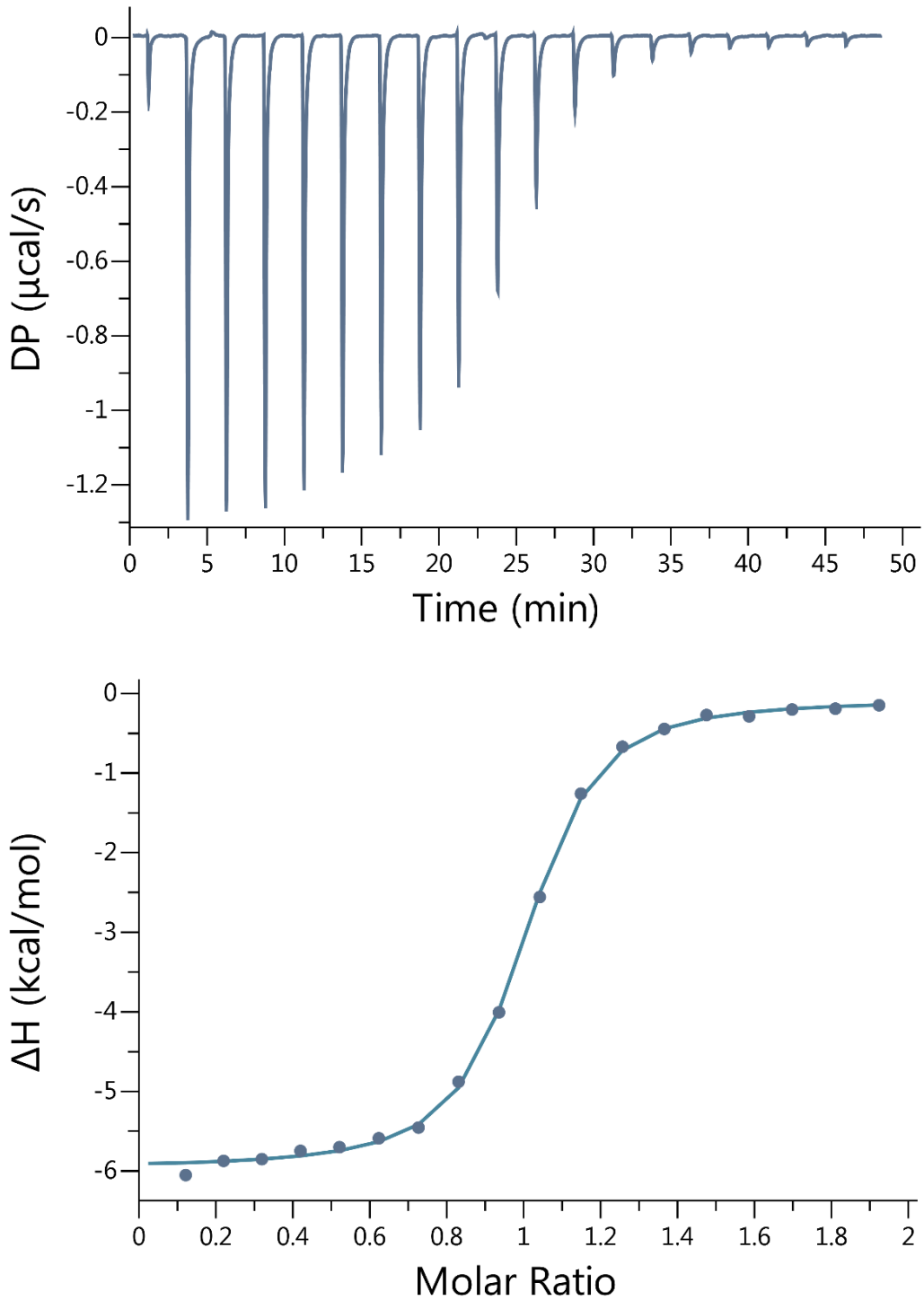

Figure III-S41. Isothermal Titration Calorimetry (ITC) curve obtained when a solution of **1** (100 µM) in the cell was titrated with **15** (1.00 mM) in the syringe at 298.0 K in 20 mM sodium phosphate buffered water at pH 7.4. $K_a = 1.11 \times 10^6\ M^{-1}$ and $\Delta H = -5.88 \pm 0.049$ kcal•mol^{-1}.

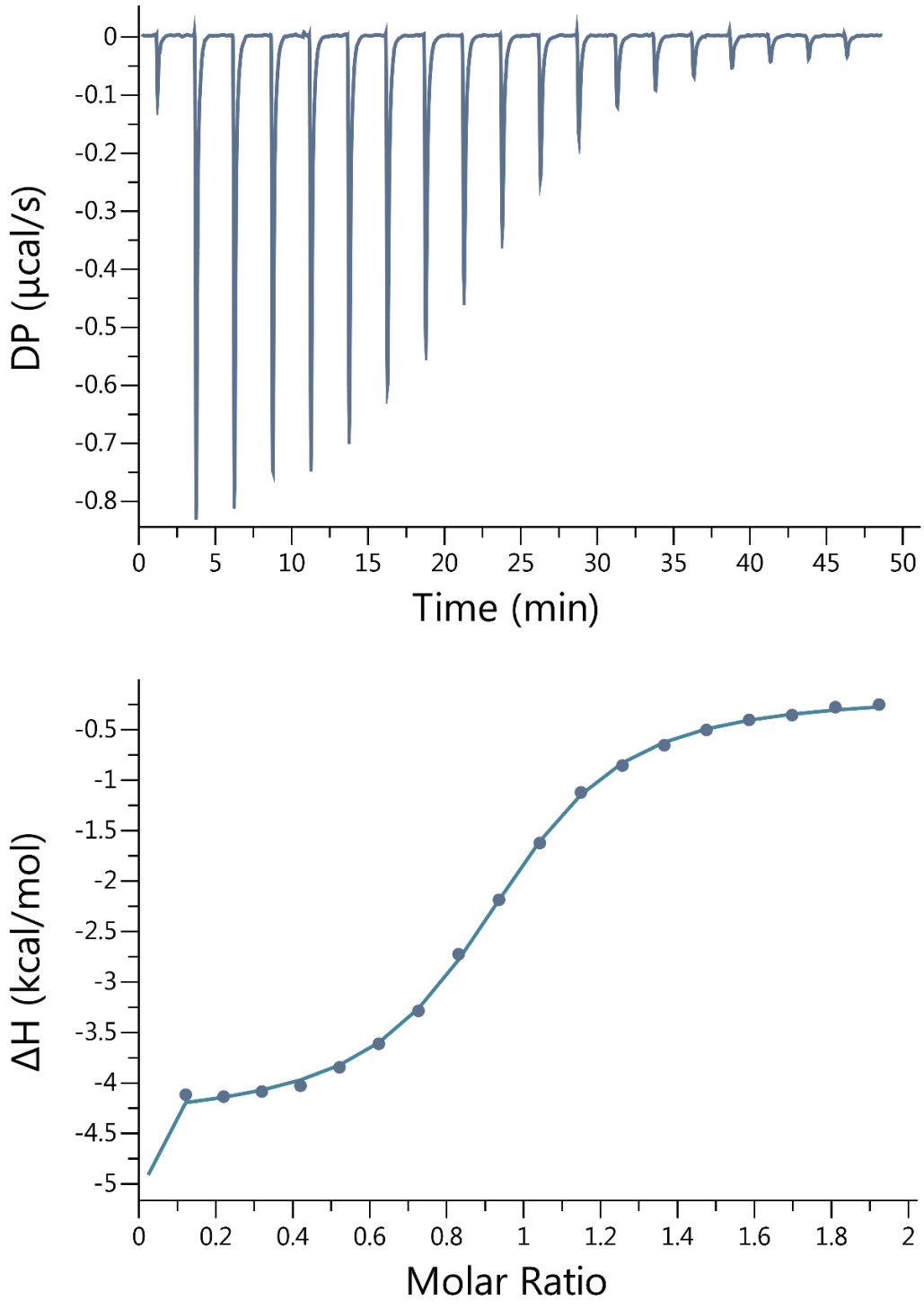

Figure III-S42. Isothermal Titration Calorimetry (ITC) curve obtained through competition binding studies. A solution of **1** (100 µM) and **19** (500 µM) in the cell was titrated with **16** (1.00 mM) in the syringe at 298.0 K in 20 mM sodium phosphate buffered water at pH 7.4. $K_a = 8.77 \times 10^6\ M^{-1}$ and $\Delta H = -10.5 \pm 0.044$ kcal•mol^{-1}.

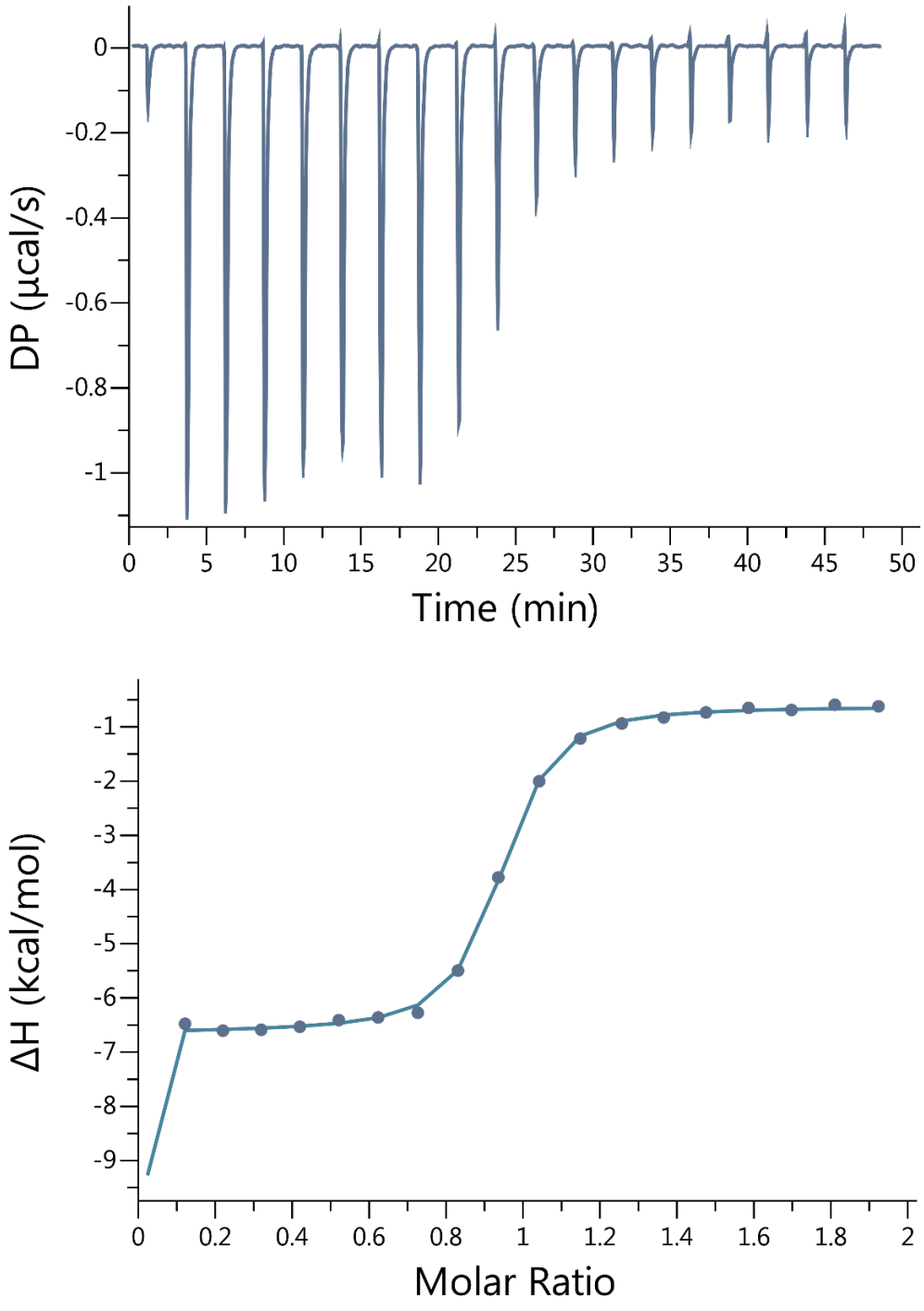

Figure III-S43. Isothermal Titration Calorimetry (ITC) curve obtained through competition binding studies. A solution of **1** (100 µM) and **19** (500 µM) in the cell was titrated with **17** (1.00 mM) in the syringe at 298.0 K in 20 mM sodium phosphate buffered water at pH 7.4. $K_a = 5.81 \times 10^7\ M^{-1}$ and $\Delta H = -12.4 \pm 0.045$ kcal•mol^{-1}.

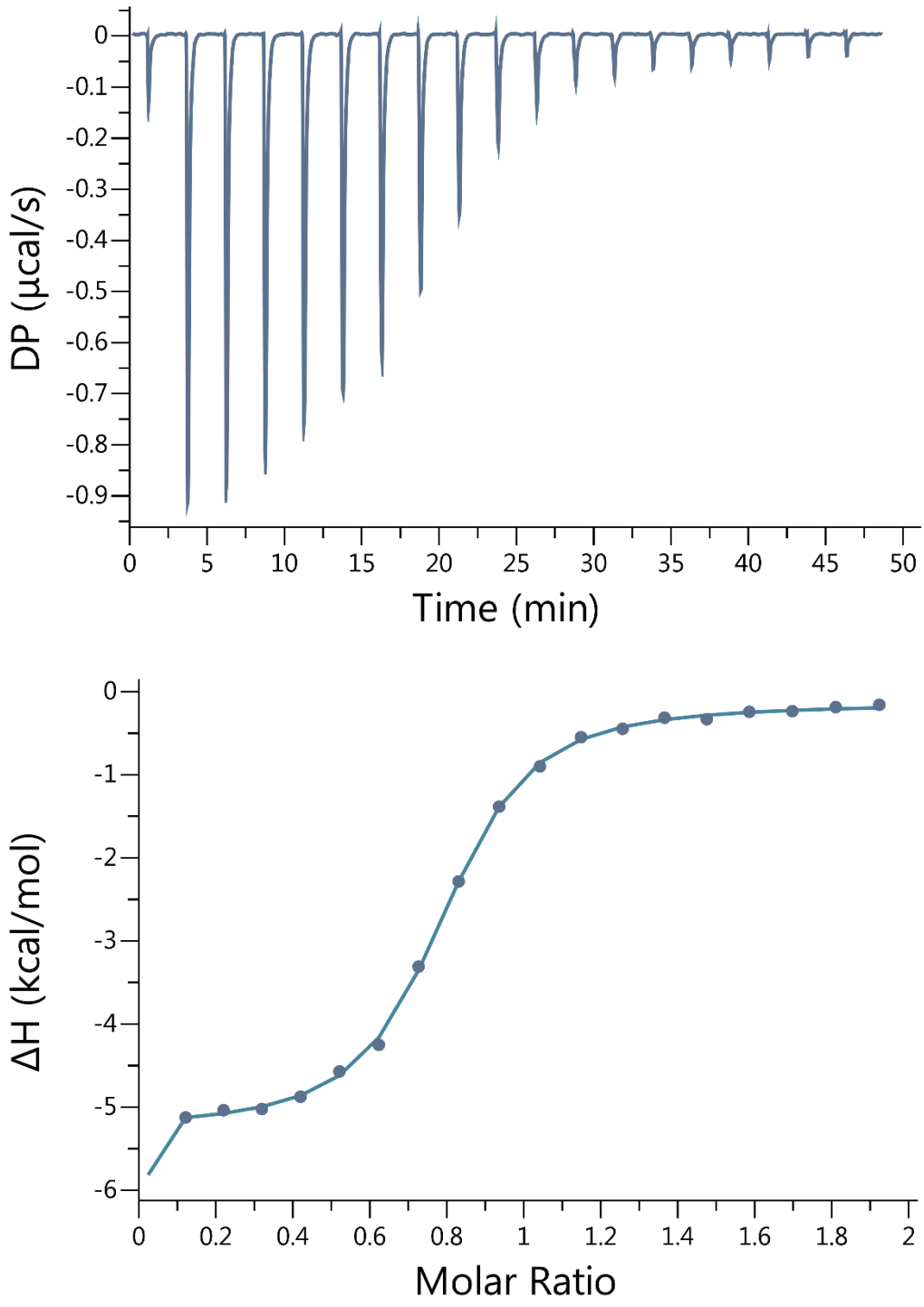

Figure III-S44. Isothermal Titration Calorimetry (ITC) curve obtained through competition binding studies. A solution of **1** (100 µM) and **5** (500 µM) in the cell was titrated with **18** (1.00 mM) in the syringe at 298.0 K in 20 mM sodium phosphate buffered water at pH 7.4. $K_a = 3.57 \times 10^8\ M^{-1}$ and $\Delta H = -13.7 \pm 0.039$ kcal•mol^{-1}.

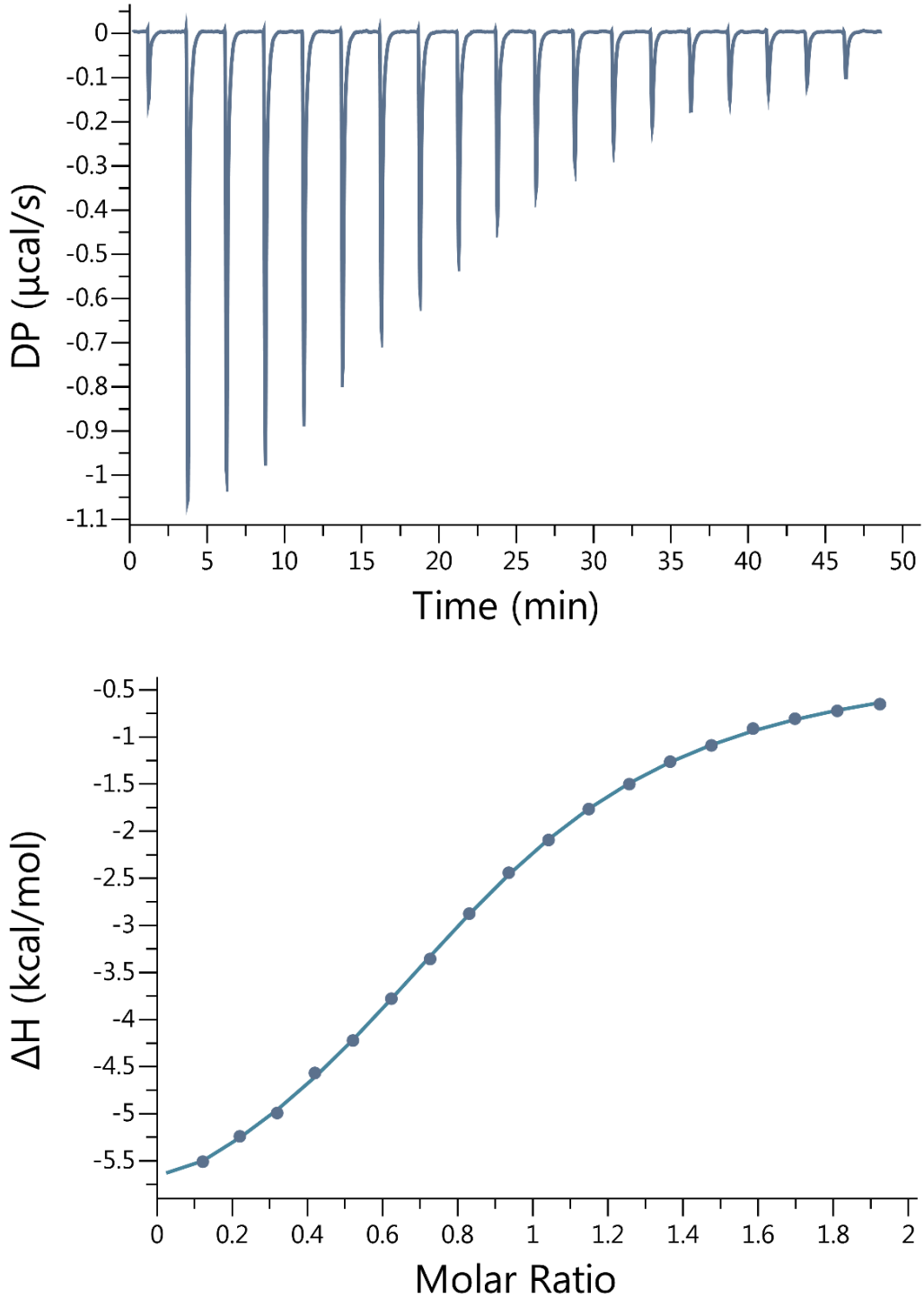

Figure III-S45. Isothermal Titration Calorimetry (ITC) curve obtained when a solution of **1** (100 µM) in the cell was titrated with **19** (1.00 mM) in the syringe at 298.0 K in 20 mM sodium phosphate buffered water at pH 7.4. $K_a = 5.95 \times 10^4\ M^{-1}$ and $\Delta H = -6.61 \pm 0.088$ kcal•mol^{-1}.

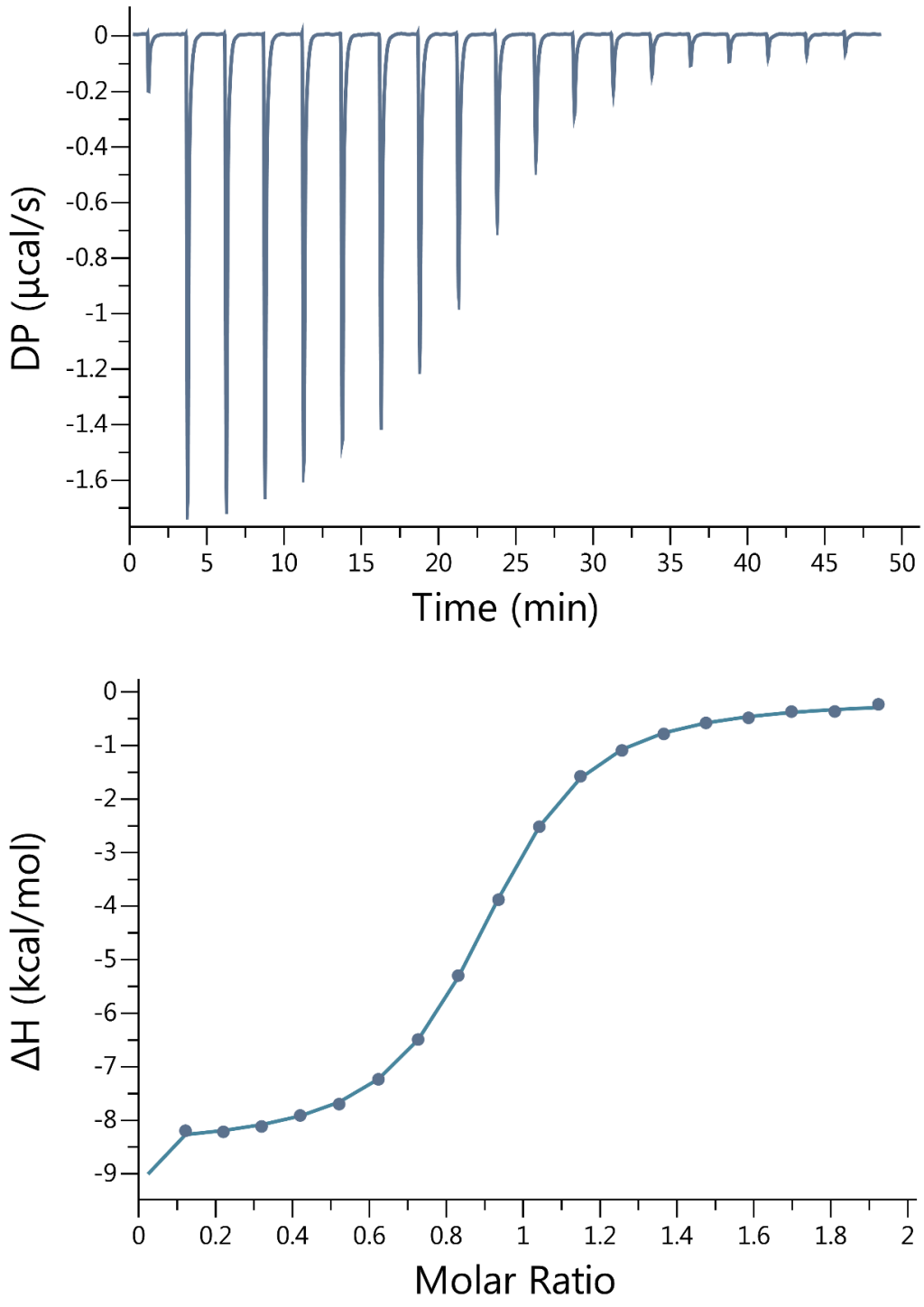

Figure III-S46. Isothermal Titration Calorimetry (ITC) curve obtained through competition binding studies. A solution of **1** (100 µM) and **19** (500 µM) in the cell was titrated with **20** (1.00 mM) in the syringe at 298.0 K in 20 mM sodium phosphate buffered water at pH 7.4. $K_a = 1.32 \times 10^7\ M^{-1}$ and $\Delta H = -14.7 \pm 0.036$ kcal•mol^{-1}.

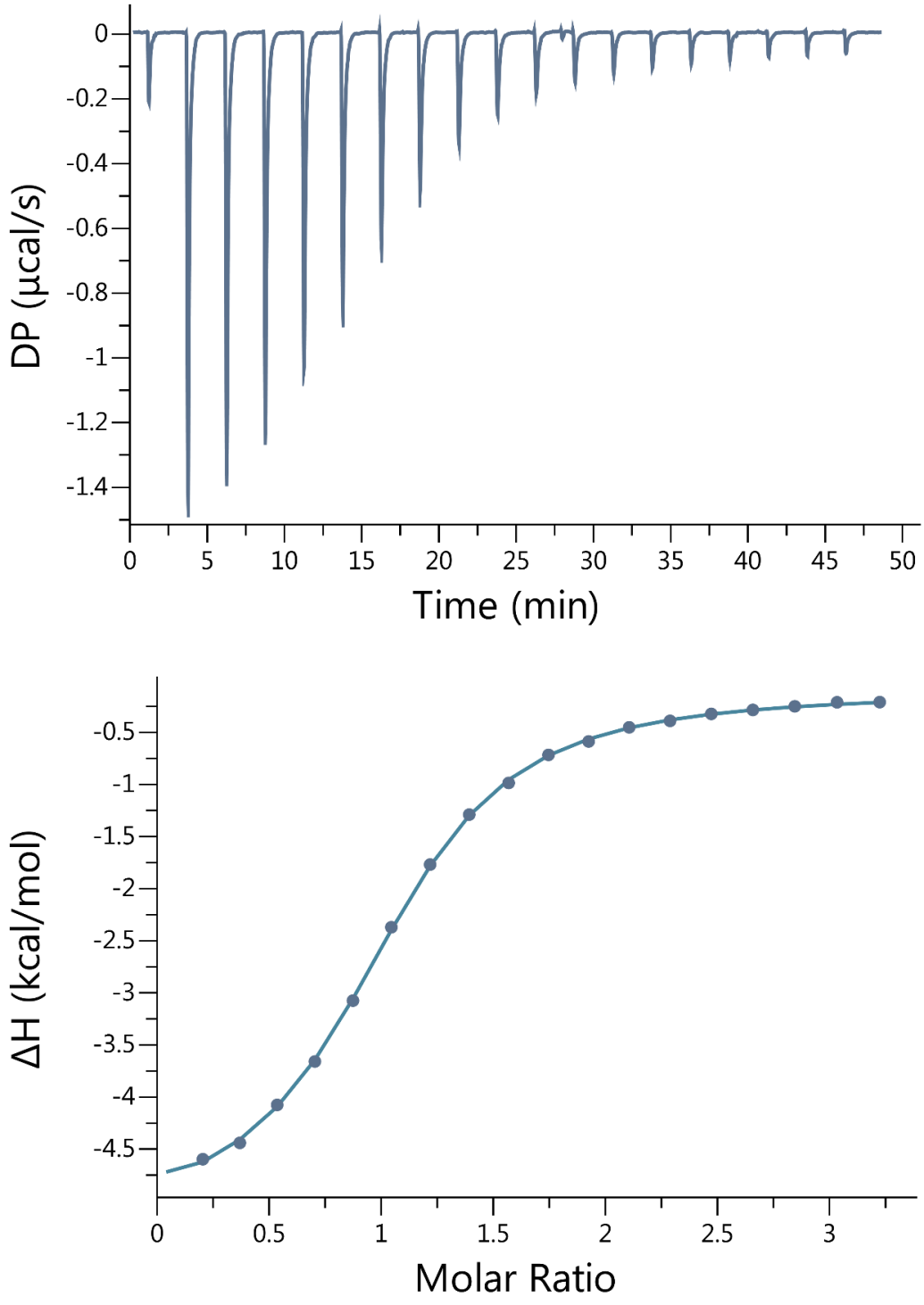

Figure III-S47. Isothermal Titration Calorimetry (ITC) curve obtained when a solution of **1** (100 µM) in the cell was titrated with **21** (1.00 mM) in the syringe at 298.0 K in 20 mM sodium phosphate buffered water at pH 7.4. $K_a = 9.80 \times 10^4$ M^{-1} and $\Delta H = -5.09 \pm 0.042$ kcal•mol^{-1}

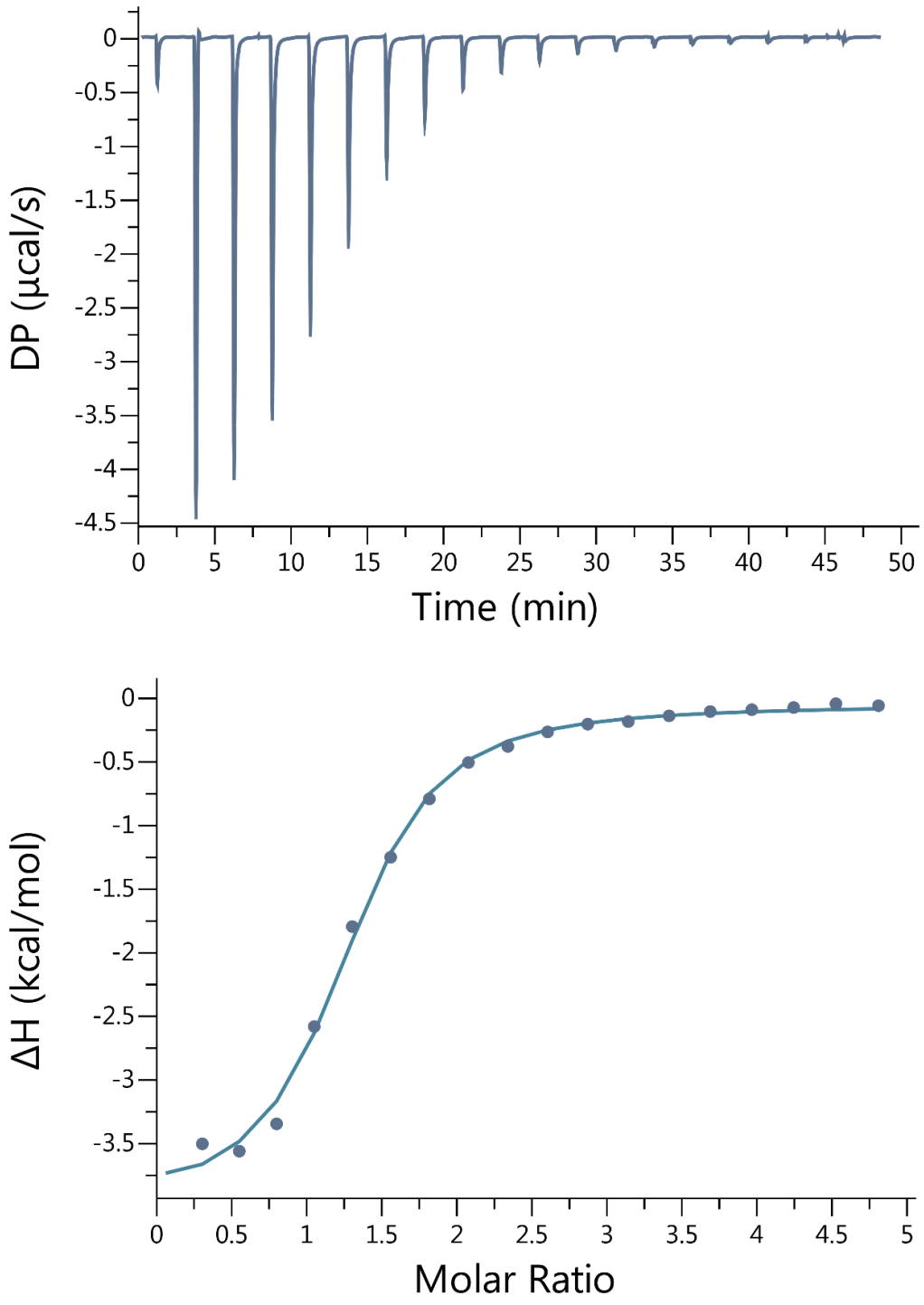

Figure III-S48. Isothermal Titration Calorimetry (ITC) curve obtained when a solution of **1** (200 µM) in the cell was titrated with **22** (5.00 mM) in the syringe at 298.0 K in 20 mM sodium phosphate buffered water at pH 7.4. $K_a = 5.61 \times 10^4\ M^{-1}$ and $\Delta H = -3.98 \pm 0.094$ kcal•mol^{-1}.

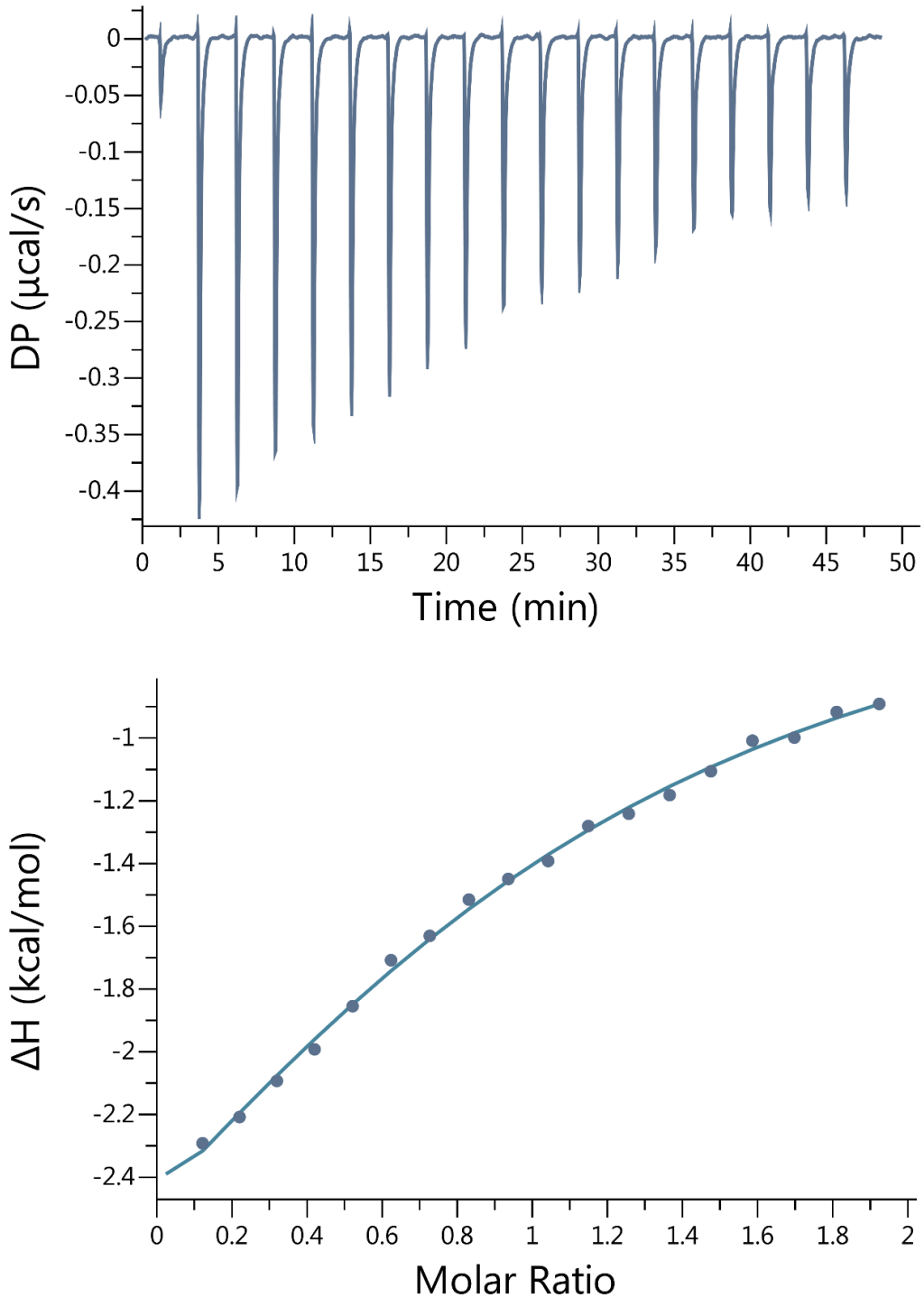

Figure III-S49. Isothermal Titration Calorimetry (ITC) curve obtained when a solution of **1** (100 µM) in the cell was titrated with **23** (1.00 mM) in the syringe at 298.0 K in 20 mM sodium phosphate buffered water at pH 7.4. $K_a = 8.47 \times 10^3\ M^{-1}$ and $\Delta H = -4.95 \pm 2.30$ kcal•mol^{-1}.

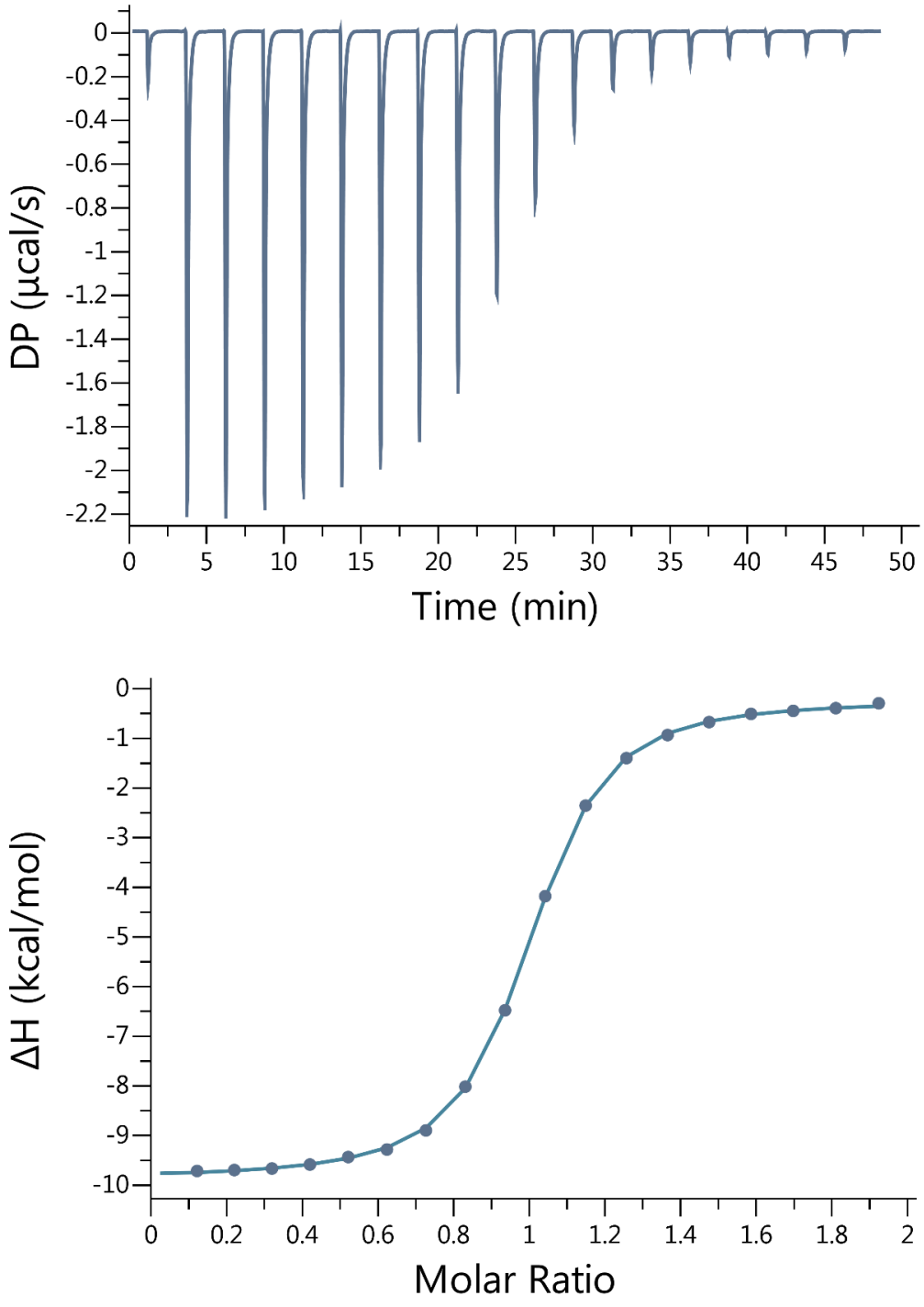

Figure III-S50. Isothermal Titration Calorimetry (ITC) curve obtained when a solution of **1** (100 µM) in the cell was titrated with **24** (1.00 mM) in the syringe at 298.0 K in 20 mM sodium phosphate buffered water at pH 7.4. $K_a = 9.43 \times 10^5\ M^{-1}$ and $\Delta H = -9.63 \pm 0.025$ kcal•mol^{-1}.

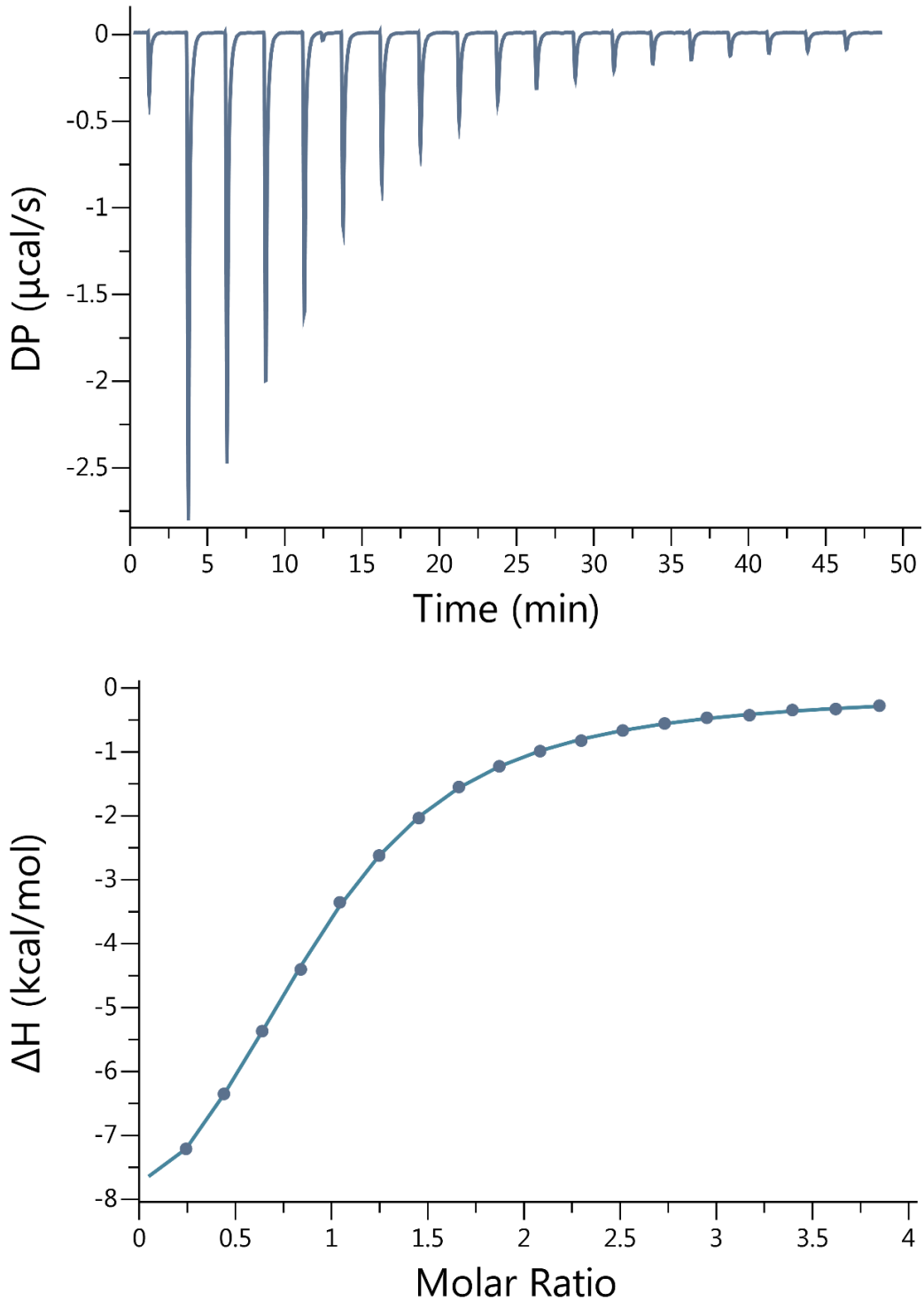

Figure III-S51. Isothermal Titration Calorimetry (ITC) curve obtained when a solution of **1** (100 µM) in the cell was titrated with **25** (2.00 mM) in the syringe at 298.0 K in 20 mM sodium phosphate buffered water at pH 7.4. $K_a = 3.70 \times 10^4\ M^{-1}$ and $\Delta H = -9.99 \pm 0.129$ kcal•mol^{-1}.

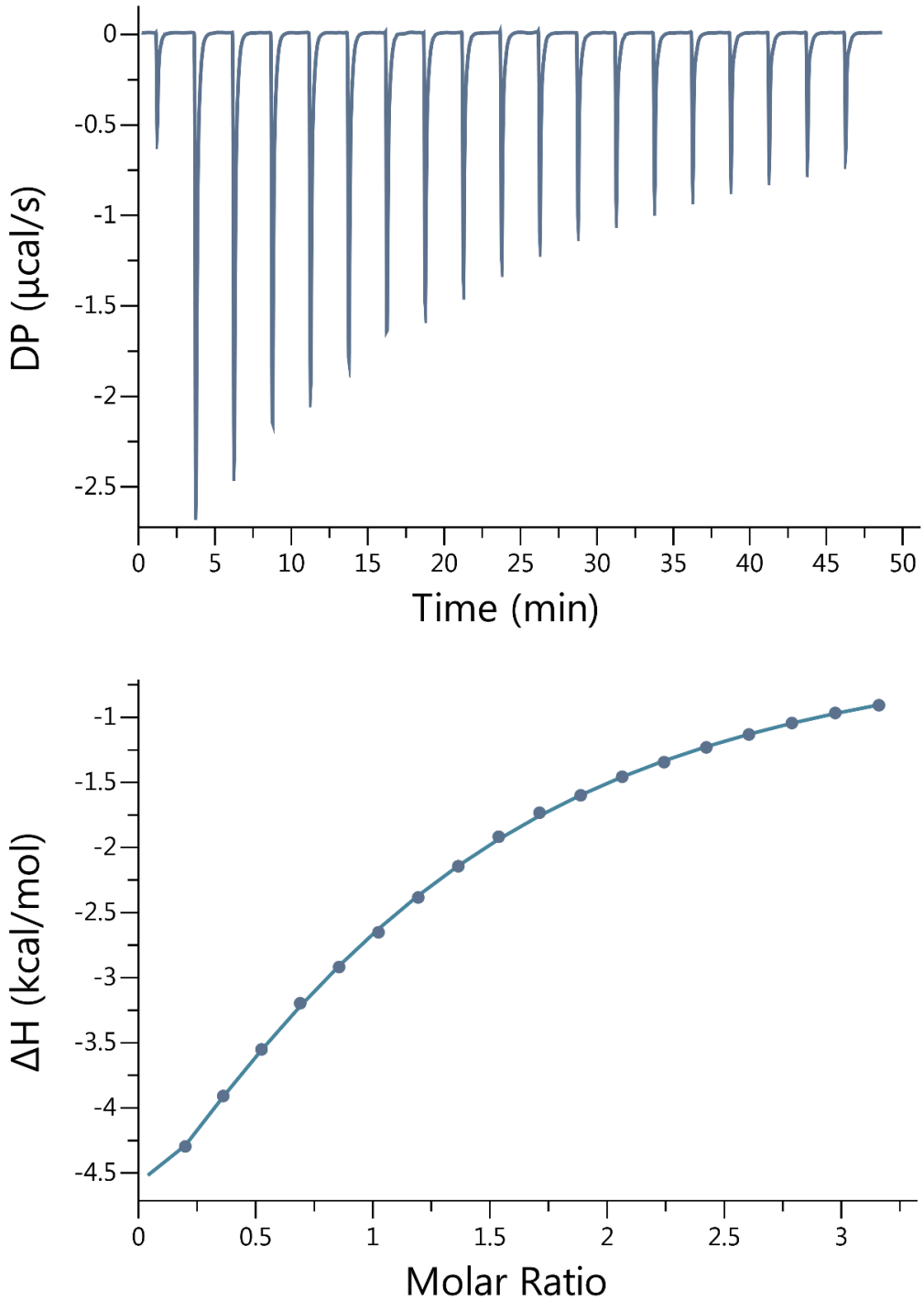

Figure III-S52. Isothermal Titration Calorimetry (ITC) curve obtained when a solution of **1** (200 µM) in the cell was titrated with **26** (2.40 mM) in the syringe at 298.0 K in 20 mM sodium phosphate buffered water at pH 7.4. $K_a = 4.67 \times 10^3\ M^{-1}$ and $\Delta H = -8.92 \pm 0.445\ kcal \bullet mol^{-1}$.

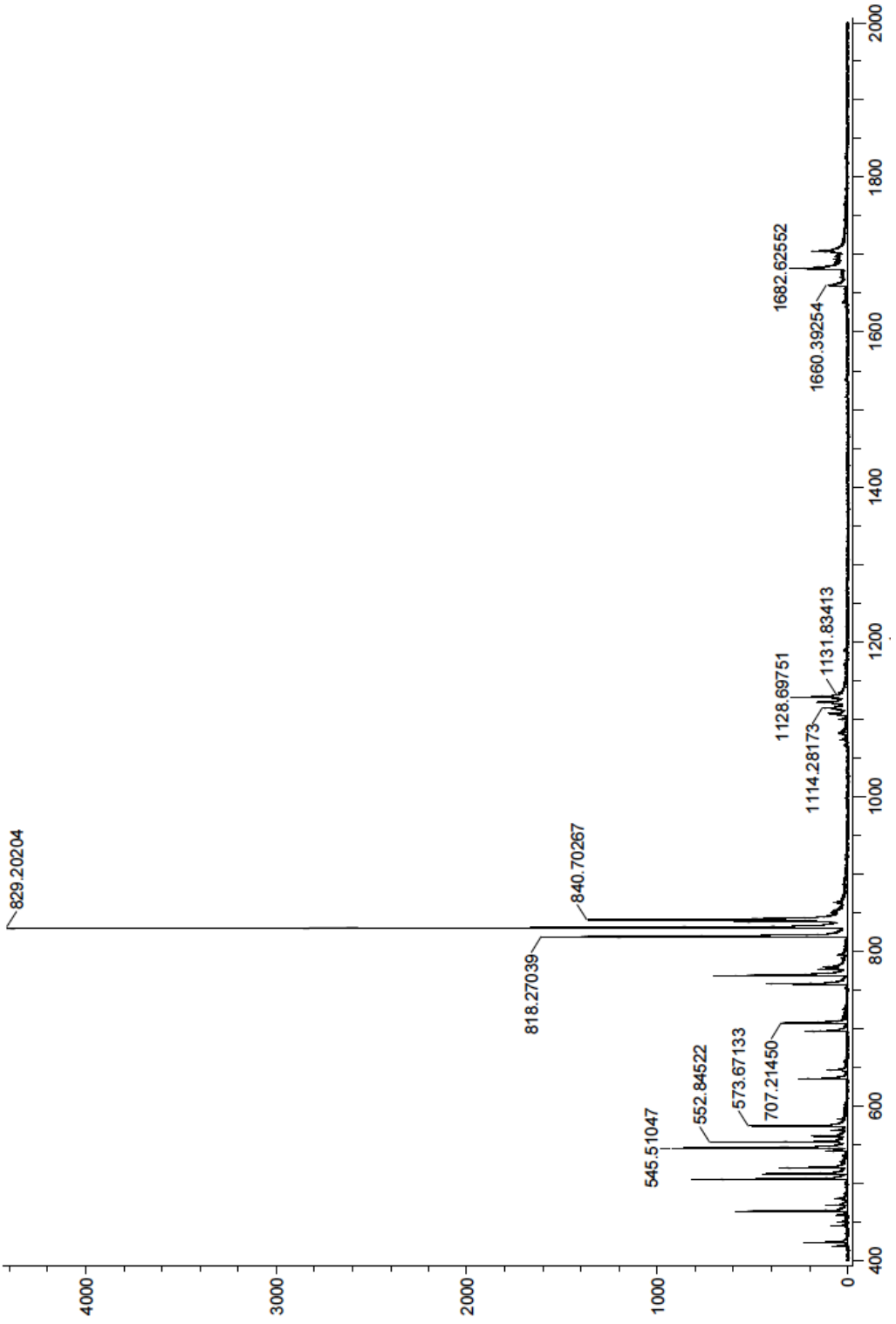

Figure III-S53. Electrospray mass spectrum for **1** recorded in the negative ion mode. The peak at 829.20204 corresponds to the $[M + 1H - 3Na]^{2-}$ ion.

Appendix III

Acyclic Cucurbit[n]uril-Type Receptors: Optimization of Electrostatic Interactions for Dicationic Guests

*By Xiaoyong Lu, Sandra A. Zebaze Ndendjio, Peter Y. Zavalij, Lyle Isaacs**

Department of Chemistry and Biochemistry, University of Maryland, College Park, College Park, MD 20742, USA

Supporting Information

Table of Contents **Pages**

General experimental

All chemicals and reagents were purchased from commercial suppliers and were used without further purification. Compound **2** was prepared as described previously.[1] NMR spectra were measured at 400, 500 or 600 MHz for ^{1}H and 100 and 125 MHz for ^{13}C. The solvent for NMR experiments was deuterated water (D_2O), deuterated chloroform ($CDCl_3$), or deuterated dimethyl sulfoxide (DMSO-d_6). Chemical shifts (δ) are referenced relative to the residual resonances for HOD (4.80 ppm), $CHCl_3$ (7.26 ppm for ^{1}H, 77.16 ppm for ^{13}C), DMSO-d_6 (2.50 ppm for ^{1}H, 39.51 ppm for ^{13}C). Isothermal titration calorimetry was performed using a MicroCal PEAQ-ITC Isothermal Titration Calorimeter using 20 mM phosphate buffered water at pH = 7.4 at 298 K. Mass spectrometry was performed using a JEOL AccuTOF electrospray instrument. Melting points were measured by a Meltemp apparatus in open capillary tubes and are uncorrected. IR spectra were measured on a Thermo Nicolet NEXUS 670 FT/IR spectrometer by attenuated total reflectance (ATR) and are reported in cm^{-1}.

1. Ma, D.; Hettiarachchi, G.; Nguyen, D.; Zhang, B.; Wittenberg, J. B.; Zavalij, P. Y.; Briken, V.; Isaacs, L. *Nature Chemistry* **2012**, *4*, 503-510.

Synthesis and characterization of compounds 4 and 1.

Container 4. To a mixture of glycoluril tetramer bisether **2** (17 g, 22.1 mmol) and hydroquinone (9.7 g, 88.2 mmol) was added trifluoroacetic acid (300 mL). The resulting heterogeneous mixture was stirred under N_2 at 25 °C for 16 hours. The reaction mixture was then poured into MeOH (600 mL) and stirred for 1 hour. The crude product was collected by filtration and subsequently washed with MeOH (400 mL), acetone (300 mL) and water (400 mL) to remove the unreacted hydroquinone. The residue was dried under the high vacuum to yield **2** as a pale-yellow solid (20.8 g, yield 99%). M.p. > 300 °C, IR (ATR, cm^{-1}): 3400w, 1713s, 1460s, 1226s, 1082m, 971w, 797s. ^{1}H NMR (DMSO-d_6, 600 MHz): δ 8.60 (s, 4H), 6.55 (s, 4H), 5.56 (d, J = 14.5 Hz, 2H), 5.49 (d, J = 15.1 Hz, 4H), 5.38 (d, J = 8.9 Hz, 2H), 5.27 (d, J = 8.9 Hz, 2H), 5.18 (d, J = 15.7 Hz, 4H), 4.09 – 4.04 (m, 10H), 1.68 (s, 6H), 1.62 (s, 6H). ^{13}C NMR (DMSO-d_6, 125 MHz): δ 155.3, 154.2, 147.0, 126.1, 116.7, 77.4, 76.4, 70.7, 70.3, 48.1, 35.0, 17.1, 15.8 ppm (13 out of the 14 expected resonances were observed). HR-MS (ESI, positive, *para*-xylenediammonium dichloride as guest): *m*/*z* 551.22446 ([M + guest- $2Cl^-$]$^{2+}$), $C_{50}H_{58}N_{18}O_{12}^{2+}$ calcd. for 551.22408.

Container 1. To a mixture of compound **2** (0.80 g, 0.83 mmol) and pyridine sulfur trioxide complex (2.6 g, 16.3 mmol) was added dry pyridine (25 mL). The resulting mixture was stirred at 90 °C under N_2 for 18 hours. The reaction mixture was cooled to RT. The product precipitated out of the solution and was collected by filtration. The solid was slurried in water (1 mL), and the pH was adjusted to 8.4 by slow addition of saturated aqueous $NaHCO_3$. After addition of EtOH (70 mL), the crude product was collected by centrifugation 7000 rpm × 7 min. The precipitate was suspended in ethanol (50 mL × 2), sonicated for 30 minutes, and solid collected by centrifugation. The crude solid was analyzed by NMR and process was repeated until the trapped pyridine was fully removed. Then the pH of the crude solution was adjusted to 7.0 by slow addition of 1 M HCl and the solvent was evaporated. The crude solid was treated with 30 mL of a mixture of CH_3CN/ H_2O (2: 1) and the heterogeneous mixture was centrifuged, the supernatant was collected and then evaporated to give a crude solid. The crude solid was redissolved in minimum amount of water and purified by size exclusion chromatography using Sephadex® G25 resin (30mm x 200mm) and eluted by water. Pure product was collected as the front fractions with violet fluorescent color under UV long wavelength (366 nm). After drying under high vacuum, the compound **1** was obtained as a light-yellow solid (0.50 g, 60% yield). M.p. > 300 °C, IR (ATR, cm^{-1}): 1720m, 1468s, 1228s, 1048s, 970m, 798s. ^{1}H NMR (D_2O, 500 MHz): δ 7.53 (s, 4H), 6.66 (d, J = 15.4 Hz, 2H), 5.57 (d, J = 15.8 Hz, 4H), 5.46 (d, J = 8.9 Hz, 2H), 5.41 (d, J = 8.9 Hz, 2H), 5.28 (d, J = 16.5 Hz, 4H), 4.41 (d, J = 16.5 Hz, 4H), 4.29 (d, J = 15.8 Hz, 4H), 4.16 (d, J = 15.4 Hz, 2H), 1.84 (s, 6H), 1.82 (s, 6H). ^{13}C NMR (D_2O, 125 MHz, dioxane as external reference): δ 156.5, 155.9, 146.0, 131.9, 123.0, 78.3, 77.3, 71.1, 70.9, 52.5, 48.1, 35.8, 15.6, 14.6 ppm (14 out of the 14 expected resonances were observed). HR-MS (ESI, positive, **6d** as guest): *m*/*z* 787.1679 ([M + **6d**-$2Cl^-$]$^{2+}$), $C_{54}H_{70}N_{18}O_{24}Na_4^{2+}$ calcd. for 787.1642.

^{1}H NMR spectra of compound 1 and 2

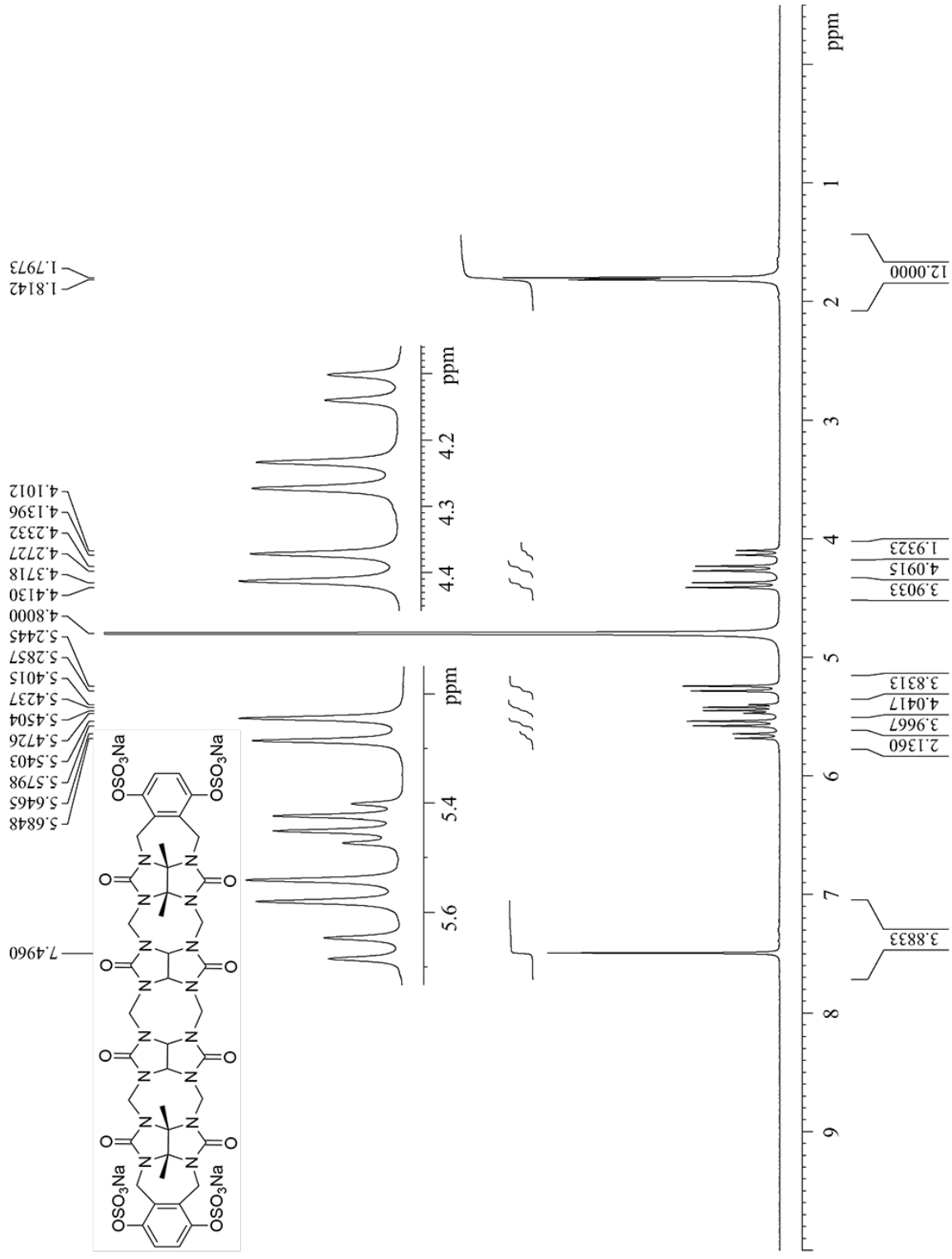

Figure IV-S1. ^{1}H NMR spectra (600 MHz, D_2O, RT) recorded for compound **1.**

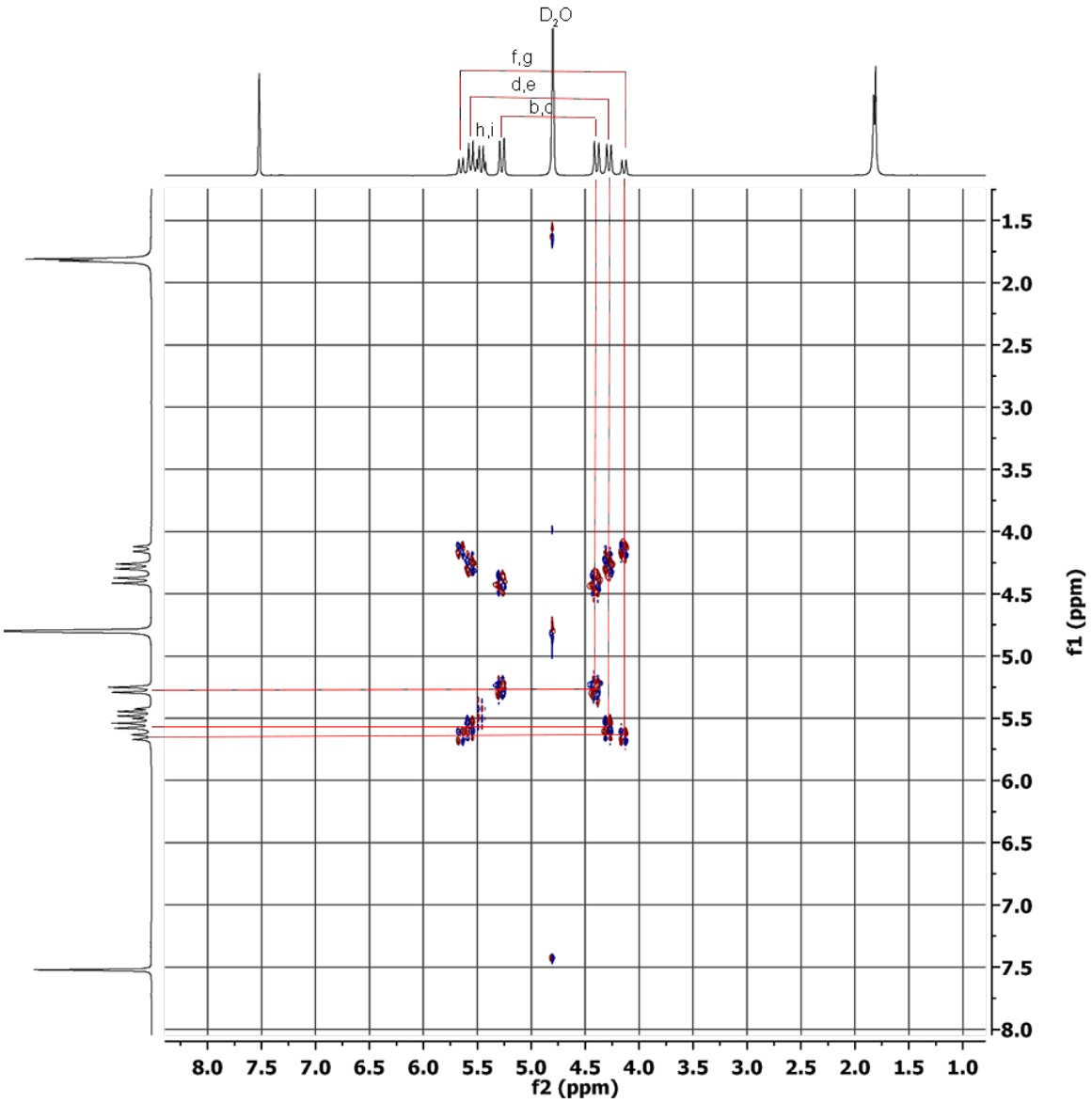

Figure IV-S2. ^{1}H, ^{1}H DQCOSY NMR spectra (600 MHz, D_2O, RT) recorded for compound **1.**

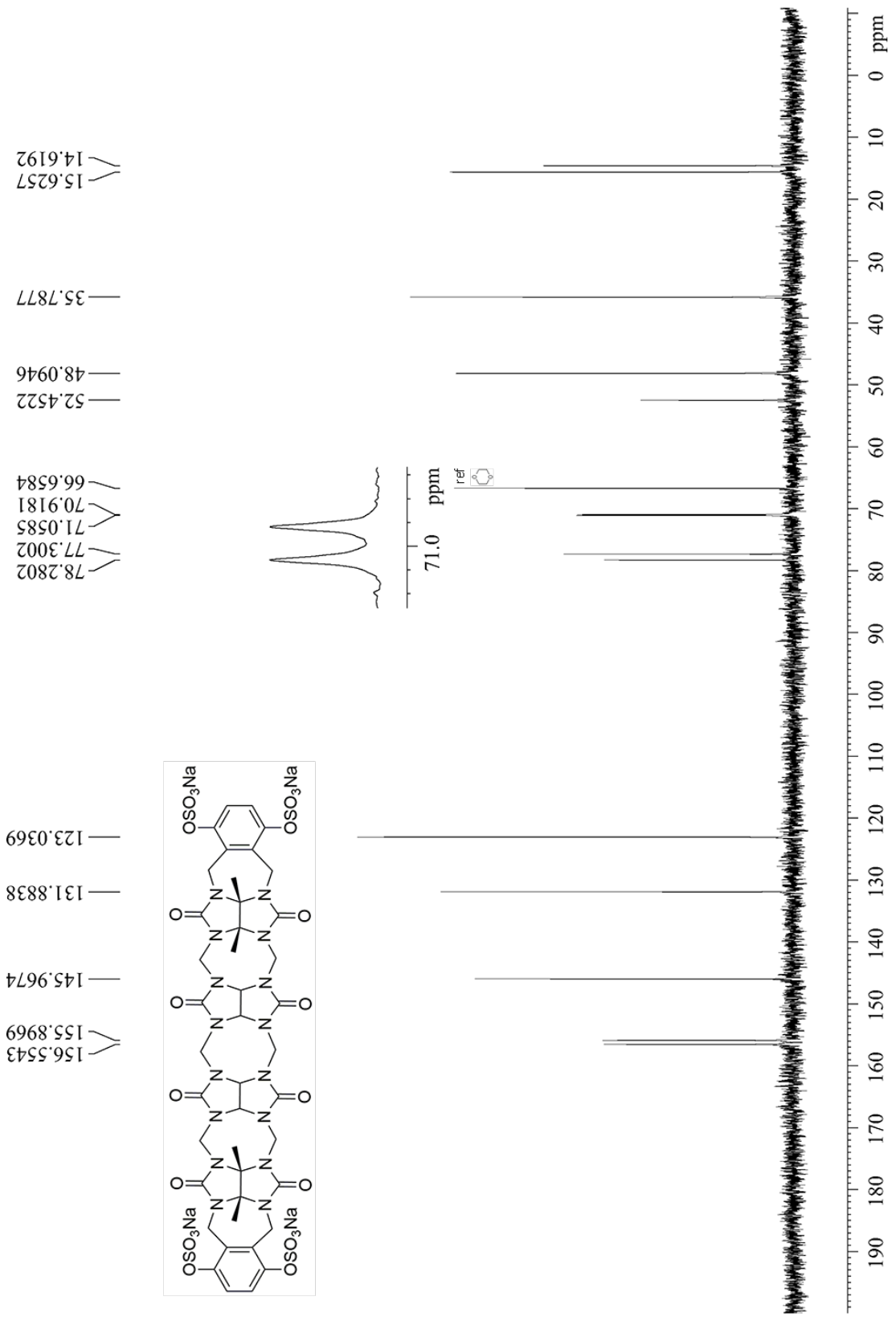

Figure IV-S3. ^{13}C NMR spectra (600 MHz, D_2O, RT) recorded for compound **1.**

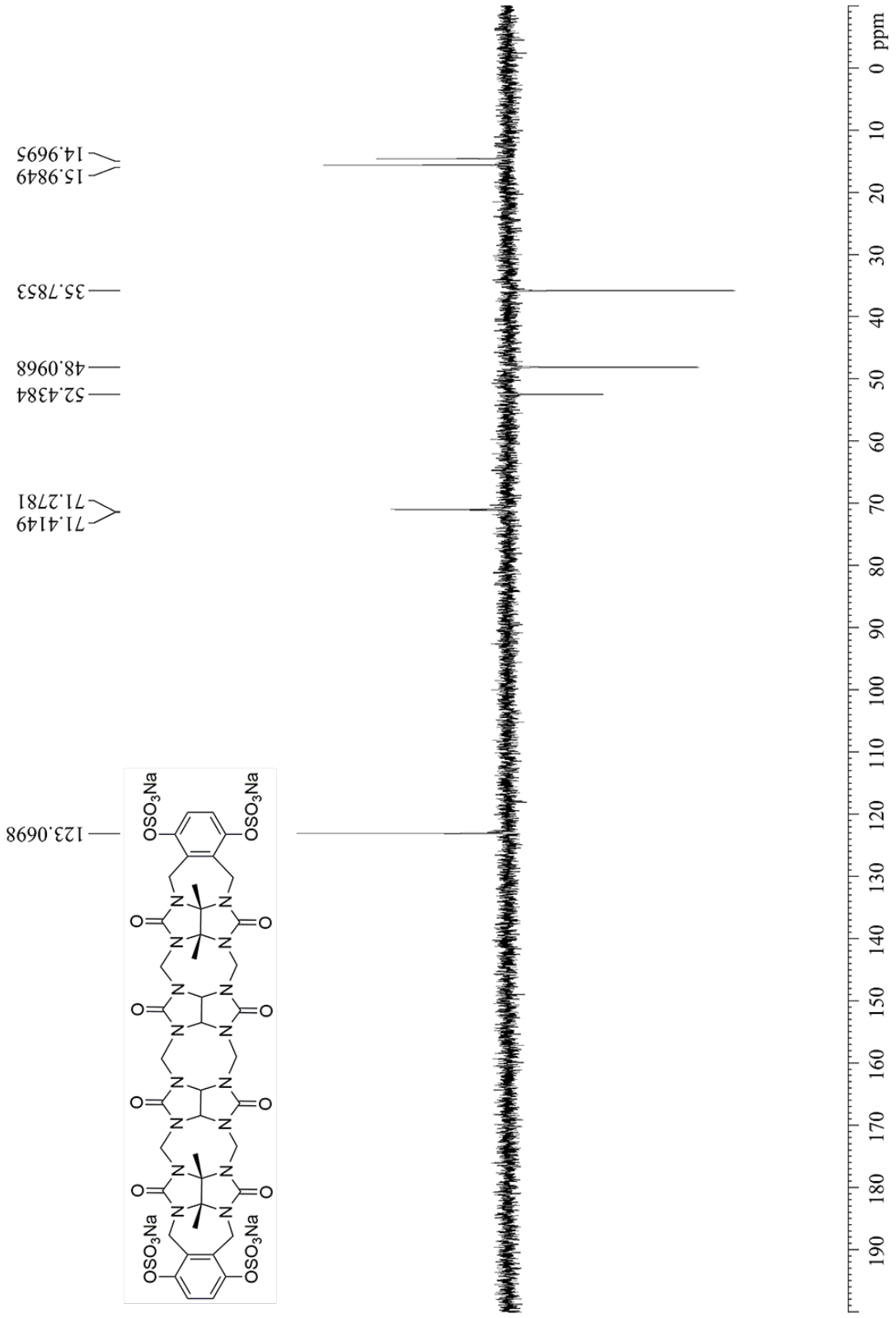

Figure IV-S4. ^{13}C DEPT135 NMR spectra (600 MHz, D_2O, RT) recorded for compound **1.**

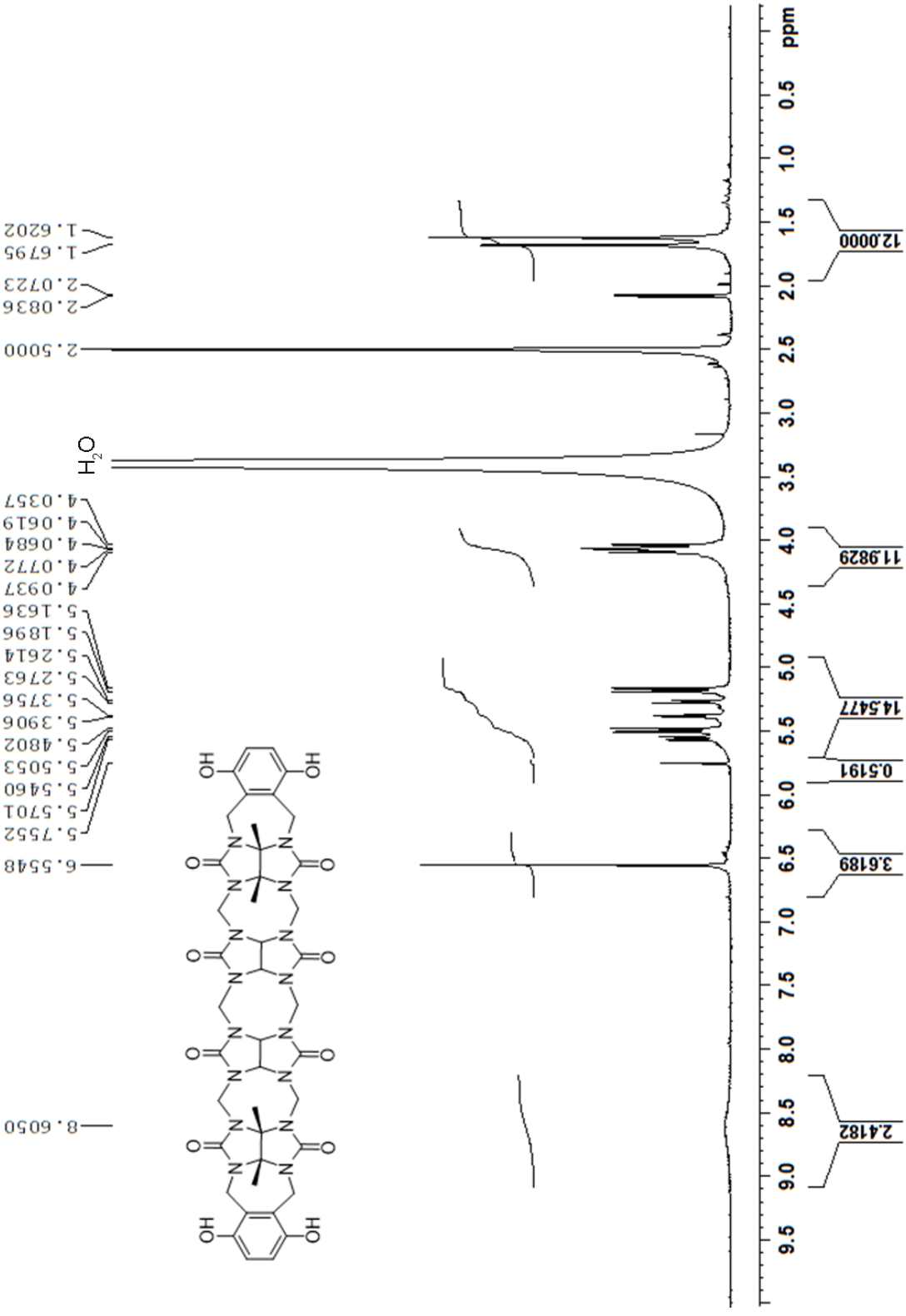

Figure IV-S5. ^{1}H NMR spectra (600 MHz, DMSO-d_6, RT) recorded for compound **2.**

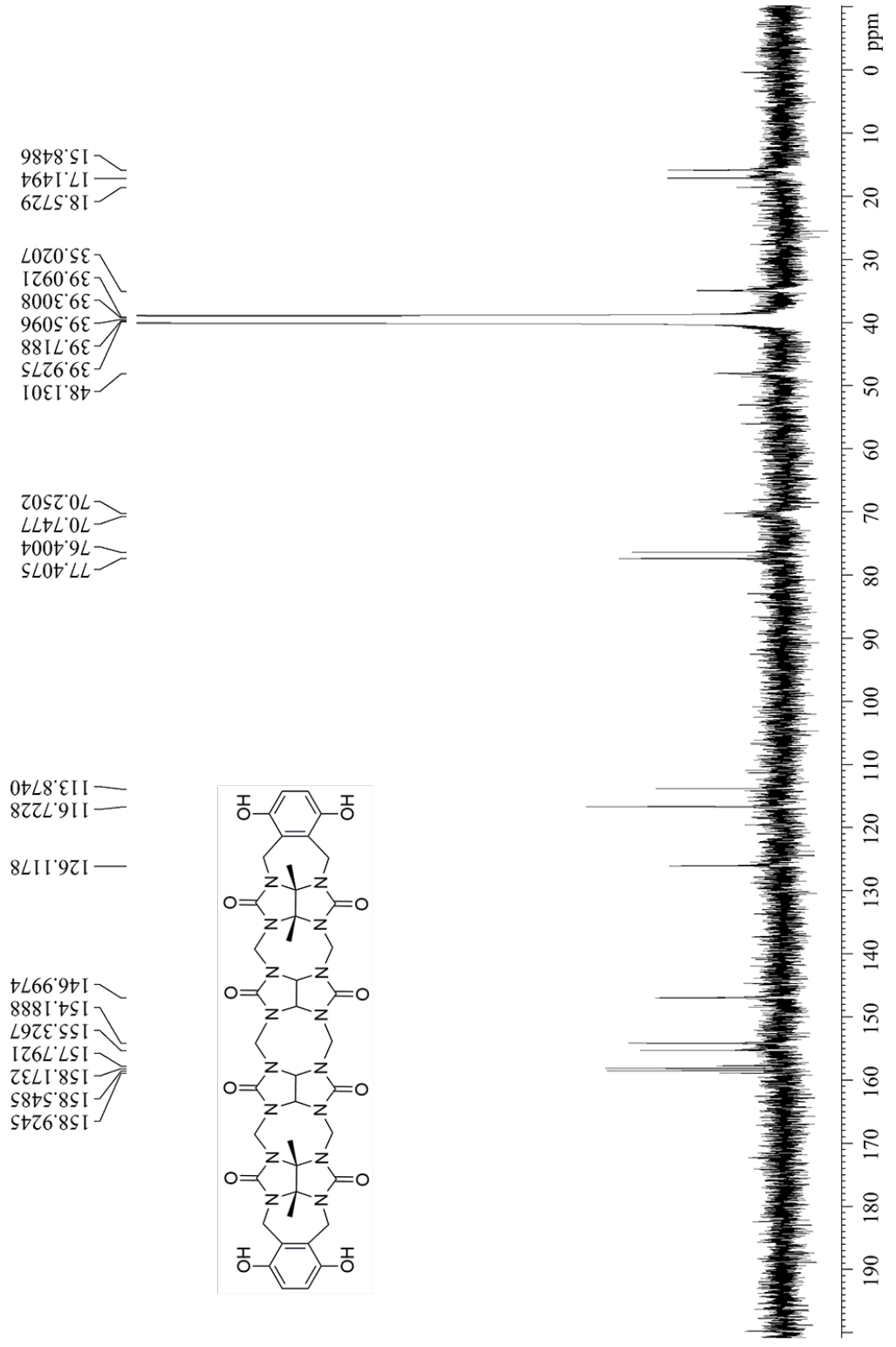

Figure IV-S6. ^{13}C NMR spectra (125 MHz, DMSO-d_6, RT) recorded for compound **2.**

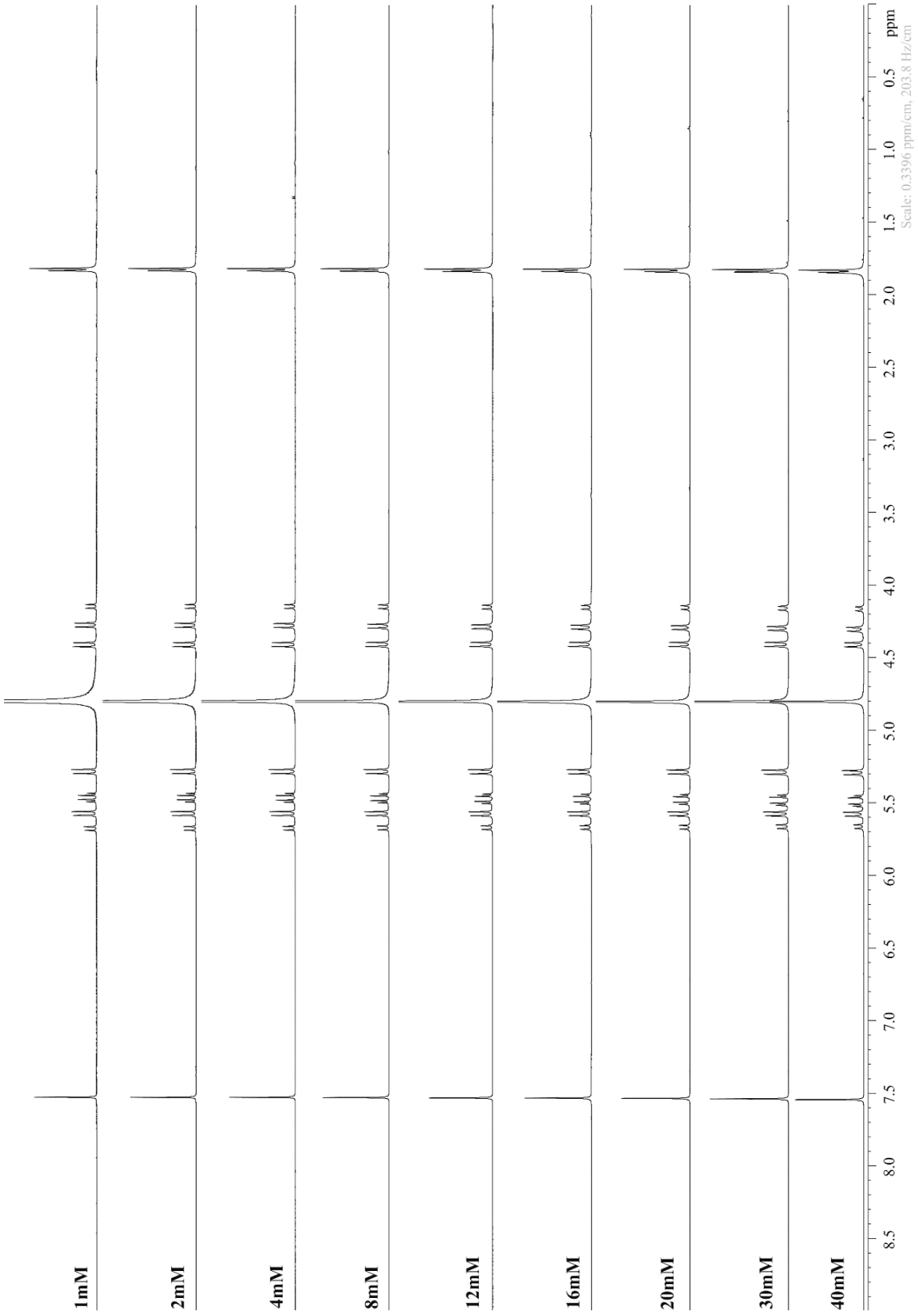

Figure IV-S7. ^{1}H NMR spectra (600 MHz, D_2O, RT) recorded for **1** as a function of concentration.

^{1}H NMR spectra of selected guests with host 1

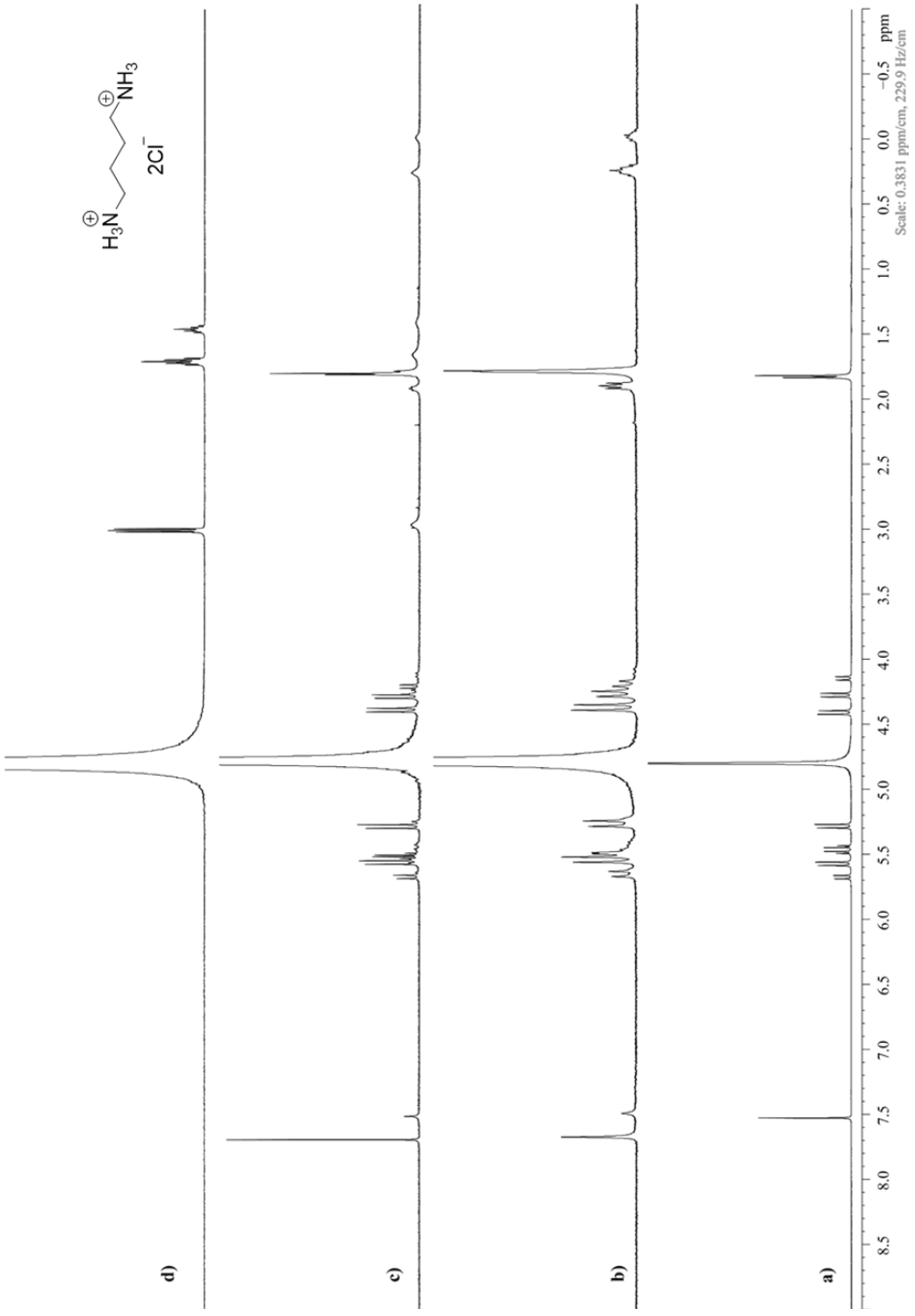

Figure IV-S8. ^{1}H NMR spectra (600 MHz, D_2O, RT) recorded for a) host **1** (1.0 mM), b) host **1** (1.0 mM) and guest **5a** (1.0 mM), c) host **1** (1.0 mM) and guest **5a** (2.0 mM), d) guest **5a** (1.0 mM).

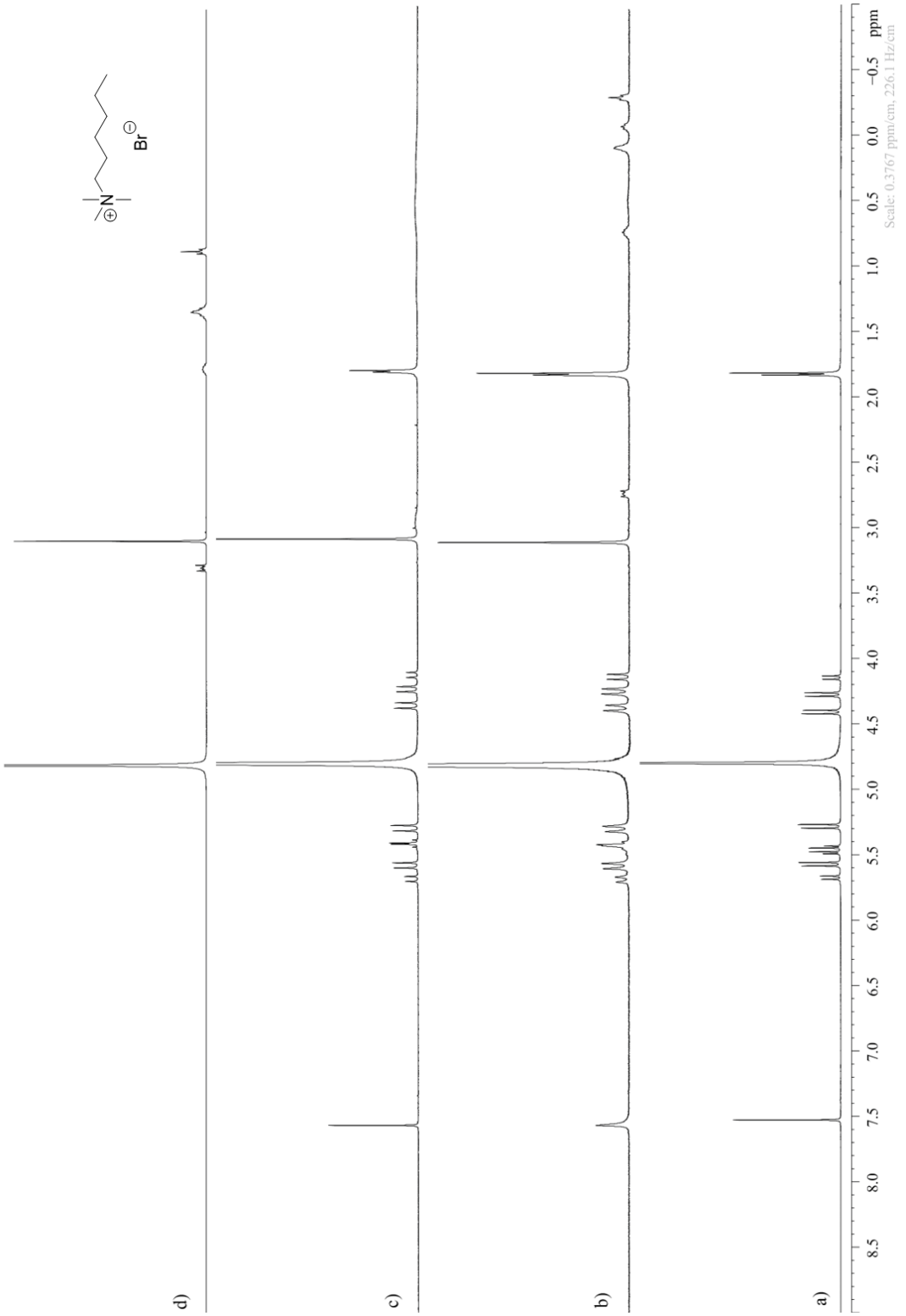

Figure IV-S9. ^{1}H NMR spectra (600 MHz, D_2O, RT) recorded for a) host **1** (1.0 mM), b) host **1** (1.0 mM) and guest **6Q** (1.0 mM), c) host **1** (1.0 mM) and guest **6Q** (2.0 mM), d) guest **6Q** (1.0 mM).

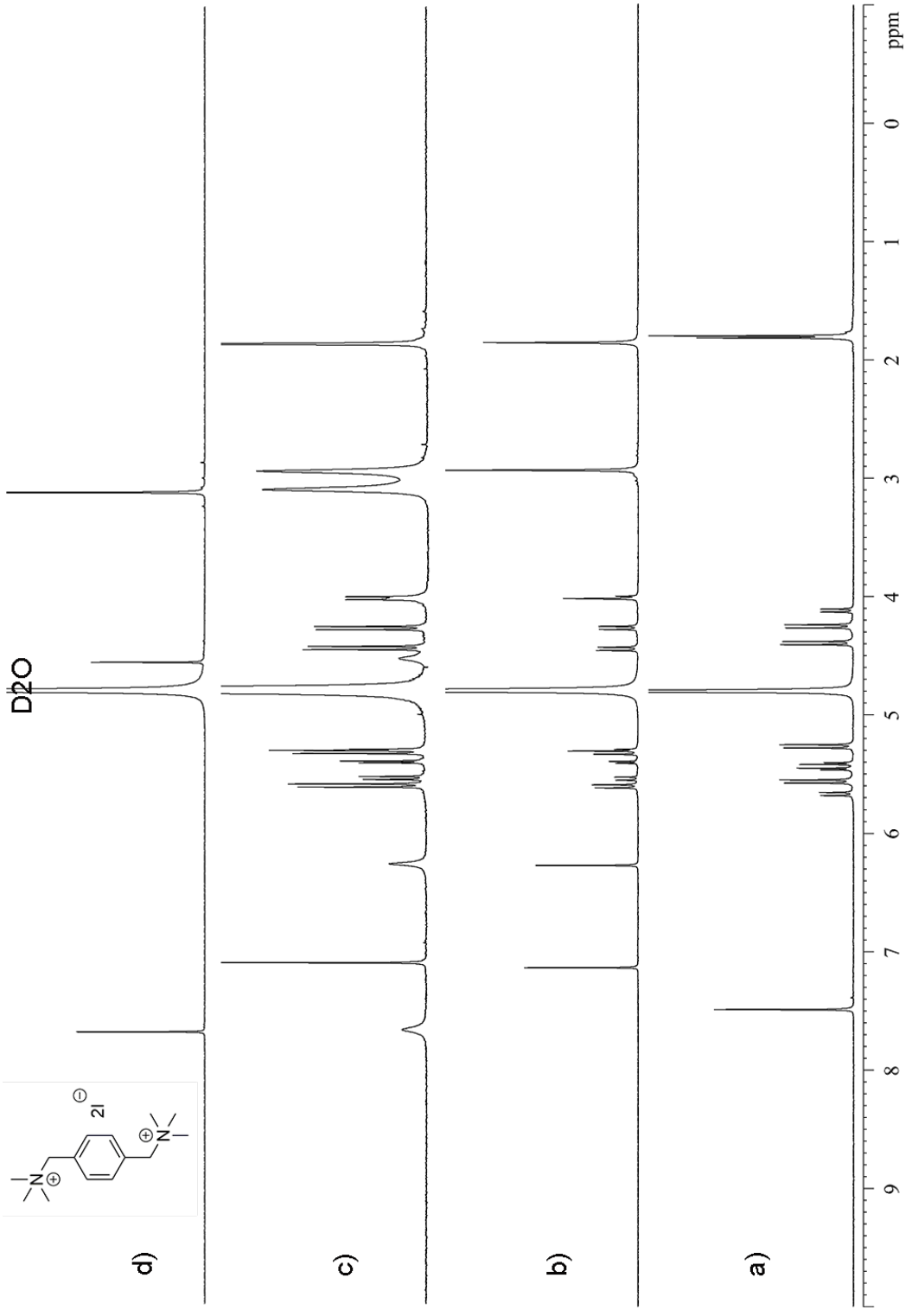

Figure IV-S10. ^{1}H NMR spectra (600 MHz, D_2O, RT) recorded for a) host **1** (1.0 mM), b) host **1** (1.0 mM) and guest **11d** (1.0 mM), c) host **1** (1.0 mM) and guest **11d** (2.0 mM), d) guest **11d** (1.0 mM)

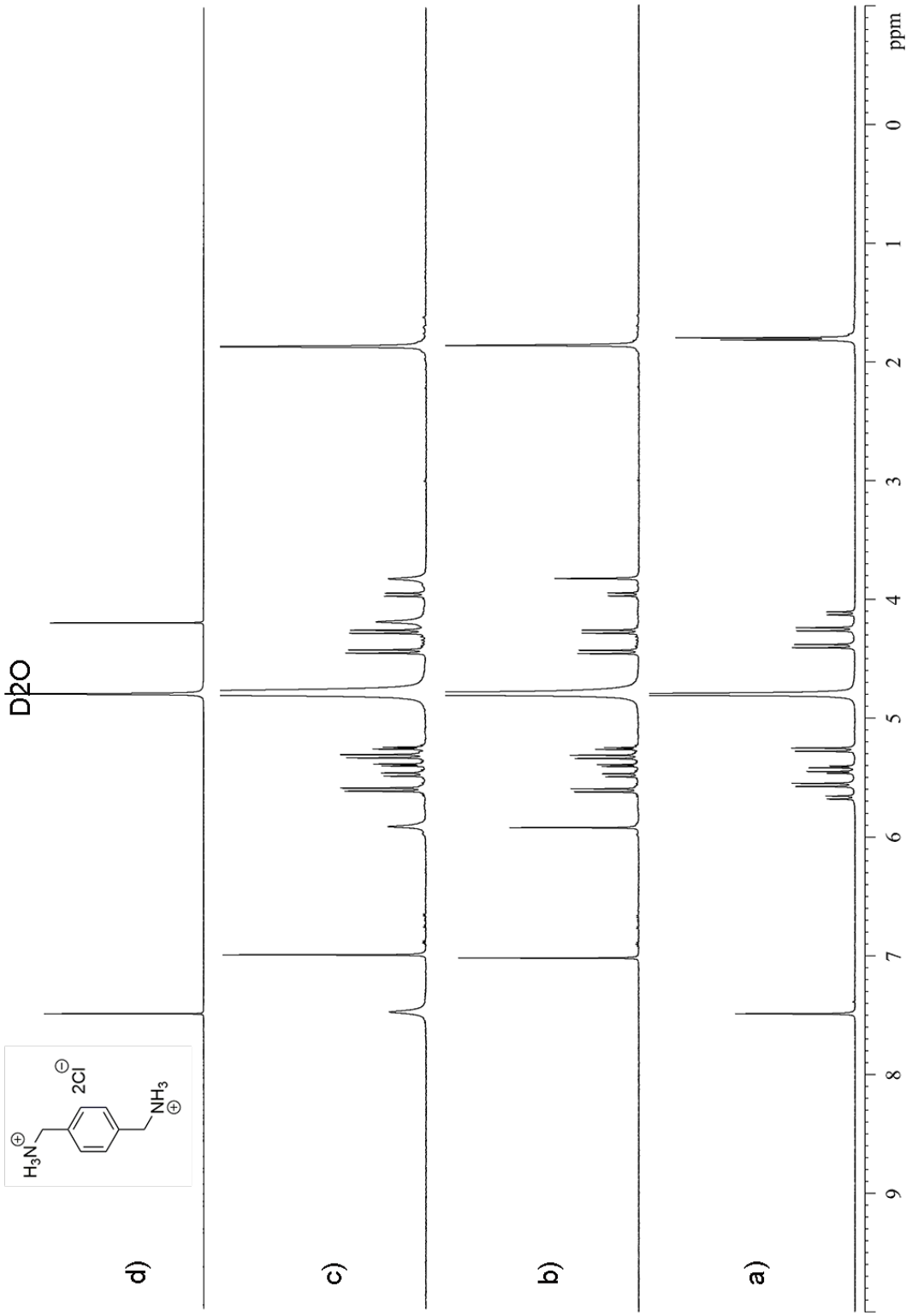

Figure IV-S11. ^{1}H NMR spectra (600 MHz, D_2O, RT) recorded for a) host **1** (1.0 mM), b) host **1** (1.0 mM) and guest **11a** (1.0 mM), c) host **1** (1.0 mM) and guest **11a** (2.0 mM), d) **11a** (1.0mM).

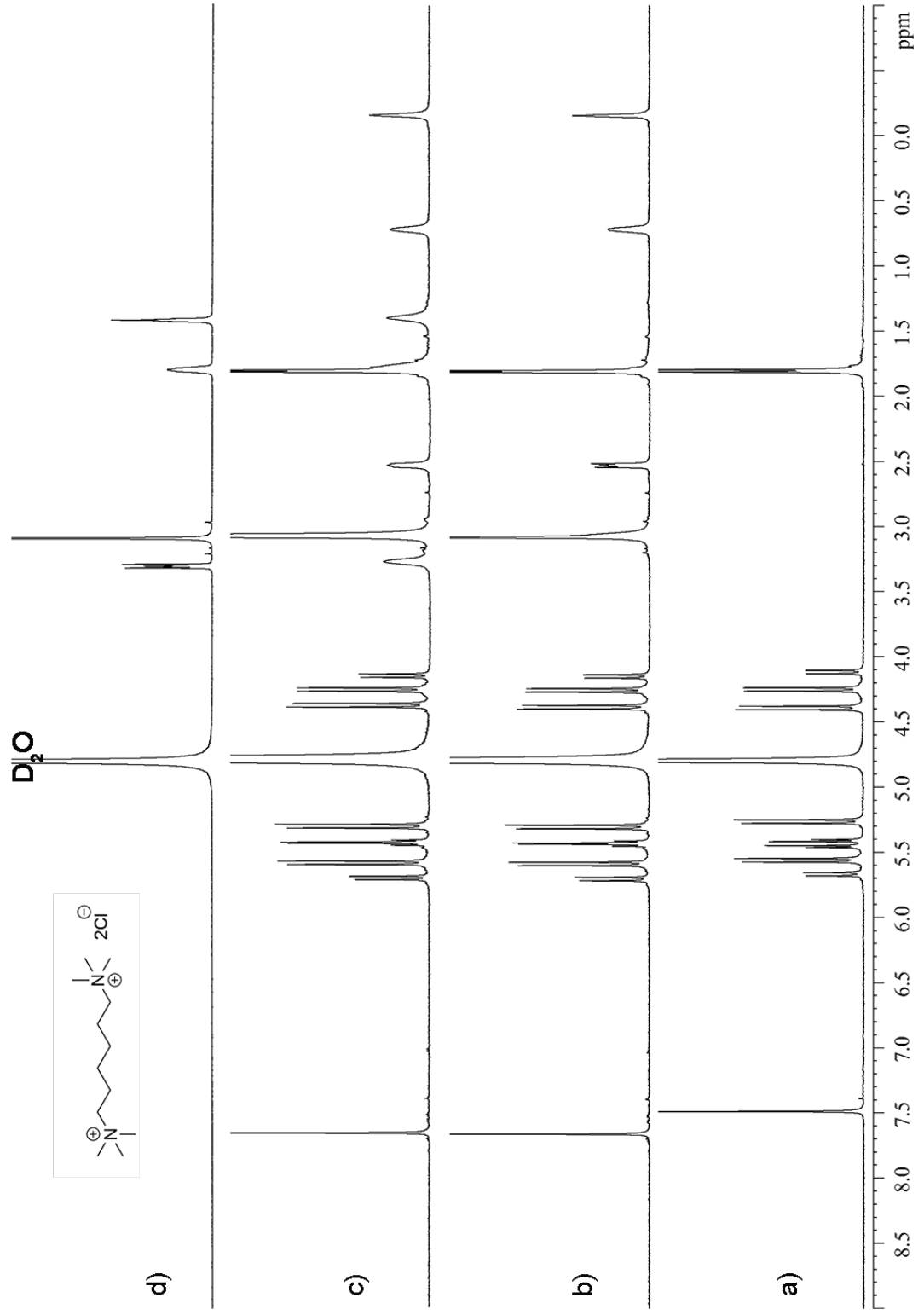

Figure IV-S12. ^{1}H NMR spectra (600 MHz, D_2O, RT) recorded for a) host **1** (1.0 mM), b) host **1** (1.0 mM) and guest **6d** (1.0 mM), c) host **1** (1.0 mM) and guest **6d** (2.0 mM), d) guest **6d** (1.0 mM).

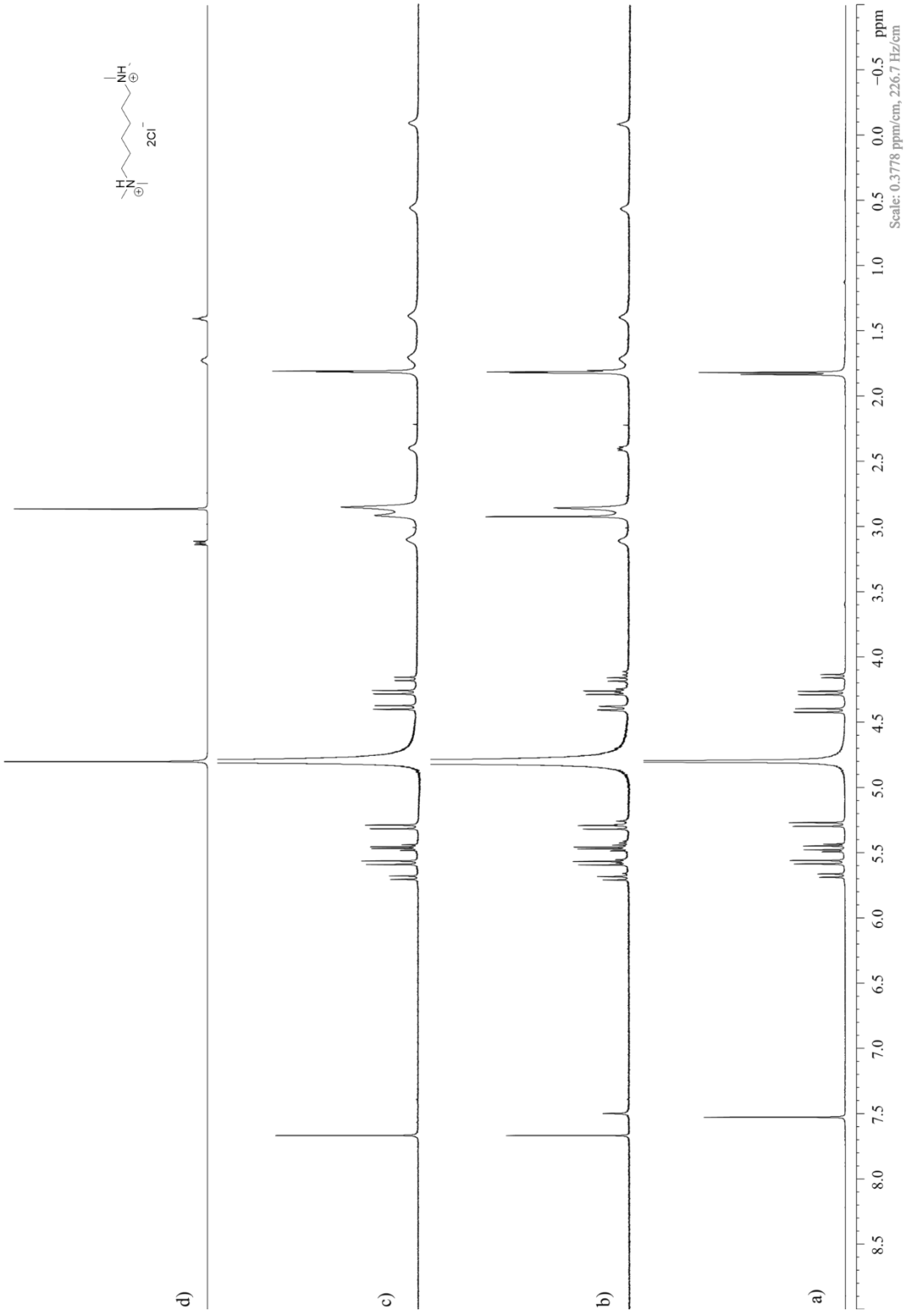

Figure IV-S13. ^{1}H NMR spectra (600 MHz, D_2O, RT) recorded for a) host **1** (1.0 mM), b) host **1** (1.0 mM) and guest **6c** (1.0 mM), c) host **1** (1.0 mM) and guest **6c** (2.0 mM), d) guest **6c** (1.0 mM).

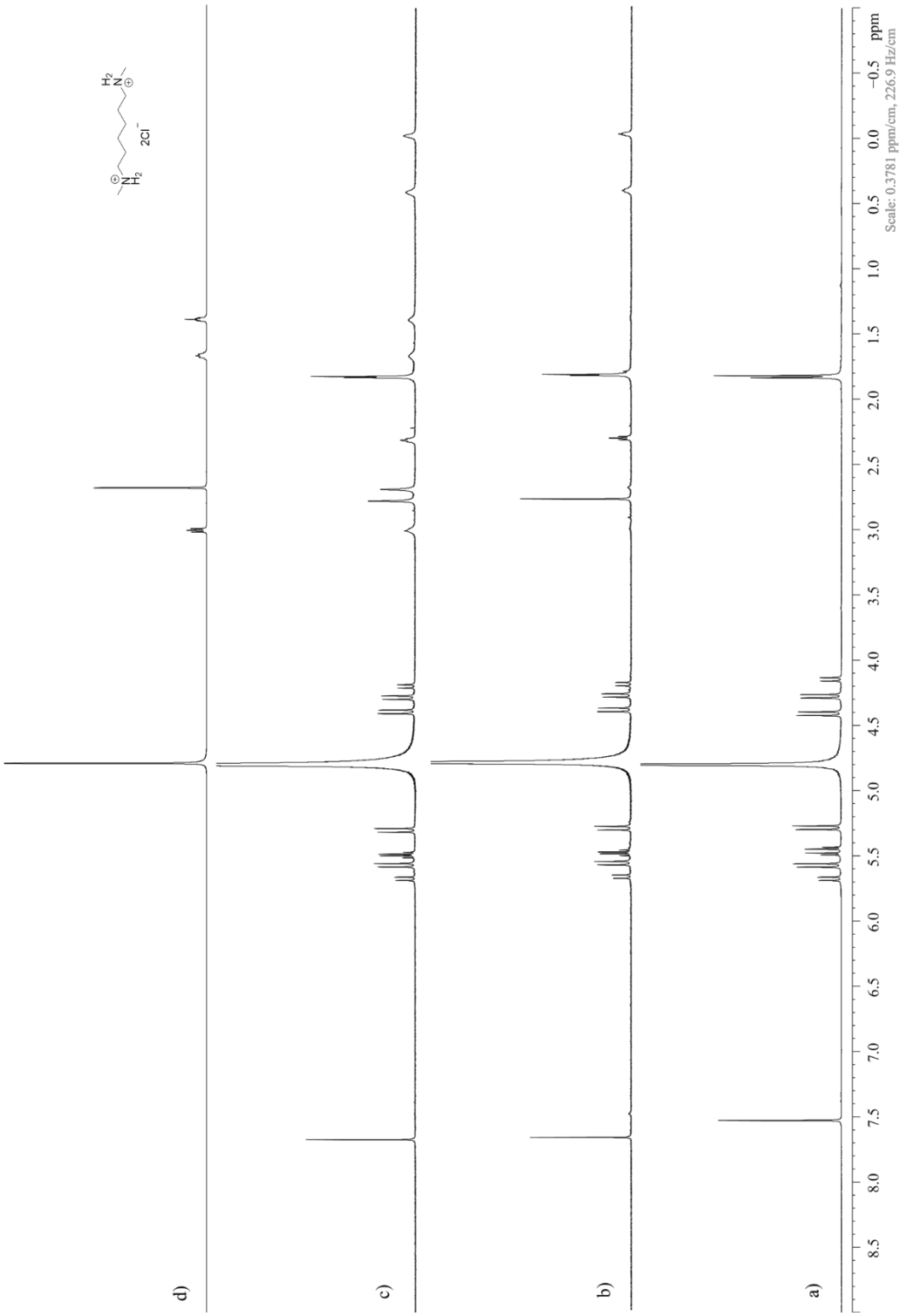

Figure IV-S14. ^{1}H NMR spectra (600 MHz, D_2O, RT) recorded for a) host **1** (1.0 mM), b) host **1** (1.0 mM) and guest **6b** (1.0 mM), c) host **1** (1.0 mM) and guest **6b** (2.0 mM), d) guest **6b** (1.0 mM).

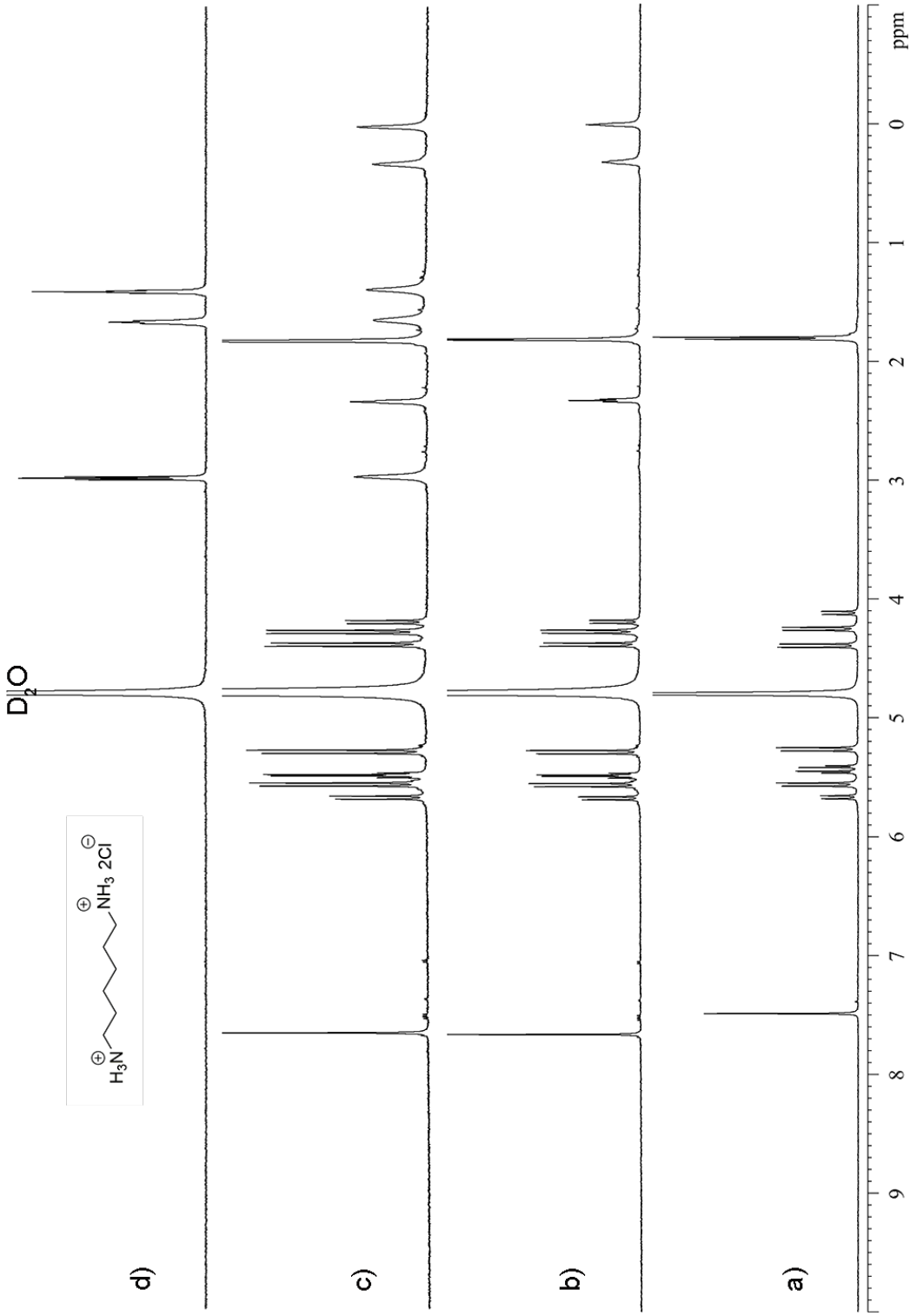

Figure IV-S15. ^{1}H NMR spectra (600 MHz, D_2O, RT) recorded for a) host **1** (1.0 mM), b) host **1** (1.0 mM) and guest **6a** (1.0 mM), c) host **1** (1.0 mM) and guest **6a** (2.0 mM), d) guest **6a** (1.0 mM).

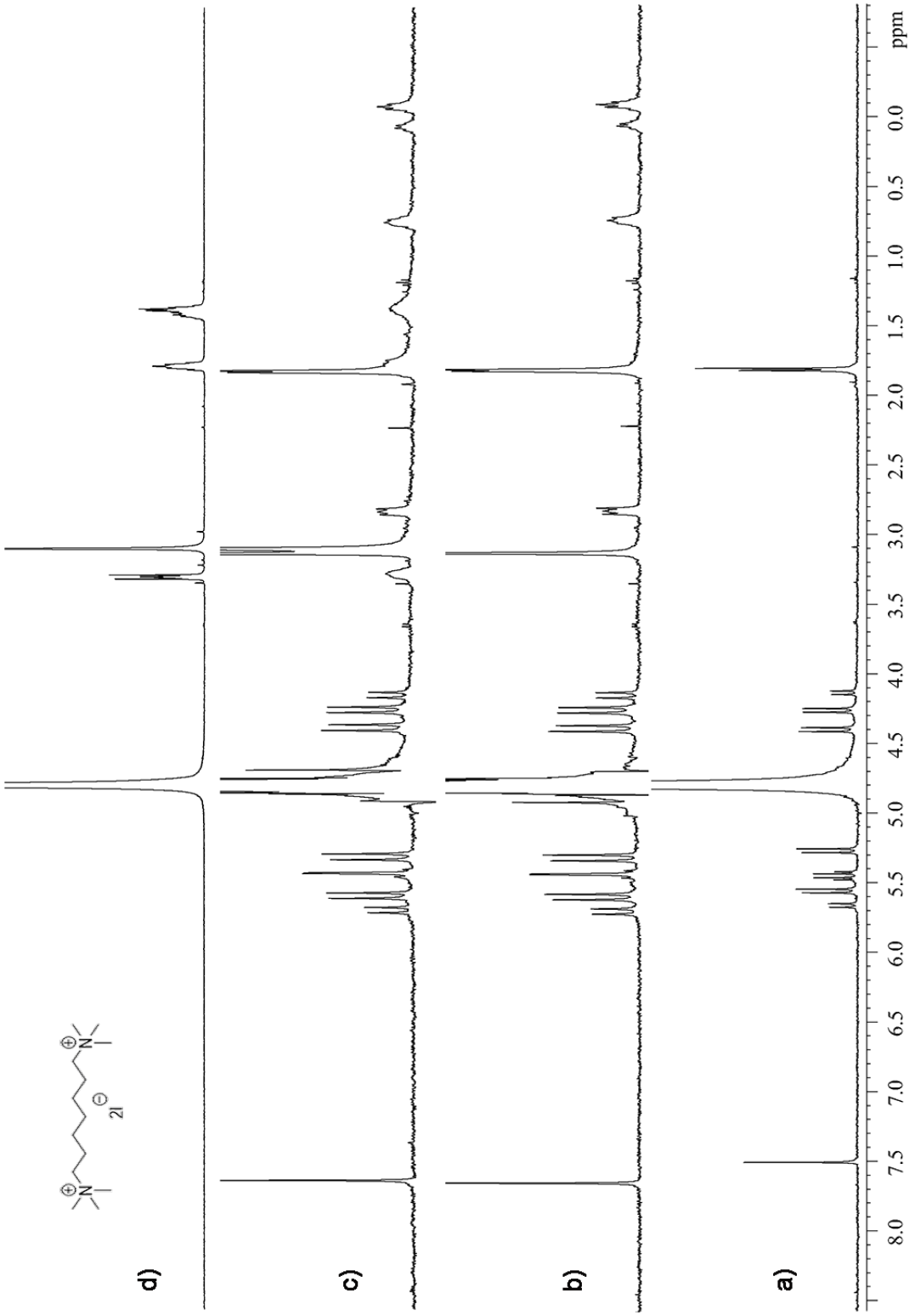

Figure IV-S16. ^{1}H NMR spectra (600 MHz, D_2O, RT) recorded for a) host **1** (1.0 mM), b) host **1** (1.0 mM) and guest **7d** (1.0 mM), c) host **1** (1.0 mM) and guest **7d** (2.0 mM), d) guest **7d** (1.0 mM).

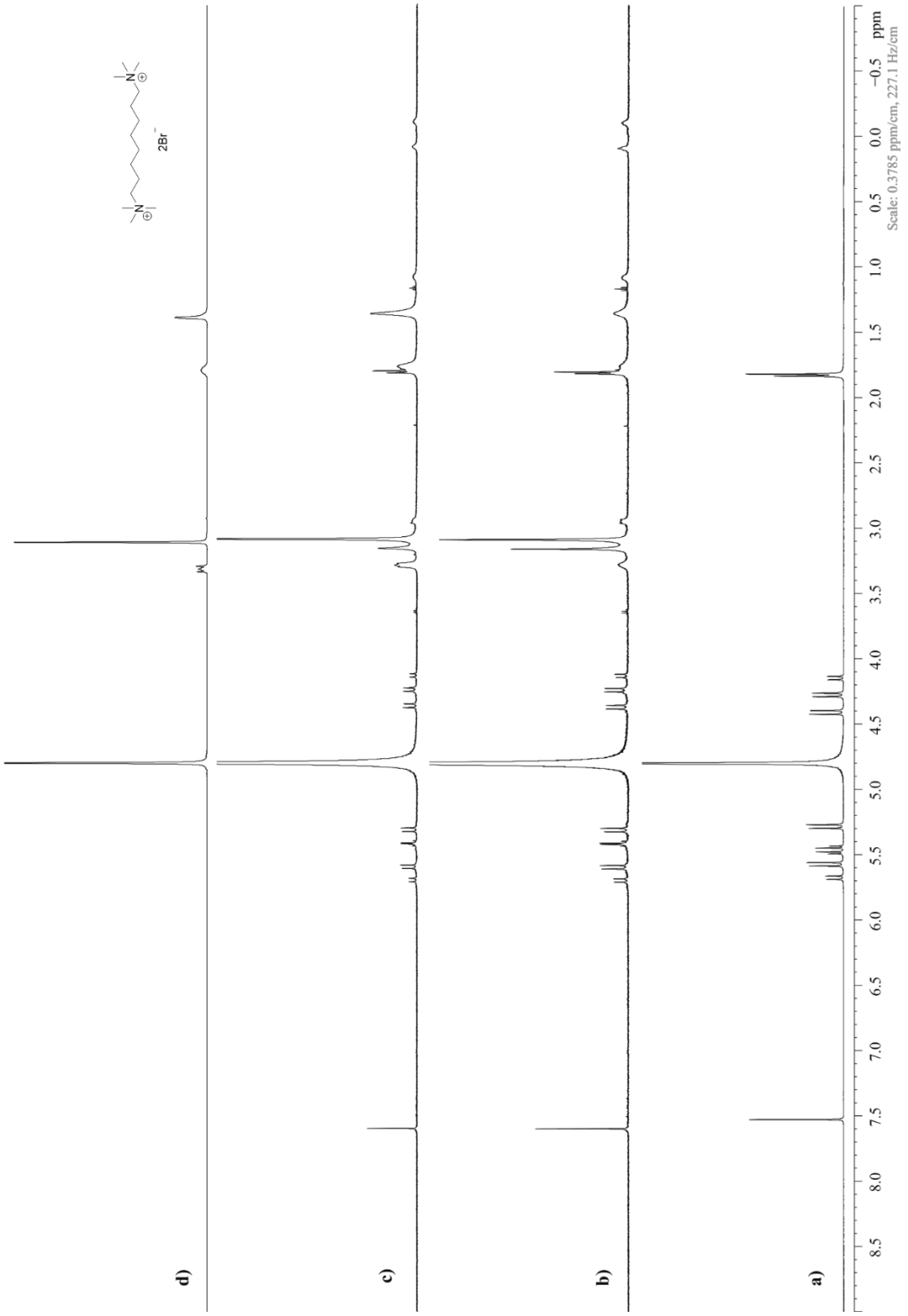

Figure IV-S17. ^{1}H NMR spectra (600 MHz, D_2O, RT) recorded for a) host **1** (1.0 mM), b) host **1** (1.0 mM) and guest **8d** (1.0 mM), c) host **1** (1.0 mM) and guest **8d** (2.0 mM), d) guest **8d** (1.0 mM).

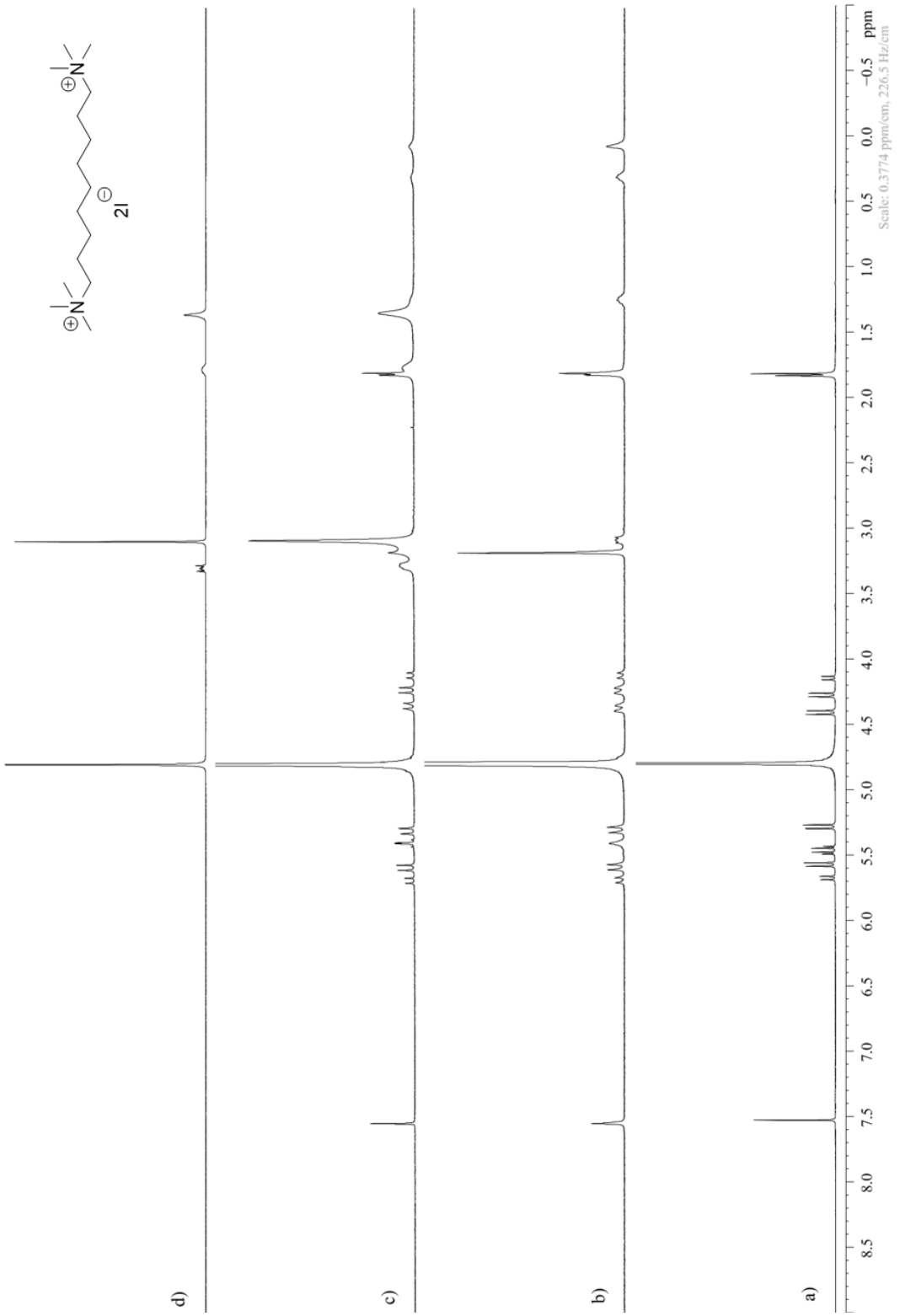

Figure IV-S18. ^{1}H NMR spectra (600 MHz, D_2O, RT) recorded for a) host **1** (1.0 mM), b) host **1** (1.0 mM) and guest **9d** (1.0 mM), c) host **1** (1.0 mM) and guest **9d** (2.0 mM), d) guest **9d** (1.0 mM).

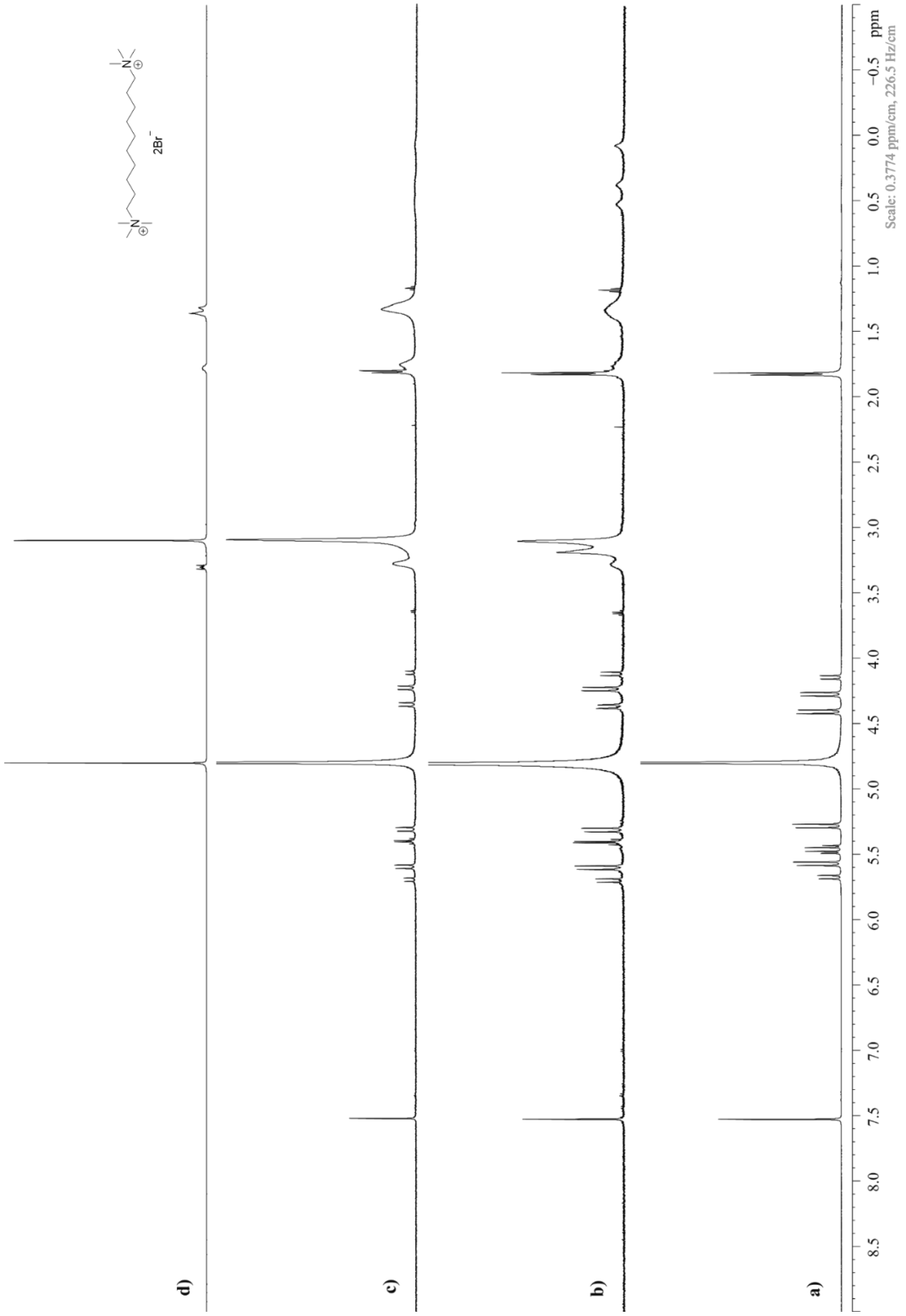

Figure IV-S19. ^{1}H NMR spectra (600 MHz, D_2O, RT) recorded for a) host **1** (1.0 mM), b) host **1** (1.0 mM) and guest **10d** (1.0 mM), c) host **1** (1.0 mM) and guest **10d** (2.0 mM), d) guest **10d** (1.0 mM).

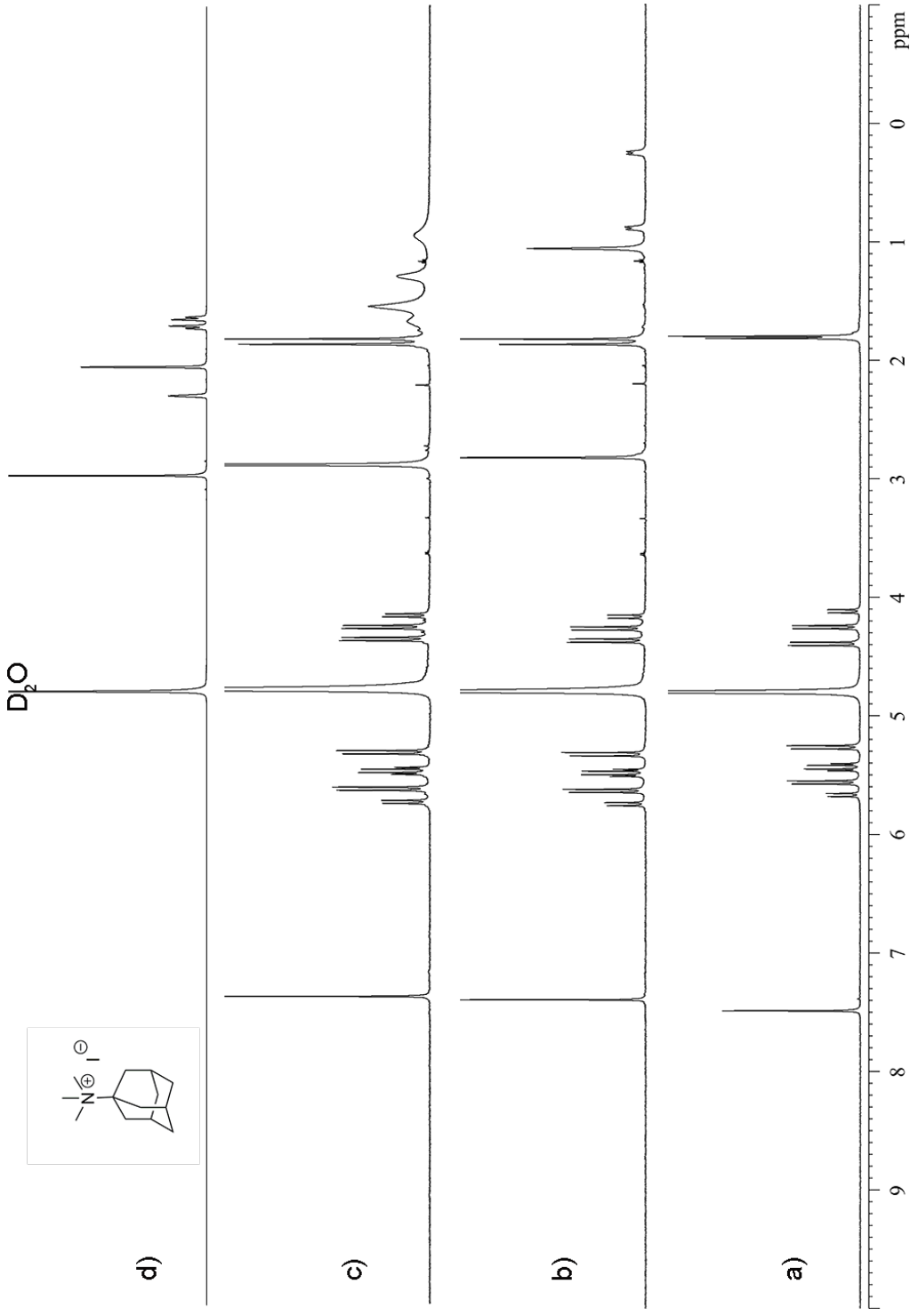

Figure IV-S20. ^{1}H NMR spectra (600 MHz, D_2O, RT) recorded for a) host **1** (1.0 mM), b) host **1** (1.0 mM) and guest **12d** (1.0 mM), c) host **1** (1.0 mM) and guest **12d** (2.0 mM), d) guest **12d** (1.0 mM).

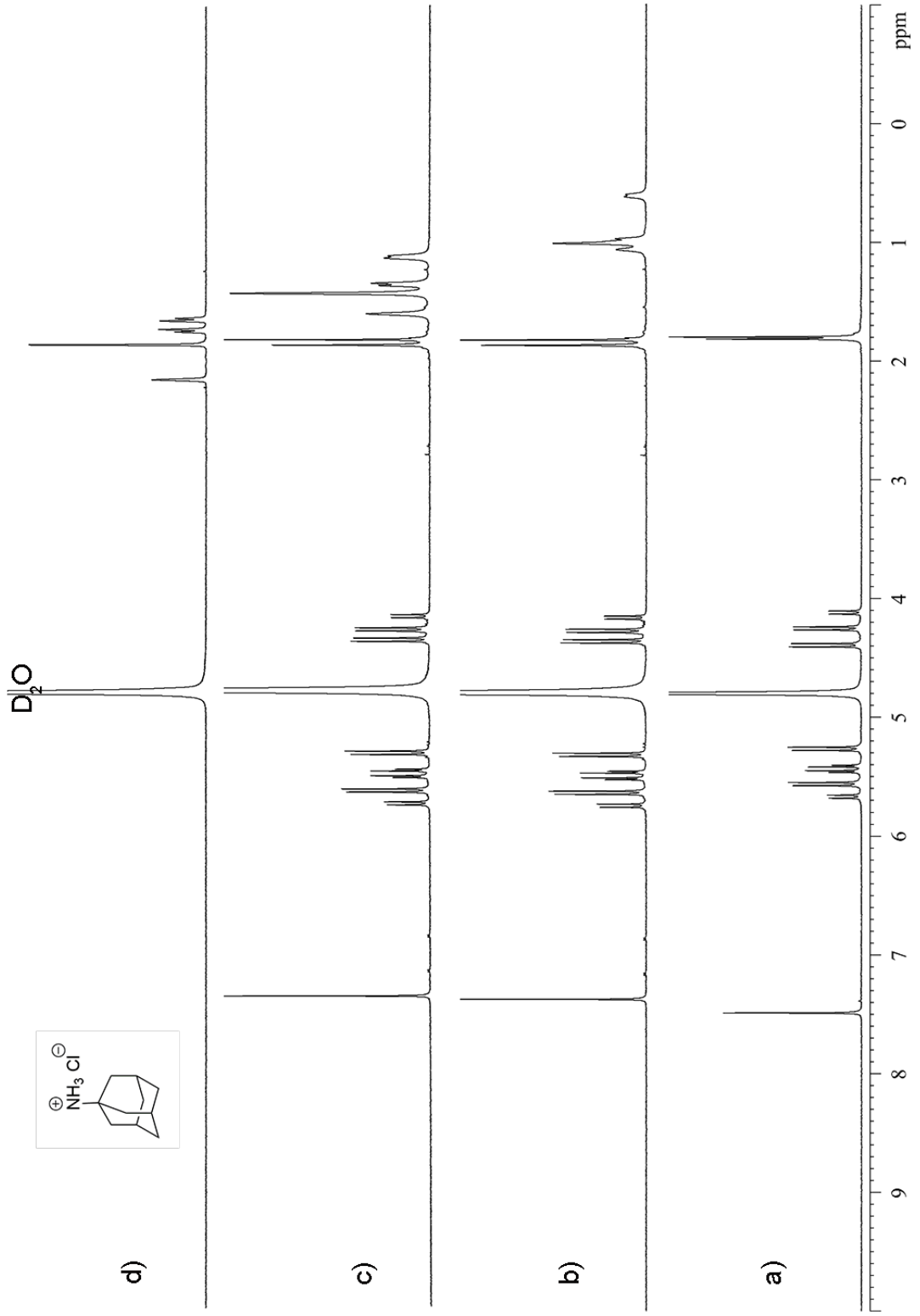

Figure IV-S21. ^{1}H NMR spectra (600 MHz, D_2O, RT) recorded for a) host **1** (1.0 mM), b) host **1** (1.0 mM) and guest **12a** (1.0 mM), c) host **1** (1.0 mM) and guest **12a** (2.0 mM), d) guest **12a** (1.0 mM).

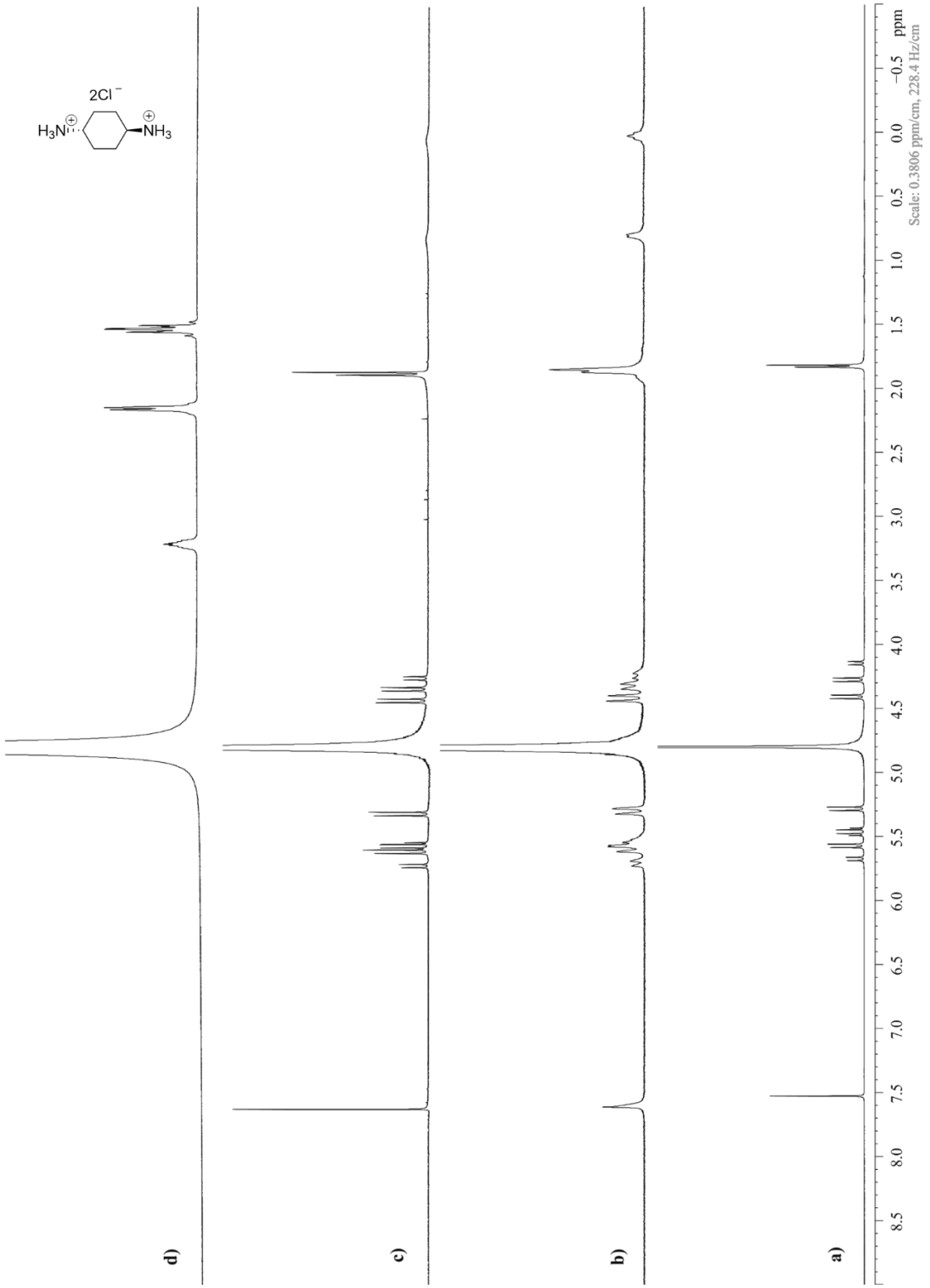

Figure IV-S22. ^{1}H NMR spectra (600 MHz, D_2O, RT) recorded for a) host **1** (1.0 mM), b) host **1** (1.0 mM) and guest **13a** (1.0 mM), c) host **1** (1.0 mM) and guest **13a** (2.0 mM), d) guest **13a** (1.0 mM).

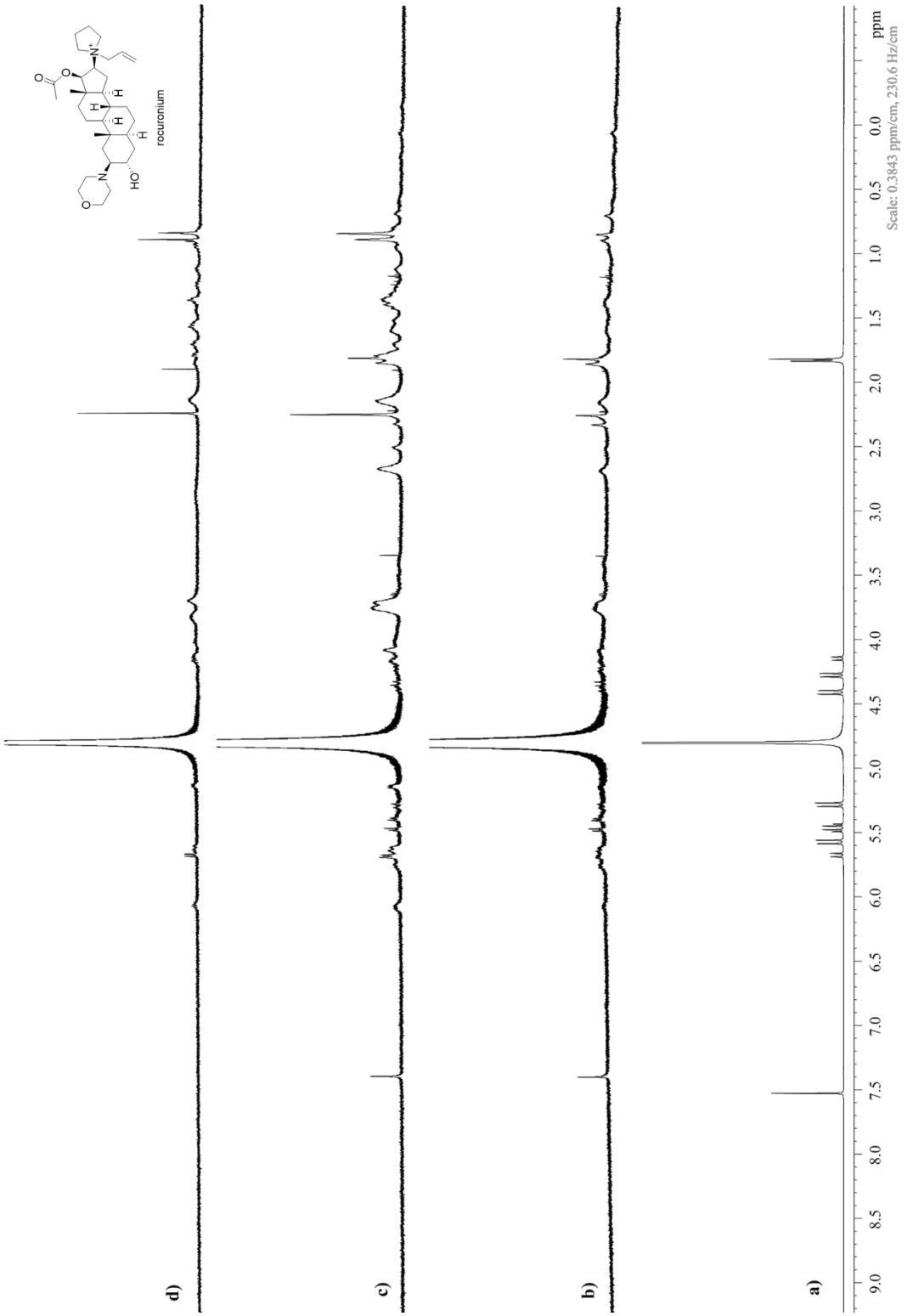

Figure IV-S23. ^{1}H NMR spectra (600 MHz, D_2O, RT) recorded for a) host **1** (1.0 mM), b) host **1** (250 µM) and guest **19** (250 µM), c) host **1** (250 µM) and guest **19** (500 µM), d) guest **19** (500 µM).

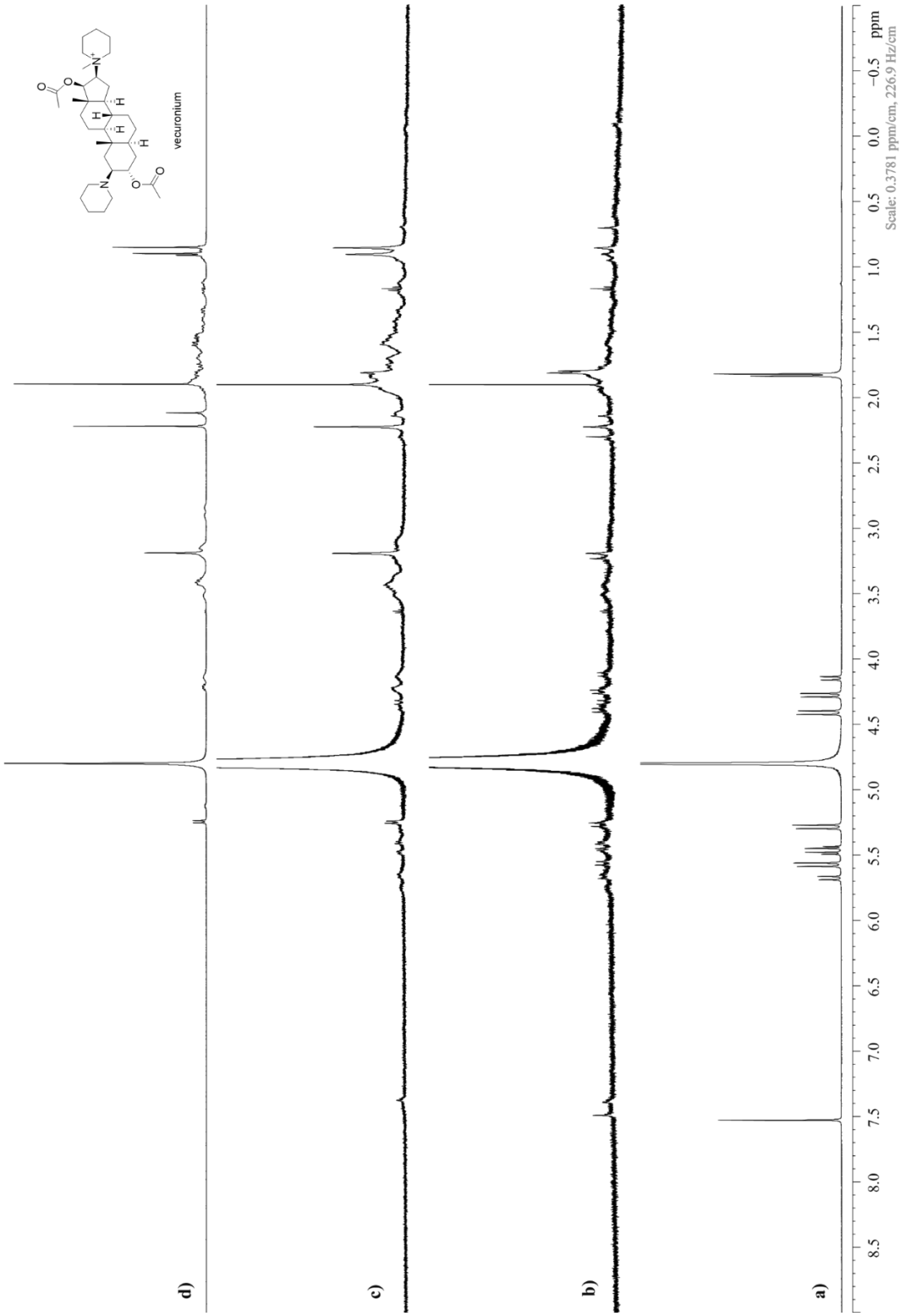

Figure IV-S24. ^{1}H NMR spectra (600 MHz, D_2O, RT) recorded for a) host **1** (1.0 mM), b) host **1** (250 µM) and guest **20** (250 µM), c) host **1** (250 µM) and guest **20** (500 µM), d) guest **20** (500 µM).

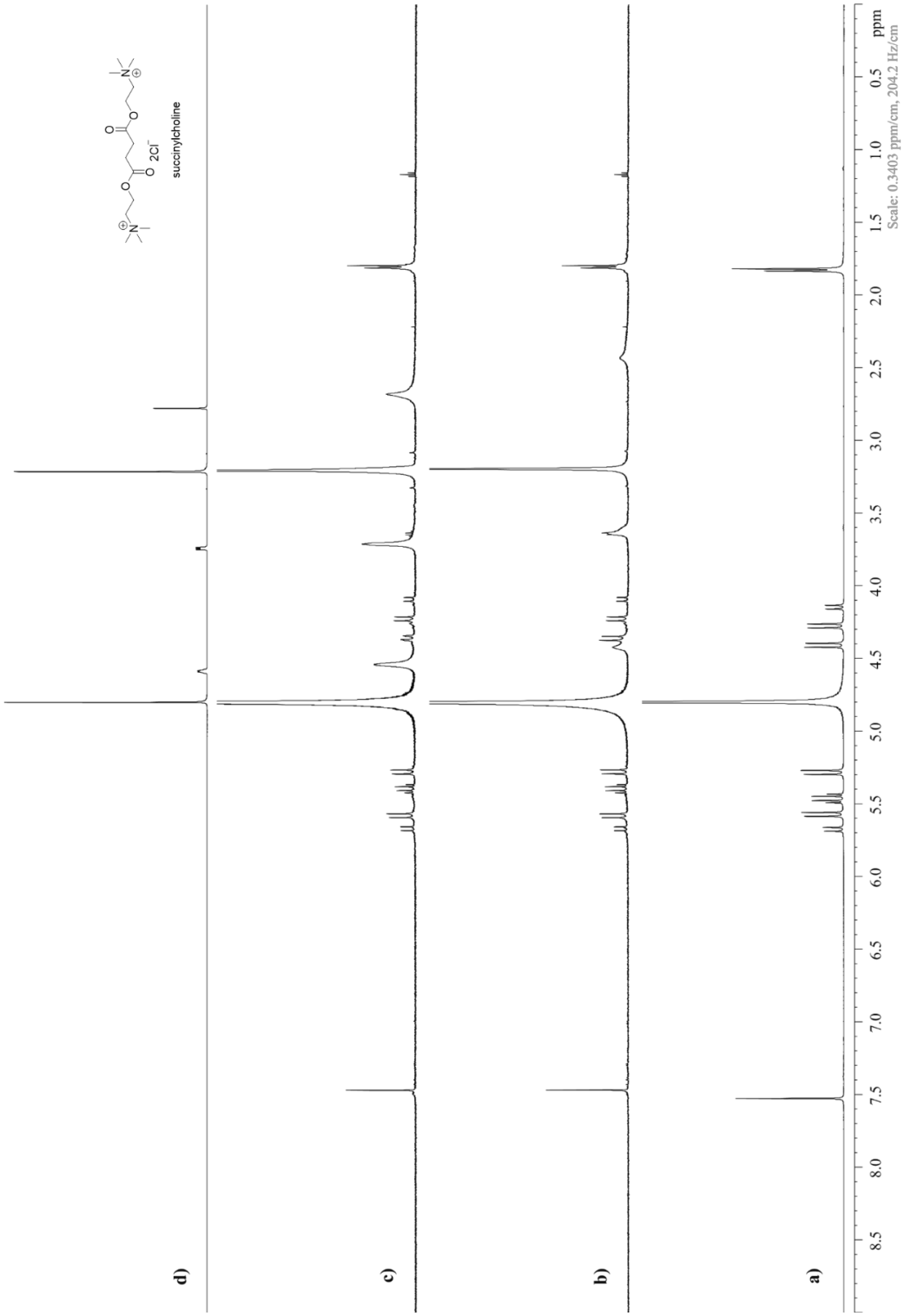

Figure IV-S25. ^{1}H NMR spectra (600 MHz, D_2O, RT) recorded for a) host **1** (1.0 mM), b) host **1** (1.0 mM) and guest **22** (1.0 mM), c) host **1** (1.0 mM) and guest **22** (2.0 mM), d) guest **22** (1.0 mM).

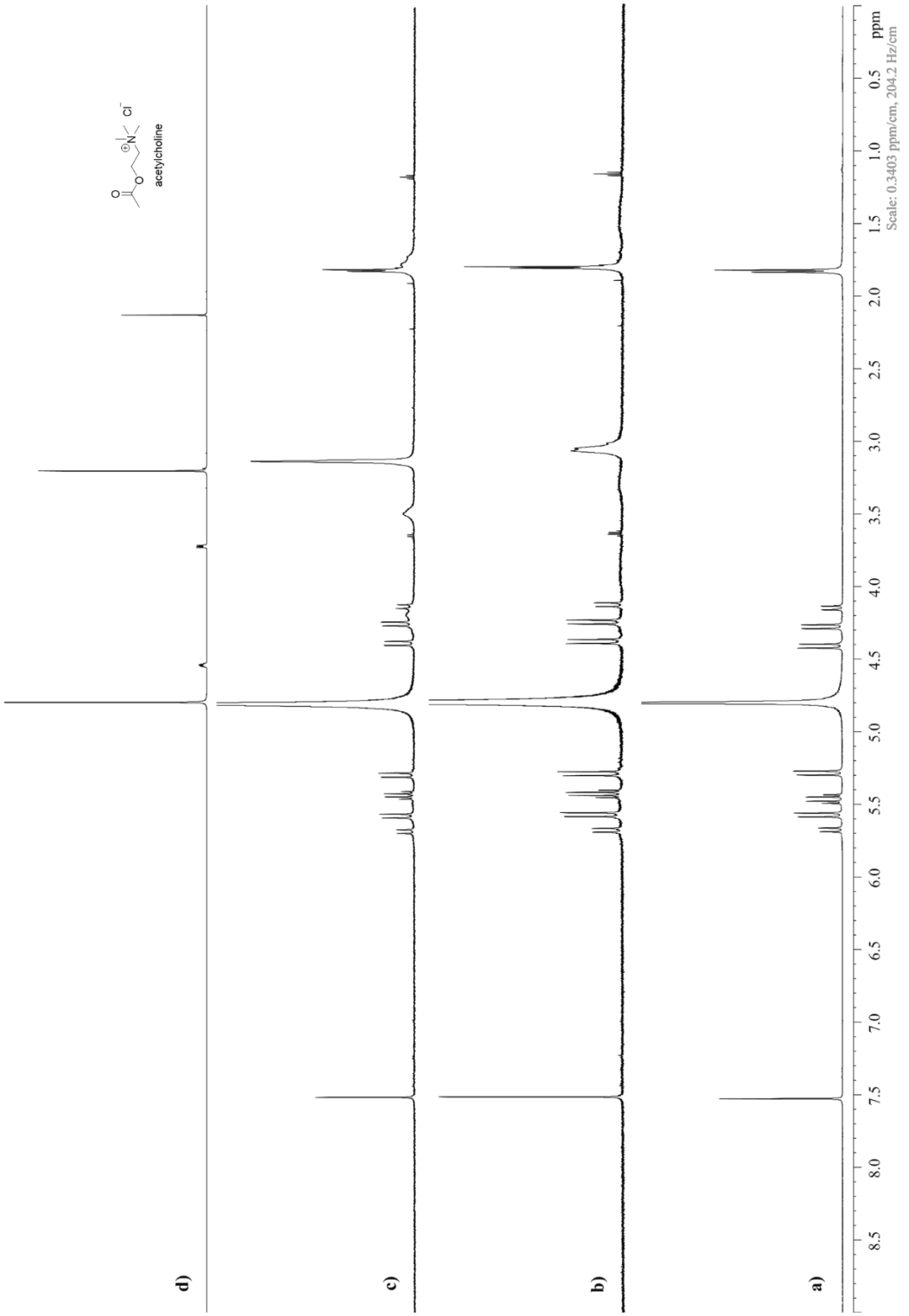

Figure IV-S26. ^{1}H NMR spectra (600 MHz, D_2O, RT) recorded for a) host **1** (1.0 mM), b) host **1** (1.0 mM) and guest **23** (1.0 mM), c) host **1** (1.0 mM) and guest **23** (2.0 mM), d) guest **23** (1.0 mM).

Isothermal Titration Calorimetry study of host 1 with selected guests

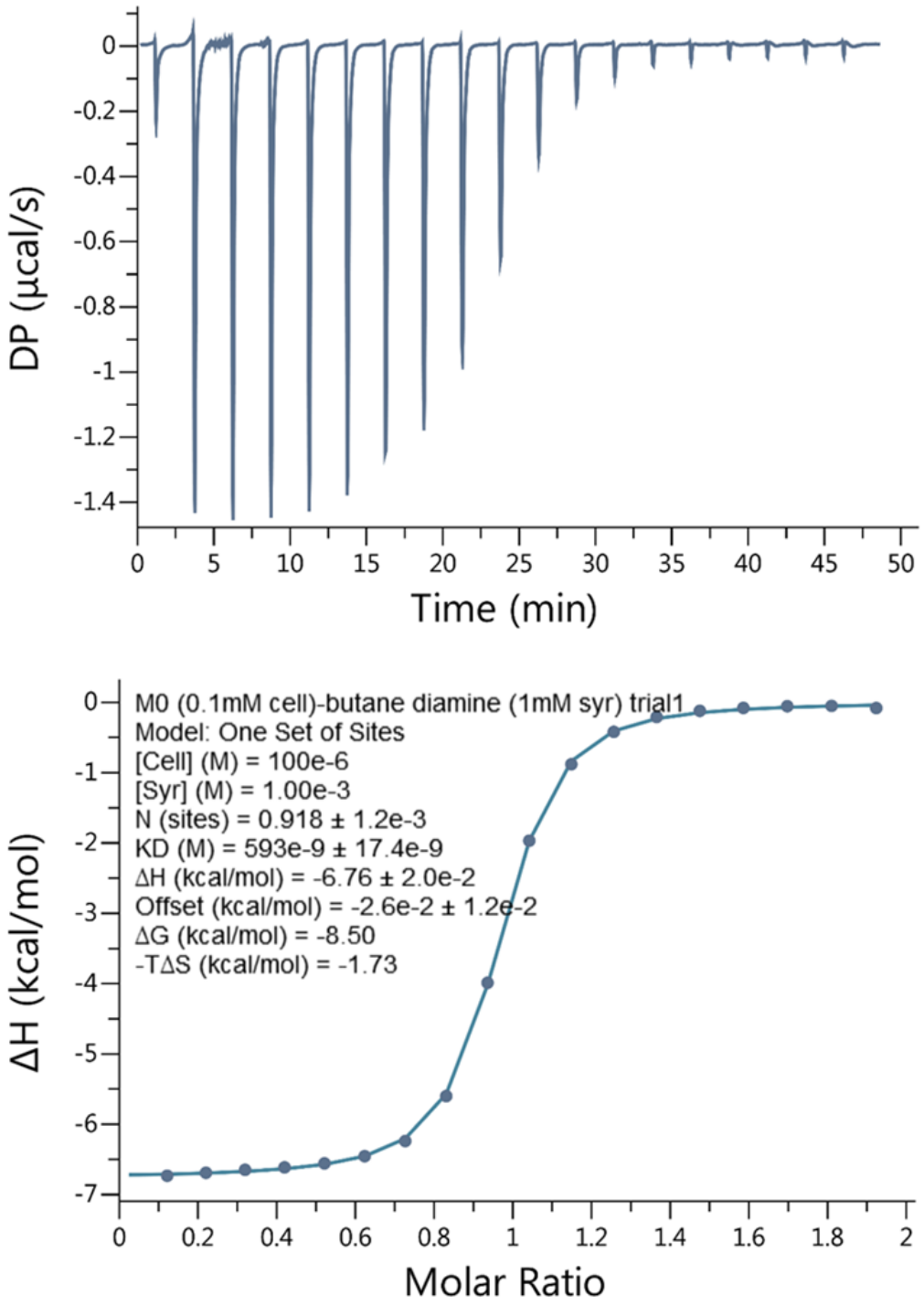

Figure IV-S27. Isothermal Titration Calorimetry (ITC) curve obtained through direct binding titration studies. A solution of **1** (100 µM) in the cell was titrated with **5a** (1.00 mM) in the syringe at 298.0 K in 20 mM sodium phosphate buffered water at pH 7.4. $K_a = 1.68 \times 10^6\ M^{-1}$.

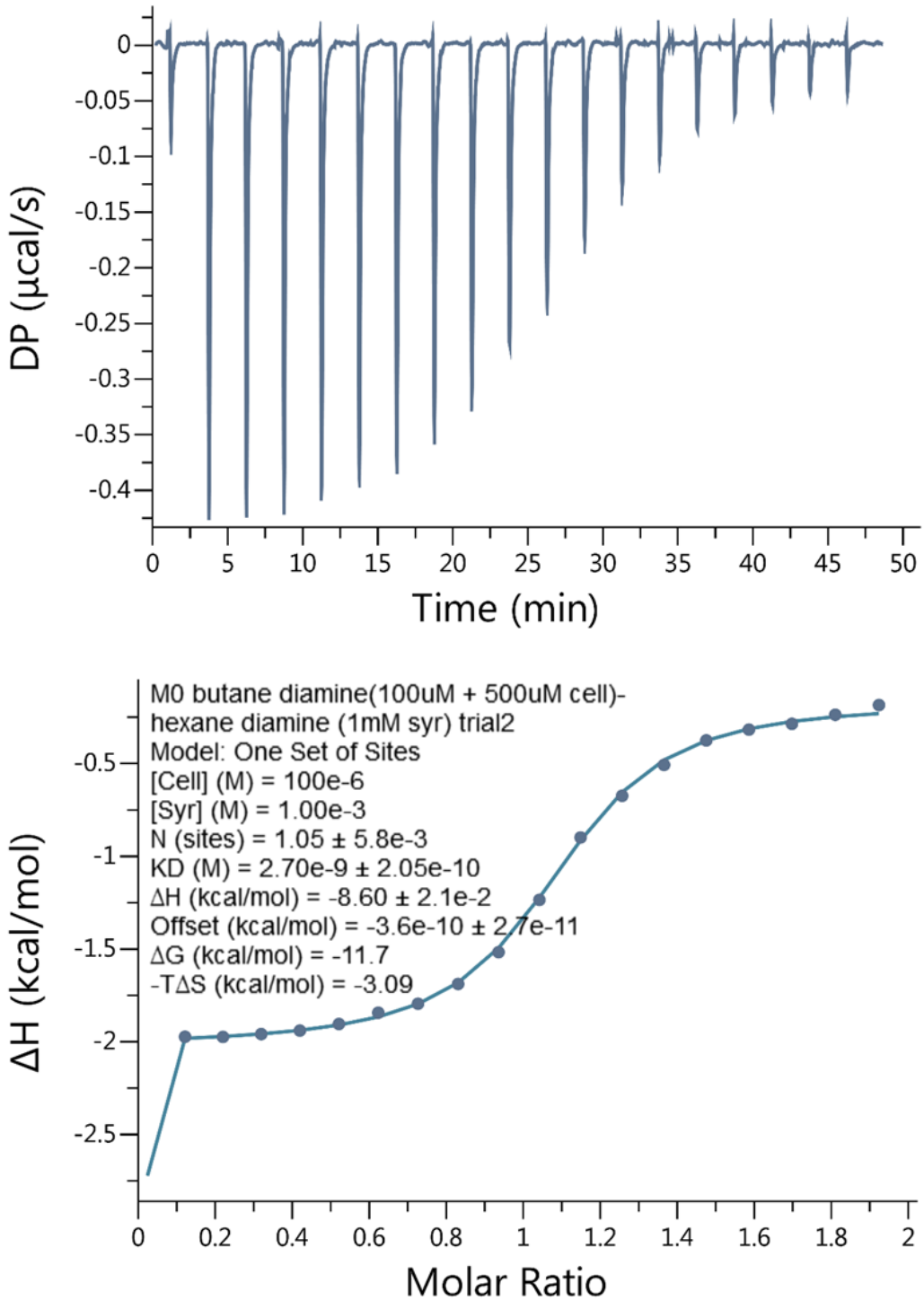

Figure IV-S28. Isothermal Titration Calorimetry (ITC) curve obtained through competition binding studies. A solution of **1** (100 µM) and **5a** (500 µM) in the cell was titrated with **6a** (1.00 mM) in the syringe at 298.0 K in 20 mM sodium phosphate buffered water at pH 7.4. $K_a = 3.70 \times 10^8\ M^{-1}$

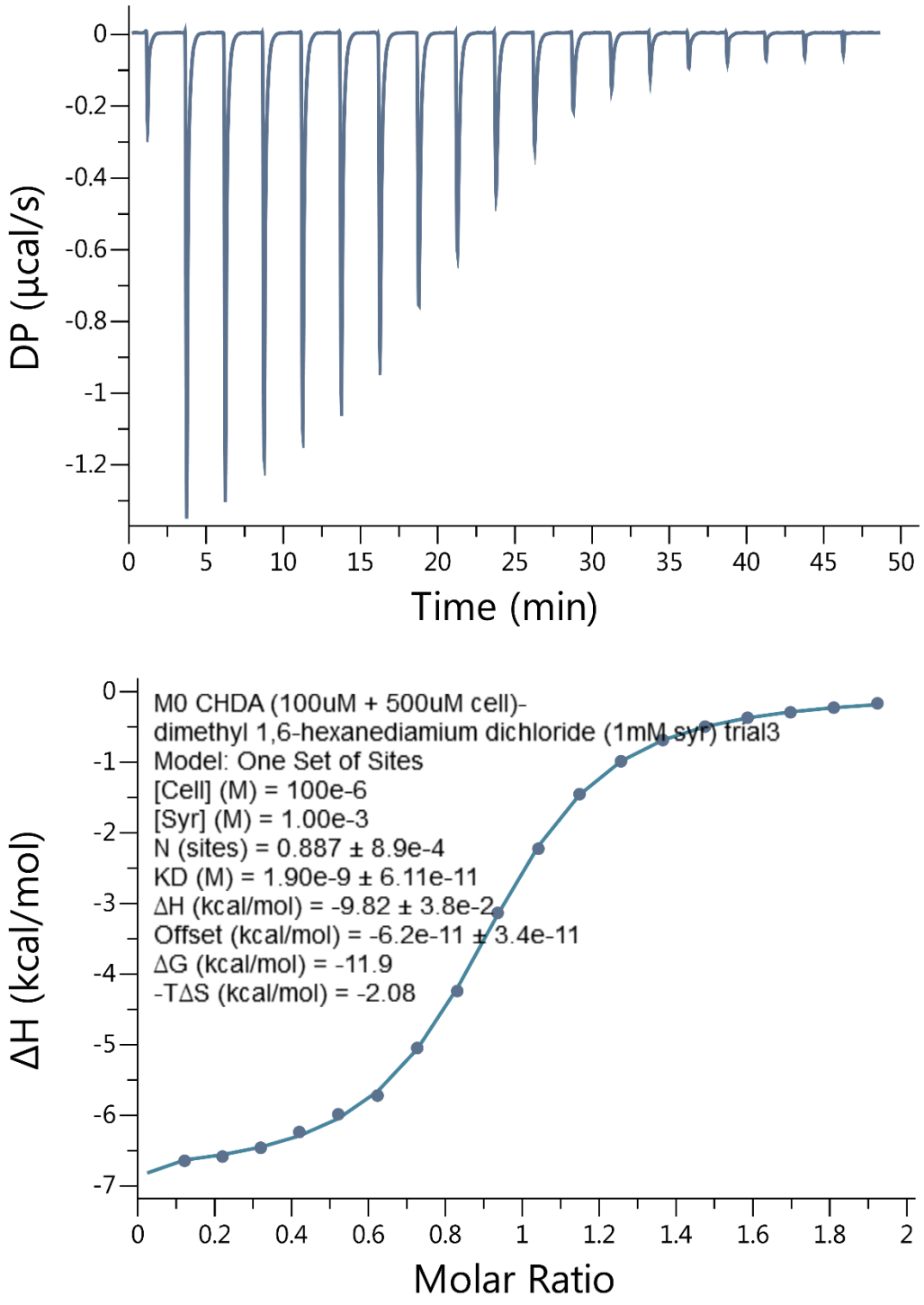

Figure IV-S29. Isothermal Titration Calorimetry (ITC) curve obtained through competition binding studies. A solution of **1** (100 µM) and **13a** (500 µM) in the cell was titrated with **6b** (1.00 mM) in the syringe at 298.0 K in 20 mM sodium phosphate buffered water at pH 7.4. $K_a = 5.26 \times 10^8\ M^{-1}$

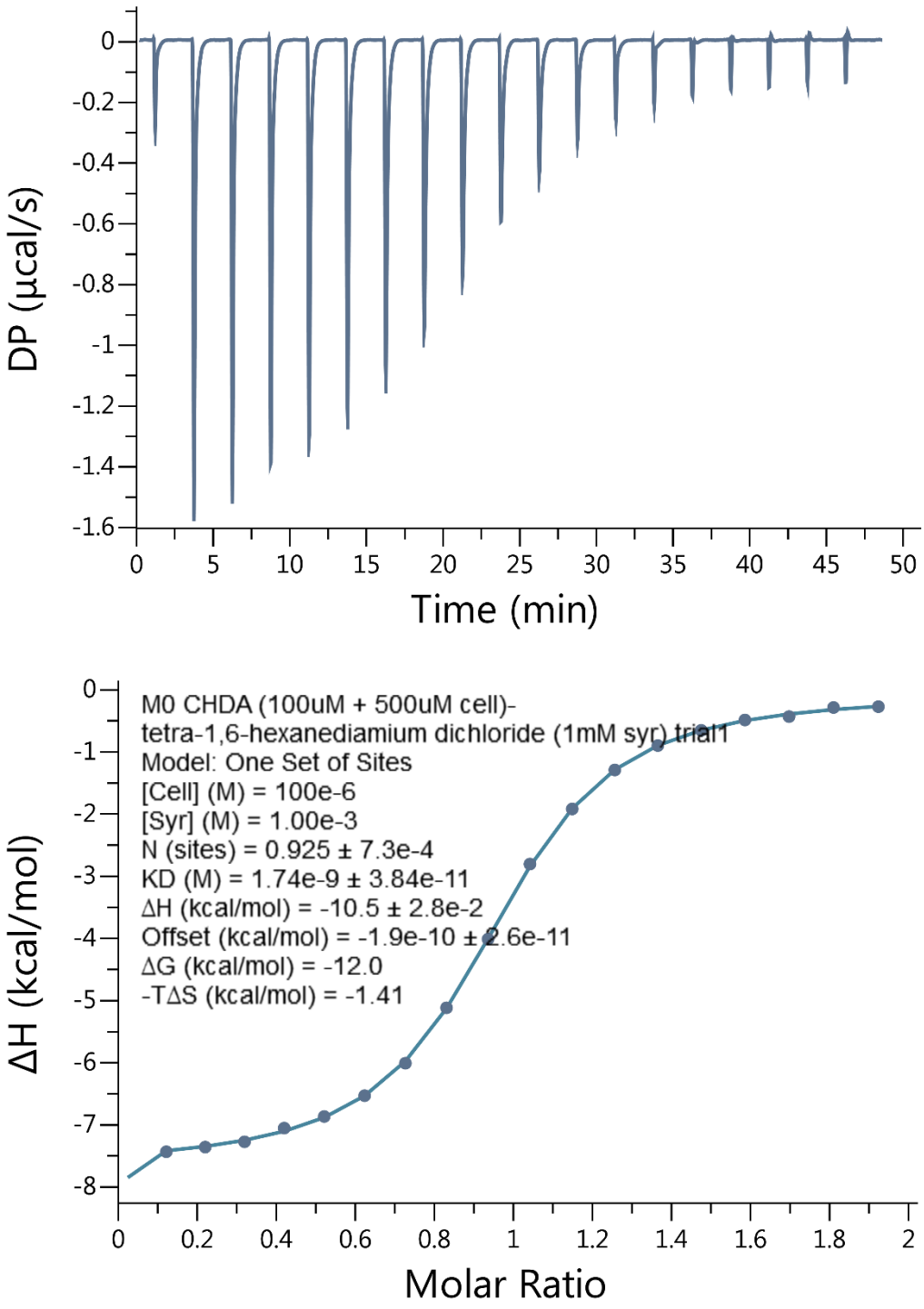

Figure IV-S30. Isothermal Titration Calorimetry (ITC) curve obtained through competition binding studies. A solution of **1** (100 µM) and **13a** (500 µM) in the cell was titrated with **6c** (1.00 mM) in the syringe at 298.0 K in 20 mM sodium phosphate buffered water at pH 7.4. $K_a = 5.74 \times 10^8\ M^{-1}$

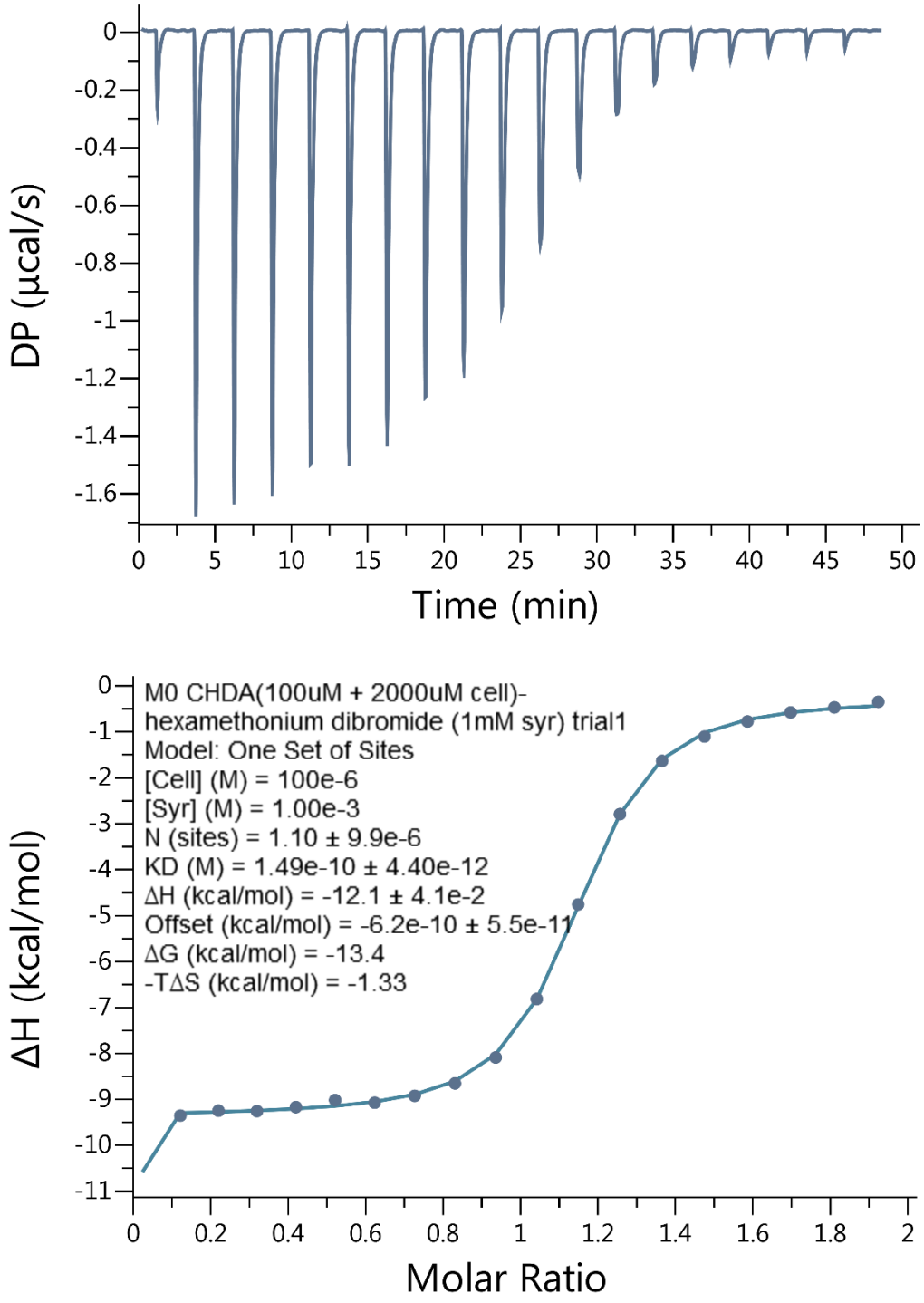

Figure IV-S31. Isothermal Titration Calorimetry (ITC) curve obtained through competition binding studies. A solution of **1** (100 µM) and **13a** (2000 µM) in the cell was titrated with **6d** (1.00 mM) in the syringe at 298.0 K in 20 mM sodium phosphate buffered water at pH 7.4. $K_a = 6.71 \times 10^9\ M^{-1}$

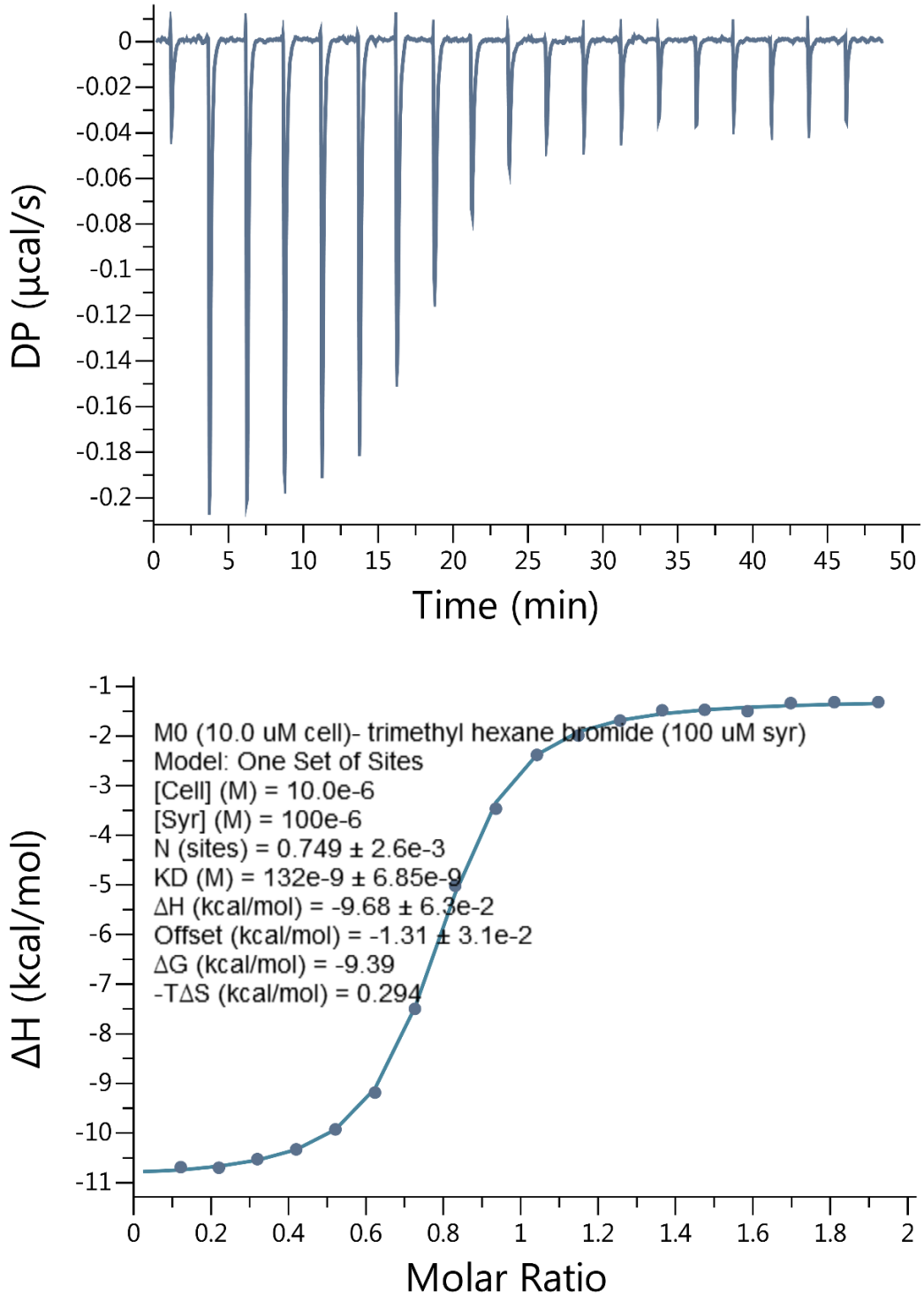

Figure IV-S32. Isothermal Titration Calorimetry (ITC) curve obtained through direct binding titration studies. A solution of **1** (10 µM) in the cell was titrated with **6Q** (100 µM) in the syringe at 298.0 K in 20 mM sodium phosphate buffered water at pH 7.4. $K_a = 7.57 \times 10^6\ M^{-1}$

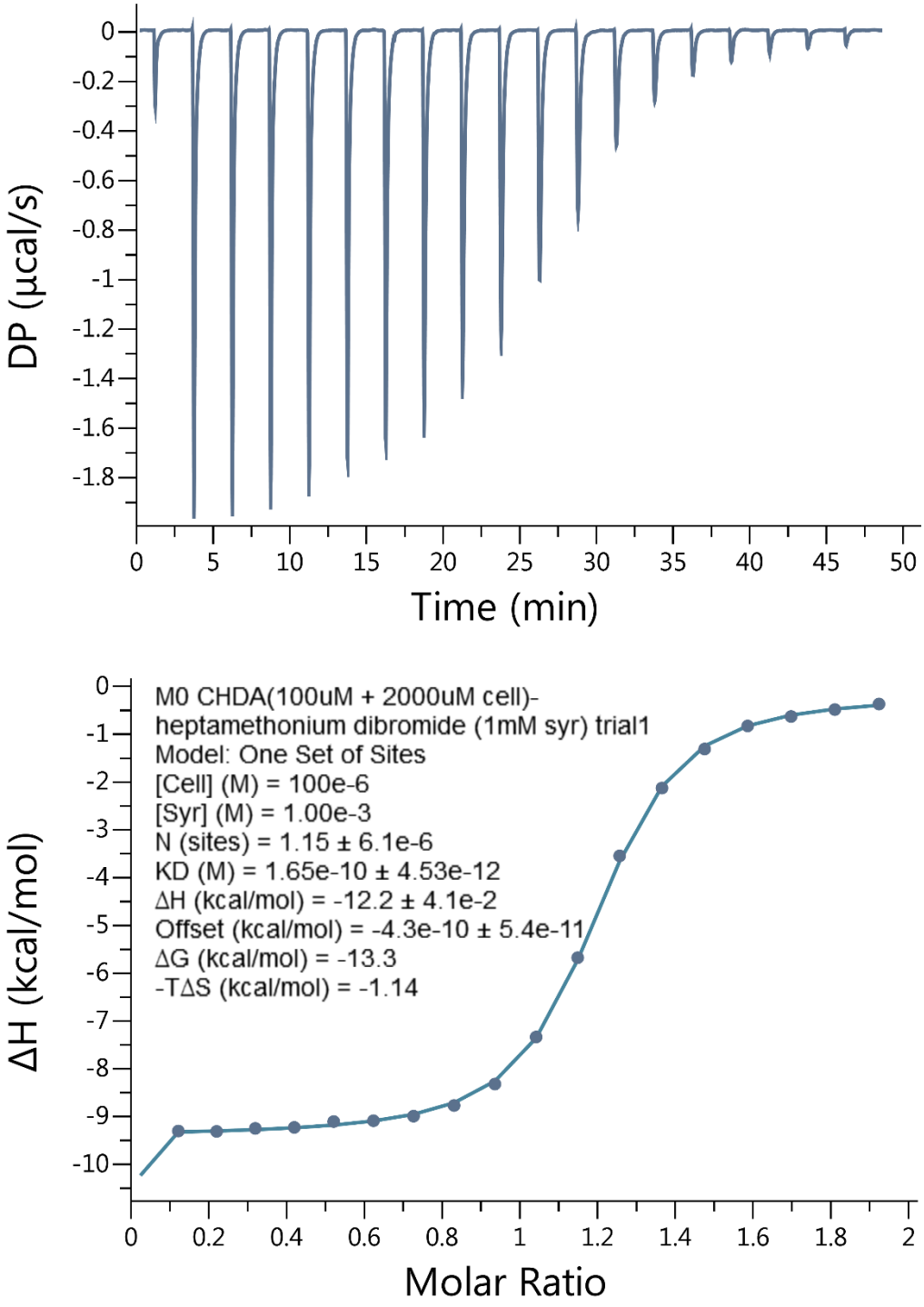

Figure IV-S33. Isothermal Titration Calorimetry (ITC) curve obtained through competition binding studies. A solution of **1** (100 µM) and **13a** (2000 µM) in the cell was titrated with **7d** (1.00 mM) in the syringe at 298.0 K in 20 mM sodium phosphate buffered water at pH 7.4. $K_a = 6.06 \times 10^9\ M^{-1}$.

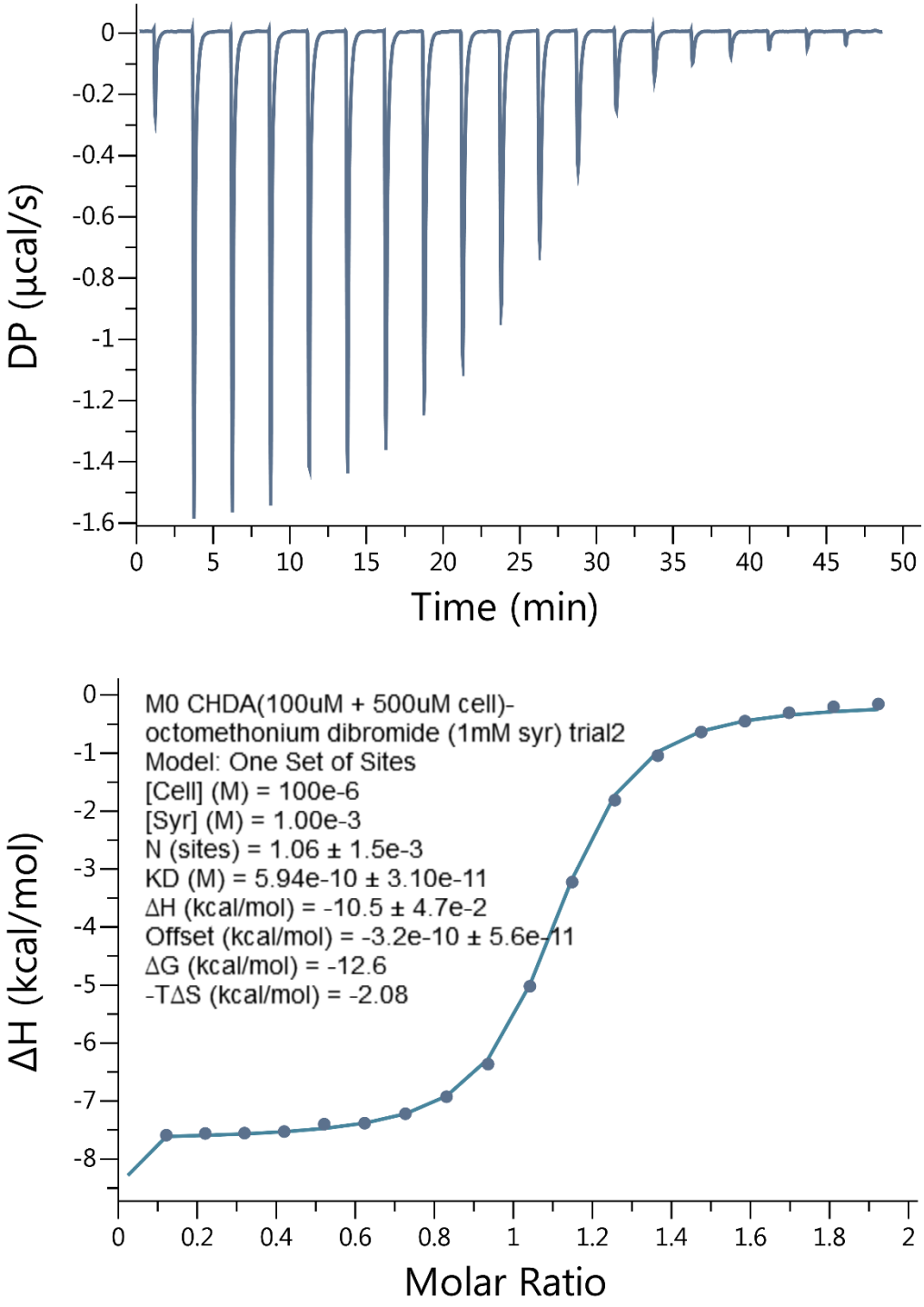

Figure IV-S34. Isothermal Titration Calorimetry (ITC) curve obtained through competition binding studies. A solution of **1** (100 µM) and **13a** (500 µM) in the cell was titrated with **8d** (1.00 mM) in the syringe at 298.0 K in 20 mM sodium phosphate buffered water at pH 7.4. $K_a = 1.75 \times 10^9\ M^{-1}$.

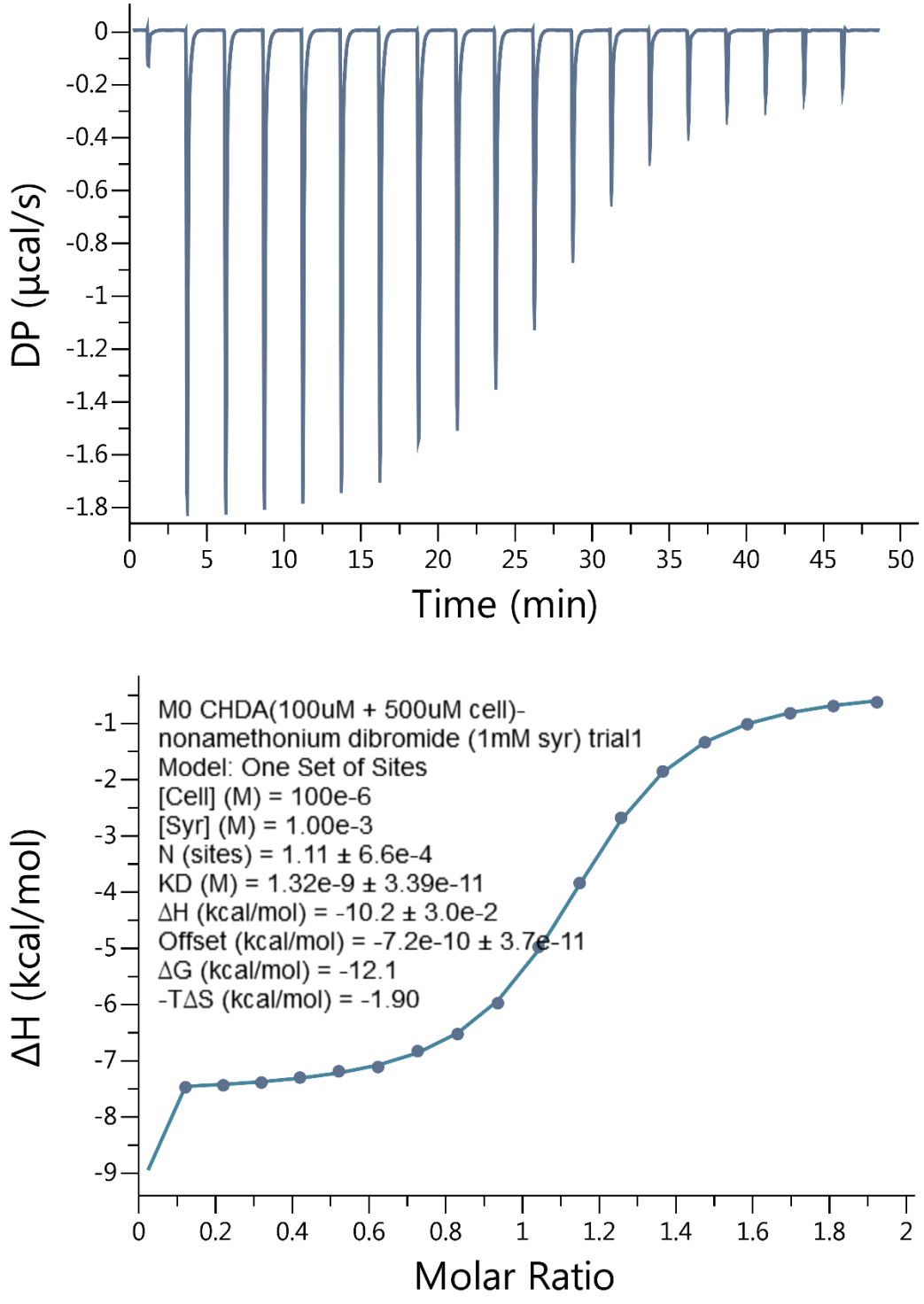

Figure IV-S35. Isothermal Titration Calorimetry (ITC) curve obtained through competition binding studies. A solution of **1** (100 µM) and **13a** (500 µM) in the cell was titrated with **9d** (1.00 mM) in the syringe at 298.0 K in 20 mM sodium phosphate buffered water at pH 7.4. $K_a = 7.57 \times 10^8\ M^{-1}$.

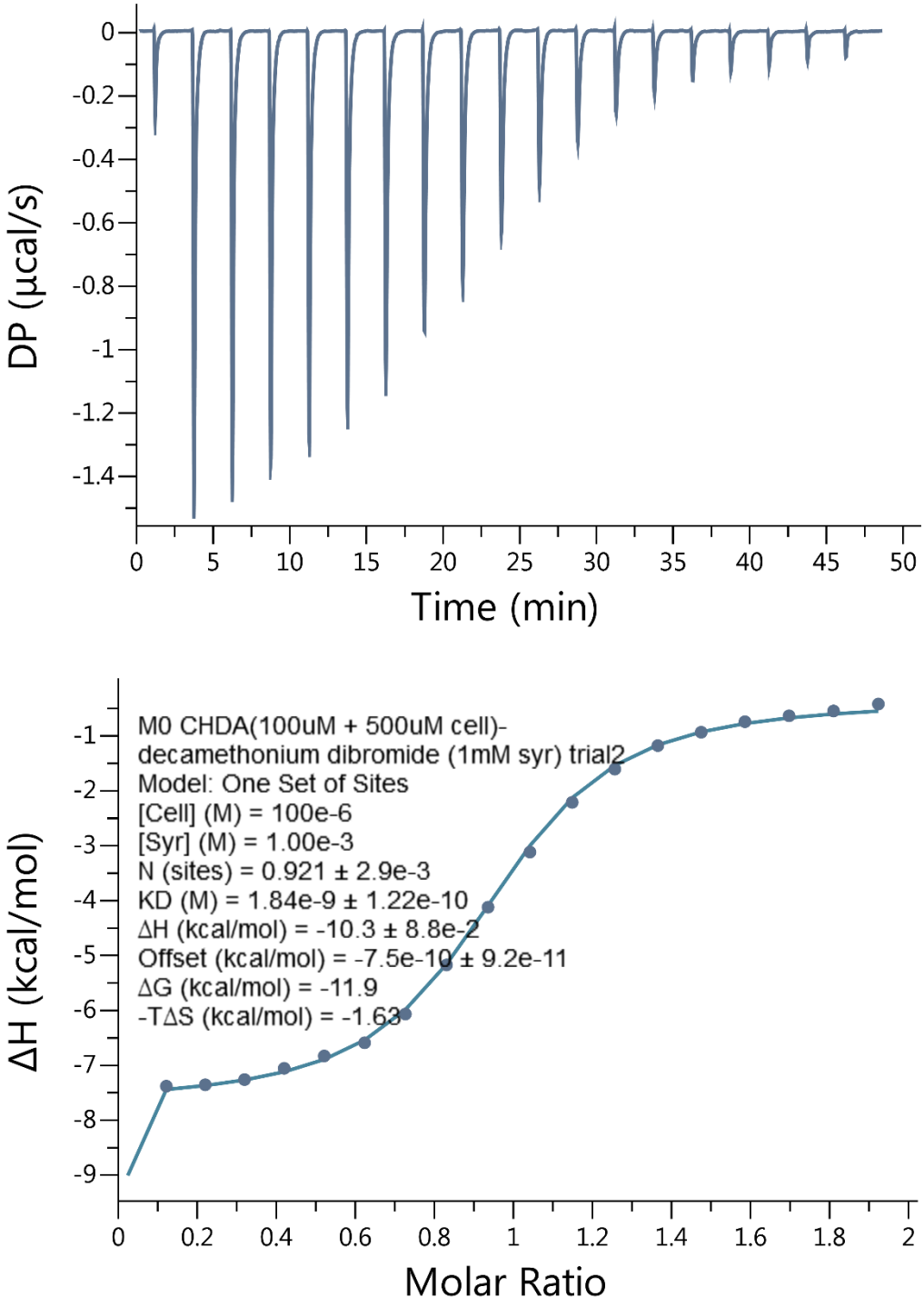

Figure IV-S36. Isothermal Titration Calorimetry (ITC) curve obtained through competition binding studies. A solution of **1** (100 µM) and **13a** (500 µM) in the cell was titrated with **10d** (1.00 mM) in the syringe at 298.0 K in 20 mM sodium phosphate buffered water at pH 7.4. $K_a = 5.43 \times 10^8\ M^{-1}$

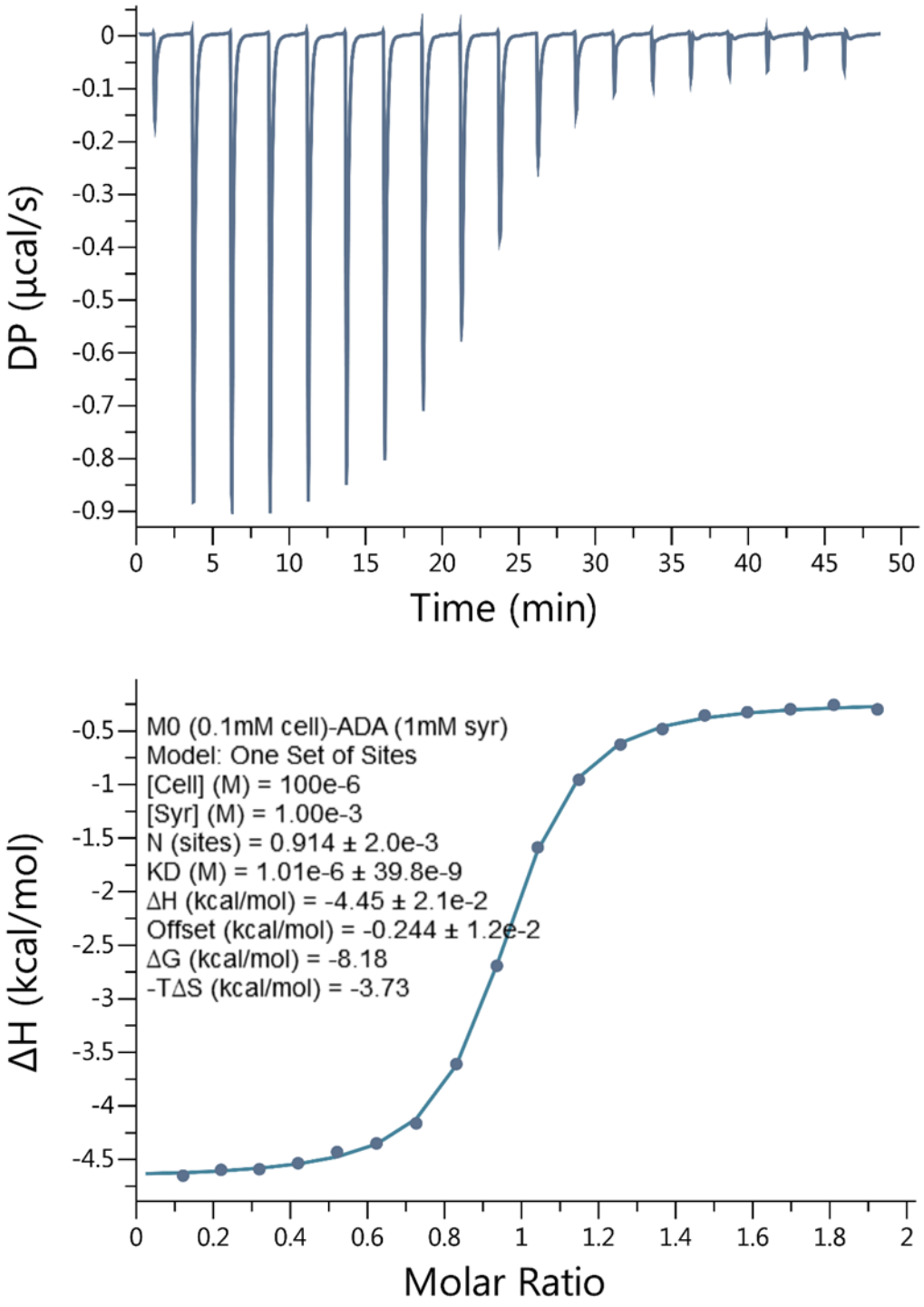

Figure IV-S37. Isothermal Titration Calorimetry (ITC) curve obtained through direct binding studies. A solution of **1** (100 µM) in the cell was titrated with **12a** (1.00 mM) in the syringe at 298.0 K in 20 mM sodium phosphate buffered water at pH 7.4. K_a = 9.90×10^5 M^{-1}

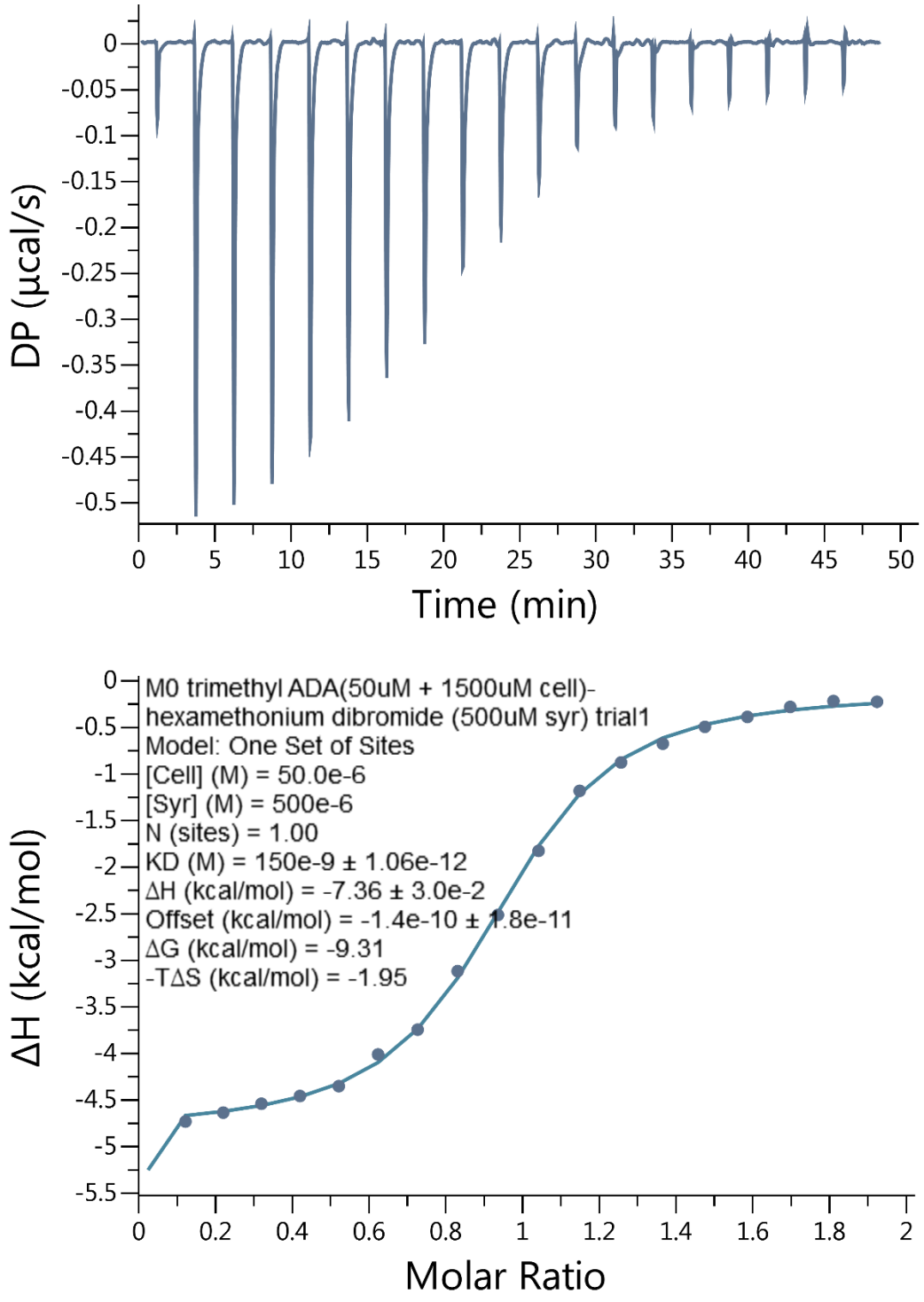

Figure IV-S38. Isothermal Titration Calorimetry (ITC) curve obtained through competition binding studies. A solution of **1** (50 µM) and **12d** (1500 µM) in the cell was titrated with **6d** (500 µM) in the syringe at 298.0 K in 20 mM sodium phosphate buffered water at pH 7.4. $K_a = 6.66 \times 10^6\ M^{-1}$

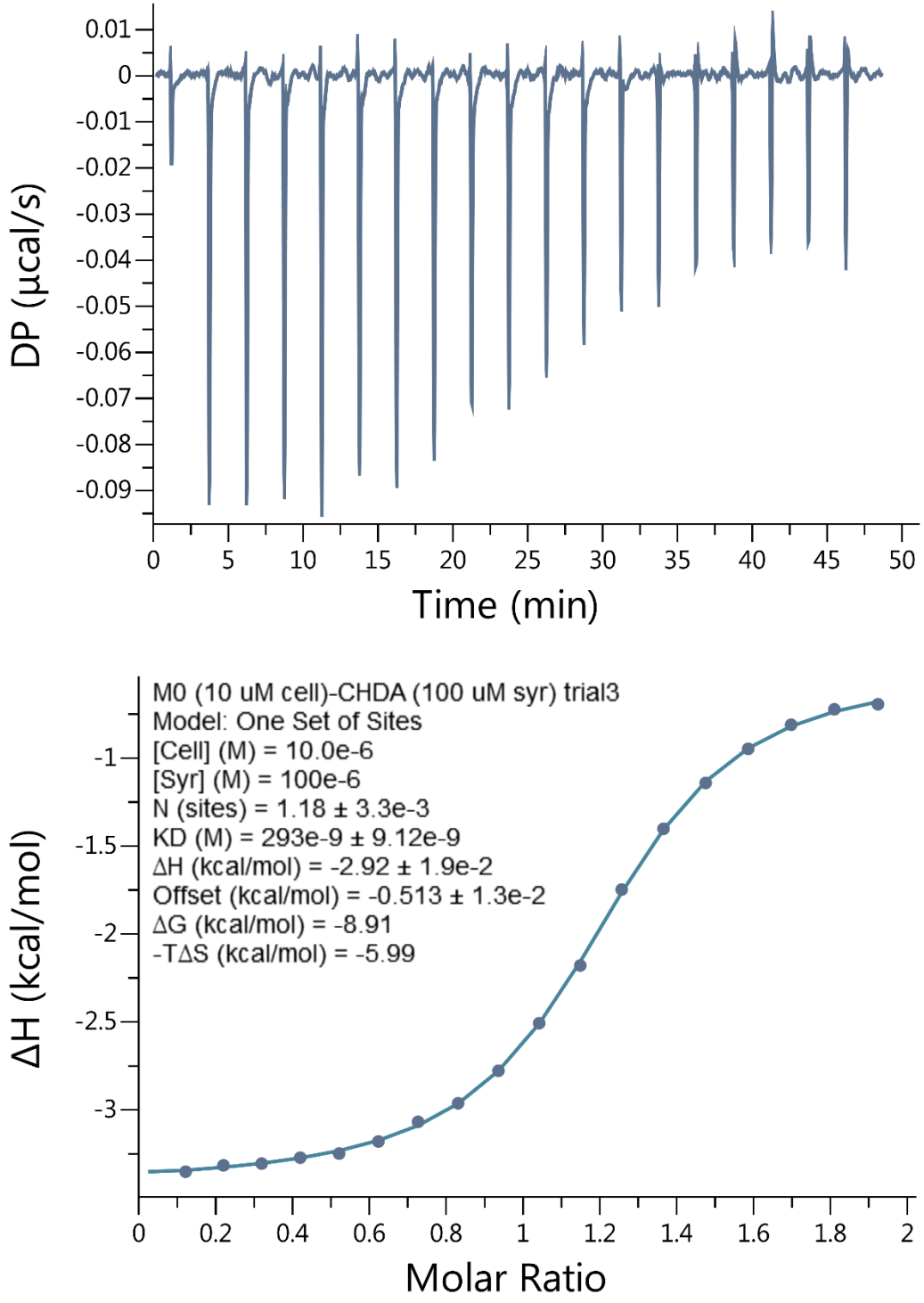

Figure IV-S39. Isothermal Titration Calorimetry (ITC) curve obtained through direct binding studies. A solution of **1** (10.0 µM) in the cell was titrated with **13a** (100 µM) in the syringe at 298.0 K in 20 mM sodium phosphate buffered water at pH 7.4. K_a = 3.41×10^6 M^{-1}.

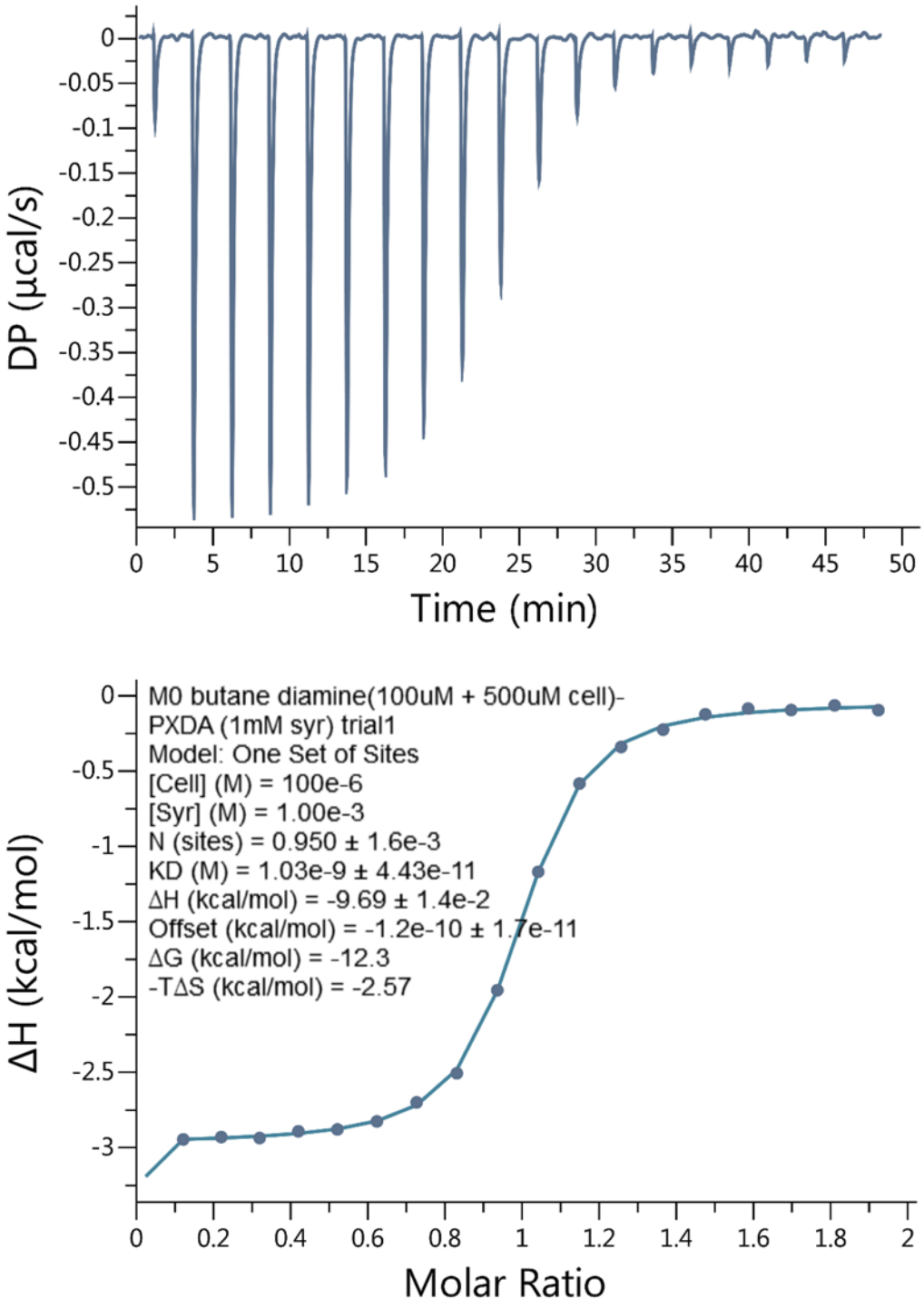

Figure IV-S40. Isothermal Titration Calorimetry (ITC) curve obtained through competition binding studies. A solution of **1** (100 µM) and **5a** (500 µM) in the cell was titrated with **11a** (1.00 mM) in the syringe at 298.0 K in 20 mM sodium phosphate buffered water at pH 7.4. $K_a = 9.71 \times 10^8\ M^{-1}$.

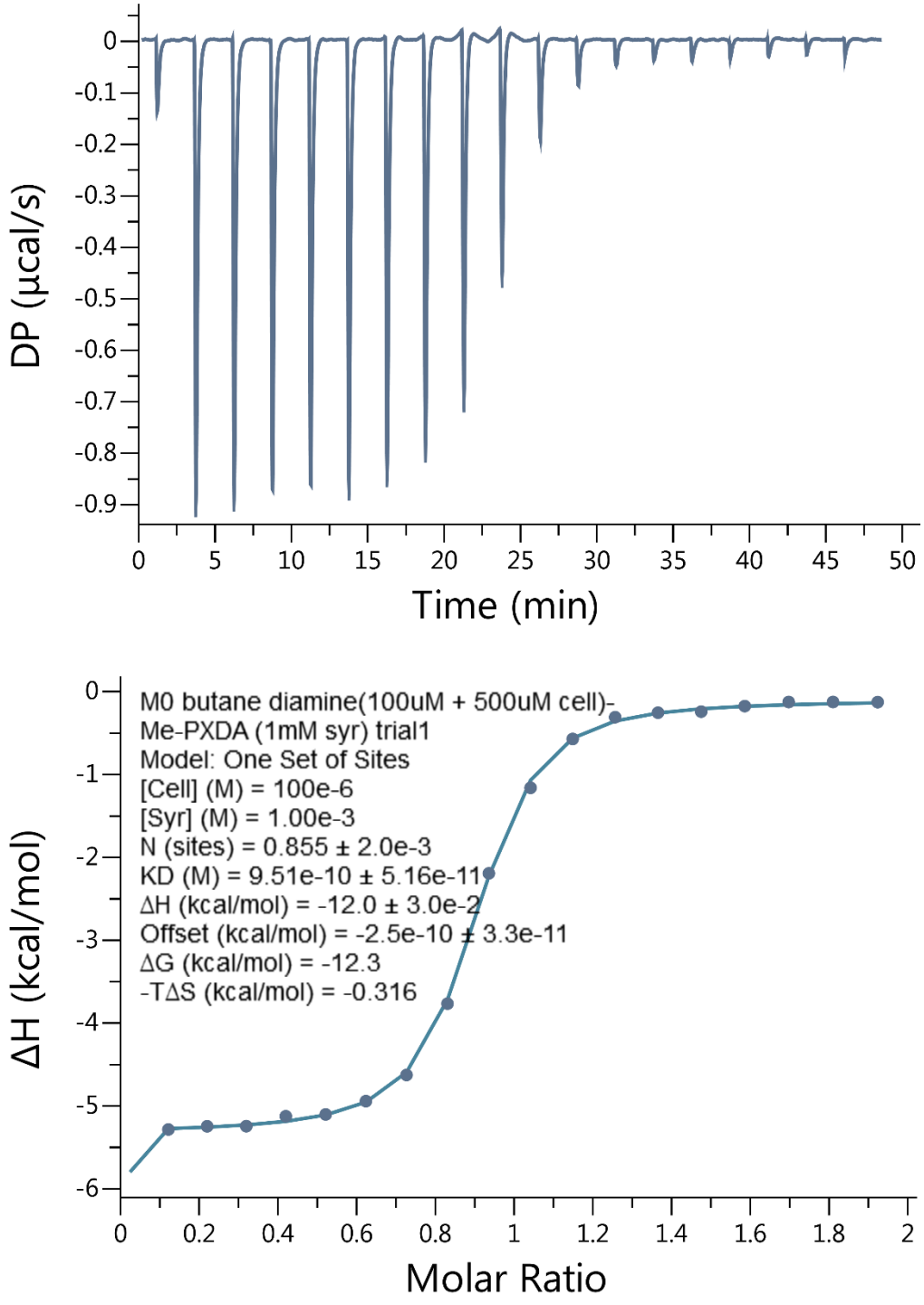

Figure IV-S41. Isothermal Titration Calorimetry (ITC) curve obtained through competition binding studies. A solution of **1** (100 µM) and **5a** (500 µM) in the cell was titrated with **11d** (1.00 mM) in the syringe at 298.0 K in 20 mM sodium phosphate buffered water at pH 7.4. $K_a = 1.05 \times 10^9\ M^{-1}$.

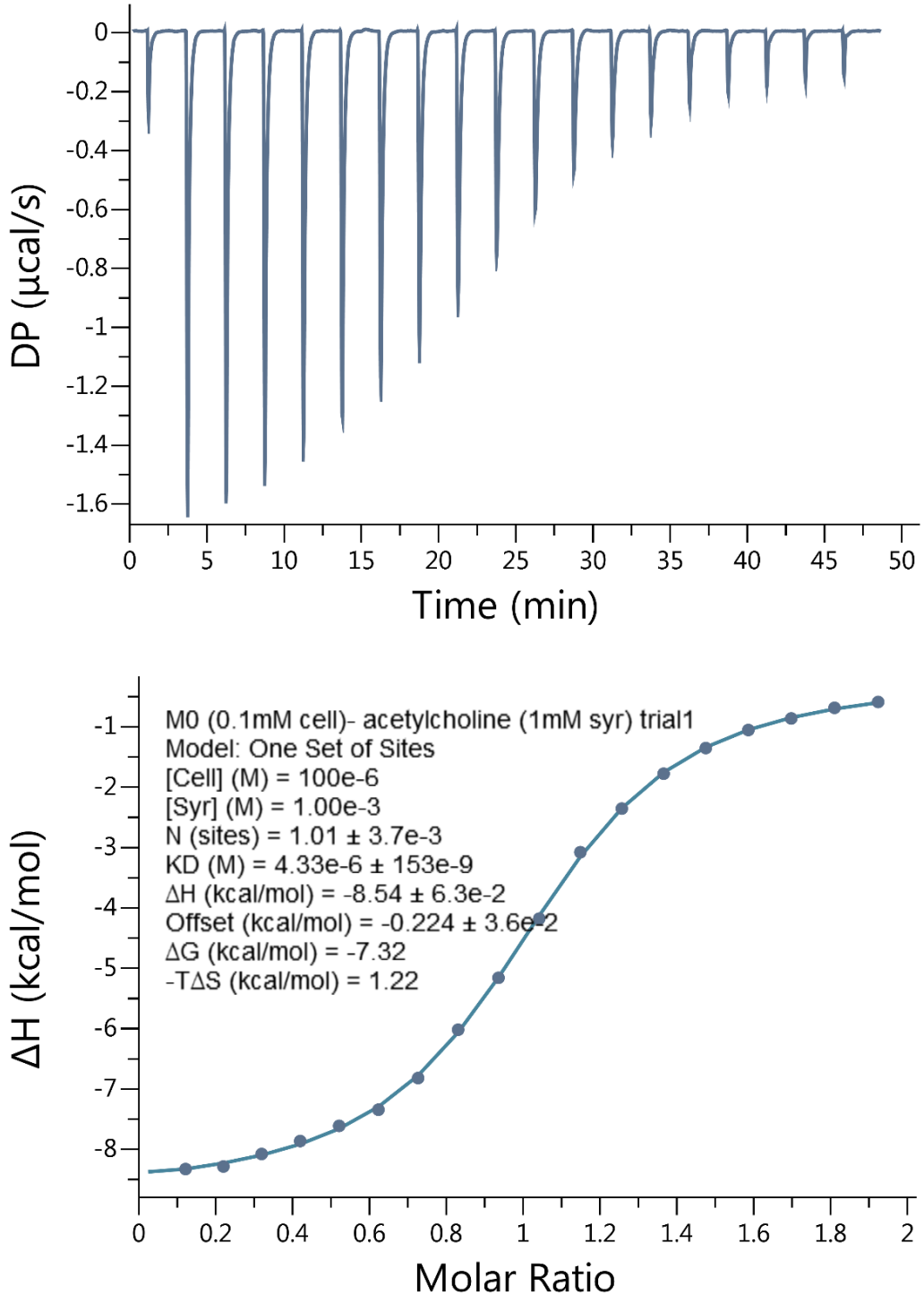

Figure IV-S42. Isothermal Titration Calorimetry (ITC) curve obtained through direct binding studies. A solution of **1** (100.0 µM) in the cell was titrated with **23** (1.00 mM) in the syringe at 298.0 K in 20 mM sodium phosphate buffered water at pH 7.4. K_a = 2.31×10^5 M^{-1}.

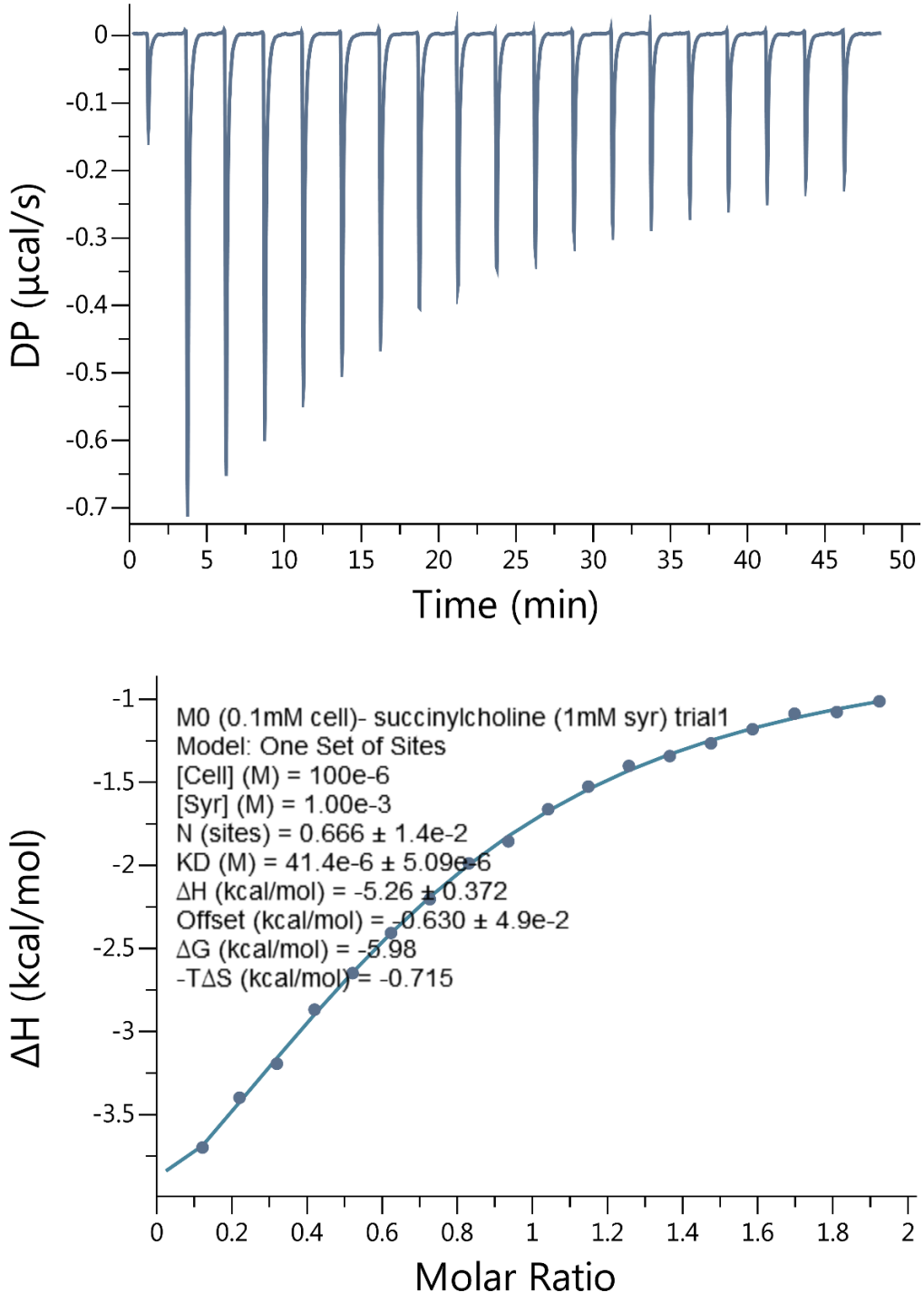

Figure IV-S43. Isothermal Titration Calorimetry (ITC) curve obtained through direct binding studies. A solution of **1** (100.0 µM) in the cell was titrated with **22** (1.00 mM) in the syringe at 298.0 K in 20 mM sodium phosphate buffered water at pH 7.4. K_a = 2.41×10^4 M^{-1}

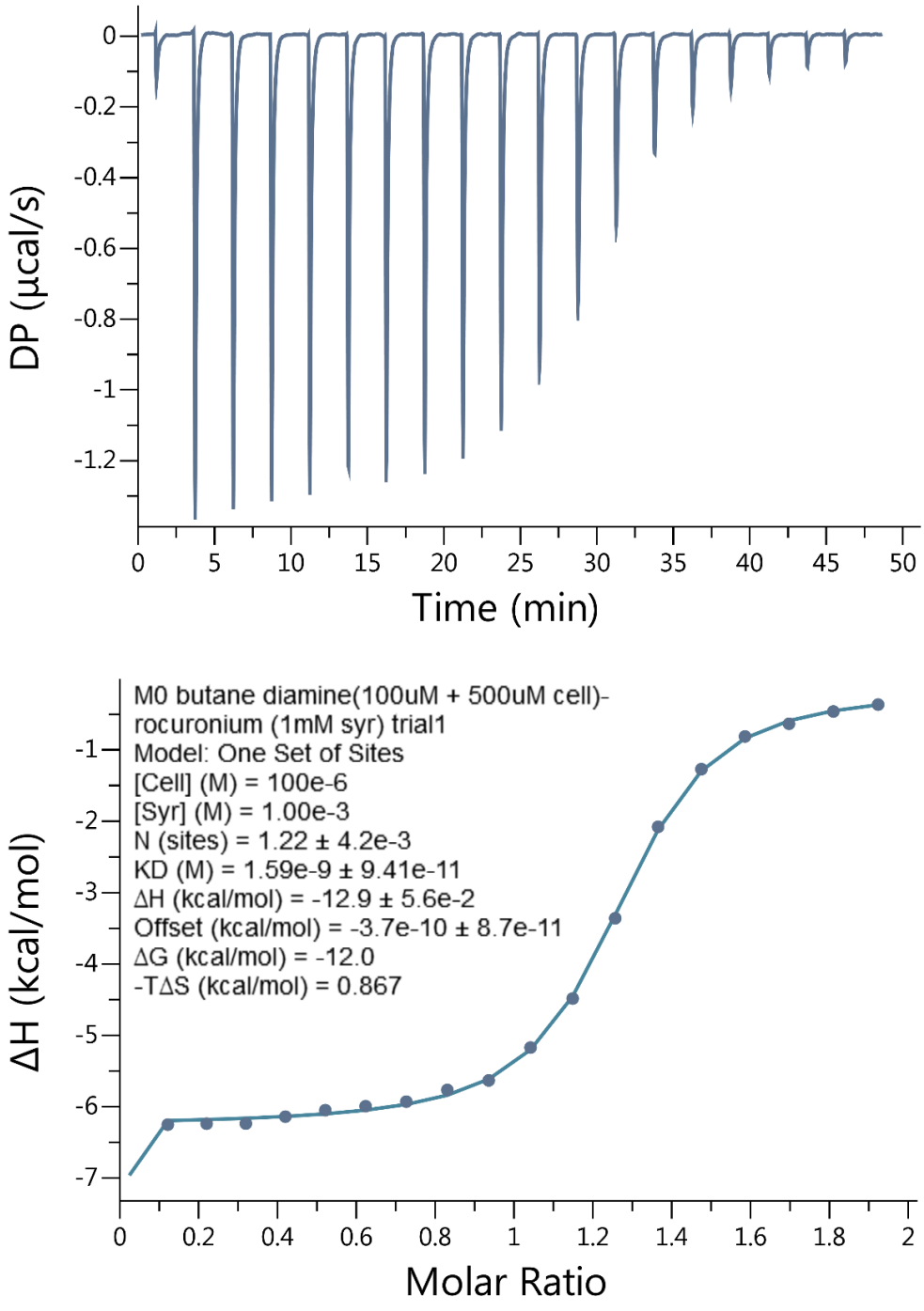

Figure IV-S44. Isothermal Titration Calorimetry (ITC) curve obtained through competition binding studies. A solution of **1** (100 µM) and **5a** (500 µM) in the cell was titrated with **19** (1.00 mM) in the syringe at 298.0 K in 20 mM sodium phosphate buffered water at pH 7.4. $K_a = 6.29 \times 10^8\ M^{-1}$.

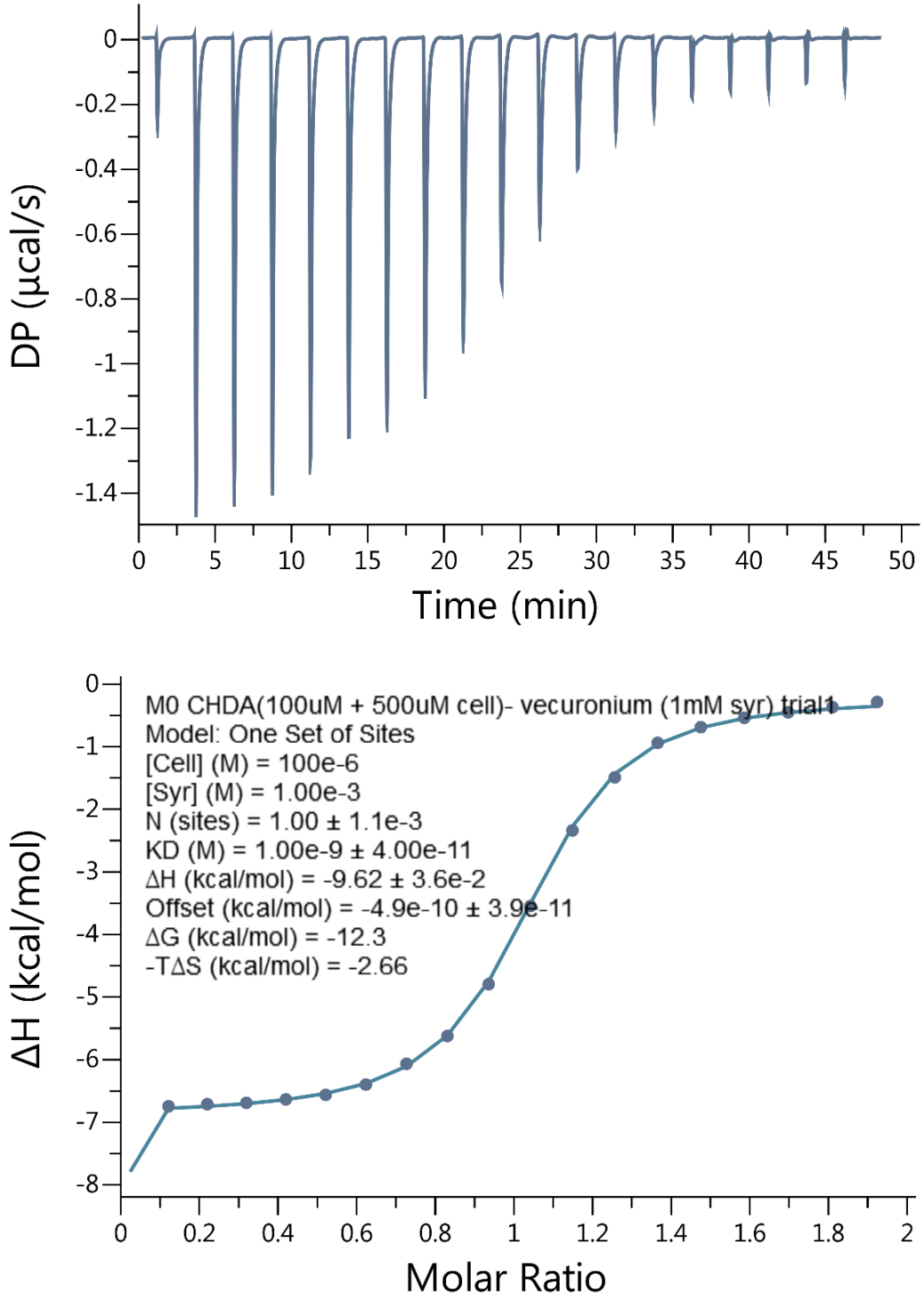

Figure IV-S45. Isothermal Titration Calorimetry (ITC) curve obtained through competition binding studies. A solution of **1** (100 µM) and **13a** (500 µM) in the cell was titrated with **20** (1.00 mM) in the syringe at 298.0 K in 20 mM sodium phosphate buffered water at pH 7.4. $K_a = 1.00 \times 10^9\ M^{-1}$.

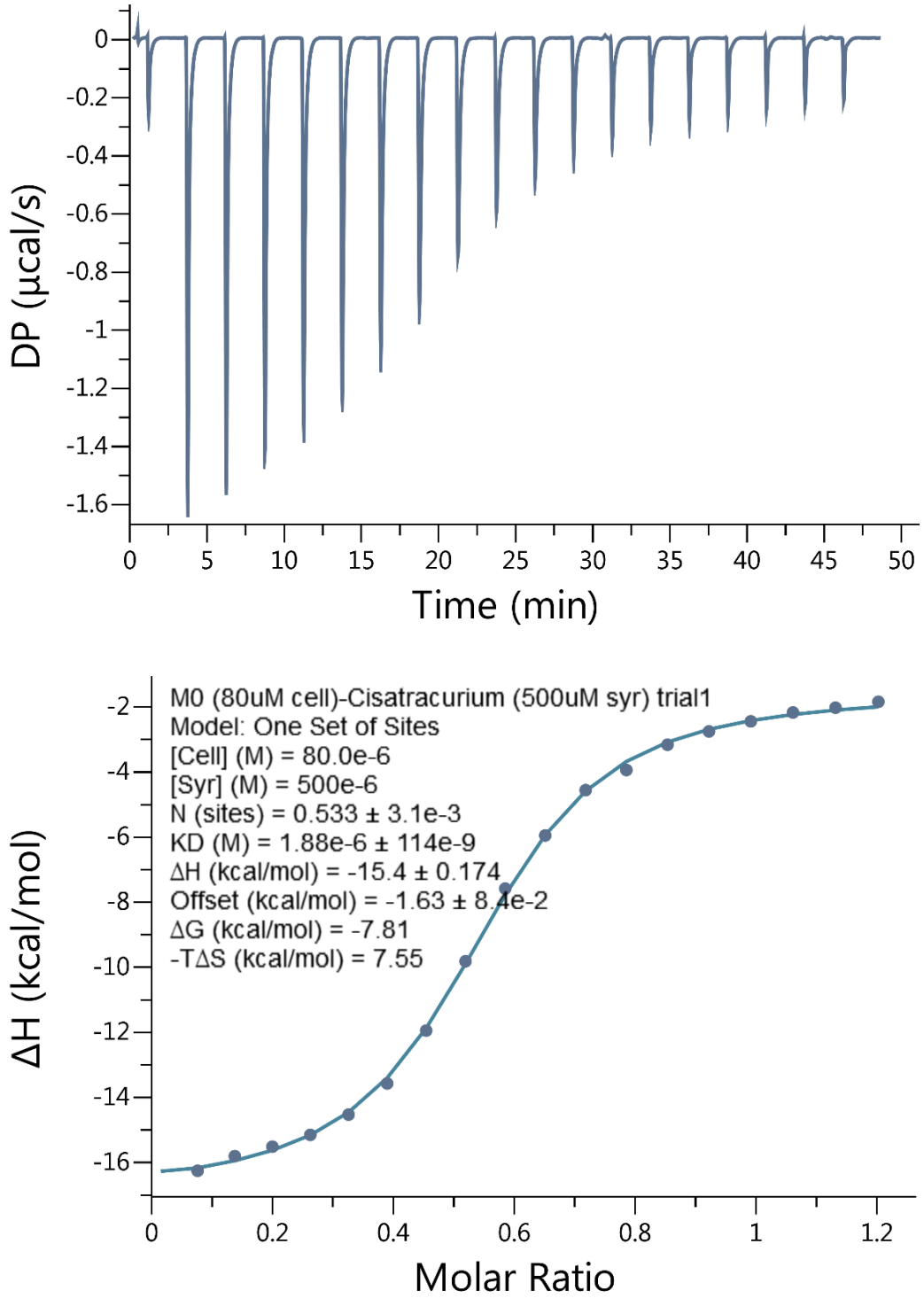

Figure IV-S46. Isothermal Titration Calorimetry (ITC) curve obtained through direct binding studies. A solution of **1** (80.0 µM) in the cell was titrated with **21** (500.0 µM) in the syringe at 298.0 K in 20 mM sodium phosphate buffered water at pH 7.4. K_a = 5.32×10^5 M^{-1}.

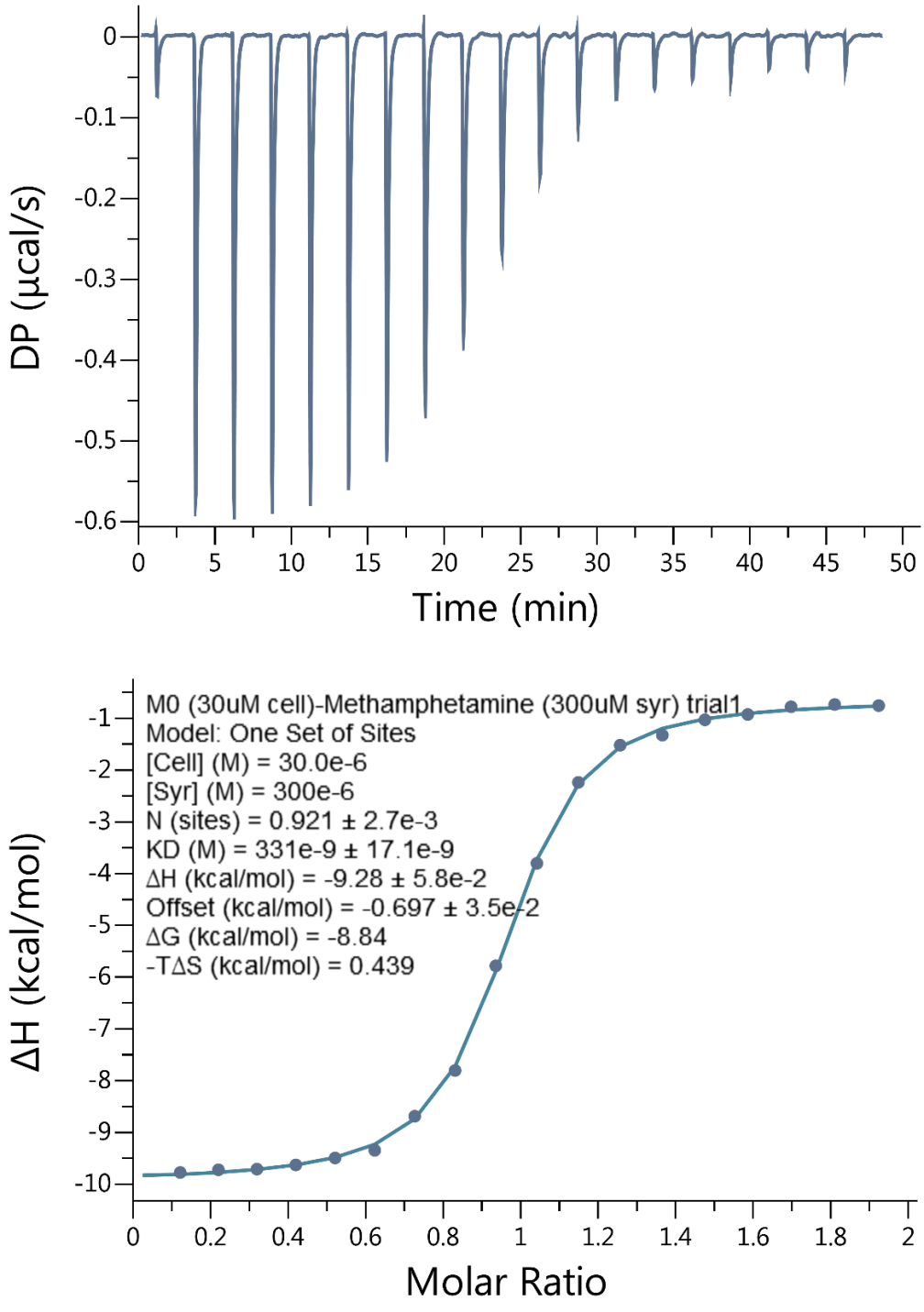

Figure IV-S47. Isothermal Titration Calorimetry (ITC) curve obtained through direct binding studies. A solution of **1** (30.0 µM) in the cell was titrated with **14** (300.0 µM) in the syringe at 298.0 K in 20 mM sodium phosphate buffered water at pH 7.4. K_a = 3.02×10^6 M^{-1}.

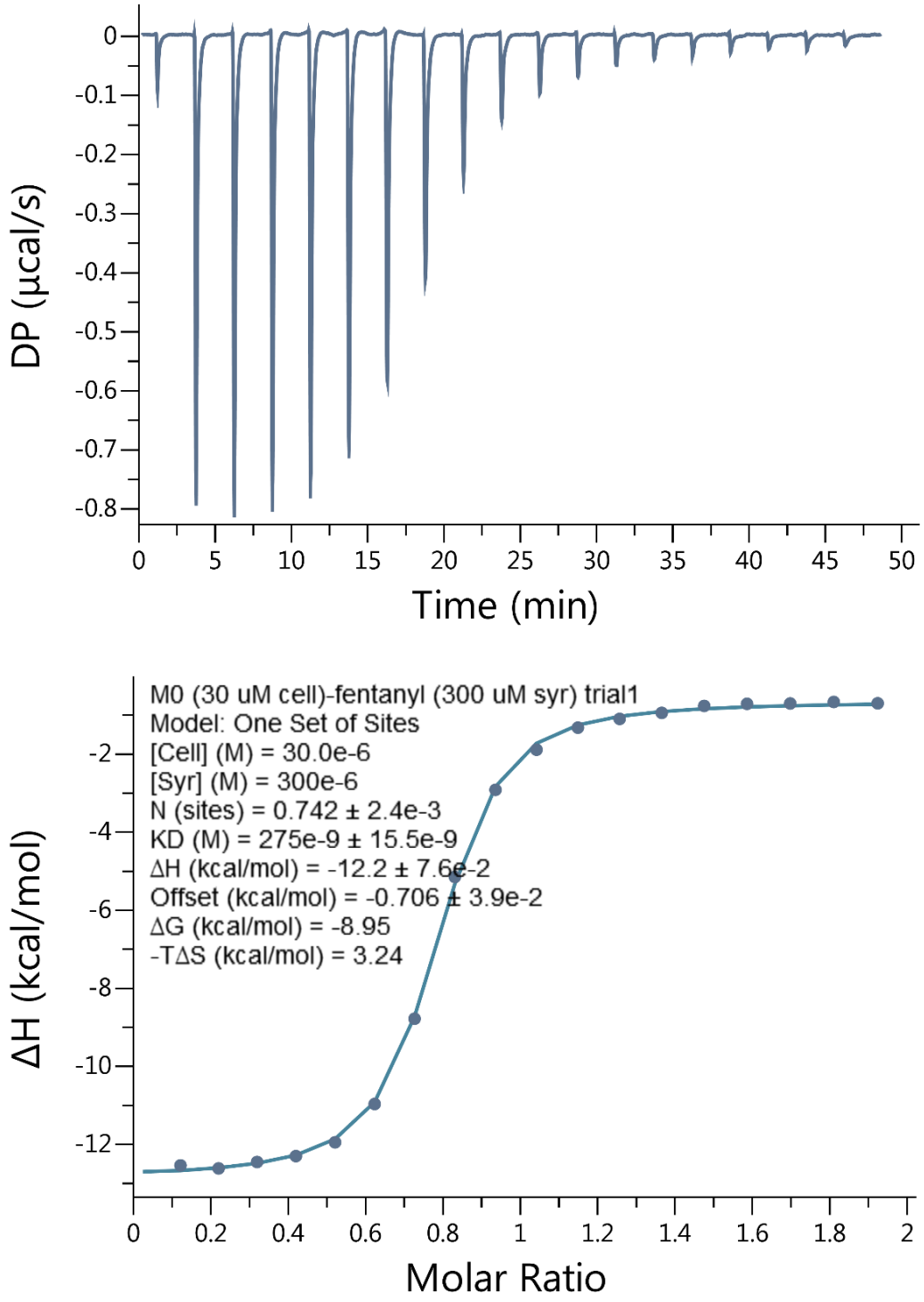

Figure IV-S48. Isothermal Titration Calorimetry (ITC) curve obtained through direct binding studies. A solution of **1** (30.0 µM) in the cell was titrated with **15** (300.0 µM) in the syringe at 298.0 K in 20 mM sodium phosphate buffered water at pH 7.4. K_a = 3.64×10^6 M^{-1}.

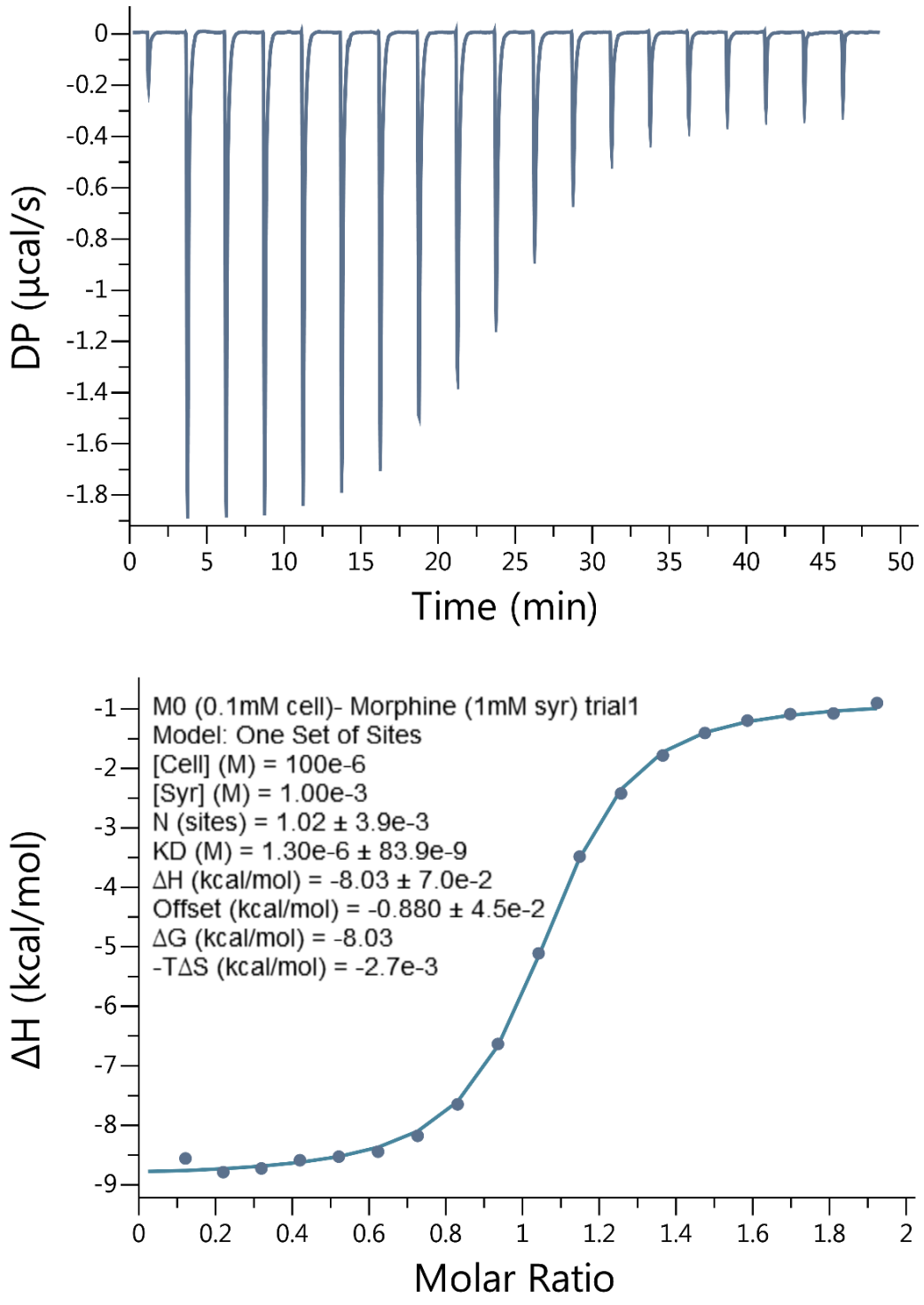

Figure IV-S49. Isothermal Titration Calorimetry (ITC) curve obtained through direct binding studies. A solution of **1** (100.0 µM) in the cell was titrated with **17** (1.00 mM) in the syringe at 298.0 K in 20 mM sodium phosphate buffered water at pH 7.4. K_a = 7.69×10^5 M^{-1}.

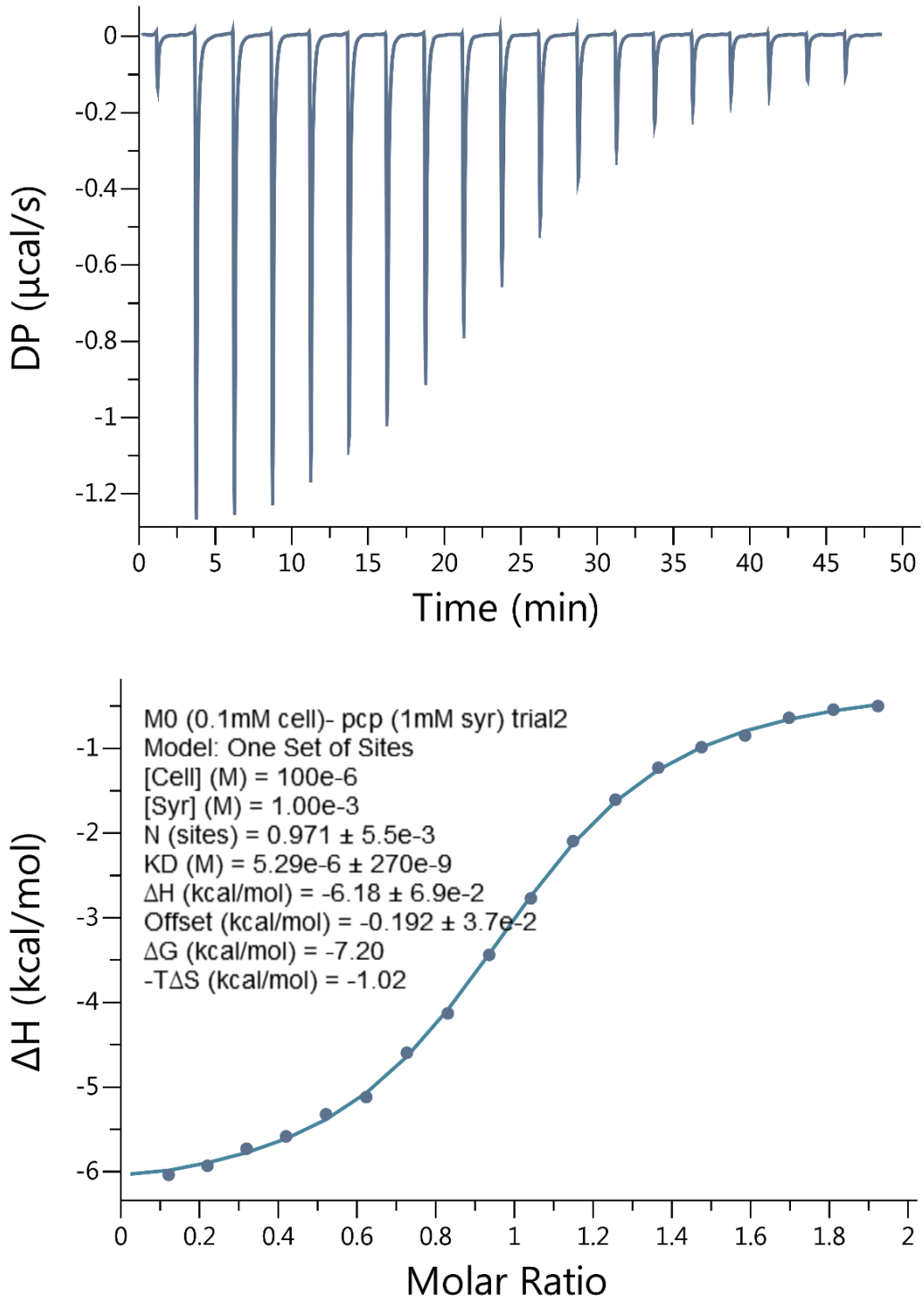

Figure IV-S50. Isothermal Titration Calorimetry (ITC) curve obtained through direct binding studies. A solution of **1** (100.0 µM) in the cell was titrated with **16** (1.00 mM) in the syringe at 298.0 K in 20 mM sodium phosphate buffered water at pH 7.4. K_a = 1.89×10^5 M^{-1}.

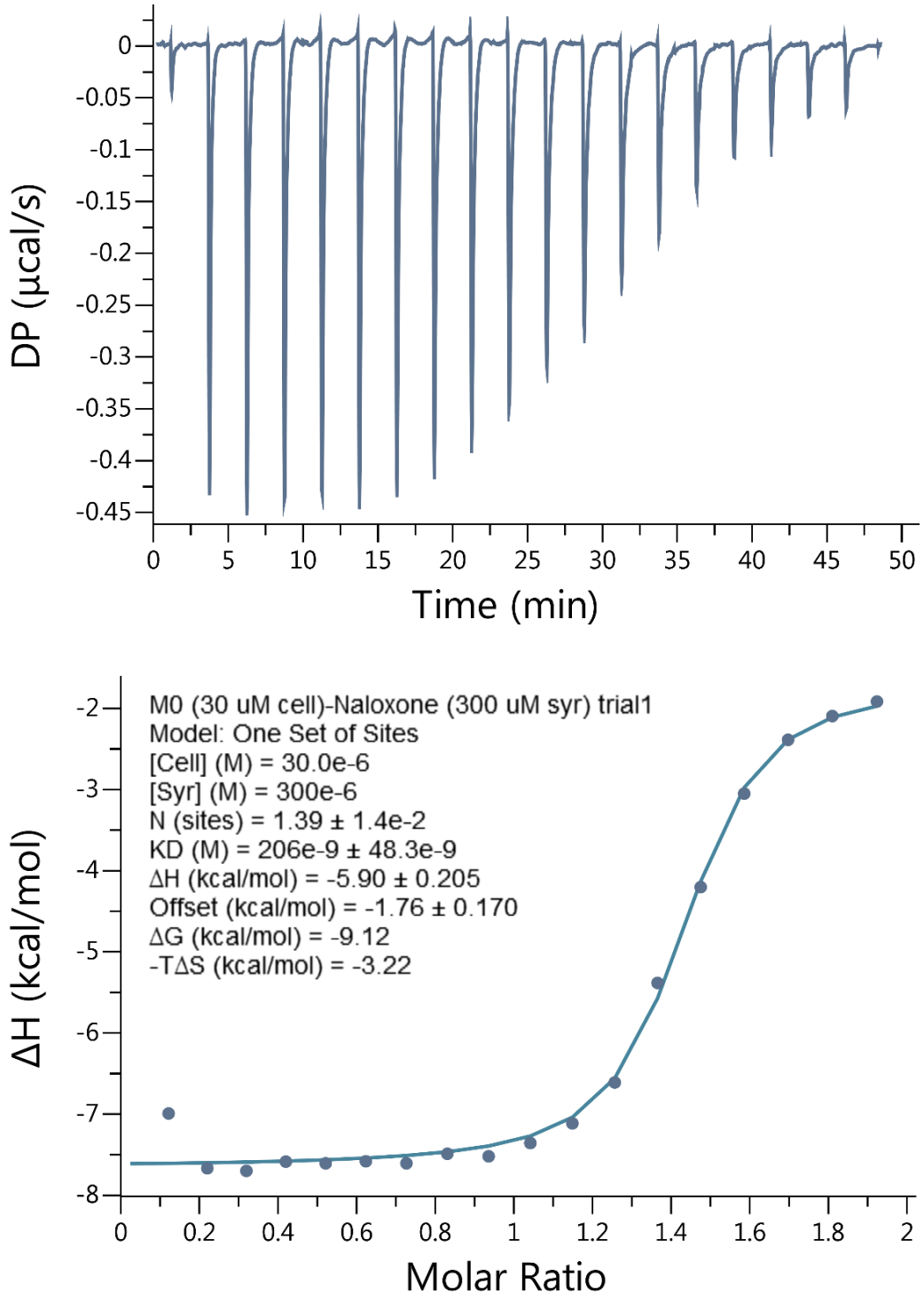

Figure IV-S51. Isothermal Titration Calorimetry (ITC) curve obtained through direct binding studies. A solution of **1** (30.0 µM) in the cell was titrated with **18** (300.00 µM) in the syringe at 298.0 K in 20 mM sodium phosphate buffered water at pH 7.4. $K_a = 4.85 \times 10^6\ M^{-1}$.

Single crystal X-ray data for host 1 and guest 6a and 6d

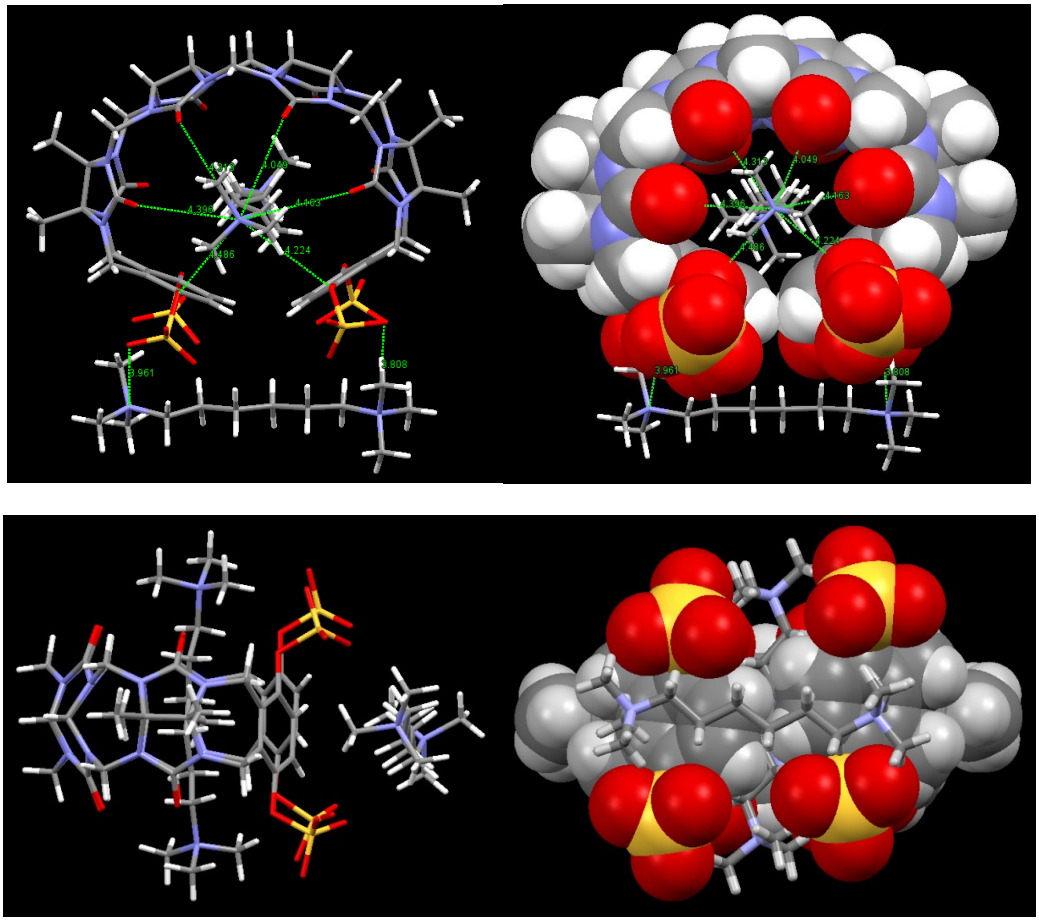

Figure IV-S52. Top view and side view of X-ray single crystal structure of host **1** and guest **6d** (capped sticks of guest **6d** and space fill model of host **1)**.

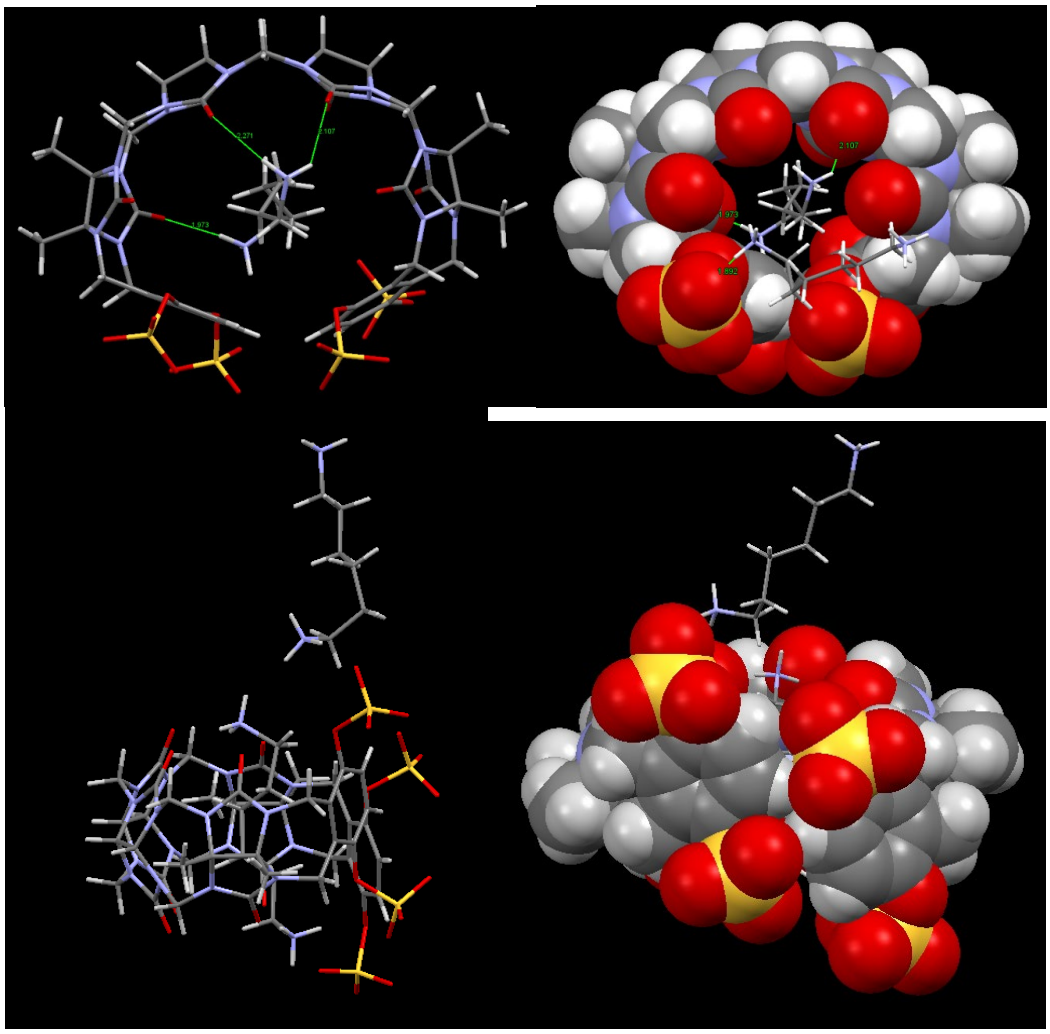

Figure IV-S53. Top view and side view of X-ray single crystal structure of host **1** and guest **6a** (capped sticks of guest 6a and space fill model of host **1**).

Bibliography

1. Lehn, J. M. *Science* **1993**, *260*, 1762-3.

2. Oshovsky, G. V.; Reinhoudt, D. N.; Verboom, W. *Angew. Chem. Int. Ed.* **2007**, *46*, 2366-2393.

3. Persch, E.; Dumele, O.; Diederich, F. *Angew. Chem. Int. Ed.* **2015**, *54*, 3290-3327.

4. Urbach, A. R.; Ramalingam, V. *Isr. J. Chem.* **2011**, *51*, 664-678.

5. Cooper, G. M.; Editor, *The Cell: A Molecular Approach, 2nd Edition*. **2000**, 625.

6. Uhlenheuer, D. A.; Petkau, K.; Brunsveld, L. *Chem. Soc. Rev.* **2010**, *39*, 2817-2826.

7. Ma, D.; Hettiarachchi, G.; Nguyen, D.; Zhang, B.; Wittenberg, J. B.; Zavalij, P. Y.; Briken, V.; Isaacs, L. *Nat. Chem.* **2012**, *4*, 503-510.

8. Doxsee, K. M.; Feigel, M.; Stewart, K. D.; Canary, J. W.; Knobler, C. B.; Cram, D. J. *J. Am. Chem. Soc.* **1987**, *109*, 3098-107.

9. Cram, D. J.; Carmack, R. A.; DeGrandpre, M. P.; Lein, G. M.; Goldberg, I.; Knobler, C. B.; Maverick, E. F.; Trueblood, K. N. *J. Am. Chem. Soc.* **1987**, *109*, 7068-73.

10. Cram, D. J. *Prix Nobel* **1988**, 105-23.

11. Mbarek, A.; Moussa, G.; Chain, J. L. *Molecules* **2019**, *24*, 1803.

12. Fokkens, M.; Schrader, T.; Klarner, F. G. *J. Am. Chem. Soc.* **2005**, *127*, 14415-14421.

13. Sinha, S.; Lopes, D. H. J.; Du, Z. M.; Pang, E. S.; Shanmugam, A.; Lomakin, A.; Talbiersky, P.; Tennstaedt, A.; McDaniel, K.; Bakshi, R.; Kuo, P. Y.; Ehrmann, M.; Benedek, G. B.; Loo, J. A.; Klarner, F. G.; Schrader, T.; Wang, C. Y.; Bitan, G. *J. Am. Chem. Soc.* **2011**, *133*, 16958-16969.

14. Bier, D.; Rose, R.; Bravo-Rodriguez, K.; Bartel, M.; Ramirez-Anguita, J. M.; Dutt, S.; Wilch, C.; Klärner, F. G.; Sanchez-Garcia, E.; Schrader, T.; Ottmann, C. *Nat Chem* **2013**, *5*, 234-9.

15. Sinha, S.; Lopes, D. H. J.; Bitan, G. *Acs Chemical Neuroscience* **2012**, *3*, 473-481.

16. Rowan, A. E.; Elemans, J. A. A. W.; Nolte, R. J. M. *Acc. Chem. Res.* **1999**, *32*, 995-1006.

17. Hernandez-Alonso, D.; Zankowski, S.; Adriaenssens, L.; Ballester, P. *Org. Biomol. Chem.* **2015**, *13*, 1022-1029.

18. Nimse, S. B.; Kim, T. *Chem. Soc. Rev.* **2013**, *42*, 366-386.

19. Gutsche, C. D.; Levine, J. A. *J. Am. Chem. Soc.* **1982**, *104*, 2652-3.

20. Gutsche, C. D. *Acc. Chem. Res.* **1983**, *16*, 161-70.

21. Ukhatskaya, E. V.; Kurkov, S. V.; Matthews, S. E.; Loftsson, T. *Journal of Pharmaceutical Sciences* **2013,** *102*, 3485-3512.

22. Fucke, K.; Anderson, K. M.; Filby, M. H.; Henry, M.; Wright, J.; Mason, S. A.; Gutmann, M. J.; Barbour, L. J.; Oliver, C.; Coleman, A. W.; Atwood, J. L.; Howard, J. A. K.; Steed, J. W. *Chem. Eur. J.* **2011**, *17*, 10259-10271.

23. Wang, K.; Guo, D.-S.; Zhang, H.-Q.; Li, D.; Zheng, X.-L.; Liu, Y. *J. Med. Chem.* **2009**, *52*, 6402-6412.

24. Guo, D.-S.; Liu, Y. *Acc. Chem. Res.* **2014**, *47*, 1925-1934.

25. Dalal, D. S.; Patil, D. R.; Tayade, Y. A. *Chem. Rec.* **2018**, *18*, 1560-1582.

26. Zare Asadabadi, A.; Hoseini, S. J.; Bahrami, M.; Nabavizadeh, S. M. *New J. Chem.* **2019**, *43*, 6513-6522.

27. Beatty, M. A.; Selinger, A. J.; Li, Y.; Hof, F. *J. Am. Chem. Soc.* **2019,** *141*, 16763-16771.

28. Motoyama, A.; Suzuki, A.; Shirota, O.; Namba, R. *J. Pharm. Biomed. Anal.* **2002**, *28*, 97-106.

29. Harada, A.; Kawaguchi, Y.; Hoshino, T. *J. Inclusion Phenom. Macrocyclic Chem.* **2001,** *41*, 115-121.

30. febreze https://www.febreze.com/en-us.

31. Lockwood, S. F.; O'Malley, S.; Mosher, G. L. *J. Pharm. Sci.* **2003**, *92*, 922-926.

32. Bom, A.; Bradley, M.; Cameron, K.; Clark, J. K.; Van Egmond, J.; Feilden, H.; MacLean, E. J.; Muir, A. W.; Palin, R.; Rees, D. C.; Zhang, M.-Q. *Angew. Chem., Int. Ed.* **2002**, *41*, 265-270.

33. Gassensmith, J. J.; Baumes, J. M.; Smith, B. D. *Chem. Commun.* **2009**, 6329-6338.

34. Diederich, F. *Angew. Chem. Intl. Ed. Engl.* **1988**, *27*, 362-386.

35. Tang, D.; Barnett, J.; Gibb, B.; Ashbaugh, H. *J. Am. Chem. Soc.* **2018**, 391.

36. Jordan, J.; Gibb, C.; Gibb, B. *J. Am. Chem. Soc.* **2017**,65.

37. Jordan, J.; Gibb, B. *J. Am. Chem. Soc.* **2016**, 609.

38. Davis, A. *Angew. Chem. Int. Ed.* **2001**, *40*, 800.

39. Yang, K.; Pei, Y.; Wen, J.; Pei, Z. *Chem. Commun.* **2016**, *52*, 9316-9326.

40. Li, C. *Chem. Commun.* **2014**, *50*, 12420-12433.

41. Stoddart, J. F. *Angew. Chem. Int. Ed.* **2017**, *56*, 11094-11125.

42. Cao; Fyfe; Stoddart; Cousins; Glink. *J. Org. Chem.* **2000**, *65*, 1937-46.

43. Balzani, V.; Credi; Raymo; Stoddart. *Angew. Chem. Int. Ed. Engl.* **2000**, *39*, 3348-3391.

44. Anamimoghadam, O.; Nguyen, M. T.; Cooper, J. A.; Pezzato, C.; Patel, H.; Stoddart, J. F. *J. Am. Chem. Soc.* **2018**, 509.

45. Rebek, J. *Acc. Chem. Res.* **2009**, *42*, 1660-1668.

46. Sijbesma, R. P.; Kentgens, A. P. M.; Lutz, E. T. G.; van der Maas, J. H.; Nolte, R. J. M. *J. Am. Chem. Soc.* **1993**, *115*, 8999-9005.

47. Lee, J. W.; Samal, S.; Selvapalam, N.; Kim, H.-J.; Kim, K. *Acc. Chem. Res.* **2003**, *36*, 621-630.

48. Nau, W. M.; Florea, M.; Assaf, K. I. *Isr. J. Chem.* **2011**, *51*, 559-577.

49. Masson, E.; Ling, X.; Joseph, R.; Kyeremeh-Mensah, L.; Lu, X. *RSC Adv.* **2012,** *2*, 1213-1247.

50. Isaacs, L. *Acc. Chem. Res.* **2014**, *47*, 2052-2062.

51. Wu, F.; Wu, L.-H.; Xiao, X.; Zhang, Y.-Q.; Xue, S.-F.; Tao, Z.; Day, A. I. *J. Org. Chem.* **2012**, *77*, 606-611.

52. Kim, J.; Jung, I.-S.; Kim, S.-Y.; Lee, E.; Kang, J.-K.; Sakamoto, S.; Yamaguchi, K.; Kim, K. *J. Am. Chem. Soc.* **2000**, *122*, 540-541.

53. Barrow, S. J.; Kasera, S.; Rowland, M. J.; del Barrio, J.; Scherman, O. A. *Chem. Rev.* **2015**, *115*, 12320-12406.

54. Assaf, K. I.; Nau, W. M. *Chem. Soc. Rev.* **2015**, *44*, 394-418.

55. Lagona, J.; Mukhopadhyay, P.; Chakrabarti, S.; Isaacs, L. *Angew. Chem. Int. Ed.* **2005**, *44*, 4844-4870.

56. Cao, L. P.; Skalamera, D.; Zavalij, P. Y.; Hostas, J.; Hobza, P.; Mlinaric-Majerski, K.; Glaser, R.; Isaacs, L. *Org. Biomol. Chem.* **2015**, *13*, 6249-6254.

57. Biedermann, F.; Uzunova, V. D.; Scherman, O. A.; Nau, W. M.; De Simone, A. *J. Am. Chem. Soc.* **2012**, *134*, 15318-15323.

58. Mock, W. L.; Shih, N. Y. *J. Org. Chem.* **1986,** *51*, 4440-6.

59. Liu, S.; Ruspic, C.; Mukhopadhyay, P.; Chakrabarti, S.; Zavalij, P. Y.; Isaacs, L. *J. Am. Chem. Soc.* **2005**, *127*, 15959-15967.

60. Cao, L.; Sekutor, M.; Zavalij, P. Y.; Mlinaric-Majerski, K.; Glaser, R.; Isaacs, L. *Angew. Chem. Int. Ed.* **2014**, *53*, 988-993.

61. Biedermann, F.; Rauwald, U.; Cziferszky, M.; Williams, K. A.; Gann, L. D.; Guo, B. Y.; Urbach, A. R.; Bielawski, C. W.; Scherman, O. A. *Chem. Eur. J.* **2010**, *16*, 13716-13722.

62. Ma, D.; Zhang, B.; Hoffmann, U.; Sundrup, M. G.; Eikermann, M.; Isaacs, L. *Angew. Chem. Int. Ed.* **2012**, *51*, 11358-11362.

63. Chinai, J. M.; Taylor, A. B.; Ryno, L. M.; Hargreaves, N. D.; Morris, C. A.; Hart, P. J.; Urbach, A. R. *J. Am. Chem. Soc.* **2011**, *133*, 8810-8813.

64. Angelos, S.; Khashab, N. M.; Yang, Y.-W.; Trabolsi, A.; Khatib, H. A.; Stoddart, J. F.; Zink, J. I. *J. Am. Chem. Soc.* **2009**, *131*, 12912-12914.

65. Hirani, Z.; Taylor, H. F.; Babcock, E. F.; Bockus, A. T.; Varnado, C. D.; Bielawski, C. W.; Urbach, A. R. *J. Am. Chem. Soc.* **2018**, *140*, 12263-12269.

66. Logsdon, L. A.; Schardon, C. L.; Ramalingam, V.; Kwee, S. K.; Urbach, A. R. *J. Am. Chem. Soc.* **2011**, *133*, 17087-17092.

67. Rekharsky, M. V.; Yamamura, H.; Ko, Y. H.; Selvapalam, N.; Kim, K.; Inoue, Y. *Chem. Commun.* **2008**, 2236-2238.

68. Sonzini, S.; Ryan, S. T. J.; Scherman, O. A. *Chem. Commun.* **2013**, *49*, 8779-8781.

69. Tian, F.; Cziferszky, M.; Jiao, D.-Z.; Wahlstrom, K.; Geng, J.; Scherman, O. A. *Langmuir* **2011**, *27*, 1387-1390.

70. Buschmann, H. J.; Jansen, K.; Schollmeyer, E. *Thermochim. Acta* **1998**, *317*, 95-98.

71. Buschmann, H. J.; Schollmeyer, E.; Mutihac, L. *Thermochim. Acta* **2003**, *399*, 203-208.

72. Kim, H.-J.; Heo, J.; Jeon, W. S.; Lee, E.; Kim, J.; Sakamoto, S.; Yamaguchi, K.; Kim, K. *Angew. Chem. Int. Ed.* **2001**, *40*, 1526-1529.

73. Kim, K.; Kim, J.; Jung, I.-s.; Kim, S.-y.; Lee, E.; Kang, J.-k. Cucurbituril derivatives, their preparation and uses. EP1094065A2, 2001.

74. Rajgariah, P.; Urbach, A. R. *Journal of Inclusion Phenomena and Macrocyclic Chemistry* **2008**, *62*, 251-254.

75. Radzicka, A.; Wolfenden, R. *Biochemistry* **1988**, *27*, 1664-70.

76. Chothia, C. *J. Mol. Biol.* **1976**, *105*, 1-12.

77. Bush, M. E.; Bouley, N. D.; Urbach, A. R. *J. Am. Chem. Soc.* **2005**, *127*, 14511-14517.

78. Assaf, K. I.; Nau, W. M. *Chem Soc Rev* **2015**, *44*, 394-418.

79. Biedermann, F.; Nau, W. M.; Schneider, H.-J. *Angew. Chem. Int. Ed.* **2014**, *53*, 11158-11171.

80. Ling, Y.; Wang, W.; Kaifer, A. E. *Chem. Commun.* **2007**, 610-612.

81. Lagona, J.; Wagner, B. D.; Isaacs, L. *J. Org. Chem.* **2006**, *71*, 1181-1190.

82. Huang, W.-H.; Zavalij, P. Y.; Isaacs, L. *Angew. Chem. Int. Ed.* **2007**, *46*, 7425-7427.

83. Rekharsky, M. V.; Mori, T.; Yang, C.; Ko, Y. H.; Selvapalam, N.; Kim, H.; Sobransingh, D.; Kaifer, A. E.; Liu, S.; Isaacs, L.; Chen, W.; Moghaddam, S.; Gilson, M. K.; Kim, K.; Inoue, Y. *Proc. Natl. Acad. Sci.* **2007**, *104*, 20737-20742.

84. Buschmann, H.-J.; Mutihac, L.; Mutihac, R.-C.; Schollmeyer, E. *Thermochim. Acta* **2005**, *430*, 79-82.

85. Zhang, H.; Grabenauer, M.; Bowers, M. T.; Dearden, D. V. *J. Phys. Chem. A* **2009**, *113*, 1508-1517.

86. Reczek, J. J.; Kennedy, A. A.; Halbert, B. T.; Urbach, A. R. *J. Am. Chem. Soc.* **2009**, *131*, 2408-2415.

87. Heitmann, L. M.; Taylor, A. B.; Hart, P. J.; Urbach, A. R. *J. Am. Chem. Soc.* **2006**, *128*, 12574-12581.

88. Rekharsky, M. V.; Yamamura, H.; Inoue, C.; Kawai, M.; Osaka, I.; Arakawa, R.; Shiba, K.; Sato, A.; Ko, Y. H.; Selvapalam, N.; Kim, K.; Inoue, Y. *J. Am. Chem. Soc.* **2006**, *128*, 14871-80.

89. Lei, W.; Jiang, G.; Zhou, Q.; Zhang, B.; Wang, X. *Phys Chem Chem Phys* **2010**, *12*, 13255-60.

90. Bhasikuttan, A. C.; Mohanty, J.; Nau, W. M.; Pal, H. *Angew. Chem. Int. Ed.* **2007**, *46*, 4120-4122.

91. Lucas, D.; Isaacs, L. *Org. Lett.* **2011**, *13*, 4112-4115.

92. Huang, W.-H.; Zavalij, P. Y.; Isaacs, L. *J. Am. Chem. Soc.* **2008**, *130*, 8446-8454.

93. Shen, C.; Ma, D.; Meany, B.; Isaacs, L.; Wang, Y. *J. Am. Chem. Soc.* **2012**, *134*, 7254-7257.

94. Ma, D.; Zavalij, P. Y.; Isaacs, L. *J. Org. Chem.* **2010**, *75*, 4786-4795.

95. Ganapati, S.; Isaacs, L. *Isr. J. Chem.* **2018**, *58*, 250-263.

96. Ganapati, S.; Zavalij, P. Y.; Eikermann, M.; Isaacs, L. *Org. Biomol. Chem.* **2016**, *14*, 1277-1287.

97. Haerter, F.; Simons, J. C. P.; Foerster, U.; Duarte, I. M.; Diaz-Gil, D.; Ganapati, S.; Eikermann-Haerter, K.; Ayata, C.; Zhang, B.; Blobner, M.; Isaacs, L.; Eikermann, M. *Anesthesiology* **2015**, *123*, 1337-1349.

98. Ganapati, S.; Grabitz, S. D.; Murkli, S.; Scheffenbichler, F.; Rudolph, M. I.; Zavalij, P. Y.; Eikermann, M.; Isaacs, L. *ChemBioChem* **2017**, *18*, 1583-1588.

99. Ndendjio, S. Z.; Liu, W.; Yvanez, N.; Meng, Z.; Zavalij, P. Y.; Isaacs, L. *New J. Chem.* **2019**, Ahead of Print.

100. Zhang, B.; Zavalij, P. Y.; Isaacs, L. *Org. Biomol. Chem.* **2014**, *12*, 2413-2422.

101. Sigwalt, D.; Zavalij, P. Y.; Isaacs, L. *Supramol. Chem.* **2016**, *28*, 825-834.

102. Zhang, B.; Isaacs, L. *J. Med. Chem.* **2014**, *57*, 9554-9563.

103. An, W. F. *Methods Mol. Biol.* **2009**, *486*, 97-107.

104. Minami T, E. N., Zhang B, Isaacs L, Anzenbacher P.J. *Chem Commun* **2013**.

105. Minami, T.; Esipenko, N. A.; Zhang, B.; Isaacs, L.; Nishiyabu, R.; Kubo, Y.; Anzenbacher, P. *J. Am. Chem. Soc.* **2012**, *134*, 20021-20024.

106. Minami, T.; Esipenko, N. A.; Akdeniz, A.; Zhang, B.; Isaacs, L.; Anzenbacher, P. *J. Am. Chem. Soc.* **2013**, *135*, 15238-15243.

107. Shcherbakova, E. G.; Zhang, B.; Gozem, S.; Minami, T.; Zavalij, P. Y.; Pushina, M.; Isaacs, L. D.; Anzenbacher, P. *J. Am. Chem. Soc.* **2017**, *139*, 14954-14960.

108. Lu, X.; Samanta, S. K.; Zavalij, P. Y.; Isaacs, L. *Angew. Chem. Int. Ed.* **2018**, *57*, 8073-8078.

109. Swager, T. M. *Acc. Chem. Res.* **2008**, *41*, 1181-1189.

110. Ansari, M.; Bera, R.; Mondal, S.; Das, N. *ACS Omega* **2019**, *4*, 9383-9392.

111. Chakraborty, S.; Mondal, S.; Li, Q.; Das, N. *Tetrahedron Lett.* **2013**, *54*, 1681-1685.

112. Chen, Z.; Swager, T. M. *Macromolecules* **2008**, *41*, 6880-6885.

113. Wang, J. G.; Wang, M.; Xiang, J. C.; Cao, L. P.; Wu, A. X.; Isaacs, L. *Crystengcomm* **2015**, *17*, 2486-2495.

114. Gilberg, L.; Zhang, B.; Zavalij, P. Y.; Sindelar, V.; Isaacs, L. *Org. Biomol. Chem.* **2015**, *13*, 4041-4050.

115.Sigwalt, D.; Moncelet, D.; Falcinelli, S.; Mandadapu, V.; Zavalij, P. Y.; Day, A.; Briken, V.; Isaacs, L. *ChemMedChem* **2016**, *11*, 980-989.

116. Ko, Y. H.; Kim, E.; Hwang, I.; Kim, K. *Chem. Commun.* **2007**, 1305-1315.

117. Palma, A.; Artelsmair, M.; Wu, G.; Lu, X.; Barrow, S. J.; Uddin, N.; Rosta, E.; Masson, E.; Scherman, O. A. *Angew. Chem. Int. Ed.* **2017**, *56*, 15688-15692.

118. Cao, L.; Hettiarachchi, G.; Briken, V.; Isaacs, L. *Angew. Chem. Int. Ed.* **2013**, *52*, 12033-12037.

119. Ghale, G.; Nau, W. M. *Acc. Chem. Res.* **2014**, *47*, 2150-2159.

120. Jang, Y.; Jang, M.; Kim, H.; Lee, S. J.; Jin, E.; Koo, J. Y.; Hwang, I.-C.; Kim, Y.; Ko, Y. H.; Hwang, I.; Oh, J. H.; Kim, K. *Chem* **2017**, *3*, 641-651.

121. Yang, H.; Yuan, B.; Zhang, X.; Scherman, O. A. *Acc. Chem. Res.* **2014**, *47*, 2106-2115.

122. van Dun, S.; Ottmann, C.; Milroy, L.-G.; Brunsveld, L. *J. Am. Chem. Soc.* **2017**, *139*, 13960-13968.

123. Bosmans, R. P. G.; Briels, J. M.; Milroy, L.-G.; de Greef, T. F. A.; Merkx, M.; Brunsveld, L. *Angew. Chem. Int. Ed.* **2016**, *55*, 8899-8903.

124. Dang, D. T.; Nguyen, H. D.; Merkx, M.; Brunsveld, L. *Angew. Chem. Int. Ed.* **2013**, *52*, 2915-2919.

125. Chinai, J. M.; Taylor, A. B.; Ryno, L. M.; Hargreaves, N. D.; Morris, C. A.; Hart, P. J.; Urbach, A. R. *J Am Chem Soc* **2011**, *133*, 8810-3.

126. Webber, M. J.; Appel, E. A.; Vinciguerra, B.; Cortinas, A. B.; Thapa, L. S.; Jhunjhunwala, S.; Isaacs, L.; Langer, R.; Anderson, D. G. *Proc. Natl. Acad. Sci. U. S. A.* **2016**, *113*, 14189-14194.

127. Zhang, M. M.; Sigwalt, D.; Isaacs, L. *Chem. Commun.* **2015**, *51*, 14620-14623.

128. Hettiarachchi, G.; Samanta, S. K.; Falcinelli, S.; Zhang, B.; Moncelet, D.; Isaacs, L.; Briken, V. *Mol. Pharmaceutics* **2016**, *13*, 809-818.

129. Chen, J.; Liu, Y.; Mao, D.; Ma, D. *Chem. Commun.* **2017**, *53*, 8739-8742.

130. Ghale, G.; Ramalingam, V.; Urbach, A. R.; Nau, W. M. *J. Am. Chem. Soc.* **2011**, *133*, 7528-7535.

131. Klaerner, F.-G.; Schrader, T. *Acc. Chem. Res.* **2013,** *46*, 967-978.

132. Jeon, W. S.; Moon, K.; Park, S. H.; Chun, H.; Ko, Y. H.; Lee, J. Y.; Lee, E. S.; Samal, S.; Selvapalam, N.; Rekharsky, M. V.; Sindelar, V.; Sobransingh, D.; Inoue, Y.; Kaifer, A. E.; Kim, K. *J. Am. Chem. Soc.* **2005**, *127*, 12984-12989.

133. Job, P. *Ann. Chim.* **1928**, *9*, 113-203.

134. Lu, X.; Isaacs, L. *Angew. Chem. Int. Ed.* **2016**, *55*, 8076-8080.

135. Moghaddam, S.; Yang, C.; Rekharsky, M.; Ko, Y. H.; Kim, K.; Inoue, Y.; Gilson, M. K. *J. Am. Chem. Soc.* **2011**, *133*, 3570-3581.

136. Zhang, X.; Xu, X.; Li, S.; Li, L.; Zhang, J.; Wang, R. *Theranostics* **2019**, *9*, 633-645.

137. Tian, J.; Xu, Z.-Y.; Zhang, D.-W.; Wang, H.; Xie, S.-H.; Xu, D.-W.; Ren, Y.-H.; Wang, H.; Liu, Y.; Li, Z.-T. *Nat. Commun.* **2016**, *7*, 11580.

138. Ahn, Y.; Jang, Y.; Selvapalam, N.; Yun, G.; Kim, K. *Angew. Chem. Int. Ed.* **2013,** *52*, 3140-3144.

139. Stancl, M.; Hodan, M.; Sindelar, V. *Org. Lett.* **2009**, *11*, 4184-4187.

140. Stancl, M.; Gilberg, L.; Ustrnul, L.; Necas, M.; Sindelar, V. *Supramol. Chem.* **2014**, *26*, 168-172.

141. Bauer, D.; Andrae, B.; Gass, P.; Trenz, D.; Becker, S.; Kubik, S. *Org. Chem. Front.* **2019**, *6*, 1719.

142. Bauer, D.; Andrae, B.; Gass, P.; Trenz, D.; Becker, S.; Kubik, S. *Org. Chem. Front.* **2019**, *6*, 1555-1560.

143. Mao, W.; Mao, D.; Yang, F.; Ma, D. *Chem. Eur. J.* **2019**, *25*, 2272-2280.

144. Hoffmann, U.; Grosse-Sundrup, M.; Eikermann-Haerter, K.; Zaremba, S.; Ayata, C.; Zhang, B.; Ma, D.; Isaacs, L.; Eikermann, M. *Anesthesiology* **2013**, *119*, 317-325.

145. Mao, D.; Liang, Y.; Liu, Y.; Zhou, X.; Ma, J.; Jiang, B.; Liu, J.; Ma, D. *Angew. Chem. Int. Ed.* **2017**, *56*, 12614-12618.

146. Liu, W.; Lu, X.; Meng, Z.; Isaacs, L. *Org. Biomol. Chem.* **2018**, *16*, 6499-6506.

147. Isaacs, L., The SAMPL7 Blind Prediction Challenges for Computational Chemistry. **2019**.

148. Wiseman, T.; Williston, S.; Brandts, J. F.; Lin, L. N. *Anal. Biochem.* **1989**, *179*, 131-7.

149. Shaikh, M.; Mohanty, J.; Singh, P. K.; Nau, W. M.; Pal, H. *Photochem. Photobiol. Sci.* **2008**, *7*, 408-414.

150. Saleh, N. i.; Koner, A. L.; Nau, W. M. *Angew. Chem. Int. Ed.* **2008**, *47*, 5398-5401.

151. Masson, E.; Shaker, Y. M.; Masson, J.-P.; Kordesch, M. E.; Yuwono, C. *Org. Lett.* **2011**, *13*, 3872-3875.

152. Xue, W.; Zavalij, P. Y.; Isaacs, L. *Org. Biomol. Chem.* **2019**, *17*, 5561-5569.

153. Ogoshi, T.; Yamagishi, T.-a.; Nakamoto, Y. *Chem. Rev.* **2016**, *116*, 7937-8002.

154. Shetty, D.; Khedkar, J. K.; Park, K. M.; Kim, K. *Chem. Soc. Rev.* **2015**, *44*, 8747-8761.

155. Dsouza, R. N.; Hennig, A.; Nau, W. M. *Chem. Eur. J.* **2012**, *18*, 3444-3459.

156. Harris, K.; Fujita, D.; Fujita, M. *Chem. Commun.* **2013**, *49*, 6703-6712.

157. NIH Alzheimer's disease fact sheet.